frontiers | Research Topics

Abiotic stresses in field crops: response, impacts and management under climate change scenario

Edited by
Aliza Pradhan, Kamal Krishna Pal, Mahesh Kumar, Ashim Datta, Milan Kumar Lal and Md Khairul Alam

Coordinated by
Basavaraj P. S.

Published in
Frontiers in Sustainable Food Systems

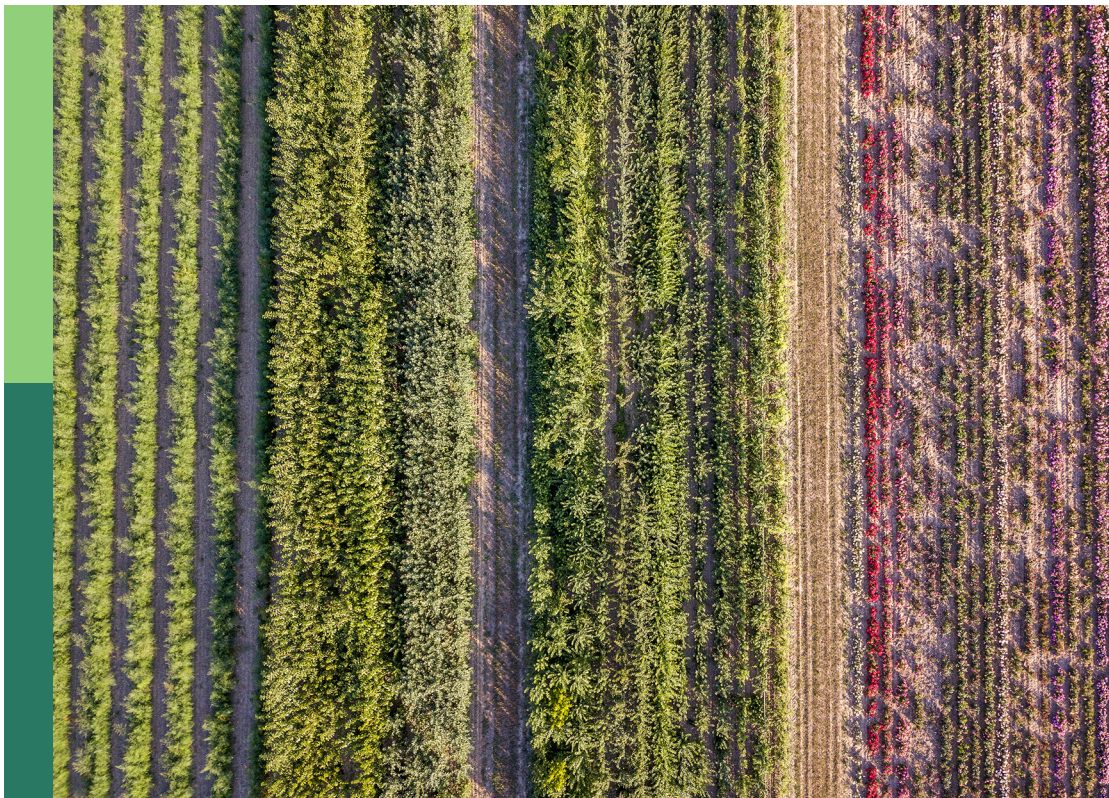

ISSN 1664-8714
ISBN 978-2-8325-5912-3
DOI 10.3389/978-2-8325-5912-3

About Frontiers

Frontiers is more than just an open access publisher of scholarly articles: it is a pioneering approach to the world of academia, radically improving the way scholarly research is managed. The grand vision of Frontiers is a world where all people have an equal opportunity to seek, share and generate knowledge. Frontiers provides immediate and permanent online open access to all its publications, but this alone is not enough to realize our grand goals.

Frontiers journal series

The Frontiers journal series is a multi-tier and interdisciplinary set of open-access, online journals, promising a paradigm shift from the current review, selection and dissemination processes in academic publishing. All Frontiers journals are driven by researchers for researchers; therefore, they constitute a service to the scholarly community. At the same time, the *Frontiers journal series* operates on a revolutionary invention, the tiered publishing system, initially addressing specific communities of scholars, and gradually climbing up to broader public understanding, thus serving the interests of the lay society, too.

Dedication to quality

Each Frontiers article is a landmark of the highest quality, thanks to genuinely collaborative interactions between authors and review editors, who include some of the world's best academicians. Research must be certified by peers before entering a stream of knowledge that may eventually reach the public - and shape society; therefore, Frontiers only applies the most rigorous and unbiased reviews. Frontiers revolutionizes research publishing by freely delivering the most outstanding research, evaluated with no bias from both the academic and social point of view. By applying the most advanced information technologies, Frontiers is catapulting scholarly publishing into a new generation.

What are Frontiers Research Topics?

Frontiers Research Topics are very popular trademarks of the *Frontiers journals series*: they are collections of at least ten articles, all centered on a particular subject. With their unique mix of varied contributions from Original Research to Review Articles, Frontiers Research Topics unify the most influential researchers, the latest key findings and historical advances in a hot research area.

Find out more on how to host your own Frontiers Research Topic or contribute to one as an author by contacting the Frontiers editorial office: frontiersin.org/about/contact

Abiotic stresses in field crops: response, impacts and management under climate change scenario

Topic editors

Aliza Pradhan — National Institute of Abiotic Stress Management (ICAR), India
Kamal Krishna Pal — Directorate of Groundnut Research (ICAR-DGR), India
Mahesh Kumar — Indian Council of Agricultural Research (ICAR), India
Ashim Datta — Central Soil Salinity Research Institute (ICAR), India
Milan Kumar Lal — National Rice Research Institute (ICAR), India
Md Khairul Alam — Bangladesh Agricultural Research Institute, Bangladesh

Topic coordinator

Basavaraj P. S. — National Institute of Abiotic Stress Management (ICAR), India

Citation

Pradhan, A., Pal, K. K., Kumar, M., Datta, A., Lal, M. K., Alam, M. K., Basavaraj P. S., eds. (2025). *Abiotic stresses in field crops: response, impacts and management under climate change scenario*. Lausanne: Frontiers Media SA.
doi: 10.3389/978-2-8325-5912-3

Table of contents

frontiers | Frontiers in Sustainable Food Systems

TYPE Editorial
PUBLISHED 07 January 2025
DOI 10.3389/fsufs.2024.1539301

OPEN ACCESS

EDITED AND REVIEWED BY
Maryke T. Labuschagne,
University of the Free State, South Africa

*CORRESPONDENCE
Aliza Pradhan
✉ alizapradhan@gmail.com

RECEIVED 04 December 2024
ACCEPTED 11 December 2024
PUBLISHED 07 January 2025

CITATION
Pradhan A, Datta A, Lal MK, Kumar M, Alam MK, Basavaraj PS and Pal KK (2025) Editorial: Abiotic stresses in field crops: response, impacts and management under climate change scenario.
Front. Sustain. Food Syst. 8:1539301.
doi: 10.3389/fsufs.2024.1539301

Editorial: Abiotic stresses in field crops: response, impacts and management under climate change scenario

Aliza Pradhan[1]*, Ashim Datta[2,3,4], Milan Kumar Lal[5], Mahesh Kumar[6], Md Khairul Alam[7], P. S. Basavaraj[1] and Kamal Krishna Pal[1,8]

[1]School of Drought Stress Management, ICAR-National Institute of Abiotic Stress Management, Baramati, Maharashtra, India, [2]Division of Soil and Crop Management, ICAR-Central Soil Salinity Research Institute, Karnal, Haryana, India, [3]W.K. Kellogg Biological Station, Michigan State University, Hickory Corners, MI, United States, [4]Great Lakes Bioenergy Research Center, Michigan State University, East Lansing, MI, United States, [5]Crop Physiology and Biochemistry Division, ICAR-National Rice Research Institute, Cuttack, India, [6]Division of Plant Physiology, ICAR-Indian Agricultural Research Institute, New Delhi, India, [7]Division of Soil Science, Bangladesh Agricultural Research Institute, Dhaka, Bangladesh, [8]Microbiology Section, ICAR-Directorate of Groundnut Research, Junagadh, India

KEYWORDS

abiotic stress, crop management, crop physiology, genotype, phenotype, soil health, sustainable production

Editorial on the Research Topic
Abiotic stresses in field crops: response, impacts and management under climate change scenario

Agriculture faces significant challenges from environmental factors like drought, heat, waterlogging, cold, soil salinity, nutrient deficiency, and heavy metal contamination (Pathak, 2023). These stresses impair plant function, limiting growth and productivity. With climate change increasing the frequency and intensity of these stresses, food and nutrition security are at risk. Plants employ various tolerance mechanisms at molecular, biochemical, physiological, and morpho-anatomical levels, which vary by species and stress type (Rane et al., 2021). This editorial highlights promising research showcasing advanced understanding of plant responses to abiotic stresses. Through 14 publications (13 original research and 1 review) editorial covers various aspects of managing the emerging and future abiotic stresses through innovative G × E × M (genotype by environment by management) practices for improving the tolerance as well as adaptation and mitigation strategies for enhanced sustainability of crop production systems.

Oat (*Avena nuda* L.) is a moderately salt-tolerant cereal crop, and understanding its salinity tolerance mechanisms can improve production in salt-affected areas. Liu et al. studied the salt tolerance of the naked oat line Bayou1, treating 17-day-old seedlings with varying NaCl concentrations for 12 days. Optimal growth was observed at 50 mM NaCl. Despite reduced water uptake and nutrient imbalances, Bayou1 maintained root growth, indicating roots play a key role in its salt tolerance through increased Na^+ concentrations in root cell sap while maintaining membrane integrity and osmotic potential.

Azrai et al. applied machine learning (ML) to predict maize grain yield and stress tolerance index (STI) under normal and drought conditions. Thirty-five genotypes were evaluated across three sites, and ML models were optimized using genetic algorithms (GA) and ensemble methods. Results showed that ensemble models optimized by grid search had

the best performance, with R^2 values of 0.92 for grain yield and 0.82 for STI. The Multi-trait Genotype-Ideotype Distance (MGIDI) approach accurately identified superior hybrids (H06, H10, H13, H35), highlighting the potential of ML and MGIDI in drought-tolerant maize breeding.

Excess soil iron (Fe) toxicity is a major challenge for rice cultivation in acidic soils. Sonu et al. assessed sixteen rice genotypes under varying iron (Fe) levels to evaluate their responses to Fe toxicity, focusing on seedling root systems. Hydroponic screening identified 460 ppm Fe as a critical threshold, significantly affecting root traits and biomass. Genotypes were classified into tolerant and sensitive categories using leaf bronzing scores and a response stability index. Tolerant varieties, such as ILS 12-5, were identified, while popular varieties like BPT 5204 and Pusa 44 showed high sensitivity to Fe toxicity.

Traditional rice monocropping in uplands is not environmentally sustainable and profitable. Pan et al. assessed the energy flow, carbon balance, and GWP of five monocropping systems (rice, finger millet, black gram, horse gram, pigeon pea) and four intercropping systems (rice+black gram, rice+horse gram, finger millet+black gram, finger millet+horse gram). Rice+black gram and rice+horse gram were the most energy-efficient, with better carbon efficiency and sustainability. Pigeon pea and finger millet+horse gram offered higher rice equivalent yields and benefit-cost ratios. Overall, pigeon pea and finger millet-based intercropping systems were the best options for eastern India's rainfed upland agro-ecosystem.

High carbon losses in Mollisols pose a substantial challenge to food security and climate regulation. Liang et al. assessed fertilization strategies on crop yield, soil organic carbon (SOC) stock, and carbon sequestration efficiency under climate change scenarios in Northeast China using the SPACSYS model. Higher temperatures reduced maize yield by 14.5% in Harbin and 13.3% in Gongzhuling, and soybean yield by 10.6%. SOC sequestration efficiency decreased with increased carbon input. Manure application resulted in higher carbon sequestration efficiency compared to other treatments, making it an effective practice for climate change mitigation in Mollisols.

Basavaraj et al. screened cowpea varieties for waterlogging tolerance by evaluating morpho-physiological and root traits under 10 days of waterlogging stress at the seedling stage. Waterlogging reduced plant height, leaf area, chlorophyll content, and NDVI, but tolerant varieties like DC15 and PL4 exhibited increased adventitious root (AR) number and length. Correlation and PCA analyses revealed a positive link between AR formation/length and waterlogging tolerance, suggesting these traits as valuable markers for breeding waterlogging-tolerant cowpeas.

Smallholder maize farming in sub-Saharan Africa is highly vulnerable to drought, threatening food security and livelihoods. Ndlovu et al. mapped genomic regions associated with water stress tolerance in tropical maize using three F3 populations (753 families) evaluated in Kenya and Zimbabwe. High-density SNP markers identified 93 QTLs under well-watered and 41 under water-stressed conditions, with significant QTLs for grain yield, plant height, ear height, and anthesis-silking interval. These findings highlight the potential of genomic selection for improving maize breeding to enhance drought tolerance and support food security in sub-Saharan Africa.

Drought is a major concern in chickpea breeding, controlled by multiple genes. Harish et al. examined 125 chickpea landraces from the West Asia and North Africa (WANA) region, and 4 varieties, to identify marker-trait associations (MTAs) and candidate genes for drought tolerance. Thirteen physio-morphological traits were analyzed over two years at two locations, revealing strong correlations between seed yield and biological yield. Using genotypic data from 6,367 SNPs, 52 significant SNPs were identified, including genes related to drought tolerance such as GHR1, WAT1, and beta-galactosidase, which will aid in improving drought tolerance in chickpea breeding.

Cadmium (Cd) contamination in agricultural soils is a global concern due to its harmful effects on human health. Iqbal et al. investigated the impact of vermicompost (VC) on soil properties, plant physiology, leaf ultrastructure, antioxidant defense, and rice yields under Cd stress. Results showed that Cd toxicity decreased soil quality, photosynthesis, and antioxidant activity, leading to lower rice yields. However, VC application improved soil health, enhanced physiological functions, and boosted antioxidant enzyme activities, reducing Cd uptake and alleviating oxidative damage. The treatment (50 mg Cd + 6 t ha^{-1} VC) significantly increased grain yields, highlighting potential of vermicompost towards sustainable rice production in Cd-contaminated soils.

Climate change directly affects cotton yield by damaging morphological development and plant growth. Fan et al. used the AquaCrop model and 30 years of meteorological data (1988–2017) to optimize irrigation and planting dates for cotton under limited water conditions. Results showed that higher irrigation quotas increased yield and biomass, with 495 mm achieving optimal water efficiency. Planting in late March to early April suits regions with abundant water, while late April to early May is better for water-scarce areas, using early-maturing varieties.

Continuous drought stress threatens food security, yet crop responses remain uncertain. Cui et al. calibrated and validated the AquaCrop model using summer maize data from 2017 to 2018 to simulate growth under various drought scenarios. The model analyzed transpiration (Tr), biomass accumulation, and yield formation at two growth stages. Results showed that drought at the seedling stage significantly reduced transpiration and biomass, with severe drought during the seedling and jointing stages causing total yield loss. The study emphasized the importance of avoiding severe drought at these stages for sustainable maize yield.

Chakrabarti et al. investigated the effects of elevated ozone (O_3) and carbon dioxide (CO_2) on rice productivity in northern India over two kharif seasons (2020–2021). Using Free Air Ozone-Carbon dioxide Enrichment (FAOCE) rings, three rice varieties (Pusa Basmati 1121, Nagina 22, IR64 Drt1) were examined under varying nitrogen (N) management. Elevated O_3 reduced photosynthesis, stomatal conductance, and transpiration, resulting a 6.9–9% yield reduction. Elevated CO_2 partially compensated for yield losses, particularly in Nagina 22. Additional N (125% RDN) improved grain N uptake under elevated O_3 and CO_2 conditions.

Siddiqui investigated the effects of cypermethrin, a widely used synthetic pyrethroid, on growth, pollen morphology,

fertility, and antioxidant activities in *Cicer arietinum* L. The exposure not only reduced plant height, branches, pods, seeds, and yield but also increased pollen wrinkling, reduced fertility, impacted chlorophyll and carotenoid content. Cypermethrin also affected hydrogen peroxide scavenging, lipid peroxidation, and antioxidant enzyme activities in a dose-dependent manner. These findings highlight the need for further research on the ecological and health risks of cypermethrin exposure.

Wang et al. conducted a review on drought and heat stress in perennial ryegrass (*Lolium perenne* L.) from 1994 to 2024 showcasing consistent publications from China and the USA. Keyword analysis revealed "growth," "endophytic fungi," and "yield" in drought studies, while "growth," "gene," and "leaf" were common in heat stress research. Most studies focused on phenotype, resistance mechanisms, and endophytes. The review emphasized the need for further molecular research on drought-heat stress interactions.

Overall, this comprehensive range of research highlights the need for a multifaceted approach to understand the interactions and impacts of combined stresses, crucial for developing stress-tolerant crops and devising mitigation strategies for various climatic challenges.

Author contributions

AP: Conceptualization, Writing – original draft, Writing – review & editing. AD: Supervision, Writing – review & editing. ML: Writing – review & editing. MK: Writing – review & editing. MA: Writing – review & editing. PB: Writing – review & editing. KP: Supervision, Writing – review & editing.

Conflict of interest

The authors declare that the research was conducted in the absence of any commercial or financial relationships that could be construed as a potential conflict of interest.

Publisher's note

References

Pathak, H. (2023). Impact, adaptation, and mitigation of climate change in Indian agriculture. *Environ. Monit. Assess.* 195:52. doi: 10.1007/s10661-022-10537-3

Rane, J., Singh, A. K., Kumar, M., Boraiah, K. M., Meena, K. K., Pradhan, A., et al. (2021). The adaptation and tolerance of major cereals and legumes to important abiotic stresses. *Int. J. Mol. Sci.* 22:12970. doi: 10.3390/ijms222312970

frontiers | Frontiers in Sustainable Food Systems

TYPE Original Research
PUBLISHED 19 January 2024
DOI 10.3389/fsufs.2023.1336350

OPEN ACCESS

EDITED BY
Md. Khairul Alam,
Bangladesh Agricultural Research Institute, Bangladesh

REVIEWED BY
Michela Janni,
Institute of Materials for Electronics and Magnetism National Research Council, Italy
Oli Fakir,
Bangladesh Agricultural Research Institute, Bangladesh

*CORRESPONDENCE
Liyun Liu
✉ liuliyun79419@163.com
Mohammad Sohidul Islam
✉ ag.islam.agn@tch.hstu.ac.bd

†PRESENT ADDRESS
Liyun Liu,
Graduate School of Engineering, Osaka University, Suita, Japan

RECEIVED 10 November 2023
ACCEPTED 28 December 2023
PUBLISHED 19 January 2024

CITATION
Liu L, Assaha DVM, Islam MS, Rajendran K, Theivasigamani P, Soufan W, Ayman ES and Ueda A (2024) Effect of NaCl on physiological, biochemical, and ionic parameters of naked oat (*Avena nuda* L.) line Bayou1.
Front. Sustain. Food Syst. 7:1336350.
doi: 10.3389/fsufs.2023.1336350

Effect of NaCl on physiological, biochemical, and ionic parameters of naked oat (*Avena nuda* L.) line Bayou1

Liyun Liu[1]*†, Dekoum V. M. Assaha[2], Mohammad Sohidul Islam[3]*, Karthika Rajendran[4], Parthasarathi Theivasigamani[4], Walid Soufan[5], El Sabagh Ayman[6,7] and Akihiro Ueda[1]

[1]Graduate School of Integrated Sciences for Life, Hiroshima University, Higashihiroshima, Japan, [2]Department of Agriculture, Higher Technical Teachers' Training College, University of Buea, Yaounde, Cameroon, [3]Department of Agronomy, Hajee Mohammad Danesh Science and Technology University, Dinajpur, Bangladesh, [4]VIT School of Agricultural Innovations and Advanced Learning (VAIAL), Vellore Institute of Technology (VIT), Vellore, India, [5]Department of Plant Production, College of Food and Agriculture Sciences, King Saud University, Riyadh, Saudi Arabia, [6]Department of Agronomy, Faculty of Agriculture, Kafrelsheikh University, Kafrelsheikh, Egypt, [7]Department of Field Crops, Faculty of Agriculture, Siirt University, Siirt, Türkiye

Oat (*Avena nuda* L.) is a globally important cereal crop grown for its nutritious grains and is considered as moderately salt-tolerant. Studying salinity tolerant mechanisms of oats could assist breeders in increasing oat production and their economic income in salt-affected areas, as the total amount of saline land in the world is still increasing. The present study was carried out to better understand the salt tolerance mechanism of the naked oat line Bayou1. A soil experiment was conducted on 17 days-old Bayou1 seedlings treated with varying concentrations of NaCl for a period of 12 days. Bayou1 plants grew optimally when treated with 50 mM NaCl, demonstrating their salinity tolerance. Reduced water uptake, decreased Ca^{2+}, Mg^{2+}, K^{+}, and guaiacol peroxidase activity, as well as increased Na^{+} concentration in leaves, all contributed to a reduction in shoot growth. However, the damage to ionic homeostasis caused by increased Na^{+} concentrations and decreased K^{+} concentrations in the roots of Bayou1 did not inhibit its root growth, indicating that the main salt-tolerant mechanism in Bayou1 existed in its roots. Further, a hydroponic experiment found that increasing Na^{+} concentration in root cell sap enhanced root growth, while maintaining the integrity of root cell membranes. The accumulated Na^{+} may have facilitated the root growth of Bayou1 exposed to NaCl by effectively adjusting cellular osmotic potential, thereby ensuring root cell turgor and expansion.

KEYWORDS

antioxidant enzymes, ionic homeostasis, relative water content, root growth, salinity tolerance

1 Introduction

Saline land is increasing in arid, semi-arid, and coastal regions due to the use of medium or high-saline water for irrigation. It is important to search for salinity-tolerant crops to meet the food demand of a growing population and to enhance the economic and ecological values of these regions, where crop production and food safety face significant challenges (Gupta and

Huang, 2014). In plants, salinity causes osmotic stress, followed by ionic stress, which induces secondary stresses including oxidative stresses (Wang et al., 2022). Osmotic stress inhibits water assimilation and ionic stress causes ionic toxicity in salt-stressed plant tissues due to excessive accumulation of sodium (Na^+) ions (Negrão et al., 2017).

In general, Na^+ ions are not essential for plant growth, and excessive concentrations of these ions are toxic to the most plant species. The increased concentration of Na^+ in salt-stressed plant tissues frequently inhibits the uptake of other nutrients, including K^+, Ca^{2+}, and Mg^{2+}, resulting in nutrient deficiency (Keutgen and Pawelzik, 2009; Assaha et al., 2017b). Thus, the maintenance of ionic homeostasis in plants by modulating ion transporters, channels, and H^+ pumps is essential for plant tolerance to salinity (Almeida et al., 2017). Plants regulate Na^+ uptake through transporters or channels to prevent excessive accumulation in the cytosol, returning Na^+ to growth medium or apoplast, or compartmentalizing it into vacuoles (Lv et al., 2012). Cytosolic Na^+ ions are compartmentalized into vacuoles for efficient Na^+ detoxification, reducing cytosol toxic effects and maintaining osmotic potential, ensuring water uptake in cells (Apse and Blumwald, 2007; Lv et al., 2012). Na^+ are employed as a cost-effective osmolyte in plant tissues subjected to salt stress (Hariadi et al., 2011). Oxidative stress disrupts the balance between reactive oxygen species production and scavenging, leading to cell membrane damage and ion leakage (Gill and Tuteja, 2010; Huang et al., 2019). Plants utilize both non-enzymatic and enzymatic antioxidant defense systems, primarily catalase (CAT), glutathione peroxidase (GPX), and guaiacol peroxidase (POX), to prevent oxidative damage.

The naked oat (*Avena nuda* L.), which originated in Mongolia and northern China, differs from the common oat (*Avena sativa* L.) in morphology, nutritional value, and growth environment (Tang et al., 2019). Because of its rich supply of vitamins, minerals, carbohydrates, lipids, and oil, naked oats constitute an essential cereal crop that is grown all over the world and utilized for both human and livestock food (Carlson and Kaeppler, 2007; Daou and Zhang, 2012; Boczkowska and Tarczyk, 2013; Diao, 2017). In recent years, oat has received more attention due to its various grain bioactive compounds, which have been linked to a lower risk of cardiovascular disease, type 2 diabetes, gastrointestinal disorders, and cancer (Martínez-Villaluenga and Peñas, 2017). This traditional Chinese cereal is gaining popularity due to its cold weather tolerance, adaptation to short growing seasons and poor soil fertility (Daou and Zhang, 2012; Boczkowska and Tarczyk, 2013; Bai et al., 2018). On the contrary, the growth of naked oats is significantly impeded and its efficient utilization and development are restricted by abiotic stresses such as salinity and drought (Liu et al., 2020a,b; Zhang et al., 2022). When treated to drought stress, Huazao2 had lower yield, grain per panicle, grain weight per thousand grains, and transpiration rate (Zhang et al., 2022). Due to an imbalance in ionic homeostasis in its leaves, the growth of a 34 days-old Mengnongda1 seedling is inhibited when exposed to 100 mM NaCl (Liu et al., 2020a). The application of 50 mM sodic-alkalinity caused a reduction in the activities of antioxidant enzymes in a 20 days-old Yanke1 seedling, which affected its growth (Liu et al., 2020b). The study of salinity-tolerant naked oat lines and their mechanisms can be beneficial for crop breeding in salt-affected areas due to increasing agricultural difficulties. Figure 1 depicts the mechanisms of salinity tolerance in oats. Enhanced salt tolerance in oats is achieved through the induction of adaptive stress mechanisms. The upregulation of NHX1 compartmentalize Na^+ into vacuole while the upregulation of SOS1 returns Na^+ to growth media, resulting in Na^+ detoxification and ionic equilibrium in the cytosol. Superoxide dismutase (SOD) and glutathione reductase (GR) catalyze the conversion of O_2^- to H_2O_2, which is further detoxified to water and oxygen by GPX and CAT. By maintaining ion homeostasis and detoxifying oxidative damage within its cellular environment, these mechanisms enable the plant to effectively endure and survive in environments with high salinity. The utilization of this adaptation mechanism confers benefits and exhibits discernible impacts in different growing regions of naked oats. Depending on the specific target organ, these mechanisms have different effects on different plant organs, such as flowers, fruits, leaves, roots, and cellular components.

Bayou1, a widely grown line in Inner Mongolia, Hebei, Shanxi, and Gansu, China, has a high recovery ability from high salinity due to its ionic homeostasis and osmolyte production in its leaves (Diao, 2017; Liu and Saneoka, 2022). This high recovery capacity from high salinity reveals its high salinity tolerance. However, its salinity tolerance mechanism remains unclear. The study aims to identify the adaptive mechanisms of Bayou1 in response to low and moderate salinity levels using soil and hydroponic experiments. We investigated various parameters including leaf antioxidative enzyme activities, growth, assimilation of Na^+ and K^+ in all organs, water status, malondialdehyde (MDA) and Mg^{2+} and Ca^{2+} ions, in the leaves of soil experiment. Furthermore, we assessed the vigor of the roots in the hydroponic experiment, osmotic potential ($\Psi\pi$), Na^+ assimilation, and MDA concentration.

2 Materials and methods

2.1 Experiment 1: growth conditions of Bayou1 in a soil experiment

The Inner Mongolia Agricultural University in China provided assistance with the cultivation of oat line Bayou1 (*Avena nuda* L.) seeds, which were stored at 4°C -until germination. Seeds were incubated at room temperature for 24 h before being sowed directly in 350 cm^3 pots filled with commercial healthy soil and a plastic mesh at the bottom of pots. Pots were irrigated twice daily for 7 days, then five uniform seedings were selected and irrigated twice with a nutrient solution including 4.2 mM NO_3-N, 0.3 mM NH_4-N, 1.1 mM K_2O, 1.0 mM CaO, 0.4 mM MgO, 0.2 mM P_2O_5, 12.1 μM Fe, 5.4 μM B_2O_3, 5.3 μM MnO, 0.3 μM Zn, 0.1 μM Cu, and 0.08 μM Mo. Seedlings were treated with a nutrient solution containing varying concentrations of NaCl [0 mM (control), 50 mM, and up to 100 mM NaCl] in increments of 50 mM to reach a final concentration on day 17 for an additional 12 days in order to prevent seedling mortality of young oat seedlings exposed to salinity. The treatment consisted of four pots, with each pot having five plants deemed a replication to ensure statistical analysis accuracy. The soil experiment was carried out in a vinyl house with natural light, with 61% humidity, 17°C–25°C day/10°C–17°C night temperature.

2.1.1 Growth analysis and relative water content in the leaves of Bayou1 under soil experiment

After 12 days of soil experiment treatment, tiller numbers of the seedlings were counted and the seedlings were washed with

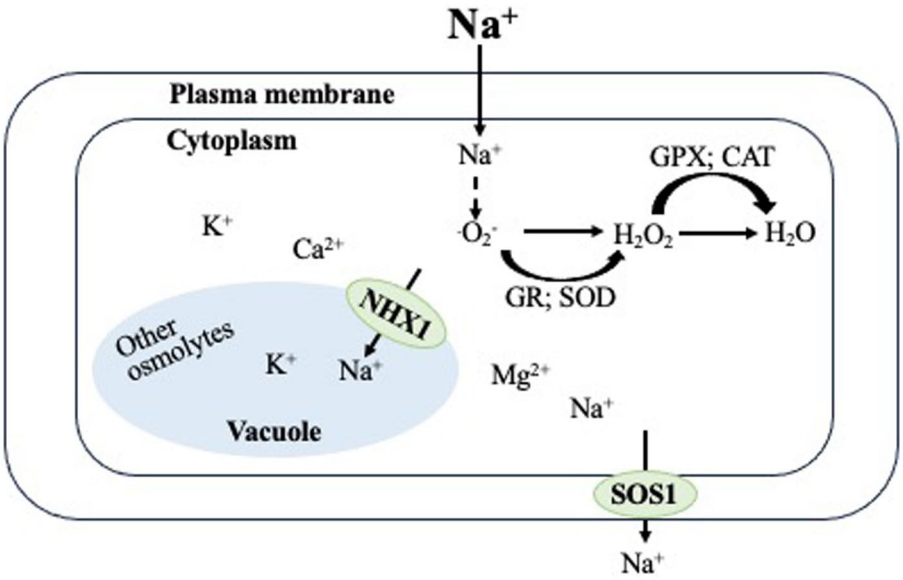

FIGURE 1
The oat plant's response mechanism to salt tolerance initiates adaptive stress mechanisms, allowing it to adapt and endure high salinity conditions by effectively managing and balancing ions within its cells. This adaptive mechanism is advantageous and manifests different effects in various plant organs. These superior mechanisms influence various plant organs, including flowers and fruits, leaves, roots, and cellular components, in a variety of ways, depending on the target organ. In addition, it upregulates a number of mechanisms, including HKT1, SOS1, and NHX1, leading to an increase in abscisic acid (ABA) levels.

tap water. Seedlings were cleaned, separated into leaves, sheaths, and roots, and oven-dried at 70°C for 3 days to determine their dry weights. The young leaf, sheath, and root tissues were flash-frozen in liquid nitrogen and stored at −80°C until use for analyses. The second fully expanded young leaves were frozen in liquid nitrogen and stored at −80°C for further analysis. Mekawy et al. (2015) provide a comprehensive account of the methodology employed to ascertain the relative water content (RWC). The fresh weight of leaves was recorded before soaking in fresh distilled water for 24 h under light. After gently removing extra water from the wet surface, the turgor weight of leaves was measured. The leaves were then oven-dried for 3 days at 80°C and the dry weight was recorded. The leaf relative water content was determined using the following formula: 100 × (fresh weight-dry weight)/(turgor weight-dry weight).

2.1.2 Na^+ and K^+ in the different organs, and Ca^{2+} and Mg^{2+} concentrations in the leaves of Bayou1 under soil experiment

Approximately 500 mg of oven-dried organs were digested with HNO_3 at 100°C for 12 h and then with HNO_3^- H_2O_2 (1:1 v/v) at 200°C for 20 min for cations. After dilution with distilled water, The Na^+ and K^+ concentrations in leaves, sheaths, and roots were measured using an ANA-135 flame photometer (Eiko Instruments Inc., Tokyo, Japan), while the Ca^{2+} and Mg^{2+} concentrations in leaves were measured using an AA-6200 atomic absorption flame emission spectrophotometer (Shimadzu Corporation Industrial Company, Kyoto, Japan). The Na^+, K^+, Ca^{2+}, and Mg^{2+} standards were used to calculate their concentrations in the organs.

2.1.3 Malondialdehyde analysis in the leaves of Bayou1 under soil experiment

The MDA concentration in the second fully expanded young leaves was evaluated to assess leaf lipid peroxidation (Draper and Hadley, 1990). Young leaves were finely pulverized in liquid nitrogen using a mortar and pestle. MDA was extracted from the powder using a 10 mM 4-(2-hydroxyethyl)-1-piperazineethanesulfonic acid (HEPES) buffer solution containing thiobarbituric acid, tricarboxylic acid, butylated hydroxytoluene, 2% ethanol, and 0.25 N HCl. After heating at 100°C for 30 min, the absorbance of the reaction supernatant was measured spectrophotometrically (U-3310; Hitachi, Tokyo, Japan) at 532 and 600 nm. The MDA concentration was determined using its extinction coefficient (1.55 mM^{-1} cm^{-1}).

2.1.4 Antioxidative enzyme activities in the leaves of Bayou1 under soil experiment

Soluble antioxidant enzymes were extracted from finely crushed powder in liquid nitrogen using a potassium phosphate buffer (pH 7.8) containing 1 mM ascorbic acid, 0.5 mM ethylenediaminetetraacetic acid, and 2% polyvinylpolypyrrolidone. Antioxidant enzyme activities in soluble protein and the concentration of soluble protein in crude extract were evaluated using the supernatant obtained after centrifugation (10,000 g, 4°C, 15 min). CAT activity was determined by measuring the initial rate of H_2O_2 disappearance at 240 nm, GPX activity by measuring tetraguaiacol absorbance at 470 nm, and GR activity by measuring the absorbance of oxidized NADPH at 340 nm in their respective reaction mixtures (Foyer and Halliwell, 1976; Aebi, 1984; Velikova et al., 2000; Liu et al., 2017). The reaction mixture for CAT activity contained 50 mM potassium phosphate buffer (pH 7.0),

10 mM hydrogen peroxide (H_2O_2), and 1% enzyme extract, and CAT activity was calculated using the molar extinction coefficient for H_2O_2 (0.04 mM^{-1} cm^{-1}). The reaction mixture for GPX activity contains 70 mM potassium phosphate buffer (pH 7.0), 15 mM guaiacol, 10 mM hydrogen peroxide (H_2O_2), and 2% enzyme extract, and GPX activity was determined using the molar extinction coefficient for tetraguaiacol (26.6 mM^{-1} cm^{-1}). The reaction mixture for GR activity contained 40 mM potassium phosphate buffer (pH 7.5), 0.78 mM glutathione, 0.4 mM EDTA, 0.02 mM NADPH, and 2% enzyme extract, and GR activity was estimated using the molar extinction coefficient for NADPH (6.22 mM^{-1} cm^{-1}). The DC protein assay kit (BioRad Laboratories, Inc.) was used to determine the amount of soluble protein in the enzyme extraction.

2.2 Experiment 2: growth conditions of Bayou1 in a hydroponic system

The seeds were germinated on damp towel paper for 3 days after being incubated at room temperature for 24 h. The seedlings were transferred to a hydroponic system comprised of plastic mesh covering 1.3 L plastic containers with tap water. After 5 days of germination, tap water was replaced with a nutrient solution according to section 2.1. Twelve-days-old seedlings were cultivated hydroponically for 6 days under 0 (control), 25 and 50 mM NaCl concentrations. Throughout the experiment, the pH of the nutrient solution was maintained between 5.9 and 6.2 with 1 N KOH. The study consisted of four containers in each treatment, with four seedlings grown in each container, representing one replicate. The tap water and nutrition solution were replaced twice a day and aerated continuously with pumps. The experiment was conducted under natural light conditions in the greenhouse, which was kept at a temperature range of 23°C–31°C during the day and 15°C–23°C at night.

2.2.1 Plant growth, and oxidative damage and vigor in the root of Bayou1 under hydroponic system

The fresh weight of shoots and roots was measured after being washed with tap water and placed on a wiper to remove any water. MDA concentration in the roots was measured in the same manner as in the soil experiment to determine oxidative damage.

Fresh root samples (0.1 g) were incubated for 10 min at room temperature in 5 mL of 0.1 M phosphate buffer (pH 7.0) containing 125 µg of -naphthylamine (Zhang et al., 2017). After incubating for one hour at 25°C, 0.2 mL of the resulting solution was combined with 1 mL of distilled water, 0.1 mL of 1% sulfanilic acid, and 0.1 mL of 0.1% sodium nitrite. After being incubated for 5 min, the mixture was once more diluted with 1.1 mL of distilled water, and results were recorded using a spectrophotometer at 510 nm. Root vigor was measured in micrograms of α -naphthylamine per gramme of FW per hour (µg α-NA g^{-1} FW h^{-1}).

2.2.2 Osmotic potential and Na^+ concentration in the roots of Bayou1 under hydroponic system

Fresh roots were filled into microtubes, then placed in a 5 mL microtube and centrifuged at 1,500 × g for 10 min to collect cell sap. The Wescor 5,500 vapor pressure osmometer (Wescor Inc., Logan, UT, United States) was used to measure the $\Psi\pi$ of the cell sap after centrifugation. Using a flame photometer (ANA-135; Eiko Instruments Inc., Tokyo, Japan), the Na^+ concentrations of 100-fold diluted root cell fluid were then determined. The $\Psi\pi$ of Na^+ was subsequently computed by applying the Van't Hoff equation derived by Liu et al. (2020a). The contribution of $\Psi\pi$ for Na^+ to the total $\Psi\pi$ was calculated using the equation: Contribution of $\Psi\pi$ for $Na^+ = 100 \times \Psi\pi$ of Na^+/ $\Psi\pi$.

2.3 Statistical analysis

All collected data were analyzed using one-way analysis of variance (ANOVA) with IBM SPSS version 25 (IBM Corp., Armonk, NY, United States). Duncan's multiple range test was used to perform multiple comparisons at $p \leq 0.05$. The values are the means (standard errors; SE) of four replicates. The values are the means (± standard errors; SE) of four replicates. The association between root biomass and other root characteristics was examined by a visual exploratory tool for correlation matrix using the corrplot package in the R programming language.

3 Results

3.1 Experiment 1

3.1.1 Effect of NaCl on biomass accumulation in soil experiment

At a concentration of 50 mM, NaCl greatly accelerated the growth of leaves and sheaths while inhibiting it at a concentration of 100 mM. When exposed to 50 mM NaCl, the DW of Bayou1 leaves and sheaths increased by 13% and 16%, respectively, but decreased by 10% and 9% when exposed to 100 mM NaCl. In contrast, neither 50 mM nor 100 mM NaCl concentrations changed root DW (Figure 2). When the concentration of NaCl was increased from 0 mM to 50 mM and then to 100 mM, the number of tillers in Bayou1 decreased by 16% and 28%, respectively (Table 1).

3.1.2 Water uptake capacity, and Mg^{2+} concentrations in the leaves of Bayou1 in soil experiment

The RWC in leaves was determined to investigate the water status of oat seedlings under salinity. When compared to control plants, RWC in the leaves was unaffected at 50 mM NaCl and considerably decreased (13%) at 100 mM NaCl (Figure 3). The Mg^{2+} in leaves was measured to examine the nutrient deficiency induced by salinity. The Mg^{2+} concentration in the leaves decreased by 13% at 100 mM NaCl, compared to 6% at 50 mM NaCl (), and by 0.15 mg g^{-1} DW (Table 1).

3.1.3 Na^+ and K^+ homeostasis in the different plant organs of Bayou1 in soil experiment

Ionic homeostasis in plant tissues is frequently disrupted as a result of the accumulation of excess Na^+ and depletion of other ions. When compared to controls, NaCl significantly increased Na^+ assimilation in all plant organs examined (Figure 4A). With an increase in salinity from 50 to 100 mM NaCl, leaf and root Na^+ concentrations did not differ significantly; Na^+ concentrations in the

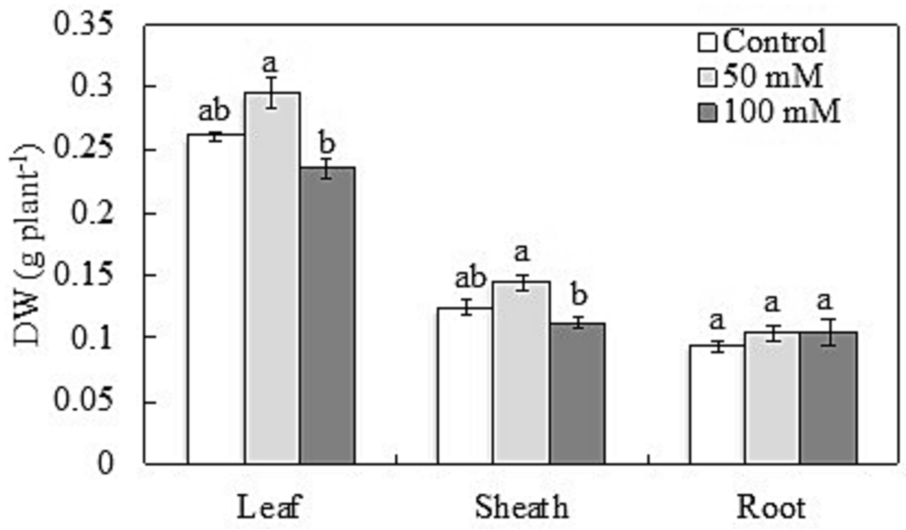

FIGURE 2
Plant dry weights in the leaves, sheathes, and roots of naked oat (*Avena nuda* L.) line Bayou1 under control conditions and 12 days of soil salinity. Values are means of four replicates ± standard error. Different lower-case letters indicate significant differences among treatments at $p \leq 0.05$.

TABLE 1 Tiller number, Mg^{2+} concentration, and activities of catalase (CAT), glutathione reductase (GR), and guaiacol peroxidase (GPX) in the leaves of naked oat (*Avena nuda* L.) cultivar Bayou1 soil grown with nutrient solution with 0 (control), 50, and 100 mM NaCl for 12 days.

Treatments	Tiller number	Mg^{2+} concentration (mg g^{-1} DW)	CAT (mM mg^{-1} protein min^{-1})	GR (μM mg^{-1} protein min^{-1})	GPX (μM mg^{-1} protein min^{-1})
Control	4.5 ± 0.65^{a}	2.05 ± 0.02^{a}	16.91 ± 1.44^{a}	21.6 ± 0.92^{a}	96.85 ± 6.27^{a}
50 mM	3.75 ± 0.25^{a}	1.93 ± 0.06^{ab}	17.73 ± 0.78^{a}	22.99 ± 1.51^{a}	100.23 ± 14.11^{a}
100 mM	3.25 ± 0.48^{a}	1.78 ± 0.05^{b}	15.9 ± 2.13^{a}	22.99 ± 1.51^{a}	36.4 ± 4.97^{b}

Values are means of four replicates ± standard error. Different lower-case letters indicate significant differences among the treatments at $p \leq 0.05$.

sheaths increased from 50 mM to 100 mM as NaCl. Compared to the controls, NaCl significantly decreased K^+ concentrations in the leaves, sheaths, and roots (Figure 4B). The K^+ concentration in the leaves and roots was reduced by 61% and 48% more at 100 mM than at 50 mM NaCl (51% and 16%). The K^+ concentration in the sheaths was reduced by 59% and 60% at 50 mM and 100 mM NaCl, respectively. All NaCl treatments increased the Na^+/K^+ ratio in the leaves, sheaths, and roots comparable to the control, with the highest ratios recorded at 100 mM (Figure 4C).

3.1.4 Effect of NaCl on the parameters related to cell membrane integrity in the leaves of Bayou1

The MDA concentration was measured to determine leaf damage under salinity (Figure 5A). MDA concentrations in the leaves increased significantly with increasing NaCl concentrations, with the highest level measured at 100 mM NaCl. However, there were no significant differences between 50 mM and 100 mM NaCl in terms of MDA concentration. Regulates A number of cell membrane functions that are associated with cell membrane integrity are regulated by Ca^{2+}. The Ca^{2+} concentration in the leaves decreased by 36% and 46% at 50 mM and 100 mM NaCl, respectively, with no significant difference between the two concentrations (Figure 5B). To investigate the antioxidative capacity of oat seedlings to salinity, antioxidant enzyme activities were measured. The activities of CAT and GR in the leaves were not affected at either by 50 mM or 100 mM NaCl. However, 50 mM NaCl had no effect on GPX activity, whereas 100 mM NaCl reduced it significantly (62%) (Table 1).

3.2 Experiment 2

3.2.1 Effect of NaCl on growth biomass of whole seedlings, and water cell membrane integrity, uptake ability, and role of Na^+ in the roots of Bayou1

The shoot FW increased by 15% at 25 mM and was unaffected at 50 mM NaCl, while the root FW increased by 22% at 25 mM and 21% at 50 mM NaCl (Table 2). MDA concentration was used to assess root damage (Figure 6A), while-naphthylamine-oxidizing activity was used to evaluate root vigor (Table 2). In comparison to the control plants, neither 25 mM nor 50 mM NaCl had any influence on MDA concentrations or root vigor (Figure 6A and Table 2).

Due to osmotic stress, the assimilation of Na^+ frequently causes water deficiency in plant tissues. To determine the effect of NaCl on water loss in Bayou1 roots, the root $\Psi\pi$ was measured (Figure 6B). In comparison to the controls, the highest root $\Psi\pi$ was observed at control, followed by 25 and 50 mM NaCl. Compared to the control plants, 25 mM and 50 mM NaCl increased Na^+ concentrations in root cell sap by 428 and 728 times, respectively (Figure 6C). To investigate the possibility of Na^+ sequestration in the vacuole of root cell vacuoles,

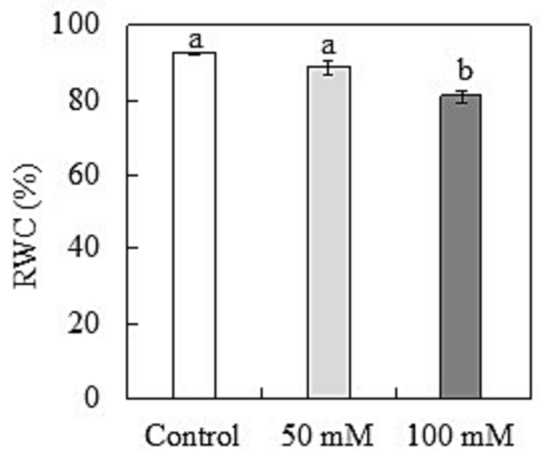

FIGURE 3
Relative water content (RWC) in the leaves of naked oat (*Avena nuda* L.) line Bayou1 under control conditions and 12 days of soil salinity. Values are means of four replicates ± standard error. Different lower-case letters indicate significant differences among treatments at $p \leq 0.05$.

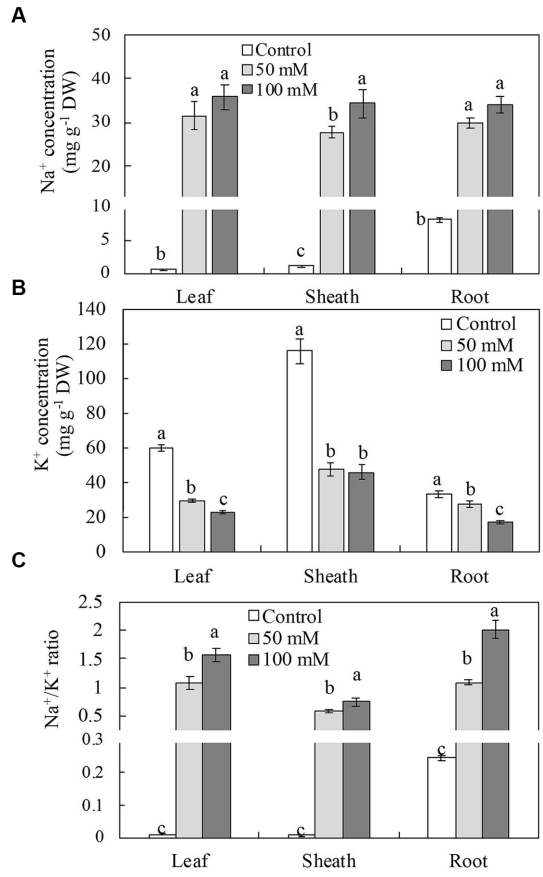

FIGURE 4
Concentrations of Na^+, **(A)** K^+ **(B)** and Na^+/K^+ ratio **(C)** in leaves, sheathes, and roots of naked oat (*Avena nuda* L.) line Bayou1 under control conditions and 12 days of soil salinity. Values are means of four replicates ± standard error. Different lower-case letters indicate significant differences among treatments at $p \leq 0.05$.

the Na^+ contribution to root Ψπ was determined. In comparison to the control plants, it increased at 25 mM (4.8-fold) and 50 mM NaCl (8.3-fold) (Figure 6D).

3.3 Correlation coefficient

The correlation coefficient of root biomass and other root characteristics in Bayou1 was significantly influenced by NaCl (Figure 7). The positive correlation between root biomass (DW-S and FW-H) and Na^+ concentration (Na-S and Na-H) in both soil and hydroponic experiments, as well as the positive correlation between the Na^+ contribution to root Ψπ ($\Psi_{Na}/\Psi\pi$-H) and FW-H, suggested that Na^+ has a beneficial effect on root growth. The negative correlation between K^+ concentration (K-S), root vigor (vigor-H), Ψπ-H, and root biomass indicated that reduced K^+, root vigor, and Ψπ had no effect on root growth. The cell membrane integrity of roots was highlighted as the positive correlation between the MDA-H and FW-H.

4 Discussion

4.1 Greater Na^+ allocation to the shoots under high salinity may be related to shoot reduction in Bayou 1

Salinity significantly decreases naked oat production, and earlier research investigated the short-term salinity tolerant mechanism in naked oats at the protein level (Chen et al., 2022). The short-term salinity tolerance mechanism in Bayou1 was determined at the physiological level in this investigation. Among plant salinity tolerance mechanisms, the exclusion of Na^+ from the shoot, i.e., the ability to restrict Na^+ transport and accumulation in the shoot, is of most importance, particularly in glycophytes (Munns and Tester, 2008; Assaha et al., 2017b; Wangsawang et al., 2018). The restriction of Na^+ allocation to young leaves is critical to Na^+ detoxification at the whole-plant level (Munns, 2002). This study found that low salinity had a positive effect on the growth and development of this line since Bayou1 did not appear to have any control over Na^+ allocation to the leaves and sheaths. Furthermore, this delivery of Na^+ coincided with improved growths of leaves and sheaths at 50 mM in the soil experiment (Figures 2, 4A). Mild salt stress improves the production and nutritional quality of several vegetable species (Rouphael and Kyriacou, 2018), which supports the observation of greater DW in leaves and sheaths in this study (Figure 2). In spinach, 50 mM NaCl enhances total yield, branch number, and antioxidant activity (Sogoni et al., 2021). It is possible that some of the Na^+ supplied to the leaves and sheaths from roots was detoxified by some mechanisms at 50 mM NaCl. However, increasing the salinity to 100 mM NaCl inhibited the growth of leaves and sheaths due to increased Na^+ buildup (Figures 2, 4A). Root Na^+ retention mechanisms are typically activated at this time, however they appeared inefficient, as Na^+ concentrations in roots levelled off with Na^+ concentrations in leaves and sheaths (Figure 4A). It is possible that the high Na^+/K^+ ratio, particularly in the leaves, caused significant damage to leaf tissues and impeded cellular activities using K^+ because the increase in shoot Na^+ coincided with a decrease in shoot K^+ (Munns and Tester, 2008). Therefore, the reduction in shoot growth may also be significantly influenced by the

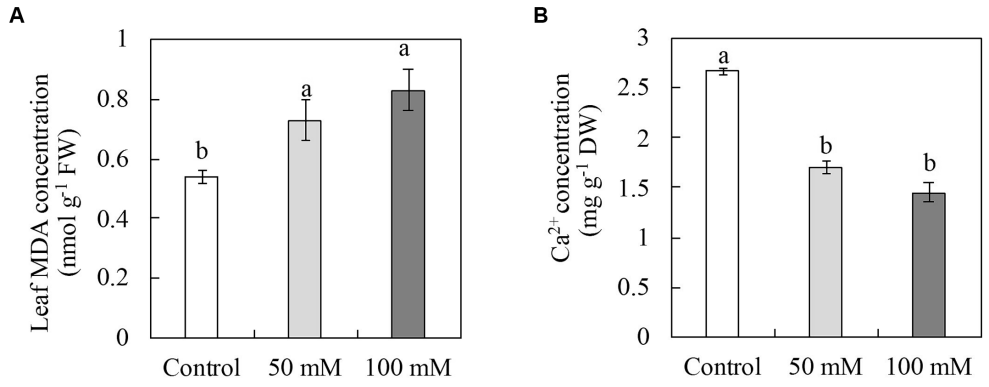

FIGURE 5
Concentrations of malondialdehyde (MDA) **(A)** and Ca^{2+} **(B)** in the leaves of naked oat (*Avena nuda* L.) line Bayou1 soil grown with nutrient solution with 0 (control), 50, and 100 mM NaCl for 12 days.

TABLE 2 **Fresh weight (FW) in the shoot, root FW and root vigor in the roots of naked oat (*Avena nuda* L.) cultivar Bayou1 hydroponically grown with nutrient solution with 0 (control), 25, and 50 mM NaCl for 6 days.**

Treatments	Shoot FW (g plant^{-1})	Root FW (g plant^{-1})	Root vigor (mg α-NA g^{-1} FW h^{-1})
Control	10.5 ± 0.02^{b}	0.58 ± 0.01^{b}	0.81 ± 0.06^{a}
25 mM	1.21 ± 0.04^{a}	0.71 ± 0.02^{a}	0.75 ± 0.02^{a}
50 mM	0.99 ± 0.04^{b}	0.70 ± 0.01^{a}	0.71 ± 0.01^{a}

Values are means of four replicates ± standard error. Different lower-case letters indicate significant differences among the treatments at $p \leq 0.05$.

decrease in shoot K^+ caused by high salt levels. However, the reduction in root growth was not related to the decrease in root K^+ and an increase in root Na^+ and the root Na^+/K^+ ratio (Figures 2, 4). It was hypothesized that increased Na^+ in roots would be compartmentalized into the vacuole rather than K^+ by NHX1 transporter, allowing roots to retain their K^+-protective functions in the cytosol. This maintenance of K^+-protective functions in root cytosol may aid in growth of roots under salinity. This effect is also demonstrated by the transformation of a barley (*Hordeum vulgare*) VP gene, HVP10, into rice (Fu et al., 2022). Transgenic rice overexpressing HVP10 exhibits greater salt tolerance than wild type, as well as Na^+ sequestration in the root vacuole and K^+ maintenance in roots (Fu et al., 2022).

4.2 NaCl treatments induce oxidative stress in the leaves of soil experiment

Under salinity, Na^+ outside of the cytosol causes oxidative stress, resulting in the production of MDA, which is the final product of peroxidation and alters cell membrane integrity (Gill and Tuteja, 2010). Due to the application of NaCl, increased MDA concentrations were observed in the leaves of Bayou1 (Figure 5A), indicating the presence of oxidative stress in the leaves. According to the findings, decreased water status (Figure 3) and Mg^{2+} concentration (Table 1), as well as increased Na^+ assimilation caused by NaCl may reduce photosynthetic capacity and, consequently, decrease photosynthetic electron transport activity, resulting in unfavorable dissipation of surplus light energy and overproduction of reactive oxygen species (ROS). Overproduction of ROS such as hydrogen peroxide (H_2O_2) in chloroplast photosystem II (PSII) induces oxidative stress in Bayou1 leaves. Plants typically utilize antioxidative enzymes such as CAT, GR, and GPX for ROS neutralization to combat oxidative stress and prevent membrane peroxidation (Couto et al., 2016; Huang et al., 2019). SOD protects against ROS-induced damage by catalyzing the conversion of O_2^- to H_2O_2, which is further catalyzed by CAT, GPX, and other peroxidases (Couto et al., 2016; Huang et al., 2019). In this instance, the maintenance of CAT activity maintained the decomposition of H_2O_2 to water and oxygen, thereby protecting the cells in the leaves from oxidative stress caused by H_2O_2. The maintenance of GR activity ensured the production of reduced glutathione, a key cellular antioxidant, and thus the protection of leaf cells against oxidative damage. However, a reduction in GPX activity decreased the capacity of the cell to eliminate excess H_2O_2 and had no effect on the cell's ability to withstand oxidative stress induced by H_2O_2 in the leaves. Meanwhile, Ca^{2+} can maintain membrane integrity, resulting in a reduction of MDA concentration under abiotic stress (Li et al., 2020); thus, the reduction of Ca^{2+} concentration (Figure 5B) may primarily weaken the permeability of cell membrane and damage the cell membrane integrity of Bayou1 leaves.

Likewise, higher shoot FW was observed at 25 mM NaCl and was maintained at 50 mM NaCl compared to the control plants in the hydroponic system (Table 2). However, the root FW increased at both 25 mM and 50 mM NaCl (Table 2), indicating that the roots are tolerant to salinity. Further analysis revealed the same MDA concentrations in the roots regardless of salinity treatment (Figure 6A), as well as a consistently increasing Na^+ concentration in root cell sap (Figure 6C), indicating that increased Na^+ concentrations in roots help maintain cell membrane integrity rather than diminish it. Moreover, root vigor is a comprehensive indicator of the number of living cells and their metabolic activity in roots; consequently, root vigor is a crucial attribute for the growth of terrestrial plants under environmental stress (Kajikawa et al., 2010; Zhang et al., 2019). The decrease in root vigor is associated with a decrease in root cell metabolism and the number of living root cells (Zhang et al., 2019). Here, the maintenance of root vigor (Table 2) suggests that the roots have maintained their capacity to adapt to either low or high salinity. Together, increased Na^+ concentrations did not affect the cell

10.3389/fsufs.2023.1336350

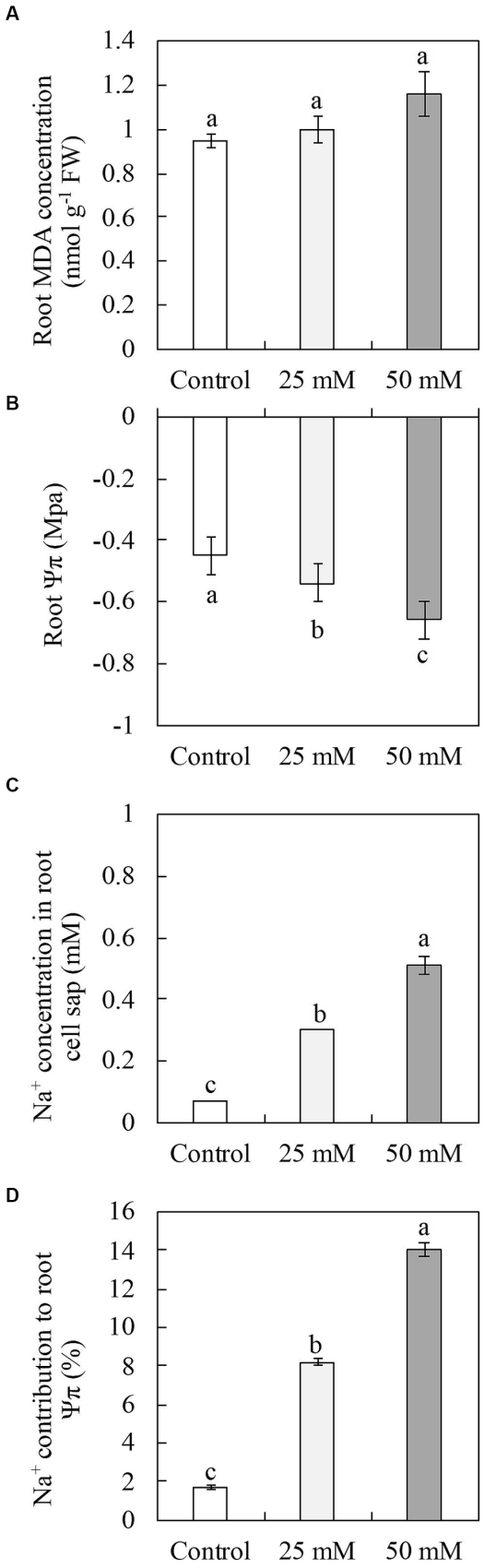

FIGURE 6
Malondialdehyde (MDA) concentration **(A)**, osmotic potential (Ψπ) **(B)**, Na^+ concentration in cell sap **(C)**, and Na^+ contribution to Ψπ **(D)** in the roots of naked oat (*Avena nuda* L.) line Bayou1 hydroponically grown with nutrient solution with 0 (control), 25, and 50 mM NaCl for 6 days.

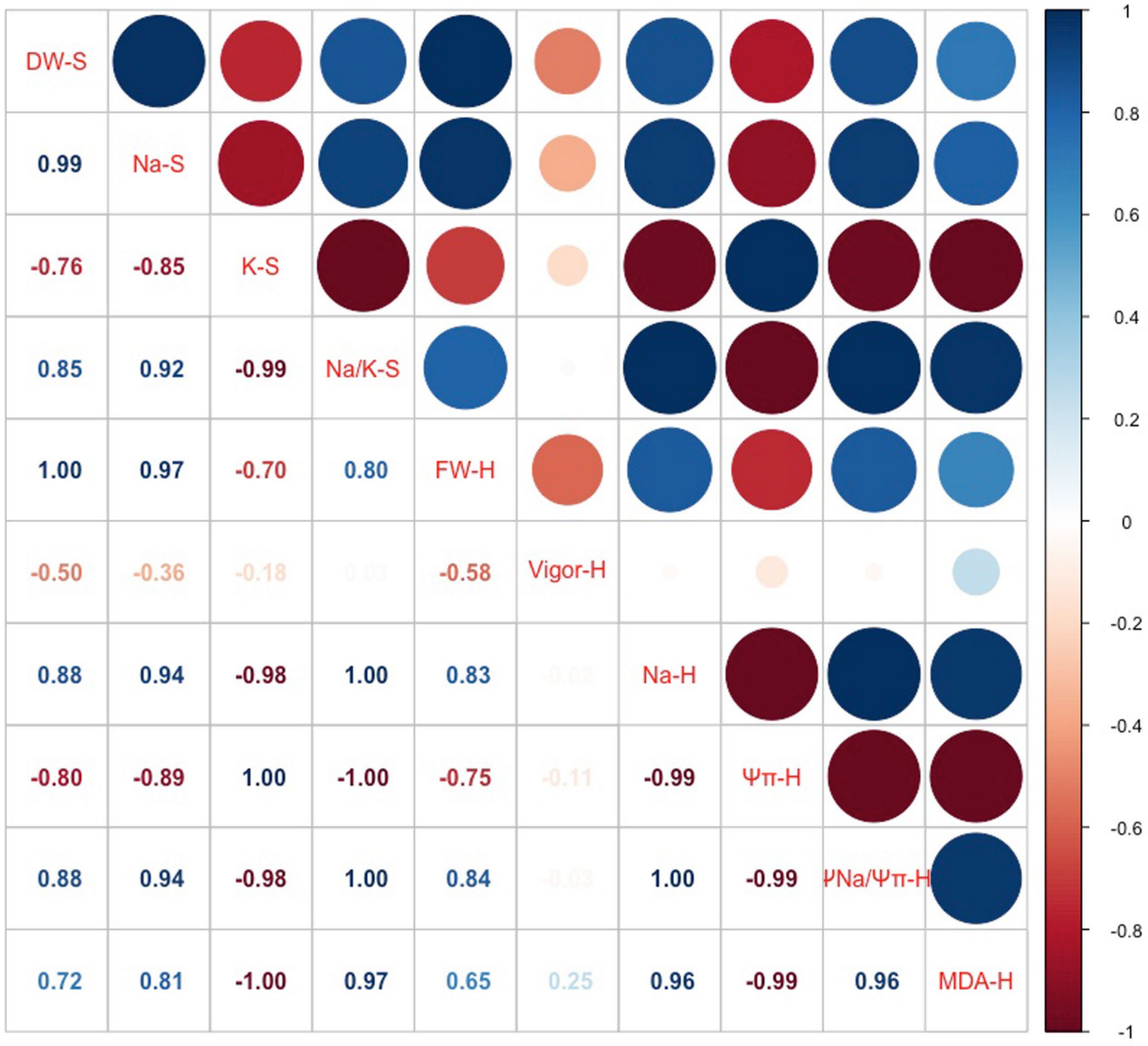

FIGURE 7
Correlation coefficients of root dry weight (DW-S) for soil experiment (S) and root fresh weight (FW-H) for hydroponic (H) system with Na^+ concentration (Na-S), K^+ concentration (K-S), and Na^+/K^+ ratio (Na/K-S) in the root of Bayou1 at different concentration of NaCl under soil experiment, and root vigor (vigor-H), Na^+ concentration in cell sap (Na-H), osmotic potential ($\Psi\pi$-H), Na^+ contribution to root $\Psi\pi$ ($\Psi_{Na}/\Psi\pi$-H), and malondialdehyde (MDA-H) in the root of Bayou1 at different concentration of NaCl under hydroponic system.

metabolic mechanisms in the roots of Bayou1 and may play a significant role in hydroponic root cell division and expansion.

4.3 Bayou1 uses Na^+ in the roots as an osmolyte to osmotically adjust to salt stress

Low water potential in the root environment causes water loss through the roots when exposed to high salinity; therefore, plants require osmolytes to continue water absorption and maintain positive turgor and root cell growth (Puniran-Hartley et al., 2014). Among the various osmolytes, soluble organic osmolytes are essential for achieving this goal. However, organic osmolytes biosynthesis is an energy-demanding process (Munns et al., 2020), making inorganic osmolytes a more cost-effective option to organic osmolytes in the short term (Puniran-Hartley et al., 2014). Numerous plants, including halophytes, withstand salinity by sequestering Na^+ in vacuoles to prevent its deleterious effects on the cytosol (Flowers et al., 2015). Here, Na^+ concentrations in roots of Bayou1 steadily increased with increasing salinity, without any growth restriction in the roots (Figures 2, 4A, 6C and Table 2), indicating that Na^+ accumulation was harmless to the roots as the stress increased from 50 to 100 mM NaCl in soil experiment or from 25 mM to 50 mM in hydroponic system. It is possible that sequestered Na^+ into vacuoles as an inorganic osmolyte supported cell expansion in roots and lateral root development. Similarly, the salinity tolerance of *Talinum paniculatum* is predominantly due to its ability to retain Na^+ in the

roots without inhibiting root growth in both low and high salinity conditions (Assaha et al., 2017a). Here, the progressively increasing root Na^+ concentrations limited the transport of this toxic ion from roots to shoots (Figure 4A), thereby partially preventing Na^+ toxicity in the shoots in the soil experiment and hydroponic system.

Certain physiological mechanisms prevent the deleterious effects of Na^+ on the roots of Bayou1 as evidenced by the fact that root DW was maintained in the soil experiment while root FW increased in the hydroponic system. To confirm these mechanisms, further research was conducted. Analyses demonstrated that osmotic adjustment was crucial and that the role of Na^+ was extremely essential, as Na^+ significantly contributed to the root $\Psi\pi$ (Figures 6B,D). These findings suggest that Bayou1 has evolved mechanisms for the selective sequestration of Na^+ into its root cell vacuoles for osmotic adjustment. This Na^+ sequestration enables the cytoplasm to sustain significantly lower Na^+ concentrations, thereby maintaining optimal cytosolic K^+ required for normal metabolic processes in the roots of Bayou1 under conditions of salt stress. The ionic homeostasis between Na^+ and K^+ in the cytosol contributed to the maintenance of normal molecular functions in root cells, as well as root vigor and growth. Therefore, in the present investigation, it was safe to predict that the root Na^+ in the cell sap was highest under 50 mM NaCl stress (Figure 6C), with a greater proportion of this Na^+ sequestered in the vacuoles in the hydroponic system. This physiological mechanism can also be demonstrated by the significant correlation between Na^+ concentration and root DW in the soil experiment and the positive correlation between Na^+ concentration in root cell sap and root FW in the hydroponic system (Figure 7).

5 Conclusion

Despite a reduction in shoot growth under high NaCl stress due to decreased water absorption capacity, Ca^{2+} and Mg^{2+} concentrations in the leaves, Bayou1 appeared to tolerate the salinity. The optimal plant growth of Bayou1 was found under low NaCl stress in either soil experiment or hydroponic system, rather than at control, implying the existence of salinity tolerant mechanisms in Bayou1. The novel discovery was the maintenance of root growth in a soil experiment (100 mM) and enhanced root FW in a hydroponic system at the highest NaCl concentration (50 mM). As a result, Bayou1's enhanced salinity tolerance is dependent on mechanisms that occur mostly inside the roots. Further investigation revealed that one of these processes is osmotic adjustment caused by Na^+ as the principal osmolyte in the roots, with a positive association between root Na^+ and root biomass in both the soil experiment and the hydroponic system. As a result, Bayou1 has a high tolerance to salinity and the ability to sequester Na^+ in root cell vacuoles. This method of Na^+ sequestration in the roots may be required to prevent Na^+ translocation to the shoots. This study provided the initial evidence demonstrating the salt tolerance of Bayou1, as indicated by the continued growth of its root system under conditions of low salinity.

Data availability statement

The datasets presented in this study can be found in online repositories. The names of the repository/repositories and accession number(s) can be found in the article/supplementary material.

Author contributions

LL: Conceptualization, Data curation, Formal analysis, Investigation, Methodology, Project administration, Resources, Software, Writing – original draft, Writing – review & editing. DVMA: Writing – review & editing, Software, Writing – original draft. MSI: Writing – review & editing, Conceptualization, Data curation, Formal analysis. KR: Software, Writing – review & editing. PT: Formal analysis, Writing – review & editing. WS: Funding acquisition, Resources, Software, Writing – review & editing. AES: Conceptualization, Funding acquisition, Resources, Writing – original draft, Writing – review & editing. AU: Conceptualization, Supervision, Writing – original draft, Writing – review & editing.

Funding

The author(s) declare financial support was received for the research, authorship, and/or publication of this article. This research was funded by the Researchers Supporting Project number (RSP2024R390) at King Saud University, Riyadh, Saudi Arabia.

Acknowledgments

All the authors are thankful to Researchers Supporting Project number (RSP2024R390), King Saud University, Riyadh, Saudi Arabia. The authors greatly appreciate the College of Grassland, Resources and Environment, Inner Mongolia Agricultural University, Inner Mongolia, China for providing the seeds of Bayou1.

Conflict of interest

The authors declare that the research was conducted in the absence of any commercial or financial relationships that could be construed as a potential conflict of interest.

Publisher's note

References

Aebi, H. (1984). Catalase *in vitro*. *Methods Enzymol.* 105, 121–126. doi: 10.1016/S0076-6879(84)05016-3

Almeida, D. M., Oliveira, M. M., and Saibo, N. J. M. (2017). Regulation of Na^+ and K^+ homeostasis in plants: towards improved salt stress tolerance in crop plants. *Genet. Mol. Biol.* 40, 326–345. doi: 10.1590/1678-4685-GMB-2016-0106

Apse, M. P., and Blumwald, E. (2007). Na^+ transport in plants. *FEBS Lett.* 581, 2247–2254. doi: 10.1016/j.febslet.2007.04.014

Assaha, D. V. M., Mekawy, A. M. M., Liu, L., Noori, S., Kokulan, K. S., Ueda, A., et al. (2017a). Na^+ retention in the root is a key adaptive mechanism to low and high salinity in the glycophyte, *Talinum paniculatum* (Jacq.) Gaertn. (Portulacaceae). *J. Agron. Crop Sci.* 203, 56–67. doi: 10.1111/jac.12184

Assaha, D. V. M., Ueda, A., Saneoka, H., Al-Yahyai, R., and Yaish, M. W. (2017b). The role of Na^+ and K^+ transporters in salt stress adaptation in glycophytes. *Front. Physiol.* 8:509. doi: 10.3389/fphys.2017.00509

Bai, J., Yan, W., Wang, Y., Yin, Q., Liu, J., Wight, C., et al. (2018). Screening oat genotypes for tolerance to salinity and alkalinity. *Front. Plant Sci.* 9:1302. doi: 10.3389/fpls.2018.01302

Boczkowska, M., and Tarczyk, E. (2013). Genetic diversity among Polish landraces of common oat (*Avena sativa* L.). *Genet. Resour. Crop Evol.* 60, 2157–2169. doi: 10.1007/s10722-013-9984-1

Carlson, A., and Kaeppler, H. F. (2007). "Oat" in *Transgenic crops IV: biotechnology in agriculture and forestry*. eds. E. C. Pua and M. R. Davey (Berlin: Springer). 59, 151–160. doi: 10.1007/978-3-540-36752-9_8

Chen, X., Xu, Z., Zhao, B., Yang, Y., Mi, J., Zhao, Z., et al. (2022). Physiological and proteomic analysis responsive mechanisms for salt stress in oat. *Front. Plant Sci.* 13:891674. doi: 10.3389/fpls.2022.891674

Couto, N., Wood, J., and Barber, J. (2016). The role of glutathione reductase and related enzymes on cellular redox homoeostasis network. *Free Radic. Biol. Med.* 95, 27–42. doi: 10.1016/j.freeradbiomed.2016.02.028

Daou, C., and Zhang, H. (2012). Oat beta-glucan: its role in health promotion and prevention of diseases. *Compr. Rev. Food Sci. Food Saf.* 11, 355–365. doi: 10.1111/j.1541-4337.2012.00189.x

Diao, X. (2017). Production and genetic improvement of minor cereal in China. *Crop J.* 5, 103–114. doi: 10.1016/j.cj.2016.06.004

Draper, H. H., and Hadley, M. (1990). Malondialdehyde determination as index of lipid peroxidation. *Methods Enzymol.* 186, 421–431. doi: 10.1016/0076-6879(90)86135-I

Flowers, T. J., Munns, R., and Colmer, T. D. (2015). Sodium chloride toxicity and the cellular basis of salt tolerance in halophytes. *Ann. Bot.* 115, 419–431. doi: 10.1093/aob/mcu217

Foyer, C. H., and Halliwell, B. (1976). The presence of glutathione and glutathione reductase in chloroplasts: a proposed role in ascorbic acid metabolism. *Planta* 133, 21–25. doi: 10.1007/BF00386001

Fu, L., Wu, D., Zhang, X., Xu, Y., Kuang, L., Cai, S., et al. (2022). Vacuolar H^{+-} pyrophosphatase HVP10 enhances salt tolerance via promoting Na^+ translocation into root vacuoles. *Plant Physiol.* 188, 1248–1263. doi: 10.1093/plphys/kiab538

Gill, S. S., and Tuteja, N. (2010). Reactive oxygen species and antioxidant machinery in abiotic stress tolerance in crop plants. *Plant Physiol. Biochem.* 48, 909–930. doi: 10.1016/j.plaphy.2010.08.016

Gupta, B., and Huang, B. (2014). Mechanism of salinity tolerance in plants: physiological, biochemical, and molecular characterization. *Int. J. Genomics* 2014:701596. doi: 10.1155/2014/701596

Hariadi, Y., Marandon, K., Tian, Y., Jacobsen, S. E., and Shabala, S. (2011). Ionic and osmotic relations in quinoa (*Chenopodium quinoa* Willd.) plants grown at various salinity levels. *J. Environ. Bot.* 62, 185–193. doi: 10.1093/jxb/erq257

Huang, H., Ullah, F., Zhou, D. X., Yi, M., and Zhao, Y. (2019). Mechanisms of ROS regulation of plant development and stress responses. *Front. Plant Sci.* 10:800. doi: 10.3389/fpls.2019.00800

Kajikawa, M., Morikawa, K., Abe, Y., Yokota, A., and Akashi, K. (2010). Establishment of a transgenic hairy root system in wild and domesticated watermelon (*Citrullus lanatus*) for studying root vigor under drought. *Plant Cell Rep.* 29, 771–778. doi: 10.1007/s00299-010-0863-3

Keutgen, A., and Pawelzik, E. (2009). Impacts of NaCl stress on plant growth and mineral nutrient assimilation in two cultivars of strawberry. *Environ. Exp. Bot.* 65, 170–176. doi: 10.1016/j.envexpbot.2008.08.002

Li, Z., Wang, L., Xie, B., Hu, S., Zheng, Y., and Jin, P. (2020). Effects of exogenous calcium and calcium chelant on cold tolerance of postharvest loquat fruit. *Sci. Hortic.* 269:109391. doi: 10.1016/j.scienta.2020.109391

Liu, L., El-Shemy, H. A., and Saneoka, H. (2017). Effects of 5-aminolevulinic acid on water uptake, ionic toxicity, and antioxidant capacity of Swiss chard (*Beta vulgaris* L.) under sodic-alkaline conditions. *J. Plant Nutr. Soil Sci.* 180, 535–543. doi: 10.1002/jpln.201700059

Liu, L., Han, G., Nagaoka, T., and Saneoka, H. (2020a). A comparative study of the growth and physiological parameters of two oat (*Avena sativa* L.) lines under salinity stress. *Soil Sci. Plant Nutr.* 66, 847–853. doi: 10.1080/00380768.2020.1820756

Liu, L., Petchphankul, N., Ueda, A., and Saneoka, H. (2020b). Differences in physiological response of two oat (*Avena nuda* L.) lines to sodic-alkalinity in the vegetative stage. *Plan. Theory* 9:1188. doi: 10.3390/plants9091188

Liu, L., and Saneoka, H. (2022). Physiological changes and subsequent recovery in seedlings of two lines of oat (*Avena nuda* L.) in response to salinity. *J. Soil. Sci. Plant Nutr.* 22, 3280–3290. doi: 10.1007/s42729-022-00886-w

Lv, S., Jiang, P., Chen, X., Fan, P., Wang, X., and Li, Y. (2012). Multiple compartmentalization of sodium conferred salt tolerance in *Salicornia europaea*. *Plant Physiol. Biochem.* 51, 47–52. doi: 10.1016/j.plaphy.2011.10.015

Martínez-Villaluenga, C., and Peñas, E. (2017). Health benefits of oat: current evidence and molecular mechanisms. *Curr. Opin. Food Sci.* 14, 26–31. doi: 10.1016/j.cofs.2017.01.004

Mekawy, A. M. M., Assaha, D. V. M., Yahagi, H., Tada, Y., Ueda, A., and Saneoka, H. (2015). Growth, physiological adaptation, and gene expression analysis of two Egyptian rice cultivars under salt stress. *Plant Physiol. Biochem.* 87, 17–25. doi: 10.1016/j.plaphy.2014.12.007

Munns, R. (2002). Comparative physiology of salt and water stress. *Plant Cell Environ.* 25, 239–250. doi: 10.1046/j.0016-8025.2001.00799.x

Munns, R., Passioura, J. B., Colmer, T. D., and Byrt, C. S. (2020). Osmotic adjustment and energy limitation to plant growth in saline soil. *New Phytol.* 225, 1091–1096. doi: 10.1111/nph.15862

Munns, R., and Tester, M. (2008). Mechanisms of salinity tolerance. *Annu. Rev. Plant Biol.* 59, 651–681. doi: 10.1146/annurev.arplant.59.032607.092911

Negrão, S., Schmöckel, S. M., and Tester, M. (2017). Evaluating physiological responses of plants to salinity stress. *Ann. Bot.* 119, 1–11. doi: 10.1093/aob/mcw191

Puniran-Hartley, J., Hartley, N., Shabala, L., and Shabala, S. (2014). Salinity-induced accumulation of organic osmolytes in barley and wheat leaves correlates with increased oxidative stress tolerance: in planta evidence for cross-tolerance. *Plant Physiol. Biochem.* 83, 32–39. doi: 10.1016/j.plaphy.2014.07.005

Rouphael, Y., and Kyriacou, M. C. (2018). Enhancing quality of fresh vegetables through salinity eustress and biofortification application facilitated by soilless cultivation. *Front. Plant Sci.* 9:1254. doi: 10.3389/fpls.2018.01254

Sogoni, A., Jimoh, M. O., Kambizi, L., and Laubscher, C. P. (2021). The impact of salt stress on plant growth, mineral composition, and antioxidant activity in *Tetragonia decumbens* mill.: an underutilized edible halophyte in South Africa. *Hort.* 7:140. doi: 10.3390/horticulturae7060140

Tang, M., Wang, L., Cheng, X., Wu, Y., and Ouyang, J. (2019). Non-starch constituents influences the *in vitro* digestibility of naked oat (*Avena nuda* L.) starch. *Food Chem.* 297:124953. doi: 10.1016/j.foodchem.2019.124953

Velikova, V., Yordanov, I., and Edreva, A. (2000). Oxidative stress and some antioxidant systems in acid rain-treated bean plants: protective role of exogenous polyamines. *Plant Sci.* 151, 59–66. doi: 10.1016/S0168-9452(99)00197-1

Wang, C. F., Han, G. L., Yang, Z. R., Li, Y. X., and Wang, B. S. (2022). Plant salinity sensors: current understanding and future directions. *Front. Plant Sci.* 13:859224. doi: 10.3389/fpls.2022.859224

Wangsawang, T., Chuamnakthong, S., Kohnishi, E., Sripichitt, P., Sreewongchai, T., and Ueda, A. (2018). A salinity-tolerant japonica cultivar has Na^+ exclusion mechanism at leaf sheaths through the function of a Na^+ transporter OsHKT1; 4 under salinity stress. *J. Agro. Crop. Sci.* 204, 274–284. doi: 10.1111/jac.12264

Zhang, X., Liu, W., Lv, Y., Li, T., Tang, J., Yang, X., et al. (2022). Effects of drought stress during critical periods on the photosynthetic characteristics and production performance of naked oat (*Avena nuda* L.). *Sci. Rep.* 12:11199. doi: 10.1038/s41598-022-15322-3

Zhang, H., Liu, X. L., Zhang, R. X., Yuan, H. Y., Wang, M. M., Yang, H. Y., et al. (2017). Root damage under alkaline stress is associated with reactive oxygen species accumulation in rice (*Oryza sativa* L.). *Front. Plant Sci.* 8:1580. doi: 10.3389/fpls.2017.01580

Zhang, G., Yang, C., Liu, R., and Ni, W. (2019). Effects of three phenolic compounds on mitochondrial function and root vigor of cotton (*Gossypium hirsutum* L.) seedling roots. *Acta Physiol. Plant.* 11:60. doi: 10.1007/s11738-019-2851-8

frontiers | Frontiers in Sustainable Food Systems

TYPE Original Research
PUBLISHED 02 February 2024
DOI 10.3389/fsufs.2024.1334421

OPEN ACCESS

EDITED BY
Mahesh Kumar,
Indian Council of Agricultural Research (ICAR), India

REVIEWED BY
Sudhir Kumar,
Indian Agricultural Research Institute (ICAR), India
R. N. Singh,
National Institute of Abiotic Stress Management (ICAR), India
Vishal Singh,
Utah State University, United States

*CORRESPONDENCE
Muhammad Azrai
azrai@agri.unhas.ac.id

RECEIVED 07 November 2023
ACCEPTED 17 January 2024
PUBLISHED 02 February 2024

CITATION
Azrai M, Aqil M, Andayani NN, Efendi R, Suarni, Suwardi, Jihad M, Zainuddin B, Salim, Bahtiar, Muliadi A, Yasin M, Hannan MFI, Rahman and Syam A (2024) Optimizing ensembles machine learning, genetic algorithms, and multivariate modeling for enhanced prediction of maize yield and stress tolerance index.
Front. Sustain. Food Syst. 8:1334421.
doi: 10.3389/fsufs.2024.1334421

Optimizing ensembles machine learning, genetic algorithms, and multivariate modeling for enhanced prediction of maize yield and stress tolerance index

Muhammad Azrai[1]*, Muhammad Aqil[2], N. N. Andayani[2], Roy Efendi[2], Suarni[2], Suwardi[2], Muhammad Jihad[2], Bunyamin Zainuddin[2], Salim[2], Bahtiar[3], Ahmad Muliadi[2], Muhammad Yasin[2], Muhammad Fitrah Irawan Hannan[2], Rahman[2] and Amiruddin Syam[4]

[1]Department of Agronomy, Faculty of Agriculture, Hasanuddin University, Makassar, Indonesia, [2]Research Center for Food Crops, National Research and Innovation Agency Republic of Indonesia—BRIN, Bogor, Indonesia, [3]Research Center for Behavioral and Circular Economics, National Research and Innovation Agency Republic of Indonesia—BRIN, Bogor, Indonesia, [4]Research Center for Macroeconomics and Finance, National Research and Innovation Agency Republic of Indonesia—BRIN, Jakarta, Indonesia

The frequent occurrence of drought, halting from unpredictable climate-induced weather patterns, presents significant challenges in breeding drought-tolerant maize to identify adaptable genotypes. The study explores the optimization of machine learning (ML) to predict both the grain yield and stress tolerance index (STI) of maize under normal and drought-induced stress. In total, 35 genotypes, comprising 31 hybrid candidates and four commercial varieties, were meticulously evaluated across three normal and drought-treated sites. Three popular ML were optimized using a genetic algorithm (GA) and ensemble ML to enhance data capture. Additionally, a Multi-trait Genotype-Ideotype Distance (MGIDI) was also involved to identify superior maize hybrids well-suited for drought conditions. The results highlight that the ensemble meta-models optimized by grid search exhibit robust performance with high accuracy across the testing datasets (R^2 = 0.92 for grain yield and 0.82 for STI). The RF optimized by GA algorithm demonstrates slightly lower performance (R^2 = 0.91 for grain yield and 0.79 for STI), surpassing the predictive performance of individual SVM-GA and KNN-GA models. Selection of the best-performing hybrids indicated that out of the six hybrids with the highest STI values, both the ensemble and MGIDI can accurately predict four hybrids, namely H06, H10, H13, and H35. Thus, combining ML with MGIDI enables researchers to discern traits for each genotype and holds promise for advancing the field of drought-tolerant maize breeding and expediting the development of resilient varieties.

KEYWORDS

drought, maize, machine learning, GA, ensemble

Introduction

The heightened concern relies on the impacts of global climate change on the intricate issue of plant water stress. The erratic shifts in precipitation patterns, coupled with increased temperatures, and the consequential elevation in evapotranspiration rates, collectively underscore a pivotal facet in the challenge of worsening drought conditions. These transformative alterations directly undermine the availability of water availability for plant growth, thereby magnifying the severity of drought scenarios. Consequently, this disruption results in a reduction in soil moisture content, while concurrently impeding the crucial uptake of water by the roots of plants. Furthermore, the heightened frequency and intensity of prolonged heatwaves, along with the changing climate, accelerate the evaporation process, which in turn intensifies the propensity for rapid water depletion, profoundly impacting the physiological well-being of plants.

The occurrence of drought in tropical regions, particularly in equatorial countries holds significant implications for agricultural productivity and necessitates adaptations in planting strategies. Bänziger et al. (2000) thoroughly investigated physical factors within the environment that exert stress on the cultivation of maize. Furthermore, Monneveux et al. (2008) underline a substantial reduction in maize productivity, ranging from 45% to 75%, due to water stress during the critical flowering period extending up to 2 weeks after silking. Moreover, in prolonged stress conditions, vulnerable genotypes exhibit an inability to produce viable seeds. The pursuit of drought-tolerant varieties demands a comprehensive plant breeding approach. It is noteworthy that the implementation of multi-location trials constitutes an essential prologue to more comprehensive field adaptation trials (Azrai et al., 2023).

As the dryland areas commonly exhibit limited water resources and low soil fertility, the process of genotype selection, usually aimed at identifying maize genotypes capable in efficient water uptake, holds significant importance within the realm of plant breeding, particularly for enhancing drought tolerance traits. The improvement of water use efficiency, achievable through the enhancement of plant water status, serves to facilitate the optimal distribution of assimilates and the improve kernel formation. Consequently, subjecting the maize genotypes assigned for development to rigorous pre-selection under water stress conditions before releasing as superior cultivars becomes imperative. Hence, the process of selecting for drought tolerance presents a multifaceted challenge, given the intricate interactions between genotypes and their environment.

Improving the selection efficiency of drought-tolerant maize genotypes involves directly observing their performance under water stress. Evaluating agronomic, morphological, and physiological traits linked to the plant's drought tolerance greatly assists in enhancing adaptation (Bänziger et al., 2000). A thorough examination of agronomic, morphological, and physiological attributes across various hybrid maize genotypes grown under intense water stress has the potential to correlate with the resulting grain yield. Numerous techniques have been utilized to assess the superiority of genotype either based on single drought-tolerant traits, including the AMMI and GGE biplot methods. However, the imperative arises to account for multiple traits due to preferences expanding beyond a single factor. To tackle this challenge, Olivoto and Nardino (2021) introduced the MGIDI index for concurrent genotype selection grounded in multiple traits.

Cutting-edge computational technologies such as high-performance computing, specialized bioinformatics tools, and advancements in artificial intelligence (AI) and ML techniques are presently employed for the comprehensive analysis of intricate datasets. These innovative approaches empower breeders to derive significant and insightful conclusions from their data, thereby enabling the formulation of enhanced and streamlined breeding strategies. Furthermore, these techniques contribute to an enhanced comprehension of the underlying genetic foundations governing plant traits (Yoosefzadeh-Najafabadi et al., 2021b). Numerous strategies encompassing ML and deep learning, have emerged for exploring genotype stability under diverse abiotic and biotic stresses. These approaches extent various abiotic stress scenarios. Cheng et al. (2021) introduced a systematic feature reduction technique within ML, substantially boosting predictive precision in gene-to-trait models. Singh et al. (2023) incorporate modern image acquisition and ML to identify key determinants of biomass accumulation, encompassing both architectural and physiological traits. Meanwhile, the use of leaf reflectance has enabled the extraction of plant water status indicators via near-infrared and short-wave infrared canopy emissions. Other studies have capitalized on the potential of ensemble ML and deep learning models in various agricultural contexts, such as rapid maize parental line identification and classification using stacking ensemble ML (Aqil et al., 2022), accurate soybean yield and biomass estimation through hyperspectral vegetation indices (Yoosefzadeh-Najafabadi et al., 2021a), genotype classification under varying light conditions (Sakeef et al., 2023), leaf chlorophyll status assessment based on SPAD readings, encompassing different nitrogen levels (Zainuddin and Aqil, 2021), and successful prediction of grain yield by utilizing these techniques across a range of environmental and phenological data (Srivastava et al., 2022). These studies exemplify the adaptability of ML and deep learning models in evaluating the performance of genotypes and making yield adjustments under a wide range of abiotic stress conditions.

Biotic stress typically become apparent during the initial stages of plant growth, posing intricate challenges concerning their manual differentiation and necessitating a substantial investment of time. Consequently, the integration of artificial intelligence (AI) and ML has yielded significant advancements in the detection and management of agricultural diseases. Noteworthy studies encompass the utilization of a novel convolution model featuring modified rectified linear unit activation for the identification of diseases in cucumber plants (Agarwal et al., 2021), underscoring the considerable potential of AI in this domain. A deeper exploration of machine vision techniques to detect diseases in corn leaves (Austria et al., 2022), coupled with the use of MobileNet for maize seedling and weed detection (Cheng et al., 2021), as well as the innovative hybridization of ResNet and YOLO for paddy leaf disease recognition (Ganesan and Chinnappan, 2022), have provided invaluable insights. Roy and Bhaduri (2021) contributed a sophisticated deep learning model capable of multi-class disease detection. The efficacy of AI in managing crop diseases extends to maize diseases, as evidenced by the boosted framework (Gokulnath and Devi, 2020). Another noteworthy contribution by Sharma et al. (2020) involves a method that combines ML techniques with image preprocessing to classify plant diseases. Furthermore, the complex field scenarios of maize leaf blight detection have been effectively addressed through the utilization of deep learning techniques (Sun

et al., 2020), and optimized neural network tailored for the identification of diseases in maize leaves (Waheed et al., 2020).

The objective of the research was to enhance the predictive accuracy of the grain yield and stress tolerance index of maize hybrids through fine-tuning via ensembles machine learning and genetic algorithms. Furthermore, the study compared the effectiveness of ML with MGIDI to select the best-performing hybrid candidates under normal and drought conditions.

Materials and methods

Experimental sites and genetic materials

The genetic material involved in the drought trials included a collection of 31 single cross hybrids, designated as H01 (DTH01) through H31 (DTH31), along with four commercial hybrids as checks, namely Bima14 (N51/MR 15), Bisi 18 (a commercial hybrid of BISI International), P 31 (hybrid of PT. Dupont Indonesia) and Pertiwi 3 (Supplementary Table S1). The N51 line was derived from Recombinant Inbred Lines (RILs) of the Syngenta genotype population through bulk selfing on a plant-to-plant basis, emphasizing drought tolerance. These hybridizations were undertaken with the intent of generating a wide spectrum of genotypes, exhibiting the potential for enhanced drought resilience. Meanwhile, the choice of the four commercial varieties was established in their proven ability to exhibit good resilience and achieve higher grain yields than other commercial varieties during cultivation in dry seasons in Indonesia.

For the assessment of potential drought-tolerant hybrid candidates during the cropping seasons of 2020–2021, three distinct locations were selected. These sites included the Maros experimental station/E1 (East longitude: 119°50; South longitude: −5°31), the Bajeng experimental station/E2 (East longitude: 119°57; South longitude: −5°33), and the Bontobili experimental station/E3 (East longitude: 119°58; South longitude: −5°01). These locations represented a diverse range of soil types, including Ultisols, Oxisols, and Inceptisols. Ultisols are rich in nutrients and suitable for farming while Oxisols are less fertile but offer good drainage and ecological importance. At the Maros site, the soil is classified as Inceptisols with varying fertility levels, ranging from low to moderate. The presence of these different soil types highlights the importance of considering soil factors when evaluating maize growth, as they significantly impact drought tolerance.

At each experimental site, there were two experimental plots: one with normal treatment involving regular plant watering and the other subjected to drought treatment, where irrigation halted at 40 DAP. The experimental plots followed a randomized complete block design (RCBD) with three replications. Plots were organized into four rows, each spanning 5 meters, with plant spacing set at 70 cm between rows and 20 cm within rows, and with 1 seed per hole. Fertilization was done twice, an initial application of 350 kg of NPK (15:15:15) and 150 kg of urea (46% N) per ha at 10 days after planting (DAP), followed by a second application of urea of 200 kg/ha at 30 DAP. Throughout the trial, negligible insect infestations were observed. Harvesting was done when plants reached physiological maturity (100–110 DAP). Maize cobs were harvested within a five-meter section from the middle rows of each replicate to ensure a representative sample for calculating yields. The collected ears from each plot were processed for yield component analysis. The moisture content of the maize kernels was measured using a digital grain moisture tester with 0.01 g resolution.

Managed water stress and phenotypic data

All tested maize genotypes under water stress conditions were subjected to the CIMMYT procedure (Bänziger et al., 2000), which involves imposing water stress on the plants from the flowering stage (50 DAP) until the milk-ripe stage (75 DAP). The water stress treatment was applied by withholding water supply when the plants were 40 DAP, causing the plants to experience water stress leading up to flowering at 50 DAP. This stress continued until the milky to kernel hardening stages (80 DAP), after which the plants were irrigated again. Observations encompassed a range of agronomic traits and yield components. From each plot, a random selection sample hybrid was gathered for analysis. The observed traits were: (1) plant height (PH), (2) ear height (EH), (3) stem diameter (SD), (4) leaf area (LA), (5) day to tasseling (DT), (6) day to silking (DS), (7) anthesis silking interval (ASI), (8) leaf angle (LAG), (9) SPAD, (10) husk cover (HC), (11) ear length (EL), (12) ear diameter (ED), (13) number of rows per cob (NR), (14) number of kernels per row (NKR), (15) 1,000 kernel weight (1,000 KW), (16) shelling percentage (SP), and (17) grain yield (GY). Both the stress tolerance index (STI) (Fernandez, 1992) and tolerance index (TOL) (Rosielle and Hamblin, 1981) were computed as metrics to quantify drought tolerance. These indices were calculated using the formulas (1) and (2) as follows:

$$\mathrm{STI} = \frac{Y_{p\times}\, Y_s}{\left(\bar{Y}_p\right)^2} \tag{1}$$

$$\mathrm{TOL} = Y_p - Y_s \tag{2}$$

Where Y_s is the mean yield of each genotype under water stress, Y_p is the mean yield of each genotype under normal condition, $\bar{Y}_p$ is the grand mean of yield under normal conditions.

Selection of ML model input

Feature selection (FS) was used to identify important attributes, eliminating irrelevant and redundant ones. This process allows for the creation of an optimized subset of features that remains unchanged by transformations, thereby improving the clarity and interpretability of learning models based on the selected feature subset. The underlying principle behind adopting feature selection includes the reduction of storage requirements and execution time, data dimensionality, and addressing concerns related to overfitting, thus promoting the refinement of model generalization. Consequently, feature selection improves the potential for enhancing model performance (Akhiat et al., 2019).

Three feature selection methods were utilized to assess the relationship between input variables and grain yield, namely Univariate Feature Selection (F-test), Recursive Feature Elimination (RFE), and LASSO (Least Absolute Shrinkage and Selection Operator) Regression. The study analyzed 17 agronomic parameters and yield

components, evaluating model performance through R^2 key metric. In the comparative analysis, LASSO and F-test demonstrated superior performance, boasting an R^2 of 0.81, which outperformed the RFE. LASSO regression is additionally favored due to its utilization of fewer model inputs, thereby effectively reducing data dimensionality. The excellence of LASSO's feature selection lay in its distinctive regularization methodology, adeptly penalizing substantial coefficients and compelling some to precisely zero, thereby eliminating irrelevant variables while maintaining model efficacy. LASSO model have also been applied as a powerful tools for reducing data dimensionality in crop yield prediction (Jhajharia et al., 2023). Feature selection using LASSO regression has selected 10 out of 16 agronomy and yield component parameters to predict grain yield and STI. The 10 selected variables as model inputs include ear height (EH), leaf area (LA), days to silking (DS), leaf angle (SD), SPAD, ear length (EL), ear diameter (ED), number of rows per cob (NR), number of kernels per row (NKR), and 1,000-kernel weight (1,000 KW). This formulation led to the refined model depicting grain yield and stress tolerance index, encapsulated by the function f (EH, LA, DS, SD, SPAD, EL, ED, NR, NKR, 1,000 KW). We examine the same model function to predict the stress tolerance index of each hybrid grown under normal and drought conditions.

Development of model prediction through fusing ML with genetic algorithm, and ensemble learning

The GA is a stochastic optimization method that operates independently of derivatives, derives its inspiration from natural selection and biological evolution. It showcases superior performance in comparison to other optimization approaches, spanning multiple dimensions. GA possesses a reduced susceptibility to being trapped in local minima. Notably, GA functions as a population-centric computational model, deeply rooted in principles of population genetics. It's recognized primarily as a function optimizer, having displayed its efficacy as a robust global optimization technique, especially adept at handling multi-modal and non-continuous processes.

Figure 1 illustrates a representation of the novel hybrid algorithms, which are rooted in the SVM-GA, KNN-GA, and RF-GA frameworks. This conceptual model delineates an amalgamated approach to artificial intelligence, fusing together various ML techniques. These chromosomes experience selection, crossover (mixing), and mutation processes to generate new solution generations. The effectiveness of each solution is assessed using a pre-defined goal. As generations progress, the algorithm moves closer to optimal or nearly optimal parameter values, allowing effective parameter adjustment for different uses. The synergy is fortified by the optimization of network hyperparameters through the utilization of GA. The hyperparameters are meticulously fine-tuned by generating a population of candidate solutions (sets of hyperparameters), assessing their performance on a testing set and subsequently evolving the population across multiple generations to discover the optimal set of hyperparameters. Afterward, the ML technique, guided by GA's processes, undertakes the training of the network.

Another predictive model that has gained popularity recently is ensemble ML. In this approach, datasets undergo a process of selecting base models followed by an ensuing meta-modelling step prior to generating predictions. The diagram of the ensemble ML process for yield prediction is shown in Figure 2. The diagram begins with thorough data preprocessing, including standardization. Afterward, the datasets are randomly divided into training and testing sets. The process of the training phase involves three specific ML models: SVM, KNN, and RF. To enhance parameter search efficiency and improve model predictions, a comprehensive search process fine-tunes the settings of each model using grid search. The algorithm generates three foundational base models, which are then input into the meta-model (SVM, KNN, and RF). This meta-model combines the separate predictions made by the SVM, KNN, and RF models mentioned earlier, resulting in an overall collective prediction. This combined prediction is applied to the testing dataset, generating yield predictions that are compared against actual yield values.

During the model running, 70% of the dataset was allocated for model training, while the remaining 30% was used for generating predictions. The accuracy of these predictions is evaluated using common metrics like R-squared (R^2), Mean Absolute Error (MAE), Root Mean Square Error (RMSE), and Normalized Root Mean Square Error (n-RMSE), n-RMSE percentages falling within the 0%–10% range are considered as "excellent," those ranging from 10%–20% are classified as "good," values between 20%–30% are categorized as "fair," and any percentages exceeding 30% are considered "poor" (Jamieson et al., 1991; Singh et al., 2023).

Nine combinations of ML and optimization models were subjected to training and prediction using cloud-based software services, GPU-based Google Colab. Nevertheless, the foundational structure of the models relies on comprehensive agronomy and yield component information for maize hybrids under both normal and drought treatment conditions. This data serves as a critical input, contributing to the accurate generation of predictions for grain yield and stress tolerance index. To construct predictive models for both grain yield and stress tolerance index, three classical ML algorithms, SVM, KNN and RF were employed, alongside traditional ML optimization using Genetic Algorithms (GA). These methods were coupled with ensemble techniques, where each SVM, KNN, and RF ML model was considered as a meta-model. In the search of enhancing predictive performance, the thoughtful adjustment of hyperparameters was integrated (Supplementary Table S2). Cross-validation was performed to some ML models to enable the training of higher-level ML models. To evaluate the effectiveness of all ML models, a comprehensive 10-fold cross-validation strategy was adopted.

The selection and manipulation of parameters for the SVM model involves a suite of hyperparameters, including the regularization parameter, kernel function and coefficient, as well as auxiliary parameters. Important parameters for KNN encompass leaf size, the number of neighbors, and the weighting scheme, while parameter configuration of RF model include n estimators for tree count, control over tree depth, and the quantity of features considered for optimal partitioning. The choice of a maximum of 50 iterations establishes a finite yet sufficient exploration horizon, balancing computational efficiency with the pursuit of optimal solutions. The modest population size of 10 individuals per generation, coupled with a 0.1 mutation probability, fosters exploration within the solution landscape. The elitism ratio of 0.01, along with the parents' portion of 0.3 and a crossover probability of 0.5 was set to optimize the adjustment of hyperparameters (Supplementary Table S2).

The study also employed an MGIDI approach to discern the most appropriate genotypes, leveraging multi trait data (Olivoto and

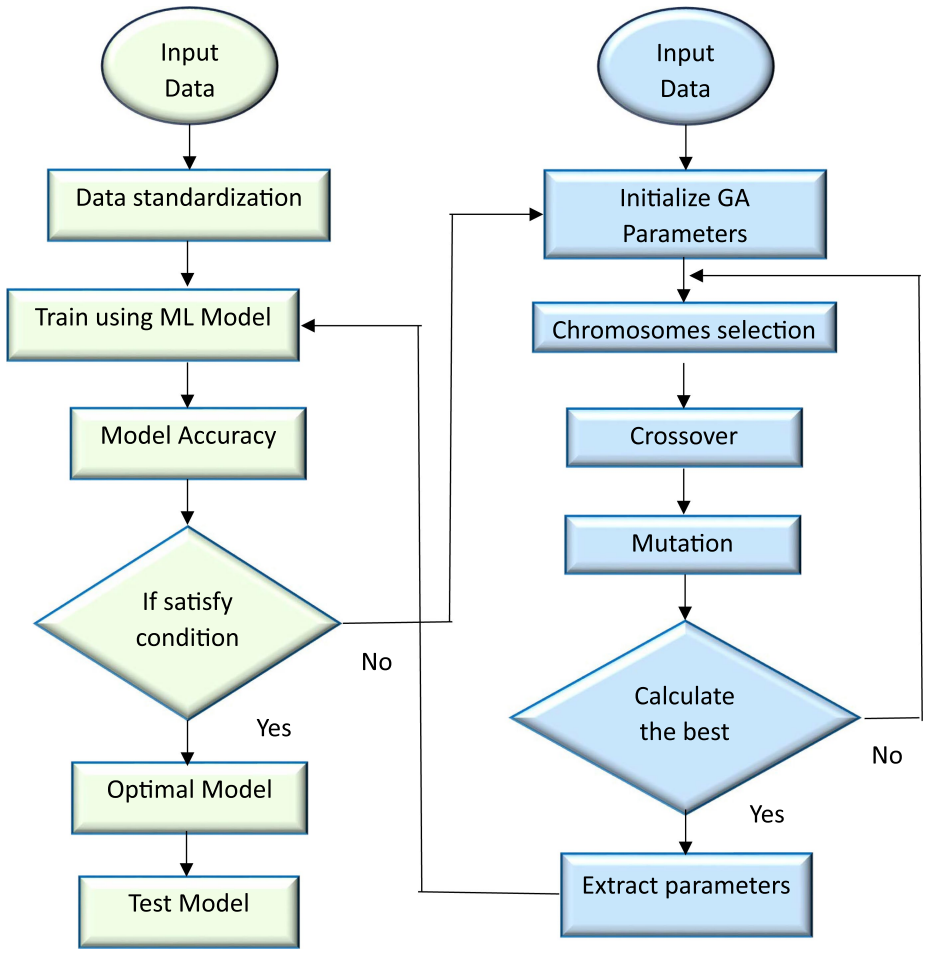

FIGURE 1
Schematic representation of ML optimized by GA for yield prediction.

Nardino, 2021). Initially, the scaling process was implemented for each individual trait under consideration. Subsequently, a Factor Analysis (FA) was performed to facilitate the reduction of data dimensions and reveal underlying relationship structures. Finally, the computation of the MGIDI was done by quantifying the Euclidean distance between genotype scores and an ideotype defined. This index was evaluated through the application of the subsequent formula:

$$\mathrm{MGIDI} = \sum_{j=1}^{f}\left[\left(\gamma_{ij} - \gamma_{j}\right)^{2}\right]^{0.5}$$

The score of the ith genotype in the jth factor ($i = 1, 2, \ldots, t$; $j = 1, 2, \ldots, f$) is represented by γ_{ij}, where t and f denote the number of genotypes and factors, respectively. The score of the jth trait for the ideal genotype is represented by γ_{j}. The genotype with the lowest MGIDI value is considered to be more closely aligned with the ideal genotype, encapsulating the desired attributes for all evaluated traits. In the genotype selection procedure, selection discrepancies were computed for all traits while maintaining a selection intensity of 30%.

The ML script was executed in Google Colaboratory (Colab) environment, which is available at https://colab.research.google.com/?utm_source=scs-index. During the process of executing ML algorithms within Google Colab, pivotal libraries, i.e., scikit-learn KNN and RF, as well as SVM implementation from sklearn.svm, were employed. To expedite computations, Colab provides GPU acceleration, enhancing the speed of model training and tuning. Moreover, GridSearchCV from the scikit-learn library was employed to optimize parameters, enabling a thorough exploration of hyperparameters for each individual algorithm. This ensemble/meta-learning process adeptly harnesses Colab's computational resources, libraries, and GPU acceleration to achieve refined predictions by amalgamating the strengths of KNN, RF, and SVM algorithms. In addition, genotype-versus-environment plots and MGIDI index calculations were generated using the "gamem" and "mgidi" functions of the "metan" package (Olivoto et al., 2019).

Results and discussion

Analysis of hybrid performance under normal and drought condition

Based on visual inspection and the analysis of grain yield and other agronomic datasets, it has been determined that trial plots subjected to normal irrigation treatment produced a more favorable

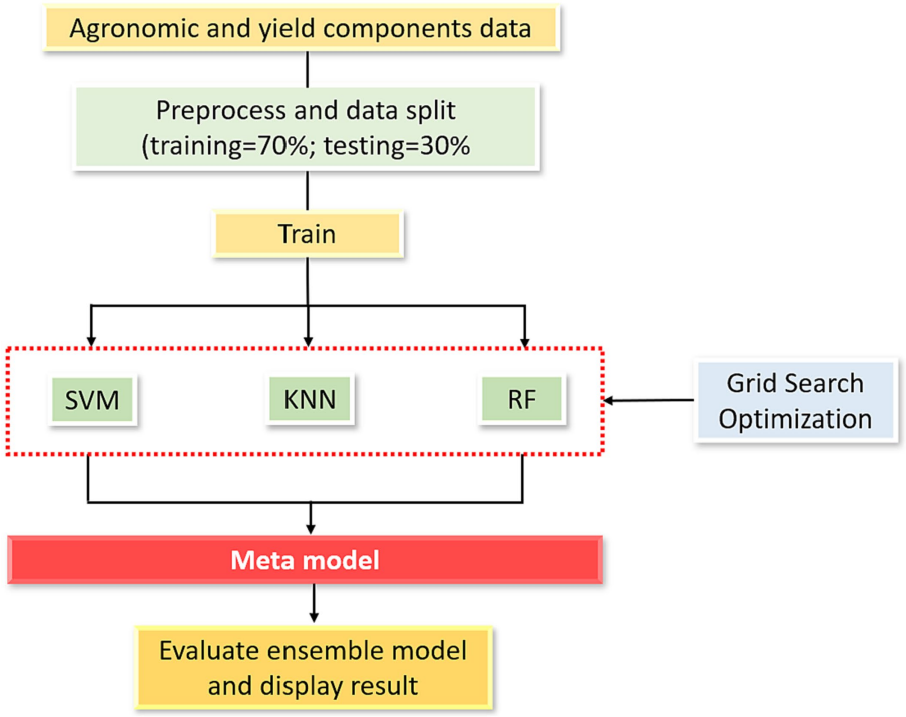

FIGURE 2
Conceptual architecture of proposed ensemble model used in the study.

conditions for obtaining yield potency, as contrasting to plots subjected to drought treatments. The combined analysis of variance revealed the distinct influence of the environment on grain yield and agronomic parameters of maize genotypes (Supplementary Table S3). The analysis involved five environments (three normal and two drought), with the environment effect separated into drought effect (df = 1) and location within the drought effect (df = 4). The effect of the drought treatment was evident across all observed traits, excluding the husk cover trait. Similarly, the effect of location within the drought treatment was significant for all 17 observed traits, except husk cover, indicating that variations in trial location have an impact on genotype performance. The genotype's effect was notable for all observed traits, except for SPAD, ED, and 1,000 KW traits, underscoring the phenotypic diversity of the hybrids in terms of agronomic, yield components, and grain yield. The interaction between genotype and location was significant for all observed traits. Additionally, the interaction between genotype and drought was significant for all traits, except husk cover and anthesis-to-silking interval. When examining the grain yields of hybrid maize, a notable finding exhibits significantly greater productivity in plots that receive regular irrigation. Figure 3 depicts the box plot graph of grain yield variation under normal and drought conditions ($n = 525$ for all environments).

Figure 3 indicated a significant difference in maize yield across the entire plot for the normal/irrigated and drought plots. Several genotypes consistently produced grain yields comparable to the best of commercial variety (Bisi 18) under both irrigated and drought conditions. The PH and EH traits of maize genotypes exhibited a significant increase under normal conditions compared to drought conditions. Physiological traits, such as chlorophyll content (SPAD), showed significantly higher levels under normal conditions compared to drought conditions. This finding affirms that drought reduces chlorophyll concentration in maize leaves, leading to a reduction in nitrogen concentration (Kira et al., 2016; Széles et al., 2023). A significant reduction was also found in LA trait under drought condition, suggesting the plant's response to water scarcity by adjusting its foliage area. Araus et al. (2021) found that the inability to maintain a larger area of green leaves under water stress conditions results in less sunlight being utilized for photosynthesis, thereby reducing yields. Several maize varieties exhibit leaf curling as a response to water stress, leading to a reduction in the photosynthetically active leaf extension of the plant. Additionally, it aids in reducing dehydration and lowering water consumption, especially during periods of high evaporation (Jordan, 1983). In addition to morphological aspect, water management such as the timing and intensity of water stress also have significant effects on maize growth (Çakir, 2004). Substantial reductions were also observed in number of kernel rows (NR), number of kernels per row (NKR), and 1,000 kernel weight (1,000 KW) under drought conditions, which might be indicative of the plant's allocation of resources towards kernel development in the face of water scarcity.

Phenotypic traits correlation

A heatmap of correlation analyses was conducted among 17 traits to identify those related to grain yield, as illustrated in Figure 4. Particularly, a significant positive correlation emerged between yield plant height and ear height ($r = 0.66^{***}$), SPAD reading with leaf area ($r = -0.43^{**}$), including highly correlated between grain yield with EL (0.75^{***}), ED (0.70^{***}), NKR (0.71^{***}), EH (0.48^{**}), LA (-0.41^{**}),

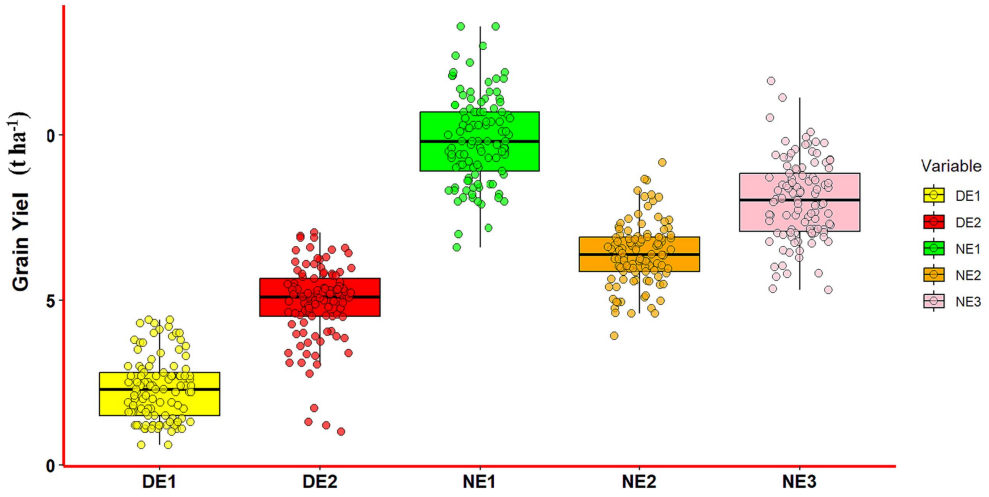

FIGURE 3
Box plots depicting the grain yield variation under normal and drought conditions (n = 105 for each environment, n = 525 for all environments, DE1 = drought E1, DE2 = drought E2, DE3 (data not available), NE1 = normal E1, NE2 = normal E2, NE3 = normal E3).

NR (0.41**), and SP (0.39**). Plants subjected to drought stress exhibit the induction of reactive oxygen species (ROS) within cells, resulting in damage to chloroplasts and cell membranes. This leads to the rapid deterioration of chloroplasts, crucial sites for photosynthesis in leaves. The compromised chloroplasts diminish the maize plant's capacity to produce energy and biomass (Sachdev et al., 2021). The impact of drought stress on chlorophyll is quantified by lower leaf chlorophyll meter (SPAD) values. Correlation analysis reveals a statistically significant correlation (r = 0.31**) between chlorophyll meter values and yield. This underscores the notion that maize plants capable of mitigating chloroplast damage under drought conditions yield higher grain quantities. Drought-tolerant plants adept at safeguarding chloroplast structures from damage enable leaves to sustain their greenness during drought stress, optimizing sunlight utilization for photosynthesis and consequently achieving elevated yields (Zahra et al., 2023).

The maize plant's ability to shield leaf structures from drought-induced damage exhibits a significant correlation (r = −0.43**) with leaf angle. Leaf angle, an imperative agronomic trait in maize, influences the plant's adaptability to drought conditions (Chotewutmontri and Barkan, 2016; Shao et al., 2016). A reduced leaf angle mitigates chloroplast exposure to intense light, preventing chloroplast damage (Zhang et al., 2022). Furthermore, a smaller leaf angle enhances planting density and maize plant biomass yield by facilitating greater light penetration through the canopy to reach lower leaves. Leaf angle demonstrates a noteworthy positive correlation with yield and yield components, with correlation coefficients ranging from 0.30 to 0.39. Therefore, manipulating leaf angles through selective breeding practices emerges as a pertinent strategy for augmenting the productivity and resilience of maize plants across diverse environmental conditions.

Yield components, such as cob length, cob diameter, seed row number, and seed number per row, manifest positive correlations with maize yield under drought stress conditions, featuring correlation coefficients ranging from 0.41** to 0.75***. These characteristics serve as reliable indicators of drought tolerance and valuable criteria for the selection of maize varieties to enhance yield under conditions of limited water availability.

Assessment of ML-GA and ensemble ML performances on grain yield prediction

The research integrates various foundational models to enhance grain yield predictive ability. The ensemble SVM, KNN, and RF models are structured with a meta-model at the helm, which employs SVM, KNN, and RF models as base models, respectively. Results of model performances during the training and prediction stages are shown in Table 1. The evaluation of the examined ML models centered around minimizing error. Moreover, model performance was assessed by minimizing the n-RMSE, which approaches below 10% for strong performance. R^2 indicated perfect correlation at 1 and no correlation at 0.

Table 1 provides metric of the individual models, with both the SVM and KNN models delivering commendable results—each exhibiting a R^2 value of 0.90 on the training set. However, in the case of SVM, there is a perceptible reduction in performance on the testing dataset (R^2 = 0.69), potentially suggesting a challenge in generalization. On the other hand, the KNN model maintains a relatively high R^2 of 0.77 on the testing set, indicating a robust balance between predictive accuracy and generalization. The RF model emerges as a standout performer, consistently achieving an R^2 of 0.97 and 0.81 on both the training and testing datasets. This striking consistency underscores RF's ability to generalize effectively, capturing complex relationships within the data. Sahu et al. (2017) reported that RF showed strong generalization capabilities for predicting grain yields in India.

The integration of RF with GA resulted in a significant enhancement in predicting grain yields, leading to an accuracy increase from 0.81 to 0.91 on testing datasets. Ensemble models, adeptly integrating predictions from multiple individual models, consistently present optimal results. These ensembles meta-model of SVM, KNN, and RF exhibit robustly high R^2 values across both

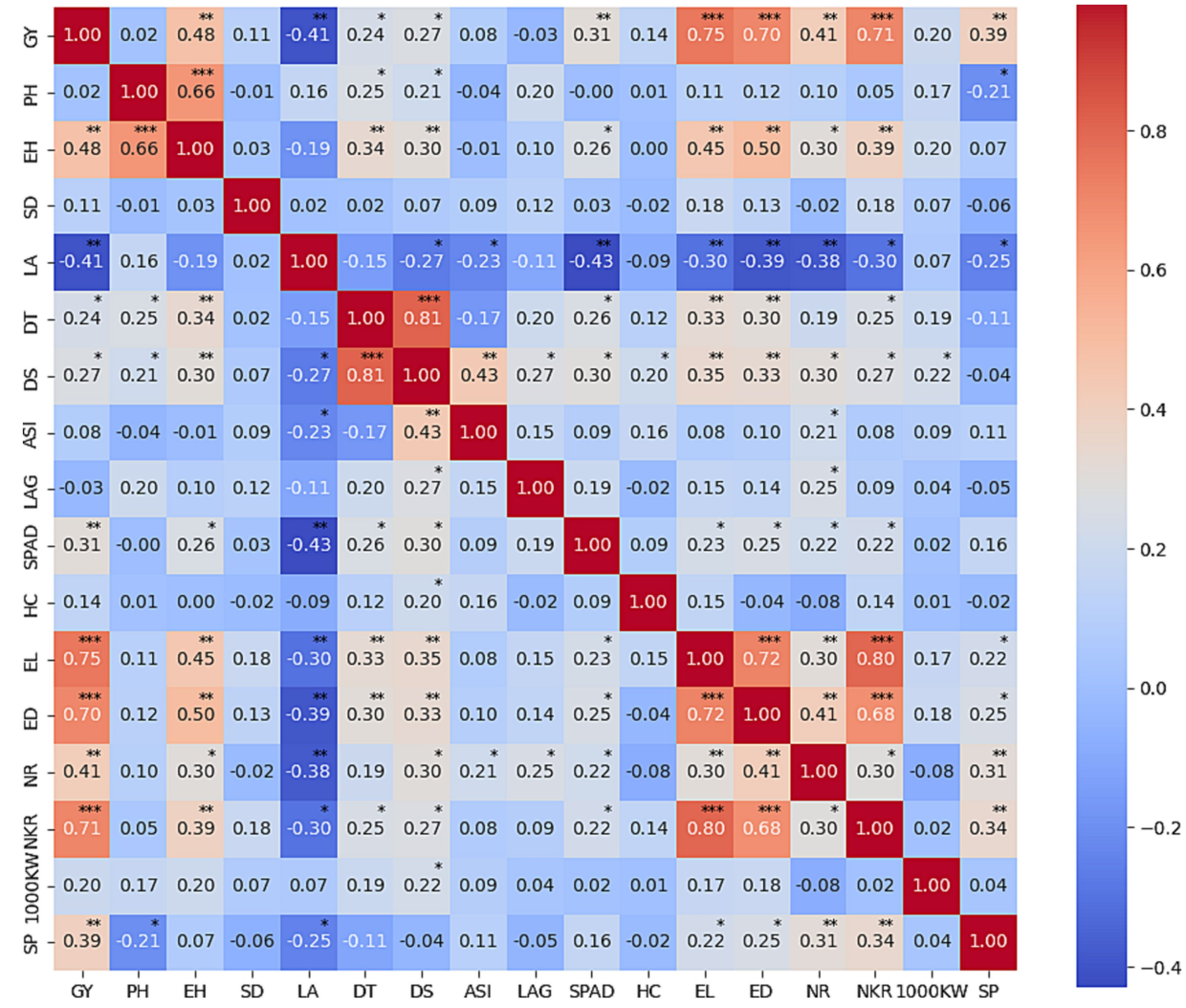

FIGURE 4
Heatmap of correlation analysis among agronomic and yield components under both normal and drought conditions.

TABLE 1 Assessment of model metrics for grain yield prediction.

MODEL	Training				Testing			
	R^2	MAE	RMSE	*n*-RMSE	R^2	MAE	RMSE (t ha^{-1})	*n*-RMSE (%)
SVM	0.90	0.68	0.905	0.071	0.69	1.21	1.772	13.91
KNN	0.90	0.65	0.894	0.069	0.77	1.04	1.415	11.10
RF	0.97	0.28	0.381	0.030	0.81	0.99	1.267	9.91
SVM + GA	0.86	0.84	1.083	0.086	0.71	1.31	1.597	12.60
KNN + GA	0.89	0.79	1.065	0.083	0.74	1.12	1.481	11.70
RF + GA	0.98	0.29	0.387	0.031	0.91	0.66	0.886	7.01
Ensemble SVM	0.97	0.28	0.451	0.035	0.91	0.64	0.876	6.93
Ensemble KNN	0.98	0.29	0.388	0.030	0.92	0.62	0.842	6.60
Ensemble RF	0.97	0.29	0.409	0.032	0.91	0.74	0.871	6.80

training and testing datasets. Utilizing an ensemble approach that incorporated three ML models as meta-models consistently resulted in high accuracy, with an R^2 consistently surpassing 0.91 (Figure 5). The excellence of these ensemble models might be rooted in the diversity of underlying models within the ensemble itself, contributing to a more thorough exploration of the feature landscape.

The analysis of the normalized *n*-RMSE values reveals distinctive performance characteristics among the considered crop yield prediction models. Ensemble modeling, combining predictions from KNN, RF, and SVM, stands out as a paradigm of excellence, showcasing an impressive *n*-RMSE range of 6.60% to 6.93%, classified as excellent prediction. This ensemble approach capitalizes on the diverse strengths of individual algorithms, resulting in a highly accurate and robust predictive model. Similarly, the standalone RF model and its optimized counterpart, RF + GA, exhibit notable excellence with *n*-RMSE values of 9.91% and 7.01%, respectively. These results underscore the significant impact of genetic algorithms in refining their predictive capabilities. In contrast, SVM emerges as the least favorable model for grain yield prediction, registering the highest *n*-RMSE value of 13.91%.

Comparative metrics for assessing model robustness in grain yield prediction in terms of R^2, MAE, RMSE and *n*-RMSE are shown in Figure 5. Ensemble algorithms demonstrated superior performance in crop yield prediction (Ahmed, 2023), while RF is the optimized algorithm for accurately forecasting maize yields at the county level through the integration of diverse data sources (Pham and Olafsson, 2018). Aqil et al. (2022) reported that incorporating ensemble machine learning may enhance the accuracy of classifying maize plants. Figure 6 depicts a simple scatter plot presenting the correlation between observed and predicted grain yields across the nine analyzed models. These results underscore the significant impact of optimizing models via GA and ensemble to enhance their predictive capabilities.

Water stress tolerance indices prediction

The performance of the developed GA and ensemble ML models was also evaluated based on a quantitative assessment. Table 2 presents a similar assessment of model performance metrics for predicting the STI of genotypes cultivated in both irrigated and drought fields. Among the individual models, the RF model exhibited remarkable performance in both the training and testing phases, achieving high R^2 values of 0.95 and 0.78, respectively. This indicates that the RF model captured a substantial portion of the variability in stress tolerance index predictions. The Ensemble KNN also demonstrated strong predictive accuracy, with R^2 values of 0.96 and 0.82 for training and testing, respectively. This suggests that the ensemble approach effectively harnessed the collective strengths of individual KNN models to enhance predictive accuracy and generalization. Additionally, the ensemble SVM and RF models yielded competitive results with R^2 values of 0.94 for both training and testing.

The analysis of the normalized *n*-RMSE values for STI indicated that none of the examined models had *n*-RMSE values falling below 10%, signifying reduced accuracy in predictive ability, although they remain within the "good" category with *n*-RMSE <20%. Ensemble KNN produced the lowest *n*-RMSE of 14.12% and is classified as a good prediction. The standalone SVM model produced the highest *n*-RMSE of 16.81%. The diminished accuracy in the predictive model is attributed to its failure to capture the underlying patterns or relationships in the data, resulting in larger prediction errors.

These ensemble methods leverage diverse models to improve predictive performance. The remaining models, including SVM, KNN, and their variants with GA optimization, displayed slightly lower R^2 values in comparison. These results emphasize that ensemble techniques, particularly the Ensemble KNN and Ensemble RF models, stand out as robust approaches for predicting the stress tolerance index. The high R^2 values achieved by these models indicate their capability to effectively capture and explain the variations in stress tolerance, making them valuable tools for accurate stress tolerance predictions. Comparative metrics for assessing model robustness in stress tolerance index prediction in terms of R^2, MAE, RMSE and

FIGURE 5
Comparative metrics for the nine examined ensembles and GA-ML models in grain yield prediction.

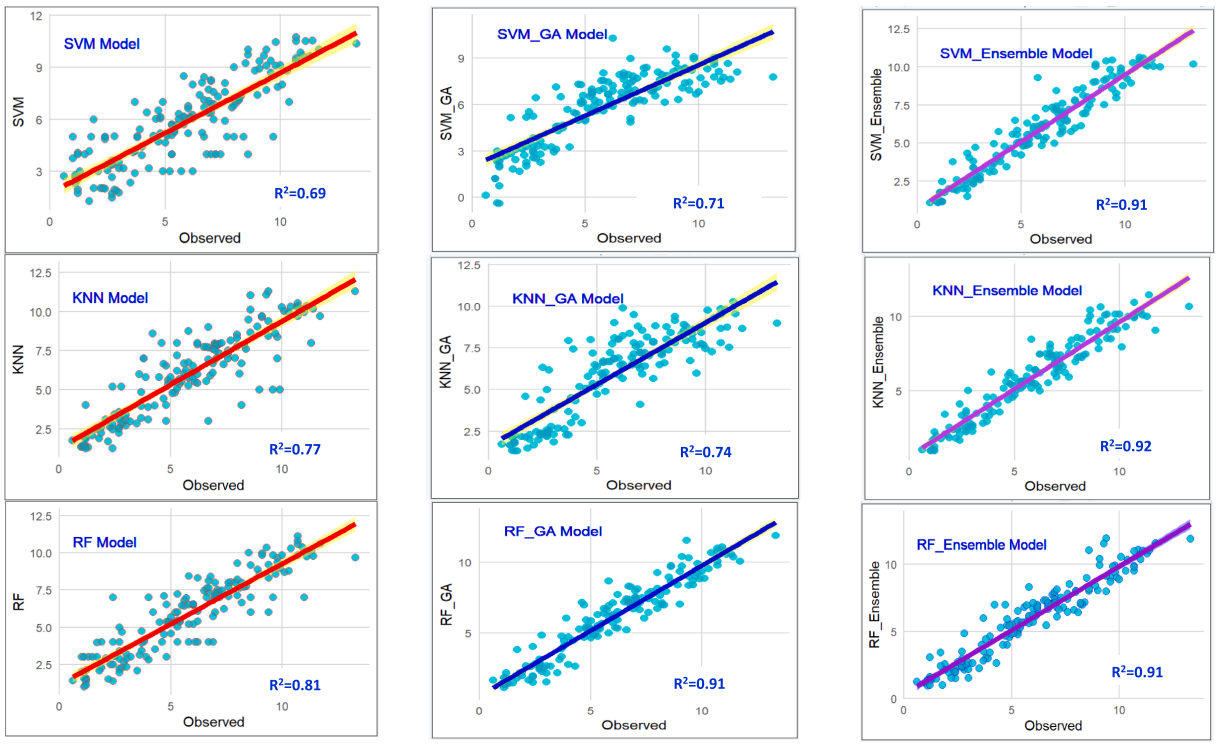

FIGURE 6
Scatter plot of the observed vs. predicted grain yield for nine examined ensemble models and GA-ML models.

TABLE 2 Assessment of model metrics for stress tolerance index prediction.

MODEL	Training				Testing			
	R^2	MAE	RMSE	*n*-RMSE	R^2	MAE	RMSE	*n*-RMSE (%)
SVM	0.92	0.08	0.09	0.92	0.77	0.11	0.143	16.81
KNN	0.84	0.09	0.12	0.84	0.73	0.23	0.148	14.72
RF	0.95	0.05	0.01	0.95	0.78	0.10	0.136	14.31
SVM + GA	0.81	0.12	0.13	0.81	0.80	0.09	0.127	14.70
KNN + GA	0.82	0.11	0.14	0.82	0.79	0.10	0.177	15.60
RF + GA	0.84	0.09	0.13	0.84	0.80	0.08	0.152	15.01
Ensemble SVM	0.94	0.06	0.07	0.94	0.80	0.08	0.129	15.12
Ensemble KNN	0.96	0.04	0.01	0.96	0.82	0.002	0.123	14.12
Ensemble RF	0.94	0.05	0.06	0.94	0.79	0.009	0.137	15.61

n-RMSE are shown in Figure 7. Aqil et al. (2022) reported that ensemble ML perform comparably with deep learning in the classification of maize tassels, reinforcing the efficacy of ensemble approaches in classification problems. The criteria for identifying a drought-tolerant maize genotype, as determined by STI value, involve a direct correlation: the greater the STI value of a maize genotype, the higher its productivity under stress conditions, including drought level. These findings highlight the potential of STI as a selective criterion for identifying maize genotypes capable of achieving high yields under stress conditions. Moradi et al. (2012) similarly reported that utilizing STI for selecting hybrid maize varieties can effectively identify tolerant genotypes with the potential for high yields in stress-prone environments.

The average yield in drought displayed a significantly positive correlation with yields in normal conditions, indicating that higher STI values corresponded to greater genotype tolerance. A three-dimensional plot was employed to visually represent the mean yield of hybrids under both irrigated and drought treatment (Figure 8). The correlation coefficient between Y_p and TOL is 0.70, suggesting a moderately positive relationship, while the correlation between Y_s and TOL is −0.51, indicating a moderate negative association. This implies that as Y_p increases, there is a tendency for TOL to increase, while as Y_s increases, TOL tends to decrease. These findings suggest that the STI and TOL could be incorporated into the selection criteria for identifying high-yielding genotypes under both normal and drought conditions. Among the test hybrids, 10 hybrids exhibited

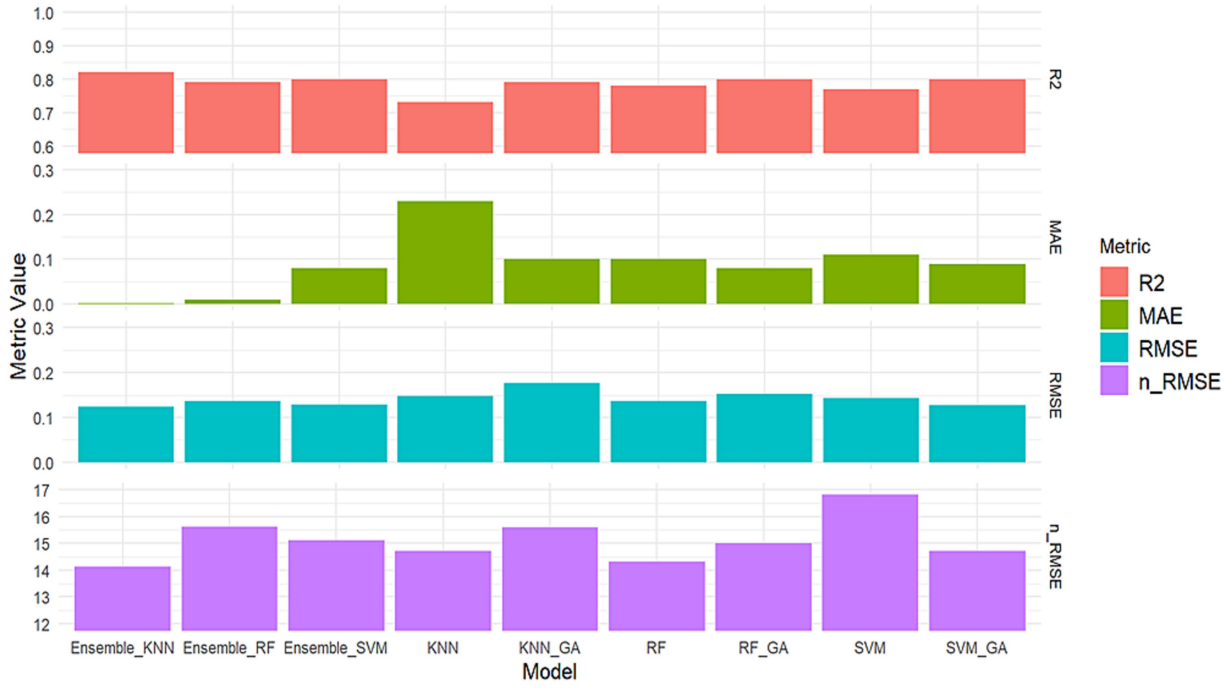

FIGURE 7
Comparative metrics for the nine examined ensembles and GA-ML models in STI prediction.

high STI values, including H33, H21, H17, H19, H14, H13, H10, H35, H30, and H06, with STI values ranging from 0.7 to 1.10. This suggests that these hybrids demonstrated greater tolerance to water stress. On the other hand, the two commercial checks, H32 and H34 displayed heightened vulnerability to drought and had lower grain yield than test varieties.

MGIDI based maize hybrid selection

A comprehensive multi-trait methodology was implemented to ascertain the optimal hybrid pairings, with due consideration not only to maize yield but also covering various plant aspects and yield attributes. The genotype selection process included an initial evaluation of traits sensitive to multicollinearity. Restricted Maximum Likelihood (REM)/Best Linear Unbiased Prediction (BLUP) was used to calculate variance aspects within a mixed-effects framework, with genotype considered as a random effect and replication as a fixed effect. The likelihood ratio test results revealed that all assessed traits demonstrated a statistically significant genotype effect, surpassing the significance threshold of $p < 0.05$. Additionally, a more in-depth examination of these traits using the REML/BLUP approach revealed six principal components, which both accounted for 93.67% of the total variation.

This indicates that the six PC effectively captured a considerable degree of diversity within the characteristics. Similarly, the communalities of the variables ranged from 0.23 for the shelling percentage to 0.79 for trait plant height, with average uniqueness's is 0.66. These figures imply that a substantial proportion of each variable's variability was elucidated by those components. The assessment of precision in determining the mean trait value reveals significant genetic diversity among the hybrid genotypes, as evidenced by an accuracy level surpassing 0.86. This remarkable level of accuracy enables precise estimation of the genetic trait value. To maintain robust interpretative power and simplify data complexity, the nine analyzed traits were categorized into two factors, designated as FA. The factorial loadings and communalities resulting from factor analysis with varimax rotation are presented in Table 3. Communality refers to the shared characteristics or traits among different genotypes, while average uniqueness indicates the distinctive features or traits specific to each genotype. FA1 is associated with attributes such as plant height, ear height, days to tasseling, and shelling percentage, whereas FA2 is linked to characteristics including grain yield, leaf area, 1,000 kernel weight, ear length, and ear diameter. Factor values offer insights into the degree of each trait's relationship with the underlying factor, with higher loadings indicating stronger associations.

FA1 prominently encapsulates traits relating to plant morphology and developmental attributes, exemplified by the involvement of variables such as plant height (PH), ear height (EH), days to tasseling (DT), and shelling percentage (SP). Notably, the distinct negative loadings exhibited by PH, EH, DT, and SP on FA1exhibit strong negative loadings (−0.86, −0.85, −0.87, and −0.36, respectively). This indicates that these variables are inversely related to FA1; when FA1 increases, these variables tend to decrease. Furthermore, FA1 markedly high communalities (0.79, 0.76, 0.76, and 0.23, respectively), underscore the robust interconnections among these traits, highlighting their mutual reliance on common underlying factors within the FA1 concept. FA2 predominantly encapsulates traits associated with crop yield and physical attributes, encompassing key variables such as grain yield (GY), leaf area (LA), ear length (EL), ear

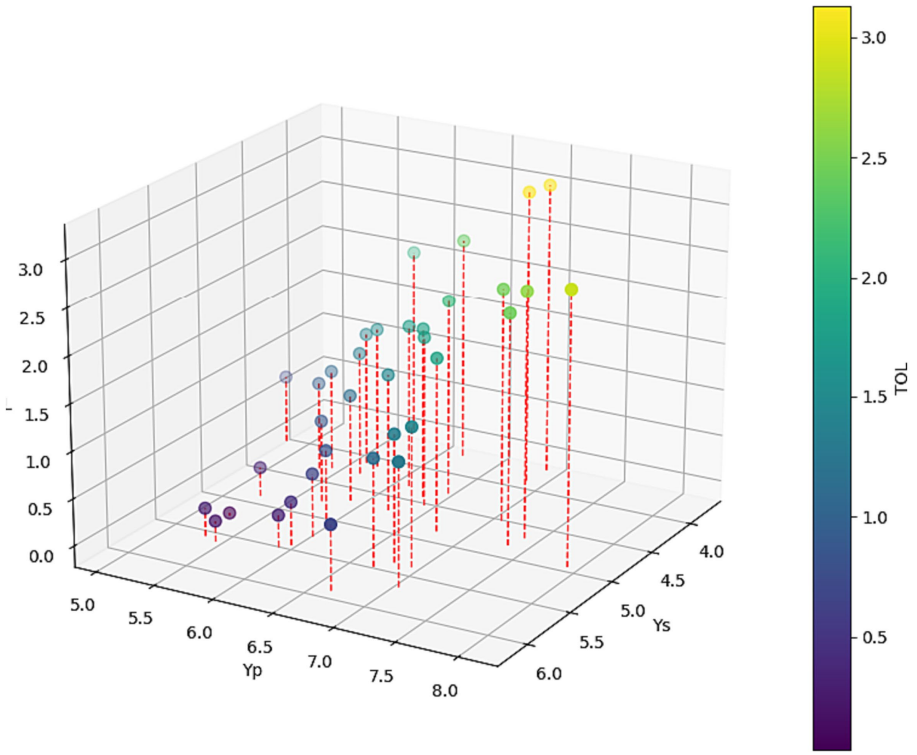

FIGURE 8
Three-dimensional plot depicting the mean yield for each hybrid under both drought and normal conditions, accompanied by their respective tolerance levels.

TABLE 3 The factorial loadings and communalities acquired through varimax rotation in the factor analysis.

VAR	FA1	FA2	Communality	Uniqueness's	Note
1 PH	−0.86	−0.22	0.79	0.21	FAI: PH, EH, DT, SP
2 EH	−0.85	−0.17	0.76	0.24	
3 DT	−0.87	−0.05	0.76	0.24	
4 GY	0.23	0.75	0.62	0.38	FA2: GY, LA, EL, ED, 1,000 KRN
5 LA	−0.16	0.79	0.65	0.35	
6 EL	0.37	0.58	0.48	0.52	
7 ED	0.54	0.62	0.67	0.33	
8 1,000 KRN	0.26	0.82	0.74	0.26	
9 SP	−0.36	−0.32	0.23	0.77	

diameter (ED), and 1,000 kernel weight (1,000 KRN). FA2 display positive loadings (ranging from 0.58 to 0.82). This signifies a positive relationship between these variables and FA2, suggesting that when FA2 scores increase, these variables tend to increase as well. These strong loadings indicate that these variables are closely linked to FA2 and contribute substantially to its definition. These intricate findings offer a nuanced perspective on the intricate architecture of these plant traits, affording researchers valuable insights into potential trait groupings and interrelationships. This newfound understanding paves the way for more refined and targeted research endeavors, ultimately enhancing the efficacy and precision of agricultural practices and crop enhancement strategies.

The MGIDI index has been employed for the comprehensive evaluation of all measured traits. The procedure involves normalizing traits through BLUP to ascertain the genotype's mean performance, followed by factor analysis and the computation of the genetic distance of hybrids from the ideotype. By utilizing a two-way table as the input dataset and applying a row-ranking approach based on desired outcomes, MGIDI provides an effective framework for evaluating the inherent strengths and weaknesses of the chosen genotypes. It offers an efficacious means of assessing the strengths and weaknesses inherent in the selected genotypes. The predicted genetic gains pertaining to the relevant traits within the MGIDI index are presented in Table 4. Specifically, an apparent

reduction of −1.09% is anticipated in plant height, a characteristic considered desirable under certain circumstances due to its potential to mitigate lodging susceptibility and harvesting efficiency. Furthermore, ear height exhibits a more substantial decline of −2.02%, a phenomenon that is poised to enhance overall crop stability. This observation aligns with Andayani et al. (2018), which explain the negative implications of excessive plant height on stability and productivity, particularly in regions characterized by heavy precipitation and strong winds, such as equatorial zones. Days to tasseling exhibits a marginal decline of −0.0572%, indicative of relatively stable performance in this trait, while grain yield demonstrates a nearly imperceptible decrease of −0.0003%, underscoring the relative success of endeavors to maintain or augment yield within the context of FA1. Within the framework of FA2, leaf area is projected to experience an incremental increase of 0.00189%, thereby potentially augmenting photosynthetic efficiency and subsequent crop yields. Ear length is anticipated to extend by 0.0726%, signifying an increase in ear length, a factor poised to positively influence overall yield. Furthermore, ear diameter is expected to expand by 0.101%, likely leading to larger and potentially more productive ears. The 1,000 kernel weight is predicted to elevate by 0.128%, which bodes well for the improvement of seed size and quality. However, it is in the context of shelling percentage that the most substantial gain is observed, registering a notable increase of 4.8%. The heritability values within this study exhibit considerable variability, ranging from 0.30 for traits such as ear length and leaf angle to values exceeding 0.50 for traits including days to shelling percentage, ear diameter, and 1,000 kernel weight.

Based on Table 4, the overall gain achieved was 5.10% for traits targeted for improvement and a reduction of −3.16% for traits designated for minimization. Figure 9 presents a concise visual representation of genotype rankings based on their MGIDI index values, highlighting specific genotypes that align with the predefined selection criteria. Among the examined genotypes, H13, H31, H35, H06, H10, and H08 emerged as distinguished performers, denoted by their prominent highlighting, signifying their remarkable accomplishments. Additionally, four other genotypes, namely H11, H25, H32, and H30, also secured positions among the top 10 best-performing genotypes, showcasing their favorable characteristics across a spectrum of traits. These genotypes exhibit attributes that make them well-suited for the intended study or purpose. It is required to acknowledge, however, that while a robust correlation exists between genotype attributes and trait values, external environmental factors may impose limitations on the realization of heightened trait values. The MGIDI provides valuable insights into the strengths and weaknesses inherent in diverse genotypes, offering a convenient framework for discerning their advantages and limitations within the intricate context of multifaceted traits (Olivoto and Nardino, 2021).

Strengths and weakness of hybrids

The comprehensive evaluation of genotype attributes, effectively categorizing their influence on MGIDI divided into two distinct factors is shown in Figure 10. Particularly, attributes directing substantial influence located in a central position within the diagram, while those exerting a more marginal effect find their placement towards the periphery. The insights derived from this data regarding attribute contributions hold a potential role in the judicious selection of suitable parental contributors for the purpose of crossbreeding programs. It is evident that FA1 exerted a obviously greater influence on the MGIDI for genotypes H35, H25, and H31. This observation implies that these hybrids exhibited a relatively less favorable performance in terms of key attributes such as PH, EH, DT and SP traits. Conversely, FA1 had a notably diminished impact on the MGIDI of hybrids H08, H10, H08, H13, H30, H32, H25, and H35, thereby indicating their proficiency and excellence in manifesting the specified traits associated with FA1. FA2 had a more substantial influence on the MGIDI of genotypes H08, H10, H08, H13, H30, H32, while manifesting a relatively moderate effect on genotypes H25 and H35. Consequently, this distinction resulted in the latter two genotypes demonstrating strengths associated with FA2 within the framework. Optimal improvements are aspired for the traits GY, LA, EL, ED and 1,000 KRN within the domain of FA2. FA2 exhibits elevated values for these specific attributes to signify favorable outcomes.

TABLE 4 Predicted genetic gain for the effective traits in the MGIDI index.

Factor	VAR	Xo	Xs	SD (%)	h^2	SG	SG (%)	Goal
FA1	PH	210	207	−2.78	−1.32	0.393	−1.09	Decrease
FA1	EH	106	103	−2.93	−2.75	0.69	−2.02	Decrease
FA1	DT	53.3	53.1	−0.203	−0.381	0.282	−0.0572	Decrease
FA1	GY	0.793	0.792	−0.000893	−0.113	0.315	−0.0003	Increase
FA2	LA	5.68	5.7	0.0239	0.421	0.0791	0.00189	Increase
FA2	EL	742	745	2.38	0.321	0.0305	0.0726	Increase
FA2	ED	15.4	15.6	0.179	1.16	0.567	0.101	Increase
FA2	1,000 KRN	45.1	45.4	0.269	0.597	0.475	0.128	Increase
FA2	SP	333	344	10.9	3.26	0.441	4.8	Increase
Total (Increase)							5.102	
Total (Decrease)							−3.16	

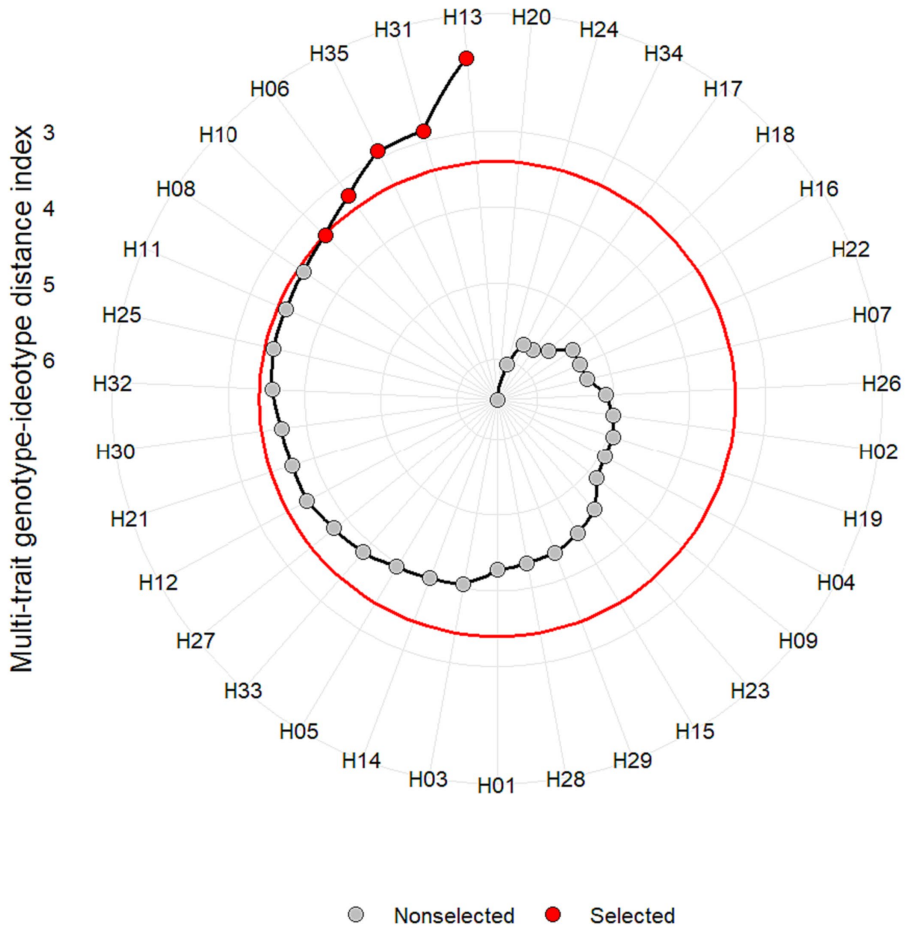

FIGURE 9
Maize hybrid ranking based on MGIDI, with highlighted top performers in red.

Through a comprehensive assessment of multiple traits, the process of genotype ranking has determined that among the chosen hybrids (H13, H31, H35, H06, H10, and H08), these six specifically exhibit the highest levels of performance. This ranking has been derived from their adeptness in seamlessly integrating grain yield with other target attributes. The practical application of the multiple trait combination index as an evaluative instrument has afforded researchers the ability to discern the traits that exert the most profound impact on each genotype. Yan and Frégeau-Reid (2018) reported that assessment of a genotype's advantage must transcend the confines of isolated trait measurements. Instead, the evaluation should focus on the genotype's proficiency in harmonizing grain yield with other meticulously chosen agronomic and yield components, thereby presenting a more holistic measure in assessment of screening or crossing program.

Conclusion

The study intricately investigated the interaction between ML techniques and a multi-trait selection model, resulting in the prediction of both grain yield and drought tolerance for maize crosses exposed to normal and drought-induced stress conditions. The results indicated that the optimized ML with GA and ensembles can substantially outperform the single ML model. Moreover, the incorporation of the Multi-trait Genotype-Ideotype Distance emerged as a crucial tool for identifying superior maize hybrids well-suited to drought-afflicted conditions, with its predictive performance benchmarked against that of the ML models. The empirical findings highlighted the elevated accuracy achieved by the RF-GA combination ($R^2 = 0.91$ for grain yield and 0.79 for stress tolerance index), while the SVM-GA and KNN-GA models exhibited less favorable predictions. The remarkable consistency in achieving optimal outcomes was exemplified by the ensemble models, which harnessed the predictive capabilities of diverse individual models. These ensemble meta-models, incorporating SVM, KNN, and RF, consistently yielded $R^2 \geq 0.92$ for grain yield and 0.82 for STI across the testing datasets. The resounding effectiveness of these ensemble models can be attributed to the inherent diversity within the ensemble itself, enabling a comprehensive exploration of the intricate feature landscape. Among the six hybrids with the highest STI values, both the ML-based optimized model and MGIDI accurately predict four hybrids with high drought tolerance index, namely H06, H10, H13, and H35.

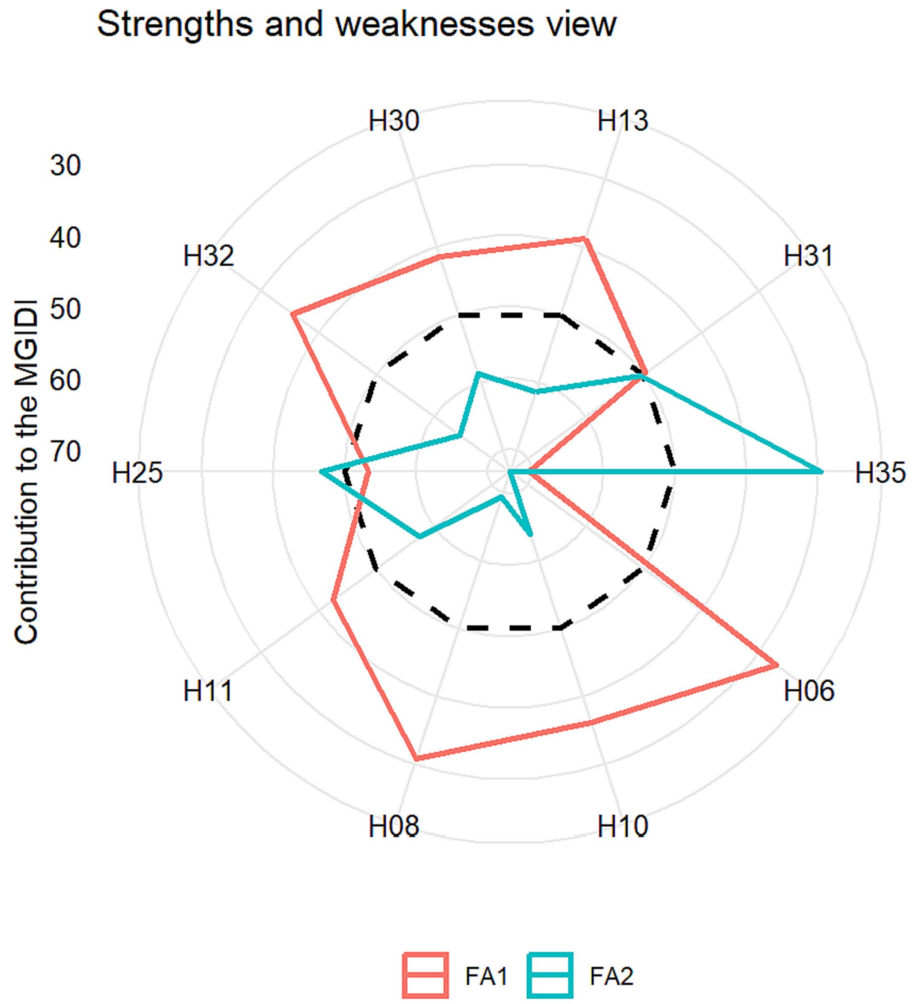

FIGURE 10
Comprehensive assessment of selected genotypes, highlighting their strengths and weaknesses weighed by MGIDI.

Data availability statement

The datasets presented in this study can be found in online repositories. The names of the repository/repositories and accession number(s) can be found in the article/Supplementary material.

Author contributions

MAz: Writing – original draft, Conceptualization. MAq: Methodology, Writing – original draft. NA: Writing – review & editing. RE: Writing – review & editing. Suarni: Writing – review & editing. Suwardi: Writing – review & editing. MJ: Writing – original draft. BZ: Writing – review & editing. Salim: Writing – original draft. Bahtiar: Writing – original draft. AM: Data analysis, Writing – original draft. MY: Writing – review & editing. MH: Writing – review & editing. Rahman: Data collection. AS: Writing – review & editing.

Funding

The author(s) declare financial support was received for the research, authorship, and/or publication of this article. We extend our gratitude to the Indonesia Endowment Fund for Education Agency (LPDP) through the Program for Funding Innovative Productive Research (Rispro Mandatori) under the National Research Priority (PRN), with reference number KEP-32/LPDP/2020. We also express our gratitude to Hasanuddin University for financing the publication of this research. Additionally, we acknowledge the IAARD, Ministry of Agriculture, Indonesia, for providing research facilities.

Acknowledgments

The research was conducted with the assistance of various genetic materials provided by CIMMYT Mexico. Thanks to the support provided by the technicians from Bajeng Experimental Station in Indonesia for this project.

Conflict of interest

The authors declare that the research was conducted in the absence of any commercial or financial relationships that could be construed as a potential conflict of interest.

Publisher's note

All claims expressed in this article are solely those of the authors and do not necessarily represent those of their affiliated organizations, or those of the publisher, the editors and the reviewers. Any product that may be evaluated in this article, or claim that may be made by its manufacturer, is not guaranteed or endorsed by the publisher.

Supplementary material

The Supplementary material for this article can be found online at: https://www.frontiersin.org/articles/10.3389/fsufs.2024.1334421/full#supplementary-material

References

Agarwal, M., Gupta, S., and Biswas, K. K. (2021). A new Conv2D model with modified ReLU activation function for identification of disease type and severity in cucumber plant. *Sustain. Comput. Informatics Syst.* 30:100473. doi: 10.1016/j.suscom.2020.100473

Ahmed, S. (2023). A software framework for predicting the maize yield using modified multi-layer perceptron. *Sustainability* 15:3017. doi: 10.3390/su15043017

Akhiat, Y., Chahhou, M., and Zinedine, A. (2019). Ensemble feature selection algorithm. *Int. J. Intell. Syst. Appl.* 11, 24–31. doi: 10.5815/ijisa.2019.01.03

Andayani, N. N., Aqil, M., Efendi, R., and Azrai, M. (2018). Line × tester analysis across equatorial environments to study combining ability of Indonesian maize inbred. *Asian J. Agric. Biol.* 6, 213–220. Available at: https://www.asianjab.com/wp-content/uploads/2018/06/15.-OK_Line-_-tester-analysis-across-equatorial-environments-to-study-combining-ability-of-Indonesian-maize-inbred.pdf

Aqil, M., Azrai, M., Mejaya, M. J., Subekti, N. A., Tabri, F., Andayani, N. N., et al. (2022). Rapid detection of hybrid maize parental lines using stacking ensemble machine learning. *Appl. Comput. Intell. Soft Comput.* 2022, 1–15. doi: 10.1155/2022/6588949

Araus, J. L., Sanchez-Bragado, R., and Vicente, R. (2021). Improving crop yield and resilience through optimization of photosynthesis: panacea or pipe dream?. *J. Exp. Bot.* 72, 3936–3955.

Austria, Y. C., Mirabueno, M. C. A., Lopez, D. J. D., Cuaresma, D. J. L., Macalisang, J. R., and Casuat, C. D. (2022). EZM-AI: a Yolov5 machine vision inference approach of the Philippine corn leaf diseases detection system. 2022 IEEE International Conference on Artificial Intelligence in Engineering and Technology (IICAIET). 1–6.

Azrai, M., Aqil, M., Efendi, R., Andayani, N. N., Makkulawu, A. T., Iriany, R. N., et al. (2023). A comparative study on single and multiple trait selections of equatorial grown maize hybrids. *Front. Sustain. Food Syst.* 7:1185102. doi: 10.3389/fsufs.2023.1185102

Bänziger, M., Edmeades, G. O., Beck, D., and Bellon, M. (2000). *Breeding for drought and nitrogen stress tolerance in maize: From theory to practice*. CIMMYT. México-Veracruz. 68.

Çakir, R. (2004). Effect of water stress at different development stages on vegetative and reproductive growth of corn. *Field Crops Res.* 89, 1–16. doi: 10.1016/j.fcr.2004.01.005

Cheng, C. Y., Li, Y., Varala, K., Bubert, J., Huang, J., Kim, G. J., et al. (2021). Evolutionarily informed machine learning enhances the power of predictive gene-to-phenotype relationships. *Nat. Commun.* 12, 5627–5615. doi: 10.1038/s41467-021-25893-w

Chotewutmontri, P., and Barkan, A. (2016). Dynamics of chloroplast translation during chloroplast differentiation in maize. *PLoS Genet.* 12:e1006106. doi: 10.1371/journal.pgen.1006106

Fernandez, G. C. J. (1992). Effective selection criteria for assessing plant stress tolerance. Proceedings of the International Symposium on Adaptation of Vegetables and Other Food Crops in Temperature and Water Stress Chapter 25, Tainan Shanhua AVRDC Publications, 257–270.

Ganesan, G., and Chinnappan, J. (2022). Hybridization of ResNet with YOLO classifier for automated paddy leaf disease recognition: an optimized model. *J. Field Robot.* 39, 1085–1109. doi: 10.1002/rob.22089

Gokulnath, B. V., and Devi, G. U. (2020). Boosted-DEPICT: an effective maize disease categorization framework using deep clustering. *Neural Comput. Applic.* doi: 10.1007/s00521-020-05303-w

Jamieson, P. D., Porter, J. R., and Wilson, D. R. (1991). A test of the computer simulation model ARCWHEAT1 on wheat crops grown in New Zealand. *Field Crops Res.* 27, 337–350. doi: 10.1016/0378-4290(91)90040-3

Jhajharia, K., Mathur, P., Jain, S., and Nijhawan, S. (2023). Crop yield prediction using machine learning and deep learning techniques. *Procedia Comput. Sci.* 218, 406–417. doi: 10.1016/j.procs.2023.01.023

Jordan, W. R. (1983). "Whole plant response to water deficit: an overview" in *Limitations to efficient water use in crop production*. ed. H. M. Taylor (Madison, WI: American Society of Agronomy), 289–317.

Kira, O., Nguy-Robertson, A. L., Arkebauer, T. J., Linker, R., and Gitelson, A. A. (2016). Informative spectral bands for remote green LAI estimation in C3 and C4. *Agric. For. Meteorol.* 218–219, 243–249. doi: 10.1016/j.agrformet.2015.12.064

Monneveux, P., Sanchez, C., and Tiessen, A. (2008). Future progress in drought tolerance in maize needs new secondary traits and cross combinations. *J. Agric. Sci.* 146, 287–300. doi: 10.1017/S0021859608007818

Moradi, H., Akbari, G. A., Khorasani, S. K., and Ramshini, H. A. (2012). Evaluation of drought tolerance in corn (*Zea mays* L.) new hybrids with using stress tolerance indices. *Eur. J. Sustain. Dev.* 1:543. doi: 10.14207/ejsd.2012.v1n3p543

Olivoto, T., Lúcio, A. D. C., da Silva, J. A. G., Sari, B. G., and Diel, M. I. (2019). Mean performance and stability in multi-environment trials II: selection based on multiple traits. *Agron. J.* 111, 2961–2969. doi: 10.2134/agronj2019.03.0221

Olivoto, T., and Nardino, M. (2021). MGIDI: toward an effective multivariate selection in biological experiments. *Bioinformatics* 37, 1383–1389. doi: 10.1093/bioinformatics/btaa981

Pham, H., and Olafsson, S. (2018). Bagged ensembles with tunable parameters: Pham and Olafsson. *Comput. Intell.* 35, 184–203. doi: 10.1111/coin.12198

Rosielle, A. A., and Hamblin, J. (1981). Theoretical aspects of selection for yield in stress and non-stress environment. *Crop Sci.* 21, 943–946. doi: 10.2135/cropsci1981.0011183X002100060033x

Roy, A. M., and Bhaduri, J. (2021). A deep learning enabled multi-class plant disease detection model based on computer vision. *AI* 2, 413–428. doi: 10.3390/ai2030026

Sachdev, S., Ansari, S. A., Ansari, M. I., Fujita, M., and Hasanuzzaman, M. (2021). Abiotic stress and reactive oxygen species: generation, signaling, and defense mechanisms. *Antioxidants* 10:277. doi: 10.3390/antiox10020277

Sahu, S., Chawla, M., and Khare, N. (2017). An efficient analysis of crop yield prediction using Hadoop framework based on random forest approach. 2017 International Conference on Computing, Communication and Automation (ICCCA). 53–57.

Sakeef, N., Scandola, S., Kennedy, C., Lummer, C., Chang, J., Uhrig, R. G., et al. (2023). Machine learning classification of plant genotypes grown under different light conditions through the integration of multi-scale time-series data. *Comput. Struct. Biotechnol. J.* 21, 3183–3195. doi: 10.1016/j.csbj.2023.05.005

Shao, R. X., Xin, L. F., Zheng, H. F., Li, L. L., Ran, W. L., Mao, J., et al. (2016). Changes in chloroplast ultrastructure in leaves of drought-stressed maize inbred lines. *Photosynthetica* 54, 74–80. doi: 10.1007/s11099-015-0158-6

Sharma, P., Hans, P., and Gupta, S. C. (2020). Classification of plant leaf diseases using machine learning and image preprocessing techniques. 10th International Conference on Cloud Computing, Data Science & Engineering. 480–484. Available at: https://api.semanticscholar.org/CorpusID:215738169.

Singh, B., Kumar, S., Elangovan, A., Vasht, D., Arya, S., Duc, N. T., et al. (2023). Phenomics based prediction of plant biomass and leaf area in wheat using machine learning approaches. *Front. Plant Sci.* 14:1214801. doi: 10.3389/fpls.2023.1214801

Srivastava, A. K., Safaei, N., Khaki, S., Lopez, G., Zeng, W., Ewert, F., et al. (2022). Winter wheat yield prediction using convolutional neural networks from environmental and phenological data. *Sci. Rep.* 12, 3215–3214. doi: 10.1038/s41598-022-06249-w

Sun, J., Yang, Y., He, X., and Wu, X. (2020). Northern maize leaf blight detection under complex field environment based on deep learning. *IEEE Access* 8, 33679–33688. doi: 10.1109/ACCESS.2020.2973658

Széles, A., Horváth, É., Simon, K., Zagyi, P., and Huzsvai, L. (2023). Maize production under drought stress: nutrient supply, yield prediction. *Plants* 12:3301. doi: 10.3390/plants12183301

Waheed, A., Goyal, M., Gupta, D., Khanna, A., Hassanien, A. E., and Pandey, H. M. (2020). An optimized dense convolutional neural network model for disease recognition and classification in corn leaf. *Comput. Electron. Agric.* 175:105456. doi: 10.1016/j.compag.2020.105456

Yan, W., and Frégeau-Reid, J. (2018). Genotype by yield*trait (GYT) biplot: a novel approach for genotype selection based on multiple traits. *Sci. Rep.* 8, 1–10. doi: 10.1038/s41598-018-26688-8

Yoosefzadeh-Najafabadi, M., Torabi, S., Tulpan, D., Rajcan, I., and Eskandari, M. (2021a). Genome-wide association studies of soybean yield-related hyperspectral reflectance bands using machine learning-mediated data integration methods. *Front. Plant Sci.* 12:777028. doi: 10.3389/fpls.2021.777028

Yoosefzadeh-Najafabadi, M., Tulpan, D., and Eskandari, M. (2021b). Using hybrid artificial intelligence and evolutionary optimization algorithms for estimating soybean yield and fresh biomass using hyperspectral vegetation indices. *Remote Sens.* 13:2555. doi: 10.3390/rs13132555

Zahra, N., Hafeez, M. B., Kausar, A., Al Zeidi, M., Asekova, S., Siddique, K., et al. (2023). Plant photosynthetic responses under drought stress: effects and management. *J. Agron. Crop Sci.* 209, 651–672. doi: 10.1111/jac.12652

Zainuddin, B., and Aqil, M. (2021). Analysis of the relationship between leaf color spectrum and soil plant analysis development. *IOP Conf. Ser.: Earth Environ. Sci* 911:012045. doi: 10.1088/1755-1315/911/1/012045

Zhang, Y., Ji, X., Xian, J., Wang, Y., and Peng, Y. (2022). Morphological characterization and transcriptome analysis of leaf angle mutant bhlh112 in maize [*Zea mays* L.]. *Front. Plant Sci.* 13:995815. doi: 10.3389/fpls.2022.995815

frontiers | Frontiers in Sustainable Food Systems

TYPE Original Research
PUBLISHED 21 February 2024
DOI 10.3389/fsufs.2023.1334487

OPEN ACCESS

EDITED BY
Md Khairul Alam,
Bangladesh Agricultural Research Institute, Bangladesh

REVIEWED BY
Heena Rani,
Agricultural Research Service (USDA), United States
Joong Hyoun Chin,
Sejong University, Republic of Korea
Naveen Puppala,
New Mexico State University, United States
Santosh Kumar Gupta,
National Institute of Plant Genome Research (NIPGR), India

*CORRESPONDENCE
Kunnummal Kurungara Vinod
✉ kkvinodh@gmail.com

RECEIVED 07 November 2023
ACCEPTED 26 December 2023
PUBLISHED 21 February 2024

CITATION
Sonu, Nandakumar S, Singh VJ, Pandey R, Gopala Krishnan S, Bhowmick PK, Ellur RK, Bollinedi H, Harshitha BS, Yadav S, Beniwal R, Nagarajan M, Singh AK and Vinod KK (2024) Implications of tolerance to iron toxicity on root system architecture changes in rice (*Oryza sativa* L.).
Front. Sustain. Food Syst. 7:1334487.
doi: 10.3389/fsufs.2023.1334487

Implications of tolerance to iron toxicity on root system architecture changes in rice (*Oryza sativa* L.)

Sonu[1], Shekharappa Nandakumar[1], Vikram Jeet Singh[2], Rakesh Pandey[3], Subbaiyan Gopala Krishnan[1], Prolay Kumar Bhowmick[1], Ranjith Kumar Ellur[1], Haritha Bollinedi[1], Bheemapura Shivakumar Harshitha[1], Sunaina Yadav[1], Ravina Beniwal[1], Mariappan Nagarajan[4], Ashok Kumar Singh[1] and Kunnummal Kurungara Vinod[1]*

[1]Division of Genetics, ICAR-Indian Agricultural Research Institute, New Delhi, India, [2]Department of Seed Science and Technology, Acharya Narendra Deva University of Agriculture & Technology, Ayodhya, India, [3]Division of Plant Physiology, ICAR-Indian Agricultural Research Institute, New Delhi, India, [4]Rice Breeding and Genetics Research Centre, Aduthurai, Tamil Nadu, India

Introduction: Toxicity due to excess soil iron (Fe) is a significant concern for rice cultivation in lowland areas with acidic soils. Toxic levels of Fe adversely affect plant growth by disrupting the absorption of essential macronutrients, and by causing cellular damage. To understand the responses to excess Fe, particularly on seedling root system, this study evaluated rice genotypes under varying Fe levels.

Methods: Sixteen diverse rice genotypes were hydroponically screened under induced Fe levels, ranging from normal to excess. Morphological and root system characteristics were observed. The onset of leaf bronzing was monitored to identify the toxic response to the excess Fe. Additionally, agronomic and root characteristics were measured to classify genotypes into tolerant and sensitive categories by computing a response stability index.

Results: Our results revealed that 460 ppm of Fe in the nutrient solution served as a critical threshold for screening genotypes during the seedling stage. Fe toxicity significantly affected root system traits, emphasizing the consequential impact on aerial biomass and nutrient deprivation. To classify genotypes into tolerant and sensitive categories, leaf bronzing score was used as a major indicator of Fe stress. However, the response stability index provided a robust basis for classification for the growth performance. Apart from the established tolerant varieties, we could identify a previously unrecognized tolerant variety, ILS 12–5 in this study. Some of the popular mega varieties, including BPT 5204 and Pusa 44, were found to be highly sensitive.

Discussion: Our findings suggest that root system damage, particularly in root length, surface area, and root volume, is the key factor contributing to the sensitivity responses under Fe toxicity. Tolerant genotypes were found to retain more healthy roots than the sensitive ones. Fe exclusion, by reducing Fe^{2+} uptake, may be a major mechanism for tolerance among these genotypes. Further field evaluations are necessary to confirm the behavior of identified tolerant and sensitive lines under natural conditions. Insights from the study provide potential scope for enhancement of tolerance through breeding programs as well as throw light on the role root system in conferring tolerance.

KEYWORDS

iron toxicity, root system response, tolerance, hydroponics, seedling stage

1 Introduction

Rice serves as a fundamental dietary staple for approximately 3.5 billion people globally, contributing to 23% of the worldwide *per capita* energy and 16% of protein intake. To accommodate the rising food needs due to the swelling global population from 2000 to 2050, projections suggest that rice production should increase by 35% between 2000 and 2050 (Jaggard et al., 2010; Timmer et al., 2010; Singh et al., 2022). Despite continuous research in past years, there has been limited noticeable genetic improvement in rice yields, indicating a saturation of yield potential in certain favorable environments (Mahender et al., 2019).

Rice yields are susceptible to a range of biotic and abiotic stresses. These stresses may operate in isolation or synergistically, with their impacts fluctuating based on local environmental conditions and the specific rice variety cultivated (Zhang et al., 2013; Ma et al., 2015; Sikirou et al., 2015; Mongon et al., 2017; Kobayashi et al., 2018). Abiotic stresses including salinity, drought, temperature extremes, nutrient imbalances, soil acidity, and ion toxicity are recognized to markedly affect rice grain yields. In acidic soils, a surplus of iron (Fe) is commonly observed, exerting a detrimental effect on the assimilation of essential nutrients, notably phosphorus and potassium (Saleem et al., 2023). Given the anticipated increase in these stress factors due to climate shifts, there is a consensus on the imperative need for cultivating rice varieties, which is resilient to multiple stresses, especially considering unforeseen future challenges. Significant strides in research are made, leading to the development of rice genotypes tolerant to several biotic and abiotic stresses across various ecosystems. However, the challenge of addressing iron (Fe) toxicity in rice remains a critical area that demands intensified and concentrated research efforts (Kar and Panda, 2020).

Fe is a crucial microelement required by all plants for their proper growth and development. It is fundamental to the structure and function of vital biomolecules, such as iron–sulfur (FeS) proteins, ferredoxins, heme proteins, and numerous other cofactors. Its pivotal role encompasses processes such as chlorophyll production and maturation, photosynthesis, and mitochondrial functions. The redox characteristics of Fe render it indispensable, underscoring its irreplaceable nature in biological mechanisms (Marschner and Römheld, 1995; Robinson et al., 1999; Waters and Eide, 2002; Rout et al., 2014; Müller et al., 2015; Bashir et al., 2017; Connorton et al., 2017; Li and Lan, 2017).

Plants primarily absorb Fe from the soil in the form of ferrous (Fe^{2+}) ions. The prevalent form of Fe in soil is ferric (Fe^{3+}), notably in its oxide form known as ferric oxide or hematite. However, soil acidification can aid in the conversion of Fe^{3+} to the bioavailable Fe^{2+} form, facilitating optimal uptake by plants. In soils abundant in sesquioxides, intense rainfall and podsolization contribute to soil acidification and subsequent accumulation of Fe ions. Fe enrichment is a distinguishing feature of acid-sulfate soils and low-lying waterlogged terrains. The spectrum of Fe concentration in soil ranges from 10 to 1,000 ppm, and a concentration > 300 ppm is considered critical for toxicity in rice (Dobermann and Fairhurst, 2000). Depending on the intervening factors, Fe toxicity can occur even at lower concentrations, and therefore, contextual intervention may be required to alleviate toxic responses in various soils.

The toxic responses of Fe can exert a significant impact on rice cultivation, as observed particularly in Southeast Asian countries such as China, India, Philippines, Thailand, Malaysia, and Indonesia (Asch et al., 2005; Fageria et al., 2008; Matthus et al., 2015). In India, the major Fe-impacted regions are spread across North-eastern states such as Assam, Arunachal Pradesh, Meghalaya, Nagaland, Mizoram, and Sikkim, along with other states such as Kerala, Odisha, and West Bengal. High acidity and leaching are the common features of soils in the North-east India. Acidity forms due to the weathering of the acidic parental rocks that are rich in Al and Fe. High rainfall together with cultivation practices such as Jhum (slash and burn) encourages continuous soil erosion in these areas, accumulating large quantity of Fe in the lower altitudes and Al in the upper regions, rendering soils marginally fertile.

Rice exhibits a sensitive reaction to toxic levels of Fe in soil. Under toxicity, 18–30% grain yield reduction was observed and under severe conditions the damage can extend to complete crop failure (Audebert and Sahrawat, 2000; Chérif et al., 2009). Rice cultivars, exposed to excess of Fe in the soil, display different adaptive mechanisms, that result in toxicity tolerance (Vose, 1982). These mechanisms invoke sequestration responses such as taking up excess Fe and storing it in vacuoles and apoplasts, followed by a detoxification process that activates antioxidant enzymes to counteract the harmful effects of Fe-induced ROS. In certain instances, roots may undergo Fe exclusion, thereby preventing the excessive absorption of the ion. Overall, these mechanisms help plants to survive and grow under conditions of Fe toxicity. In regions characterized by persistent iron toxicity, effective management techniques include soil amendment and water management (Becker and Asch, 2005; Audebert and Fofana, 2009). However, the most sustainable and effective approach involves the identification and cultivation of rice varieties tolerant to Fe toxicity (Abifarin, 1989; Onaga et al., 2016; Pawar et al., 2017). When used alongside proper soil management practices, tolerant varieties can reduce the need for soil amendments and increase rice yields in lowland areas (Sahrawat et al., 1996; Mahender et al., 2019). Therefore, breeding for tolerance is imperative for Fe-prone areas and ecosystems.

The identification of cultivars resistant to Fe toxicity involves various methodologies, including field-based trials, pot experiments, and hydroponic studies (Hoan et al., 1992; Silveira et al., 2007; Vasconcelos and Grusak, 2014). Though field screening replicates the real time stress originating from the intricate chemical composition of flooded soil, it proves to be laborious, costly, and cumbersome due to the considerable variability in the soil. Conducting the pot experiments, on the other hand, necessitates a substantial quantity of pots and experimental space, leading to increased expenses. Furthermore, it involves the challenge of maintaining consistent stress levels uniformly across all pots (Elec et al., 2013). Among these methods, hydroponics has been widely used to screen for Fe toxicity

tolerance as it is the most convenient in maintaining uniform stress levels for a large number of plants in various crops such as maize, chickpea including rice (Mahmoudi et al., 2007; Carvalhais et al., 2011; Dotaniya et al., 2013; Mamidi et al., 2014; Kabir et al., 2016). It has also been used in screening for parameters related to other essential nutrients, such as nitrogen and phosphorus use efficiency (Archana et al., 2021). Although hydroponic experiments may not simulate the actual field conditions, it is reasonably useful in identifying tolerant responses among the genotypes that can be used for further practical use.

Among the various response traits, leaf bronzing is considered one of the most important criteria for screening Fe toxicity tolerance. However, root attributes, such as total root length, root average diameter, root surface area, root projected area, root volume, and number of root tips play a significant role in differentiation between tolerant and resistant genotypes (Pathirana et al., 2002). Besides, the reports of critical Fe concentrations for identifying tolerant and sensitive genotypes were also found to vary across studies, making it difficult to choose a common threshold. Several of these studies lack confidence since they are made on a few genotypes or carried out in one season/location. Therefore, in this report, we present standardization of protocol for Fe toxicity screening along with the effect of Fe toxicity on different morphophysiological parameters leading to the identification and grouping of tolerant and susceptible genotypes. The objective of our investigation is to ascertain the threshold of Fe toxicity concentration, employing it as a criterion for screening and distinguishing between tolerant and susceptible rice genotypes. This selection process is crucial for subsequent integration into breeding programs and investigations at identifying specific genes/QTLs associated with this trait.

2 Materials and methods

2.1 Plant materials

The experiment materials comprised 16 rice genotypes collected from the Division of Genetics, ICAR-Indian Agricultural Research Institute, New Delhi (IARI), details of which are briefed in Table 1. Among these, Shahsarang was an established Fe toxicity tolerant variety (Debnath et al., 2021) while IR 64 was a known sensitive cultivar (Sikirou et al., 2016; Turhadi et al., 2019). The remaining genotypes represented popular cultivars in Basmati, non-basmati, *aus* and *japonica* type.

TABLE 1 Plant material used in hydroponic experiment.

Genotype	Source/Origin	Description
ILS 12–5	ICAR-IARI	Breeding line
NPT 34	India	New plant type breeding line
Pusa 1,176	IARI	Breeding line
Pusa 1,342	IARI	Breeding line
Megha SA2	Meghalaya	Cultivar., Fe toxicity tolerant
Shahsarang	Meghalaya	Cultivar., Fe toxicity tolerant
IRGC 127653	Indian cultivar	Selection from NCS102
Sonasal	West Bengal	Indian aromatic landrace
RTN 10B	ICAR-IARI	Maintainer parent
BPT 5204	IARI	Mega-variety
Nagina 22	India	Drought tolerant *aus* variety
PB 1	IARI	Popular Basmati variety
PB 1121	IARI	Popular Basmati variety
PR 126	PAU, Ludhiana	Green super rice variety
Pusa 44	ICAR-IARI	Mega-variety, high yielding
IR 64	IRRI	Mega-variety, Fe toxicity sensitive

2.2 Hydroponic screening

The hydroponic system was set up at the National Phytotron Facility at IARI with 1X modified Hoagland mixture as the basic nutrient solution for providing optimal nutrients for rice seedlings (Hoagland and Arnon, 1950; Gamborg and Wetter, 1975). In total, 1 L of the nutrient solution consisted of 610.0 mg of KNO_3, 120.0 mg of $NH_4H_2PO_4$, 950.0 mg of Ca $(NO_3)_2.4H_2O$, 490.0 mg of $MgSO_4.7H_2O$, 50.0 mg of $FeSO_4.7H_2O$, 2.0 mg of $MnCl_2.4H_2O$, 0.02 mg of H_2MoO_4, 3.0 mg of H_3BO_3, 0.25 mg of $ZnSO_4.7H_2O$, 0.1 mg of $CuSO_4.5H_2O$, and 33.0 mg of Na_2EDTA. The pH of the nutrient solution was maintained between 5.0 and 5.5.

Initially, the seeds of all the genotypes were surface sterilized using 3% sodium hypochlorite solution by shaking for 1 min, and subsequently, washing with ultrapure water three times. Sterilized seeds are then placed on a germination paper and kept in an incubator for germination at 25–30°C. After 6–7 days, seedlings presenting uniform shoot and root growth were transferred to 100 mm^2 wells punched on an expanded polystyrene (EPS) float sheet of size 24 × 36 × 2 cm. Each sheet had 80 wells spaced at 10 × 20 mm.

The sheet was layered with a nylon net of 2 mm mesh size on the underside to prevent seedlings from drowning in the nutrient solution. Each well supported one seedling. The EPS floats were placed in a 10 L rectangular plastic trough of inner dimensions of 24 × 36 × 12 cm filled with 7 L nutrient solutions, with all the roots submerged. Each EPS float supported 16 genotypes with two genotypes accommodated in one row with five plants each. Two such trays per treatment were maintained, which represented two replications. The basic nutrient medium contained 10 ppm (0.2 mM) of Fe, and therefore, the treatment system included varying Fe levels, such as 10p pm (T_0), 260 ppm (T_1), 360 ppm (T_2), and 460 ppm (T_3) equivalent to 0.2, 4.7, 6.5, and 8.3 mM of Fe. For imposing treatments, for each replication, 36.5 g of $FeSO_4.7H_2O$ was freshly dissolved in 400 mL of basic nutrient solution and made up to 500 mL. In addition, 55.0 g of citric acid monohydrate was dissolved separately in 500 mL of nutrient solution. For making T_1 treatment, 119 mL of $FeSO_4$ solution and 125 mL of citric acid solution were added to the trough, and the volume was made up to 7 L. Similarly, for T_2 and T_3 treatments, 167 mL and 214 mL of Fe solution were added respectively, together with 260 ppm of citric acid solution each. The T_0 treatment received only 250 mL of citric acid solution. Citric acid was added to improve the effective availability of Fe in plants (Hoagland and Arnon, 1950).

The nutrient solution was changed every 7 days, and the pH of the nutrient solution was maintained between 5.0 and 5.5 using 0.1 M HCl or 0.1 M NaOH daily. Initially, all the trays were maintained uniformly for 7 days in the basic nutrient solution. On the 8th day, in different

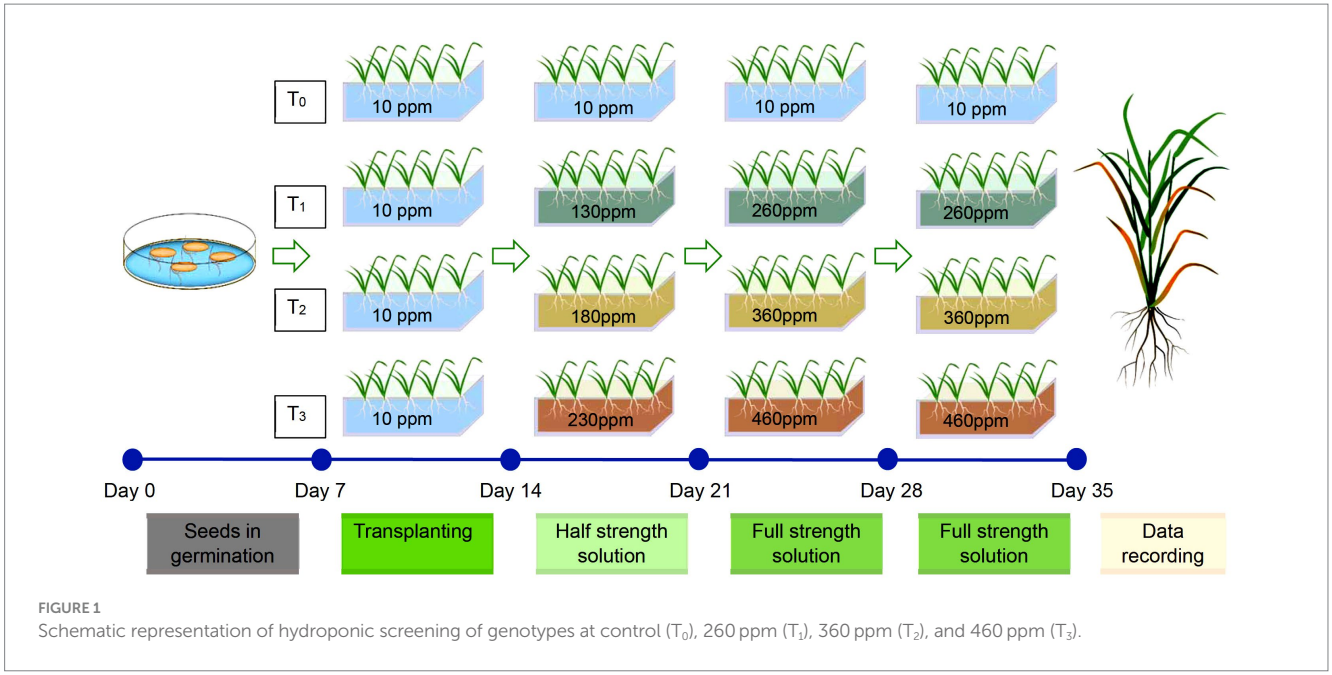

FIGURE 1
Schematic representation of hydroponic screening of genotypes at control (T_0), 260 ppm (T_1), 360 ppm (T_2), and 460 ppm (T_3).

TABLE 2 Modified score scale used to score leaf bronzing.

Score	Leaf area affected (%)	Description
0	0	Healthy leaves, no symptoms
1	1–10	Very few small brown specks on oldest leaves
3	11–29	Brown specks on oldest leaves more spread and enlarged; few brown specks on middle leaves
5	30–69	>50% of old leaves covered by brown lesions; enlarged brown specks on middle leaves
7	70–89	Old leaves entirely covered by brown lesions more than 50% of middle leaves covered by brown lesions
9	90–99	Whole plant covered with brown lesions; youngest leaf may look green
10	100	Whole plant dying or dead

treatments, half the strength of the Fe concentrations was added to prevent the sudden shock of Fe flooding in the plants. On the 15th day, the strength was increased to full strength. Thereafter, the genotypes were critically observed for the appearance of the symptoms. The data on both root and shoot-related traits were recorded after 35 days of sowing (Figure 1).

2.3 Phenotyping

The plants were evaluated non-destructively for leaf bronzing score (LBS) after 10 days of the full-strength stress treatment using a modified score scale (Table 2 and Supplementary Figure S1), integrating the observations from the study by Shimizu et al. (2005) and Wissuwa et al. (2006). Thirty-five days after sowing, all five sample plants per genotype were individually picked from the wells, and measurements of maximum root length (RL) and shoot length (SL) were taken. Subsequently, the plants were dissected into root and shoot sections. After blotting dry with an absorbent paper, the fresh weight of the shoot was measured. The root section was immediately scanned with a WinRHIZO® optical scanner (model Expression 12000XL, Epson Inc.), to measure root system architectural traits (Arsenault et al., 1995), such as root volume (RV), total root length (TRL), average diameter (AD), and surface area (SA). Following measurement, the root samples were blotted dry with an absorbent paper, and their fresh weight was measured. Both root and shoot samples were then oven-dried at 60°C for 72 h, to determine the corresponding dry weight, and the biomass (BM) was calculated by summing up the shoot and root dry weight. Oven-dried shoot samples were subsequently used to estimate shoot Fe concentration (SFC). For this purpose, all five dry samples per genotype were pooled and ground in a porcelain mortar. A 250 mg portion of these powdered samples was then wet-digested in 4 mL of 65% HNO_3 at 180°C for 8 h. The digest was subsequently diluted to 25 mL with distilled water and filtered. The filtrate was used to measure the Fe content using atomic absorption spectroscopy (AAS). Standard Fe solutions were prepared through serial dilutions ranging from 1 to 10 ppm.

2.4 Data analyses

The experiment was conducted in a completely randomized design with two factors, different levels of Fe and genotypes. The experiment was repeated twice, by setting the second experiment immediately after the first with the same setup, treatments and the management. The experimental data were subjected to analysis of variance using PBTools v.1.4.1 The degree of concordance (DoC) of the screening was calculated from the squared correlations between the experiment for every trait. The adjusted mean values were used for further analyses. The box plots were drawn from the average data, and the means were compared using Duncan's multiple range test.

Response stability of different traits relative to the unstressed treatment (T_0) was calculated for the treatment with maximum stress (T_3) by calculating the response stability index (RSI), which was similar to the yield stability index proposed by Bouslama and Schapaugh (1984). A correlogram of all the traits was visualized using the *corrplot* package in the R statistical environment. A principal component analysis (PCA) was performed to identify the most variable traits using *princomp()* function in the R *stats* package, and the biplots were drawn using the *factoextra* package. The contribution of different traits to principal components is graphically visualized using Circos Table Viewer v0.63–10 (Krzywinski et al., 2009). Principal component scores were utilized for the hierarchical clustering of genotypes, employing the Euclidean distances and the farthest neighbor clustering method. The clustering was performed using the *pheatmap* package under the R statistical environment.

3 Results

In both the screenings, a similar response to Fe concentration was observed among the genotypes. Combined analysis of variance indicated a significant variation of genotypes, Fe levels, and their interaction on all the root-related and shoot-related traits, except for root length in the screening 1. However, variation due to time of screening and respective interaction with genotypes was found non-significant except for LBS and RDW (Table 3 and Supplementary Table S1). The concordance of both experiments was high and significant as revealed by the degree of concordance, which was above 80% for all the traits except for RL.

3.1 Phenotypic variation for Fe levels

Comparison based on the significant difference of treatment mean values for the traits indicated that, irrespective of the genotypes, there was a significant increase in LBS and SFC while there was a reduction in SL, SFW, SDW, RFW, RDW, TRL, and SA as the Fe concentration increased (Figure 2). The mean LBS substantially increased from 0.34 in T_0 condition to 1.69 at T_1, 5.28 at T_2, and 6.62 at T_3. The range of leaf bronzing was from 0.4 to 3.8 at T_1, 3.0 to 7.0 at T_2, and 3.0 to 9.0 at T_3 of Fe, implying that the highest variability for LBS was observed at T_3 of Fe treatment compared with T_2 and T_1 of Fe treatment (Table 4). A similar effect could also be observed for SFC among the treatments with the lowest mean 1.76 at T_0, 6.41 ppm at T_1, 11.01 ppm at T_2, and 14.87 ppm at T_3. Beyond T_0, the treatment means did not vary significantly for SL, TRL, and SA. The SL was found reduced from 48.57 cm in T_0 to an average of 27.2 cm among the rest of the Fe levels. Significant change in treatment mean could be observed beyond T_2 for several traits, such as SFW, SDW, RL, RFW, RV, and AD (Table 4). The lowest values for most of the traits were encountered in T_3, which was significantly lower than T_2 for RV and RL. The relative differences over mean (RDM) among the treatments also showed distinct variations after T_2 for almost all the traits, except SL and SA, for which no significant reduction could be observed. Among the treatments with high Fe levels, RDM values were higher in T_3 for traits, such as RL, RDW, and RV, whereas this level showed effects at par with T_2 for the remaining traits, except for SFW, SDW, and RFW. Coupled with the highest variance, T_3 was the treatment that could reveal significant variation among the genotypes for the Fe toxicity response and was therefore considered as the critical concentration.

3.2 Response of genotypes

The response stability index of the genotypes under maximum stress exhibited varying degrees of response across the traits (Table 5). As mentioned previously, the most significant deviations were observed for LBS and SFC. In the case of LBS, the lowest index values were found in the already known tolerant cultivars such as Shahsarang

TABLE 3 Combined analysis of variance showing the partitioned variance across various components.

Traits	Mean squares							DoC
	Season (S)	Fe level (Fe)	S:Fe	Genotype (G)	Fe:G	S:G	S:Fe:G	
LBS	52.9**	1394.6**	20.7**	34.8**	9.6**	5.6**	2.3**	0.88
SFC	0.5	5161.3**	8.7**	57.3**	51.4**	0.4	7.5**	0.92
SL	1.78	18573.4**	32.4	1515.2**	247.9**	14.9	22.1	0.96
SFW	0.3	15.7**	0.1	1.5**	0.3**	0.01	0.01	0.98
SDW	0.01	1.3**	0.01	0.08**	0.03**	0.01	0.01	0.96
RL	0.4	53.7**	8.2**	65.8**	5.7**	0.5	1.9	0.76
TRL	501.7	132297.4**	424.2	23272.7**	3432.8**	80.6	171.4	0.96
RFW	0.01	2.2**	0.02	0.8**	0.1**	0.01	0.01	0.94
RDW	0.02**	0.9**	0.01**	0.03**	0.01**	0.01**	0.01**	0.85
RV	0.01	0.6**	0.01	0.2**	0.03**	0.01	0.01	0.92
AD	0.01	0.8**	0.01	0.06**	0.01**	0.01	0.01	0.85
SA	1.46	2213.2**	31.2	750.4**	65.1**	3.8	16.8	0.88

LBS, leaf bronzing score; SFC, shoot iron concentration in mg/kg; SL, shoot length in cm; RL, maximum root length in cm; SFW, shoot fresh weight in g; SDW, shoot dry weight in g; RFW, root fresh weight in g; RDW, root dry weight in g; TRL, total root length in cm; RV, root volume in cm^3; AD, average diameter in mm; SA, surface area in cm^2; DoC; degree of concordance; ** significant at 1% level.

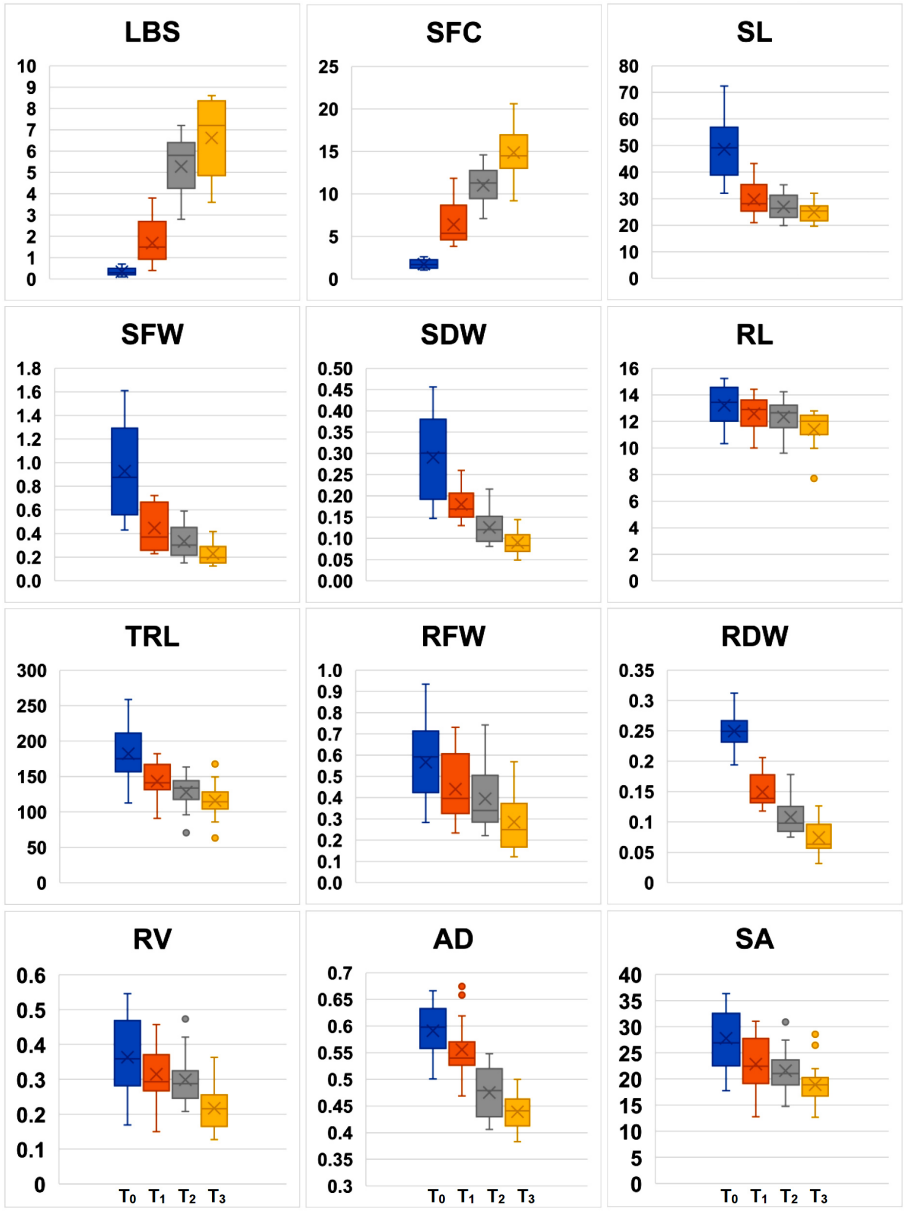

FIGURE 2
Box plots showing mean variability in root and shoot traits under four Fe concentrations. LBS, leaf bronzing score; SFC, shoot iron concentration in mg/kg; SL, shoot length in cm; RL, maximum root length in cm; SFW, shoot fresh weight in mg; SDW, shoot dry weight in mg; RFW, root fresh weight in mg; RDW, root dry weight in mg; TRL, total root length in cm; RV, root volume in mm^3; AD, average diameter in μm; SA, surface area in cm^2.

(6.3) and Megha SA2 (7.2), while the high index values were observed in RTN 10B (62.0), Pusa 1,342, and IR 64 (43.0 each), as well as BPT 5204 (41.0). Similarly, for SFC, the lowest index values were recorded for NPT 34 (3.5), followed by ILS 12–5 (5.2). The remaining traits did not show significant differences among the index values. Consequently, the index sum was used to compare the overall response of the genotypes. Based on this analysis, Shahsarang (17.4), ILS 12–5 (20.4), and Megha SA2 (21.3) were identified as the genotypes, displaying a high level of tolerance to Fe toxicity. Among the sensitive genotypes, RTN 10B had the highest index sum (78.0), followed by IR 64 (57.3), BPT 5204 (55.6), and Pusa 1,342 (54.3).

At the maximum toxicity level, Shahsarang and Megha SA2 displayed LBS values of 4.0 and 3.4, respectively, whereas the susceptible variety IR 64 had an LBS value of 8.6 (Supplementary Table S2). The lowest SFC was observed in NPT 34 (9.34), while the highest was found in IR 64 (20.6). PB 1121 exhibited the highest SL at 32.3 cm, followed closely by Shahsarang at 32.1 cm, with BPT 5204 having the shortest SL with an average value of 19.6 cm. In terms of SFW among genotypes under the highest toxicity, it ranged from 0.5 mg (ILS 12–5) to 0.1 g for IRGC 127653. A similar pattern was observed for SDW. Among the root traits, RL ranged from 7.8 cm (NPT 34) to 14.0 cm (ILS 12–5) under high toxic conditions. As for RFW, ILS 13–5 had the highest value at 569.0 mg, followed by Megha SA2 and Shahsarang with an average dry weight of 506.0 mg. The same genotypes showed a similar response for RDW. Root biomass, as determined by RFW and RDW, was low

TABLE 4 Phenotypic means of Fe level treatment across different traits.

Trait	Fe level treatments							
	T_0 (10 ppm)		T_1 (260 ppm)		T_2 (360 ppm)		T_3 (460 ppm)	
	Mean	RDM	Mean	RDM	Mean	RDM	Mean	RDM
LBS	0.34 ^{d}	0.0	1.69 ^{c}	−38.8	5.28 ^{b}	−103.1	6.62 ^{a}	−38.5
SFC	1.76 ^{d}	0.0	6.41 ^{c}	−54.6	11.01 ^{b}	−54.0	14.87 ^{a}	−45.3
SL	48.57 ^{a}	0.0	28.65 ^{b}	61.2	27.35 ^{b}	4.0	25.53 ^{b}	5.6
SFW	928.7 ^{a}	0.0	447.1 ^{b}	99.0	333.6 ^{bc}	24.7	229.5 ^{c}	20.6
SDW	290.4^{a}	0.0	179.9 ^{b}	63.8	125.7 ^{c}	29.0	90.1 ^{c}	23.2
RL	12.97 ^{a}	0.0	12.67 ^{ab}	2.4	12.27 ^{b}	3.2	11.63 ^{c}	5.2
TRL	182.14 ^{a}	0.0	143.41 ^{b}	27.2	128.02 ^{b}	10.8	116.07 ^{b}	8.4
RFW	566.6 ^{a}	0.0	440.2 ^{b}	30.6	395.1 ^{bc}	9.4	285.3 ^{c}	25.9
RDW	249.4 ^{a}	0.0	149.3 ^{b}	69.0	107.9 ^{c}	27.6	74.7 ^{d}	27.6
RV	363.3 ^{a}	0.0	314.8 ^{a}	16.8	298.8 ^{a}	3.4	217.1 ^{b}	26.9
AD	591.3 ^{a}	0.0	555.7 ^{a}	5.8	475.3 ^{b}	15.5	439.2 ^{b}	7.7
SA	27.76 ^{a}	0.0	22.83 ^{b}	21.7	21.56 ^{b}	5.6	18.88 ^{b}	11.8

LBS, leaf bronzing score; SFC, shoot iron concentration in mg/kg; SL, shoot length in cm; RL, maximum root length in cm; SFW, shoot fresh weight in g; SDW, shoot dry weight in g; RFW, root fresh weight in g; RDW, root dry weight in g; TRL, total root length in cm; RV, root volume in cm^3; AD, average diameter in mm; SA, surface area in cm^2. Trait means superscripted with same letters are significantly not significant across different Fe treatments at $p < 0.05$ by Duncan's multiple range test.

TABLE 5 Response stability index of different genotypes at maximum Fe toxicity stress.

Genotype	Response stability index												Index sum*
	LBS	SFC	SL	SFW	SDW	RL	TRL	RFW	RDW	SA	AD	RV	
BPT 5204	41.0	9.8	0.6	0.8	0.3	0.4	0.3	0.4	0.5	0.6	0.6	0.7	55.6
ILS 12–5	11.5	5.2	0.6	1.0	0.3	0.3	0.7	0.4	0.7	0.8	0.8	0.8	20.4
IR 64	43.0	9.8	0.6	1.0	0.2	0.2	0.4	0.2	0.7	0.6	0.7	0.7	57.3
IRGC 127653	35.0	9.3	0.4	0.9	0.2	0.2	0.4	0.2	0.5	0.6	0.6	0.7	49.6
Megha SA2	7.2	10.3	0.5	0.9	0.3	0.4	0.6	0.4	0.8	0.8	0.8	0.8	21.3
Nagina 22	28.0	18.9	0.4	1.1	0.2	0.2	0.3	0.2	0.7	0.6	0.6	0.8	51.9
NPT 34	24.7	3.5	0.5	0.8	0.4	0.6	0.6	0.3	0.5	0.7	0.7	0.7	32.4
PB 1	28.0	11.3	0.6	0.9	0.2	0.2	0.4	0.3	0.6	0.7	0.6	0.6	44.2
PB 1121	12.4	9.2	0.6	0.9	0.2	0.2	0.4	0.2	0.5	0.6	0.5	0.8	26.5
PR 126	15.0	7.2	0.6	0.8	0.4	0.5	0.7	0.1	0.8	0.8	0.8	0.7	26.0
Pusa 1,176	10.9	9.7	0.6	1.0	0.2	0.3	0.6	0.3	0.9	0.9	0.8	0.7	24.3
Pusa 1,342	43.0	7.4	0.6	0.9	0.4	0.3	0.5	0.3	0.9	0.7	0.6	0.8	54.3
Pusa 44	28.0	7.0	0.7	0.9	0.2	0.4	0.4	0.2	0.7	0.7	0.8	0.7	39.5
RTN 10B	62.0	11.9	0.6	0.9	0.3	0.5	0.5	0.2	0.7	0.8	0.8	0.7	78.0
Shahsarang	6.3	7.2	0.5	0.9	0.3	0.4	0.8	0.6	0.6	0.7	0.7	0.7	17.4
Sonasal	13.3	9.3	0.5	0.7	0.2	0.3	0.5	0.3	0.5	0.6	0.5	0.7	27.9

LBS, leaf bronzing score; SFC, shoot iron concentration in mg/kg; SL, shoot length in cm; RL, maximum root length in cm; SFW, shoot fresh weight in mg; SDW, shoot dry weight in mg; RFW, root fresh weight in mg; RDW, root dry weight in mg; TRL, total root length in cm; RV, root volume in mm^3; AD, average diameter in μm; SA, surface area in cm^2; * index sum is the sum of index values across traits – for traits where the response reduces with increase in Fe level, the value of (1-index) was used while summing.

among sensitive genotypes, such as RTN 10B, IR 64, BPT 5204, and others.

Root system architectural traits, such as SA, AD, and RV, under high toxicity levels, also highlighted the differences between tolerant and sensitive genotypes. SA was greater in Megha SA2 (31.0 cm^2), ILS 12–5 (30.8 cm^2), and Shahsarang (28.8 cm^2), whereas Pusa 1,342 (13.3 cm^2), BPT 5204 (14.3 cm^2), IR 64 (18.5 cm^2), and others had lower values for this trait. However, the AD of the roots showed relatively low variation among the genotypes under T_3. RV was more robust in the tolerant genotypes, particularly in ILS 12–5 (363.0 mm^3) and Megha SA2 (314.0 mm^3), while the lowest RV was observed in NPT 24 (127.0 mm^3).

3.3 Trait correlations and modelling the genotypic response for biomass

Correlation of component traits at maximum toxicity showed LBS having a negative but significant association with SFC, SFW, SDW, BM, PA, SA, AD, and RV. Trait pairs such as SFW:SDW and PA:SA:RV were autocorrelated. SFC exhibited high a positive association with SL, while SL indicated positive and significant associations with biomass traits, such as SFW, SDW, and BM and PA, SA, and RV. RL showed a positive association with TRL, SA, and RV. TRL also had a positive association with RFW, PA, SA, and RV. All the root system architecture traits indicated high association among themselves (Figure 3). Since several traits showed autocorrelations, further analyses were carried out with eight traits, *viz.*, LBS, SFC, SL, BM, RL, TRL, AD, and RV.

Considering the total dry matter (weight) as the important response variable under Fe toxicity among the rice seedlings, 25 regression models with best fit were identified using seven dependent variables (Supplementary Table S3). Among the models, the best-fit model with the highest R^2 value, lowest Akaike information criterion (AIC), and lowest Mallow's Cp was the model having two parameters, LBS and AD. This model explained 72% of the total variation in BM with the following coefficients. Additionally, the model also provided the lowest error variance of 850.0 among all the models. The Durbin–Watson (DW) statistic *p*-value shows no serial autocorrelation in the residuals at the 95.0% confidence level. The model coefficients are provided in following equation.

$$BM \sim 23.24 - 17.65 * LBS + 0.59 * AD$$

The model statistics are presented in Table 6. Although this mode accounted for the maximum variation in BM, the value of *ps* of AD remained at a non-significant level, signifying an inconspicuous contribution to this trait. Therefore, the model was modified as $BM \sim 313.5 - 22.51 * LBS$, accounting for 62.5% of the total variation.

3.4 Multidimensional classification of genotypes

Taking into consideration of the variables that exhibited weak association among themselves, eight principal components (PCs) were extracted by PCA. The first two components were identified significant as they accounted for 74.3% of the total variation (Figure 4). The biplot of PC1 versus PC2 showed that the Fe toxicity tolerant genotypes Megha SA2, ILS 12–5, Shahsarang, and Sonasal located at the upper right quadrant. The upper left quadrant consisted of moderately sensitive genotypes such as NPT 34, Pusa 1,342, and BPT 5204. The lower right quadrant encompassed the moderately tolerant genotypes PB 1121 and PB 1, while sensitive genotypes IR 64, IRGC 127653, Nagina 22, and Pusa 44 fell in the lower left quadrant. Analyzing the influence of traits on PC1, greater contribution could be observed from traits like RV, BM, LBS, AD, and TRL, all demonstrating nearly equal levels of contributions. Conversely, on PC2, RL and FSC exhibited significant contributions.

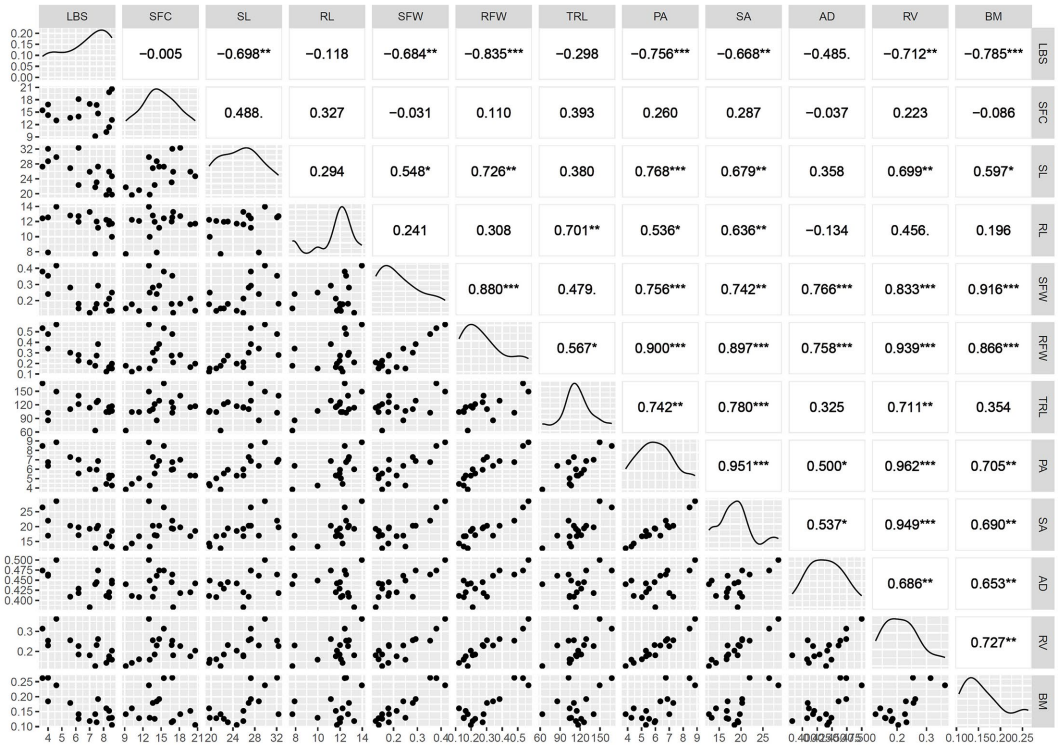

FIGURE 3
Correlogram showing Pearson correlation coefficient among the traits under the maximum Fe toxicity treatment. LBS, leaf bronzing score; SFC, shoot iron concentration in mg/kg; SL, shoot length in cm; RL, maximum root length in cm; SFW, shoot fresh weight in mg; RFW, root fresh weight in mg; TRL, total root length in cm; RV, root volume in mm^3; AD, average diameter in μm; PA, projected area in cm2; SA, surface area in cm^2; BM, Biomass in mg, ns, not significant at $p \leq 0.05$; *$p < 0.05$; **$p < 0.01$, ***$p < 0.001$.

PCA-based clustering generated three clusters of genotypes. Cluster 1 comprised of NPT 34, Pusa 1,342, Pusa 44, and BPT 5204, making it a group of sensitive genotypes. ILS 12–5, Megha SA2, and Shahsarang formed the Cluster 3, having tolerance to Fe toxicity. The Cluster 2 comprised of remaining genotypes that showed an intermediate response. Surprisingly, IR 64 was found included in this cluster, even though it is a well-known sensitive cultivar. Other members in the Cluster 2 were Pusa 1,176, PB 1, Sonasal, PB 1121, IRGC 127653, RTN 10B, PR 126, IR 64, and Nagina 22 (Figure 4).

4 Discussion

Fe toxicity is a nutritional stress that commonly affects lowland rice. In India, approximately 11.7 mha of rice area is affected by excess Fe in soil, potentially interfering with crop production. Identifying genotypes that can significantly withstand excess Fe stress is crucial for sustaining rice production in affected soils. Given that Fe affects the rice crop at all stages, an early-stage evaluation can help in identifying tolerant genotypes, justifying the usefulness of artificial screening. Although several studies have been reported, there seem to be many disagreements regarding the level of critical toxicity imposed (Elec et al., 2013; Rout et al., 2014; Reddy et al., 2015; Suma et al., 2022). Dobermann and Fairhurst (2000) identified 300–500 ppm to be a critical level of toxicity in soil for rice; however, the level changes with respect to soil properties and crop growth stage. Therefore, Fe toxicity screening requires standardization of screening conditions before setting up of experiments. Furthermore, conditions for soil-based screening needed to be customized depending on the soil type and properties, which warrants multiple testing, making it a cumbersome process. Soil-based or field-based screening (Gridley et al., 2006; Sikirou et al., 2016), pot culture (Sikirou et al., 2016), and hydroponics (Wan et al., 2003; Shimizu et al., 2005) are the major ways of studying genotype response. However, hydroponics is considered to be quick, efficient, and reliable (Suma et al., 2022). Among the various traits, LBS is considered as the most important parameter to study genotype response (Sikirou et al., 2016; Rumanti et al., 2017; Devi et al., 2018; Siriwardana et al., 2018). This is because the plants under excess Fe level produce a characteristic 'bronzing' symptom, due to the formation of numerous brown specks on the leaves (Wu et al., 2014). Bronzing occurs when the plants are deprived of oxygen supply from roots, and excess Fe accumulates in the leaves and shoots, leading to the Fenton reaction, cellular damage, and consequent yellowing and browning of tissues (Aung and Masuda, 2020). Plants that are adapted to Fe toxic ecologies show lesser bronzing than the un-adapted sensitive genotypes (Turhadi et al., 2019). Bronzing typically occurs on the lower leaves, starting to tip downward, and entire leaves can turn yellow or brown in severe cases. Bronzing is accompanied with growth retardation and plaque formation on the roots. Although many reports are available on various

TABLE 6 Refining the model for biomass (BM) under high toxicity treatment.

Parameter	Model 1	value of p	Model 2	*P*-value
Intercept	23.24	0.87	313.54	0.00
LBS	−17.65	0.00	−22.51	0.00
AD	0.59	0.06		
Variance	14167.70	0.00	24609.00	0.00
Residual	850.00		1055.46	
R^2	71.94		62.48	
Adjusted *R*	67.63		59.80	
SE	29.15		32.49	
Durbin-Watson statistic	1.94	0.44	1.88	0.39

LBS, leaf bronzing score; AD, average diameter in cm^2; SE, standard error.

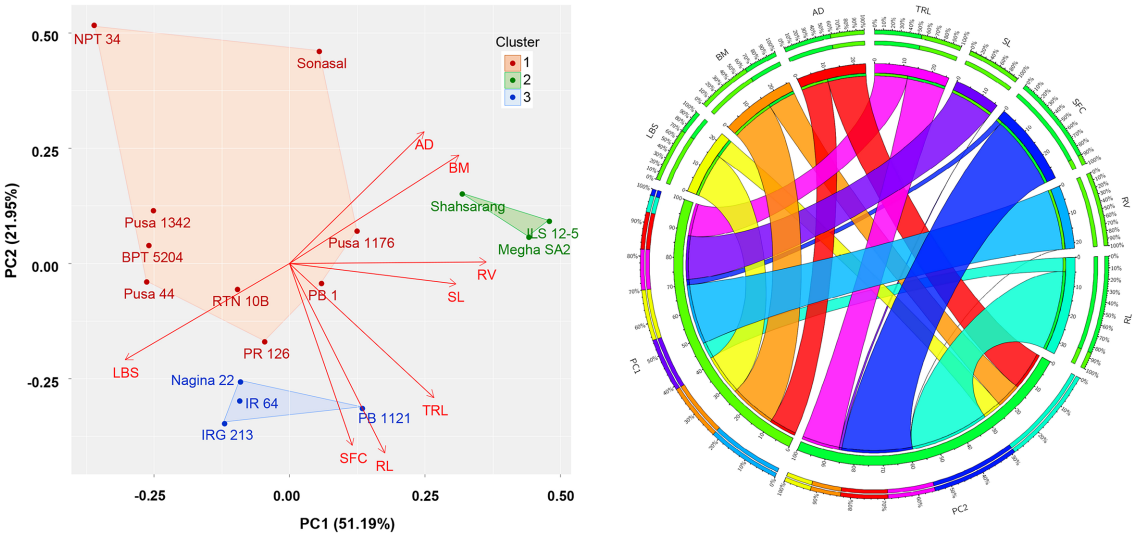

FIGURE 4
PCA-biplots depicting genotype clusters and trait contribution visualized via Circos-diagram for major principal components. LBS, leaf bronzing score; SFC, shoot iron concentration in mg/kg; SL, shoot length in cm; RL, maximum root length in cm; TRL, total root length in cm; RV, root volume in mm^3; AD, average diameter in μm; BM, Biomass in mg.

morphophysiological traits in different genotypes, not many deals with the effect of Fe toxicity on root system architecture (RSA) attributes. This study forms one such preliminary attempt to detail the effect of Fe toxicity stress on root system in rice.

We have selected 16 genotypes, of which two were well-known Fe tolerant cultivars adapted to North-eastern ecology. These genotypes, Shahsarang and Megha SA2, are widely cultivated in the North-east states of India, such as Meghalaya, Mizoram, Manipur, and Nagaland. Shahsarang is a high-yielding hybrid derivative of Mirikrak/Rasi, with semi-dwarf and non-lodging habit. Among the several features of this variety, traits such as tolerance to Fe toxicity and adaptation to cold and low light stand out as typical. Megha SA 2 (Megha Semi-Aromatic 2) or RCPL 1–160 is a fine grain high-yielding semi-dwarf variety, with adaptation to lowlands of low-altitude ecology. Being established and tolerant to excess Fe, these varieties would help in comparative evaluation. In addition, IR 64 was included, a mega variety that was established as sensitive to excess Fe from various studies (Wu et al., 1997; Mackill and Khush, 2018; Turhadi et al., 2019). The remaining genotypes were selected at random but represented mega varieties, Basmati cultivars, stress-tolerant cultivars, and green super rice. The selection of an optimal set of genotypes provided an opportunity to evaluate the response to different Fe concentrations on various morphological traits and identify the critical iron concentration for screening. Critical iron concentration is a parameter influenced by tested genotypes, a form of Fe applied, and solution pH (De Dorlodot et al., 2005; Nozoe et al., 2008). Sharp contrast between tolerant and sensitive genotypes with respect to Fe toxicity symptoms and variation for traits was the main criterion to choose the optimum combination (Elec et al., 2013). Accordingly, 460 ppm of Fe was selected as critical, as it provided larger variance among the traits and could display remarkable contrasts between known tolerant and sensitive genotypes, and largest decrease in most of the morphologic traits from normal.

High contrast among various traits is desirable to differentiate genotypes from extreme responses under stress (Rinyu et al., 1995; Houle, 1998). Although significant variation could be observed on all the traits under normal Fe concentration, LBS and SFC increased with Fe level, indicating the progressive influence of toxicity. These observations are in concordance with several previous reports (Zhang et al., 2017; Onyango et al., 2018). A sharp increase in LBS among the genotypes with increased levels of Fe could imply an increased accumulation of toxic levels of Fe ions, driving Fenton reactions and cellular damage. One of the important features of excess Fe uptake in plants is the accumulation of Fe in the cellular component as revealed by the increase in SFC with increasing toxicity stress. In tolerant genotypes, accumulation of excess Fe^{2+} ions in vacuoles (plastids) forms a mode of tolerance (Asch et al., 2005; Wu et al., 2014; Santos et al., 2018). However, tolerant varieties, Shahsarang and Megha SA2, accumulated less Fe in the shoot as compared with IR 64, which indicated a different mechanism in operation in these genotypes. These varieties may have exclusion (type I) mechanism, wherein excess Fe is prevented from uptake by oxidation and precipitation on the root surface (Becker and Asch, 2005; Saikia and Baruah, 2012; Wu et al., 2014; Dufey et al., 2015; Sikirou et al., 2016; Turhadi et al., 2018; Bresolin et al., 2019; Aung and Masuda, 2020). As reported earlier, leaf bronzing remained the most important parameter and straightforward indicator of the intensity of Fe toxicity stress in this study (Wan et al., 2003; Asch et al., 2005; Dufey et al., 2009). As a result, increased bronzing with increasing levels of Fe indicated a strong positive correlation. Since the stress induced a reduction in all other traits, SFC, LBS showed a strong negative relationship with all those traits that showed a progressive reduction with increasing Fe levels. However, although the SFC exhibited a positive correlation with LBS, earlier studies indicate that the iron content in plant tissue may not always be associated with bronzing scores (Nugraha et al., 2016b; Turhadi et al., 2018; Sitaresmi et al., 2021).

Several earlier studies have reported a reduction in SL under Fe toxicity (Rout et al., 2014; Bresolin et al., 2019; Suma et al., 2022), we did not observe any significant difference in the height of seedlings at different Fe concentrations. However, reduction in RL was significant at critical Fe level, confirming root growth inhibition as one of the primary damages due to Fe toxicity. Toxic levels of Fe interfere with and inhibit cell division and elongation of the primary roots and, subsequently, the growth of lateral roots (Li et al., 2016a; Hamim et al., 2018; Suma et al., 2022). Since RL reduction appears after the primary damage to the root system, a concomitant reduction in nutrient uptake can be expected as a consequence. However, in the seedling stage evaluation, no apparent reduction in shoot growth was observed because of the short-term exposure to stress. Therefore, shoot traits cannot be considered as reliable parameters for screening genotypes for Fe toxicity response particularly in the seedling stage. Nevertheless, shoot and root biomass (fresh and dry weight) showed significant differences with increasing Fe stress, aligning with earlier studies (Dufey et al., 2009; Wu et al., 2014; Nugraha et al., 2016b; Reddy et al., 2019).

With the increasing reduction in biomass observed beyond 360 ppm, the relative deviation from the biomass under normal Fe level could clearly differentiate tolerant and sensitive genotypes at the critical level. As with the earlier reports, the reduction in biomass is reflective of the retardation in the growth of the plants as a result of stress due to Fe toxicity (Onaga et al., 2013; Nugraha et al., 2016b; Theerawitaya et al., 2022). Among the biomass traits, RDW, in particular, is reported to be influenced by the presence of Fe coating on the root surface, which comes as a result of the exclusion mechanism (De Dorlodot et al., 2005; Saikia and Baruah, 2012; Sikirou et al., 2016; Wu et al., 2017). In this study, higher relative root and shoot dry weight observed among the tolerant rice lines signifies better growth among these genotypes under stress, which aligns well with the previous reports by Wu et al. (2014) and Devi et al. (2018).

Notwithstanding the importance of aerial morphologic changes, the major focus of this study was on the root system architecture. Although much-needed attention was not provided to these traits earlier, the root system has recently recognized as an effective selection parameter to determine the ability of plants to manage various soil stresses (Mahender et al., 2019). However, the information on the effects of excess Fe on the root system architecture in rice is still scanty (Li et al., 2016a). Roots being the primary plant organ involved in Fe uptake from the soil solution, the first line of defense against excess Fe, must initiate at the rhizosphere (Onaga et al., 2016). Hence, Fe toxicity is considered to affect and alter the root system architectural traits (Mahender et al., 2019). The experiences from the other soil-based stresses, such as drought and phosphorus starvation, showed that highly dynamic adjustments in overall root system architecture (RSA) determine root plasticity and allow plants to efficiently adapt to environmental

constraints. Irrespective of the sensitive or tolerant behavior of genotypes, we could observe a marked decrease in TRL, SA, AD, and TV, with maximum reduction occurring with the exposure to the highest toxicity level. Therefore, the reduction in RSA traits could occur due to the damage in the root system in sensitive genotypes, while it can also be a part of the root development adaptation strategy in the tolerant genotypes to restrict excess Fe absorption (Li et al., 2016b). Reduction in the TRL due to Fe toxicity was also reported by Ward et al. (2008) in *Arabidopsis thaliana*, where the primary root length was inhibited. Excess Fe inhibited the formation of 1st, 2nd, and 3rd order lateral roots confirmed by a decrease in the number of roots. Earlier studies have concluded that arrested cell division and elongation due to excess Fe could significantly distort the root system architecture (Reyt et al., 2015; Li et al., 2016b).

Among the various root traits, SA contributed >15% to the total genotypic variation both in control and stress conditions. A reduced root surface area can be explained as a strategy to restrict nutrient absorption (Kirk et al., 2022). Nurmalasari et al. (2016) observed a reduction in SA due to Fe toxicity in oil palm. The reduction in the SA may be considered as a potential mechanism for Fe exclusion, evidenced by a decrease in the number of root hairs. Reduction in SA could also be occurring due to reduced AD. Wu et al. (2014) reported a marked reduction in AD in the susceptible variety IR 29 as compared with the tolerant line Pokkali, which is similar to the observation in the tolerant varieties, Shahsarang and Megha SA2, as compared with IR 64. Higher AD in the tolerant genotypes facilitates the formation of aerenchyma in roots, enhancing air transport and the ability to oxidize Fe^{2+} in the rhizosphere, ultimately contributing to Fe exclusion. A decrease in RV among the sensitive genotypes could be interpreted as a reduction in RL, SA, and AD (Hussain et al., 2020).

Stress indices can serve as effective parameters to identify tolerant and sensitive genotypes (Kakar et al., 2019; Dwivedi et al., 2021). The response stability index used in this study was the ratio of response under stress to the un-stressed (Bouslama and Schapaugh, 1984), which is an indicator or genotype's resilience to stress. When challenged with stress, if any genotype could respond similarly or better than the unstressed conditions, the index will tend toward one and above. Therefore, lower values of the index indicated tolerance, while higher values indicated sensitiveness. Accordingly, based on the index sum, we could identify genotypes such as Shahsarang, Megha SA2, and ILS 12–5 as the most resilient genotypes among all. Interestingly, most of the sensitive genotypes showed an index sum of >50, which included RTN 10B, IR 64, BPT 5204, Nagina 22, and Pusa 1,342. Genotypes such as PB 1121, Pusa 1,176, PR 126, NPT 34, Sonasal, and Pusa 44 showed moderate tolerance, while PB 1 and IRGC 127653 were moderately sensitive. Several stress evaluation studies reported the usefulness of stress indices for identifying tolerant genotypes and classifying them (Dhawan et al., 2021; Joshi et al., 2023). The grouping of 16 rice genotypes, based on their morphophysiological responses to Fe toxicity, also indicated conspicuous polarization of tolerant and sensitive genotypes. PCA-based clustering has been previously utilized in studies by Nugraha et al. (2016a,b), Pawar et al. (2017), Dziwornu et al. (2018), Theerawitaya et al. (2022), and Ahmed et al. (2023) for identification of sensitive and tolerant genotypes. Using the index sum and PCA the sensitive genotypes could be separated clearly from the tolerant genotypes with, the moderately responding genotypes falling in between. The results also indicated that the index sum was robust enough to differentiate between tolerant and sensitive genotypes. In previous studies, LBS served as the exclusive criterion for classifying tolerant and sensitive genotypes (Engel et al., 2012; Harahap et al., 2014; Nugraha et al., 2016b). However, in this study, we were able to show that changes in the root system can function as a significant criterion for classification.

5 Conclusion

The present study concluded that 460 ppm of Fe in the nutrient solution was critical for screening genotypes for their response to Fe toxicity. Based on the significant effect of excess Fe on morphological and root system characteristics in rice genotypes, these genotypes could be classified into tolerant and sensitive ones. Leaf bronzing was the major response to Fe stress in plants, indicating a high level of contrast between tolerant and sensitive genotypes. The response stability index across traits provided ample opportunity for classification. In addition to the known tolerant genotypes, ILS 12–5 was identified as a tolerant, qualifying it to be tested under Fe-rich field conditions. Some of the most sensitive genotypes included mega varieties such as BPT 5204 and Pusa 44, making them suitable candidates for Fe toxicity tolerance improvement. This would enable these mega-varieties to be recommended for Fe-toxic regions of Northeastern India. Fe toxicity had a severe effect on RSA traits, such as RL, SA, and RV. This report provides insight into the influence of toxic levels of Fe on the root system. There is a reasonable indication that the responses in aerial biomass are consequential to root system damage, resulting from the nutrient deprivation. Furthermore, Fe exclusion could be a major mechanism for conditioning toxicity tolerance in tolerant genotypes, enabling them to reduce Fe^{2+} uptake. These valuable inferences will be useful for managing Fe toxicity and improving tolerance in rice through selection strategies in breeding programs. Field evaluation of identified tolerant/sensitive lines is still required to confirm their behavior under field conditions and use them in breeding programs. The effect of Fe toxicity on RSA traits can be further investigated for a better understanding of intrinsic mechanisms of root system variations, differentiating tolerant and sensitive genotypes.

Data availability statement

The original contributions presented in the study are included in the article/Supplementary material, further inquiries can be directed to the corresponding author.

Author contributions

So: Data curation, Formal analysis, Investigation, Methodology, Validation, Writing – original draft. SN: Formal analysis, Validation. VS: Data curation, Investigation, Writing – review & editing. RP: Methodology, Investigation. SG: Supervision, Resources. PB: Methodology, Resources, Validation. RE: Formal analysis. HB: Validation. BH: Investigation. SY: Investigation. RB: Data curation. MN: Resources. AS: Project administration. KV: Conceptualization,

Data curation, Investigation, Methodology, Resources, Supervision, Visualisation, Writing – review & editing.

Funding

The author(s) declare financial support was received for the research, authorship, and/or publication of this article. The author(s) declare financial support received in the form of a senior research fellowship received by the senior author from ICAR-IARI. The author(s) declare publication support of this article from the Crop Research Platform - Hybrid Technology (CRP-HT) project code 12-142A from the Indian Council of Agricultural Research (ICAR).

Acknowledgments

The authors greatly acknowledge the facilities provided by the National Phytotron Facility and the Divisions of Genetics and Crop Physiology in conducting this study.

Conflict of interest

The authors declare that the research was conducted in the absence of any commercial or financial relationships that could be construed as a potential conflict of interest.

Publisher's note

Supplementary material

The Supplementary material for this article can be found online at: https://www.frontiersin.org/articles/10.3389/fsufs.2023.1334487/full#supplementary-material

References

Abifarin, A. O. (1989). Progress in breeding rice for tolerance to iron toxicity. *WARDA Ann. Rep.*, 34–39.

Ahmed, S. F., Ullah, H., Aung, M. Z., Tisarum, R., Cha-Um, S., and Datta, A. (2023). Iron toxicity tolerance of rice genotypes in relation to growth, yield and physiochemical characters. *Rice Sci.* 30, 321–334. doi: 10.1016/j.rsci.2023.02.002

Archana, R., Bollinedi, H., Nagarajan, M., Gangadhara, K. N., Ellur, R. K., Singh, V. J., et al. (2021). Stay green behaviour of a novel mutant, PSG16 shows complex inheritance and functional relations with grain yield in rice. *Indian J. Genet Plant Breed.* 81, 495–504. doi: 10.31742/IJGPB.81.4.1

Arsenault, J. L., Poulcur, S., Messier, C., and Guay, R. (1995). WinRHlZO™, a root-measuring system with a unique overlap correction method. *Hortic. Sci.* 30:906D. doi: 10.21273/HORTSCI.30.4.906D

Asch, F., Becker, M., and Kpongor, D. S. (2005). A quick and efficient screen for resistance to iron toxicity in lowland rice. *J. Plant. Nutr. Soil Sci.* 168, 764–773. doi: 10.1002/jpln.200520540

Audebert, A., and Fofana, M. (2009). Rice yield gap due to iron toxicity in West Africa. *J. Agron. Crop. Sci.* 195, 66–76. doi: 10.1111/j.1439-037X.2008.00339.x

Audebert, A., and Sahrawat, K. L. (2000). Mechanisms for iron toxicity tolerance in lowland rice. *J. Plant Nutr.* 23, 1877–1885. doi: 10.1080/01904160009382150

Aung, M. S., and Masuda, H. (2020). How does rice defend against excess iron? Physiological and molecular mechanisms. *Front. Plant Sci.* 11:1102. doi: 10.3389/fpls.2020.01102

Bashir, K., Nozoye, T., Nagasaka, S., Rasheed, S., Miyauchi, N., Seki, M., et al. (2017). Paralogs and mutants show that one DMA synthase functions in iron homeostasis in rice. *J. Exp. Bot.* 68, 1785–1795. doi: 10.1093/jxb/erx065

Becker, M., and Asch, F. (2005). Iron toxicity in rice—conditions and management concepts. *J. Plant. Nutr. Soil Sci.* 168, 558–573. doi: 10.1002/jpln.200520504

Bouslama, M., and Schapaugh, W. T. (1984). Stress tolerance in soybeans. I. Evaluation of three screening techniques for heat and drought tolerance 1. *Crop Sci.* 24, 933–937. doi: 10.2135/cropsci1984.0011183X002400050026x

Bresolin, A. P. S., Dos Santos, R. S., Wolter, R. C. D., de Sousa, R. O., da Maia, L. C., and Costa de Oliveira, A. (2019). Iron tolerance in rice: an efficient method for performing quick early genotype screening. *BMC Res. Note.* 12, 361–366. doi: 10.1186/s13104-019-4362-5

Carvalhais, L. C., Dennis, P. G., Fedoseyenko, D., Hajirezaei, M. R., Borriss, R., and von Wirén, N. (2011). Root exudation of sugars, amino acids, and organic acids by maize as affected by nitrogen, phosphorus, potassium, and iron deficiency. *J. Plant. Nutr. Soil Sci.* 174, 3–11. doi: 10.1002/jpln.201000085

Chérif, M., Audebert, A., Fofana, M., and Zouzou, M. (2009). Evaluation of iron toxicity on lowland irrigated rice in West Africa. *Tropicultra* 27, 88–92.

Connorton, J. M., Balk, J., and Rodríguez-Celma, J. (2017). Iron homeostasis in plants – a brief overview. *Metallomics* 9, 813–823. doi: 10.1039/C7MT00136C

De Dorlodot, S., Lutts, S., and Bertin, P. (2005). Effects of ferrous iron toxicity on the growth and mineral composition of an interspecific rice. *J. Plant Nutr.* 28, 1–20. doi: 10.1081/PLN-200042144

Debnath, A., Rai, M., and Tyagi, W. (2021). Identification of Swarna x *O. Nivara* (RPBio4918) advanced backcross lines performing well under acidic soil conditions. *J. Environ. Biol.* 42, 240–246. doi: 10.22438/jeb/42/2/MRN-1481

Devi, A. G., Rangappa, K., Yadav, G. S., Devi, H. L., Barman, K. K., Kandpal, B. K., et al. (2018). Physiological tolerance mechanism of selected rice germplasm of Northeast India to iron toxicity. *Indian J. Hill Farm.* 31, 75–81.

Dhawan, G., Kumar, A., Dwivedi, P., Gopala Krishnan, S., Pal, M., Vinod, K. K., et al. (2021). Introgression of *qDTY1. 1. Agronomy* 11:202. doi: 10.3390/agronomy11020202

Dobermann, A., and Fairhurst, T. (2000). *Rice: Nutrient disorders and nutrient management*, International Rice Research Institute: Los Baños.

Dotaniya, M. L., Meena, H. M., Lata, M., and Kumar, K. (2013). Role of phyto-siderophores in iron uptake by plants. *Agric. Sci. Dig.* 33, 73–76.

Dufey, I., Draye, X., Lutts, S., Lorieux, M., Martinez, C., and Bertin, P. (2015). Novel QTLs in an interspecific backcross *Oryza sativa*× *Oryza glaberrima* for resistance to iron toxicity in rice. *Euphytica* 204, 609–625. doi: 10.1007/s10681-014-1342-7

Dufey, I., Hakizimana, P., Draye, X., Lutts, S., and Bertin, P. (2009). QTL mapping for biomass and physiological parameters linked to resistance mechanisms to ferrous iron toxicity in rice. *Euphytica* 167, 143–160. doi: 10.1007/s10681-008-9870-7

Dwivedi, P., Ramawat, N., Dhawan, G., Gopala Krishnan, S., Vinod, K. K., Singh, M. P., et al. (2021). Drought tolerant near isogenic lines (NILs) of Pusa 44 developed through marker assisted introgression of *qDTY2.1* and *qDTY3.1* enhances yield under reproductive stage drought stress. *Agriculture* 11:64. doi: 10.3390/agriculture11010064

Dziwornu, A. K., Shrestha, A., Matthus, E., Ali, B., Wu, L. B., and Frei, M. (2018). Responses of contrasting rice genotypes to excess manganese and their implications for lignin synthesis. *Plant Physiology and Biochemistry* 123, 252–259. doi: 10.1016/j.plaphy.2017.12.018

Elec, V., Quimio, C. A., Mendoza, R., Sajise, A. G. C., Beebout, S. E., Gregorio, G. B., et al. (2013). Maintaining elevated Fe 2+ concentration in solution culture for the development of a rapid and repeatable screening technique for iron toxicity tolerance in rice (*Oryza sativa* L.). *Plant Soil.* 372, 253–264. doi: 10.1007/s11104-013-1739-4

Engel, K., Asch, F., and Becker, M. (2012). Classification of rice genotypes based on their mechanisms of adaptation to iron toxicity. *J. Plant. Nutr. Soil Sci.* 175, 871–881. doi: 10.1002/jpln.201100421

Fageria, N. K., Santos, A. B., Barbosa Filho, M. P., and Guimarães, C. M. (2008). Iron toxicity in lowland rice. *J. Plant Nutr.* 31, 1676–1697. doi: 10.1080/01904160802244902

Gamborg, O. L., and Wetter, L. R. (1975). *Plant tissue culture methods*. Saskatoon: National research council of Canada. Prairie regional laboratory.

Gridley, HE, Efisue, A, Tolou, B, and Bakayako, T (2006) *Breeding for tolerance to iron toxicity at WARDA. Iron toxicity in rice-based systems in West Africa*, Africa Rice Center (WARDA): Cotonou 96–111.

Hamim, H., Miftahudin, M., and Setyaningsih, L. (2018). "Cellular and ultrastructure alteration of plant roots in response to metal stress" in *Plant growth and regulation-alterations to sustain unfavorable conditions*, eds. D. Ratnadewi and Hamim (London: IntechOpen), 21–41.

Harahap, S. M., Ghulamahdi, M., Aziz, S. A., and Sutandi, A. (2014). Relationship of ethylene production and aerenchyme formation on oxidation ability and root surfaced-iron (Fe^{+2}) accumulation under different iron concentrations and rice genotypes. *Int. J. Appl. Sci. Technol.* 4, 186–194.

Hoagland, D. R., and Arnon, D. I. (1950). The water-culture method for growing plants without soil. *Circular. Calif. Agric. Exp. Stn.* 347:32.

Hoan, N. T., Prasada Rao, U., and Siddiq, E. A. (1992). Genetics of tolerance to iron chlorosis in rice. *Plant Soil.* 146, 233–239. doi: 10.1007/BF00012017

Houle, D. (1998). How should we explain variation in the genetic variance of traits? *Genetica* 102, 241–253. doi: 10.1023/A:1017034925212

Hussain, H. A., Men, S., Hussain, S., Zhang, Q., Ashraf, U., Anjum, S. A., et al. (2020). Maize tolerance against drought and chilling stresses varied with root morphology and antioxidative defense system. *Plants* 9:720. doi: 10.3390/plants9060720

Jaggard, K. W., Qi, A., and Ober, E. S. (2010). Possible changes to arable crop yields by 2050. *Phil. Trans. R. Soc. B.* 365, 2835–2851. doi: 10.1098/rstb.2010.0153

Joshi, N., Pappula Reddy, S. P., Kumar, N., Bharadwaj, C., Tapan, K., Patil, B. S., et al. (2023). Siphoning novel sources of seedling salinity tolerance from the diverse chickpea landraces. *Crop Pasture Sci.* 74, 1080–1093. doi: 10.1071/CP22319

Kabir, A. H., Begum, M. C., Haque, A., Amin, R., Swaraz, A. M., Haider, S. A., et al. (2016). Genetic variation in Fe toxicity tolerance is associated with the regulation of translocation and chelation of iron along with antioxidant defence in shoots of rice. *Funct. Plant Biol.* 43, 1070–1081. doi: 10.1071/FP16068

Kakar, N., Jumaa, S. H., Redoña, E. D., Warburton, M. L., and Reddy, K. R. (2019). Evaluating rice for salinity using pot-culture provides a systematic tolerance assessment at the seedling stage. *Rice* 12, 57–14. doi: 10.1186/s12284-019-0317-7

Kar, S., and Panda, S. K. (2020). Iron homeostasis in rice: deficit and excess. *Proc. Natl. Acad. Sci. India Sect. B Biol. Sci.* 90, 227–235. doi: 10.1007/s40011-018-1052-3

Kirk, G. J., Manwaring, H. R., Ueda, Y., Semwal, V. K., and Wissuwa, M. (2022). Below-ground plant–soil interactions affecting adaptations of rice to iron toxicity. *Plant Cell Environ.* 45, 705–718. doi: 10.1111/pce.14199

Kobayashi, N. I., Ogura, T., Takagi, K., Sugita, R., Suzuki, H., Iwata, R., et al. (2018). Magnesium deficiency damages the youngest mature leaf in rice through tissue-specific iron toxicity. *Plant Soil.* 428, 137–152. doi: 10.1007/s11104-018-3658-x

Krzywinski, M., Schein, J., Birol, I., Connors, J., Gascoyne, R., Horsman, D., et al. (2009). Circos: an information aesthetic for comparative genomics. *Genome Res.* 19, 1639–1645. doi: 10.1101/gr.092759.109

Li, G., Kronzucker, H. J., and Shi, W. (2016a). Root developmental adaptation to Fe toxicity: mechanisms and management. *Plant Signal. Behav.* 11:e1117722. doi: 10.1080/15592324.2015.1117722

Li, G., Kronzucker, H. J., and Shi, W. (2016b). The response of the root apex in plant adaptation to iron heterogeneity in soil. *Front. Plant Sci.* 7:344. doi: 10.3389/fpls.2016.00344

Li, W., and Lan, P. (2017). The understanding of the plant iron deficiency responses in strategy I plants and the role of ethylene in this process by omic approaches. *Front. Plant Sci.* 8:40. doi: 10.3389/fpls.2017.00040

Ma, C., Burd, S., and Lers, A. (2015). Mi R 408 is involved in abiotic stress responses in *Arabidopsis*. *Plant J.* 84, 169–187. doi: 10.1111/tpj.12999

Mackill, D. J., and Khush, G. S. (2018). IR64: a high-quality and high-yielding mega variety. *Rice* 11, 1–11. doi: 10.1186/s12284-018-0208-3

Mahender, A., Swamy, B. M., Anandan, A., and Ali, J. (2019). Tolerance of iron-deficient and-toxic soil conditions in rice. *Plants* 8:31. doi: 10.3390/plants8020031

Mahmoudi, H., Labidi, N., Ksouri, R., Gharsalli, M., and Abdelly, C. (2007). Differential tolerance to iron deficiency of chickpea varieties and Fe resupply effects. *C. R. Biol.* 330, 237–246. doi: 10.1016/j.crvi.2007.02.007

Mamidi, S., Lee, R. K., Goos, J. R., and McClean, P. E. (2014). Genome-wide association studies identifies seven major regions responsible for iron deficiency chlorosis in soybean (*Glycine max*). *PLoS One* 9:e107469. doi: 10.1371/journal.pone.0107469

Marschner, H., and Römheld, V. (1995). "Strategies of plants for acquisition of iron" in *Iron nutrition in soils and plants. Developments in plant and soil sciences*. ed. J. Abadía, vol. *59* (Dordrecht: Springer)

Matthus, E., Wu, L. B., Ueda, Y., Höller, S., Becker, M., and Frei, M. (2015). Loci, genes, and mechanisms associated with tolerance to ferrous iron toxicity in rice (*Oryza sativa* L.). *Theor. Appl. Genet.* 128, 2085–2098. doi: 10.1007/s00122-015-2569-y

Mongon, J., Chaiwong, N., Bouain, N., Prom-U-Thai, C., Secco, D., and Rouached, H. (2017). Phosphorus and iron deficiencies influences rice shoot growth in an oxygen dependent manner: insight from upland and lowland rice. *Int. J. Mol. Sci.* 18:607. doi: 10.3390/ijms18030607

Müller, J., Toev, T., Heisters, M., Teller, J., Moore, K. L., Hause, G., et al. (2015). Iron-dependent callose deposition adjusts root meristem maintenance to phosphate availability. *Dev. Cell* 33, 216–230. doi: 10.1016/j.devcel.2015.02.007

Nozoe, T., Agbisit, R., Fukuta, Y., Rodriguez, R., and Yanagihara, S. (2008). Characteristics of iron tolerant rice lines developed at IRRI under field conditions. *JARQ* 42, 187–192. doi: 10.6090/jarq.42.187

Nugraha, Y., Ardie, S. W., Ghulammahdi, M., Suwarno, , and Aswidinnoor, H. (2016a). Nutrient culture media with agar is effective for early and rapid screening of iron toxicity tolerance in rice. *J. Crop Sci. Biotechnol.* 19, 61–70. doi: 10.1007/s12892-015-0075-z

Nugraha, Y., Utami, D. W., Rosdianti, I. D. A., Ardie, S. W., Ghulammahdi, M., Suwarno, S., et al. (2016b). Markers-traits association for iron toxicity tolerance in selected Indonesian rice varieties. *Biodiversitas* 17, 753–763. doi: 10.13057/biodiv/d170251

Nurmalasari, A. I., Putra, E. T. S., and Yudono, P. (2016). Root morphology of eight hybrid oil palms under iron (Fe) toxicity. *Ilmu Pertanian* 1, 013–018. doi: 10.22146/ipas.11254

Onaga, G., Dramé, K. N., and Ismail, A. M. (2016). Understanding the regulation of iron nutrition: can it contribute to improving iron toxicity tolerance in rice? *Funct. Plant Biol.* 43, 709–726. doi: 10.1071/FP15305

Onaga, G., Edema, R., and Asea, G. (2013). Tolerance of rice germplasm to iron toxicity stress and the relationship between tolerance, Fe2+, P and K content in the leaves and roots. *Arch. Agron. Soil Sci.* 59, 213–229. doi: 10.1080/03650340.2011.622751

Onyango, D. A., Entila, F., Dida, M. M., Ismail, A. M., and Drame, K. N. (2018). Mechanistic understanding of iron toxicity tolerance in contrasting rice varieties from Africa: 1. Morpho-physiological and biochemical responses. *Funct. Plant Biol.* 46, 93–105. doi: 10.1071/FP18129

Pathirana, R., Wijithawarna, W. A., Jagoda, K., and Ranawaka, A. L. (2002). Selection of rice for iron toxicity tolerance through irradiated caryopsis culture. *Plant Cell Tissue Organ Cult.* 70, 83–90. doi: 10.1023/A:1016025728740

Pawar, S., Pandit, E., Arjun, P., Wagh, M., Bal, D., Panda, S., et al. (2017). Genetic variation and association of molecular markers for iron toxicity tolerance in rice. *ORYZA-An International Journal on Rice* 54, 356–366. doi: 10.5958/2249-5266.2017.00066.2

Reddy, M. A., Francies, R. M., Abida, P. S., and Kumar, P. S. (2019). Correlation among morphological, biochemical and physiological responses under iron toxic conditions in rice. *Int. J. Curr. Microbiol. App. Sci.* 8, 37–44. doi: 10.20546/ijcmas.2019.801.005

Reddy, M. A., Francies, R. M., Elsy, C. R., Jiji, J., Kumar, P. S., and Abida, P. S. (2015). Screening of rice genotypes for iron toxicity tolerance through hydroponics. *Trends Biosci.* 8, 3087–3090.

Reyt, G., Boudouf, S., Boucherez, J., Gaymard, F., and Briat, J.-F. (2015). Iron- and ferritin-dependent reactive oxygen species distribution: impact on *Arabidopsis* root system architecture. *Mol. Plant* 8, 439–453. doi: 10.1016/j.molp.2014.11.014

Rinyu, E., Varga, J., and Ferenczy, L. (1995). Phenotypic and genotypic analysis of variability in *Aspergillus fumigatus*. *J. Clin. Microbiol.* 33, 2567–2575. doi: 10.1128/jcm.33.10.2567-2575.1995

Robinson, N. J., Procter, C. M., Connolly, E. L., and Guerinot, M. L. (1999). A ferric-chelate reductase for iron uptake from soils. *Nature* 397, 694–697. doi: 10.1038/17800

Rout, G. R., Sunita, S., Das, A. B., and Das, S. R. (2014). Screening of iron toxicity in rice genotypes on the basis of morphological, physiological and biochemical analysis. *J. Exp. Biol. Agric.* 2, 567–582.

Rumanti, I., Wening, R. H., and Sitaresmi, T. (2017). Leaf bronzing symptom score as related to grain yield of rice under iron toxicity of acid-sulfate soil area. Proceedings of PERIPI-2017 International Seminar, October 2nd 2017, Bogor, Indonesia. 154–161.

Sahrawat, K. L., Mulbah, C. K., Diatta, S., Delaune, R. D., Patrick, W. H., Singh, B. N., et al. (1996). The role of tolerant genotypes and plant nutrients in the management of iron toxicity in lowland rice. *J. Agric. Sci.* 126, 143–149. doi: 10.1017/S002185960007307X

Saikia, T., and Baruah, K. K. (2012). Iron toxicity tolerance in rice (*Oryza sativa*) and its association with anti-oxidative enzyme activity. *J. Crop Sci.* 3:90.

Saleem, A., Zulfiqar, A., Saleem, M. Z., Ali, B., Saleem, M. H., Ali, S., et al. (2023). Alkaline and acidic soil constraints on iron accumulation by Rice cultivars in relation to several physio-biochemical parameters. *BMC Plant Biol.* 23:397. doi: 10.1186/s12870-023-04400-x

Santos, F. I. D. C. D., Marini, N., Santos, R. S. D., Hoffman, B. S. F., Alves-Ferreira, M., and de Oliveira, A. C. (2018). Selection and testing of reference genes for accurate RT-qPCR in rice seedlings under iron toxicity. *PLoS One* 13:e0193418. doi: 10.1371/journal.pone.0193418

Shimizu, A., Guerta, C. Q., Gregorio, G. B., Kawasaki, S., and Ikehashi, H. (2005). QTLs for nutritional contents of rice seedlings (*Oryza sativa* L.) in solution cultures and its implication to tolerance to iron-toxicity. *Plant Soil* 275, 57–66. doi: 10.1007/s11104-004-4683-5

Sikirou, M., Saito, K., Achigan-Dako, E. G., Drame, K. N., Ahanchede, A., and Venuprasad, R. (2015). Genetic improvement of iron toxicity tolerance in rice-progress, challenges and prospects in West Africa. *Plant Prod. Sci.* 18, 423–434. doi: 10.1626/pps.18.423

Sikirou, M., Saito, K., Dramé, K. N., Saidou, A., Dieng, I., Ahanchédé, A., et al. (2016). Soil-based screening for iron toxicity tolerance in rice using pots. *Plant Prod. Sci.* 19, 489–496. doi: 10.1080/1343943X.2016.1186496

Silveira, V. C. D., Oliveira, A. P. D., Sperotto, R. A., Espindola, L. S., Amaral, L., Dias, J. F., et al. (2007). Influence of iron on mineral status of two rice (*Oryza sativa* L.) cultivars. *Braz. J. Plant Physiol.* 19, 127–139. doi: 10.1590/S1677-04202007000200005

Singh, V. J., Bhowmick, P. K., Vinod, K. K., Krishnan, S. G., Nandakumar, S., Kumar, A., et al. (2022). Population structure of a worldwide collection of tropical *japonica* rice indicates limited geographic differentiation and shows promising genetic variability associated with new plant type. *Genes* 13:484. doi: 10.3390/genes13030484

Siriwardana, K. G. D. I., Weerasinghe, W. D. P., Priyantha, G. D. A., Chandrasekara, K. K. D., Rupasinghe, M. D. N., Wickramasinghe, W. R. K. D. W. K. V., et al. (2018). Screening of selected rice varieties and advanced breeding lines against iron toxicity under field conditions in the low country wet zone of Sri Lanka. *Trop. Agric. Res.* 30, 33–46. doi: 10.4038/tar.v30i2.8307

Sitaresmi, T., Dewi, K., Rumanti, I. A., Herlinda, S., and Nugraha, Y. (2021). Response of Indonesian rice varieties to iron toxicity under field and green house condition. In E3S Web of Conferences 306, 01012. E3S Web Conf. 306, 01012

Suma, A., Francies, R. M., Radhakrishnan, V. V., Sureshkumar, P., and Varghese, E. (2022). Elucidating the response of rice genotypes to iron toxicity through hydroponics. *Ind. J. Plant Genet. Res.* 35, 66–72. doi: 10.5958/0976-1926.2022.00010.9

Theerawitaya, C., Wanchana, S., Ruanjaichon, V., Tisaram, R., Samphumphuang, T., Sotesaritkul, T., et al. (2022). Determination of traits responding to iron toxicity stress at different stages and genome-wide association analysis for iron toxicity tolerance in rice (*Oryza sativa* L.). *Front. Plant Sci.* 13:994560. doi: 10.3389/fpls.2022.994560

Timmer, C. P., Block, S., and Dawe, D. (2010). "Long-run dynamics of rice consumption, 1960-2050" in *Rice in the global economy: Strategic research and policy issues for food security*. eds. S. Pandey, D. Byerlee, D. Dawe, A. Dobermann, S. Mohanty and S. Rozelleet al. (Los Baños, Philippines: International Rice Research Institute), 139–173.

Turhadi, T., Hamim, H., Ghulamahdi, M., and Miftahudin, M. (2018). Morpho-physiological responses of rice genotypes and its clustering under hydroponic iron toxicity conditions. *Asian J. Agric. Biol.* 6, 495–505.

Turhadi, T., Hamim, H., Ghulamahdi, M., and Miftahudin, M. (2019). Iron toxicity-induced physiological and metabolite profile variations among tolerant and sensitive rice varieties. *Plant Signal. Behav.* 14:1682829. doi: 10.1080/15592324.2019.1682829

Vasconcelos, M. W., and Grusak, M. A. (2014). Morpho-physiological parameters affecting iron deficiency chlorosis in soybean (*Glycine max L.*). *Plant Soil* 374, 161–172. doi: 10.1007/s11104-013-1842-6

Vose, P. B. (1982). Iron nutrition in plants: a world overview. *J. Plant. Nutr.* 5, 233–249. doi: 10.1080/01904168209362954

Wan, J. L., Zhai, H. Q., Wan, J. M., and Ikehashi, H. (2003). Detection and analysis of QTLs for ferrous iron toxicity tolerance in rice, *Oryza sativa* L. *Euphytica* 131, 201–206. doi: 10.1023/A:1023915710103

Ward, J. T., Lahner, B., Yakubova, E., Salt, D. E., and Raghothama, K. G. (2008). The effect of iron on the primary root elongation of *Arabidopsis* during phosphate deficiency. *Plant Physiol.* 147, 1181–1191. doi: 10.1104/pp.108.118562

Waters, B. M., and Eide, D. J. (2002). Combinatorial control of yeast *FET4* gene expression by iron, zinc, and oxygen. *J. Biol. Chem.* 277, 33749–33757. doi: 10.1074/jbc.M206214200

Wissuwa, M., Ismail, A. M., and Yanagihara, S. (2006). Effects of zinc deficiency on rice growth and genetic factors contributing to tolerance. *Plant Physiol.* 142, 731–741. doi: 10.1104/pp.106.085225

Wu, P., Luo, A., Zhu, J., Yang, J., Huang, N., and Senadhira, D. (1997). Molecular markers linked to genes underlying seedling tolerance for ferrous iron toxicity. *Plant Soil* 196, 317–320. doi: 10.1023/A:1004288427140

Wu, L. B., Shhadi, M. Y., Gregorio, G., Matthus, E., Becker, M., and Frei, M. (2014). Genetic and physiological analysis of tolerance to acute iron toxicity in rice. *Rice* 7, 8–12. doi: 10.1186/s12284-014-0008-3

Wu, L. B., Ueda, Y., Lai, S. K., and Frei, M. (2017). Shoot tolerance mechanisms to iron toxicity in rice (*Oryza sativa* L.). *Plant Cell Environ.* 40, 570–584. doi: 10.1111/pce.12733

Zhang, J., Chen, K., Pang, Y., Naveed, S. A., Zhao, X., Wang, X., et al. (2017). QTL mapping and candidate gene analysis of ferrous iron and zinc toxicity tolerance at seedling stage in rice by genome-wide association study. *BMC Genom.* 18, 828–815. doi: 10.1186/s12864-017-4221-5

Zhang, J., Soomro, A. A., Chai, L., Cui, Y., Wang, X., Zheng, T., et al. (2013). Mapping of QTL for iron and zinc toxicity tolerance at seedling stage using a set of reciprocal introgression lines of rice. *Acta Agron. Sin.* 39, 1754–1765. doi: 10.3724/SP.J.1006.2013.01754

frontiers | Frontiers in Sustainable Food Systems

TYPE Original Research
PUBLISHED 27 February 2024
DOI 10.3389/fsufs.2024.1340638

OPEN ACCESS

EDITED BY
Ashim Datta,
Central Soil Salinity Research Institute (ICAR), India

REVIEWED BY
Jayanta Layek,
The ICAR Research Complex for North Eastern Hill Region (ICAR RC NEH), India
Jatish Chandra Biswas,
Bangladesh Rice Research Institute, Bangladesh
Yuan Li,
Lanzhou University, China

*CORRESPONDENCE
Pravin Kumar Upadhyay
✉ pravin.ndu@gmail.com
Rakesh Kumar
✉ rakeshbhu08@gmail.com
Santosh S. Mali
✉ santosh.icar@gmail.com

RECEIVED 18 November 2023
ACCEPTED 29 January 2024
PUBLISHED 27 February 2024

CITATION
Pan RS, Mali SS, Kumar R, Naik SK, Upadhyay PK, Shinde R, Jha BK, Jeet P and Das A (2024) An evaluation of energy and carbon budgets in diverse cropping systems for sustainable diversification of rainfed uplands in India's eastern hill and plateau region.
Front. Sustain. Food Syst. 8:1340638.
doi: 10.3389/fsufs.2024.1340638

An evaluation of energy and carbon budgets in diverse cropping systems for sustainable diversification of rainfed uplands in India's eastern hill and plateau region

Rabi Sankar Pan[1], Santosh S. Mali[1]*, Rakesh Kumar[2]*, Sushanta Kumar Naik[1], Pravin Kumar Upadhyay[3]*, Reshma Shinde[1], Bal Krishna Jha[1], Pawan Jeet[2] and Anup Das[2]

[1]ICAR-Research Complex for Eastern Region, Farming System Research Centre for Hill and Plateau Region, Ranchi, India, [2]ICAR-Research Complex for Eastern Region, Patna, Bihar, India, [3]Division of Agronomy, ICAR-Indian Agricultural Research Institute, New Delhi, India

With increasing cost and use of energy in agriculture, the traditional practice of mono-cropping of rice in upland is neither sustainable nor eco-friendly. It is necessary to identify crop diversification options with high energy efficiency, productivity, and low global warming potential (GWP). In this experiment, an inclusive system analysis was accomplished for 3 years (2016–2019) of five mono-cropping production (MCP) systems namely rice (R), finger millet (FM), black gram (BG), horse gram (HG), pigeon pea (PP), and four intercropped systems viz. R+BG, R+HG, FM+ BG, and FM + HG. The key objective was to evaluate the flow of energy, carbon balance, and GWP of these varied production systems. Puddled rice was recorded as an energy-exhaustive crop (27,803 MJ ha^{-1}), while horse gram was noted to have the lowest energy use (26,537 MJ ha^{-1}). The total energy output from pigeon pea (130,312 MJ ha^{-1}) and diversified intercropped systems (142,135 MJ ha^{-1}) was 65.3% and 80.3% higher than mono-cultured systems, respectively. Rice and rice-based intercropping production systems showed higher carbon footprints (1,264–1,392 kg CO_2 eq. ha^{-1}). Results showed that R+BG and R+HG were the most energy-efficient production systems, having higher energy ratio (5.8 and 6.0), higher carbon efficiency (7.41 and 8.24), and carbon sustainability index (6.41 and 7.24) as against 3.30, 3.61, and 2.61 observed under sole cropping production systems. On average, rice and rice-based production systems had 7.4 times higher GWP than other production systems. In productivity terms, pigeon pea and FM+HG had higher rice equivalent yields of 8.81 and 5.79 t ha^{-1} and benefit-cost ratios of 2.29 and 1.87, respectively. Thus, the present study suggests that pigeon pea and finger millet-based intercropping systems were the most appropriate crop diversification options for the rainfed upland agro-ecosystem of the eastern region of India.

KEYWORDS

carbon budgeting, carbon sustainability index, climate resilient cropping system, energy productivity, global warming potential, system productivity

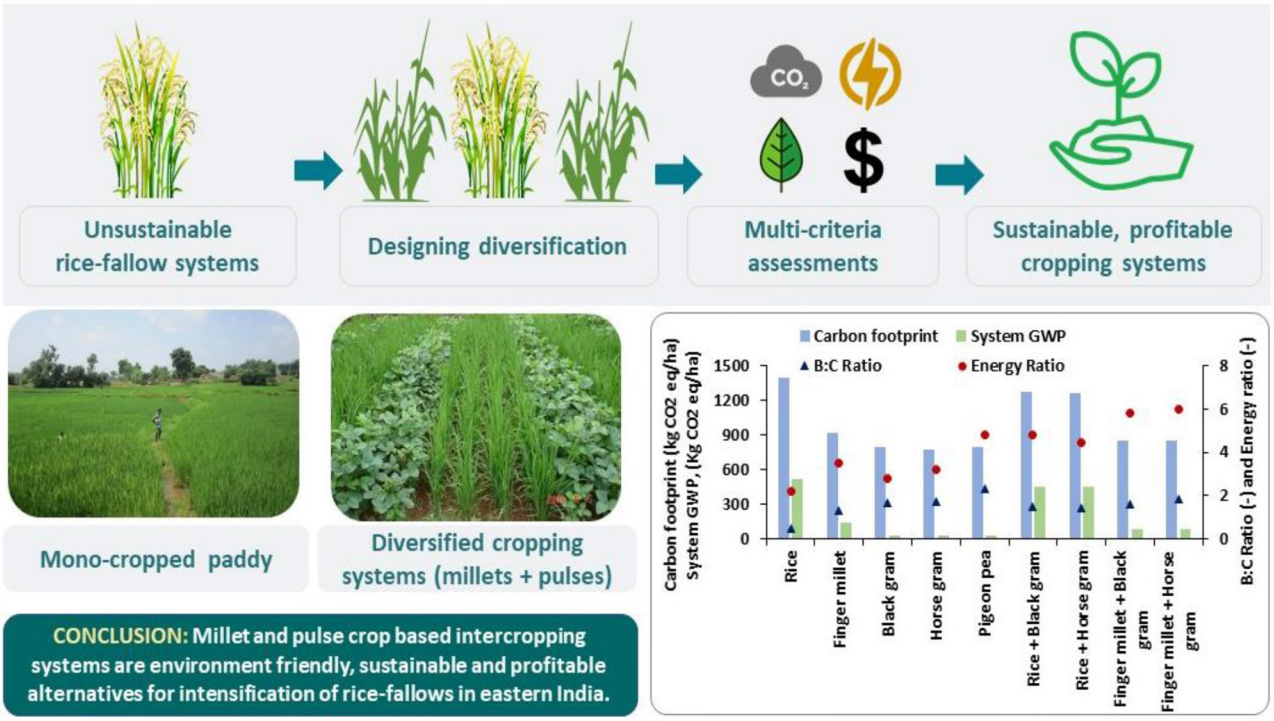

GRAPHICAL ABSTRACT

1 Introduction

Energy use efficiency (Fatima et al., 2023), economic returns, and environmental sustainability (Shyam et al., 2023) of agriculture enterprises are greatly influenced by the quantum and form of energy used in a cropping system. A production system with comparatively lower input requirements and higher outputs is the most efficient one (Upadhyay et al., 2022). The sustainability and profitability of the production systems in the rainfed upland of India's eastern region are in question due to unsustainable energy use practices, the backdrop of widespread natural resource degradation, climate aberrations, and low crop productivity (Praharaj et al., 2016; Singh et al., 2017). The principal cropping system in the rainfed upland of India's eastern region is rice-fallow, constituting ~83% (9.7 M ha) of the nation's total rice-fallow area (11.7 M ha) (Ali et al., 2014; Ghosh et al., 2016; Li et al., 2024). The sustainability of conventional production systems in rainfed upland ecosystems is threatened by declining water availability, limited soil residual moisture, free grazing of cattle, and the poor socio-economic condition of the farming communities (NAAS, 2013).

Energy is a fundamental component of modern agriculture, as it relies significantly on fossil fuels and other energy resources. Production and environmental sustainability are directly related to the type of energy inputs and the total energy output from a production system. Studies have shown that crop production systems are very energy-intensive. In the eastern plateau region, rice-rice systems and rice-fallow-fallow systems recorded energy use of 2.14 and 1.91 MJ kg^{-1}, respectively (Ray et al., 2020). Research into energy flows within diverse production systems gained prominence among the researchers in 1970s, driven by the worldwide fossil-fuel crunch and the growing demand for food to sustain the constantly growing population (Alam et al., 2019). Evaluating the energy dynamics of a system and conducting carbon auditing are crucial steps in choosing the most suitable crop production system, considering factors such as energy efficiency, carbon footprints (CFs), and their environmental implications (Babu et al., 2020). Effective use of energy in agriculture is a prerequisite for sustainable agricultural production which will ensure higher production and productivity, save financial resources, and conserve fossil fuels. Following the Green Revolution era, Indian agriculture has been characterized by the promotion of high input (John and Babu, 2021), mechanized, and irrigated cropping systems. This has led to substantial energy consumption, both directly and indirectly, due to the energy-intensive nature of production activities, inputs, and supplementary requirements (Soni et al., 2018). Hence, enhancing energy efficiency has emerged as a primary goal for both farmers and policymakers. Nevertheless, ongoing initiatives have not fully realized the comprehensive economic potential of energy utilization in agriculture (World Energy Outlook, 2012). Agricultural production systems should be smart enough to sensibly use all the energy inputs so that the twin goals of environmental sustainability and system productivity can be achieved at minimal energy cost.

The agricultural sector is anticipated to play an important role in the share of greenhouse gas (GHG) emissions attributed to climate change. In 2018, global agricultural and associated land

use emissions amounted to 9.30 billion tons of carbon dioxide equivalent (FAO, 2018). With growing demands for food grains production, energy use in the agriculture sector will amplify significantly leading to increased greenhouse gas (GHG) emissions (FAO, 2022). As per Czyzewski and Kryszak (2018), agricultural practices account for ∼25–30% of GHG emissions. Furthermore, it is well-established that rice cultivation is a significant source of GHGs, including methane (CH_4), nitrous oxide (N_2O), and carbon dioxide (CO_2). This phenomenon is believed to be partially responsible for global warming and subsequent climate change, as indicated by Linquist et al. (2012). Evidence from eastern India showed that GHG emissions were highest (1.265 ± 0.29 t CO_2eq. t^{-1}) for rice-fallow-fallow systems and lowest for rice-vegetable systems (Ray et al., 2020;). Rice-based cropping systems have always been predominant in India and are believed to be a major contributor to CH_4 and N_2O emissions (Yadav et al., 2017; Ray et al., 2018). Rice fields can alone contribute to ∼19% and 11% of the total N_2O and CH_4 emissions, respectively (IPCC, 2007). The impact of crop production systems on GHG emissions is multifaceted, influenced by factors such as variations in energy efficiency, temperature and water management, carbon sequestration, nutrient inputs, fossil fuel utilization for machinery and pesticides, differing crop growth durations, and variations in the crop yields (Alam et al., 2019). Due to increasing environmental impacts and rising energy costs, upland rice-based production systems of eastern India are becoming unsustainable and non-profitable. In this context, the diversification of crops has been recognized as a significant agricultural practice aimed at enhancing agroecosystem productivity while reducing CF (Singh et al., 2017).

There are a few studies focusing on energy budgeting and CFs of cropping systems in India, the majority of which accounted for energy and carbon budgeting in a sole rice production system (Chaudhary et al., 2017; Singh et al., 2019) and sole wheat system (Singh et al., 2020). Some studies considered different cropping systems such as maize-wheat (Saad et al., 2016), pearl millet-wheat (Choudhary et al., 2017), and maize-wheat-mungbean (Parihar et al., 2018). However, the main aim of these studies was to assess the energy and carbon budgeting under the varying tillage, crop establishment, and residue management practices. Studies focusing on the evaluation of diverse cropping systems in a region with consideration of millet and pulse-based systems as alternate cropping systems are lacking for the eastern part of the country. There is an immediate need to identify the most environmentally friendly and efficient millet-based production systems that offer increased productivity and profitability, while also being economical in their use of energy, water, and carbon inputs, all in an environmentally sustainable manner in longer perspectives. We hypothesized that diversified crop rotations and intercropping production systems result in a reduction in energy consumption and carbon footprints and provide more yields and income in the climate change scenario. Over a span of 3 years, from 2016 to 2019, a comprehensive study was undertaken to intensify the cropping systems in South Asia, with the objective of replacing the extensively practiced rice-fallow production system. The outcomes of this study can be applied to enhance the utilization of unutilized rice-fallow lands by introducing the appropriate post-rainy-season/winter crops and employing effective crop establishment practices. Additionally, a deeper understanding of the ecology of rice-fallow areas can facilitate the development of suitable crop rotations and moisture conservation practices to enhance the income of the farmers in eastern India.

2 Materials and methods

2.1 Experiment site

The field study was conducted at a research farm situated in Ranchi, Jharkhand, India (23.35°N and 85.33°E at an altitude of 629 m), spanning *kharif* seasons from 2016 to 2019. The soil of the experimental site was Typic Haplustalf type (Order: Alfisol) and sandy loam in texture (sand: 69%; silt: 20%; clay: 11%)/The soil exhibited low fertility, characterized by low organic carbon content at 0.43% and a deficiency in available nitrogen (N) (195.5 kg ha^{-1}) and was acidic in nature. However, it had moderate levels of available phosphorus (P) (35.7 kg ha^{-1}) and potassium (K) (241.2 kg ha^{-1}). Monsoon rainfall is the main source of water in the region which is concentrated mostly in 4 months (June–September). During the other periods, agriculture is largely dependent on the groundwater sources.

2.2 Experiment design

The experiment was laid out in a randomized block design with three replications. The treatments consisted of five sole corps and four intercropped systems. The experiment included five sole crop-based production systems namely, rice (*Oryza sativa*) (T1), finger millet (*Eleusine coracana*) (T2), black gram (*Vigna mungo*) (T3), horse gram (*Macrotyloma uniflorum*) (4), and pigeon pea (*Cajanus cajan*) (T5) and four diversified intercropped systems, namely, Rice+ Black gram (T6), Rice+ Horse gram (T7), Finger millet + Black gram (T8), and Finger millet + Horse gram (T9). Crops were sown at their respective recommended plant geometry and fertilizer rate (Table 1). In diversified production systems, individual crops were planted in a ratio of 1:1. The selection of sole crops was based on nutritional requirements and the preference of farm families for a particular crop. The cultivars/varieties of the particular crops were the same across all the treatments during the experimentation.

2.3 Crop management

Prior to the start of the experiment each year, the experimental plots were plowed using a tractor-drawn plow and subsequently harrowed to pulverize the soil. In rice-based treatments, the initiation of nursery raising started at the same time as the planting date of other intercropping and sole crop treatments. A uniform dose of 1.0 t ha^{-1} of vermicompost was applied across all the treatment plots before the start of the experiment. In rice-based treatments, 21-day-old seedlings (2–3 seedlings per hill) with a spacing of 30 × 10 cm were used. The recommended dose of fertilizers (RDF) was applied in each of the cropping systems

TABLE 1 Crop yield, total biomass production and system productivity of diverse cropping systems in rice-fallow systems in the eastern hill and plateau region of eastern India (average of 3 years).

Cropping systems	Crop yield (Mg ha^{-1})			Straw biomass (Mg ha^{-1})			Root biomass (Mg ha^{-1})			Total biomass production (Mg ha^{-1})	System productivity (REY Mg ha^{-1})
	MC	IC	Total	MC	IC	Total	MC	IC	Total		
Rice	1.38	–	1.38^{f}	2.59	-	2.59^{f}	0.71	–	0.71^{h}	4.68^{f}	1.38
Finger millet	2.45	–	2.45^{bc}	4.96	-	4.96^{d}	1.39	–	1.39^{f}	8.80^{d}	3.96^{e}
Black gram	1.74	–	1.74^{e}	3.19	-	3.19^{ef}	0.84	–	0.84^{g}	5.77^{e}	5.40^{bc}
Horse gram	1.97	–	1.97^{de}	3.60	-	3.60^{e}	0.92	–	0.92^{gd}	6.49^{e}	5.43^{bc}
Pigeon pea	2.81	–	2.81^{a}	4.76	-	4.76^{d}	1.83	–	1.83^{d}	9.40^{d}	8.81^{a}
Rice+ Black gram	1.04	1.09	2.13^{d}	2.31	3.82	6.13^{c}	1.01	0.97	1.98^{c}	10.24^{c}	4.39^{dc}
Rice+ Horse gram	0.64	1.31	1.95^{de}	1.80	4.96	6.76^{c}	0.62	0.98	1.60^{e}	10.31^{c}	4.24^{e}
Finger millet+ Black gram	1.24	0.98	2.22^{cd}	2.85	5.23	8.08^{b}	1.39	1.32	2.71^{a}	13.01^{b}	5.04^{cd}
Finger millet+ Horse gram	1.21	1.39	2.60^{ab}	3.77	5.68	9.45^{a}	1.21	1.07	2.29^{b}	14.34^{a}	5.79^{bc}

REY, Rice equivalent yield; SPE, System production efficiency; MC, Main crop; IC, Inter crop. Values with different superscripts in a column are significantly different at $p < 0.05$ according to Duncan Multiple Range Test (DMRT).

(Supplementary Table 1). For nutrient application, 50% of the required N, along with a full dosage of P and K, was applied as a basal dose. The outstanding 50% of N was administered in two equal portions, divided into applications at maximum tillering and panicle initiation stages of respective crop growth. Weed control was done through manual weeding at the relevant growth stages of crops. Details of crops/cultivars are provided in Supplementary Table 1. Except for sole rice and sole finger millet, an insecticide spray of Imidacloprid 200 SL (17.8 % w w^{-1}) at the rate of 1 ml l^{-1} was advocated in all treatments.

2.4 Energy budgeting

In the current investigation, an analysis of energy input-output flows was conducted and compared across varied tillage systems. The management of energy input flows in different tillage systems was determined based on their input intensiveness. Energy flows in various tillage systems were calculated by considering the crop management practices, which encompassed machinery operations and input utilization, as well as the quantity of biomass produced. Energy inputs were categorized into direct (operational) and indirect (non-operational) categories. Direct energy inputs encompassed labor (manual), fuel, and farm implements usage, while indirect energy inputs included seeds, farmyard manure (FYM), fertilizers, and pesticides. A comprehensive inventory was prepared encompassing inputs of different crops (such as seeds, pesticides, fertilizers, manpower, farm implements, etc.) and principle/by-product (output) to establish the energy input-output flow for individual crops. Based on total fuel consumption, diesel energy was calculated. Soil fertility, solar radiation, wind, etc. (renewable and natural energy sources) were not considered, as they are not associated with opportunity costs and are not contingent on experiments. Manpower (human labor) and the input of draft animals (bullock power) were measured during the study, as these inputs played a significant role in conventional tillage (CT) production systems. Physical units of total input and output were transformed into energy units using available energy equivalents (published data) (Supplementary Table 2). Various energy use indices were computed using the below formulas (See Equations 1–8).

Energy inputs: The energy equivalent for all inputs was totaled to give an estimation of total energy inputs in respective crop production.

Energy outputs: The energy output from grains/seeds and straw/haulm was computed by multiplying its consequent energy equivalents.

$$Net\ energy\ return = Gross\ energy\ output - Total\ energy\ input \quad (1)$$

$$Energy\ ratio = \frac{Energy\ output\ \left(MJ\ ha^{-1}\right)}{Energy\ input\ \left(MJ\ ha^{-1}\right)} \quad (2)$$

$$Energy\ profitibility = \frac{Net\ energy\ gain\ \left(MJ\ ha^{-1}\right)}{Energy\ input\ \left(MJ\ ha^{-1}\right)} \quad (3)$$

$$Energy\ productivity = \frac{Crop\ economic\ yield\ \left(INR\ ha^{-1}\right)}{Input\ energy\ \left(MJ\ ha^{-1}\right)} \quad (4)$$

$$Specific\ energy = \frac{Energy\ input\ \left(MJ\ ha^{-1}\right)}{System\ productivity\ \left(kg\ ha^{-1}\right)} \quad (5)$$

$$Human\ profitability = \frac{Energy\ output\ \left(MJ\ ha^{-1}\right)}{Labor\ energy\ input\ \left(MJ\ ha^{-1}\right)} \quad (6)$$

$$Non-renewable\ energy\ use\ efficiency = \frac{Total\ energy\ output}{Non-renewable\ energy\ input} \quad (7)$$

$$Energy\ intensiveness = \frac{Energy\ input\ (MJ)}{Cost\ of\ cultivation\ (USD)} \quad (8)$$

2.5 GHG emissions and GWP

The impact on the environment by the diverse tillage systems was measured by computing the carbon footprint in spatial scale (CFs) and yield scale carbon footprint (CFy). CFs is the total greenhouse gas emissions which include CO_2, N_2O, and CH_4 emitted (directly and indirectly) in carbon dioxide equivalent (CE). The CO_2, CH_4, and N_2O emissions were altered into CE use of GWP equivalents factor of 1, 28, and 265 for CO_2, CH_4, and N_2O, respectively (Padre et al., 2016). The C-footprint (CF) was assessed through the emission of GHG from fossil fuels (diesel) various agronomic operations (tillage, insecticide, plantings, fertilizers) (operational GHG flux), and the production of fertilizer/seed (input GHG flux). The amount of GHG emissions in CE is linked with agronomic input and different operations computed by multiplied inputs (diesels, fertilizers) with corresponding carbon-emission coefficients (C-emission coefficient) (Supplementary Table 3). However, C-emission coefficients were not available for specific applied pesticides. Hence, it is presumed that emissions associated with diverse stages of pesticide production, its transportation, storage, and application in the field were comparable for similar groups of pesticides (Lal, 2004). The periodic CH_4 emissions from puddled transplanted rice (PTR) and direct seeded rice (DSR) were 13 and 6 kg cycle^{-1} hectare^{-1}, respectively (Padre et al., 2016). GHG emissions resulting from nitrogenous fertilizers (Equation 9) were computed by the formula suggested by Padre et al. (2016).

$$N_2O\ emission\ (kg\ ha^{-1} year^{-1}) = \frac{(Factor \times 44 \times total\ N\ applied\ to\ the\ crop)}{(100 \times 28)} \quad (9)$$

The emission factor for N_2O (% of applied *N*) for a rice paddy was 0.51 (Padre et al., 2016; Kumar et al., 2018). Data on GHG (CO_2, CH_4, N_2O) emissions were used to compute the GWP as shown in the Equation 10:

$$GWP = (emission\ of\ CH_4 \times 28 + emissions\ of\ N_2O \times 265) + emissions\ of\ CO_2 \quad (10)$$

The cumulative photosynthates of the crops, which represent the total carbon (C) output, were calculated by multiplying them with their respective crop yield, considering the total above-ground biomass and the average carbon content of biomass, ~44% on a dry weight (DW) basis (Lal, 2004). The carbon budgeting for various tillage production systems was computed using the Equations 11–14.

$$Carbon\ output = Total\ biomass\ (economic\ yields + by-product\ yields) \times 0.44 \quad (11)$$

$$Carbon\ efficiency\ (CE) = \frac{Carbon\ outputs}{Carbon\ inputs} \quad (12)$$

$$Carbon\ sustainability\ index\ (CSI) = \frac{Carbon\ outputs - Carbon\ inputs}{Carbon\ inputs} \quad (13)$$

$$Carbon\ footprint\ in\ yield\ scale\ (CFy) = \frac{CFs}{System\ productivity} \quad (14)$$

Where, CFs: carbon footprint in spatial scale

The Eco-efficiency Index (EEI) considers both economic and ecological aspects in the context of diverse cropping systems. EEI1 (Equation 15) represents the ratio of economic returns to the overall environmental impact (Gómez-Limón et al., 2012) (Equation 15). Sustainable agricultural production aims to enhance the EEI by reducing the environmental impact, which includes factors such as energy input and greenhouse gas emission, while simultaneously improving the economic outputs (Cicek et al., 2011). The EEI expresses how efficient a diverse production system is, linked to its impact on nature. EEI2 (Equation 16) can also be computed considering GHG emissions (EEI2), representing economic returns per kilogram of GHG emitted. These indices were computed by the following formula:

$$EEI1\ \left(US\ MJ^{-1}\right) = \frac{Amount\ of\ economic\ returns\ \left(US\ ha^{-1}\right)}{Environmental\ impact\ \left(MJ\ ha^{-1}\right)} \quad (15)$$

$$EEI2\ \left(US\ per\ kg\ GHG\right) = \frac{Amount\ of\ economic\ returns\ \left(US\ ha^{-1}\right)}{GHG\ emissions\ \left(kg\ GHG\ ha^{-1}\right)} \quad (16)$$

In the present investigation, the environmental impacts of diverse tillage production systems were computed using energy input (MJ) and the amount of greenhouse gas emitted (kg CE ha^{-1}) during the investigation.

2.6 Yield attributing traits and yield

The economic yield and by-product (straw/haulm) of each crop in diverse production systems were calculated by harvest of 50 m^2 areas in all plots. The root biomass was estimated using destructive sampling of five plants from each experimental plot. The extracted roots were placed in a paper bag and dried in an oven at 60°C for 48 h. The dry weight of five plants was upscaled to obtain the per hectare root biomass under each treatment. Economic yields were obtained by threshing at a moisture content of ~12% (ww^{-1}). Rice equivalent yield (REY) of different crops was calculated by adapting grain yields to rice yields with MSP factors using the Equation 17:

$$REY = \frac{Grain\ yield\ of\ the\ winter/summer\ crop \times MSP\ of\ winter/summer\ crops\ )}{Price\ of\ rice} \quad (17)$$

The minimum support price (MSP) of crops for the corresponding year (Indian rupee, INR) was taken into account for the calculation of REY. The calculation of system rice equivalent yield (SREY) was done using the following formula (See Equation 18):

$$SREY = Grain\ yield\ of\ rice + REY\ of\ winter\ crops + REY\ of\ summer\ crops \quad (18)$$

Emissions from vermicompost were calculated by scaling the equivalent compost emissions by the relative N content (Equation 19).

$$CO_2\ emissions\ from\ vermicompost = \frac{W_{vermi}(kg)xEF_{compost}\ x\ N_{vermi}(\%)}{N_{compost}(\%)} \quad (19)$$

Where, W_{vermi} is the amount of vermicompost applied, kg; $EF_{compost}$ is the CO_2 emission factor for compost, and N_{vermi} and $N_{compost}(\%)$ are the nitrogen contents in vermicompost and compost, respectively.

2.7 Economics

The cultivation cost of various production systems in different tillage practices was calculated by adding the cost of the entire input (seed, fertilizer, pesticide, fuels, labor) and farm machinery (Mandal et al., 2015). These inputs cost was computed based on prevailing market rates. The price of economic yield was acquired from the minimum support price (MSP) from the Government of India (GOI). Selling charges of straw (by-products) were computed based on native price. The following economic parameters were calculated based on input cost and gross return (Equations 20, 21):

$$Net\ returns = Gross\ returns\ (Product\ cost + By - product\ cost) - Cost\ of\ cultivation\ (Input\ cost) \quad (20)$$

$$Benefit : cost\ ratio = \frac{Gross\ returns}{Cost\ of\ cultivation} \quad (21)$$

2.8 Data analysis

Collected data underwent an analysis of variance (ANOVA) to facilitate comparisons between treatments and to draw statistical interpretations. The treatment comparison was made using Duncan's Multiple Range Test (DMRT) *post hoc* with the help of the SPSS program (version 16.0) with a windows-based interface. Principal Component Analysis (PCA) was conducted using PAST 3.14 statistical software with a windows-based interface.

3 Results

3.1 Crop yield, total biomass production, and system productivity

In the present investigation, crop economic yields and total biomass production were significantly influenced by diverse cropping systems due to differentiation in bio-physical and management factors (Table 1). The yield of rice varied from 1.38 Mg ha^{-1} in sole cropping systems to 0.64–1.04 Mg ha^{-1} in intercropping systems. Among the intercropped systems, the finger millet + horse gram system had higher crop yield, which was 22.2, 33.2, and 17.3% higher than the rice + black gram, rice + horse gram, and finger millet + black gram systems, respectively. On average, intercropped systems recorded 99% and 88.6% higher straw and root biomass, respectively, over mono-cropped systems. Finger millet-based intercropping systems, finger millet + black gram and finger millet + horse gram, showed significantly higher ($p < 0.05$) straw as well as root biomass yields. The annual biomass production varied across the crops and intercropping systems (Table 1). Intercropping systems produced higher total biomass (10.24–14.34 Mg ha^{-1} year^{-1}). The highest biomass production was noted in the finger millet + horse gram system (T9:14.34 Mg ha^{-1} year^{-1}), which was higher by 206.4, 63, 148.5, 121, 52.6, 40, 39.1, and 10.2% than T1, T2, T3, T4, T5, T6, T7, and T8, respectively. Regardless of the cropping system, treatments T9 and T8 exhibited higher root biomass (2.29–2.74 Mg ha^{-1} year^{-1}). Among the different crops, pigeon pea (2.81 Mg ha^{-1}), finger millet (24.5 Mg ha^{-1}), horse gram (1.97 Mg ha^{-1}), and black gram (1.74 Mg ha^{-1}) were the most productive. However, rice had the lowest crop yield (1.38 Mg ha^{-1}). System productivity of rice and finger millet-based intercropping systems was 3.2 and 1.34 times higher than respective sole cropping system productivity.

3.2 Energy use and input-output relationships

In general, millet-based intercropping production systems exhibited lower energy input requirements compared to rice-based intercropping systems (Table 2). Based on the energy use patterns, T1 was the most energy-intensive (27,803 MJ ha^{-1}), followed by T5 (27,289 MJ ha^{-1}). In contrast, production systems based on millet (T9: 26,714 and T8: 26,885 MJ ha^{-1}) required lower energy. Amongst the diverse intercropping systems, treatments T4, T3, T8, and T2 demonstrated the lowest energy requirements.

The total energy output varied across a range from T1 (61,604 MJ ha^{-1}) to T9 (160,049 MJ ha^{-1}) (Table 2). Irrespective of the crops/intercropping system, the highest energy output was noted in T9 (160,049 MJ ha^{-1}). The same trends were observed for the net returns. Additionally, energy ratio and energy profitability were notably higher in T9 (6.0 and 5.0), with T8 following closely (5.8 and 4.8). Similar trends were followed in energy productivity also. As evident from the data, the specific energy was significantly higher in the case of sole crop-based systems (Table 2). Among the intercropping systems, millet-based systems had markedly lower specific energy compared to rice-based intercropping systems. The

TABLE 2 Energy flow as influenced by diverse cropping systems in rice-fallow systems in the eastern hill and plateau region of eastern India (average of 3 years).

Cropping systems	Energy input (MJ ha^{-1})	Energy output (MJ ha^{-1})	Net energy return (MJ ha^{-1})	Energy ratio	Energy productivity (kgMJ^{-1})	Specific energy (MJ kg^{-1})	Energy profitability
Rice	27,803^{a†}	61,604^{f}	33,801^{g}	2.22^{e}	0.048^{e}	20.22^{a}	1.22^{e}
Finger millet	26,891^{bc}	93,637^{d}	66,746^{e}	3.49^{c}	0.092^{b}	11.02^{ef}	2.49^{c}
Black gram	26,879^{bc}	74,705^{e}	47,826^{f}	2.78^{d}	0.063^{d}	15.54^{b}	1.78^{d}
Horse gram	26,537^{c}	85,454^{d}	58,917^{e}	3.22^{c}	0.075^{c}	13.86^{cd}	2.22^{c}
Pigeon pea	27,289^{ab}	130,312^{b}	103,023^{bc}	4.78^{b}	0.103^{a}	9.75^{f}	3.78^{b}
Rice + Black gram	27,341^{ab}	131,806^{b}	104,465^{b}	4.82^{b}	0.078^{c}	12.93^{cd}	3.82^{b}
Rice + Horse gram	27,170^{abc}	120,839^{c}	93,670^{d}	4.45^{b}	0.072^{cd}	14.04^{bc}	3.45^{b}
Finger millet+ Black gram	26,885^{bc}	155,846^{a}	128,961^{a}	5.80^{a}	0.082^{c}	12.21^{de}	4.80^{a}
Finger millet+ Horse gram	26,714^{bc}	160,049^{a}	133,335^{a}	6.00^{a}	0.097^{ab}	10.31^{f}	5.00^{a}

†Values with different superscripts in a column are significantly different at $p<0.05$ according to Duncan Multiple Range Test (DMRT).

TABLE 3 Share of various energy inputs (MJ ha^{-1}) under diverse cropping systems in rice-fallow systems in the eastern hill and plateau region of eastern India (average of 3 years).

Cropping system	Fertilizers	Diesel	Plant protection chemical	Machinery	Human power	Seed
Rice	3,430	7,602	–	322^{c}	15,233^{b}	1,216
Finger millet	3,409	7,602	–	322^{c}	15,512^{b}	47
Black gram	2,693	7,602	103^{a}	376^{a}	15,688^{ab}	419
Horse gram	2,259	7,602	51^{b}	376^{a}	15,955^{ab}	294
Pigeon pea	2,693	7,602	51^{b}	378^{a}	16,284^{ab}	281
Rice + Black gram	3,062	7,602	51^{b}	348^{b}	15,461^{b}	817
Rice + Horse gram	2,845	7,602	26^{c}	349^{b}	15,594^{ab}	755
Finger millet + Black gram	3,051	7,602	51^{b}	348^{b}	15,600^{ab}	233
Finger millet + Horse gram	2,834	7,602	26^{c}	349^{b}	15,733^{ab}	170

Values with different superscripts in a column are significantly different at $p < 0.05$ according to Duncan Multiple Range Test (DMRT).

lowest specific energy (10.3 MJ ha^{-1}) was recorded in the millet-based system treatment (T9).

It was observed that human power comprised the highest percentage of total energy inputs (54.8%-60.1%). The energy input used for diesel in the millet-based intercropping system was 7,602 MJ ha^{-1} (Table 3). Energy inflow through crop nutrition, i.e., fertilizers, ranged between 8.5 and 12.7%, being higher in rice (3,430 MJ ha^{-1}) and finger millet (3,409 MJ ha^{-1}). Among the intercropping system, maximum energy input was noted in the rice-based system compared to the millet-based production system (Table 3). Irrespective of intercropping systems, higher energy input was used through human power followed by diesel and fertilizer.

Among the different agronomic management practices, land preparation was the most energy-intensive (10,650–11,481 MJ ha^{-1}). The maximum consumption of energy input was noted in intercropping systems compared to sole cropping (Table 4). Irrespective of the crops/intercropping system, harvesting, threshing, and storage consumed the highest energy input (4,875–6,020 MJ ha^{-1}). Seed and intercultural operations shared similar energy inputs toward total energy inputs in cropping systems.

Direct and non-renewable energy sources represented 86–88.8% and 59.7–63.1% of the energy inputs, respectively. In general, these categories constituted the most substantial portions of the total energy inputs, followed by non-direct and renewable energy sources (Figure 1). Irrespective of the crops/intercropping system, the highest human energy profitability (HEP) was noted in intercropping systems in comparison to sole-cropping systems. Amongst the intercropping systems, finger millet + horse gram had the highest HEP and the lowest was the rice-monocropping system. The millet-based production systems had a higher HEP than the rice-based intercropping systems (Figure 2). Intercropping systems

TABLE 4 Energy consumption (MJ ha^{-1}) under different agronomic management practices of diverse cropping systems in rice-fallow systems in the eastern hill and plateau region of eastern India (average of 3 years).

Agronomic practice	Rice	Finger millet	Black gram	Horse gram	Pigeon pea	Rice +Black gram	Rice + Horse gram	Finger millet + Black gram	Finger millet + Horsegram
Land preparation	10,650^{b}	10,650^{b}	11,481^{a}	11,481^{a}	11,481^{a}	11,065^{ab}	11,065^{ab}	11,065^{ab}	11,065^{ab}
Fertilizer application	3,556	3,535	2,819	2,385	2,819	3,187	2,970	3,177	2,960
Seed sowing	4,352^{a}	3,496^{c}	3,555^{c}	3,493^{c}	3,417^{c}	3,953^{b}	3,922^{b}	3,526^{c}	3,495^{c}
Intercultural operations	4,273^{a}	4,336^{a}	3,896^{a}	4,085^{a}	3,394^{b}	4,085^{a}	4,179^{a}	4,116^{a}	4,211^{a}
Plant protection	–	–	209^{a}	158^{ab}	158^{ab}	105^{b}	79^{b}	105^{b}	79
Harvesting, threshing, storage	4,972^{b}	4,875^{b}	4,919^{b}	4,935^{b}	6,020^{a}	4,946^{b}	4,953^{b}	4,897^{b}	4,905^{b}

Values with different superscripts in a row are significantly different at $p < 0.05$ according to the Duncan Multiple Range Test (DMRT).

recorded higher renewable and non-renewable energy efficiency over the rice-sole system (Figure 3). These attributes were highest for T9 (finger millet + horse gram) and lowest for T1 (rice-sole cropping). Energy intensiveness (EI) was markedly influenced by diverse cropping systems (Figure 4). Among the sole cropping, T1 (rice sole) recorded the highest EI whereas the lowest EI was pigeon pea (T5). Similarly, the rice-based intercropping systems had a comparatively higher EI in comparison to the millet-based systems. The rice + horse gram system had the highest EI. A comparable pattern was also observed within the millet-based systems (Figure 4).

Among the different cropping systems, the total energy input requirement was highest in the rice-sole cropping system for T1 (27,803 Mg ha^{-1}), notably surpassing that of the millet-based production systems (Table 1). In terms of diverse farm operations, diesel (27.3–28.5%) and inorganic fertilizers (8.5–12.7%) constituted the most substantial share of the energy input, following land preparation (Table 3).

Generally, millet-based production systems demonstrated higher energy outputs compared to rice-sole cropping. The system-based energy ratio ranged from 2.22 to 6.0, with the values contingent on the total biomass production and energy input utilization. Among the treatments, T9 was recognized as the most energy-efficient. In the current investigation, the millet-based production systems displayed lower energy requirements, ranging from 26,714 to 26,891 MJ ha^{-1}, in contrast to the rice-based systems (27,803 MJ ha^{-1}).

3.3 Carbon budgeting

The CF was markedly influenced by diverse crop and intercropping production systems. Irrespective of the crops/intercropping system, land preparation, fertilizer application, and seed sowing contributed ~82.2–89.5% toward the total carbon footprint (Table 5). Among these, land preparation had the highest share of 59.2–69.3%. Intercultural operations, chemical plant protection, and harvesting/threshing operations had comparatively lower contributions toward the total carbon footprint. Among the various crops/intercropping systems, rice had the highest total carbon footprint (814 kg CE ha^{-1}). The millet-based intercropping systems had a comparatively lower total carbon footprint in comparison to the rice-based production systems (Table 5).

Irrespective of crops/cropping system, rice had the highest share toward the total carbon input (Figure 5). Among the tested crops, pulses (black gram, horse gram, pigeon pea) contributed comparatively lower carbon inputs to the total carbon input due to being low input requiring crops. As the cropping system intensified, overall contribution toward C-input was increased markedly during the present study. Sole cropping had comparatively lower C-input as compared to intercropping systems. Millet-based intercropping systems (T8 and T9) had comparatively lower C-input than rice and or cereal-based systems. The lowest carbon output was recorded with sole rice (T1). The millet-based intercropping systems had markedly higher carbon output compared to cereals-based systems. The highest levels of C-outputs

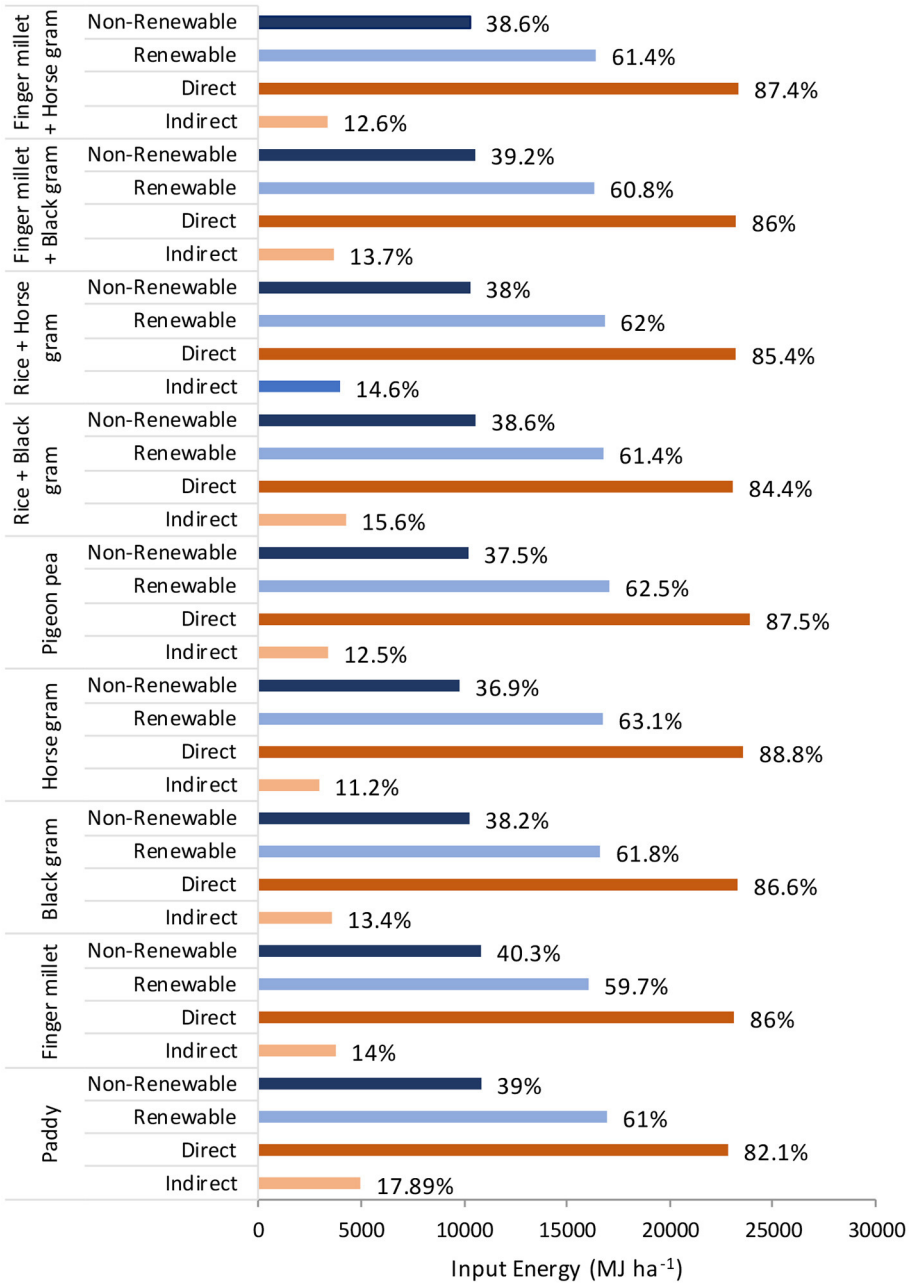

FIGURE 1
Source-wise distribution of direct, indirect, renewable, and non-renewable input energy as influenced by diverse cropping systems in rice-fallow systems in the eastern hill and plateau region of eastern India (average of 3 years).

were observed in T9. Conversely, the highest CF was recorded in T1 (1.4 kg CE kg SREY^{-1}).

Diesel usage during land preparation and irrigation represented the most substantial contributor to carbon emissions in cereal-based production systems, while these values were minimized with the adoption of a millet-based cropping system (Table 6). The total CE emissions were higher in cereal-based cropping systems (814–874 kg CE ha^{-1}) compared to the millet-based production systems (766–779 kg CE ha^{-1}). Cereal-based production systems exhibited significantly higher ($p < 0.05$) C-footprints (1.04–2.05 CE kg SREY^{-1}) compared to the millet-based production systems (0.23–0.44 CE kg SREY^{-1}). An interesting observation is that pulses had the lowest CFs (778 kg CE ha^{-1}) due to their inherently low input requirements (Table 6).

3.4 Eco-efficiency index (EEI)

In general, pulses (black gram, horse gram, and pigeon pea) recorded a higher EEI in economic (0.02 and−0.04 US $ MJ^{-1})

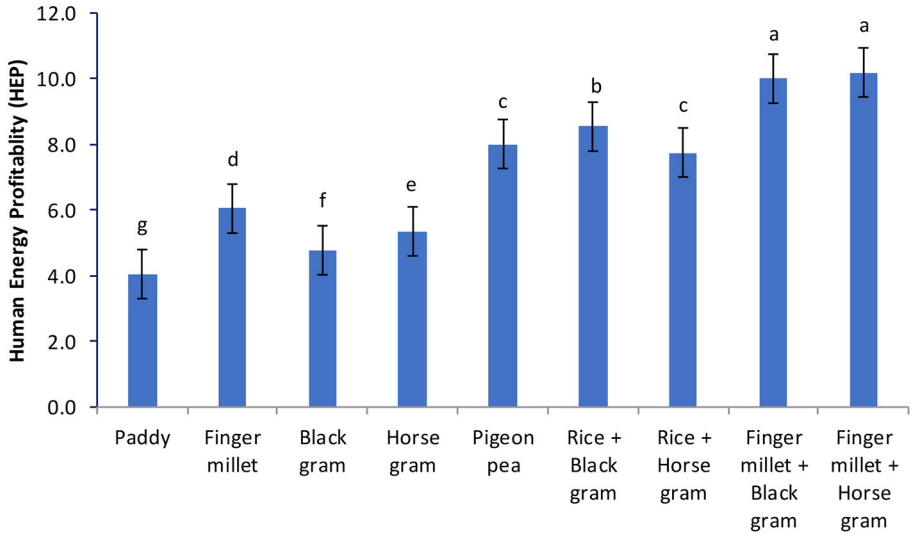

FIGURE 2
Human energy profitability as influenced by diverse cropping systems in rice-fallow systems in the eastern hill and plateau region of eastern India (average of 3 years). Values with lower case letters provided in graph are significantly different at $p < 0.05$ according to Duncan Multiple Range Test (DMRT).

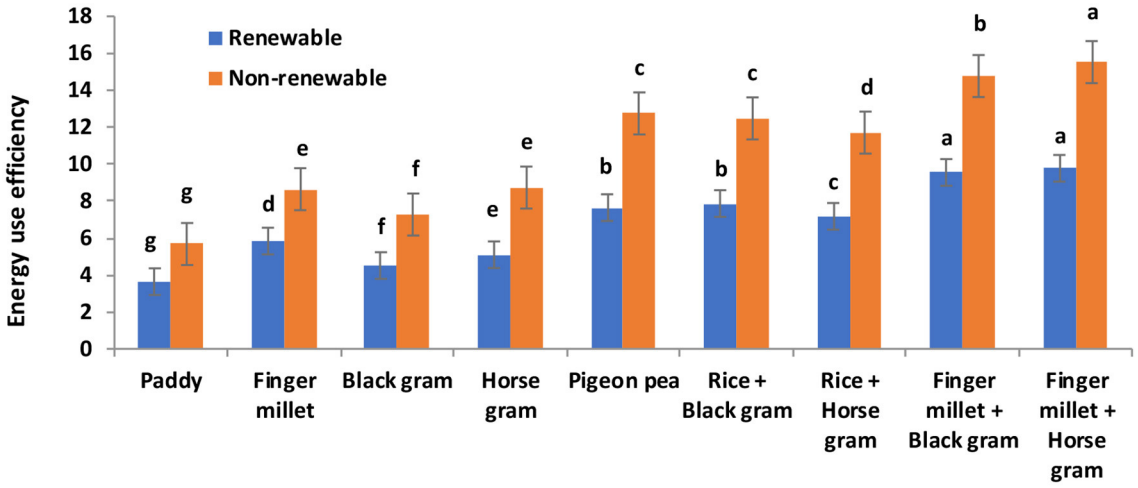

FIGURE 3
Renewable and non-renewable energy use efficiency as influenced by diverse cropping systems in rice-fallow systems in the eastern hill and plateau region of eastern India (average of 3 years). Values with lower case letters provided in graph are significantly different at $p < 0.05$ according to Duncan Multiple Range Test (DMRT).

as well as in ecological terms (0.7 and 1.75 US $ kg CO_2eq^{-1}) (Figure 6). In terms of input energy and GHG emission, millet-based intercropping had a lower EEI than cereal-based production systems. The EEI (economic terms) in pulses and millet was found to be 1.92 and 2.64 times higher, respectively, than rice alone. A similar pattern was noted in the case of the EEI concerning GHG emissions.

3.5 Environmental impact

Assessment of GHG emissions and evaluation of GWP were conducted to determine the effect of diverse cropping systems on environmental sustainability. Horse gram, black gram, and pigeon pea had the lowest N_2O emissions (0.09–0.11 kg ha^{-1} $season^{-1}$) as against finger millet and rice crops (0.51–0.60 kg ha^{-1} $season^{-1}$) (Table 7), while only rice-based systems were assessed for CH_4 emissions with 12.8 kg ha^{-1} $season^{-1}$. The N_2O-GWP of rice and finger millet-based sole cropping systems was 1.7 to 6.6 times higher than other sole or intercropped production systems. The N_2O-GWP of intercropped systems ranged between 80.0 and 95.0 kg CO_2 eq. ha^{-1} $season^{-1}$. Among the sole crop systems, the GWP of black gram (30.08 kg CO_2 eq. ha^{-1} $season^{-1}$) and horse gram (24.42 kg CO_2 eq. ha^{-1} $season^{-1}$) was 5.8% and 22.2% of the GWP of sole rice, while in comparison to finger millet, it was 4.7% and 18%, respectively.

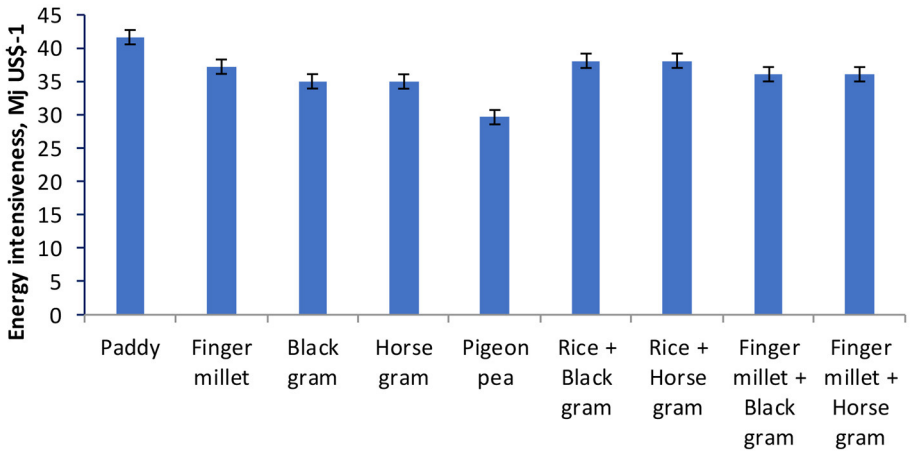

FIGURE 4
Energy intensiveness as influenced by diverse cropping systems in rice-fallow systems in the eastern hill and plateau region of eastern India (average of 3 years).

3.6 Production economics

The higher average expenditures that were incurred in cereal-based production systems compared to pulse-based production systems were attributed to excessive tillage operations, increased fertilizer and irrigation usage, and higher labor costs (Table 8). Rice-based production systems recorded comparatively less B:C while millet-based systems observed higher net returns.

4 Discussion

4.1 Productivity of the cropping systems

In the present investigation, crop yields and total biomass production were significantly affected by diverse cropping systems due to variations in bio-physical and management factors (Table 1). Pan et al. (2022) also observed that the introduction of black gram and horse gram as intercrops in paddy and finger millet crops increased the system productivity and efficiency as compared to sole-cropping systems. Crop rotations involving a variety of crop cultivars and cropping systems, a widely adopted agricultural practice globally, have proven effective in addressing the challenges posed by the adverse climatic changes in intensive production systems, ultimately promoting environmental sustainability (Lal et al., 2020). Crop diversification through climate-resilient cropping systems represents a primary strategy for enhancing overall ecosystem productivity and mitigating ecological sustainability concerns (Chaudhary et al., 2009). This approach also contributes to a reduction in CFs and energy use (Yang et al., 2014). Consequently, the design of a resilient crop production system should prioritize the optimization of energy inputs and CFs throughout the entire production process. Assessment of GHG emissions and CFs for individual crops is imperative when creating an efficient cropping system. Selection of crops and cultivars that demand minimal input and have lesser carbon footprints is essential, regardless of the cropping systems (Yadav et al., 2017).

Across all the cropping systems, the T9 treatment consistently exhibited the highest biomass production. Variations in biomass production can be attributed to differences in the genetic potential of individual crops (Lal et al., 2020). Increased total biomass production in finger millet and horse gram systems can be attributed to the superior production capabilities of C4 plants. Finger millet (dual purpose) and horse gram efficiently harness solar energy, resulting in an overall higher total biomass production (Tuti et al., 2012). This study has been also authenticated under upland rainfed conditions, where soil moisture is a primary constraint to achieving a higher crop yield (Choudhary et al., 2017). Furthermore, improved crop management practices, including residual fertility and moisture management, significantly contributed to higher yield benefits (Samal et al., 2017).

4.2 Energy and input use efficiencies

Energy requirements for crop production are directly influenced by the management techniques applied and inputs utilized. In general, millet-based intercropping systems exhibited lower energy input requirements compared to rice-based intercropping systems (Table 2). The need for energy and its production potential is significantly influenced by factors such as inputs used, choice of crops and cultivars, type of cropping system, and crop establishment methods (Kumar et al., 2020). Among the different cropping systems, the total energy input requirement was higher in rice alone (27,803 MJ ha^{-1}), notably surpassing millet-based production systems (Table 1). The primary factor contributing to the increase in energy input was the intensive crop management practices involving human labor, diesel, fertilizers, seeds, and machinery to enhance crop productivity in the rice-sole cropping system (Kumar et al., 2019). Crop production based on conventional tillage systems exhibited high energy input requirements and relatively lower resource use efficiency.

TABLE 5 C-footprint (kg CO_2 eq. ha^{-1}) in different agronomic management practices of diverse cropping systems in rice-fallow systems in the eastern hill and plateau region of eastern India (average of 3 years).

Agronomic management practice	Rice	Finger millet	Black gram	Horse gram	Pigeon pea	Rice + Black gram	Rice + Horse gram	Finger millet + Black gram	Finger millet + Horse gram
Land preparation	517	517	522	522	522	520	520	520	520
Fertilizer application	147	130	63	60	63	105	103	96	95
Seed sowing	119	33	58	46	46	89	83	46	40
Intercultural operations	29	30	27	28	23	28	29	28	29
Plant protection	0	0	30	28	28	15	14	15	14
Harvesting, threshing	62	69	68	68	86	65	65	68	69
Total	874	779	767	753	768	821	814	773	766

Approximately 54.8–57.4% of energy input was allocated for land preparations and crop establishment management, a trend supported by various researchers (Yadav et al., 2017). In terms of diverse farm operations, crop diesel (27.3–28.5%) and inorganic fertilizers (8.5–12.7%) constituted the most substantial share of energy inputs, following land preparation (Table 3). After fertilizers, diesel was the most energy-intensive item, and this variance stemmed from the adoption of high-yielding crop cultivars and various farm operations, including plowing, irrigation, and machinery, under different production systems (Chaudhary et al., 2017). However, millet-based production systems exhibited lower energy requirements due to reduced tillage and minimal inter-cultural operations (Saad et al., 2016). Tuti et al. (2012) also reported that land preparation, fertilizer, and seeds were primary contributors to energy consumption, accounting for ~83% of the total energy use.

Under the varied production system, the energy output is majorly determined by the total biomass production, which includes the main product as well as by-products (Fatima et al., 2023). Intercropping systems exhibit more energy productivity by yielding higher grain, seeds, straw, and total biomass production (Table 1). Regardless of the cropping systems, the highest energy input contribution was attributed to land preparation, followed by diesel and fertilizers, particularly due to the elevated levels of nitrogenous fertilization in rice cultivation. In terms of energy productivity, millet-based production systems outperformed rice-based production systems. Generally, millet-based production systems demonstrated higher energy outputs compared to rice-sole cropping. The system-based energy ratio ranged from 2.22 to 6.0, with values contingent on total biomass production and energy input utilization. The energy ratio of millet-based cropping systems was notably higher, primarily due to the production of more biomass with minimal energy input (Choudhary et al., 2017; Pan et al., 2022). Among the treatments, T9 was identified as the most energy-efficient. In contrast, rice-sole cropping (T1) exhibited the lowest energy efficiency, largely owing to the increased energy input in terms of fertilizer and human power (Kumar et al., 2019). The treatment T1, which involved sole cropping, exhibited higher energy input and relatively lower energy output, leading to a reduced energy ratio. Notably, a higher energy ratio and productivity were observed in the treatments with higher economic yields (Tuti et al., 2012). Rice treatment (T1) demonstrated the lowest energy productivity. Efficiency of energy utilization was more pronounced in millets and pulses, as evidenced by improved energy ratios. The treatment T1 emerged as an energy-intensive system due to the utilization of increased energy inputs to generate comparable energy outputs (Yadav et al., 2020). Consequently, judicious selection of crops and varieties is essential for designing resource-efficient, energy-efficient, and carbon-efficient production systems (Benbi, 2018).

Millet-based production systems exhibited the highest energy outputs while utilizing lower energy inputs. The superior energy output of millet-based production systems was attributed to higher yields of finger millet, expressed in terms of REY (Chaudhary et al., 2017). The primary factors contributing to higher energy inputs in conventional rice-production systems were increased energy input in terms of fertilizers, machinery, diesel, and

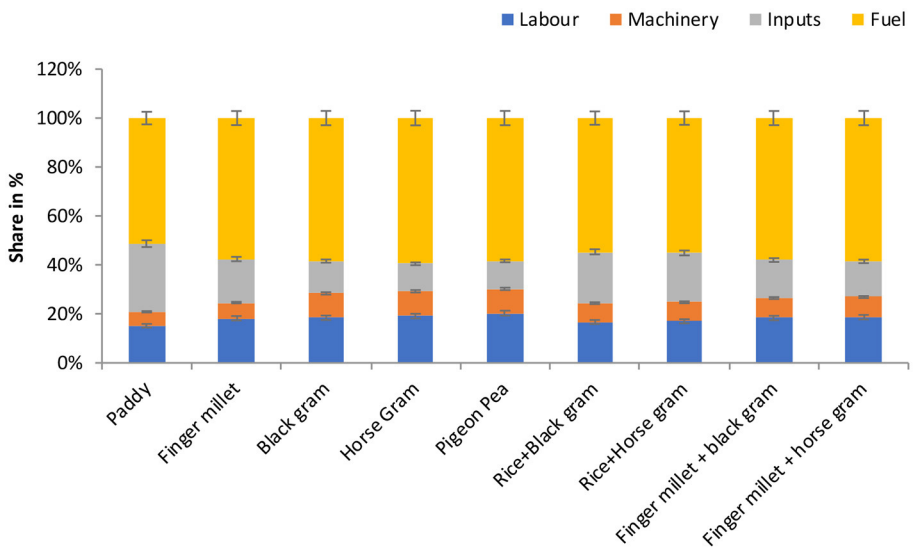

FIGURE 5
Percentage share of different inputs toward carbon input under diverse tillage production systems in rice-fallow systems in the eastern hill and plateau region of eastern India (average of 3 years).

TABLE 6 Carbon input and output efficiency of diverse cropping systems in rice-fallow systems in the eastern hill and plateau region of eastern India (average of 3 years).

Cropping systems	Carbon input (kg CO_2 eq. ha^{-1})	Carbon output (kg CO_2 eq. ha^{-1})	Carbon efficiency	Carbon sustainability index	Carbon footprint (kg CO_2 eq. ha^{-1})	CF on yield scale (kg CO_2 eq. kg^{-1} SREY)
Rice	874^{a}	$2{,}061^{g}$	2.36^{g}	1.36^{g}	$1{,}392^{a}$	1.04^{c}
Finger millet	779^{d}	$3{,}869^{e}$	4.97^{d}	3.97^{d}	914^{d}	0.23^{e}
Black gram	767^{e}	$2{,}540^{f}$	3.31^{f}	2.31^{f}	797^{g}	0.15^{ef}
Horse gram	753^{f}	$2{,}855^{f}$	3.79^{e}	2.79^{e}	778^{h}	0.15^{ef}
Pigeon pea	768^{e}	$4{,}135^{e}$	5.38^{cd}	4.38^{cd}	798^{g}	0.09^{f}
Rice + Black gram	821^{b}	$4{,}503^{d}$	5.49^{c}	4.49^{c}	$1{,}274^{b}$	1.30^{b}
Rice + Horse gram	814^{c}	$4{,}539^{c}$	5.58^{c}	4.58^{c}	$1{,}264^{b}$	2.05^{a}
Finger millet + Black gram	773^{de}	$5{,}725^{b}$	7.41^{b}	6.41^{b}	856^{e}	0.43^{d}
Finger millet + Horse gram	766^{e}	$6{,}310^{a}$	8.24^{a}	7.24^{a}	846^{f}	0.44^{d}

Values with different superscripts in a column are significantly different at $p < 0.05$ according to Duncan Multiple Range Test (DMRT).

weeding (Bohra and Kumar, 2015). Therefore, minimizing these constituents in crop management is essential to enhance the energy ratio.

In the current investigation, millet-based production systems displayed lower energy requirements mainly due to reduced fertilizer usage and intercultural operations, while intensive tillage in rice as a sole cropping system increased energy consumption (Nassiri and Singh, 2009; Houshyar et al., 2015). Adoption of the millets in cropping systems led to a partial reduction in energy use, although the use of pesticides somewhat increased energy consumption compared to conventional tillage (Choudhary et al., 2017). Consequently, a greater biological yield of millet-based systems resulted in elevated energy outputs, even under conditions of limited resources (Barut et al., 2011).

4.3 Carbon footprints

Carbon footprints were markedly influenced by diverse crops and intercropping systems (Table 5). Rice-based intercropping systems exhibited the highest levels of C-inputs (Table 6). This could be attributed to extensive land preparation and increased use of fertilizers. Variations in C-inputs were primarily the result of changes in crop and cropping systems (Yadav et al., 2020). In general, C-inputs in cereals, including rice-based production systems, were significantly consumed during land preparation, fertilizer application, and seed sowing. Amongst the various agronomic management practices, the largest shares of C-inputs were attributed to land preparation and fertilizer application (Jat et al., 2019).

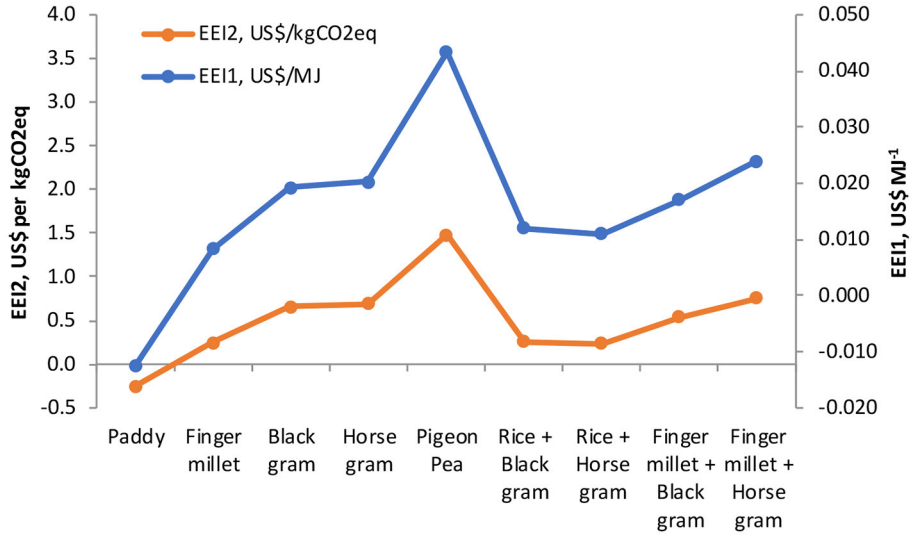

FIGURE 6
Eco-efficiency index (EEI) as influenced by diverse cropping systems in rice-fallow systems in the eastern hill and plateau region of eastern India (average of 3 years).

TABLE 7 Greenhouse gas emission and GWP of diverse cropping systems in rice-fallow systems in the eastern hill and plateau region of eastern India (average of 3 years).

Cropping systems	N_2O emission (kg ha^{-1} $season^{-1}$)	CH_4 emission (kg ha^{-1} $season^{-1}$)	GWP of N_2O (kg CO_2 eq. ha^{-1} $season^{-1}$)	GWP of CH_4 (kg CO_2 eq. ha^{-1} $season^{-1}$)	System GWP (kg CO_2 eq. ha^{-1} $season^{-1}$)
Rice	0.60	12.80	159.99	358.40	518.39[a]
Finger millet	0.51	–	135.56	–	135.56[b]
Black gram	0.11	–	30.08	–	30.08[c]
Horse gram	0.09	–	24.42	–	24.42[c]
Pigeon pea	0.11	–	30.08	–	30.08[c]
Rice + Black gram	0.36	12.80	95.04	358.40	453.44[a]
Rice + Horse gram	0.35	12.80	92.21	358.40	450.61[a]
Finger millet + Black gram	0.31	–	82.82	–	82.82[bc]
Finger millet + Horse gram	0.30	–	79.99	–	79.99[bc]

Values with different superscripts in a column are significantly different at $p < 0.05$ according to Duncan Multiple Range Test (DMRT).

Irrespective of the crops/cropping system, rice had the highest share of the total C-input (Figure 5). Millet-based intercropping systems (T8 and T9) had comparatively lower C-input compared to rice/cereal-based systems. Field investigations by Babu et al. (2020) also reported that non-renewable energy sources, mainly chemical fertilizer applications, had a major share in total C-input followed by diesel use in all the cropping systems. Compared to cereals-based systems, intercropping systems based on millet had markedly higher C-output which may primarily be attributed to substantial biomass production. The transition from a cereal-based system to a millet-based system resulted in a significant reduction in CFs. This trend underscores the idea that the CF of crop production largely depends on the crop/cultivar's ability to efficiently convert mineral nutrition into total biomass (Yadav et al., 2020). These findings align with the perspective of others who have emphasized that the CF of cereal-based production systems can be notably reduced through improved management approaches and sustainable cropping intensification, particularly through the adoption of climate-resilient production systems (Babu et al., 2020). Irrespective of crops or cropping systems, the greatest contributions to GHG emissions came from land preparation, fertilizer application, and seed sowing, followed by harvesting, threshing, and plant protection chemicals. Consequently, focus should be directed toward the selection of crops/cultivars for intensification of rice-based systems that require reduced land preparation and fertilizer inputs while exhibiting comparatively higher conversion efficiency of inputs into outputs.

Enhancing energy use efficiency (EUE) and carbon use efficiency (CUE) in all crops within diverse crop/intercropping production systems plays a pivotal role in promoting environmental sustainability by reducing carbon emissions.

TABLE 8 Production economics of diverse cropping systems in rice-fallow systems in the eastern hill and plateau region of eastern India (average of 3 years).

Cropping systems	SCOC (US$ ha^{-1})	SGR (US$ ha^{-1})	SNR (US$ ha^{-1})	B:C ratio	SEE (US$ ha^{-1} d^{-1})	SPE (kg ha^{-1} d^{-1})	EI (MJ US^{-1})
Rice	667.5^{i}	320.3^{i}	−347.3^{i}	0.48^{g}	−72.3^{f}	3.78^{f}	41.7^{a}
Finger millet	722.4^{f}	945.0^{h}	222.6^{gh}	1.31^{f}	46.4^{e}	10.85^{e}	37.2^{c}
Black gram	767.5^{b}	1289.2^{cd}	521.7^{cd}	1.68^{bcd}	108.6^{bc}	14.79^{bc}	35.0^{e}
Horse gram	758.1^{bc}	1296.4^{c}	538.3^{c}	1.71^{bc}	112.1^{bc}	14.88^{bc}	35.0^{e}
Pigeon pea	920.4^{a}	2104.5^{a}	1184.1^{a}	2.29^{a}	246.5^{a}	24.14^{a}	29.6^{f}
Rice + Black gram	717.5^{fg}	1048.1^{f}	330.6^{f}	1.46^{def}	68.8^{de}	12.03^{de}	38.1^{b}
Rice + Horse gram	712.8^{fgh}	1012.2^{fg}	299.4^{fg}	1.42^{ef}	62.3^{de}	11.62^{e}	38.1^{b}
Finger millet + Black gram	744.9^{cd}	1203.1^{de}	458.2^{de}	1.62^{cde}	95.4^{cd}	13.81^{cd}	36.1^{d}
Finger millet + Horse gram	740.3^{cde}	1382.3^{b}	642.1^{b}	1.87^{b}	133.7^{bc}	15.86^{b}	36.1^{d}

SCOC, System cost of cultivation; SGR, System gross returns; SNR, System net returns; B:C ratio, Benefit cost ratio; SEE, System economic efficiency; SPE, system production efficiency; EI, Energy intensiveness, Values with different superscripts in a column are significantly different at $p < 0.05$ according to Duncan Multiple Range Test (DMRT).

The elevated CUE/CSI observed in T8 and T9 can be attributed to lower C-inputs resulting from reduced input usage, including fertilizers, pesticides, and irrigations. Conversely, the highest C-footprint recorded for treatment T1 (1.4 kg CE kg SREY^{-1}) may be due to minimal emissions of carbon from fossil fuels (Choudhary et al., 2017). These findings are consistent with the results reported by Jat et al. (2019). Increased C-input in cereal-based production systems primarily resulted from higher inorganic fertilizer application. Higher values of CE/CSI in millet-based systems were associated with reduced C-inputs during land preparation, fertilizer application, and fossil fuel (diesel) usage, in addition to increasing the production of C-outputs (Yadav et al., 2020).

Diesel usage during land preparation and irrigation represented the most substantial contributor to carbon emissions in cereal-based rotation, while these values were minimized by the inclusion of a millet-based production system (Table 6). This difference in GHG emissions amongst these cropping systems may be attributed to differences in the amount of diesel used (Pratibha et al., 2015). Notably, minimum tillage practices resulted in lower GHG emissions compared to conventional tillage systems (Yadav et al., 2018). Pulse-based cropping systems had the lowest CFs due to their inherently low input requirements (Table 6) which is consistent with the finding reported by Choudhary et al. (2017). The substantial impact of crop establishment and tillage practices on CE/CSI has been emphasized by other researchers (Singh et al., 2020).

Considering the backdrop of climate change and human-induced emissions, the feasibility of diverse cropping systems hinges on carbon efficiency. Consequently, the transition from a rice-based production system to a millet-based cropping system reduces the reliance on fossil fuels and enhances environmental sustainability. Therefore, the implementation and advancement of millet-based production systems contribute to energy conservation, improved EUE, reduced CFs, and the harmonization of food security, nutritional quality, and environmental sustainability in the Indo-Gangetic Plain of South Asia.

4.4 Environmental sustainability

Assessment of environmental sustainability for any system can be achieved through the application of eco-efficiency indices, which encompass both economic and ecological dimensions of a production system (Keating et al., 2010). In general, the EEI (economic term) in pulses and millets was 1.92 and 2.64 times higher than the rice alone system, respectively. This pattern underscores that rice monocropping is not environmentally robust because it significantly degrades the ecosystem (Gupta et al., 2016). An improved EEI in terms of economic gains suggests that pulses and millets generate higher net income over their adverse impact on the environment (Lal et al., 2020). These findings indicate that the addition of pulses/millet in intercropping systems enhances economic profitability while minimizing environmental losses. Several studies have also recommended incorporating energy-efficient crops into cereal-based cropping systems to enhance the EEI (Kulak et al., 2013; Babu et al., 2020). Therefore, the adoption of a pulse/millet production system under a rice-fallow system in eastern India significantly enhances the EEI in terms of energy use and GHG emissions when compared to rice monocropping.

Elevated GWP observed in rice cultivation can be attributed to the increased CH_4 emissions from anaerobic paddy fields. The practice of puddling and flooding in paddy fields promotes methanogenesis, resulting in heightened CH_4 emissions. Conventional-till-direct-seeded rice (CTDSR) recorded lower CH_4 emissions due to the prevalence of aerobic conditions in this practice (Chaudhary et al., 2017). Comparatively, lower energy intensiveness of the management practices and reduced CH_4 emission due to foregoing puddling led to significantly lower GWP in solely millet-based as well as intercropped cropping production systems (Babu et al., 2020).

4.5 Comparative economic gains

Net returns serve as a primary evaluation tool for assessing the efficiency of enterprises, management strategies, and production economics (Yadav et al., 2017). The 3-year average expenditures incurred in the rice-based production systems were higher, attributed to excessive tillage operations, increased fertilizer and irrigation usage, and higher labor costs (Table 8). Comparatively lower B:C ratios in the rice-based production systems were due to lower returns and higher per-unit production expenditures (Kumar et al., 2018). Consequently, the higher net returns observed in the millet-based intercropping production systems in this study suggest that these alternative production systems are highly profitable due to their lower investments and equivalent economic yields as compared to cereal-based production systems. Therefore, efficient utilization of natural resources (energy, water, labor) through the adoption of millet-based production systems in diverse agro-ecosystems offers a feasible and viable option for enhancing productivity and profitability, and providing a cleaner and safer environment for resource-poor farmers in the region (Lal et al., 2020).

4.6 Millet-based diversification—barriers and policy

While millet-based production systems have demonstrated remarkable efficiency in terms of system productivity, profitability, energy ratio, and the reduction of C-footprints and GHG emissions, their adoption and substitution for rice-based cropping systems with millet face challenges on the eastern Indo-Gangetic Plains (IGP). This is primarily because rice and wheat are the major staple food in the region. Diversification with new crops or changing the existing cropping systems to environment-friendly and productive ones requires changing the mindset of the farmers which can be achieved through large-scale participatory technology demonstration programs across the region. Apart from these social concerns, some advanced research on millet-based cropping systems is also required. For example, considering increasing temperatures and rainfall variability, it is an imperative to identify and target areas suitable for millet-based production systems. Millet, being rich in nutrients and dietary fiber, should be actively promoted as a nutri-cereal in the diets of the rural poor. Government policies need to be oriented toward millet-based production systems to facilitate wider promotion and adoption. The Food and Agriculture Organization's (FAO) recognition of the year 2023 as the International Year of Millets has left a footprint in people's minds about the benefits and potential of millet.

5 Conclusion

The study demonstrated that adopting a millet-based production system resulted in a ~12% reduction in carbon input and a 14.2% reduction in energy intensiveness compared to cereal-based cropping systems. The CF and GWP of millet-based systems were 38.9 and 15.7% of the values observed in rice-based cropping systems. This study recommends that existing rice-fallow systems be diversified by incorporating climate-resilient millet-based production systems such as Finger millet + Horse gram and Finger millet + Black Gram. The addition of millet in prevailing systems can enhance energy and system productivity, and economic efficiency. The cultivation of pigeon pea as a sole crop also showed the potential for environmental as well as monetary gains. These climate-resilient production systems are not only more productive but are also resource-efficient, energy-efficient, and C-efficient, and exhibit lower GHG emissions. These systems can be incorporated into the policy for large upscaling and out-scaling in the eastern plateau region of the country. The persisting mindset of the farmers and the lack of technological innovations can be the major barriers in achieving the suggested crop diversification at regional scales. This calls for policy interventions (perhaps in terms of subsidy programs and irrigation schemes) for the promotion and adoption of millet and pulse-based cropping systems. The insights generated from this study have the potential to enhance the knowledge base and empower policymakers and researchers to promote safer, cleaner, more sustainable, and more productive climate-resilient cropping systems in the Indo-Gangetic Plains of South Asia, aligning with the United Nations Sustainable Development Goals (SDGs).

Data availability statement

The original contributions presented in the study are included in the article/supplementary material, further inquiries can be directed to the corresponding author/s.

Author contributions

RP: Formal analysis, Investigation, Writing – review & editing, Conceptualization, Writing – original draft. SM: Conceptualization, Investigation, Methodology, Writing – original draft, Writing – review & editing. RK: Data curation, Formal analysis, Investigation, Writing – review & editing, Writing – original draft. SN: Data curation, Formal analysis, Investigation, Methodology, Writing – review & editing, Writing – original draft. RS: Formal analysis, Investigation, Writing – original draft, Writing – review & editing. PU: Data curation, Formal analysis, Investigation, Writing – review & editing. BJ: Data curation, Formal analysis, Writing – original, Writing – review & editing draft. PJ: Data curation, Formal analysis, Writing – original, Writing – review & editing draft. AD: Data curation, Supervision, Formal analysis, Writing – original, Writing – review & editing draft.

Funding

The author(s) declare that no financial support was received for the research, authorship, and/or publication of this article.

Acknowledgments

Authors are grateful to the ICAR-Research Complex for Eastern Region, Patna, Bihar, India for providing necessary facilities during the experimentation.

Conflict of interest

The authors declare that the research was conducted in the absence of any commercial or financial relationships that could be construed as a potential conflict of interest.

Publisher's note

All claims expressed in this article are solely those of the authors and do not necessarily represent those of their affiliated organizations, or those of the publisher, the editors and the reviewers. Any product that may be evaluated in this article, or claim that may be made by its manufacturer, is not guaranteed or endorsed by the publisher.

Supplementary material

The Supplementary Material for this article can be found online at: https://www.frontiersin.org/articles/10.3389/fsufs.2024.1340638/full#supplementary-material

References

Alam, M. K., Bell, R. W., and Biswas, W. K. (2019). Decreasing the carbon footprint of an intensive rice-based cropping system using conservation agriculture on the Eastern Gangetic Plains. *J. Clean. Prod.* 218, 259–272. doi: 10.1016/j.jclepro.2019.01.328

Ali, M., Ghosh, P. K., and Hazra, K. K. (2014). "Resource conservation technologies in rice fallow," in *Resource Conservation Technology in Pulses*, eds P. K. Ghosh, N. Kumar, M. S. Venkatesh, K. K. Hazra, N. Nadarajan (Jodhpur: Scientific Publishers), 83–88.

Babu, S., Mohapatra, K. P., Das, A., Yadav, G. S., Tahasildar, M., Singh, R., et al. (2020). Designing energy-efficient, economically sustainable, and environmentally safe cropping system for the rainfed maize–fallow land of the Eastern Himalayas. *Sci Total Environ.* 722, 137874. doi: 10.1016/j.scitotenv.2020.137874

Barut, Z. B., Ertekin, C., and Karaagac, H. A. (2011). Tillage effects on energy use for corn silage in Mediterranean Coastal of Turkey. *Energy* 36, 5466–5475. doi: 10.1016/j.energy.2011.07.035

Benbi, D. K. (2018). Carbon footprint and agricultural sustainability nexus in an intensively cultivated region of Indo-Gangetic Plains. *Sci. Total Environ.* 644, 611–623. doi: 10.1016/j.scitotenv.2018.07.018

Bohra, J. S., and Kumar, R. (2015). Effect of crop establishment methods on productivity, profitability, and energetics of rice (Oryza sativa)-wheat (Triticum aestivum) system. *Ind. J. Agric. Sci.* 85, 217–223.

Chaudhary, V. P., Gangwar, B., Pandey, D. K., and Gangwar, K. S. (2009). Energy auditing of diversified rice–wheat cropping systems in Indo-Gangetic plains. *Energy* 34, 1091–1096. doi: 10.1016/j.energy.2009.04.017

Chaudhary, V. P., Singh, K. K., Pratibha, G., Bhattacharyya, R., Shamim, M., Srinivas, I., et al. (2017). Energy conservation and greenhouse gas mitigation under different production systems in rice cultivation. *Energy* 130, 307–317. doi: 10.1016/j.energy.2017.04.131

Choudhary, M., Rana, K. S., Bana, R. S., Ghasal, P. C., Choudhary, G. L., Jakhar, P., et al. (2017). Energy budgeting and carbon footprint of pearl millet–mustard cropping system under conventional and conservation agriculture in rainfed semi-arid agro-ecosystem. *Energy* 141, 1052–1058. doi: 10.1016/j.energy.2017.09.136

Cicek, A., Altintas, G., and Erdal, G. (2011). Energy consumption patterns and economic analysis of irrigated wheat and rain-fed wheat production: case study for Tokat Region, Turkey. *Bulgarian J. Agric. Sci.* 17, 378–388.

Czyzewski, B., and Kryszak, L. (2018). Impact of different models of agriculture on greenhouse gases (GHG) emissions: a sectoral approach. *Outlook Agric.* 47, 68–76. doi: 10.1177/0030727018759092

FAO (2018). *Food and Agriculture Statistics*. FAO.

FAO (2022). *Greenhouse Gas Emissions From Agrifood Systems. Global, Regional and Country Trends, 2000-2020. FAOSTAT Analytical Brief Series No. 50*. Rome:FAO.

Fatima, A., Singh, V. K., Babu, S., Singh, R. K., Upadhyay, P. K., Rathore, S. S., et al. (2023). Food production potential and environmental sustainability of different integrated farming system models in northwest India. *Front. Sustain. Food Syst.* 7, 959464. doi: 10.3389/fsufs.2023.959464

Ghosh, P. K., Hazra, K. K., Nath, C. P., Das, A., and Acharya, C. L. (2016). Scope, constraints and challenges of intensifying rice (Oryza sativa) fallows through pulses. *Indian J. Agron.* 61, S122–128.

Gómez-Limón, J. A., Picazo-Tadeo, A. J., and Reig-Martínez, E. (2012). Eco-efficiency assessment of olive farms in Andalusia. *Land Use Policy* 29, 395–406. doi: 10.1016/j.fcr.2012.06.007

Gupta, D. K., Bhatia, A., Kumar, A., Das, T. K., Jain, N., Tomer, R., et al. (2016). Mitigation of greenhouse gas emission from rice–wheat system of the Indo-Gangetic plains: through tillage, irrigation, and fertilizer management. *Agric. Ecosyst. Environ.* 230, 1–9. doi: 10.1016/j.agee.2016.05.023

Houshyar, E., Dalgaard, T., Tarazkar, M. H., and Jørgensen, U. (2015). Energy input for tomato production. What economy says, and what is good for the environment? *J. Clean Prod.* 89, 99–109. doi: 10.1016/j.jclepro.2014.11.022

IPCC (2007). *Climate Change 2007: Synthesis Report Contribution of Working Groups I, II and III to the Fourth Assessment Report of the Intergovernmental Panel on Climate Change*. Geneva: IPCC, 104.

Jat, S. L., Parihar, C. M., Singh, A. K., Kumar, B., Choudhary, M., Nayak, H. S., et al. (2019). Energy auditing and carbon footprint under long-term conservation agriculture-based intensive maize systems with diverse inorganic nitrogen management options. *Sci. Total Environ.* 664, 659–668. doi: 10.1016/j.scitotenv.2019.01.425

John, D. A., and Babu, G. R. (2021). Lessons from the aftermaths of green revolution on food system and health. *Front. Sustain. Food Syst.* 5:644559. doi: 10.3389/fsufs.2021.644559

Keating, B. A., Carberry, P. S., Bindraban, P. S., Asseng, S., Meinke, H., and Dixon, J. (2010). Eco-efficient agriculture: concepts, challenges, and opportunities. *Crop Sci.* 50, S-109–S-119. doi: 10.2135/cropsci2009.10.0594

Kulak, M., Nemecek, T., Frossard, E., and Gaillard, G. (2013). How eco-efficient are low-input cropping systems in Western Europe, and what can be done to improve their eco-efficiency? *Sustainability* 5, 3722–3743. doi: 10.3390/su5093722

Kumar, R., Mishra, J. S., Rao, K. K., Bhatt, B. P., Hazra, K. K., Hans, H., et al. (2019). Sustainable intensification of rice fallows of Eastern India with suitable winter crop and appropriate crop establishment technique. *Environ. Sci. Poll. Res.* 26, 29409–29423. doi: 10.1007/s11356-019-06063-4

Kumar, R., Mishra, J. S., Rao, K. K., Mondal, S., Hazra, K. K., and Choudhary, J. S., et al. (2020). Crop rotation and tillage management options for sustainable intensification of rice-fallow agro-ecosystem in eastern India. *Sci. Rep.* 10, 1–15. doi: 10.1038/s41598-020-67973-9

Kumar, V., Jat, H. S., Sharma, P. C., Gathala, M. K., Malik, R. K., Kamboj, B. R., et al. (2018). Can productivity and profitability be enhanced in intensively managed cereal systems while reducing the environmental footprint of production? Assessing sustainable intensification options in the breadbasket of India. *Agric. Ecosyst. Environ.* 252, 132–147. doi: 10.1016/j.agee.2017.10.006

Lal, B., Gautama, P., Panda, B. B., Tripathi, R., Shahid, M., Bihari, P., et al. (2020). Identification of energy and carbon efficient cropping system for ecological sustainability of rice fallow. *Ecol. Indic.* 115, 106431. doi: 10.1016/j.ecolind.2020.106431

Lal, R. (2004). Carbon emission from farm operations. *Environ. Int.* 30, 981–990. doi: 10.1016/j.envint.2004.03.005

Li, Y., Li, Y., Zhang, Q., Xu, G., Liang, G., Kim, D. G., et al. (2024). Enhancing soil carbon and nitrogen through grassland conversion from degraded croplands in China: assessing magnitudes and identifying key drivers of phosphorus reduction. *Soil Till. Res.* 236, 105943. doi: 10.1016/j.still.2023.105943

Linquist, B. A., Adviento-Borbe, M. A., Pittelkow, C. M., Van Kessel, C., and Van Groenigen, K. J. (2012). Fertilizer management practices and greenhouse gas emissions from rice systems: a quantitative review and analysis. *Field Crops Res.* 135, 10–21.

Mandal, S., Roy, S., Das, A., Ramkrushna, G. I., Lal, R., and Verma, B. C., et al. (2015). Energy efficiency and economics of rice cultivation systems under sub-tropical Eastern Himalaya. *Energy Sustain. Dev.* 28, 115–121. doi: 10.1016/j.esd.2015.08.002

NAAS (2013). *Improving Productivity of Rice Fallows*. Policy Paper No. 64. New Delhi: National Academy of Agricultural Sciences.

Nassiri, S. M., and Singh, S. (2009). Study on energy use efficiency for paddy crop using data envelopment analysis (DEA) technique. *Appl. Energy* 86, 1320–1325. doi: 10.1016/j.apenergy.2008.10.007

Padre, T. A., Rai,. M., Kumar, V., Gathala, M., Sharma, P. C., Sharma, S., et al. (2016). Quantifying changes to the global warming potential of rice-wheat systems with the adoption of conservation agriculture in north-western India. *Agric. Ecosyst. Environ.* 219, 125–137. doi: 10.1016/j.agee.2015.12.020

Pan, R. S., Kumar, R., Bhatt, B. P., Mishra, J. S., Singh, A. K., Naik, S. K., et al. (2022). Production potential and soil health of diversified production system of hill and plateau region of eastern India. *Indian J. Agric. Sci.* 92, 101–104. doi: 10.56093/ijas.v92i1.120849

Parihar, C. M., Jat, S. L., Singh, A. K., Kumar, B., Rathore, N. S., Jat, M. L., et al. (2018). Energy auditing of long-term conservation agriculture based irrigated intensive maize systems in semi-arid tropics of India. *Energy* 142, 289–302. doi: 10.1016/j.energy.2017.10.015

Praharaj, C. S., Singh, U., Singh, S. S., Singh, N. P., and Shivay, Y. S. (2016). Supplementary and life-saving irrigation for enhancing pulses production, productivity and water-use efficiency in India. *Ind. J. Agric. Sci.* 61, 249–261.

Pratibha, G., Srinivas, I., Rao, K. V., Raju, B. M. K., Thyagaraj, C. R., and Korwar, G. R. (2015). Energy auditing of long-term conservation agriculture based irrigated intensive maize systems in semi-arid tropics of India. *Energy* 142, 289–302.

Ray, K., Hasan, S. S., and Goswami, R. (2018). Techno-economic and environmental assessment of different rice-based cropping systems in an inceptisol of West Bengal, India. *J Clean Prod*. 205, 350–363. doi: 10.1016/j.jclepro.2018.09.037

Ray, K., Sen, P., Goswami, R., Sarkar, S., Brahmachari, K., Ghosh, A., et al. (2020). Profitability, energetics and GHGs emission estimation from rice-based cropping systems in the coastal saline zone of West Bengal, India. *PLoS ONE* 15, e0233303. doi: 10.1371/journal. pone.0233303

Saad, A. A., Das, T. K., Rana, D. S., Sharma, A. R., Bhattacharyya, R., and Lal, K. (2016). Energy auditing of a maize–wheat–greengram cropping system under conventional and conservation agriculture in irrigated north-western Indo-Gangetic Plains. *Energy* 116, 293–305. doi: 10.1016/j.energy.2016.09.115

Samal, S. K., Rao, K. K., Poonia, S. P., Kumar, R., Mishra, J. S., Prakash, V., et al. (2017). Evaluation of long-term conservation agriculture and crop intensification in rice-wheat rotation of Indo–Gangetic Plains of South Asia: carbon dynamics and productivity. *Eur. J. Agron.* 90, 98–208. doi: 10.1016/j.eja.2017.08.006

Shyam, C. S., Shekhawat, K., Rathore, S. S., Babu, S., Singh, R. K., Upadhyay, P. K., et al. (2023). Development of integrated farming system model-a step towards achieving biodiverse, resilient and productive green economy in agriculture for small holdings in India. *Agronomy* 13:955. doi: 10.3390/agronomy13040955

Singh, P., Singh, G., and Sodhi, G. P. S. (2019). Energy auditing and optimization approach for improving energy efficiency of rice cultivation in south-western Punjab, India. *Energy* 174, 269–279. doi: 10.1016/j.energy.2019.02.169

Singh, P., Singh, G., and Sodhi, G. P. S. (2020). Energy and carbon footprints of wheat establishment following different rice residue management strategies vis-à-vis conventional tillage coupled with rice residue burning in north-western India. *Energy* 200, 117554. doi: 10.1016/j.energy.2020.117554

Singh, R. N., Praharaj, C. S., Kumar, R., Singh, S. S., Kumar, N., and Singh, U. (2017). Influence of rice (Oryza sativa) habit groups and moisture conservation practices on soil physical and microbial properties in rice + lathyrus relay cropping system under rice fallows in Eastern Plateau of India. *Ind. J. Agric. Sci.* 87, 1633–1639.

Soni, P., Sinha, R., and Perret, S. R. (2018). Energy use and efficiency in selected rice-based cropping systems of Middle-Indo Gangetic Plains in India. *Energy Rep.* 4, 554–564. doi: 10.1016/j.egyr.2018.09.001

Tuti, M. D., Prakash, V., Pandey, B. M., Bhattacharya, R., Mahanta, D., Bisht, J. K., et al. (2012). Energy budgeting of colocasia–based cropping systems in the Indian sub-Himalayas. *Energy* 45, 986–993. doi: 10.1016/j.energy.2012.06.056

Upadhyay, P. K., Sen, A., Singh, Y., Singh, R. K., Prasad, S. K., Sankar, A., et al. (2022). Soil health, energy budget, and rice productivity as influenced by cow products application with fertilizers under south Asian Eastern Indo-Gangetic plains zone. *Front. Agron.* 3, 758572. doi: 10.3389/fagro.2021.758572

World Energy Outlook (2012). *International Energy Agency*. Tokyo: World Energy Outlook.

Yadav, G. S., Babu, S., Das, A., Mohapatra, K. P., Singh, R., Avasthe, R. K., et al. (2020). No-till and mulching enhance energy use efficiency and reduce carbon footprint of a direct-seeded upland rice production system. *J. Clean. Prod.* 271, 122700. doi: 10.1016/j.jclepro.2020. 122700

Yadav, G. S., Das, A., Lal, R., Babu, S., Meena, R. S., Saha, P., et al. (2018). Energy budget and carbon footprint in a no-till and mulch-based rice-mustard cropping system. *J. Clean. Prod.* 191, 144–157. doi: 10.1016/j.jclepro.2018.04.173

Yadav, G. S., Lal, R., Meena, R. S., Datta, M., Babu, S., Das, A., et al. (2017). Energy budgeting for designing sustainable and environmentally clean/safer cropping systems for rainfed rice fallow lands in India. *J. Clean. Prod.* 158, 29–37. doi: 10.1016/j.jclepro.2017.04.170

Yang, X., Gao, W., Zhang, M., Chen, Y., and Sui, P. (2014). Reducing agricultural carbon footprint through diversified crop rotation systems in the North China Plain. *J. Clean. Prod.* 76, 131–139. doi: 10.1016/j.jclepro.2014.03.063

frontiers | Frontiers in Sustainable Food Systems

TYPE Original Research
PUBLISHED 02 April 2024
DOI 10.3389/fsufs.2024.1332483

OPEN ACCESS

EDITED BY
Ashim Datta,
Central Soil Salinity Research Institute (ICAR), India

REVIEWED BY
Dibakar Roy,
National Bureau of Soil Survey and Land Use Planning (ICAR), India
Samrat Ghosh,
Emergent Ventures India, India

*CORRESPONDENCE
Minggang Xu
xuminggang@caas.cn
Nan Sun
sunnan@caas.cn

RECEIVED 13 November 2023
ACCEPTED 14 March 2024
PUBLISHED 02 April 2024

CITATION
Liang S, Sun N, Longdoz B, Meersmans J, Ma X, Gao H, Zhang X, Qiao L, Colinet G, Xu M and Wu L (2024) Both yields of maize and soybean and soil carbon sequestration in typical Mollisols cropland decrease under future climate change: SPACSYS simulation. *Front. Sustain. Food Syst.* 8:1332483. doi: 10.3389/fsufs.2024.1332483

Both yields of maize and soybean and soil carbon sequestration in typical Mollisols cropland decrease under future climate change: SPACSYS simulation

Shuo Liang[1,2], Nan Sun[1]*, Bernard Longdoz[2], Jeroen Meersmans[2], Xingzhu Ma[3], Hongjun Gao[4], Xubo Zhang[5], Lei Qiao[1], Gilles Colinet[2], Minggang Xu[1,6]* and Lianhai Wu[7]

[1]State Key Laboratory of Efficient Utilization of Arid and Semi-Arid Arable Land in Northern China, Key Laboratory of Arable Land Quality Monitoring and Evaluation, Ministry of Agriculture and Rural Affairs/Institute of Agricultural Resources and Regional Planning, Chinese Academy of Agricultural Sciences, Beijing, China, [2]TERRA Teaching and Research Centre, Gembloux Agro-Bio Tech, University of Liège, Gembloux, Belgium, [3]Heilongjiang Academy of Black Soil Conservation and Utilization, Harbin, China, [4]Institute of Agricultural Resources and Environment, Jilin Academy of Agricultural Sciences, Changchun, China, [5]Key Laboratory of Ecosystem Network Observation and Modeling, Institute of Geographic Sciences and Natural Resources Research, Chinese Academy of Sciences, Beijing, China, [6]Institute of Eco-Environment and Industrial Technology, Shanxi Agricultural University, Taiyuan, China, [7]Net Zero and Resilient Farming, Rothamsted Research, North Wyke, United Kingdom

Although Mollisols are renowned for their fertility and high-productivity, high carbon (C) losses pose a substantial challenge to the sustainable provision of ecosystem services, including food security and climate regulation. Protecting these soils with a specific focus on revitalizing their C sequestration potential emerges as a crucial measure to address various threats associated with climate change. In this study, we employed a modeling approach to assess the impact of different fertilization strategies on crop yield, soil organic carbon (SOC) stock, and C sequestration efficiency (CSE) under various climate change scenarios (baseline, RCP 2.6, RCP 4.5, and RCP 8.5). The process-based SPACSYS model was calibrated and validated using data from two representative Mollisol long-term experiments in Northeast China, including three crops (wheat, maize and soyabean) and four fertilizations (no-fertilizer (CK), mineral nitrogen, phosphorus and potassium (NPK), manure only (M), and chemical fertilizers plus M (NPKM or NM)). SPACSYS effectively simulated crop yields and the dynamics of SOC stock. According to SPACSYS projections, climate change, especially the increased temperature, is anticipated to reduce maize yield by an average of 14.5% in Harbin and 13.3% in Gongzhuling, and soybean yield by an average of 10.6%, across all the treatments and climatic scenarios. Conversely, a slight but not statistically significant average yield increase of 2.5% was predicted for spring wheat. SOC stock showed a decrease of 8.2% for Harbin and 7.6% for Gonghzuling by 2,100 under the RCP scenarios. Future climates also led to a reduction in CSE by an average of 6.0% in Harbin (except NPK) and 13.4% in Gongzhuling. In addition, the higher average crop yields, annual SOC stocks, and annual CSE (10.15–15.16%) were found when manure amendments were performed under all climate scenarios compared with the chemical fertilization. Soil CSE displayed an exponential decrease with the C accumulated input, asymptotically approaching a constant. Importantly, the CSE asymptote associated with manure application was higher than that of other treatments. Our findings emphasize the consequences of climate change on crop yields,

SOC stock, and CSE in the Mollisol regions, identifying manure application as a targeted fertilizer practice for effective climate change mitigation.

KEYWORDS

yield, SOC stock, carbon sequestration efficiency, Mollisols, SPACSYS model, long-term fertilization, climate change

1 Introduction

Mollisols, characterized by their thick, dark and well-structured surface horizon, stand out as one of the most fertile and productive soils on Earth (Durán et al., 2011). Comprising approximately 7% of the world's ice-free land surface, these soils account for 28.6% of global farmland across all soil types (Durán et al., 2011; Liu et al., 2012; Xu et al., 2020). Their unique characteristics make Mollisols exceptionally suitable for cultivating cereal crops and establishing pasture and forage systems (Durán et al., 2011; Xu et al., 2020), playing a vital role in agricultural productivity and global food security (Liu et al., 2012). Mollisols are primarily distributed in four regions: the majority of Russia and Ukraine (45%), the central plains of North America (29%), Northeast China (10%), and a substantial portion of South America (10%) (Liu et al., 2012; Xu et al., 2020). Mollisols face challenges due to the conversion of natural grassland to croplands and consecutive planting and tillage practices. These practices have resulted in insufficient carbon (C)inputs, leading to significant soil organic C (SOC) loss in these regions (Sanford et al., 2012). Reports indicate Mollisols in Russia and Ukraine have lost approximately 15–40% of their original organic C pool, while those in America and Northeast China have seen a decline of around 50% over the past several decades (Gollany et al., 2011; Xu et al., 2020). This accelerated land degradation is often accompanied by decreases in crop yield. For example, crop yields in North America have declined by 20–40% over the past century, as a result of unsustainable cultivation practices (Posner et al., 2008). Similarly, Mollisols in Northeast China have experienced a decrease in thickness of approximately 30–50 cm, with each 1 cm reduction corresponding to a 2% reduction in crop yield (Liu H. et al., 2013). In addition, even a slight reduction in C from the substantial SOC pool (approximately 4 Pg) in Mollisols could lead to significant CO_2 emissions within these regions (Cheng et al., 2010). For instance, the average C release rate from Mollisols in Northeast China ranged from 0.17 to 2.17 Tg C $yr.^{-1}$, significantly surpassing the global average of 0.09–0.78 Tg C $yr.^{-1}$ from the pedological C pool (Lal et al., 2007; Li et al., 2013). Therefore, strategic C sequestration in Mollisols is crucial not only for ensuring food security and promoting soil stability but also for effectively mitigating global climate change.

The potential to sequester C in soils depends not only on the quantity of C input but also on the retention coefficient of the applied C, a concept referred to as C sequestration efficiency (i.e., CSE, $\triangle$SOC/$\triangle$C input) (Stewart et al., 2007; Maillard and Angers, 2014). Stewart et al. (2007) established an asymptotically increasing relationship between C inputs and changes in SOC, based on data from 14 long-term experiments conducted over 12 to 96 years of fertilization. This highlighted a decreasing CSE as the soil approached C saturation (Hassink and Whitmore, 1997; Six et al., 2002). However, our previous study (Liang et al., 2023) indicated that CSE remained nearly constant within four decades of fertilization. This was accompanied by a linear relationship between C inputs and SOC changes, as validated by eight extensive long-term experimental datasets, including the Mollisol site at Gongzhuling. Therefore, a narrow range of C input levels, corresponding to shorter fertilization durations, did not necessarily reflect the full spectrum of linear-to-asymptotic behaviors for SOC content (Stewart et al., 2007), and, consequently, the CSE characteristics. Further, examining SOC dynamics that encompasses Mollisols across a broad range of C input levels is essential and urgent to comprehensively elucidate their CSE characteristics.

Optimal fertilizer practices play a critical role in promoting SOC restoration in degraded Mollisols (Xu et al., 2020). Manure application, especially when combined with chemical fertilizers, has demonstrated the potential to enhance CSE due to the beneficial effects of additional organic C and nutrients on soil fertility and soil structure (Liang et al., 2023). However, the sustainability of this benefit under long-term fertilization conditions as soil C approaches saturation requires further investigation. In addition, most Mollisol regions experience cool, moist, and semi-humid climates (Xu et al., 2020), and the warmer and wetter future climates in these regions might significantly impact SOC sequestration by influencing crop production and soil ecological processes (Chu et al., 2017; Lin et al., 2017). Thus, predicting SOC changes and crop yields (associated with C input) in Mollisols is necessary to explore the dynamics of CSE and its response to future climate change under different fertilization strategies.

Process-based models have become essential decision support tools for addressing climate change issues in agriculture management and production, as these models enable the integration of diverse data sources and knowledge concerning the impacts of phenological and environmental variables allowing for valuable evaluations of specific hypotheses and scenarios (Smith et al., 2005). Among the widely used process-based models, the SPACSYS model stands out for its comprehensive consideration of processes in C, nitrogen (N) and phosphorus (P) cycling. Numerous studies have demonstrated its robust capabilities in accurately simulating plant growth, N and P uptake, SOC and soil total nitrogen (TN) stocks, as well as CO_2 and N_2O emissions across cropland and grassland in diverse regions of Europe and China (Wu et al., 2015; Perego et al., 2016; Li et al., 2017; Liang et al., 2018). Furthermore, validated using data from the Broadbalk continuous wheat experiment over a century of fertilization, the SPACSYS model has successfully captured the dynamics of SOC stock in the plow layer (Liang et al., 2024). These results confirm the SPACSYS model's reliability in simulating SOC changes and crop yields in response to different long-term fertilization strategies and various climatic conditions. The Mollisol long-term experiments established in the 1980 s in Northeast China offer a valuable resource with well-documented and comprehensive records, detailing fertilization practices, cultivation methods, crop management, climate conditions, grain and straw yields, and soil properties. These detailed

records provide a solid foundation for the modeling study and enable accurate predictions of the impacts of fertilizer management and climate change on CSE.

In this study, we aimed to elucidate the responses of crop yield and CSE to climate change in the typical Mollsiol regions of China, while proposing a sustainable strategy to enhance both crop productivity and C sequestration. Specifically, firstly we initially calibrated and validated the SPACSYS model using data from two Mollisol long-term experiments in Northeast China. Subsequently, we quantified the impacts of various future climate scenarios and fertilizer application practices on crop yield, SOC stock, and CSE within the plow layer (0–20 cm) of Mollisols. Finally, we elucidated the comprehensive CSE characteristics when a substantial amount of C has accumulated in the future.

2 Materials and methods

2.1 Study sites background information

2.1.1 Study sites and experimental design

Two typical Mollisols long-term experiments located in Northeast China at Harbin (45°40′ N, 126°35′ E) and Gongzhuling (43°30′ N, 124°48′ E) have been selected for this study. The essential background information, including the locations, initial soil properties, cropping systems and climatic conditions, is given in Table 1. For both experiments, four fertilizer treatments common were chosen, namely (1) no fertilizer (CK), (2) combinations of chemical nitrogen (N), phosphorus (P) and potassium (K) fertilizers (NPK), (3) manure application (M), and (4) chemical fertilizers (N or NPK) plus manure (NM/NPKM) (refer to Supplementary Table S1 for details). Detail information can be found in the works of Jiang et al. (2014, 2018).

TABLE 1 General information and initial soil properties of two experimental sites.

Site	Harbin	Gongzhuling
Starting year	1979	1989
Location	45°40′ N, 126°35′ E	43°30′ N, 124°48′ E
Climate type	Mild temperate Semi-humid	Mild temperate Semi-humid
Annual temperature, °C	3.5	4.5
Annual precipitation, mm	533	595
Crop rotation system	Maize-soybean-wheat	Maize
Initial soil properties		
Initial SOC[a], g kg^{-1}	15.66	13.23
Total N[b], g kg^{-1}	1.47	1.40
Available N, mg kg^{-1}	151	114
Total P[c], g kg^{-1}	1.07	1.39
Olsen P, mg kg^{-1}	51	27.0
Total K[d], g kg^{-1}	25.16	22.1
Available K, mg kg^{-1}	200	190
pH	7.2	7.6
Bulk density, g cm^{-3}	1.37	1.19
Clay, %	30	32

[a]SOC means soil organic carbon.
[b]N means nitrogen.
[c]P means phosphorus.
[d]K means potassium.

2.1.2 Soil sampling and analysis

The soil samples of Gongzhuling in the plow layer (0–20 cm) were collected from 1989 to 2018 annually in approximately 15 days after harvest ($n = 28$ for each treatment). The soil samples of Harbin in the plow layer (0–20 cm) were collected annually from 1979 to 1988 and almost every 3 years from 1988 to 2018 in approximately 15 days after harvest ($n = 23$ for each treatment). The SOC content was determined using dichromate oxidation following the modified Walkley & Black method (i.e., heated for 12 min at 220°C) with a correction factor of 1.1 (Walkley and Black, 1934; Xu et al., 2016). While the factor may vary between samples with and without manure applications, a very high heating temperature of 220°C results in a nearly complete oxidation of the organic carbon, and as such, also the more recalcitrant fractions. This strongly limits the potential error introduced to the application of it across all treatments. In this context, we assumed that the error introduced in SOC measurements due to variations in the correction factor among the different treatments could be considered negligible.

2.2 Model parameterization and prediction

2.2.1 Model description

The SPACSYS model is a field-scale, weather-driven with flexible time steps (ranging from minutes to daily), employing a process-based approach that quantifies the biogeochemical processes related to C, N, and P cycling, as well as the water and heat budgets within the soil-plants-and atmosphere continuum. In the current version (6.0) the model incorporates the Farquhar method for photosynthesis (Yin and Struik, 2009) coupled with a modified stomatal conductance sub-model based on Leuning et al. (1995) and Tuzet et al. (2003). This integration enables simulation of the plant photosynthesis rates accounting for the impacts of atmospheric CO_2 concentration on photosynthesis and transpiration.

Compared to other widely cited process-based simulation models, SPACSYS stands out due to its detailed representation biogeochemical processes (refer to Supplementary Table S2) and a substantial number of organic matter pools (five). Additionally, SPACSYS includes a detailed root architecture that significantly influences nutrients and water capture, comprehensive descriptions of above- and below-ground plant growth and a nutrient recycling (Wu et al., 2007). More information about SPACSYS can be found in previous articles (Wu et al., 2007, 2015; Bingham and Wu, 2011).

2.2.2 Calibration, validation, and prediction

SPACSYS was operated from the starting year of the experiments (1979 for Harbin and 1989 for Gongzhuling) until 2020 using a daily time-step. Daily weather data (maximum and minimum temperatures, precipitation, wind speed, relative humidity, and solar radiation) were obtained as inputs from the National Meteoritical Information Center.[1] Agronomic management details including soil

1 http://data.cma.cn/

work (plowing depth and date), plant management (seeding and harvesting dates), and fertilizer application (date, amount and type) for each treatment in the Harbin and Gongzhuling long-term experiments, were sourced from records maintained by the Heilongjiang Academy of Black Soil Conservation and Utilization and Jilin Academy of Agricultural Sciences, respectively. Soil properties in the top 20 cm deep at each site (Table 1) were acquired through field surveys. Other missing properties that the model required were estimated from soil texture using pedo transfer functions (PTFs) implemented in the model. The atmospheric CO_2 concentration was set from 330 to 380 ppm for Harbin and from 348 to 380 ppm for Gongzhuling, following a linear increase over the experimental period, as per IPCC (2021) guidelines. Grain yields and straw dry matter (if recorded) of maize, wheat and soybean, as well as SOC and total nitrogen (TN) stocks from the NPK and NPKM/NM treatments, were randomly chosen for the model calibration. Data from the other treatments served for model validation. Parameters related to C and N cycling, soil water movement, heat transformation, and plant photosynthesis were adopted from previous studies (Bingham and Wu, 2011; Wu et al., 2015; Liu et al., 2020). The parameters related to the manure decomposition and transformation were from our previous reports (Zhang et al., 2016; Liang et al., 2018). The built-in Multi-Objective Shuffled Complex Evolution Metropolis algorithm (MOSCEM-UA) (Vrugt et al., 2003) was applied to determine the other parameters, primarily those linked to phenology and vegetation characteristics. The optimized parameters and their values for maize, wheat, soybean, and soil C and N cycling are listed in Supplementary Tables S3, S4.

For crop yield and SOC predictions, four climate scenarios were considered, encompassing the baseline and three representative concentration pathways (RCP 2.6, RCP 4.5, and RCP 8.5; Riahi et al., 2011; van Vuuren et al., 2011). The baseline scenario involved historic meteorological data rotated between 1979 and 2020 for Harbin and between 1989 and 2020 for Gongzhuling with a constant CO_2 concentration of 380 ppm. Weather data for the RCP scenarios between 2021 and 2,100 were extracted from the HadGEM2-ES model with a spatial resolution of 0.5° × 0.5° (Collins et al., 2011; Jones et al., 2011). The annual average of maximum and minimum temperatures, precipitation, and CO_2 concentration under the three RCP scenarios are shown in Supplementary Figure S1 and Supplementary Table S5. The climate projections indicated warmer and wetter future conditions in the studied regions, with average increases of 0.8–3.5°C and 0.4–2.5°C observed in Harbin and Gongzhuling, respectively, when compared to the baseline. The mean annual precipitation (MAP) was projected to rise by 43–121 mm in Harbin and 137–207 mm in Gongzhuling. The RCP 8.5 scenario demonstrated the most significant alteration, nearly doubling CO_2 concentrations by 2,100.

Crop varieties and field management practices were fixed as identical to those before 2021 for both sites and scenario. To simplify the assessment of future climate change on crop phenology and yield, the sowing dates were fixed on 30th April for maize, 23rd April for wheat, and 29th April for soybean in Harbin and 26th April in Gongzhuling each year in this study. Harvest dates were determined based on simulated physiological maturity. Simulations were run for each of the four treatments under the various proposed climate scenarios.

2.3 Soil carbon sequestration rate and efficiency

2.3.1 Soil organic carbon sequestration rate

Since SOC predominately undergoes changes in the plow layer (0–20 cm) in Mollisol (Liang et al., 2009), our report concentrates on SOC within this layer. The SOC sequestration rate in the plow layer of the field with fertilization (C_r, t C ha^{-1} yr.$^{-1}$) in year t is calculated using the Equation (1) as follows:

$$C_r = \frac{SOC_F - SOC_{CK}}{t} \quad (1)$$

where SOC_F and SOC_{CK} are the SOC stock in the layer for the NPK, NPKM, NM, or M treatment and the CK treatment in year t, respectively.

2.3.2 Carbon sequestration efficiency

CSE for a fertilization treatment is defined as the percentage of the SOC stock change relative to the net C input between the treatment and CK (Jiang et al., 2018). It is calculated using the Equation (2) as follows:

$$CSE\,(\%) = \frac{SOC_F - SOC_{CK}}{\sum_{i=1}^{t}\left(C_{I-F} - C_{I-CK}\right)} \times 100\% \quad (2)$$

where $C_{I\text{-}F}$ and $C_{I\text{-}CK}$ are the annual C input rate for a fertilization treatment (NPK, NPKM, NM, or M) and CK, respectively, which are the cumulative amounts in both manure and crop residue.

2.4 Statistical analysis

We used three statistical criteria to evaluate the model performance: (1) the coefficient of determination (R^2) that measures the degree of agreement between simulation and observation; (2) the root mean squared error (RMSE), providing a measure of the average deviation of the estimates from observed values; and (3) the relative error (RE) that reflects the overall difference between simulated and observed data.

Two-way analysis of variance (ANOVA) and Tukey tests ($p < 0.05$) were used to compare the effects of fertilizer practices and future climate scenarios on grain yield, SOC stock, C input, and CSE. All statistical analyses were conducted using SPSS 24.0 (SPSS, Inc., 2017, Chicago, United States).

3 Results

3.1 Model calibration and validation

The simulated crop yields for different treatments at both sites closely aligned with observations, demonstrating an RMSE below 24% (Supplementary Figures S2–S5; Table 2). Linear regression analysis further revealed a satisfactory correlation between the observed and

simulated values ($R^2 > 0.54$) (Figure 1), despite a tendency for the model to overestimate low observed yields and underestimate high observed ones. It was noted that SPACSYS underestimated maize grain and straw yields at Gongzhuling by an average of 16 and 20%, respectively, from 2010 to 2012 (Supplementary Figure S3).

Moreover, SPACSYS effectively simulated SOC and TN stocks, with R^2 values ranging from 0.60 to 0.79 and RMSE ranging from 6.8 to 8.2% (Figure 1; Table 2). This favorable agreement with measurements is particularly evident in the first decade of the simulation period (Supplementary Figures S4, S5). In general, the model exhibited a 20% underestimation of SOC stock and a 37% underestimation of TN stock during model validation (Figure 1). However, it overestimated TN stock by an average of 7.3% for CK, 10.2% for NPK, 8.5% for NM, and 9.0% for M after 2000 in Harbin (Supplementary Figure S4).

3.2 Crop yield and SOC stock

Average yields of wheat, maize, and soybean from 2021 to 2,100 under each climate scenario with different fertilizer practices are shown in Figure 2. Notably, a slight but not statistically significant average yield increase of 2.5% was predicted for spring wheat ($p < 0.05$). Under all climate scenarios, there was also no significant difference ($p < 0.05$) between the NPK and NPKM/NM fertilizer treatments for maize (1005–12,101 vs. 1,112–12,573 kg ha^{-1}), wheat (2729–5,548 vs. 2,727–5,287 kg ha^{-1}), and soybean (975–4,314 vs. 1,024–4,350 kg ha^{-1}) at both sites. However, the yields for these treatments were significantly higher than those for the M and CK treatments ($p < 0.05$). Compared with the baseline, the maize yield decreased by an average of 14.5 and 13.3% for Harbin and Gongzhuling, respectively, across all RCP scenarios and under all considered fertilizer practices (Table 3). The decreases in maize yield under the RCP scenarios were ranked as follows: RCP 8.5 (20.6–40.8%) > RCP 4.5 (5.5–25.4%) > RCP 2.6 (0.1–7.8%). The soybean yield decreased by 10.6% on average in Harbin, with the highest decline under RCP 8.5 ($p < 0.05$) (Table 3).

SOC stock decreased by 8.2% in Harbin and 7.6% in Gongzhuling by 2,100 across all RCP scenarios and fertilizer treatments when compared with the baseline (Figure 3; Table 3). The decline under RCP 8.5 (10.5–15.6%) was significantly higher than those under RCP 4.5 (5.3–8.5%) and RCP 2.6 (3.9–6.8%). The ranking of SOC stocks in 2100 was generally as follows: baseline > RCP 2.6 > RCP 4.5 > RCP 8.5. In addition, manure amendment resulted in the highest SOC stock among the treatments, with the values of 38.9–50.3 t C ha^{-1} in Harbin and 60.6–69.2 t C ha^{-1} in Gonghzuling, respectively ($p < 0.05$) (Table 3).

3.3 Annual carbon input and SOC sequestration rate

The average annual C inputs from different sources under different fertilizer practices are presented in Figure 4. When considering the impacts of future climate change on C inputs, compared with the baseline, the C inputs from crops decreased by an average of 2.8% in Harbin and 9.5% in Gongzhuling under all RCP scenarios (Supplementary Table S6). For total C input, no significant difference was observed between the baseline and RCP 2.6 for all treatments, and the lowest C input was observed under RCP 8.5.

Soil C sequestration rates for various fertilization treatments across the different periods are shown in Table 4. The rates for manure-amended treatments exceeded those without manure ranging from 62 to 154 kg C ha^{-1} yr.$^{-1}$ in Harbin and 311 to 429 kg C ha^{-1} yr.$^{-1}$ in Gongzhuling. Furthermore, the rates for NPK and NPKM/NM fertilizer practices in Gongzhuling were higher than

TABLE 2 Statistical criteria of model performance for crop grain yield, straw dry matter, and SOC and TN stocks.

Index	Calibration	Validation	Calibration	Validation
	Maize grain yield		Maize straw dry matter	
R^2	0.58**	0.58**	0.72**	0.60**
RMSE (%)	15	23	16	15
RE (%)	−12	−11	9	4
n	81	54	56	28
	Wheat grain yield[a]		Soybean grain yield[a]	
R^2	0.66**	0.60**	0.54**	0.56**
RMSE (%)	21	17	23	18
RE (%)	−7	−6	−24	−11
n	26	26	26	26
	SOC stock		TN stock	
R^2	0.79**	0.71**	0.67**	0.60**
RMSE (%)	8.2	6.8	8.6	7.5
RE (%)	−0.8	0.4	−2.0	−3.3
n	102	79	102	79

[a]There was no record about the wheat and soybean straw dry matter in the Harbin long-term experiment.
**means $p < 0.01$.

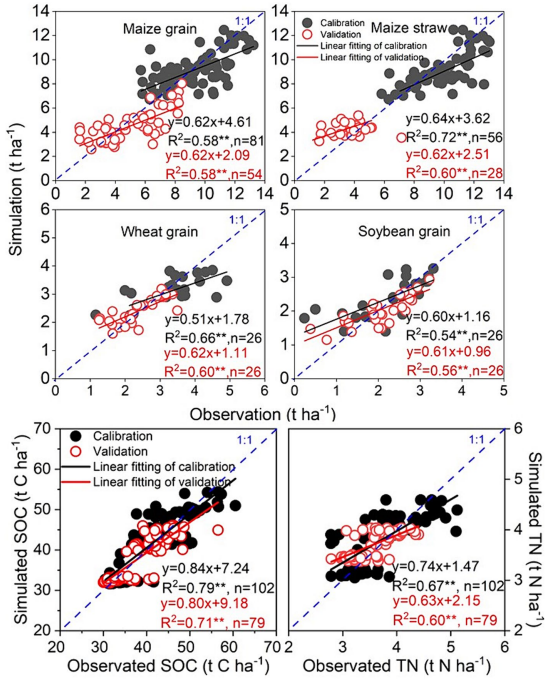

FIGURE 1
Comparison between simulated and observed grain yields and straw dry matter of maize, wheat and soybean for model calibration and validation. Note: wheat and soybean were only planted in Harbin, and data on straw dry matter for all crops in Harbin are unavailable.

those in Harbin. Overall, the rates under the RCP scenarios were lower than those under the baseline, with the lowest rates observed under RCP 8.5.

3.4 Carbon sequestration efficiency

As outlined in Table 3, the annual CSE averaged over the simulation period showed significantly reduction compared to the baseline across RCP scenarios at both sites (except those for NPK in Harbin). The decreased CSE due to climate change was 6.0% in Harbin (except for NPK) and 13.4% in Gongzhuling. In Harbin, excluding NPK, the CSE values were ranked as follows: baseline > RCP 2.6, RCP 4.5 ≥ RCP 8.5 ($p < 0.05$). Among the treatments, those with manure amendment (10.15–15.16%) were higher than those for NPK (3.99–6.68%).

The relationship between CSE and cumulative C input (C_{input}) was accurately captured by an exponential decreasing function ($CSE = b + a \times e^{-k \times Cinput}$, $p < 0.001$) for all the treatments (Figure 5; Table 5). The CSE asymptotic value, denoted by the parameter 'b' in the function, consistently exhibited higher values for M (Harbin: 7.62–9.78%) and NM/NPKM (Harbin: 9.80–11.29% and Gonghzuling: 8.93–10.91%) under all climate scenarios compared to NPK (Harbin: 3.54–4.54% and Gongzhuling: 5.29–6.36%). In addition, the asymptotic CSE values under all RCP scenarios (5.29–10.61%) generally were lower than those under the baseline (6.36–11.29%) for the majority of treatments in both Harbin (except for NPK) and Gongzhuling.

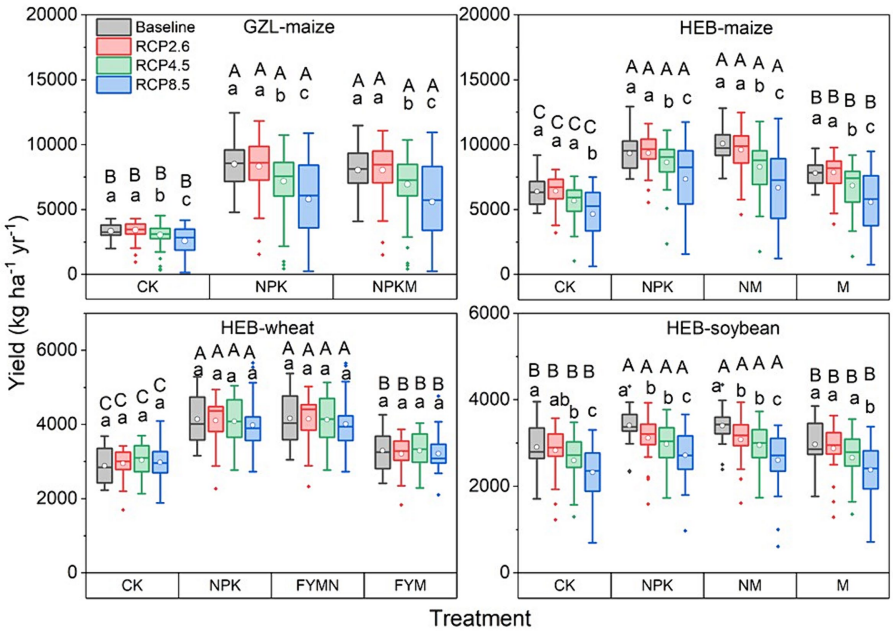

FIGURE 2
Boxplots of simulated grain yields of maize, wheat and soybean with various fertilizer practices under future climate scenarios between 2021 and 2,100 in Harbin (HEB) and Gongzhuling (GZL). Different lowercase letters over the boxes indicate significant difference ($p < 0.05$) under different climate scenarios for a specific fertilizer treatment, and different capital letters over the boxes indicate significant difference ($p < 0.05$) among different fertilizer treatments under a specific climate scenario.

TABLE 3 Relative change of crop yield (%) and average annual CSE (%) between 2021 and 2,100, annual SOC stock in 2100 (t C ha^{-1}), and their relative changes (%) with each fertilizer treatments under RCP climate scenarios compared with the baseline.

Treatment	Harbin								Gongzhuling				
	Climate scenario	Maize $Yield_C$[a]	Wheat $Yield_C$	Soybean $Yield_C$	SOC	SOCc[b]	CSE	CSE_C[c]	Maize $Yield_C$	SOC	SOCc	CSE	CSEc
CK	Baseline				35.88					29.12			
	RCP2.6	3.76	5.39	1.26	34.43	−4.02			5.27	27.82	−4.46		
	RCP4.5	−8.83	8.58	−8.72	33.99	−5.26			−6.16	27.31	−6.23		
	RCP8.5	−26.79	6.46	−19.89	31.36	−12.59			−20.60	26.06	−10.51		
NPK	Baseline				37.77		3.99bC			33.92		6.68aB	
	RCP2.6	2.42	2.14	−6.62	36.14	−4.32	4.28bC	7.78	1.98	32.57	−3.98	5.65bB	−15.61
	RCP4.5	−5.53	1.65	−11.61	35.64	−5.65	4.36bC	9.65	−11.64	31.65	−6.69	5.80bB	−13.03
	RCP8.5	−20.66	−1.12	−21.13	33.37	−11.65	5.02aC	26.56	−28.46	30.07	−11.35	5.65bB	−15.43
NM/NPKM	Baseline				50.31		12.16aA			69.19		15.16aA	
	RCP2.6	−7.82	2.48	−4.13	46.91	−6.76	11.49bA	−5.36	3.97	66.01	−4.60	13.44bA	−11.52
	RCP4.5	−25.41	2.44	−8.15	46.03	−8.51	11.41bA	−6.08	−9.55	63.51	−8.20	13.41bA	−11.69
	RCP8.5	−40.77	−1.44	−20.04	42.45	−15.63	11.22cA	−8.32	−27.10	60.56	−12.46	13.16cA	−13.30
M	Baseline				45.34		11.42aB						
	RCP2.6	−0.14	0.41	0.55	43.57	−3.90	10.94bB	−3.92					
	RCP4.5	−13.32	1.95	−8.65	42.47	−6.33	10.76bB	−5.86					
	RCP8.5	−30.87	0.42	−20.00	38.85	−14.31	10.15cB	−11.98					

[a]Yieldc means the relative change of crop yield under an individual RCP scenario to the baseline (%).

[b]SOCc means the relative change of SOC stock under an individual RCP scenario to the baseline (%).

[c]CSEc means the relative change of CSE under an individual RCP scenario to the baseline (%).Numbers with different lowercase letters indicate significant difference ($P < 0.05$) in an individual fertilizer treatment under different climate scenarios and those with different capital letters indicate significant difference ($p < 0.05$) among different fertilizer treatments under an individual climate scenario.

10.3389/fsufs.2024.1332483

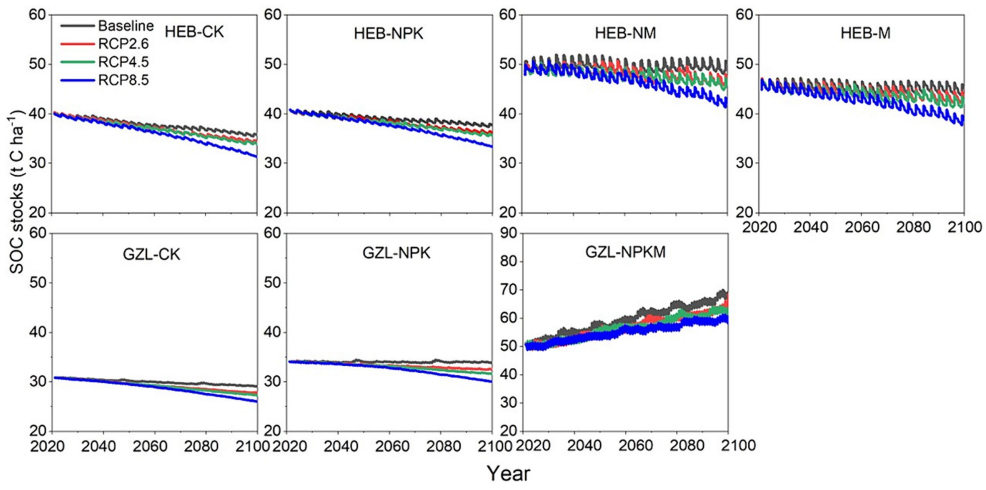

FIGURE 3
Simulated dynamics of soil organic carbon (SOC) stocks with different fertilization practices under future climate scenarios from 2021 and 2,100 in Harbin (HEB) and Gongzhuling (GZL).

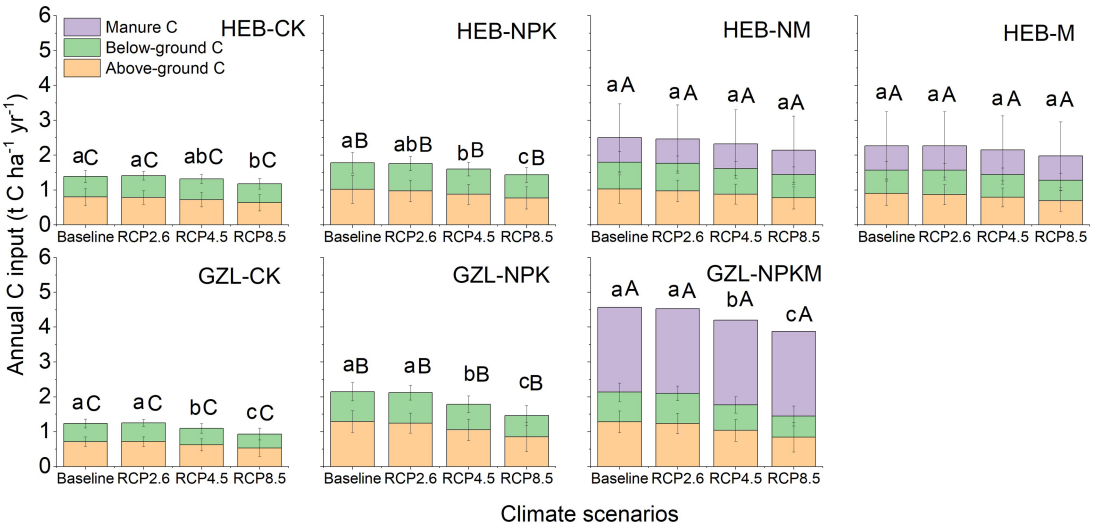

FIGURE 4
Average annual carbon (C) inputs from different sources with different fertilizer practices in Harbin (HEB) and Gonzghuling (GZL). Different lowercase letters over the columns indicate significant difference ($p < 0.05$) in total annual C input among different RCP scenarios under a specific treatment at a site, and different capital letters over the columns indicate significant difference ($p < 0.05$) in total annual C input among different fertilizer treatments under a specific climate scenario at a site.

4 Discussion

4.1 Model performance

Our results highlight that SPACSYS emerges as a competitive model for simulating maize yield in typical Mollisol regions of Northeast China achieving R^2 values of 0.58–0.72 (Figure 1; Table 2). This performance compares favorably with the PRYM-Maize model ($R^2 = 0.57$) and the CERES-Maize ($R^2 = 0.80$) model (Jiang et al., 2021; Zhang et al., 2021). Similarly, SPACSYS demonstrated a competitive soybean yield simulation with an RMSE of 18–23%, comparable to the performance of the DSSAT model with an RMSE of 15–22% in Northeast China (Liu S. et al., 2013). It should be noted that SPACSYS has previously employed for simulating winter wheat yield (Liang et al., 2018; Liu et al., 2020), and our study further validates its effectiveness in simulating spring wheat, expanding the application scope of SPACSYS. Furthermore, SPACSYS adequately simulated SOC stocks in the study regions for all treatments (Figure 1; Supplementary Figures S3, S4; Table 2), despite underestimating SOC stocks by 20% during validation. Jiang et al. (2014) applied the Roth-C model to the same sites, our study demonstrated superior performance with R^2 values of 0.79 for calibration and 0.71 for validation, while

TABLE 4 Soil organic carbon sequestration rates (kg C ha^{-1} $yr.^{-1}$) for various fertilization treatments across the different periods.

Treatment	Climate scenario	Harbin		Gongzhuling	
		2021–2060	2061–2,100	2021–2060	2061–2020
NPK	Baseline	15.7	15.7	57.1	43.2
	RCP2.6	15.4	14.1	57.0	42.8
	RCP4.5	15.1	13.7	55.3	39.1
	RCP8.5	16.8	16.6	54.5	36.1
NM/NPKM	Baseline	154.0	119.3	429.0	361.0
	RCP2.6	147.3	103.1	400.3	344.0
	RCP4.5	138.0	99.5	401.4	326.2
	RCP8.5	141.8	91.6	397.1	310.8
M	Baseline	98.5	78.2		
	RCP2.6	95.7	75.5		
	RCP4.5	96.3	70.1		
	RCP8.5	88.2	61.9		

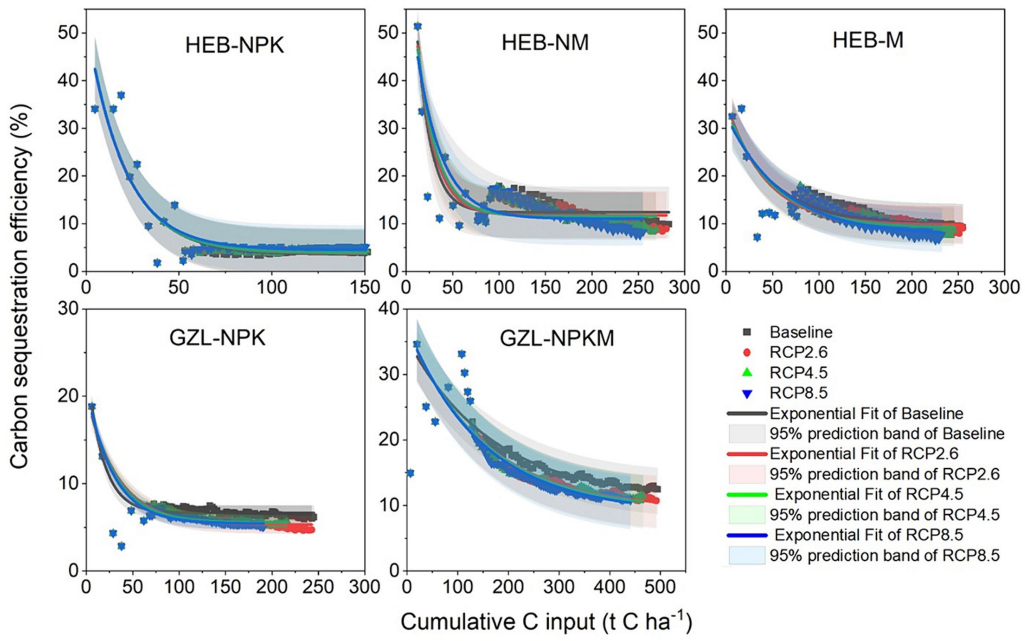

FIGURE 5
Dynamics of carbon sequestration efficiency (CSE) with carbon input cumulation for all fertilizer practices from the beginning to 2,100 under future climate scenarios in Harbin (HEB) and Gongzhuling (GZL).

Roth-C achieved R^2 values of 0.25 for Harbin and 0.77 for Gongzhuling. In terms of TN stock, SPACSYS also performed well with R^2 values of 0.60–0.67 and RMSE of 7.5–8.6% (Table 2), surpassing the GWRK model ($R^2 = 0.50$ and RMSE = 29%) when applied to data from the central Northeast China, including Gongzhuling (Li et al., 2020).

Nevertheless, the model still exhibited certain inevitable errors. For example, it consistently overestimated TN stock for all treatments after 2000 in Harbin. This discrepancy could be partially due to the relocation of the long-term experiment in Chi et al. (2016), despite the soil at a depth of 1.5 m being transferred under frozen soil conditions. Moreover, the model's excessive reliance on stomatal resistance to soil water could lead to underestimations of maize grain and straw yields (Supplementary Figure S3) during the prolonged droughts from April to June in 2010, 2011 and 2012 in Gongzhuling. In addition, the extreme drought experienced after flowering in 2008, with the precipitation about 80–100 mm lower than those of adjacent years in Harbin, might have contributed to the overestimation of soybean yield by 2.5 times (Supplementary Figure S2). Improvements are needed in the model's representation of how drought impacts crop growth and development in future iterations.

TABLE 5 Relationship between carbon sequestration efficiency (CSE) and cumulative carbon input to the plow soil layer over the simulation period in Harbin and Gongzhuling.

Site	Treatment	Climate scenario	Model
HEB	NPK	Baseline	$CSE = 3.54 + 49.08e^{-0.048Cinput}$
		RCP2.6	$CSE = 3.75 + 48.65e^{-0.048Cinput}$
		RCP4.5	$CSE = 3.87 + 48.97e^{-0.049Cinput}$
		RCP8.5	$CSE = 4.54 + 48.24e^{-0.050Cinput}$
	NM	Baseline	$CSE = 11.29 + 47.40e^{-0.030Cinput}$
		RCP2.6	$CSE = 10.61 + 49.08e^{-0.031Cinput}$
		RCP4.5	$CSE = 10.40 + 48.05e^{-0.029Cinput}$
		RCP8.5	$CSE = 9.80 + 45.09e^{-0.025Cinput}$
	M	Baseline	$CSE = 9.78 + 23.47e^{-0.020Cinput}$
		RCP2.6	$CSE = 9.74 + 25.79e^{-0.023Cinput}$
		RCP4.5	$CSE = 9.14 + 25.23e^{-0.021Cinput}$
		RCP8.5	$CSE = 7.62 + 25.19e^{-0.017Cinput}$
GZL	NPK	Baseline	$CSE = 6.36 + 17.09e^{-0.056Cinput}$
		RCP2.6	$CSE = 5.29 + 14.78e^{-0.029Cinput}$
		RCP4.5	$CSE = 5.53 + 15.14e^{-0.033Cinput}$
		RCP8.5	$CSE = 5.43 + 15.69e^{-0.035Cinput}$
	NPKM	Baseline	$CSE = 10.91 + 24.52e^{-0.006Cinput}$
		RCP2.6	$CSE = 9.50 + 27.54e^{-0.007Cinput}$
		RCP4.5	$CSE = 9.29 + 27.86e^{-0.007Cinput}$
		RCP8.5	$CSE = 8.93 + 28.30e^{-0.007Cinput}$

4.2 Climate and fertilizer impacts on crop yield

In our study, climate change was projected to decrease maize yield in the typical Mollisol regions of Northeast China. The increased temperature might be the primary factor contributing the decline in maize yield, inducing crop early development (i.e., anthesis precocity) and accelerating the reproductive stage compared to the cooler conditions under the baseline (Supplementary Figure S6). While a warming climate might alleviate the effects of chilling damage on maize growth in Harbin and Gongzhuling, our study supported the previous conclusion that the overall impact of future temperatures would be more negative than positive for maize growth (Lin et al., 2017). Furthermore, several studies have suggested that the maize yield increase resulting from the "CO_2 fertilization effect" could not offset the reduction caused by the increased temperature in study regions of Northeast China (Wang et al., 2011; Lin et al., 2017; Jiang et al., 2021). Consequently, future climate was expected to significantly decrease maize yield in the Mollisol regions of Northeastern China, especially at the end of the simulation period (2090–2,100) under RCP 8.5 (57.6–69.2% for Harbin and 54.8–67.1% for Gongzhuling), coinciding with the largest increments in both CO_2 concentration and temperature (Supplementary Table S7).

The decrease in soybean yield in Harbin was less pronounced (10.6%) compared to maize (14.5%). According to Jin et al. (2017), the impact of enhanced CO_2 concentration on offsetting yield gaps caused by changes in temperature and precipitation is more substantial for soybean than for maize. On the other hand, earlier studies have indicated that soybean yield in Northeast China could potentially increase with rising precipitation and temperature, considering the effects of "CO_2 fertilization" (Yin et al., 2015; Lin et al., 2017). However, our findings corroborate previous studies (Jin and Zhu, 2008; Guo et al., 2022) when temperatures reach high levels (e.g., a 4°C increase) as projected at our study sites. The maximum temperature enhancement under RCP 4.5 was generally above 4°C after 2080 and ranged from 4.0 to 8.5°C after 2060 under RCP 8.5 (Supplementary Figure S1). In such conditions, soybean yield would decline without cultivar improvement in response to temperature extremes, leading to a reduction in the number of grains by shortening the grain-filling period. Climate change did not significantly affect spring wheat yield in the study regions, being consistent with the earlier reports (Jin and Zhu, 2008; Yin et al., 2015). The anticipated warmer climate is expected to result in a shortened growing period, leading to a diminished accumulation of photosynthate (Supplementary Figure S6). For major C3 crops, the current atmosphere CO_2 concentration constrains crop photosynthesis. Elevated CO_2 concentration can increase crop net photosynthesis by increasing the availability of intercellular CO_2 as a substrate and restraining competition with photorespiration for the Rubisco enzyme (Dermody et al., 2008).

4.3 Response of the carbon sequestration to climate change

Our simulations revealed a significant decrease in SOC stock under all future climate scenarios, consistent with previous studies conducted in Mollisol regions (Gao et al., 2008; Ramírez et al., 2019; Bao et al., 2023). The decline in C input for each fertilizer practice, due to the reduction of maize and soybean productions under the RCP scenarios, likely played a predominant role in the SOC decline. Consequently, SOC stock under RCP 8.5 was significantly lower than those under RCP 4.5 and RCP 2.6 ($p < 0.05$). Furthermore, the combined application of manure with chemical N treatments simultaneously showed the highest SOC stock and crop yield at both sites under each climate scenario (Figures 2, 3; Table 3). It has been reported that manure combined with chemical fertilizer treatment has the beneficial effects of both C inputs and readily available nutrients for plant growth, enhancing C inputs from crop residues and sequestrating a greater amount of C compared to other treatments (Triberti et al., 2016; Jiang et al., 2018; Gross and Glaser, 2021). Notably, the impact of fertilization on SOC stock was more pronounced with the manure-only treatment compared to NPK. The significantly higher annual C input (Figure 4) could be the primary reason for the observed difference, along with the very close amount of C inputs from crop residues for both treatments (Supplementary Table S6). However, a contrary conclusion was found when C inputs from manure into croplands were transferred from other ecosystems within the same region, rather than relying on consistent C inputs from fertilization (Schmidt et al., 2011).

Our results showed that fields with manure application had greater efficiencies in C sequestration than those receiving chemical fertilizer alone. Applied manure creates a favorable growth environment for plants and microorganisms (Mandal et al., 2007). Our simulations demonstrated that manure amendments led to

increased C inputs and microbial biomass. Those might be beneficial for retaining massive amounts of total C in the Mollisol regions of Northeast China (Yu et al., 2006; Ding et al., 2016; Wang et al., 2020). Consistently, compared to the practice using chemical fertilizer alone, manure application exhibited significantly higher SOC stocks and change rates (Figure 3; Table 4), supporting a higher value of CSE.

Our investigation revealed a pronounced negative exponential correlation between CSE and the cumulative C input. Specifically, CSE showed an initial rapid decline following the onset of C input, then a decelerated decrease, ultimately settling into a slow decay until reaching a stable asymptotic value with a substantial accumulation of C input. This dynamics pattern has been directly or indirectly supported by previous findings (Stewart et al., 2007, 2008; Yan et al., 2013; Maillard and Angers, 2014; Jiang et al., 2018). Stewart et al. (2007), in their synthesis of data from 14 long-term experiments in the USA and Canada, identified an asymptotic increase in the relationship between C inputs and SOC content, ascribable to the soil C saturation phenomena at high C inputs. Furthermore, Stewart et al. (2008) proposed that the stabilization efficiency of added C would decrease with increasing C input levels. These studies collectively supported our observation of a negative exponential relationship between CSE and C inputs. Warmer and wetter environmental conditions are likely to enhance the mineralization rate of added C (Fang et al., 2022; Bao et al., 2023), leading to a reduction in CSE. Our predictions indicated that the soil respiration rate under the RCP scenarios which soil temperature is a primary control factor increased 3.10–9.36% in Gongzhuling and 1.67–16.18% in Harbin compared to the baseline (Supplementary Table S8). Similar findings have been reported (Wang et al., 2022).

Notably, the average annual CSE for NPK under future climate scenarios in Harbin increased, contrasting with the absence of such a trend in Gongzhuling (Table 3). The incorporation of soybean into the crop rotation in Harbin likely contributed to the divergent responses observed in CSE. Biologically fixed N by soyabean can be available for subsequent crops, which can increase biomass accumulation in non-leguminous crops within the rotation (Stagnari et al., 2017). This results in an increase of C input to the soils. Additionally, root exudation and senescence of legume roots and nodules further contribute to the C input to the soils, offering benefits for SOC sequestration (Virk et al., 2022). The findings suggested that integrating leguminous crop in a rotation cropping system could contribute to improved C retention in soils, especially in situations where manure is not readily available.

4.4 Adaptation strategies for climate change

In our study, the average CSE for NPKM/NM/M treatments ranged from 9.54 to 15.16%, aligning closely with the reported global manure C conversion ratio of 12±4%, derived from a meta-analysis of 130 observations spanning 4–82 years of manure applications (Maillard and Angers, 2014). Furthermore, predictions regarding the CSE of manure application in the soils of 20 long-term experiments in China, including the two Mollisols examined in our research, indicated that CSE approaching the stable stage ranged from 8.8 to 10.4% under baseline and RCP 4.5 conditions (Jiang et al., 2018). Our findings, ranging from 9.1 to 11.3%, closely resembled these results (Table 5). This suggested that our results can serve as a useful reference for investigating the characteristics of CSE under long-term fertilization conditions in Chinese Mollisols, especially with a substantial amount of C input. Our predictions indicated a worse situation for both food security and soil fertility for Mollisols in the future, in comparison to the current condition. In addition to spring wheat, the production of maize and soybean, which are the primary crops in the world's Mollisol regions (Durán et al., 2011; Xu et al., 2020), would decline under future climate change. In addition, the goal of sequestrate more C in Mollisols to mitigate global warming cannot be achieved through the sole application of chemical fertilizers, as both the SOC sequestration rate and CSE decreased under all climatic scenarios. To address this, our predictions suggest the following interventions: (1) the development of new cultivars that better adapt to the anticipated warmer and wetter climates; (2) an earlier planting of crops to prevent the negative effects of heat and drought during the growing season; and (3) the optimization of nutrient application rates and the ratio of chemical fertilizers to manure.

5 Conclusion

Our study successfully validated the SPACSYS model for simulating yields of maize, spring wheat and soybean, and the SOC stock in typical Mollisol regions in China. SPACSYS predicted a decline in both yields and SOC stock under future climate scenarios compared with the baseline. The anticipated reduction in maize and soybean yields was primarily attributed to increased temperatures with maize being more significantly affected than soybean. Interestingly, the warmer and wetter future had no significant effects on spring wheat yield in this region. Future climate conditions led to a decrease in SOC stocks and CSE at the two typical Mollisol sites for fertilization treatments. Our prediction confirmed that CSE initially decreased rapidly following C inputs, exhibited a decelerated decline, and eventually decayed slowly until reaching a stable asymptotic value due to substantial C accumulation. Notably, the combined application of manure and chemical fertilizers demonstrated the highest potential to mitigate the negative impacts of climate change on crop yields and CSE. Our findings suggest that future research should prioritize improving crop cultivars, optimizing planting timings, and establishing effective fertilizer management strategies to mitigate climate change risks in Mollisol regions.

Data availability statement

The original contributions presented in the study are included in the article/Supplementary material, further inquiries can be directed to the corresponding authors.

Author contributions

SL: Conceptualization, Data curation, Formal analysis, Methodology, Software, Writing - original draft, Writing - review & editing. NS: Conceptualization, Funding acquisition, Supervision, Writing – review & editing. BL: Methodology, Supervision, Writing – review & editing. JM: Methodology, Supervision, Writing – review & editing. XM: Data curation and Writing – review & editing. HG: Data curation and Writing – review & editing. XZ: Methodology and

Writing – review & editing. LQ: Funding acquisition and Writing – review & editing. GC: Methodology, Supervision, Writing – review & editing. MX: Conceptualization, Funding acquisition, Supervision, Writing – review & editing. LW: Conceptualization, Methodology, Writing – review & editing.

Funding

The author(s) declare that financial support was received for the research, authorship, and/or publication of this article. This study was supported by the National Key Research and Development Program of China (2021YFD1500205) and the National Natural Science Foundation of China (42177341). SL was supported by the China Scholarship Council (No. 202003250099).

Acknowledgments

We acknowledge the Chinese Academy of Agricultural Sciences - Gembloux Agro-Bio Tech joint PhD program and all the colleagues from the long-term fertilization experimental sites for their unremitting assistance.

Conflict of interest

The authors declare that the research was conducted in the absence of any commercial or financial relationships that could be construed as a potential conflict of interest.

The author(s) declared that they were an editorial board member of Frontiers, at the time of submission. This had no impact on the peer review process and the final decision.

Publisher's note

Supplementary material

The Supplementary material for this article can be found online at: https://www.frontiersin.org/articles/10.3389/fsufs.2024.1332483/full#supplementary-material

References

Bao, Y., Yao, F., Meng, X., Fan, J., Zhang, J., Liu, H., et al. (2023). Dynamic modeling of topsoil organic carbon and its scenarios forecast in global Mollisols regions. *J. Clean. Prod.* 421:138544. doi: 10.1016/j.jclepro.2023.138544

Bingham, I. J., and Wu, L. (2011). Simulation of wheat growth using the 3D root architecture model SPACSYS: validation and sensitivity analysis. *Eur. J. Agron.* 34, 181–189. doi: 10.1016/j.eja.2011.01.003

Cheng, S., Fang, H., Zhu, T., Zheng, J., Yang, X., Zhang, X., et al. (2010). Effects of soil erosion and deposition on soil organic carbon dynamics at a sloping field in Black soil region, Northeast China. *Soil Sci. Plant Nutr.* 56, 521–529. doi: 10.1111/j.1747-0765.2010.00492.x

Chu, Z., Guo, J., and Zhao, J. (2017). Impacts of future climate change on agroclimatic resources in Northeast China. *J. Geogr. Sci.* 27, 1044–1058. doi: 10.1007/s11442-017-1420-6

Chi, F., Liu, J., Kuang, E., Zhang, J., and Su, Q. (2016). Effects of the relocation of undisturbed black soil after long-term test on soil fungal community diversity. *China Soil Fert.* 6, 141–150. (in Chinese). doi: 10.11838/sfsc.20160607

Collins, W. J., Bellouin, N., Gedney, N., and Halloran, P. (2011). Development and evaluation of an earth-system model – HadGEM2. *Geosci. Model Dev. Discuss.* 4:997. doi: 10.5194/gmdd-4-997-2011

Dermody, O., Long, S. P., McConnaughay, K., and DeLucia, E. H. (2008). How do elevated CO_2 and O_3 affect the interception and utilization of radiation by a soybean canopy? *Glob. Chang. Biol.* 14, 556–564. doi: 10.1111/j.1365-2486.2007.01502.x

Ding, J., Jiang, X., Ma, M., Zhou, B., Guan, D., Zhao, B., et al. (2016). Effect of 35 years inorganic fertilizer and manure amendment on structure of bacterial and archaeal communities in black soil of Northeast China. *Appl. Soil Ecol.* 105, 187–195. doi: 10.1016/j.apsoil.2016.04.010

Durán, A., Morrás, H., Studdert, G., and Liu, X. (2011). Distribution, properties, land use and management of Mollisols in South America. *Chinese Geogr. Sci.* 21, 511–530. doi: 10.1007/s11769-011-0491-z

Fang, R., Li, Y., Yu, Z., Xie, Z., Wang, G., Liu, X., et al. (2022). Warming offsets the beneficial effect of elevated CO_2 on maize plant-carbon accumulation in particulate organic carbon pools in a Mollisol. *Catena* 213:106219. doi: 10.1016/j.catena.2022.106219

Gao, C. S., Wang, J. G., Zhang, X. Y., and Sui, Y. Y. (2008). The evolution of organic carbon in Chinese Mollisol under different farming systems: validation and prediction by using century model. *Agric. Sci. China* 7, 1490–1496. doi: 10.1016/S1671-2927(08)60407-1

Gollany, H. T., Rickman, R. W., Liang, Y., Albrecht, S. L., Machado, S., and Kang, S. (2011). Predicting agricultural management influence on long-term soil organic carbon dynamics: implications for biofuel production. *Agron. J.* 103, 234–246. doi: 10.2134/agronj2010.0203s

Gross, A., and Glaser, B. (2021). Meta-analysis on how manure application changes soil organic carbon storage. *Sci. Rep.* 11, 5516–5513. doi: 10.1038/s41598-021-82739-7

Guo, S., Guo, E., Zhang, Z., Dong, M., Wang, X., Fu, Z., et al. (2022). Impacts of mean climate and extreme climate indices on soybean yield and yield components in Northeast China. *Sci. Total Environ.* 838:156284. doi: 10.1016/j.scitotenv.2022.156284

Hassink, J., and Whitmore, A. P. (1997). A model of the physical protection of organic matter in soils. *Soil Sci. Soc. Am. J.* 61, 131–139. doi: 10.2136/sssaj1997.03615995006100010020x

IPCC (2021). "Climate change 2021: the physical science basis" in *Contribution of working group I to the sixth assessment report of the intergovernmental panel on climate change*. eds. V. Masson-Delmotte, P. Zhai, A. Pirani, S. L. Connors, C. Péan and S. Berger, et al. Cambridge: Cambridge University Press.

Jiang, R., He, W., He, L., Yang, J. Y., Qian, B., Zhou, W., et al. (2021). Modelling adaptation strategies to reduce adverse impacts of climate change on maize cropping system in Northeast China. *Sci. Rep.* 11, 810–813. doi: 10.1038/s41598-020-79988-3

Jiang, G., Xu, M., He, X., Zhang, W., Huang, S., Yang, X., et al. (2014). Soil organic carbon sequestration in upland soils of northern China under variable fertilizer management and climate change scenarios. *Global Biogeochem. Cycles* 28, 319–333. doi: 10.1002/2013GB004746.Received

Jiang, G., Zhang, W., Xu, M., Kuzyakov, Y., Zhang, X., Wang, J., et al. (2018). Manure and mineral fertilizer effects on crop yield and soil carbon sequestration: a Meta-analysis and modeling across China. *Global Biogeochem. Cycles* 32, 1659–1672. doi: 10.1029/2018GB005960

Jin, Z. Q., and Zhu, D. W. (2008). Impacts of changes in climate and its variability on food production in Northeast China. *Acta Agron. Sin.* 34, 1588–1597. doi: 10.1016/S1875-2780(09)60005-5

Jin, Z., Zhuang, Q., Wang, J., Archontoulis, S. V., Zobel, Z., and Kotamarthi, V. R. (2017). The combined and separate impacts of climate extremes on the current and future US rainfed maize and soybean production under elevated CO_2. *Glob. Chang. Biol.* 23, 2687–2704. doi: 10.1111/gcb.13617

Jones, C. D., Hughes, J. K., Bellouin, N., Hardiman, S. C., Jones, G. S., Knight, J., et al. (2011). The HadGEM2-ES implementation of CMIP5 centennial simulations. *Geosci. Model Dev. Discuss.* 4, 689–763. doi: 10.5194/gmdd-4-689-2011

Lal, R., Follett, R. F., Stewart, B. A., and Kimble, J. M. (2007). Soil carbon sequestration to mitigate climate change and advance food security. *Soil Sci.* 172, 943–956. doi: 10.1097/ss.0b013e31815cc498

Leuning, R., Kelliher, F. M., De Pury, D. G. G., and Schulze, E.-D. (1995). Leaf nitrogen, photosynthesis, conductance and transpiration: scaling from leaves to canopies. *Plant Cell Environ.* 18, 1183–1200. doi: 10.1111/j.1365-3040.1995.tb00628.x

Li, Y., Liang, S., Zhao, Y., Li, W., and Wang, Y. (2017). Machine learning for the prediction of *L. chinensis* carbon, nitrogen and phosphorus contents and understanding of mechanisms underlying grassland degradation. *J. Environ. Manag.* 192, 116–123. doi: 10.1016/j.jenvman.2017.01.047

Li, H., Peil, J. B., Wang, J. K., Li, S. Y., and Gao, G. W. (2013). Organic carbon density and storage of the major black soil regions in Northeast China. *J. Soil Sci. Plant Nutr.* 13, 883–893. doi: 10.4067/S0718-95162013005000070

Li, X., Shang, B., Wang, D., Wang, Z., Wen, X., and Kang, Y. (2020). Mapping soil organic carbon and total nitrogen in croplands of the Corn Belt of Northeast China based on geographically weighted regression kriging model. *Comput. Geosci.* 135:104392. doi: 10.1016/j.cageo.2019.104392

Liang, S., Li, Y., Zhang, X., Sun, Z., Sun, N., Duan, Y., et al. (2018). Response of crop yield and nitrogen use efficiency for wheat-maize cropping system to future climate change in northern China. *Agric. For. Meteorol.* 262, 310–321. doi: 10.1016/j.agrformet.2018.07.019

Liang, S., Sun, N., Meersmans, J., Longdoz, B., Colinet, G., Xu, M., et al. (2024). Impacts of climate change on crop production and soil carbon stock in a continuous wheat cropping system in Southeast England. *Agric. Ecosyst. Environ.* 365:108909. doi: 10.1016/j.agee.2024.108909

Liang, S., Sun, N., Wang, S., Colinet, G., Longdoz, B., Meersmans, J., et al. (2023). Manure amendment acts as a recommended fertilization for improving carbon sequestration efficiency in soils of typical drylands of China. *Front. Environ. Sci.* 11:1173509. doi: 10.3389/fenvs.2023.1173509

Liang, A. Z., Zhang, X. P., Yang, X. M., McLaughlin, N. B., Shen, Y., and Li, W. F. (2009). Estimation of total erosion in cultivated Black soils in Northeast China from vertical profiles of soil organic carbon. *Eur. J. Soil Sci.* 60, 223–229. doi: 10.1111/j.1365-2389.2008.01100.x

Lin, Y., Feng, Z., Wu, W., Yang, Y., Zhou, Y., and Xu, C. (2017). Potential impacts of climate change and adaptation on maize in Northeast China. *Agron. J.* 109, 1476–1490. doi: 10.2134/agronj2016.05.0275

Liu, X., Lee Burras, C., Kravchenko, Y. S., Duran, A., Huffman, T., Morras, H., et al. (2012). Overview of Mollisols in the world: distribution, land use and management. *Can. J. Soil Sci.* 92, 383–402. doi: 10.4141/CJSS2010-058

Liu, C., Wang, L., Cocq, K.Le, Chang, C., Li, Z., Chen, F., et al. (2020). Climate change and environmental impacts on and adaptation strategies for production in wheat-rice rotations in southern China. *Agric. For. Meteorol.* 292,:108136. doi: 10.1016/j.agrformet.2020.108136

Liu, S., Yang, J. Y., Zhang, X. Y., Drury, C. F., Reynolds, W. D., and Hoogenboom, G. (2013). Modelling crop yield, soil water content and soil temperature for a soybean-maize rotation under conventional and conservation tillage systems in Northeast China. *Agric. Water Manag.* 123, 32–44. doi: 10.1016/j.agwat.2013.03.001

Liu, H., Zhang, T., Liu, B., Liu, G., and Wilson, G. V. (2013). Effects of gully erosion and gully filling on soil depth and crop production in the black soil region, Northeast China. *Environ. Earth Sci.* 68, 1723–1732. doi: 10.1007/s12665-012-1863-0

Maillard, É., and Angers, D. A. (2014). Animal manure application and soil organic carbon stocks: a meta-analysis. *Glob. Chang. Biol.* 20, 666–679. doi: 10.1111/gcb.12438

Mandal, A., Patra, A. K., Singh, D., Swarup, A., and Ebhin Masto, R. (2007). Effect of long-term application of manure and fertilizer on biological and biochemical activities in soil during crop development stages. *Bioresour. Technol.* 98, 3585–3592. doi: 10.1016/j.biortech.2006.11.027

Perego, A., Wu, L., Gerosa, G., Finco, A., Chiazzese, M., and Amaducci, S. (2016). Field evaluation combined with modelling analysis to study fertilizer and tillage as factors affecting N2O emissions: a case study in the Po valley (northern Italy). *Agric. Ecosyst. Environ.* 225, 72–85. doi: 10.1016/j.agee.2016.04.003

Posner, J. L., Baldock, J. O., and Hedtcke, J. L. (2008). Organic and conventional production systems in the Wisconsin integrated cropping systems trials: I. Productivity 1990-2002. *Agron. J.* 100, 253–260. doi: 10.2134/agronj2007.0058

Ramírez, P. B., Calderón, F. J., Fonte, S. J., and Bonilla, C. A. (2019). Environmental controls and long-term changes on carbon stocks under agricultural lands. *Soil Tillage Res.* 186, 310–321. doi: 10.1016/j.still.2018.10.018

Riahi, K., Rao, S., Krey, V., Cho, C., Chirkov, V., Fischer, G., et al. (2011). RCP 8.5-a scenario of comparatively high greenhouse gas emissions. *Clim. Chang.* 109, 33–57. doi: 10.1007/s10584-011-0149-y

Sanford, G. R., Posner, J. L., Jackson, R. D., Kucharik, C. J., Hedtcke, J. L., and Lin, T. L. (2012). Soil carbon lost from Mollisols of the north Central U.S.a. with 20 years of agricultural best management practices. *Agric. Ecosyst. Environ.* 162, 68–76. doi: 10.1016/j.agee.2012.08.011

Schmidt, M. W. I., Torn, M. S., Abiven, S., Dittmar, T., Guggenberger, G., Janssens, I. A., et al. (2011). Persistence of soil organic matter as an ecosystem property. *Nature* 478, 49–56. doi: 10.1038/nature10386

Six, J., Conant, R. T., Paul, E. A., and Paustian, K. (2002). Stabilization mechanisms of SOM implications for C saturation of soils. *Plant Soil* 241, 155–176. doi: 10.1023/A:1016125726789

Smith, J., Smith, P., Wattenbach, M., Zaehle, S., Hiederer, R., Jones, R. J. A., et al. (2005). Projected changes in mineral soil carbon of European croplands and grasslands, 1990-2080. *Glob. Chang. Biol.* 11, 2141–2152. doi: 10.1111/j.1365-2486.2005.001075.x

Stagnari, F., Maggio, A., Galieni, A., and Pisante, M. (2017). Multiple benefits of legumes for agriculture sustainability: an overview. *Chem. Biol. Technol. Agric.* 4, 1–13. doi: 10.1186/s40538-016-0085-1

Stewart, C. E., Paustian, K., Conant, R. T., Plante, A. F., and Six, J. (2007). Soil carbon saturation: concept, evidence and evaluation. *Biogeochemistry* 86, 19–31. doi: 10.1007/s10533-007-9140-0

Stewart, C. E., Paustian, K., Conant, R. T., Plante, A. F., and Six, J. (2008). Soil carbon saturation: evaluation and corroboration by long-term incubations. *Soil Biol. Biochem.* 40, 1741–1750. doi: 10.1016/j.soilbio.2008.02.014

Triberti, L., Nastri, A., and Baldoni, G. (2016). Long-term effects of crop rotation, manure and mineral fertilisation on carbon sequestration and soil fertility. *Eur. J. Agron.* 74, 47–55. doi: 10.1016/j.eja.2015.11.024

Tuzet, A., Perrier, A., and Leuning, R. (2003). A coupled model of stomatal conductance, photosynthesis and transpiration. *Plant Cell Environ.* 26, 1097–1116. doi: 10.1046/j.1365-3040.2003.01035.x

van Vuuren, D. P., Stehfest, E., den Elzen, M. G. J., Kram, T., van Vliet, J., Deetman, S., et al. (2011). RCP 2.6: exploring the possibility to keep global mean temperature increase below 2°C. *Clim. Chang.* 109, 95–116. doi: 10.1007/s10584-011-0152-3

Virk, A. L., Lin, B. J., Kan, Z. R., Qi, J. Y., Dang, Y. P., Lal, R., et al. (2022). Simultaneous effects of legume cultivation on carbon and nitrogen accumulation in soil. *Adv. Agron.* 171, 75–110. doi: 10.1016/bs.agron.2021.08.002

Vrugt, J. A., Gupta, H. V., Bastidas, L. A., Bouten, W., and Sorooshian, S. (2003). Effective and efficient algorithm for multiobjective optimization of hydrologic models. *Water Resour. Res.* 39, 1–19. doi: 10.1029/2002WR001746

Walkley, A., and Black, I. A. (1934). An examination of the degtjareff method for determining soil organic matter, and a proposed modification of the chromic acid titration method. *Soil Sci.* 37, 29–38. doi: 10.1097/00010694-193401000-00003

Wang, M., Li, Y., Ye, W., Bornman, J. F., and Yan, X. (2011). Effects of climate change on maize production, and potential adaptation measures: a case study in Jilin province, China. *Clim. Res.* 46, 223–242. doi: 10.3354/cr00986

Wang, Y., Tao, F., Chen, Y., and Yin, L. (2022). Interactive impacts of climate change and agricultural management on soil organic carbon sequestration potential of cropland in China over the coming decades. *Sci. Total Environ.* 817:153018. doi: 10.1016/j.scitotenv.2022.153018

Wang, S., Zhao, Y., Wang, J., Gao, J., Zhu, P., Cui, X., et al. (2020). Estimation of soil organic carbon losses and counter approaches from organic materials in black soils of northeastern China. *J. Soils Sediments* 20, 1241–1252. doi: 10.1007/s11368-019-02520-2

Wu, L., McGechan, M. B., McRoberts, N., Baddeley, J. A., and Watson, C. A. (2007). SPACSYS: integration of a 3D root architecture component to carbon, nitrogen and water cycling-model description. *Ecol. Model.* 200, 343–359. doi: 10.1016/j.ecolmodel.2006.08.010

Wu, L., Rees, R. M., Tarsitano, D., Zhang, X., Jones, S. K., and Whitmore, A. P. (2015). Simulation of nitrous oxide emissions at field scale using the SPACSYS model. *Sci. Total Environ.* 530-531, 76–86. doi: 10.1016/j.scitotenv.2015.05.064

Xu, X., Pei, J., Xu, Y., and Wang, J. (2020). Soil organic carbon depletion in global Mollisols regions and restoration by management practices: a review. *J. Soils Sediments* 20, 1173–1181. doi: 10.1007/s11368-019-02557-3

Xu, H., Shen, H. P., Zhou, S. W., Wang, X. L., and Sun, N. (2016). Determination of soil organic matter content by heating method with an aluminum module digesting device. *China Soil Fert.* 3, 140–144. (in Chinese). doi: 10.11838/sfsc.20160323

Yan, X., Zhou, H., Zhu, Q. H., Wang, X. F., Zhang, Y. Z., Yu, X. C., et al. (2013). Carbon sequestration efficiency in paddy soil and upland soil under long-term fertilization in southern China. *Soil Tillage Res.* 130, 42–51. doi: 10.1016/j.still.2013.01.013

Yin, X., and Struik, P. C. (2009). C3 and C4 photosynthesis models: an overview from the perspective of crop modelling. *NJAS Wageningen J. Life Sci.* 57, 27–38. doi: 10.1016/j.njas.2009.07.001

Yin, Y., Tang, Q., and Liu, X. (2015). A multi-model analysis of change in potential yield of major crops in China under climate change. *Earth Syst. Dynam.* 6, 45–59. doi: 10.5194/esd-6-45-2015

Yu, G., Fang, H., Gao, L., and Zhang, W. (2006). Soil organic carbon budget and fertility variation of black soils in Northeast China. *Ecol. Res.* 21, 855–867. doi: 10.1007/s11284-006-0033-9

Zhang, S., Bai, Y., Zhang, J. H., and Ali, S. (2021). Developing a process-based and remote sensing driven crop yield model for maize (PRYM–maize) and its validation over the Northeast China plain. *J. Integr. Agric.* 20, 408–423. doi: 10.1016/S2095-3119(20)63293-2

Zhang, X., Xu, M., Sun, N., Xiong, W., Huang, S., and Wu, L. (2016). Modelling and predicting crop yield, soil carbon and nitrogen stocks under climate change scenarios with fertiliser management in the North China plain. *Geoderma* 265, 176–186. doi: 10.1016/j.geoderma.2015.11.027

frontiers | Frontiers in Sustainable Food Systems

TYPE Original Research
PUBLISHED 04 April 2024
DOI 10.3389/fsufs.2024.1373183

OPEN ACCESS

EDITED BY
Pushp Sheel Shukla,
Centre for Cellular and Molecular Platforms, India

REVIEWED BY
Kapil Gupta,
Siddharth University Kapilvastu, India
Birinchi Kumar Sarma,
Banaras Hindu University, India
Nivetha Nagarajan,
Sea6 Energy Pvt Ltd, India

*CORRESPONDENCE
P. S. Basavaraj
✉ bassuptl@gmail.com

RECEIVED 19 January 2024
ACCEPTED 20 March 2024
PUBLISHED 04 April 2024

CITATION
Basavaraj PS, Jangid KK, Babar R, Gangana Gowdra VM, Gangurde A, Shinde S, Tripathi K, Patil D, Boraiah KM, Rane J, Harisha CB, Halli H, Sammi Reddy K and Prabhakar M (2024) Adventitious root formation confers waterlogging tolerance in cowpea (*Vigna unguiculata* (L.) Walp.). *Front. Sustain. Food Syst.* 8:1373183. doi: 10.3389/fsufs.2024.1373183

Adventitious root formation confers waterlogging tolerance in cowpea (*Vigna unguiculata* (L.) Walp.)

P. S. Basavaraj[1]*, Krishna Kumar Jangid[1], Rohit Babar[1], Vinay M. Gangana Gowdra[1], Anuja Gangurde[1], Shweta Shinde[1], Kuldeep Tripathi[2], Deepak Patil[3], K. M. Boraiah[1], Jagadish Rane[1,4], C. B. Harisha[1], Hanamant Halli[1], K. Sammi Reddy[1] and M. Prabhakar[5]

[1]ICAR-National Institute of Abiotic Stress Management, Malegaon, India, [2]ICAR- National Bureau of Plant Genetic Resources, New Delhi, India, [3]Agriculture Research Station, Badnapur, VNMKV, Parbhani, India, [4]ICAR-Central Institute of Arid Horticulture, Bikaner, India, [5]ICAR-Central Research Institute for Dryland Agriculture, Hyderabad, India

Crop adaptation to waterlogging stress necessitates alterations in their morpho-physiological and biochemical characteristics. Cowpeas, which serve as a dual-purpose legume crop (food and fodder), are sensitive to waterlogging stress, especially when exposed to extended periods of water stagnation during the early growth stage. In this study, we subjected five distinct and superior cowpea varieties to 10 days of waterlogging stress at the early seedling stage (V2, 15 days post emergence for 10 days) under controlled conditions. The aim was to comprehend the response of these varieties and identify the ideal trait for screening a large collection of cowpea genetic resources for waterlogging tolerance. We measured and analyzed changes in morpho-physiological and root parameters to gain a deeper understanding of the mechanism underlying waterlogging tolerance. The treatment (waterlogging and control), genotype, and their interactions had a significant impact on the most studied traits ($p < 0.05$). The results indicated a significant reduction in morpho-physiological parameters such as plant height, leaf area, leaf number, Normalized Difference Vegetation Index (NDVI), chlorophyll content, and chlorophyll fluorescence parameters under stress treatment than control conditions. However, root parameters like the number of adventitious roots (AR) and their length (ARL) significantly increased under waterlogging stress in tolerant cowpea varieties like DC15 and PL4. Correlation and PCA analyses further revealed a positive and significant association between cowpeas' waterlogging tolerance and AR formation and its AR length. Therefore, the current study reveals that swift development of AR and ARL may serve as potential traits conferring waterlogging tolerance in cowpeas. Using suitable mapping populations, these traits could reveal genomic regions associated with waterlogging tolerance in cowpeas. The tolerant varieties and key traits identified in this study could be beneficial in breeding programs aimed at enhancing waterlogging tolerance in cowpeas.

KEYWORDS

legumes, aerial roots, lateral roots, waterlogging, flood, abiotic stress, climate change

Introduction

Excess soil moisture due to heavy and high-frequency precipitation and poor soil drainage constraints negatively affects more than 16% of global arable land (Zhang et al., 2015; Olorunwa et al., 2022a). Episodes of flooding or waterlogging have become more frequent in recent years, posing a severe threat to global food security (Ward et al., 2020). Furthermore, NASA climate simulation models predict that by 2030, there will be a 30% increase in heavy rainfall and flood events due to the impact of climate change, making the situation worse. Crops, except rice, are susceptible to waterlogging stress, showing significant yield reduction when exposed to prolonged water stagnation (Zhang et al., 2015). Cowpea is a dual-purpose legume crop sensitive to waterlogging stress, with 10–52% yield loss reported when waterlogging occurs during the vegetative period. If it is during the reproductive stage, more than 52% yield reduction was observed. This sensitivity and yield loss vary depending on the variety grown, soil type, and crop growth stage (Olorunwa et al., 2022a,b).

Oxygen deprivation in the root zone from waterlogging is the main factor influencing plants' growth and development. Lack of oxygen results in reduced ATPs and leads to modification in physiological and biochemical parameters and the final yield of the crops (Olorunwa et al., 2022a,b). During waterlogging conditions, a decrease in leaf area, reduced shoot growth, reduced leaf nitrogen content, and reduction in net photosynthesis rates, transpiration, and stomatal conductance are reported in cowpeas (Zhang et al., 2015; Olorunwa et al., 2022a,b, 2023).

The negative impact of waterlogging stress on crops can be managed by soil application or foliar spray of nutrients, providing drainage, and sowing on raised beds (Pang et al., 2007). However, developing and deploying inherent waterlogging tolerant cultivars is the most economical and plausible approach. Nevertheless, the low heritability of the trait and complexity in phenotyping are the main bottlenecks in the genetic improvement of cowpea cultivars for waterlogging tolerance (Olorunwa et al., 2022a,b, 2023).

Deeper insight into the underlying mechanism of waterlogging tolerance in cowpeas is essential to identify relevant trait(s) that can improve waterlogging tolerance. Plants have evolved various tolerance mechanisms and developed adaptive trait(s) for waterlogging stress. For instance, rice survives and reproduces by the mechanism of shoot elongation and formation of aerenchyma (Steffens et al., 2010), whereas lysigenous aerenchyma formation confers tolerance to waterlogging in barley (Barrett-Lennard, 2003). Similarly, the formation of aerenchyma cells, lenticels, and adventitious roots in the tolerant genotypes was associated with waterlogging tolerance in pigeonpea (Hingane et al., 2015). Therefore, the main objective of the investigation is to identify key trait(s) contributing to waterlogging tolerance in cowpeas. Those traits can be targeted in future cowpea breeding programs to improve waterlogging tolerance.

Materials and methods

Experimental setup

The experiment was conducted under controlled conditions at the Green House (®Allice Biotechnology) of ICAR-National Institute of Abiotic Stress Management, Pune, India, from June to December 2022. The treatments were arranged in a factorial completely randomized design with five replications. Five popular cowpea varieties, *viz.*, RC101, DC15, PL3, PL4, and GC3, were selected for the study. The selection was based on popularity among farmers and cultivation in large areas. The average daily temperature of 28.1 ± 4.6°C and relative humidity of 68.2 ± 10.8% were maintained in the greenhouse conditions using a water-cooling pad system throughout the experiment.

The plants were grown in plastic pots of 20 cm diameter and height of 20 cm with three perforations at the base. Pots were filled with a mixture of black soil and farmyard manure (FYM) at the proportion of 50:1 (V/V). Nutrients (nitrogen, phosphorus, and potassium) were applied as per the recommended dose of 10: 20: 10 kg ha^{-1}, respectively. The amount of NPK added to each pot was calculated on a soil weight basis and blended adequately into the soil. After filling, each pot was weighed to 13 kg soil to ensure the same amount of soil mixture and constant moisture in each pot. Ten pots were used for each genotype (Five pots were used for imposing waterlogging stress treatment, and five were kept as a control). Filled pots were sown with six seeds per pot at 17–20 mm depth, and after seven days, the seedlings were thinned, and two healthy plants per pot were retained.

Waterlogging treatments

At the V2 leaf stage (15 days after emergence, 15 DAE), one set of uniformly emerged seedlings was subjected to waterlogging and the other set was retained as control for ten days (Olorunwa et al., 2022a). Waterlogging stress was achieved by placing the pots in a water-filled cement tank (8 × 5 × 1 m). The water level was maintained at least 20 mm above the soil surface throughout the stress. At the same time, five pots of each variety were kept at optimum soil moisture below field capacity as a control (<80% of FC). After ten days of stress treatment, excess water in the pots was drained and allowed to recover for five days.

Physiological parameters

Leaf area was measured using a leaf area meter (LI-3100C®Licor), Normalized Difference Vegetation Index (NDVI) was recorded during the recovery period (5 days post completion of stress treatment) using a hand-held device (GreenSeeker®, Trimble, United States) from 1.0 m above the soil surface of the experimental pot by following the method of Verhulst and Govaerts (2010), canopy temperature was measured by Infrared thermal Camera (Vario CAM hr. inspect 575, Jenoptic, Germany) with spatial resolution of 768 × 576 pixels. Chlorophyll fluorescence in leaves was measured during recovery (5 days post-completion of stress treatment) to study changes in maximum PSII efficiency in response to waterlogging. Leaves were adapted to dark for 30 min before measurement, and lights in the chlorophyll fluorescence imaging chamber were turned off to avoid any effect of light on maximum PSII efficiency. The temperature in the imaging chamber was set around 25 ± 1°C. The leaf images were captured at given time points by chlorophyll fluorescence measuring system (FC 1000-H/GFP, Handy Fluor Cam, P.S.I., Brno, Czech Republic) as described in Nedbal et al. (2000). Fluorescence was detected by a

high-sensitivity charge-coupled device (CCD) camera. It was driven by the FluorCam software package (FluorCam 7). First, the minimum fluorescence level (F0) of dark-adapted leaves was determined using non-actinic measuring flashes provided by super-bright light emitting diodes (LEDs) followed by a saturation pulse of light radiation [2,500 μmol (photon) m^{-2} s^{-1}] to obtain the maximum fluorescence (Fm). The maximum photochemical efficiency of PSII (Fv/Fm) was calculated according to Krause and Weis (1991).

$$Qmax = (Fm - F0) / Fm$$

where the difference between Fm and F0 represents the variable fluorescence (Fv).

For assessing response to waterlogging stress by image analysis, four colors were set manually for taking fluorescent images: blue (corresponding to Fv/Fm; 0.8), yellow, green, and red (related to Fv/Fm; 0.1). Photosynthetic pigments such as Chlorophyll a, b, and carotenoids in the leaf sample of cowpea (both stress and control sample) were estimated following the protocol of Lichtenthaler and Wellburn (1983).

Root and shoot parameters

Parameters such as root length (cm), shoot length (cm), root fresh weight (g/plant), root dry weight (g/plant), shoot fresh biomass (g/plant), and shoot dry biomass (g/plant), number of roots in each plant, nodules per plant, number of adventitious roots per plant and adventitious root length were measured destructively at the end of the stress treatment in each set manually.

Crop growth, morphology, and yield traits

Growth and yield attributes such as plant height (cm), number of branches per plant, number of leaves per plant, pod length (cm), the weight of 5 pods/plant (g), test weight (g), number of pods per plant and grain yield per plant (g) were measured in both the control and waterlogged plants in each replication after harvest of the crop.

Statistical analysis

The Analysis of variance and significant treatment differences (LSD) was carried out using SAS (version 9.4; SAS Institute, Cary, NC). The Spearman correlation coefficient was determined to assess the relationship between different parameters. Furthermore, Principal component analysis (PCA), biplot analysis, and box plots were drawn using R v 4.3.1. software.

Results

Analysis of variance

The Analysis of variance revealed a significant difference between control and stress treatment and their interaction for all the root traits, physiological parameters, and yield and its attributing traits ($p < 0.05$). Results presented in Table 1 imply considerable genetic variability among cowpea varieties, as evidenced by significant genotype and genotype x treatment interaction.

Physiological parameters

Waterlogging stress significantly ($p < 0.05$, Tables 1, 2) influenced the physiological parameters of all cowpea varieties. Waterlogging reduced the leaf area (31.89%), Normalized Difference Vegetation Index value (51.89%), chlorophyll a (33.08%), chlorophyll b (34.54%) and total chlorophyll content (32.44%) and maximum quantum efficiency (Qmax) by 4.93%. In contrast, waterlogging led to an increase in the canopy temperature by 3.38°C, ground fluorescence (F0), maximum fluorescence (Fm), and variable chlorophyll fluorescence (Fv) by 40.71, 15.75 and 9.76%, respectively, compared to plants under control conditions.

The physiological performance of the varieties was also found to be significant under both treatments. Among all the varieties, DC15 was found to perform better for leaf area (45.24 cm^2 $plant^{-1}$), chlorophyll a, b and total chlorophyll (1.60, 0.66 and 2.18, respectively), carotenoids (2.35), maximum quantum efficiency (0.80) and lower canopy temperature (28.94°C) followed by variety PL4. Meanwhile, RC101 performed the lowest in terms of physiological parameters (Table 2).

The interaction of waterlogging and cowpea varieties was also found to be significant. All the varieties performed better under control than stress conditions for most of the studied physiological traits. Among those, the performance of DC15 was significantly superior with higher leaf area (58.21 cm^2 $plant^{-1}$), Normalized Difference Vegetation Index I (0.80), total chlorophyll (2.72) and maximum quantum efficiency (0.82). Similarly, the same variety has performed better under stress with higher Normalized Difference Vegetation Index (0.44), total chlorophyll (1.63), carotenoids (1.63) and lower canopy temperature (30.96°C) followed by variety PL4. Maximum quantum efficiency was high in the variety PL4 variety, followed by DC15. Nevertheless, higher leaf area (35.43 cm^2 $plant^{-1}$), ground fluorescence (155.72), maximum fluorescence (649.12) and variable chlorophyll fluorescence were observed in the GC3 variety.

Root morphological parameters

Waterlogging stress significantly ($p < 0.05$) affected the root morphological traits of cowpea varieties (Tables 1, 3). In response to waterlogging, there was a reduction in the root length (27.90%), the number of roots per plant (7.44%), and root nodules per plant (79.73%), while an increase in the root fresh weight (383.46%) and root dry weight (118.18%) due to the formation of adventitious roots under stress compared to plants grown under non-stress conditions. Irrespective of waterlogging stress, the performance of cowpea varieties differed regarding root morphological traits; among them, the DC15 variety was found to be more promising with significantly distinct root morphological parameters such as root length (11.80 cm), number of roots (20.88 $plant^{-1}$), root nodules (7.66 $plant^{-1}$), root fresh weight (1.32 g $plant^{-1}$) and adventitious roots followed by GC3 and PL4 varieties. Root dry weight (0.26 g $plant^{-1}$) recorded in the PL4 variety was more than that of DC15 or GC3.

TABLE 1 Analysis of variance in response to waterlogging stress (WL) and varieties (V) in cowpea for different physiological, root, growth and yield-attributing traits.

Physiological parameters												
Source of variation	DF*	LA	Chla	Chlb	TCH	Car	CT	NDVI	F0	Fm	Qmax	Fv
Treatments (Control & Waterlogging) T	1	0.001	0.000	0.000	0.000	0.000	0.000	0.000	0.000	0.000	0.000	0.000
Varieties (V)	4	0.002	0.000	0.000	0.000	0.000	0.004	0.000	0.000	0.000	0.000	0.000
T × V	4	0.002	0.001	0.001	0.006	0.003	0.005	0.000	0.000	0.000	0.000	0.000

Root and shoot parameters								
Source of variation	DF	RL	SL	RFW	RDW	NR	AR	ARL
Treatments (Control & Waterlogging) T	1	0.000	0.000	0.000	0.000	0.000	0.000	0.001
Varieties (V)	4	0.000	0.000	0.000	0.000	0.001	0.000	0.000
T × V	4	0.001	0.000	0.001	0.001	0.000	0.000	0.000

Growth and yield attributes											
Source of variation	DF	PH	LPP	NBP	SFW	SDW	NPP	PL	PW	TW	GY
Treatments (Control & Waterlogging) T	1	0.001	0.000	0.000	0.001	0.002	0.000	0.002	0.000	0.000	0.001
Varieties (V)	4	0.002	0.000	0.000	0.000	0.001	0.000	0.001	0.000	0.000	0.002
T × V	4	0.002	0.000	0.004	0.002	0.001	0.000	0.001	0.000	0.000	0.002

*DF, Degrees of freedom; NS, Non-significant; RL, Root length; SL, Shoot length; RFW, Root fresh weight; RDW, Root dry weight; NR, No. of roots/plant; NN, Root nodules/plant; AR, Adventitious roots/plant; ARL, Adventitious root length; LA, Leaf area; NDVI, Normalized difference in vegetative index; CT, Canopy temperature; Chla, Chlorophyll a; Chlb, Chlorophyll b; TChl, Total chlorophyll; Car, Carotenoids; F0, Ground fluorescence; Fm, Maximum chlorophyll fluorescence; Fv, Variable chlorophyll fluorescence; QYmax, Maximum quantum efficiency; PH, Plant height, NBP, No. of branches per plant; LPP, Leaves per plant; SFW, Shoot fresh weight; SDW, Shoot dry weight; PP, Pods per plant; PL, Pod length; PW, Pod weight; TW, 100 seed weight; GY, Grain yield; T, Treatment (Control & waterlogging Stress); V, Cowpea Varieties.

The interaction between waterlogging stress and varieties was also significant (Tables 1, 3). All the varieties recorded better root growth under control than waterlogging stress. The minimum reduction in the root length (3.66%), root dry weight (19.04%) and number of roots (7.15%) was observed in the DC15 variety under stress. Meanwhile, the maximum reduction in root morphological parameters is recorded in RC101 and PL3 varieties compared to their performance under control conditions. Among all the varieties, the DC15 variety has registered higher root length (11.58 cm), root fresh weight (1.60 g plant^{-1}), number of roots per plant (20.11), number of nodules per plant (4) and adventitious roots per plant (38.33) followed by PL4 and GC3 varieties.

Growth and yield attributes of cowpea

The effect of waterlogging on plant growth and yield attributes was significant ($p < 0.05$, Table 1), as shown in Table 4. Under waterlogging stress, there was a reduction in shoot length (5.77%), plant height (15.43%), number of branches per plant (21.34%), number of leaves per plant (65.74%), pods per plant (64.70%), pod length (23.93%), pod weight (42.40%), test weight (17.53%) and yield (60.81%) compared to control condition.

Evaluation of cowpea varieties showed that DC15 performed better in terms of growth (plant height, 108.13 cm; number of branches, 5.50 and leaves per plant, 54.66) and yield attributes (pods per plant, 54.66; pod weight, 10.43 g; test weight, 10.26 g and grain yield, 48.16 g) followed by PL4. Meanwhile, the performance of the RC101 variety (in terms of growth and yield) was less than all other four cowpea varieties.

Compared to the other varieties, the performance of DC15 was better under both control and stress conditions with higher growth and yield parameters. This variety has had better growth attributes such as plant height (116.16, 100.11 cm), number of branches (6.33, 4.66), and leaves per plant (26.78, 11.66) as well as yield attributes such as number of pods (25.57 and 17.59), pod weight (13.12 and 7.12 g) and test weight (12.42, 10.70 g), respectively under control and stress conditions.

The higher grain yield was recorded by DC 15, followed by PL4, under both control and stress conditions. The same varieties have recorded a minimum decrease in grain yield, i.e., 23.68 and 18.88% under stress conditions relative to their yield under control, respectively. Meanwhile, GC3, PL3, and RC 101 recorded 44.56, 64.86, and 65.09% yield reductions, respectively, under stress, compared to control.

Association between traits under control and stress conditions

Correlation studies were conducted to determine the association between different parameters and grain yield under control and

10.3389/fsufs.2024.1373183

TABLE 2 Influence of waterlogging on physiological parameters of cowpea varieties.

Treatments (T)		LA	NDVI	CT	Chla	Chlb	TChl	Car	F0	Fm	Qmax	Fv
Control		47.66a	0.79a	28.56b	1.36a	0.55a	1.88a	2.37a	94.74b	498.90b	0.81a	404.6b
Stress		32.46b	0.38b	31.94a	0.91b	0.36b	1.27b	1.31b	133.31a	577.51a	0.77b	444.11a
CD		0.55	0.006	0.51	0.10	0.04	0.16	0.204	5.87	14.24	0.009	12.15
Varieties (V)												
DC15		45.24a	0.61a	28.94b	1.60a	0.66a	2.18a	2.35a	91.28c	474.62b	0.80a	383.34b
GC3		40.46c	0.56c	31.46a	1.04c	0.39c	1.44c	1.54bc	125.17b	575.39a	0.78b	450.22a
PL4		41.45b	0.62a	29.10b	1.23b	0.50b	1.74b	2.34a	89.98c	466.32b	0.80a	376.34b
PL3		41.07bc	0.59b	31.11a	1.00c	0.41c	1.42c	1.25c	127.73ab	589.34a	0.78b	461.60a
RC101		32.060d	0.55d	31.56a	0.78d	0.32d	1.11d	1.71b	136.17a	585.35a	0.77c	449.18a
CD		0.87	0.009	0.55	0.16	0.07	0.25	0.323	9.28	22.52	0.013	19.21
Interaction (T × V)												
Control	DC15	58.21a	0.80a	28.88d	2.04a	0.84a	2.72a	3.04a	92.70 cd	515.01c	0.82a	422.31c
	GC3	45.50d	0.79ab	31.83ab	1.17b	0.53b	1.63bc	2.51b	94.63 cd	501.67 cd	0.81ab	407.04c
	PL4	55.78b	0.80a	29.56d	1.35b	0.54b	1.90b	2.90ab	86.14d	488.6 cd	0.82a	402.46c
	PL3	49.33c	0.78b	31.06bc	1.31b	0.47b	1.85b	1.87c	100.23c	519.25c	0.81ab	419.02c
	RC101	34.64e	0.78b	31.83ab	1.16b	0.37 cd	1.63bc	1.53 cd	100.00c	470.0de	0.79b	370.00d
Stress	DC15	32.28f	0.44c	30.967c	1.17b	0.47b	1.63bc	1.78c	89.86 cd	434.24f	0.79b	344.38d
	GC3	35.43e	0.40e	31.10c	0.92 cd	0.36c	0.94e	1.21de	155.72b	649.12b	0.76c	493.40b
	PL4	27.127 h	0.42d	30.967	0.15bc	0.45bc	1.63bc	1.66 cd	93.82 cd	444.04ef	0.81a	350.22d
	PL3	32.82f	0.34e	31.96a	0.66e	0.28de	1.25de	0.97e	155.24b	659.44b	0.79b	504.19ab
	RC101	29.47 g	0.32f	32.16a	0.64e	0.27e	0.93e	0.91e	172.34a	700.71a	0.75c	528.37a
CD		1.24	0.01	0.15	0.23	0.09	0.36	0.45	13.12	31.84	0.001	27.16

LA, Leaf Area; NDVI, Normalized difference in vegetative index; CT, Canopy temperature (°C); Chla, Chlorophyll a (mg/mL); Chlb, Chlorophyll b (mg/mL); TChl, Total Chlorophyll (mg/mL); Car, Carotenoids(mg/mL); F0, ground fluorescence; Fm, Maximum chlorophyll fluorescence; Fv, Variable chlorophyll fluorescence; Qmax, Maximum quantum efficiency. Any two means having a common letter resulted from DMRT, are not significantly different at the 5% level of significance, CD, Critical difference.

stress conditions, and results were presented in the form of a correlogram (Figures 1, 2). Results revealed that traits *viz.*, plant height (PH), number of branches per plant (NBP), no. of leaves per plant (LPP), Normalized Difference Vegetation Index (NDVI), shoot length (SL), number of roots (NR), number of pods per plant (NPP) and initial fluorescence/ground fluorescence (F0) are negatively associated with grain yield under control conditions. In contrast, all the other traits such as leaf area (LA), canopy temperature (CT), chlorophyll a (Chla), chlorophyll b (Chlb), total chlorophyll (TotalChl), carotenoids (Car), root length (RL), root fresh weight (RFW), shoot fresh weight (SFW), root dry weight (RDW), shoot dry weight (SDW), nodules, pod length (PL), pod weight (PW), maximum fluorescence (Fm), variable fluorescence (Fv) and Qmax were positively associated with grain yield under control conditions (Figure 1). Similarly, under stress conditions, traits such as plant height, number of branches per plant, no. of leaves per plant, root length, Qmax, test weight, no. of pods per plant, and adventitious roots had a strong significant positive association with grain yield ($r = 0.5$ to1). Traits *viz.*, shoot fresh weight, shoot dry weight, adventitious root length, and pod length had a moderate positive association with grain yield under stress ($r = 0.25$ to 0.5). In contrast, traits such as canopy temperature, chlorophyll a, b total chlorophyll, shoot length, no. of roots and nodules per plant had weak to moderate positive correlation with grain yield under stress ($r = 0$ to 0.25) (Figure 2).

Principal component analysis

To assess how cowpea varieties responded to waterlogging, Principal Component Analysis (PCA) was employed to determine the morpho-physiological traits that most effectively explained their response (Figures 3A,B). This helped identify which genotypes are tolerant and sensitive to waterlogging. The analysis revealed four principal components (PCs), with PC1 (42.95%) and PC2 (28.88%) accounting for 71.83% of the total variation (Figures 3A,B). Among the different variables, AR, Qmax, F0, Fm, Fv, and GY showed the highest variation in PC1, while in PC2, variables such as Chla, Chlb, TotalChl, Car, and NR contributed significantly compared to other variables. Furthermore, the biplot analysis revealed that traits such as Chla, b, total chlorophyll content, no. of roots, number of branches per plant, plant height, no. of pods per plant, shoot dry weight, pod length, nodules per plant, shoot length, adventitious roots, root length, test weight, Qmax, root dry weight, grain yield and adventitious root length are in the same direction as PC1. Hence, they are positively correlated with PC1. Further, cowpea varieties DC15 and PL4 are on the positive side of PC1, suggesting their tolerance nature toward waterlogging. On the other hand, leaf area, maximum florescence, variable florescence, and root fresh weight are in the opposite direction of PC1, which implies a negative association. Further, varieties PL3, GC3 and RC101 were situated in the opposite direction of PC, indicating the sensitive nature of these varieties (Figure 4). Further,

TABLE 3 Influence of waterlogging on root parameters of cowpea varieties.

Treatments (T)		RL*	RFW	RDW	NR	NN	AR	ARL
Control		11.72a	0.913b	0.11b	19.08	7.55a	0.00b	0.00b
Stress		8.45b	4.414a	0.24a	17.66	1.53b	27.33a	8.87a
CD		0.37	1.13	0.12	1.00	2.59	3.79	2.48
Varieties (V)								
DC15		11.80a	1.32a	0.19b	20.88	7.66a	19.16a	5.6a
GC3		10.40b	0.76c	0.19b	18.33	3.33bc	13.66b	4.66b
PL4		10.39a	0.95b	0.26a	20.83	5.33ab	19.66a	5.5a
PL3		9.46c	0.73c	0.11c	14.83	2.33c	6.83c	3.68c
RC101		8.38d	0.53d	0.12c	17.00	4.06bc	10.00bc	2.66d
CD		0.58	0.21	0.13	1.33	1.64	2.40	1.45
Interaction (T × V)								
Control	DC15	12.02a	1.04b	0.21b	21.66a	11.32a	0.00e	0.00e
	GC3	11.80a	1.08b	0.32a	19.33b	8.10b	0.00e	0.00e
	PL4	12.17a	0.88c	0.31a	18.00b	8.19b	0.00e	0.00e
	PL3	11.41a	0.78d	0.13 cd	17.66c	5.6c	0.00e	0.00e
	RC101	11.63a	0.77d	0.22b	20.33ab	4.66 cd	0.00e	0.00e
Stress	DC15	11.58a	1.60a	0.17bc	20.11ab	4.00d	38.33a	11.33a
	GC3	9.00b	0.45f	0.07de	17.21c	1.02f	27.33b	9.33b
	PL4	8.62b	1.02b	0.22b	16.56d	2.66e	39.36a	11.00a
	PL3	7.51c	0.65e	0.10 cd	12.78e	0.00 g	13.66d	7.31c
	RC101	5.14d	0.30 g	0.02e	20.1ab	0.00 g	20.00c	5.18d
CD		0.82	0.15	0.10	1.26	1.56	5.37	2.24

*RL, Root length (cm); RFW, Root fresh weight (g/plant); RDW, Root dry weight (g/plant); NR, No. of roots/plant; NN, Root nodules/plant; AR, Adventitious roots/plant; ARL, Adventitious root length (cm). Any two means having a common letter resulted from DMRT, are not significantly different at the 5% level of significance, CD, Critical difference.

the length of the vector indicated the significance of the traits. In the present study, adventitious roots, no. of pods per plant, no. of roots, and total chlorophyll content had higher contributions to the waterlogging tolerance of the DC15 variety. Similarly, root dry weight, Qmax, test weight, adventitious root length, and pod weight significantly contributed to the PL4 variety.

Discussion

In response to waterlogging stress, a series of modifications in morpho-physiological, root, growth and development-related parameters were observed in cowpeas, which eventually hindered the potential yield of cowpea genotypes (Olorunwa et al., 2022a,b, 2023). Additionally, projections have suggested that climate change factors intensify this situation, resulting in declined cowpea productivity, which could worsen world food security (Ray et al., 2019). Therefore, it is imperative to find an appropriate solution to this problem. A possible approach to managing waterlogging stress includes agronomic interventions (sowing on raised beds), growth regulators, chemical applications/spay, and the genetic improvement of cowpea cultivars resilient to waterlogging. However, among the approaches mentioned above, developing and deploying waterlogging tolerant cowpeas would be the most ideal, economical, and eco-friendly approach (Olorunwa et al., 2022a,b).

However, due to the poor heritability and extremely unpredictable waterlogging conditions, little success has been achieved in breeding cowpea genotypes for waterlogging tolerance (Olorunwa et al., 2022a,b). Breeders mostly screened genotypes that were tolerant to waterlogging through field-based trials rather than laboratory-based physiological features (Khabaz-Saberi et al., 2005). Direct selection for waterlogging tolerance in the field may not be efficient due to the intricacy of waterlogging tolerance and variation in field conditions. Deeper insight into the underlying mechanisms of waterlogging tolerance allows plant breeders to target specific physiological trait (s) and pyramid different tolerance-related traits to generate cowpea pre-breeding material with enhanced tolerance to waterlogging. Therefore, identifying physiological characteristics associated with waterlogging tolerance in cowpeas is essential to accomplish this task. Therefore, we have studied morpho-physiological, root responses to waterlogging stress under controlled situations, as it avoids variation arising due to field heterogeneity.

Waterlogging tolerance is associated with adventitious root formation

The rate of oxygen diffusion in water is 104 times slower than that of air (Armstrong, 1980). Therefore, roots under waterlogging conditions lack or have minimal oxygen uptake. As a result of oxygen

TABLE 4 Influence of waterlogging on growth and yield attributing parameters of cowpea varieties.

Treatments (T)		PH	NBP	LPP	SL	SFW	SDW	NPP	PL	PW	TW	GY
Control		102.2a	5.34a	18.10a	34.40a	9.58a	1.69a	59.86a	18.01a	10.33a	11.35a	40.99a
Stress		86.43b	4.20b	6.20b	27.41b	8.55b	1.30b	21.13b	13.70b	5.95b	9.36b	24.93b
CD		0.76	0.30	0.39	1.12	1.10	0.34	1.33	0.40	0.16	0.09	0.52
Varieties (V)												
DC15		108.13a	5.50a	16.39a	32.63b	10.31a	1.92a	54.66a	21.58a	10.43a	10.26b	48.16a
GC3		90.98c	4.91b	11.44c	31.26c	10.38a	1.91a	43.66b	14.21c	7.95d	9.36	26.44c
PL4		77.22d	5.33ab	12.58b	28.20d	9.74a	1.26b	45.66b	12.93d	9.20b	9.58 cd	45.88b
PL3		103.89a	4.11c	9.5d	34.55a	8.39b	1.32b	27.83d	17.32b	8.29c	13.48a	23.31d
RC101		91.38c	4.00c	10.833c	28.71d	6.50c	1.07b	30.66c	13.21d	4.85w	9.09e	21.02e
CD		1.21	0.48	0.62	0.71	1.18	0.54	2.11	0.64	0.25	0.14	0.82
Interaction (T × V)												
Control	DC15	116.16a	6.33a	26.78a	37.60a	11.89a	2.73a	88.33a	25.57a	13.12a	12.42b	54.63a
	GC3	101.61 cd	5.49b	16.33c	35.19b	10.95a	1.52b	64.66b	16.31d	10.42c	9.90f	34.02e
	PL4	80.30f	6.31a	17.89b	31.24c	10.22a	2.30a	64.00b	14.48ef	13.12b	14.54a	50.67b
	PL3	110.45b	4.55c	16.0c	37.75a	10.22a	1.44b	41.33c	19.96b	9.38d	9.82f	36.43d
	RC101	102.54c	4.33 cd	13.50d	30.24c	8.90c	1.08b	41.00c	14.68e	8.50de	10.20e	29.22f
Stress	DC15	100.11d	4.66c	11.667e	31.66c	9.81b	1.70b	27.33d	17.59c	7.20e	10.70d	41.69c
	GC3	80.36f	4.33 cd	5.12 g	27.33d	8.74c	1.10b	22.66e	12.12 g	5.48 g	8.82 g	18.86 g
	PL4	74.15 g	5.4b	5.33f	25.16e	9.25b	1.44b	21.00e	11.94 g	6.38f	11.42c	41.10c
	PL3	97.34e	3.667d	3.00 h	31.35c	6.57d	1.18b	20.00e	11.10 g	5.29 g	7.99 h	12.80 h
	RC101	80.23f	3.66d	5.00 g	23.18f	4.11e	0.96b	14.66f	12.20 g	3.32 h	7.74i	10.20i
CD		1.71	0.69	0.88	1.59	1.15	0.76	2.98	0.91	0.36	0.21	2.10

*PH, Plant height (cm); NBP, No. of Branches per plant; LPP, Leaves per plant; SFW, Shoot fresh weight (g/plant); Shoot dry weight (g/plant), NPP, Pods per plant; PL, Pod length (cm); PW, Pod weight (g/5pods); TW, 100 seed weight (g); GY, Grain yield (g/plant), Any two means having a common letter resulted from DMRT, are not significantly different at the 5% level of significance, CD, Critical difference.

deprivation, ATP production is affected severely, causing an energy crisis in the waterlogged plants (Colmer and Voesenek, 2009). Plants have developed many adoptive strategies to withstand O_2 deficiency conditions, including aerenchyma formation, adventitious root (AR) development, and regulation of shoot elongation (Suralta and Yamauchi, 2008). Different crop plants have different survival mechanisms; for instance, rice, maize, and barley can form aerenchyma tissue in response to waterlogging (Steffens et al., 2010; Zhang et al., 2015). The primary roots of cowpeas under waterlogged conditions decay or deteriorate quickly due to lack of oxygen, leading to an energy crisis. A fundamental response in cowpeas is developing adventitious roots to replace the damaged original root system under flooded conditions (AR). The development of AR has been observed in many species, including rice (Mhimdi and Pérez-Pérez, 2020), maize (Mano and Omori, 2013), grain legumes such as mungbean and Blackgram (Kyu et al., 2021). The AR develops as a part of the existing root system; however, they primarily differ in terms of emergence, i.e., from the base of stem, nodes, mesocotyl and hypocotyls and have more aerenchyma than the primary root system (Della Rovere et al., 2013).

Consequently, under anoxygenic conditions, ARs support and enhance gas diffusion and water and nutrient uptake in plants along and across the roots via air-filled space known as aerenchyma (Steffens and Rasmussen, 2016). Therefore, plants that can quickly form AR under waterlogged conditions are expected to be a better adaptation trait for waterlogging environments (Yang et al., 2023). In the current study, no tested varieties developed AR under control conditions (Figures 5, 6). Contrasting to this, all the varieties formed AR under waterlogging conditions. However, oxygen transport efficiency depends on AR formation and the number of AR formed during waterlogging stress. In the present experiment, the number of AR varied significantly among the varieties; this signifies the variation in waterlogging tolerance among varieties.

Further, tolerant varieties had significantly higher and longer AR than sensitive varieties. Akin to our results, Thomas et al. (2005) reported that faster AR formation is associated with the recovery of N metabolism in the roots of legumes. Further, the formation of AR enhances the internal oxygen transport from shoot to waterlogged roots, increasing the oxygen concentration in the root zone (Shimamura et al., 2010; Teakle et al., 2011).

Waterlogging induces morphological changes in varieties

Waterlogging significantly influenced the growth and development of cowpea varieties. Ten days of waterlogging treatment on cowpeas induced significant changes in morphological parameters, including decreased plant height, leaf area, number of leaves, and biomass accumulation to varying degrees in different cowpea varieties. In the

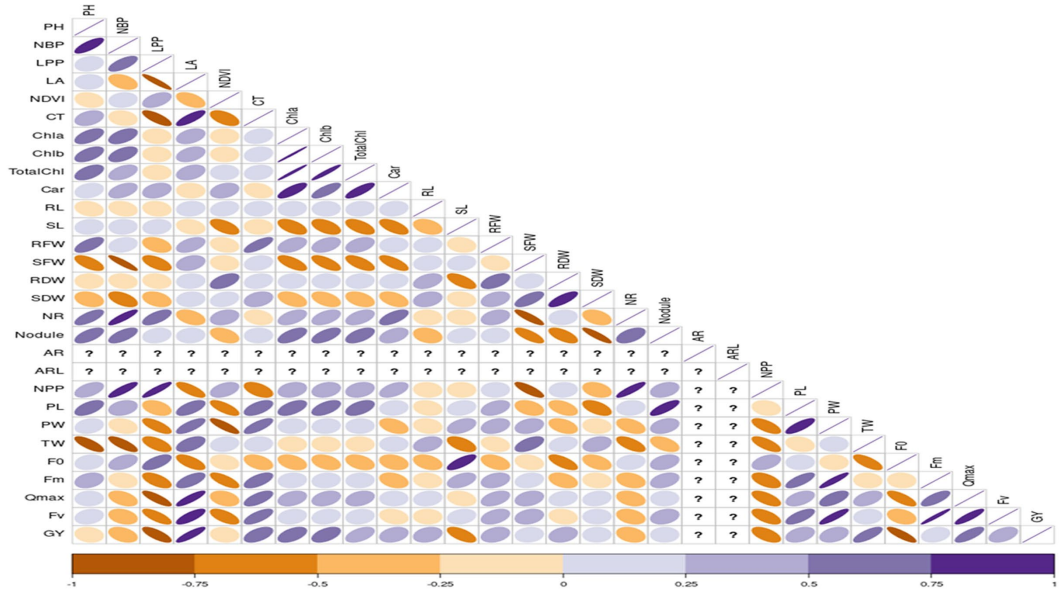

FIGURE 1
Correlation coefficient between grain yield with, root, shoot, growth and physiological parameters under control conditions RL, Root length (cm); SL, Shoot Length (cm); RFW, Root Fresh Weight (g/plant); SFW, Shoot Fresh Weight (g/plant); RDW, Root Dry Weight (g/plant); SDW, Shoot Dry Weight (g/plant); NR, No. of Roots/plant; NN, Root Nodules/plant; AR, Adventitious Roots/plant; ARL, Adventitious Root Length (cm); LA, Leaf Area; NDVI, Normalized Difference in Vegetative Index; CT, Canopy Temperature; Chla, Chlorophyll a (mg/mL); Chlb, Chlorophyll b (mg/mL); TChl, Total Chlorophyll (mg/mL); Car, Carotenoids (mg/mL); F0, ground fluorescence; Fm, maximum chlorophyll fluorescence; Fv, Variable chlorophyll fluorescence; QYmax, maximum quantum efficiency; PH, Plant Height (cm); NBP, No. of Brancher per plant; LPP, Leaves per plant; NPP, Pods per plant; PL, Pod Length (cm); PW, Pod Weight (g/5pods); TW, 100 seed weight (g); GY, Grain Yield (g/plant).

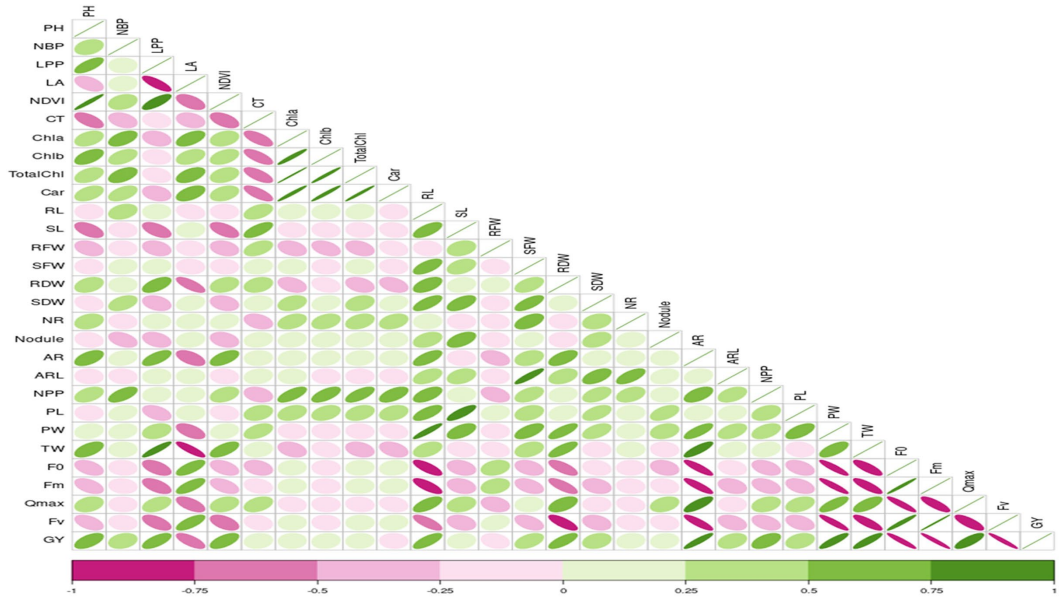

FIGURE 2
Correlation coefficient between grain yield with, root, shoot, growth and physiological parameters under waterlogging stress conditions RL, Root length (cm); SL, Shoot Length (cm); RFW, Root Fresh Weight (g/plant); SFW, Shoot Fresh Weight (g/plant); RDW, Root Dry Weight (g/plant); SDW, Shoot Dry Weight (g/plant); NR, No. of Roots/plant; NN, Root Nodules/plant; AR, Adventitious Roots/plant; ARL, Adventitious Root Length (cm); LA, Leaf Area; NDVI, Normalized Difference in Vegetative Index; CT, Canopy Temperature; Chla, Chlorophyll a (mg/mL); Chlb, Chlorophyll b (mg/mL); TChl, Total Chlorophyll (mg/mL); Car, Carotenoids (mg/mL); F0, ground fluorescence; Fm, maximum chlorophyll fluorescence; Fv, Variable chlorophyll fluorescence; QYmax, maximum quantum efficiency; PH, Plant Height (cm); NBP, No. of Brancher per plant; LPP, Leaves per plant; NPP, Pods per plant; PL, Pod Length (cm); PW, Pod Weight (g/5pods); TW, 100 seed weight.

present study, waterlogging for ten days significantly decreased plant height, number of branches per plant, and number of leaves per plant in all the tested cowpea varieties compared to the control. Similar modifications and decreases in plant height and number of leaves were reported in cowpea (Olorunwa et al., 2022a,b), decrease in plant height of soybean (Dhungana et al., 2019), mung (Kumar et al., 2013), and

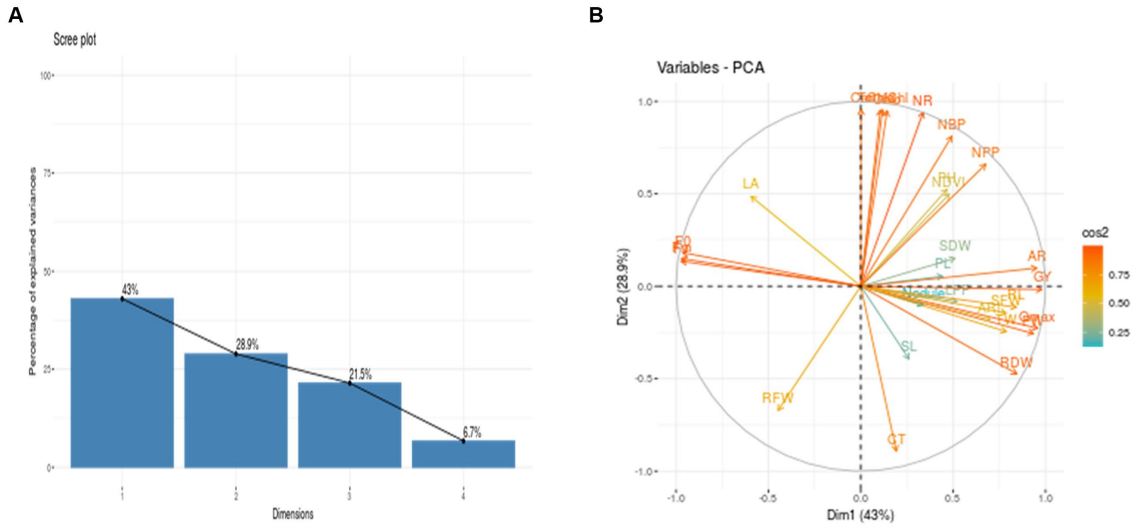

FIGURE 3
(A) Scree plot depicting percentage of variance explained for various growth, physiology, root, and yield parameters of cowpea genotypes under water- logging stress. 1 to 4 number indicates component numbers. **(B)** Contribution of each variable to total variability in PC1 and PC2 and correlation between them.

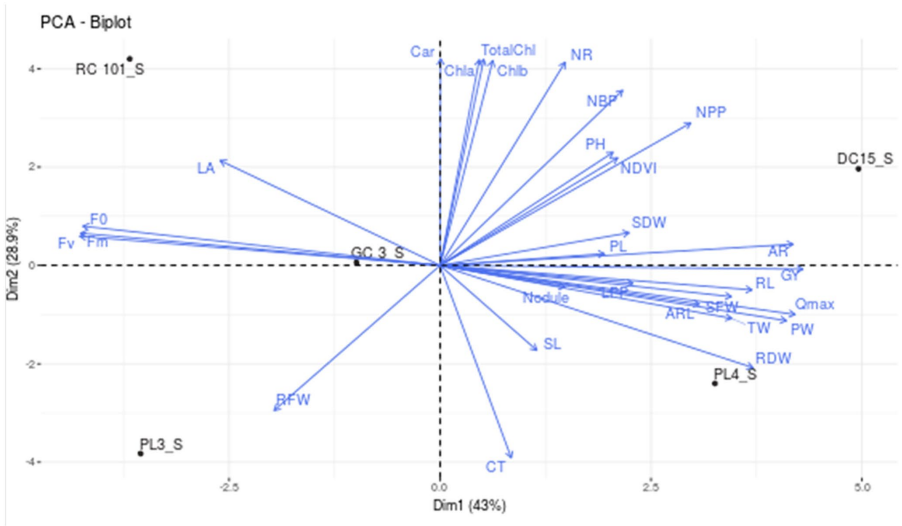

FIGURE 4
Biplot depicting the interrelationship between various growth, physiology, root, and yield parameters of cowpea genotypes under waterlogging stress.

pigeonpea (Basavaraj et al., 2023) under waterlogging stress at vegetative stage, this supports the present results. As a result of waterlogging, a decrease in plant height and resultant stunted growth was observed in all the tested varieties; this is akin to observations of the previous reports in cowpea (Umaharan et al., 1997; Olorunwa et al., 2022a,b). Although we have not measured ethylene production in the present investigation, the decrease in plant height under waterlogging is mainly due to increased production of ethylene compound, 1-aminocyclopropane-1-carboxylic acid (ACC), production of which enhanced under waterlogging conditions (Pan et al., 2019). Further, increased ACC levels might have inhibited the abscisic acid biosynthesis, thereby inhibiting shoot elongation and overall plant growth (Ntukamazina et al., 2017; Ploschuk et al., 2018; Olorunwa et al., 2022a).

Additionally, plants under waterlogging stress during the vegetative stage respond in various ways to sustain their growth and development by utilizing their morphological characteristics, particularly those associated with their leaves, which are the site of photosynthesis. The onset of leaf senescence and a notable decrease in leaf area and leaf number are typical signs of waterlogging stress, which worsens depending on the severity of waterlogging, particularly in legumes (Hingane et al., 2015; Olorunwa et al., 2022a,b; Basavaraj et al., 2023). A similar trend was observed in the present study: a decrease in leaf area and number of leaves per plant in stress treatment compared to control plants of all tested cowpea varieties. This decrease in leaf area is mainly due to decreased photosynthesis (Pn) caused by stomata closure under waterlogging

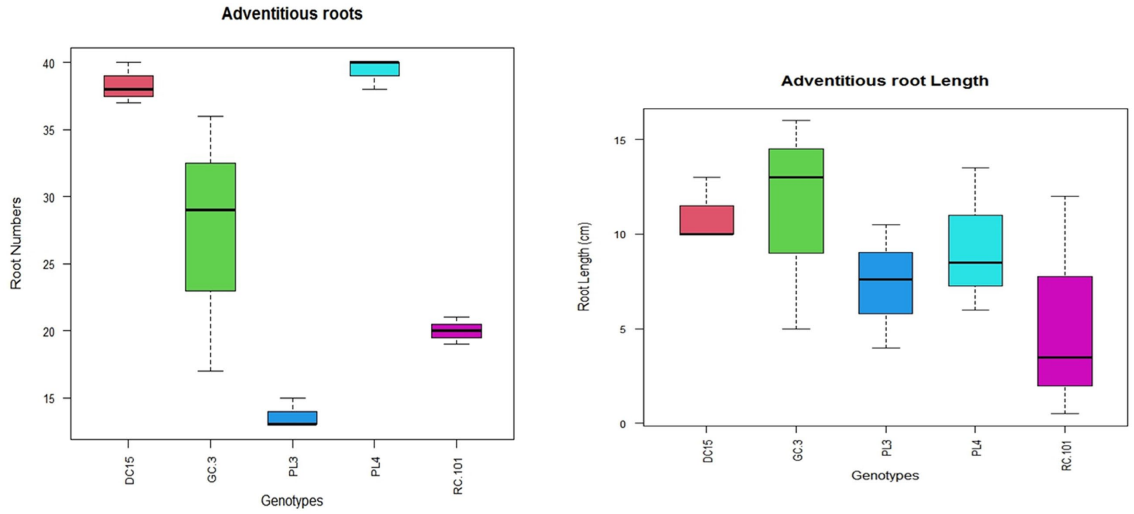

FIGURE 5
Variation in the number and length of adventitious roots of different cowpea varieties under waterlogging stress.

FIGURE 6
Variation in root and shoot parameters of cowpea varieties under control and waterlogging stress (picture is taken immediately after 10th day of waterlogging treatment).

stress (Takele and McDavid, 1994; Olorunwa et al., 2022a). Changes in photosynthetic capacity are mainly due to modifications in enzyme carboxylation, reduction in chlorophyll content and reduced leaf area. Further, tolerant varieties such as DC15 and PL4 in the present study could maintain higher leaf area and leaf number under waterlogging conditions, resulting in optimum photosynthesis, growth, development, and economic yield. Kumutha et al. (2009) made similar observations on leaf area in waterlogging tolerant pigeonpea genotypes with higher leaf area than sensitive genotypes under waterlogging stress.

Waterlogging induces physiological changes in cowpea varieties

Waterlogging stress significantly affected the morpho-physiological functions of cowpea varieties, notably altered shoot morphology and physiology, which had an adverse impact on carbon fixation and stomatal conductance (Ploschuk et al., 2018). Since the waterlogging condition has 10,000 times less oxygen diffusion, the stomata and cell walls find it difficult to exchange the CO_2 needed for the plant's fundamental functions (Voesenek and Bailey-Serres, 2015).

Further, reduced CO_2 availability under waterlogging/flooding causes a reduction in heterotrophic energy production in mitochondria, therefore decreasing photosynthesis. In addition, waterlogging stress caused a decline in the photosynthetic capacity of tested cowpea varieties, inhibiting the electron transport rate and leading to photo-inhibition in PSII. In the present study, we observed a decrease in chlorophyll fluorescence parameters such as F0, Fv, Fm and Fv/Fm, which are signs of damaged PSII. Alternatively, a reduction of photosynthetic pigments (Chlorophyll and carotenoids) contributed to a decline in photosynthesis in the sensitive cowpea varieties in the present study. Under waterlogging, the drop in Fv/Fm indicates that the light energy absorbed by PSII was utilized to reduce PSII's potential vigor change and the efficiency of the principal electron acceptor (Rao et al., 2021). These alterations represent the plants' ability to withstand a range of environmental stressors, such as hypoxia and anoxia (Zhu et al., 2016).

Additionally, cowpea genotypes under waterlogging in the early phases of vegetative growth had lower Fv, Fm, F0 and Fv/Fm, suggesting that cowpeas are susceptible to waterlogging stress. These results aligned with those of Ploschuk et al. (2018), who reported that field peas are sensitive to waterlogging because of impaired PSII. Further, a decrease in quantum efficiency of PSII (Fv/Fm) was observed under stress treatment compared to optimum conditions and tolerant cowpea varieties such as DC15 and PL4 had higher PSII values under stress compared to sensitive RC101 cowpea variety, indicating that tolerant cowpea genotypes can prevent photodamage during waterlogging stress more effectively than susceptible genotypes. According to Zhu et al. (2016), the xanthophyll cycle's capacity to shield the photosynthetic machinery from photo-inhibitory damage under waterlogging is responsible for this waterlogging tolerance. Previously, Olorunwa et al. (2022a,b) also reported similar results.

Association between morpho-physiological and root traits under waterlogging stress

Waterlogging tolerance is a complex quantitative trait involving plants' morphological, physiological, anatomical, and molecular characteristics (Yamauchi et al., 2018; Zeng et al., 2020; Basavaraj et al., 2023). More than one criterion is required to reflect plants' waterlogging tolerance precisely. Therefore, correlation and principal component analysis were used to evaluate cowpea varieties in the present study. Association analysis indicated that grain yield in the present study is significantly positively associated with forming adventitious roots (root length, root number). Therefore, adventitious root traits provide selection criteria for screening waterlogging-tolerant cowpea genotypes. Thus, these findings illustrated the significance of root characteristics in selecting genotypes tolerant of waterlogging stress. Further, significant differences for various morpho-physiological and root traits were observed among the tested cowpea varieties, suggesting inherent genetic variation. These results are consistent with Olorunwa et al. (2022a,b) studies in cowpeas and beans (Velasco et al., 2019).

Conclusion

The present study highlighted the significance of morpho-physiological and root parameters tolerant to waterlogging, and the study revealed the quantitative complex nature of tolerance traits among the cowpea varieties. There is a significant positive association between adventitious root number and root length with grain yield under waterlogging stress, suggesting that while screening cowpea genotypes, tolerance to waterlogging, priority should be given to root traits, especially AR and ARL. Cowpea varieties like PL4 and DC15 could aid in developing novel genotypes of cowpeas that are tolerant to waterlogging. These tolerant genotypes can be crossed with them to transfer waterlogging tolerance genes into high-yielding commercial cowpea varieties without compromising their natural performance under waterlogging stress. However, before crossing programs, these findings must be validated under field conditions to evaluate their growth, development, and yield performance under waterlogging conditions to guarantee sustainable cowpea production.

Data availability statement

The raw data supporting the conclusions of this article will be made available by the authors, without undue reservation.

Author contributions

PB: Conceptualization, Data curation, Formal analysis, Funding acquisition, Investigation, Methodology, Project administration, Resources, Software, Supervision, Validation, Visualization, Writing – original draft, Writing – review & editing. KJ: Visualization, Writing – review & editing. RB: Formal analysis, Software, Writing – review & editing. VG: Writing – review & editing. AG: Resources, Validation, Writing – review & editing. SS: Formal analysis, Resources, Validation, Writing – review & editing. KT: Software, Writing – review & editing. DP: Resources, Writing – review & editing. KB: Investigation, Methodology, Supervision, Writing – review & editing. JR: Formal analysis, Supervision, Writing – review & editing. CH: Methodology, Writing – review & editing. HH: Data curation, Formal analysis, Writing – review & editing. KS: Funding acquisition, Supervision, Writing – review & editing. MP: Writing – review & editing.

Funding

The author(s) declare financial support was received for the research, authorship, and/or publication of this article. The research was carried out under the ICAR-NICRA project "Phenotyping of Pulses for Enhanced Tolerance to Drought and Heat (OXX01737)."

Acknowledgments

The authors thank ICAR-NICRA for funding the project "Phenotyping of Pulses for Enhanced Tolerance to Drought and Heat" and ICAR-NIASM for the logistic support.

Conflict of interest

The authors declare that the research was conducted without any commercial or financial relationships that could be construed as a potential conflict of interest.

Publisher's note

References

Armstrong, W. (1980). Aeration in higher plants. *Adv. Bot. Res.* 7, 225–332. doi: 10.1016/S0065-2296(08)60089-0

Barrett-Lennard, E. G. (2003). The interaction between waterlogging and salinity in higher plants: causes, consequences and implications. *Plant Soil* 253, 35–54. doi: 10.1023/A:1024574622669

Basavaraj, P. S., Rane, J., Boraiah, K. M., Gangashetty, P., and Harisha, C. B. (2023). Genetic analysis of the tolerance to transient waterlogging stress in pigeonpea (*Cajanus cajan* L. Millspaugh). Indian J. Genet. *Plant Breed.* 83, 316–325. doi: 10.31742/ISGPB.83.3.3

Colmer, T. D., and Voesenek, L. A. C. J. (2009). Flooding tolerance: suites of plant traits in variable environments. *Funct. Plant Biol.* 36, 665–681. doi: 10.1071/FP09144

Della Rovere, F., Fattorini, L., D'angeli, S., Veloccia, A., Falasca, G., and Altamura, M. (2013). Auxin and cytokinin control formation of the quiescent Centre in the adventitious root apex of *Arabidopsis*. *Ann. Bot.* 112, 1395–1407. doi: 10.1093/aob/mct215

Dhungana, S. K., Kim, H. S., Kang, B. K., Seo, J. H., Kim, H. T., Shin, S. O., et al. (2019). Evaluation of flooding tolerance of soybean (*Glycine max* L. Merr.) in greenhouse under upland and paddy soil conditions. *J. Crop. Sci. Biotechnol.* 22, 283–290. doi: 10.1007/s12892-019-0106-0

Hingane, A., Saxena, K., Patil, S., Sultana, R., Srikanth, S., Mallikarjuna, N., et al. (2015). Mechanism of water-logging tolerance in pigeonpea. *Indian J. Genet. Plant Breed.* 75, 208–214. doi: 10.5958/0975-6906.2015.00032.2

Khabaz-Saberi, H., Setter, T. L., and Waters, I. (2005). Waterlogging induces high to toxic concentrations of iron, aluminum, and manganese in wheat varieties on acidic soil. *J. Plant Nutr.* 29, 899–911. doi: 10.1080/01904160600649161

Krause, G. H., and Weis, E. (1991). Chlorophyll fluorescence and photosynthesis—the basics. Annu rev plant Physiol. *Plant Mol. Biol.* 42, 313–349. doi: 10.1146/annurev.pp.42.060191.001525

Kumar, P., Pal, M., Joshi, R., and Sairam, R. K. (2013). Yield, growth and physiological responses of mung bean [*Vigna radiata* (L.) Wilczek] genotypes to waterlogging at vegetative stage. *Physiol. Mol. Biol. Plants* 19, 209–220. doi: 10.1007/s12298-012-0153-3

Kumutha, D., Ezhilmathi, K., Sairam, R. K., Srivastava, G. C., Deshmukh, P. S., and Meena, C. R. (2009). Waterlogging induced oxidative stress and antioxidant activity in pigeonpea genotypes. *Biol. Plant.* 53, 75–84. doi: 10.1007/s10535-009-0011-5

Kyu, K. L., Malik, A. I., Colmer, T. D., Siddique, K. H. M., and Erskine, W. (2021). Response of mungbean (cvs. Celera II-AU and jade-AU) and blackgram (cv. Onyx-AU) to transient waterlogging. *Front. Plant Sci.* 12:709102. doi: 10.3389/fpls.2021.709102

Lichtenthaler, H. K., and Wellburn, A. R. (1983). Determinations of total carotenoids and chlorophylls a and b of leaf extracts in different solvents. *Biochem. Soc. Trans.* 11:592.

Mano, Y., and Omori, F. (2013). Relationship between constitutive root aerenchyma formation and flooding tolerance in *Zea nicaraguensis*. *Plant Soil* 370, 447–460. doi: 10.1007/s11104-013-1641-0

Mhimdi, M., and Pérez-Pérez, J. M. (2020). Understanding of adventitious root formation: what can we learn from comparative genetics? *Front. Plant Sci.* 11:582020. doi: 10.3389/fpls.2020.582020

Nedbal, L., Soukupová, J., Kaftan, D., Whitmarsh, J., and Trtílek, M. (2000). Kinetic imaging of chlorophyll fluorescence using modulated light. *Photosynth. Res.* 66, 3–12. doi: 10.1023/A:1010729821876

Ntukamazina, N., Onwonga, R. N., Sommer, R., Mukankusi, C. M., Mburu, J., and Rubyogo, J. C. (2017). Effect of excessive and minimal soil moisture stress on agronomic performance of bush and climbing bean (*Phaseolus vulgaris* L.). *Cogent Food Agric.* 3:1373414. doi: 10.1080/23311932.2017.1373414

Olorunwa, O. J., Adhikari, B., Brazel, S., Bheemanahalli, R., Barickman, T. C., and Reddy, K. R. (2023). Waterlogging stress reduces cowpea (*Vigna unguiculata* L.) genotypes growth, seed yield, and quality at different growth stages: implications for developing tolerant cultivars under field conditions. *Agric. Water Manag.* 284:108336. doi: 10.1016/j.agwat.2023.108336

Olorunwa, O. J., Adhikari, B., Brazel, S., Shi, A., Popescu, S. C., Popescu, G. V., et al. (2022b). Growth and photosynthetic responses of cowpea genotypes under waterlogging at the reproductive stage. *Plan. Theory* 11:2315. doi: 10.3390/plants11172315

Olorunwa, O. J., Adhikari, B., Shi, A., and Barickman, T. C. (2022a). Screening of cowpea (*Vigna unguiculata* (L.) Walp.) genotypes for waterlogging tolerance using morpho-physiological traits at early growth stage. *Plant Sci.* 315:111136. doi: 10.1016/j.plantsci.2021.111136

Pan, R. W., Jiang, Q., Wang, L., Xu, S., Shabala, W. Y., and Zhang, L. (2019). Differential response of growth and photosynthesis in diverse cotton genotypes under hypoxia stress. *Photo-Dermatology* 57, 772–779. doi: 10.32615/ps.2019.087

Pang, J., Ross, J., Zhou, M., Mendham, N., and Shabala, S. (2007). Amelioration of detrimental effects of waterlogging by foliar nutrient sprays in barley. *Funct. Plant Biol.* 34, 221–227. doi: 10.1071/fp06158

Ploschuk, R. A., Miralles, D. J., Colmer, T. D., Ploschuk, E. L., and Striker, G. G. (2018). Waterlogging of winter crops at early and late stages: impacts on leaf physiology, growth and yield. *Front. Plant Sci.* 9:425885. doi: 10.3389/fpls.2018.01863

Rao, L., Li, S., and Cui, X. (2021). Leaf morphology and chlorophyll fluorescence characteristics of mulberry seedlings under waterlogging stress. *Sci. Rep.* 11:13379. doi: 10.1038/s41598-021-92782-z

Ray, D. K., West, P. C., Clark, M., Gerber, J. S., Prishchepov, A. V., and Chatterjee, S. (2019). Climate change has likely already affected global food production. *PLoS One* 14:e0217148. doi: 10.1371/journal.pone.0217148

Shimamura, S., Yamamoto, R., Nakamura, T., Shimada, S., and Komatsu, S. (2010). Stem hypertrophic lenticels and secondary aerenchyma enable oxygen transport to roots of soybean in flooded soil. *Ann. Bot.* 106, 277–284. doi: 10.1093/aob/mcq123

Steffens, B., Geske, T., and Sauter, M. (2010). Aerenchyma formation in the rice stem and its promotion by H_2O_2. *New Phytol.* 190, 369–378. doi: 10.1111/j.1469-8137.2010.03496.x

Steffens, B., and Rasmussen, A. (2016). The physiology of adventitious roots. *Plant Physiol.* 170, 603–617. doi: 10.1104/pp.15.01360

Suralta, R. R., and Yamauchi, A. (2008). Root growth, aerenchyma development, and oxygen transport in rice genotypes subjected to drought and waterlogging. *Environ. Experiment. Bot.* 64, 75–82. doi: 10.1016/j.envexpbot.2008.01.0

Takele, A., and McDavid, C. R. (1994). Effects of short-term waterlogging on cultivars of cowpea (*Vigna uniguiculata* (L.) Walp.). *Trop. Agric.* 71, 275–280.

Teakle, N. L., Armstrong, J., Barrett-Lennard, E. G., and Colmer, T. D. (2011). Aerenchymatous phellem in hypocotyl and roots enables O_2 transport in *Melilotus siculus*. *New Phytol.* 190, 340–350. doi: 10.1111/j.1469-8137.2011.03655.x

Thomas, A. L., Guerreiro, S. M. C., and Sodek, L. (2005). Aerenchyma formation and recovery from hypoxia of the flooded root system of nodulated soybean. *Ann. Bot.* 96, 1191–1198. doi: 10.1093/aob/mci272

Umaharan, P., Ariyanayagam, R. P., and Haque, S. Q. (1997). Effect of short-term waterlogging applied at various growth phases on growth, development and yield in *Vigna unguiculata*. *J. Agric. Sci.* 128, 189–198. doi: 10.1017/S0021859696004121

Velasco, N. F., Ligarreto, G. A., Díaz, H. R., and Fonseca, L. P. M. (2019). Photosynthetic responses and tolerance to root-zone hypoxia stress of five bean cultivars (*Phaseolus vulgaris* L.). *South Afr. J. Bot.* 123, 200–207. doi: 10.1016/j.sajb.2019.02.010

Verhulst, N., and Govaerts, B. (2010). The normalized difference vegetation index (NDVI) GreenSeekerTM handheld sensor: toward the integrated evaluation of crop management. Part A: concepts and case studies. Mexico: CIMMYT.

Voesenek, L. A. C. J., and Bailey-Serres, J. (2015). Flood adaptive traits and processes: an overview. *New Phytol.* 206, 57–73. doi: 10.1111/nph.13209

Ward, P. J., De Ruiter, M. C., Mård, J., Schröter, K., Van Loon, A., Veldkamp, T., et al. (2020). The need to integrate flood and drought disaster risk reduction strategies. *Water Security.* 11:100070. doi: 10.1016/j.wasec.2020.100070

Yamauchi, T., Colmer, T. D., Pedersen, O., and Nakazono, M. (2018). Regulation of root traits for internal aeration and tolerance to soil waterlogging-flooding stress. *Plant Physiol.* 176, 1118–1130. doi: 10.1104/pp.17.01157

Yang, L., Li, N., Liu, Y., Miao, P., Liu, J., and Wang, Z. (2023). Updates and prospects: morphological, physiological, and molecular regulation in crop response to waterlogging stress. *Agronomy* 13:2599. doi: 10.3390/agronomy13102599

Zeng, R., Chen, L., Wang, X., Cao, J., Li, X., Xu, X., et al. (2020). Effect of waterlogging stress on dry matter accumulation, photosynthesis characteristics, yield, and yield components in three different ecotypes of peanut (*Arachis hypogaea* L.). *Agronomy* 10:1244. doi: 10.3390/agronomy10091244

Zhang, X., Shabala, S., Koutoulis, A., Shabala, L., Johnson, P., Hayes, D., et al. (2015). Waterlogging tolerance in barley is associated with faster aerenchyma formation in adventitious roots. *Plant Soil* 394, 355–372. doi: 10.1007/s11104-015-2536-z

Zhu, M., Li, F. H., and Shi, Z. S. (2016). Morphological and photosynthetic response of waxy corn inbred line to waterlogging. *Photo-Dermatology* 54, 636–640. doi: 10.1007/s11099-016-0203-0

frontiers | Frontiers in Sustainable Food Systems

TYPE Original Research
PUBLISHED 15 May 2024
DOI 10.3389/fsufs.2024.1391989

OPEN ACCESS

EDITED BY
Aliza Pradhan,
National Institute of Abiotic Stress Management (ICAR), India

REVIEWED BY
Anilkumar C,
National Rice Research Institute (ICAR), India
Bharadwaj Chellapilla,
Indian Agricultural Research Institute (ICAR), India

*CORRESPONDENCE
Manje Gowda
m.gowda@cgiar.org

RECEIVED 26 February 2024
ACCEPTED 19 April 2024
PUBLISHED 15 May 2024

CITATION
Ndlovu N, Gowda M, Beyene Y, Chaikam V, Nzuve FM, Makumbi D, McKeown PC, Spillane C and Prasanna BM (2024) Genomic loci associated with grain yield under well-watered and water-stressed conditions in multiple bi-parental maize populations. *Front. Sustain. Food Syst.* 8:1391989. doi: 10.3389/fsufs.2024.1391989

Genomic loci associated with grain yield under well-watered and water-stressed conditions in multiple bi-parental maize populations

Noel Ndlovu[1,2], Manje Gowda[1]*, Yoseph Beyene[1], Vijay Chaikam[1], Felister M. Nzuve[3], Dan Makumbi[1], Peter C. McKeown[2], Charles Spillane[2] and Boddupalli M. Prasanna[1]

[1]International Maize and Wheat Improvement Center (CIMMYT), Nairobi, Kenya, [2]Agriculture & Bioeconomy Research Centre, Ryan Institute, University of Galway, Galway, Ireland, [3]Department of Plant Science and Crop Protection, University of Nairobi, Nairobi, Kenya

Smallholder maize farming systems in sub-Saharan Africa (SSA) are vulnerable to drought-induced yield losses, which significantly impact food security and livelihoods within these communities. Mapping and characterizing genomic regions associated with water stress tolerance in tropical maize is essential for future breeding initiatives targeting this region. In this study, three biparental F_3 populations composed of 753 families were evaluated in Kenya and Zimbabwe and genotyped with high-density single nucleotide polymorphism (SNP) markers. Quantitative trait loci maping was performed on these genotypes to dissect the genetic architecture for grain yield (GY), plant height (PH), ear height (EH) and anthesis-silking interval (ASI) under well-watered (WW) and water-stressed (WS) conditions. Across the studied maize populations, mean GY exhibited a range of 4.55–8.55 t/ha under WW and 1.29–5.59 t/ha under WS, reflecting a 31–59% reduction range under WS conditions. Genotypic and genotype-by-environment (G × E) variances were significant for all traits except ASI. Overall broad sense heritabilities for GY were low to high (0.25–0.60). For GY, these genetic parameters were decreased under WS conditions. Linkage mapping revealed a significant difference in the number of QTLs detected, with 93 identified under WW conditions and 41 under WS conditions. These QTLs were distributed across all maize chromosomes. For GY, eight and two major effect QTLs (>10% phenotypic variation explained) were detected under WW and WS conditions, respectively. Under WS conditions, Joint Linkage Association Mapping (JLAM) identified several QTLs with minor effects for GY and revealed genomic region overlaps in the studied populations. Across the studied water regimes, five-fold cross-validation showed moderate to high prediction accuracies (–0.15–0.90) for GY and other agronomic traits. Our findings demonstrate the polygenic nature of WS tolerance and highlights the immense potential of using genomic selection in improving genetic gain in maize breeding.

KEYWORDS

water stress, maize, sub-Saharan Africa, QTL mapping, grain yield, genomic selection

1 Introduction

Across Africa, *circa* 40% of maize-growing areas are exposed to recurrent drought (Fisher et al., 2015), with a frequency of 10-20% (Tesfaye et al., 2016). These droughts are responsible for substantial grain yield losses exceeding 20% in smallholder farming systems. Previous studies have shown that with each additional degree day above 30°C, maize grain yield under water-stressed (WS) conditions is reduced by 1.7% (Lobell et al., 2011). These drought-induced yield losses can be attributed to several trait-related factors - including reduced kernel size, inhibited ear elongation (Wang et al., 2019) and delayed silking (Sah et al., 2020). Water stress can also have negative effects on the nutritional quality of maize grain (Barutcular et al., 2016; Sehgal et al., 2018), which is a concern for the already malnourished smallholder farmer communities in sub-Saharan Africa (SSA). Over the past decades, the adverse effects of WS have been more pronounced in rainfed (Lunduka et al., 2019) maize-dependent smallholder farming systems in SSA. In this region, maize grain yield [range: 1–3 tonne ha^{-1} (Prasanna et al., 2020)] and quality losses are further compounded by other limiting factors such as heat stress (Chukwudi et al., 2021), low soil nitrogen stress (Ndlovu et al., 2022; Kimutai et al., 2023), insect pest infestations (Deutsch et al., 2018), disease incidences (Beyene et al., 2017) and limited access to quality seeds among smallholders (Breen et al., 2024).

Despite the widely reported unpredictability of drought (Seleiman et al., 2021), farmers and researchers can adopt a range of strategies to curb yield losses (Muroyiwa et al., 2022). Such strategies include the development, release, and adoption of WS-tolerant maize varieties. On-farm trials conducted in SSA have shown that WS-tolerant varieties of maize can have a 5–40% grain yield advantage over traditional varieties under WS conditions (Tesfaye et al., 2016). Such yield advantage has been reported to generate extra income for maize-dependent households [e.g., up to US$240/ha or > 9 months of food sufficiency in Zimbabwean households (Lunduka et al., 2019)]. Advancing genetic gains for WS-tolerant maize varieties is, therefore, an essential component of the basket of technology options for improving the resilience of smallholder maize farming systems (Habte et al., 2023) in SSA. However, breeding for WS-tolerant maize varieties presents several challenges due to the complex nature of WS and the need to advance genetic gain concurrently for a range of yield-related traits.

Breeding for higher maize grain yields under WS has been limited by genotype-by-environment (G × E) effects and low heritability (Collins et al., 2008). As water stress tolerance is a multigenic trait, investigations of grain yield under WS also involve evaluating a range of secondary traits, including anthesis-silking interval (ASI) (Bolaños and Edmeades, 1996; Gopalakrishna K. et al., 2023), reduced water potential and root development (Thirunavukkarasu et al., 2014), ear height-to-plant height ratio (Zhao et al., 2019) and number of ears per plant (Badu-Apraku et al., 2019). Other studies have also measured high water-holding capacity, enhanced cell wall biosynthesis and stability of photosynthesis (Zhang et al., 2020). Most of these traits have higher heritabilities than grain yield and can be good secondary traits to enhance selection for drought tolerance in maize. Using conventional breeding to improve traits associated with WS tolerance presents a range of challenges, including its laborious and slow nature (Nikolić et al., 2013). However, there is significant potential to overcome some WS-tolerance breeding challenges by incorporating molecular breeding [e.g., quantitative-trait loci (QTL) mapping (Zhao et al., 2019; Hu et al., 2021; Sarkar et al., 2023), genome-wide association studies (GWAS) (Khan et al., 2022; Anilkumar et al., 2023; Chen et al., 2023) and genomic selection (GS) (Beyene et al., 2015; Cerrudo et al., 2018; He et al., 2019; Ndlovu et al., 2022, 2024; Zhang et al., 2022)] and phenomics-assisted breeding [i.e., high-throughput phenotyping (Wu et al., 2021)] approaches. To unravel the genetic architecture of WS tolerance in tropical maize, molecular breeding approaches have become crucial for improving this complex trait.

A range of studies have identified genomic regions associated with the tolerance of maize lines to WS conditions. These studies have shown that WS tolerance is a complex trait governed by many minor QTLs (Choudhary et al., 2023). For instance, Osuman et al. (2022) identified 27 single nucleotide polymorphisms (SNPs), with four SNPs [*SNP_138825271* (Chr. 3), *SNP_244895453* (Chr. 4), *SNP_168561609* (Chr. 5), and *SNP_62970998* (Chr. 6)] having pleiotropic effects on anthesis days, silking days and husk cover under terminal drought. Under both WS and well-watered (WW) conditions, Zaidi et al. (2016) identified 37 SNPs for grain yield and shoot biomass. Two of these SNPs (SNPs *S1_211520521* and *S2_20017716*) were associated with shoot biomass and transpiration efficiency under WS. For plant height, 120 SNPs were identified by Wallace et al. (2016) from 15 tropical maize populations grown under WS in SSA. Thirunavukkarasu et al. (2014) identified SNPs associated with functional traits such as stomatal closure, root development, flowering, detoxification, and reduced water potential under drought stress, Yuan et al. (2019) identified 46 differentially expressed candidate genes under both WS and WW conditions. At the seedling stage, Chen et al. (2023) identified 15 candidate genes for water stress tolerance in maize.

Combining QTL mapping with GWAS can enhance the identification of markers associated with various traits of interest (Chen et al., 2016; Zhou et al., 2018; Li et al., 2020; Ndlovu et al., 2022; Sallam et al., 2022). The identified markers can then be utilized in marker-assisted recurrent selection (MARS) for improving WS tolerance in tropical maize (Beyene et al., 2016). GS is also a promising tool for improving polygenic traits (like WS tolerance in maize). Unlike MARS, GS can capture the effects of many small-effect QTLs (Bentley et al., 2014; Cerrudo et al., 2018). Several studies also showed that incorporation of markers linked to major effect QTLs as a fixed effect in genomic prediction model can improve the prediction accuracy as observed for *Striga* resistance (Gowda et al., 2021) and maize lethal necrosis resistance in maize (Gowda et al., 2015). To understand the effectiveness of QTL mapping and GS in dissecting the genetic basis of WS tolerance, a set of tropical bi-parental maize populations evaluated in Kenya and Zimbabwe were used in this study. The study sought to (i) compare the quantitative genetic parameters (i.e., heritability, variance, and genetic correlation) of grain yield and secondary traits under WW and WS conditions; (ii) identify the genomic regions through linkage mapping and joint linkage association mapping for grain yield and other traits in three F_3 populations evaluated in multiple locations; and (iii) assess the potential of GS in improving grain yield and related traits under WW and WS conditions.

2 Materials and methods

2.1 Plant materials, experimental design, and crop management

Three biparental F_3 maize populations comprised of 753 families developed by the Global Maize Program of the International Maize and Wheat Improvement Centre (CIMMYT) were evaluated under WW and managed WS conditions. Population 1 comprised 240 F_3 families from the cross CML543 × CML444, Population 2 comprised 255 F_3 families from the cross CML543 × LaPostaSeqC7-F71 and Population 3 comprised 258 F_3 families from the cross CKL5009 × LaPostaSeqC7-F71. CML444 and LaPostaSeqC7-F7 are known WS-tolerant lines; CML543, on the other hand, perform better under WW and is resistant to foliar diseases. CML444 from heterotic group B is extensively used as a drought tolerant donor line in SSA and is adapted to mid-altitude region. It is also known to be tolerant to low soil N stress and resistant to maize streak virus, ear rot, and northern corn leaf blight. CML543 is another promising elite line that was developed from a CML202xCML395 derived population known for being tolerant to foliar diseases like gray leaf spot, northern corn leaf blight and common rust. LapostaSeqC7-F71 and CKL5009 are the other parents used in population development. LapostaSeqC7-F71 was derived from the LapostaSequia germplasm, a known source for developing WS-tolerant elite donors. In addition to WS-tolerance, LapostaSeqC7-F71 also exhibits tolerance to ear rot. CKL5009, developed from Kenya Agricultural and Livestock Research Organization's germplasm, is known to be moderately tolerant to drought and tolerant to low soil N conditions. All 753 F_3 families from the three bi-parental populations were test-crossed to a single cross-tester for phenotypic evaluation. The testcross progenies were evaluated across six sites in Kenya and one site in Zimbabwe (Table 1). Field trials in Kakamega and Kiboko were all evaluated over a two-year period.

Trials of each test cross were planted in single row (4 m) plots with 2 replications at all locations. The field layout was an alpha (0,1) lattice design. Experiments were laid out in a 40 × 6, 51 × 5 and 43 × 6 alpha lattice design for F_3 pop 1, pop 2 and pop 3, respectively. Four commercial checks (DKC8031, H513, WH504 and WH505) and two parents of each population were used so that the total of the experimental genotypes were 240, 255 and 258 for F_3 pop 1, pop 2 and pop 3, respectively. Standard agronomic management practices were followed. All populations were planted in the same season in adjacent plots. The genotypes were subjected to WW and WS management conditions. In the WS trial, drought stress was imposed following the CIMMYT-established protocol (Bänziger et al., 2000). Trials for WS evaluations were irrigated once a week until 2 weeks prior to the expected flowering date in each population. Irrigation was withdrawn and the water stress condition was maintained till harvest. For WW trials, planting was done in the main rainy season and whenever needed, irrigation was provided to avoid any stress.

2.2 Phenotypic data collection and analyses

A total of ten traits (i.e., grain yield (GY), anthesis date (AD), silking date (SD), anthesis-silking interval (ASI), plant height (PH), ear height (EH), ear rot (ER), ears per plant (EPP), ear position (EPO) and ear aspect (EA)) were measured for all bi-parental populations under WW and WS regimes. All ears harvested from each plot were shelled and weighed to determine total GY (in kg), then converted to t/ha by dividing the total GY per plot by the plot area. The grain moisture content (MOI) of the shelled grains at harvest was determined using a hand-held moisture meter and recorded in percentages. The ASI was calculated as the difference between SD and AD in days. SD was recorded as the number of days from sowing to at least 50% silk emergence in each plot, while AD was recorded as the number of days from sowing to when 50% of the plants per plot had shed pollen. PH was measured in centimetres (cm) from the base of the plant to the tip of the tassel. EH was measured in cm from the ground to the node bearing the highest ear. Five representative plants were measured at maturity in each plot for both PH and EH. EA was measured on a scale of 1–5, where 1 = nice and uniform cobs with the preferred texture; 5 = cobs with undesirable texture. EPO was calculated as the ratio of EH to PH.

Analyses of variance for each bi-parental population at each and across environments (i.e., WW and WS regimes) were performed using ASREML-R (Gilmour et al., 2009) and META-R (Alvarado et al., 2020). The following statistical mixed model was used to estimate variance components:

$$Y_{ijko} = \mu + G_i + E_j + (GE)_{ij} + R(E)_{kj} + B(R.E)_{ojk} + e_{ijko},$$

where Y_{ijko} is the phenotypic performance of the ith genotype at the jth environment in the k^{th} replication of the oth incomplete block, μ is an intercept term, G_i is the genetic effect of the i^{th} genotype, E_j is the effect of the jth environment, $(GE)_{ij}$ is the interaction effect between genotype and environment, $R(E)_{kj}$ is the effect of the k^{th}

TABLE 1 Agro-climatic characteristics and management at seven field sites used for the evaluation of the bi-parental populations of tropical maize.

Location	Country	Longitude	Latitude	Altitude (masl)	Management
Kiboko-1	Kenya	37°75′E	02°15′ S	975	Water-stressed
Kiboko-2	Kenya	37°75′E	02°15′ S	975	Water-stressed
Chiredzi	Zimbabwe	31°34′E	21°01′S	430	Water-stressed
Embu	Kenya	37°27′E	01°31′N	1,350	Well-watered
Kakamega-1	Kenya	34°45′E	00°16′N	1,585	Well-watered
Kakamega-2	Kenya	34°45′E	00°16′N	1,585	Well-watered
Kitale	Kenya	01°01E	39°59N	1849	Well-watered

replication at the j^{th} environment, $B(R.E)_{ojk}$ is the effect of the o^{th} incomplete block in the k^{th} replication at the j^{th} environment, and e_{ijko} is the residual. The genotypic effect (G_i), genotype by environment interaction (GEI) and effect of incomplete blocks were treated as random effects to estimate their variances and residual error. Environments and replications were treated as fixed effects. Assuming fixed genotypic effects, a mixed linear model was fitted to obtain the best linear unbiased estimates (BLUEs). Broad-sense heritability (H^2) was estimated as the ratio of genotypic to phenotypic ratio from the variance components. META-R software (Alvarado et al., 2015) was used to obtain the best linear unbiased prediction (BLUP) for each genotype across environments. BLUEs and BLUPs across the population were also obtained with the mixed model through META-R software.

2.3 Molecular data analysis

All three bi-parental populations used in this study were also used in earlier QTL mapping studies for maize lethal necrosis (MLN) disease (Gowda et al., 2018). Detailed description of the molecular markers used and the linkage map construction are also described in our earlier study (Gowda et al., 2018). In brief, DNA of all lines of the bi-parental populations was extracted from seedlings at the 3–4 leaf stage and genotyped using the genotype-by-sequencing (GBS) platform at the Institute for Genomic Diversity, Cornell University, Ithaca, USA, using high density markers, as per the protocol described in (Elshire et al., 2011). For SNP calling, raw data in a FASTQ file together with the barcode information and Tags On Physical Map (TOPM) data, which had SNP position information was used. We used TOPM data from AllZeaGBSv2.7 downloaded from Panzea,[1] which contained information for 955,690 SNPs mapped with B73 AGPv2 coordinates. The TASSEL-GBS pipeline was used for calling SNPs (Glaubitz et al., 2014). TASSEL ver. 5.2 (Bradbury et al., 2007) was used to exclude SNPs with heterozygosity of >5%, minor allele frequency (MAF) of <0.05, and a minimum count of 90% by filtering from raw GBS SNP markers in all populations. The number of SNPs was further reduced by selecting homozygous and polymorphic markers between the parents in each population. SNPs were further filtered based on the minimum distance between the markers. We used the criteria of minimum distance between adjacent SNPs as ≥200 Kilo base pairs (Kbps) to ensure uniform distribution of markers throughout the genome. For joint linkage association mapping (JLAM), markers from all three bi-parental populations were combined, and markers with <1% missing value and > 5% MAF and Heterozygosity of <5% were retained. Finally, a set of 5,490 SNPs that are uniformly distributed across the genome were used for JLAM analyses.

QTL IciMapping ver. 4.1 (Meng et al., 2015) was used to construct the linkage map based on data from all three biparental populations. QTL IciMapping was used to remove the highly correlated SNPs that do not provide any additional information by using an inbuilt tool BIN. This resulted in the retention of 560, 556 and 555 high-quality SNPs in populations 1, 2 and 3, respectively. These SNPs were used to construct linkage maps using the MAP function, by selecting the most significant markers using stepwise regression. A likelihood ratio test was used to calculate the logarithm of odds (LOD) for each marker at a score of >3 with a 30 cM maximum distance between two loci. The Kosambi mapping function (Kosambi, 1944) was used to transform the recombination frequencies between two linked loci. BLUPs across environments were used to detect QTLs based on Inclusive interval mapping (ICIM) for each population. The phenotypic variation explained by individual QTLs and the total variation explained by QTLs was estimated. QTL naming was done with the letter "q" indicating QTL, followed by an abbreviation of the trait name, the chromosome, and the marker position, respectively.

2.4 Joint linkage association mapping

For JLAM, high-quality and uniformly distributed 5,490 SNPs across three F_3 populations were selected. The SNPs were then used to construct a linkage map based on their physical positions. A biometric model (Würschum et al., 2012; Kibe t al., 2020) was used to perform JLAM, with BLUPs across environments and populations being applied for analysis. After testing several biometric models, one which performed well for association studies in multiple segregating biparental populations (Würschum et al., 2012) was used to conduct the JLAM. This model controls the differences in population means by incorporating population effect, and the genetic background by using cofactors and marker effects across populations. This model was explained in detail by Liu et al. (2011) and Würschum et al. (2012). With this model, first-step cofactors were selected based on the Schwarz Bayesian Criterion (Schwarz, 1978) by including a population effect and in the second step, p values were calculated for the F-test by using a full model (including SNP effect) versus a reduced model (without SNP effect). Cofactors were selected by using PROC GLM SELECT from SAS 9.4 (SAS Institute Inc. 2015) and genome-wide scans for QTLs were applied in R (ver. 4.3.1) (R Core Team, 2023).

2.5 Genomic prediction

Genome-wide prediction was applied for GY and all other traits within and across three F_3 populations with five-fold cross-validation. BLUEs across locations obtained under WW and WS management were used with a ridge-regression BLUP prediction model (Zhao et al., 2012; Sitonik et al., 2019). For genomic prediction, 4,000 common SNPs for each of the three populations which were distributed uniformly across the genome with no missing values were selected. To understand the effect of different training populations on accuracy, genomic prediction was carried out in three scenarios of cross-validation within and across biparental populations. Scenario 1: both training and testing populations are drawn from within each segregating population. In Scenario 2, the training population is derived from across populations, and the testing population was drawn from within each population whereas, for Scenario 3, both the training and testing population was derived from across populations. For Scenarios 2 and 3, the estimation of marker effects was based on the genotypic variance of the total populations. For Scenario 1, the estimates of the genotypic variance and heritability within segregating

1 https://www.panzea.org/

populations were used in the rr-BLUP model. The prediction accuracy of GS was calculated as $r_{GS} = r_{MP}/h$, where h refers to the square root of heritability and r_{MP} is the correlation between observed and predicted phenotypes (Dekkers, 2007). For each trait in each population and each scenario, 100 iterations were done for sampling the training and testing sets.

3 Results

3.1 Effect of water stress on maize grain yield and related traits

The mean GY of the four parents CML543, CML444, LapostasequiaC7-F71 and CKL5009 (used to develop the studied bi-parental maize populations) were 6.97, 6.30, 6.31 and 5.87 t/ha under WW conditions, and 2.32, 2.68, 5.08 and 3.69 t/ha under managed WS conditions, respectively. Across the three bi-parental maize populations, significant variations were observed for GY, EH, PH and ASI in both WW and WS regimes (Figure 1; Tables 2, 3). Mean GY for pop 1 (CML543 × CML444), pop 2 (CML543 × LPSC7-F71) and pop 3 (CKL5009 × LPSC7-F71), and across populations were 6.38, 7.04, 6.04 and 6.41 t/ha under WW and 2.66, 3.72, 4.08 and 3.50 t/ha under WS management, respectively (Figure 1). Across the three bi-parental maize populations, mean GY ranged from 4.55 to 8.55 t/ha and 1.29 to 5.59 t/ha under WW and WS conditions, respectively. Overall analysis showed that under WS environments, GY reductions were 59, 48, and 31% in pop 1, pop 2 and pop 3, respectively. The ranges of ASI values were wider under WS conditions than under WW conditions (Figure 1). Across all populations, we observed ASI, PH and EH means of 1.48 days, 241.65 cm, and 127.76 cm, respectively under WW conditions. Under WS conditions, the recorded means for ASI, PH and EH were 2.12 days, 210.71 cm, and 127.1 cm, respectively. Interestingly, mean ASI across the studied maize populations was 2.6 days longer under WS conditions than under WW conditions. The BLUEs and BLUPs for each and combined populations and markers used in this study are presented in Supplementary Table S1.

Analyses of variance for 'within' and 'across' environments revealed significant genotypic and genotype by environment (G × E) variances for all traits except for ASI (under WW conditions) and EH (under WS conditions) in pop 1 (Table 2). For GY, we observed low to moderate heritability estimates of 0.60, 0.54, 0.25 and 0.65 under WW conditions and 0.30, 0.32, 0.58 and 0.54 under WS management for pop 1, pop 2, pop 3 and all combined, respectively (Table 2). It is important to highlight that the lowest broad sense heritabilities under WS conditions were greater than the lowest values achieved under WW conditions, yet they remained below the highest values achieved under WW conditions. For individual populations, broad sense heritabilities for ASI ranged from 0.43–0.53 and 0.18–0.50 under WW and WS conditions, respectively. For PH, heritability ranged from 0.68–0.79 (WW) and 0.43–0.65 (WS). The estimates of broad-sense heritability for EH ranged between 0.72–0.85 (WW) and 0.39–0.79 (WS). Under WW conditions and for all studied populations, the broad sense heritability of GY was highest (65%), followed by EH (51%), PH (45%) and ASI (35%). While, under WS environments, broad sense heritabilities were estimated at 54, 47, 23 and 17% for GY, EH, PH and ASI, respectively. Generally, the broad-sense heritability of all studied maize traits was low under WS compared to WW conditions (Table 2).

Correlation analyses showed that GY was significantly and negatively correlated with *Turcicum* leaf blight (TLB) severity (−0.53), husk cover (−0.24), ear rot (−0.20), and ear aspect (−0.60) under WW conditions. GY was also shown to be positively and significantly correlated with PH (0.60), EH (0.41), anthesis date (0.28), silking date (0.22), and ears per plant (0.40) (Figure 2) under the same conditions. Under WS conditions, GY was significantly and negatively correlated with anthesis date (−0.69), silking date (−0.7), ASI (−0.27), ear rot (−0.4), ear aspect (−0.38) and ear position (−0.25). It was also significantly and positively correlated with ears per plant (0.71).

3.2 QTLs associated with grain yield and related traits under well-watered and water-stressed conditions

The linkage map was constructed for F_3 pop 1, pop 2 and pop 3 using 560, 556 and 555 high-quality polymorphic SNPs, respectively. The mean distances between adjacent markers were recorded at 8.07, 7.50 and 8.04 cM for F_3 pop 1, pop 2 and pop 3, respectively. The identified QTLs for GY, ASI, PH and EH at WW and WS conditions for each population are presented in Tables 3–6. Our QTL analyses identified totals of 93 and 41 QTLs for GY, ASI, PH and EH, under WW and WS conditions, respectively. For the studied four traits, 23, 39 and 31 QTLs (under WW conditions) and 8, 4, and 29 QTLs (under WS conditions) in pop 1, pop 2 and pop 3 were detected, respectively.

In F_3 pop 1, QTL analysis revealed a total of 23 QTLs for GY (8), PH (9) and EH (6) under WW conditions and 8 QTLs for ASI (4), PH (3) and EH (1) under WS conditions (Supplementary Table S2). For this population, no QTLs were detected for GY under WS conditions (Table 3). In pop 2, QTL analysis revealed 39 QTLs for GY (8), ASI (5), PH (12) and EH (14) under WW conditions and four QTLs for GY (1), ASI (1), and PH (2) under WS conditions. In pop 3, 31 and 29 QTLs were detected for the four traits under WW and WS conditions, respectively. Interestingly, the highest number of QTLs detected in this population were for PH (13) and EH (13) under WS conditions. Furthermore, no QTLs were detected for ASI under WS conditions in this population (Tables 5, 6).

The phenotypic variation explained (PVE) for all the detected QTLs ranged from 2.51 to 27.77%. Interestingly, these two extremes were observed in pop 3 for WS_PH (2.51%) and WW_GY (27.77%). Significant QTLs with major effects, explaining >10% of the PVE, were identified for GY (nine QTLs under WW and two QTLs under WS conditions). Noteworthy, a few significant major effect QTLs were also identified for ASI, PH and EH under both WW and WS conditions (Tables 4–6).

JLAM QTL analysis across the three bi-parental populations identified 25 QTLs for GY under the WW conditions and 4 under the WS (Table 7). For this analysis, PVE ranged from 0.80–3.9% and 1.4–11.8% for WW and WS environments, respectively. For GY, most of the QTLs were identified in chromosomes 4 and 6 (5 QTLs each). For ASI, 16 and 15 QTLs were identified under WW and WS environments, respectively (Table 8). PVE for ASI ranged from 0.1–4.9% and 1.3–10.9% for WW and WS environments,

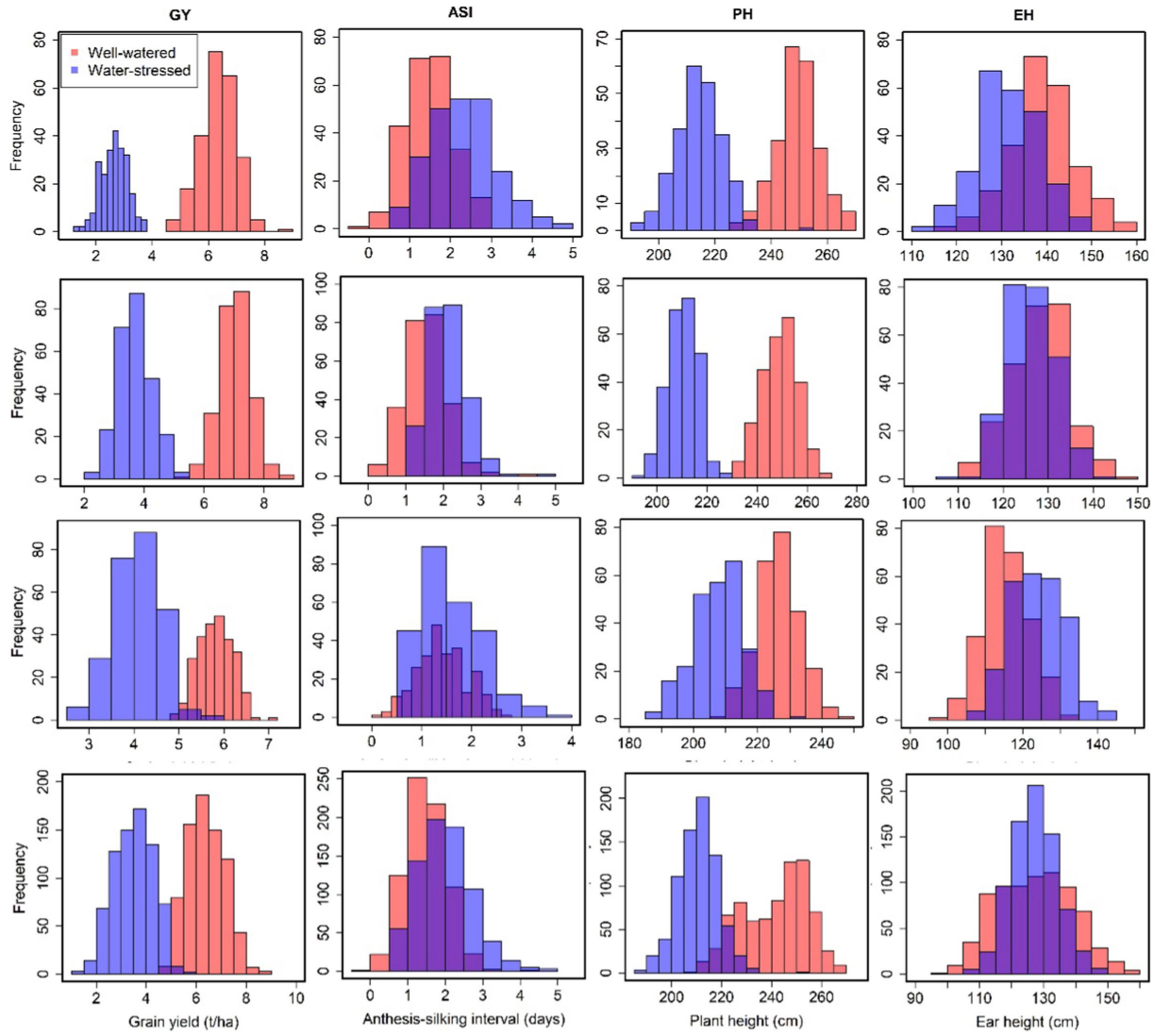

FIGURE 1
Phenotypic distribution of grain yield and related traits tested under well-watered and water-stressed conditions in Kenya and Zimbabwe. The orange and purple color plots represent the field trials conducted under well-watered and water-stressed conditions, respectively.

respectively. Interestingly, most of the QTLs associated with ASI were identified in chromosomes 8 (n = 4) and 1 (n = 6) under WW and WS conditions, respectively. However, across the two water regimes, no QTLs were identified for ASI in chromosomes 4 and 10. We also identified 19 QTLs for PH under WW (12) and WS (7) environments (Table 9). Notably, chromosome 1 had no QTLs for PH under both WW and WS conditions. For EH, our analysis identified 20 QTLs under WW (6) and WS (14) environments. Unlike the other traits, chromosomes 9 and 10 had no QTLs for EH across the two studied management conditions. For GY, the QTL on chromosome 6 (*qGY6_89*) had the largest effect with 11.80% of PVE under WS condition and was found overlapping with QTL for WW_PH (*qPH6_87*) in F_3 pop 2 and with WW_EH (*qEH6_90*) in F_3 pop 1 (Tables 5–7). Another major effect was QTL identified for ASI (*qASI1_107*) which explained 10.9% of the PVE and did not overlap with any QTL detected in the individual population analyses.

3.3 Prediction accuracies of grain yield and related traits under WW and WS conditions

Five-fold cross-validation was used to assess the prediction accuracy for GY, ASI, PH and EH traits by combining data from three populations and within each population. Prediction accuracies for the training and testing within-within (WW scenario 1) populations were 0.67, 0.58 and 0.57 for GY under well-watered conditions and 0.38, −0.15 and 0.20 under water stress conditions for pop 1, pop 2 and pop 3, respectively (Figure 3). For ASI, prediction accuracies for pop 1, pop 2 and pop 3 were 0.55, 0.74 and 0.61 under WW conditions and 0.30, 0.31 and 0.41 under WS conditions, respectively. For PH, prediction accuracies of 0.75 and 0.67, 0.68 under WW conditions and 0.48, 0.30 and 0.62 under WS conditions were recorded for pop 1, pop 2 and pop 3, respectively. For EH, prediction accuracies of 0.38, 0.20 and 0.60 under WW management and 0.67, 0.58 and 0.60 under WS management were recorded for pop 1, pop 2 and pop 3, respectively.

TABLE 2 Genetic parameters for the individual and combined three bi-parental populations evaluated under well-watered and water-stressed conditions in multiple environments.

	Well-watered				Water stressed			
Trait	GY (t/ha)	ASI (days)	PH (cm)	EH (cm)	GY (t/ha)	ASI (days)	PH (cm)	EH (cm)
CML543 × CML444 F_3 pop 1								
Mean	6.38	1.49	249.43	139.21	2.66	2.67	194.59	119.17
σ^2_G	0.23**	0.17**	41.25**	40.97**	0.02*	0.15*	21.99**	20.69**
σ^2_{GE}	0.26**	0.00	3.91*	8.77**	0.02*	0.23**	7.83**	0.00
σ^2_e	0.71	1.23	150.62	108.93	0.19	1.33	97.86	87.19
h^2	0.60	0.53	0.68	0.72	0.30	0.33	0.54	0.59
CML543 × LapostaSequiaF71 F_3 pop 2								
Mean	7.04	1.50	241.91	124.06	3.72	2.65	195.44	118.51
σ^2_G	0.15**	0.12**	29.45**	26.88**	0.03*	0.04*	11.39*	8.13*
σ^2_{GE}	0.17**	0.11**	9.97**	8.19**	0.05**	0.10**	0.15*	5.46*
σ^2_e	0.73	1.01	54.50	31.11	0.29	0.91	88.62	64.81
h^2	0.54	0.43	0.76	0.82	0.32	0.18	0.43	0.39
CML543 × LapostaSequiaF71 F_3 pop 3								
Mean	6.04	1.38	225.83	115.60	4.08	1.65	207.45	126.94
σ^2_G	0.03*	0.13**	27.96**	27.38**	0.06**	0.13**	22.63**	27.41**
σ^2_{GE}	0.12**	0.02*	2.60*	1.23*	0.01	0.01	3.32*	2.68*
σ^2_e	0.51	0.85	54.84	36.73	0.23	0.76	67.64	39.40
h^2	0.25	0.53	0.79	0.85	0.58	0.50	0.65	0.79
Across three bi-parental maize populations								
Mean	6.41	1.48	241.65	127.76	3.50	2.12	210.71	127.10
σ^2_G	0.35**	0.10**	21.59**	21.37**	0.32**	0.14**	13.74*	22.85**
σ^2_{GE}	0.20**	0.15**	44.79**	40.29**	0.05*	0.25**	20.00**	11.00**
σ^2_e	1.06	1.24	120.78	84.54	1.03	2.17	147.34	81.56
h^2	0.65	0.35	0.45	0.51	0.54	0.17	0.23	0.47

* and ** indicate significance at $p < 0.05$ and $p < 0.01$, respectively. σ^2G, σ^2GxE, σ^2e, and h^2, refer to genotypic variance, genotype x environment interaction variance, error variance and broad sense heritability, respectively.

For across-within scenario (AW scenario 2) where training population is derived by combining all three populations and testing population is derived from within single population, prediction accuracies for GY were higher under well-watered conditions with 0.56, 0.59 and 0.44 compared to WS conditions (0.25, −0.01 and 0.15) for pop 1, pop 2, and pop 3, respectively. For ASI, PH and EH, the prediction accuracies were varied from 0.58 to 0.70, 0.63 to 0.78 and 0.62 to 0.70 under well-watered conditions, respectively. Whereas under water stress conditions prediction accuracies for ASI, PH and EH were ranged from 0.34 to 0.44, 0.31 to 0.72 and 0.35 to 0.61, respectively. The prediction accuracy across all populations combined showed high values for all traits in both well-watered (0.53–0.90) and water stress (0.41–0.89) conditions (Figure 3).

4 Discussion

Water stress is one of the most significant abiotic factors impacting GY and quality in maize-dependent farming systems of SSA. WS-tolerant maize varieties can offer an inexpensive solution to low-input farming systems in drought-prone regions. Improving WS tolerance in maize cultivars using advanced tools such as doubled haploid technology and marker-assisted selection necessitates a deeper knowledge of its genetic basis (Hu et al., 2021). Mapping of QTLs associated with WS tolerance, and its related secondary traits can facilitate the use of molecular markers for improving WS tolerance in tropical maize. In this study, three bi-parental populations were evaluated under WW and WS conditions in Kenya and Zimbabwe. The populations were mapped for QTL associated with GY, PH, EH and ASI. These related complex quantitative traits have been widely used for selection in the development of WS-tolerant maize lines and hybrids (Zhao et al., 2019).

4.1 Well-watered and water-stressed conditions induced significant variations in phenotypic mean, variance, and heritability

Our phenotypic analyses showed that GY, PH and EH were substantially decreased under WS conditions across the studied bi-parental populations. This is consistent with the findings of previous studies (Adebayo and Menkir, 2014; Wang et al., 2019; Balbaa

TABLE 3 Number of QTLs associated with grain yield under well-watered and water-stressed conditions detected in three F_3 populations.

	QTL name	Chr	Position (cM)	LOD	PVE (%)	TPVE (%)	Add	Dom	QTL confidence interval	
									Left SNP	Right SNP
F_3 pop 1 CML543 × CML444										
WW_GY	*qGY1_199*	1	588	7.48	9.32	42.59	0.23	0.08	*S1_198739875*	*S1_199756190*
	qGY2_194	2	430	3.77	5.20		0.16	0.09	*S2_193189169*	*S2_198859260*
	qGY3_208	3	39	9.54	13.04		0.30	−0.02	*S3_212501788*	*S3_207551089*
	qGY3_206	3	44	5.59	11.18		−0.27	−0.04	*S3_207551089*	*S3_206260377*
	qGY4_150	4	295	9.65	13.16		−0.28	−0.01	*S4_149725104*	*S4_150813768*
	qGY5_50	5	306	3.21	3.74		0.17	−0.04	*S5_55216459*	*S5_46946857*
	qGY8_155	8	216	4.74	6.03		−0.18	−0.13	*S8_153860376*	*S8_159336080*
	qGY9_155	9	10	3.14	16.19		0.19	−0.46	*S9_155445883*	*S9_146872747*
F_3 pop 2 CML543 × LapostaSeqF71										
WW_GY	*qGY3_85*	3	275	5.41	7.41	34.76	0.04	−0.32	*S3_85662699*	*S3_81746578*
	qGY4_210	4	79	3.07	16.76		−0.29	−0.01	*S4_210692761*	*S4_209568060*
	qGY4_191	4	117	5.94	19.27		0.26	−0.27	*S4_192238206*	*S4_190672218*
	qGY4_70	4	259	3.79	5.15		−0.01	0.24	*S4_49729965*	*S4_73097597*
	qGY8_135	8	156	6.32	8.10		0.21	−0.04	*S8_136138158*	*S8_134078364*
	qGY8_133	8	161	3.48	6.64		−0.19	−0.01	*S8_134078364*	*S8_132170809*
	qGY9_9	9	346	5.71	7.98		−0.20	−0.04	*S9_9640583*	*S9_6794782*
	qGY10_6	10	3	3.08	4.47		0.15	0.02	*S10_4308155*	*S10_6530067*
WS_GY	*qGY4_70*	4	262	3.07	24.45	20.92	0.28	0.10	*S4_73097597*	*S4_54124398*
F_3 pop 3 LapostaSeqF71 × CKL5009										
WW_GY	*qGY4_60*	4	458	3.31	27.77	34.65	−0.24	−0.13	*S4_60944899*	*S4_49729965*
	qGY10_70	10	278	3.83	28.25		0.09	−0.10	*S10_42442641*	*S10_71472634*
WS_GY	*qGY1_195*	1	212	3.81	6.28	25.18	0.05	−0.01	*S1_190394399*	*S1_199640380*
	qGY2_215	2	132	4.01	24.98		0.10	−0.04	*S2_217686135*	*S2_212803577*
	qGY2_185	2	211	3.98	7.39		0.05	0.01	*S2_185019543*	*S2_181424849*

LOD, logarithm of odds; Add, additive effect; Dom, dominance effect; PVE, phenotypic variance explained; GY, grain yield; WW, well-watered; WS, water-stressed. The exact physical position of the SNP can be inferred from the marker's name, for example, S1_82702920: chromosome 1; 82,702,920 bp.

et al., 2022; Gopalakrishna K. et al., 2023; Huang et al., 2023), which demonstrated that WS has an impact on GY and its related traits in maize. In our study, the average GY was highest (4.55–8.55 t/ha) and lowest (1.29–5.59 t/ha) for WW and WS conditions, respectively. The observed discrepancy in GY between those for WW and WS conditions underscores the influence of WS on maize crop productivity in SSA. We also found that, across environments, WS-induced GY reductions were highest for pop 1 (59%) and lowest for pop 3 (31%). Our results indicate that under conditions of WS, all studied bi-parental populations experienced reductions in GY. Notably, among the three tested genotypes, Pop 3 exhibited a comparatively higher level of WS tolerance, as evidenced by its lower GY losses under WS and also the contribution of favourable alleles from known WS tolerant parent (LaPostaSequiaC7-F71).

Like GY, ASI serves as one of the traits utilized in maize breeding initiatives (Silva et al., 2022) for selecting water stress tolerance. In our study, significantly wide ranges (2.6 days longer) were observed for ASI under WS compared to WW conditions across the studied genotypes. A wider ASI in maize under WS indicates an extended duration between the initiation of anthesis and silking – i.e., likely due to slowed reproductive development. This asynchrony can have adverse effects on pollination, potentially leading to low GY. Araus et al. (2012) alluded that maize plants exhibiting a wider ASI during WS conditions tend to either produce no seeds or yield only a limited number of grains per ear. The specific causes of the elongated ASI triggered by WS remain uncertain (Liu et al., 2021). Like GY response across genotypes, the mean values of PH and EH exhibited their lowest points under conditions of WS compared to WW conditions. These findings serve to highlight the adverse influence of WS on these GY-related traits and, by extension, maize crop performance in SSA. In this respect, further research into the mechanisms governing the observed GY and related trait variations can provide valuable insights for enhancing the resilience of smallholder maize systems in SSA.

Earlier studies have reported that the slow rate of genetic gain in breeding for WS tolerance can be attributed to high GxE interaction and low heritability and the polygenic nature of this trait (Mathew et al., 2019; Sallam et al., 2019; Zhang et al., 2022). Across the studied bi-parental populations and field conditions, broad-sense heritabilities were low (0.17) to high (0.85) for the studied traits. Most importantly,

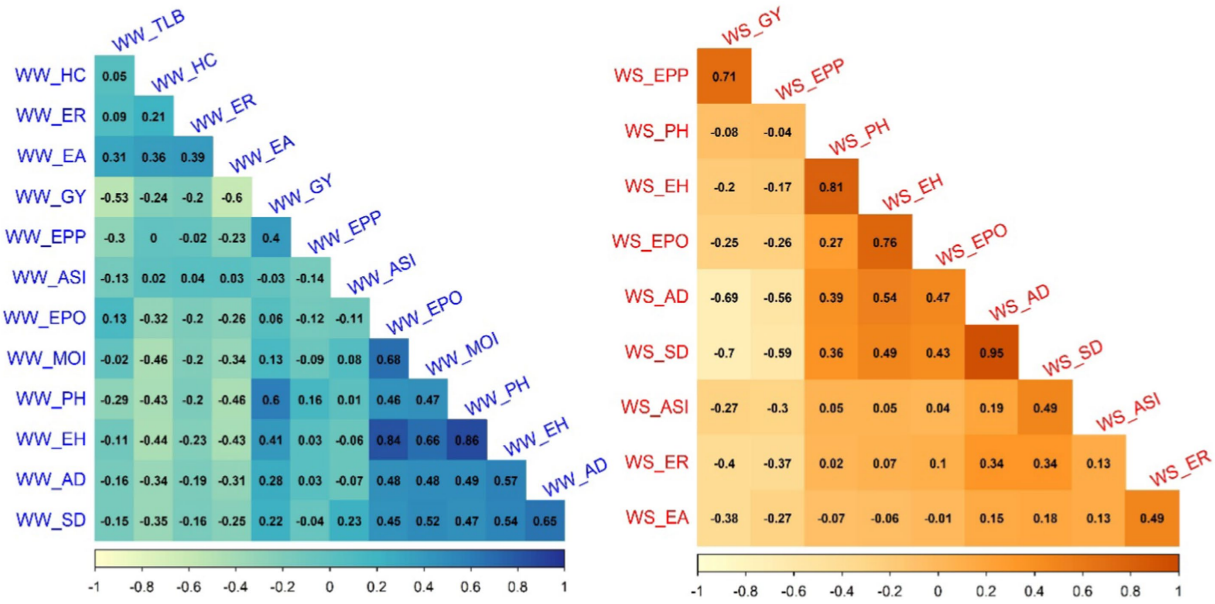

FIGURE 2
Phenotypic correlations between grain yield and other agronomic traits evaluated under well-watered and water-stressed conditions. The correlation values <0.11 were interpreted as 'not significant' at $p < 0.05$. GY, grain yield; AD, days to anthesis; SD, days to silking; ASI, anthesis silking interval; PH, plant height; EH, ear height; EPO, ear position; EPP, number of ears per plant; HC, husk cover; TLB, Turcicum leaf blight; MOI, grain moisture content; EA, ear aspect; and ER, ear rot.

TABLE 4 Number of QTLs associated with anthesis-to-silking interval under well-watered and water-stressed conditions detected in three F_3 populations.

	QTL name	Chr	Position (cM)	LOD	PVE (%)	TPVE (%)	Add	Dom	QTL confidence interval	
									Left SNP	Right SNP
F_3 pop 1 CML543 × CML444										
WS_ASI	*qASI1_265*	1	124	3.64	6.36	16.08	−0.22	−0.11	*S1_264962509*	*S1_267153406*
	qASI1_39	1	301	3.14	5.43		−0.13	0.26	*S1_38609777*	*S1_39743833*
	qASI2_14	2	36	3.01	18.88		0.39	0.14	*S2_9920694*	*S2_14334182*
	qASI7_125	7	266	3.87	6.79		−0.24	−0.03	*S7_123586636*	*S7_127579232*
F_3 pop 2 CML543 × LapostaSeqF71										
WW_ASI	*qASI1_245*	1	143	3.72	5.37	22.41	−0.07	0.07	*S1_248287688*	*S1_244472614*
	qASI2_156	2	255	4.24	6.57		0.00	−0.14	*S2_155786568*	*S2_157235338*
	qASI4_175	4	183	3.43	5.09		0.08	−0.01	*S4_177124549*	*S4_172996349*
	qASI8_165	8	24	3.01	9.94		−0.11	0.04	*S8_168275493*	*S8_160531262*
	qASI9_155	9	11	5.31	12.93		0.12	−0.04	*S9_155445883*	*S9_148918231*
WS_ASI	*qASI10_35*	10	95	3.57	20.99	16.58	−0.31	0.02	*S10_36380033*	*S10_34023708*
F_3 pop 3 LapostaSeqF71 × CKL5009										
WW_ASI	*qASI4_175*	4	252	3.14	5.64	16.78	0.15	−0.09	*S4_177124549*	*S4_172996349*
	qASI9_91	9	248	3.18	5.84		−0.15	0.09	*S9_92486034*	*S9_90971499*
	qASI9_91	9	256	4.70	8.22		0.18	0.04	*S9_90971499*	*S9_98491971*
	qASI10_90	10	159	3.60	6.50		0.17	0.00	*S10_90243627*	*S10_79537481*
WS_ASI	*qASI5_175*	5	124	3.26	6.18	27.85	0.19	0.07	*S5_180440672*	*S5_167276704*
	qASI5_175	5	452	3.32	24.59		−0.52	−0.31	*S5_217608792*	*S5_29623366*
	qASI6_130	6	354	3.74	20.71		0.55	−0.15	*S6_128790659*	*S6_139874840*
	qASI7_13	7	423	3.11	19.01		0.59	−0.40	*S7_5146124*	*S7_13176585*

LOD, logarithm of odds; Add, additive effect; Dom, dominance effect; PVE, phenotypic variance explained; ASI, anthesis-silking interval; WW, well-watered; WS, water-stressed. The exact physical position of the SNP can be inferred from the marker's name, for example, S1_82702920: chromosome 1; 82,702,920 bp.

TABLE 5 Number of QTLs associated with plant height under well-watered and water-stressed conditions detected in three F_3 populations.

	QTL name	Chr	Position (cM)	LOD	PVE (%)	TPVE (%)	Add	Dom	QTL confidence interval	
									Left SNP	Right SNP
F_3 pop 1 CML543 × CML444										
WW_PH	*qPH1_240*	1	59	3.91	4.68	43.96	0.08	2.32	*S1_238752622*	*S1_241001627*
	qPH3_175	3	113	3.56	15.29		2.69	0.55	*S3_179251623*	*S3_171703625*
	qPH4_50	4	416	4.71	11.06		2.07	1.15	*S4_41839869*	*S4_130024331*
	qPH5_45	5	334	3.37	3.84		1.34	0.33	*S5_51427709*	*S5_43147454*
	qPH6_70	6	210	4.31	4.97		−1.52	0.25	*S6_74462121*	*S6_67218451*
	qPH6_160	6	382	6.44	7.67		−2.02	−0.20	*S6_156878226*	*S6_167594329*
	qPH8_100	8	123	5.40	18.11		2.39	−1.80	*S8_65785251*	*S8_111044893*
	qPH8_150	8	239	3.04	8.71		1.73	−2.03	*S8_163655109*	*S8_149891724*
	qPH8_145	8	261	7.16	10.59		2.19	−1.01	*S8_149891724*	*S8_114742936*
WS_PH	*qPH7_149*	7	327	3.30	5.88	20.23	−1.91	−1.15	*S7_149852693*	*S7_148148303*
	qPH8_130	8	178	6.84	12.56		−2.79	−1.39	*S8_130328693*	*S8_131340896*
	qPH10_30	10	419	3.34	14.63		2.68	2.59	*S10_4244837*	*S10_34023708*
F_3 pop 2 CML543 × LapostaSeqF71										
WW_PH	*qPH2_130*	2	233	3.13	9.37	50.59	1.88	0.36	*S2_81807776*	*S2_139435119*
	qPH3_230	3	5	8.87	8.69		1.84	−0.13	*S3_230439536*	*S3_228551502*
	qPH3_227	3	10	7.61	9.52		−1.96	0.02	*S3_228551502*	*S3_226806334*
	qPH3_137	3	215	3.63	3.91		−0.33	−1.60	*S3_137679135*	*S3_136337566*
	qPH4_210	4	71	4.95	8.85		−1.72	−0.56	*S4_213777313*	*S4_210692761*
	qPH6_87	6	204	7.23	7.45		−1.91	0.52	*S6_89123242*	*S6_86182651*
	qPH7_170	7	10	3.96	3.80		−1.15	0.25	*S7_172496672*	*S7_170251440*
	qPH7_130	7	106	3.91	3.97		1.16	−0.09	*S7_136855242*	*S7_128139766*
	qPH8_143	8	137	4.18	4.29		1.25	−0.35	*S8_142011621*	*S8_144367600*
	qPH8_140	8	144	7.96	7.73		−1.73	−0.37	*S8_144367600*	*S8_138521503*
	qPH8_100	8	243	3.53	4.89		−1.46	0.20	*S8_101670845*	*S8_98766563*
	qPH8_5	8	457	4.11	4.40		−1.22	−0.11	*S8_5319373*	*S8_2288877*
WS_PH	*qPH9_120*	9	134	3.11	6.15	8.27	1.74	0.75	*S9_122035076*	*S9_112333377*
	qPH9_80	9	245	3.21	5.82		−0.77	−0.19	*S9_86530554*	*S9_64295850*
F_3 pop 3 LapostaSeqF71 × CKL5009										
WW_PH	*qPH1_246*	1	338	3.35	11.10	42.77	−2.52	−1.71	*S1_245744980*	*S1_248615699*
	qPH1_275	1	433	3.45	4.24		−1.30	−1.17	*S1_276683320*	*S1_275032102*
	qPH3_213	3	143	3.11	7.74		−2.18	0.04	*S3_213548502*	*S3_212501788*
	qPH4_132	4	334	3.89	4.24		−1.57	0.32	*S4_131701338*	*S4_134995001*
	qPH5_180	5	108	6.22	7.05		−2.18	−0.61	*S5_182032257*	*S5_180440672*
	qPH6_08	6	275	4.00	4.46		−1.74	0.28	*S6_8143156*	*S6_5442499*
	qPH7_24	7	162	3.95	5.50		1.91	−0.44	*S7_24795707*	*S7_23352528*
	qPH8_90	8	317	3.83	5.43		−0.22	2.87	*S8_95129491*	*S8_85101441*
	qPH8_65	8	340	8.89	12.34		−2.97	−0.20	*S8_38701797*	*S8_65781214*
	qPH8_65	8	348	13.57	17.37		3.20	0.31	*S8_65781214*	*S8_64174106*
WS_PH	*qPH1_245*	1	329	3.71	2.89	58.35	0.11	−1.26	*S1_241001627*	*S1_245744980*
	qPH1_245	1	336	7.43	8.43		1.49	0.00	*S1_245744980*	*S1_248615699*
	qPH1_250	1	342	10.80	9.29		−1.56	−0.13	*S1_248615699*	*S1_253109076*
	qPH2_210	2	141	3.16	4.21		−0.23	−1.47	*S2_212803577*	*S2_201799296*

(Continued)

TABLE 5 (Continued)

	QTL name	Chr	Position (cM)	LOD	PVE (%)	TPVE (%)	Add	Dom	QTL confidence interval	
									Left SNP	Right SNP
	qPH3_05	3	559	6.92	5.29		0.96	0.99	*S3_8122530*	*S3_3525325*
	qPH4_214	4	146	9.69	9.49		−0.94	1.76	*S4_215105658*	*S4_213777313*
	qPH4_135	4	341	3.07	2.51		−0.70	0.12	*S4_134995001*	*S4_136178733*
	qPH5_180	5	106	9.90	8.52		−1.37	−0.76	*S5_182032257*	*S5_180440672*
	qPH6_140	6	52	3.89	3.17		−0.86	−0.13	*S6_143755461*	*S6_140908415*
	qPH6_140	6	59	5.08	4.94		1.08	0.08	*S6_140908415*	*S6_138562829*
	qPH6_10	6	297	9.49	7.81		−1.41	−0.05	*S6_6901831*	*S6_10346160*
	qPH7_95	7	268	4.29	6.61		1.36	0.24	*S7_98849992*	*S7_94238156*
	qPH8_65	8	353	17.66	15.68		1.92	0.32	*S8_65781214*	*S8_64174106*

LOD, logarithm of odds; Add, additive effect; Dom, dominance effect; PVE, phenotypic variance explained; PH, plant height; WW, well-watered; WS, water-stressed. The exact physical position of the SNP can be inferred from the marker's name, for example, S1_82702920: chromosome 1; 82,702,920 bp.

heritability estimates for GY and EH were low to high for both WW and WS conditions. High heritability estimates indicate the potential for traits to be improved through recurrent selection processes (Gowda et al., 2021; Ndlovu et al., 2022). High broad-sense heritability estimates hint at the possibility of even greater narrow-sense heritability, suggesting the feasibility of achieving substantial genetic advancement for these traits. We also found that the broad sense heritabilities of all studied maize traits at individual population levels decreased under WS conditions compared to WW conditions. This was consistent with studies by Chen et al. (2023) and Zhao et al. (2019), who also presented lower heritabilities for traits under WS conditions.

For genotypic variance, statistical significance at $p \leq 0.05$ was observed for all traits (Table 2). Genotypic variance decreased for GY and PH under WS. A study by Badu-Apraku et al. (2017) on early white maize in Nigeria also reported a decreased GY heritability and magnitude of genotypic variance under WS conditions. G×E interaction variance was also significant ($p \leq 0.05$) for all traits in pop 1 and pop 2 indicating the substantial variation observed in terms of the performance of genotypes in different environments. We also observed significant negative correlations between GY and other yield-related traits in both WW and WS conditions (Figure 2). This suggests adopting a cautious approach when trying to improve multiple traits simultaneously under both WW and WS conditions.

4.2 Multiple QTLs identified for well-watered and water-stressed environments

Linkage mapping in three bi-parental maize populations identified multiple QTLs for GY, PH, EH and ASI under WW (93) and WS (41) conditions. Previous studies have also found multiple QTLs for WS-related traits and GY in maize (Sanguineti et al., 1999; Li et al., 2016; Zhao et al., 2018; Abdelghany et al., 2019; Zhao et al., 2019; Hu et al., 2021; Sarkar et al., 2023). Although previous studies have identified QTLs and genes associated with improved GY and related traits, untapped maize populations probably harbour additional genetic variations. In our study, QTL analyses in individual bi-parental populations identified 22, 18, 49 and 45 QTLs for GY, ASI, PH and EH, respectively. The highest number of QTLs was identified in pop 3 (n = 60) and pop 2 (n = 43) under WW and WS conditions, respectively. Notably, four QTLs were identified for GY under WS (*qGY4_70* (Chr. 4), *qGY2_215*, *qGY2_185* (Chr. 2), and *qGY1_195* (Chr. 1)). Under both WW and WS environments, GY-associated QTLs were distributed across all chromosomes except chr 6 and 7 (Table 3). Agrama et al. (1999) found genomic regions associated with WS tolerance on chromosomes 1, 3, 5, 6 and 8. Hu et al. (2021) reported QTLs on chromosomes 3, 5, 7 and 10 for yield-related traits under different water regimes. Comparison of QTL detected across populations revealed several common genomic regions across populations, like two QTLs, *qGY1_199* in pop 1 and *qGY1_195* on pop 3 were overlapped at 190–200 Mbp on chromosome 1 (Table 3). Another QTL for GY on chromosome 4 (*qGY4_70*) detected on pop 2 overlapped with QTL (*qGY4_60*) detected on pop 3. For ASI, one QTL (*qASI4_175*) was detected in both pop 2 and pop 3 under WW conditions (Table 4). For PH, one QTL (*qPH8_130*) detected under WS was located within the region of the QTL (*qPH8_145*) detected under WW management (Table 5). These genomic regions are most interesting to know their role in trait improvement and bring most of these favourable alleles into elite lines through marker-assisted selection. In the case of ASI, nine QTLs each were identified under WW and WS conditions. In both water regimes, chromosome 3 did not harbour any QTLs for ASI. Significant QTLs with major effects (explaining more than 10% of the phenotypic variance) were identified for GY (*qGY6_89*) and ASI (*qASI1_107*) under WS conditions.

The absence of QTLs associated with GY and related traits on certain chromosomes in our analysis, compared to previous studies, highlights the complex interplay of genes and environmental pressures that significantly shape QTL identification in tropical maize. The observed disparities can be attributed to distinct maize populations and growing/management conditions employed (Ndlovu et al., 2024). This further emphasizes the need to consider these prevailing interactions when investigating genetic influences on maize traits under WS conditions.

Linkage mapping uses variation within a population whereas JLAM is known to explore variations both within and across populations. This allows JLAM to detect new QTLs which are not detected through individual linkage mapping. In our study, among the 25 QTLs detected for GY under WW conditions, only two

TABLE 6 Number of QTLs associated with ear height under well-watered and water-stressed conditions detected in three F_3 populations.

	QTL name	Chr	Position (cM)	LOD	PVE (%)	TPVE (%)	Add	Dom	QTL confidence interval	
									Left SNP	Right SNP
F_3 pop 1 CML543 × CML444										
WW_EH	*qEH2_25*	2	74	4.10	4.99	42.07	1.52	0.73	*S2_26004514*	*S2_24257802*
	qEH4_165	4	259	5.88	7.78		2.00	−0.09	*S4_165637692*	*S4_166866479*
	qEH6_90	6	65	5.08	6.67		−1.86	0.94	*S6_90931126*	*S6_86257555*
	qEH6_160	6	376	6.05	14.00		−2.64	−1.17	*S6_156878226*	*S6_167594329*
	qEH8_70	8	314	13.63	20.00		3.19	−1.01	*S8_69119155*	*S8_72750921*
	qEH8_65	8	321	11.65	18.50		−3.19	−0.65	*S8_72750921*	*S8_59316871*
WS_EH	*qEH8_130*	8	180	9.29	17.82	15.98	−3.09	−1.30	*S8_130328693*	*S8_131340896*
F_3 pop 2 CML543 × LapostaSeqF71										
WW_EH	*qEH2_55*	2	348	5.85	4.85	58.97	−1.23	−0.42	*S2_55249812*	*S2_50644503*
	qEH3_227	3	6	3.77	4.33		1.29	−0.34	*S3_228551502*	*S3_226806334*
	qEH3_220	3	17	6.62	7.78		−1.57	−0.71	*S3_226806334*	*S3_212501788*
	qEH3_170	3	108	8.52	7.74		−1.66	0.22	*S3_171639585*	*S3_169577878*
	qEH3_150	3	183	5.15	3.90		−1.24	−0.18	*S3_153858200*	*S3_148833306*
	qEH5_200	5	322	3.24	3.08		−1.01	−0.18	*S5_196508562*	*S5_201580291*
	qEH5_205	5	333	5.34	4.44		1.27	−0.08	*S5_201580291*	*S5_207514182*
	qEH7_171	7	8	7.98	13.01		−2.16	−0.19	*S7_172496672*	*S7_170251440*
	qEH7_88	7	233	5.62	4.24		−1.08	−0.61	*S7_87193242*	*S7_88803418*
	qEH8_143	8	136	7.41	5.94		1.47	−0.51	*S8_143280651*	*S8_142011621*
	qEH8_143	8	143	5.07	5.35		−1.44	−0.42	*S8_142011621*	*S8_144367600*
	qEH8_115	8	200	8.67	7.46		1.70	−0.59	*S8_118858352*	*S8_114638748*
	qEH8_114	8	208	10.19	8.58		−1.84	−0.63	*S8_114638748*	*S8_111824358*
	qEH6_16	9	307	4.85	3.93		−1.09	−0.51	*S9_16728498*	*S9_15608594*
F_3 pop 3 LapostaSeqF71 × CKL5009										
WW_EH	*qEH1_200*	1	216	4.45	6.07	48.83	−0.12	−2.85	*S1_199640380*	*S1_200910153*
	qEH3_213	3	137	3.64	4.95		1.68	−0.06	*S3_213548502*	*S3_212501788*
	qEH3_212	3	148	8.37	9.72		−2.29	−0.38	*S3_212501788*	*S3_206481439*
	qEH5_181	5	108	6.03	6.12		−2.03	0.12	*S5_182032257*	*S5_180440672*
	qEH7_24	7	162	6.57	8.69		2.29	−0.60	*S7_24795707*	*S7_23352528*
	qEH7_95	7	168	5.94	9.03		−2.26	−0.54	*S7_23352528*	*S7_95431651*
	qEH8_144	8	89	3.66	4.95		−1.68	0.18	*S8_146891047*	*S8_144367600*
	qEH8_144	8	94	3.23	3.78		1.45	−0.24	*S8_144367600*	*S8_143280651*
	qEH8_40	8	339	8.80	9.23		−2.41	1.11	*S8_43051270*	*S8_38701797*
	qEH8_40	8	345	8.63	11.40		2.38	1.25	*S8_38701797*	*S8_65781214*
	qEH10_145	10	52	3.39	8.59		−2.07	−0.10	*S10_140851297*	*S10_149390708*
WS_EH	*qEH1_225*	1	298	4.82	5.91	60.37	−1.44	0.38	*S1_225033350*	*S1_229482334*
	qEH3_214	3	126	5.19	4.80		−1.30	0.36	*S3_214830240*	*S3_213548502*
	qEH4_230	4	113	3.19	5.15		0.86	1.57	*S4_225687739*	*S4_231141298*
	qEH5_180	5	109	10.71	8.69		−1.90	−0.22	*S5_180440672*	*S5_167276704*
	qEH6_140	6	52	3.63	2.87		−1.02	0.19	*S6_143755461*	*S6_140908415*
	qEH6_140	6	63	3.80	2.95		−1.03	0.08	*S6_140908415*	*S6_138562829*
	qEH6_140	6	372	4.27	4.40		−1.59	−2.69	*S6_155235957*	*S6_122406660*
	qEH7_165	7	5	5.23	5.08		−0.62	−1.86	*S7_167104322*	*S7_164828478*

(Continued)

TABLE 6 (Continued)

	QTL name	Chr	Position (cM)	LOD	PVE (%)	TPVE (%)	Add	Dom	QTL confidence interval	
									Left SNP	Right SNP
	qEH7_160	7	24	3.14	2.88		−0.84	−0.97	*S7_161855642*	*S7_154741580*
	qEH7_25	7	161	6.50	7.45		1.74	−0.12	*S7_28818246*	*S7_24795707*
	qEH7_25	7	167	4.87	3.70		−1.21	0.17	*S7_23352528*	*S7_95431651*
	qEH8_144	8	90	4.08	4.21		−1.22	−0.45	*S8_144367600*	*S8_143280651*
	qEH8_65	8	351	16.06	14.23		2.21	0.63	*S8_65781214*	*S8_64174106*

LOD, logarithm of odds; Add, additive effect; Dom, dominance effect; PVE, phenotypic variance explained; GY, grain yield; WW, well-watered; WS, water-stressed. The exact physical position of the SNP can be inferred from the marker's name, for example, S1_82702920: chromosome 1; 82,702,920 bp.

QTLs (*qGY3_208* and *qGY4_70*) overlapped with QTLs detected through linkage mapping. JLAM analyses revealed 25 and 4 QTLs under WW and WS conditions for GY, respectively, which were distributed across all chromosomes and individually explained 0.8–11.8% of the phenotypic variance (Table 7). JLAM results indicated that GY is controlled by many minor effect genes, as shown in low PVE for each QTL (Table 7). However, we found one major effect QTL on chromosome 6 (*qGY6-89*) which explained 11.8% of phenotypic variation and was found overlapping with the PH QTL (*qPH6-87*) on pop 2 (Tables 5, 7). Because of limited recombination events during population development, linkage mapping identifies the genomic region with 10-20 cM intervals. On the contrary, JLAM identifies the single marker which is closely linked to the causative gene for the trait of interest. Two QTLs (qGY3_208 and qGY4_70) detected through JLAM overlapped with the QTL detected in linkage mapping helped to reduce the confidence interval of the QTLs and may even be closer to the causal variant responsible for GY. On the other hand, a comparison of QTLs detected across WW and WS conditions revealed no common QTL for GY, PH and EH. On the contrary, we found four QTLs for ASI (*qASI1_234, qASI8_22, qASI9_105* and *qASI9_108*) were consistently detected across WW and WS regimes. ASI is critical in hybrid breeding, specifically in commercial seed production and also in drought-prone regions for good seed setting. Therefore, these genomic regions are important to achieve synchrony in flowering time in diverse management.

4.3 Genomic prediction accuracies under different water regimes

Genomic prediction demonstrated its usefulness in maize breeding by facilitating the rapid selection of superior genotypes. This was achieved by using molecular markers which help to capture maximum favourable alleles for various traits of interest. Breeding for drought tolerance is resource and time-intensive. Genomic prediction offers an alternative and complementary tool to achieve high selection efficiency with optimum resources (Beyene et al., 2015, 2019, 2021; Atanda et al., 2021). Several studies reported that genomic-prediction-based models are effective in identifying better-performing genotypes for GY and other agronomic and disease resistance traits (Crossa et al., 2017; Sitonik et al., 2019; Ertiro et al., 2020; Kibe et al., 2020a; Gowda et al., 2021; Ndlovu et al., 2022; Kimutai et al., 2023; Ndlovu et al., 2024). The effectiveness of GS compared to traditional phenotypic selection plays a significant role in determining its likelihood of adoption in breeding programs (Beyene et al., 2019; Kibe et al., 2020b). In our study, the moderate to high levels of prediction accuracy observed across the bi-parental populations hold the potential for enhancing breeding efforts to improve WS tolerance in tropical maize germplasm. The same trends were observed in previous studies which reported moderate to high accuracies for GY and related traits under WS (Dias et al., 2018; Zhang et al., 2022). The moderate to high prediction accuracy we report here indicates that the methodology used is reliable in predicting the performance of GY and related traits in bi-parental maize populations under different water regimes. This reliability enhances the effectiveness of breeding for WS tolerance programs by enabling the selection of genotypes for desired traits more efficiently.

Combining the three populations and forming the training set and testing set from the total populations resulted in substantial improvement in the prediction accuracy (Figure 3). This was due to the increase in the population size of the training set and the high relatedness between training and testing sets. Unlike other traits, GY exhibited a negative prediction accuracy for drought tolerance in population 2 under within-within and across-within prediction scenarios (Figure 3). Similar results were also reported for prediction among biparental populations of maize (Riedelsheimer and Melchinger, 2013; Sitonik et al., 2019) and sugar beet (Würschum et al., 2013). Mismatched alleles between markers linked with WS tolerance in pop 2 could explain the negative prediction accuracy. Moreover, low genotypic variation and heritability for GY response to WS conditions might have also contributed.

Under WW management, the prediction accuracy for GY was 0.67, 0.58 and 0.57 in the within-within scenario for pop 1, pop 2 and pop 3, respectively (Figure 3). In scenario 2, a training population combining individuals from three populations achieved prediction accuracies of 0.56, 0.59 and 0.44 for pop 1, pop 2 and pop 3, respectively (Figure 3). Though there is a reduction in accuracy for scenario 2, the recorded accuracies are still comparable to those of phenotypic selection. The recorded moderate to high prediction accuracies likely stems from the shared parentage between the studied maize populations. Breeding for WS tolerance remains a challenging task. While the reported prediction accuracies indicate some success in achieving this goal, they still fall short of those achievable through phenotypic selection. However, since it's possible to fit three maize cycles per agricultural calendar (Beyene et al., 2019), GS is expected to get a similar or higher genetic gain over phenotypic selection in the coming years. For ASI, PH and EH, accuracies are relatively high

TABLE 7 Analysis of GY-associated markers under well-watered and water-stressed conditions, allele substitution (α) effects, and the total phenotypic variance (R^2) of the joint linkage association mapping based on combined three F_3 populations.

WW_GY	QTL name	chr	Position (Mbp)	α-effect	*p* value	PVE (%)
S1_42012727	*qGY1_42*	1	42.01	−0.19	6.46E-06	1.00
S1_99283222	*qGY1_99*	1	99.28	0.3	2.20E-06	1.10
S1_262175904	*qGY1_262*	1	262.18	−0.24	1.37E-06	1.10
S2_204872338	*qGY2_205*	2	204.87	−0.15	5.23E-07	1.20
S2_208974622	qGY2_209	2	208.98	0.13	7.87E-06	0.90
S3_114352108	qGY3_114	3	114.35	0.13	4.96E-05	0.80
S3_207898219	qGY3_208	3	207.9	−0.33	3.16E-11	2.10
S4_38028976	*qGY4_38*	4	38.03	−0.22	4.26E-10	1.90
S4_69920709	*qGY4_70*	4	69.92	−0.26	3.01E-05	0.80
S4_152397975	*qGY4_152*	4	152.4	0.2	6.01E-07	1.20
S4_231141298	*qGY4_231*	4	231.14	−0.22	4.28E-09	1.60
S4_232139676	*qGY4_232*	4	232.14	−0.17	2.16E-05	0.80
S5_190481535	*qGY5_191*	5	190.48	0.15	2.06E-05	0.90
S5_199231742	*qGY5_199*	5	199.23	−0.19	6.35E-07	1.20
S5_206027675	*qGY5_206*	5	206.03	0.14	4.63E-05	0.80
S6_96673215	*qGY6_97*	6	96.67	−0.21	9.23E-08	1.40
S6_112123594	*qGY6_112*	6	112.12	0.27	1.56E-05	0.90
S6_124667680	*qGY6_125*	6	124.67	−0.31	1.27E-05	0.90
S6_158689057	*qGY6_159*	6	158.69	−0.22	3.30E-08	1.50
S6_162690530	*qGY6_163*	6	162.69	−0.15	1.42E-05	0.90
S8_115294871	*qGY8_115*	8	115.3	−0.26	2.92E-10	1.90
S8_173704036	*qGY8_173*	8	173.7	0.22	4.48E-19	3.90
S9_143177138	*qGY9_143*	9	143.18	0.16	5.61E-07	1.20
S10_88396836	*qGY10_88*	10	88.4	0.23	2.23E-09	1.70
S10_100028254	*qGY10_100*	10	100.03	0.14	3.05E-07	1.20
WS_GY						
S5_16303706	*qGY5_16*	5	16.3	0.13	3.93E-13	4.30
S6_29639026	*qGY6_30*	6	29.64	0.07	3.26E-05	1.40
S6_89403767	*qGY6_89*	6	89.4	−0.29	2.96E-31	11.80
S7_99206507	*qGY7_99*	7	99.21	0.12	5.46E-12	3.90

*Chr, Chromosome; PVE, proportion of phenotypic variance explained; GY, grain yield; WW, well-watered; WS, water-stressed; Mbp, Mega base pairs. The exact physical position of the SNP can be inferred from the marker's name, for example, S1_82702920: chromosome 1; 82,702,920 bp.

which clearly supports the usefulness of GS in their improvement under both WW and WS conditions.

5 Conclusion

The negative impact of drought on maize production has been profound, significantly impairing the livelihoods and food security of millions of people in SSA. Drought tolerance, an important trait, can play a vital role in mitigating the yield losses caused by drought in smallholder maize farming systems. Here, we investigated the genetic parameters (i.e., heritabilities and genetic-based variances), mapped QTLs for WS tolerance and assessed the potential of using GS in bi-parental maize populations evaluated under WW and WS conditions in Kenya and Zimbabwe. For these genotypes, broad sense heritabilities were low to high and genetic variances were significant for the studied traits. For GY, these parameters were decreased under WS. According to our QTL mapping results, WS tolerance in maize is controlled by multiple genes with small effects. Several QTLs identified in this study were found to be overlapping across different analyses and with earlier studies. The genomic regions consistently detected more than one population and/or traits that are promising and need to be prioritised for inclusion in marker-assisted recurrent selection. This is vital in our efforts to increase favourable alleles in selected elite maize germplasm. The specific genomic loci identified in this study can also be used in selecting for improved GY and related trait performances under WS conditions. Additionally, our results demonstrated that incorporating GS into maize breeding for WS

TABLE 8 Analysis of ASI-associated markers under well-watered and water-stressed conditions, allele substitution (α) effects, and the phenotypic variance (PVE) of the joint linkage association mapping based on combined three F_3 populations.

WW_ASI	QTL name	chr	Position (Mbp)	α-effect	*p* value	PVE (%)
S1_219379659	*qASI1_219*	1	219.38	0.19	8.64E-05	1.3
S1_233633174	*qASI1_233*	1	233.63	0.24	3.31E-06	1.2
S1_234787174	*qASI1_234*	1	234.79	0.48	4.08E-13	7.0
S2_9982799	*qASI2_10*	2	9.98	0.23	3.78E-05	0.5
S3_44094305	*qASI3_44*	3	44.09	0.38	1.52E-09	0.5
S3_48807819	*qASI3_49*	3	48.81	−0.52	3.08E-08	3.1
S5_39671048	*qASI5_40*	5	39.67	0.17	5.88E-05	1.1
S5_69514509	*qASI5_70*	5	69.52	0.85	8.23E-12	0.1
S5_70773399	*qASI5_71*	5	70.77	−0.75	3.37E-09	4.9
S7_117541299	*qASI7_118*	7	117.54	−0.18	1.40E-05	2.1
S8_19830105	*qASI8_20*	8	19.83	−0.29	2.82E-08	0.7
S8_21847291	*qASI8_22*	8	21.85	0.36	2.14E-07	1.1
S8_113714982	*qASI8_114*	8	113.72	−0.23	2.20E-06	2.9
S8_141395117	*qASI8_141*	8	141.40	−0.33	7.21E-05	0.7
S9_104993163	*qASI9_105*	9	104.99	0.49	8.85E-11	0.5
S9_108293552	*qASI9_108*	9	108.29	0.24	3.98E-05	4.5
WS_ASI						
S1_48660741	*qASI1_49*	1	48.66	−0.19	1.24E-05	1.7
S1_100991498	*qASI1_101*	1	100.99	1.68	3.27E-12	4.4
S1_105951838	*qASI1_106*	1	105.95	0.99	2.00E-06	2
S1_106498930	*qASI1_107*	1	106.50	−2.66	6.85E-27	10.9
S1_188742138	*qASI1_189*	1	188.74	0.20	2.67E-05	1.6
S1_234787174	*qASI1_235*	1	234.79	0.29	1.57E-06	2
S3_39217617	*qASI3_39*	3	39.22	0.27	5.61E-05	1.4
S6_92390840	*qASI6_92*	6	92.39	0.22	9.03E-05	1.4
S6_154887691	*qASI6_155*	6	154.89	−0.29	2.03E-13	4.9
S7_124507887	*qASI7_125*	7	124.51	−0.33	1.31E-07	2.5
S7_173489659	*qASI7_173*	7	173.49	0.29	7.12E-06	1.8
S8_21847291	*qASI8_22*	8	21.85	0.30	1.11E-06	2.1
S8_142370328	*qASI8_142*	8	142.37	−0.24	9.85E-05	1.3
S9_104993163	*qASI9_105*	9	104.99	0.33	4.12E-05	1.5
S9_108399137	*qASI9_108*	9	108.40	−0.45	4.77E-06	1.9

*Chr, Chromosome; PVE, proportion of phenotypic variance explained; GY, grain yield; WW, well-watered; WS, water-stressed; Mbp, Mega base pairs. The exact physical position of the SNP can be inferred from the marker's name, for example, S1_82702920: chromosome 1; 82,702,920 bp.

tolerance can effectively complement traditional phenotypic selection. In addition, future research should also prioritize the validation of the QTLs identified in this study to further improve the efficiency of WS-tolerance maize breeding efforts in SSA.

Data availability statement

The datasets presented in this study can be found in online repositories. The names of the repository/repositories and accession number(s) can be found in the article/Supplementary material.

Author contributions

NN: Conceptualization, Data curation, Formal analysis, Methodology, Validation, Writing – original draft, Writing – review & editing. MG: Conceptualization, Data curation, Funding acquisition, Investigation, Project administration, Software, Supervision, Writing – original draft, Writing – review & editing. YB: Conceptualization, Investigation, Project administration, Validation, Visualization, Writing – review & editing. VC: Data curation, Formal analysis, Methodology, Visualization, Writing – review & editing. FN: Conceptualization, Project administration, Supervision, Validation,

TABLE 9 Analysis of PH and EH-associated markers under well-watered and water-stressed conditions, allele substitution (α) effects, and the phenotypic variance (PVE) of the joint linkage association mapping based on combined three F_3 populations.

WW_PH	QTL name	chr	Position (Mbp)	α-effect	*P value*	PVE (%)
S3_172198924	*qPH3_172*	3	172.20	−2.10	6.11E-07	1.8
S4_38288565	*qPH4_382*	4	38.29	−5.36	4.10E-28	9.4
S4_60360208	*qPH4_60*	4	60.36	5.73	9.81E-13	3.8
S4_202224476	*qPH4_202*	4	202.22	−2.23	5.27E-07	1.8
S5_4303244	*qPH5_04*	5	4.30	−2.04	3.12E-05	1.3
S5_29809776	*qPH5_30*	5	29.81	1.36	7.42E-04	0.8
S5_178925335	*qPH5_179*	5	178.93	−1.97	1.10E-04	1.1
S8_117747254	*qPH8_118*	8	117.75	−2.14	1.17E-05	1.4
S8_132202657	*qPH8_132*	8	132.20	−4.23	6.22E-10	2.8
S9_23759221	*qPH9_24*	9	23.76	−1.59	8.34E-04	0.8
S9_139761585	*qPH9_140*	9	139.76	1.77	1.96E-04	1.0
S10_2839563	*qPH10_03*	10	2.84	−1.64	3.07E-05	1.3
WS_PH						
S2_30548333	*qPH2_31*	2	30.55	2.28	1.90E-05	4.6
S5_200649357	*qPH5_201*	5	200.65	1.16	1.36E-03	0.8
S6_160675816	*qPH6_161*	6	160.68	1.60	9.70E-05	1.7
S7_2292978	*qPH7_02*	7	2.29	2.28	1.84E-05	8.5
S8_21847291	*qPH8_22*	8	21.85	−2.73	9.31E-06	0.2
S8_107231702	*qPH8_107*	8	107.23	−1.77	9.49E-05	4.0
S8_124937569	*qPH8_125*	8	124.94	1.86	5.34E-03	0.7
WW_EH						
S2_212803577	*qEH2_213*	2	212.80	−3.25	1.41E-09	2.9
S2_219293267	*qEH2_219*	2	219.29	−4.74	2.86E-15	4.9
S3_3204077	*qEH3_03*	3	3.20	1.23	3.32E-03	0.7
S4_164095194	*qEH4_164*	4	164.10	6.50	1.93E-18	6.2
S5_33980430	*qEH5_34*	5	33.98	5.39	9.93E-13	4.0
S7_25812716	*qEH7_26*	7	25.81	1.41	1.14E-03	0.8
WS_EH						
S1_45928305	*qEH1_46*	1	45.93	−0.83	5.08E-03	0.4
S1_279913054	*qEH1_280*	1	279.91	−1.74	2.30E-03	0.9
S1_283431481	*qEH1_283*	1	283.43	−1.78	2.14E-04	0.3
S1_286399533	*qEH1_286*	1	286.40	−3.01	8.78E-09	3.6
S2_178096547	*qEH2_178*	2	178.10	−0.89	2.27E-03	0.8
S2_204467855	*qEH2_204*	2	204.47	0.96	2.28E-03	0.2
S4_232139676	*qEH4_232*	4	232.14	−1.25	1.24E-04	5.1
S5_200649357	*qEH5_201*	5	200.65	1.09	2.68E-04	0.8
S6_35061159	*qEH6_35*	6	35.06	2.78	3.18E-04	1.2
S6_88731794	*qEH6_89*	6	88.73	−2.53	4.50E-04	5.0
S6_159257304	*qEH6_159*	6	159.26	1.44	7.69E-06	4.8
S6_167688609	*qEH6_168*	6	167.69	3.15	2.91E-10	3.3
S7_2292978	*qEH7_03*	7	2.29	2.29	2.88E-06	6.3
S8_21847291	*qEH8_22*	8	21.85	−3.35	2.27E-13	1.1

*Chr, Chromosome; PVE, proportion of phenotypic variance explained; GY, grain yield; WW, well-watered; WS, water-stressed; Mbp, Mega base pairs. The exact physical position of the SNP can be inferred from the marker's name, for example, S1_82702920: chromosome 1; 82,702,920 bp.

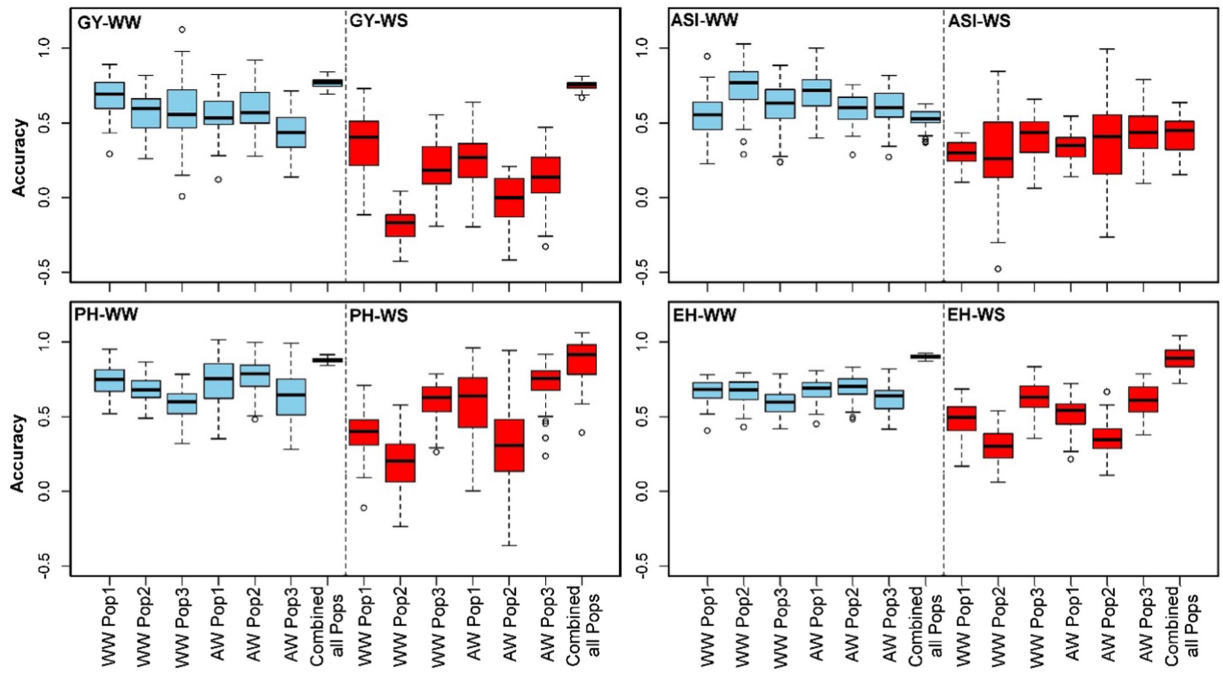

FIGURE 3
Genome-wide prediction accuracies for GY, ASI, PH and EH in within-within (WW) population, across-within (AW) population and all combined populations scenarios. Blue and red box plots illustrate trait evaluations conducted under well-watered and water-stressed conditions, respectively.

Writing – review & editing. DM: Conceptualization, Resources, Validation, Visualization, Writing – review & editing. PM: Resources, Supervision, Validation, Visualization, Writing – review & editing. CS: Investigation, Project administration, Resources, Supervision, Validation, Writing – review & editing. BP: Conceptualization, Funding acquisition, Investigation, Project administration, Resources, Supervision, Writing – review & editing.

Funding

The author(s) declare that financial support was received for the research, authorship, and/or publication of this article. The success of this paper is highly attributed to the mother projects which include DTMA, WEMA, and IMAS projects. The research was supported by the Bill and Melinda Gates Foundation (B&MGF), Foundation for Food and Agriculture Research (FFAR) and the United States Agency for International Development (USAID) through AGG (Accelerating Genetic Gains in Maize and Wheat for Improved Livelihoods; B&MGF Investment ID INV-003439). NN, PM and CS acknowledge funding from the European Commission DESIRA funded LEG4DEV Project [FOOD/2020/418–901] and the Science Foundation Ireland Principal Investigator Grant [13/IA/1820].

Acknowledgments

The authors thank the CIMMYT field technicians for phenotypic evaluations and Laboratory technicians for sample preparation for genotyping. More gratitude to Dr. Kassa Semagn, for his excellent and noble guidance throughout the processes of this research. We also thank Dr. Edward S Buckler and the Institute of Genomic Diversity, Cornell University, for the high-density genotyping (GBS) and imputation service.

Conflict of interest

The authors declare that the research was conducted in the absence of any commercial or financial relationships that could be construed as a potential conflict of interest.

Publisher's note

Supplementary material

The Supplementary material for this article can be found online at: https://www.frontiersin.org/articles/10.3389/fsufs.2024.1391989/full#supplementary-material

References

Abdelghany, M., Liu, X., Hao, L., Gao, C., Kou, S., Su, E., et al. (2019). QTL analysis for yield-related traits under different water regimes in maize. *Maydica*. 64:10. Available at: https://core.ac.uk/reader/270269270.

Adebayo, M. A., and Menkir, A. (2014). Assessment of hybrids of drought tolerant maize (*Zea mays* L.) inbred lines for grain yield and other traits under stress managed conditions. *Niger. J. Genet.* 28, 19–23. doi: 10.1016/j.nigjg.2015.06.004

Agrama, H., Zakaria, A., Said, F., and Tuinstra, M. (1999). Identification of quantitative trait loci for nitrogen use efficiency in maize. *Mol. Breed.* 5, 187–195. doi: 10.1023/A:1009669507144

Alvarado, G., López, M., Vargas, M., Pacheco, Á., Rodríguez, F., Burgueño, J., et al. (2015). *META-R (multi Environment Trail analysis with R for windows) version 6.04*: CIMMYT Research Data & Software Repository Network, V23. Available at: https://hdl.handle.net/11529/10201

Alvarado, G., Rodríguez, F. M., Pacheco, A., Burgueño, J., Crossa, J., Vargas, M., et al. (2020). META-R: A software to analyze data from multi-environment plant breeding trials. *Crop J.* 8, 745–756. doi: 10.1016/j.cj.2020.03.010

Anilkumar, C., Muhammed Azharudheen, T. P., Sah, R. P., Sunitha, N. C., Devanna, B. N., Marndi, B. C., et al. (2023). Gene based markers improve precision of genome-wide association studies and accuracy of genomic predictions in rice breeding. *Heredity* 130, 335–345. doi: 10.1038/s41437-023-00599-5

Araus, J. L., Serret, M. D., and Edmeades, G. O. (2012). Phenotyping maize for adaptation to drought. *Front. Physiol.* 3:305. doi: 10.3389/fphys.2012.00305

Atanda, S. A., Olsen, M., Burgueño, J., Crossa, J., Dzidzienyo, D., Beyene, Y., et al. (2021). Maximizing efficiency of genomic selection in CIMMYT's tropical maize breeding program. *Theor. Appl. Genet.* 134, 279–294. doi: 10.1007/s00122-020-03696-9

Badu-Apraku, B., Oyekunle, M., Talabi, A., Annor, B., and Akaogu, I. (2017). Changes in genetic variances and heritabilities in an early white maize population following S1 selection for grain yield, Striga resistance and drought tolerance. *J. Agric. Sci.* 155, 629–642. doi: 10.1017/S0021859616000770

Badu-Apraku, B., Talabi, A., Fakorede, M., Fasanmade, Y., Gedil, M., Magorokosho, C., et al. (2019). Yield gains and associated changes in an early yellow bi-parental maize population following genomic selection for Striga resistance and drought tolerance. *BMC Plant Biol.* 19, 1–17. doi: 10.1186/s12870-019-1740-z

Balbaa, M. G., Osman, H. T., Kandil, E. E., Javed, T., Lamlom, S. F., Ali, H. M., et al. (2022). Determination of morpho-physiological and yield traits of maize inbred lines (*Zea mays* L.) under optimal and drought stress conditions. *Front. Plant Sci.* 13:959203. doi: 10.3389/fpls.2022.959203

Bänziger, M., Edmeades, G., Beck, D., and Bellon, M. (2000). *Breeding for drought and nitrogen stress tolerance in maize: From theory to practice*. Mexico, D.F.: CIMMYT. Available at: http://hdl.handle.net/10883/765.

Barutcular, C., Dizlek, H., el-Sabagh, A., Sahin, T., Elsabagh, M., and Islam, S. (2016). Nutritional quality of maize in response to drought stress during grain-filling stages in Mediterranean climate condition. *J. Exp. Biol. Agric. Sci.* 4, 644–652. doi: 10.18006/2016.4(Issue6).644.652

Bentley, A. R., Scutari, M., Gosman, N., Faure, S., Bedford, F., Howell, P., et al. (2014). Applying association mapping and genomic selection to the dissection of key traits in elite European wheat. *Theor. Appl. Genet.* 127, 2619–2633. doi: 10.1007/s00122-014-2403-y

Beyene, Y., Gowda, M., Olsen, M., Robbins, K. R., Pérez-Rodríguez, P., Alvarado, G., et al. (2019). Empirical comparison of tropical maize hybrids selected through genomic and phenotypic selections. *Front. Plant Sci.* 10:1502. doi: 10.3389/fpls.2019.01502

Beyene, Y., Gowda, M., Pérez-Rodríguez, P., Olsen, M., Robbins, K. R., Burgueño, J., et al. (2021). Application of genomic selection at the early stage of breeding pipeline in tropical maize. *Front. Plant Sci.* 12:685488. doi: 10.3389/fpls.2021.685488

Beyene, Y., Gowda, M., Suresh, L. M., Mugo, S., Olsen, M., Oikeh, S. O., et al. (2017). Genetic analysis of tropical maize inbred lines for resistance to maize lethal necrosis disease. *Euphytica* 213:224. doi: 10.1007/s10681-017-2012-3

Beyene, Y., Semagn, K., Crossa, J., Mugo, S., Atlin, G. N., Tarekegne, A., et al. (2016). Improving maize grain yield under drought stress and non-stress environments in sub-saharan africa using marker-assisted recurrent selection. *Crop Sci.* 56, 344–353. doi: 10.2135/cropsci2015.02.0135

Beyene, Y., Semagn, K., Mugo, S., Tarekegne, A., Babu, R., Meisel, B., et al. (2015). Genetic gains in grain yield through genomic selection in eight bi-parental maize populations under drought stress. *Crop Sci.* 55, 154–163. doi: 10.2135/cropsci2014.07.0460

Bolaños, J., and Edmeades, G. (1996). The importance of the anthesis-silking interval in breeding for drought tolerance in tropical maize. *Field Crop Res.* 48, 65–80. doi: 10.1016/0378-4290(96)00036-6

Bradbury, P. J., Zhang, Z., Kroon, D. E., Casstevens, T. M., Ramdoss, Y., and Buckler, E. S. (2007). TASSEL: software for association mapping of complex traits in diverse samples. *Bioinformatics* 23, 2633–2635. doi: 10.1093/bioinformatics/btm308

Breen, C., Ndlovu, N., McKeown, P. C., and Spillane, C. (2024). Legume seed system performance in sub-Saharan Africa: barriers, opportunities, and scaling options. A review. *Agron. Sustain. Dev.* 44:20. doi: 10.1007/s13593-024-00956-6

Cerrudo, D., Cao, S., Yuan, Y., Martinez, C., Suarez, E. A., Babu, R., et al. (2018). Genomic selection outperforms marker assisted selection for grain yield and physiological traits in a maize doubled haploid population across water treatments. *Front. Plant Sci.* 9:366. doi: 10.3389/fpls.2018.00366

Chen, S., Dang, D., Liu, Y., Ji, S., Zheng, H., Zhao, C., et al. (2023). Genome-wide association study presents insights into the genetic architecture of drought tolerance in maize seedlings under field water-deficit conditions. *Front. Plant Sci.* 14:1165582. doi: 10.3389/fpls.2023.1165582

Chen, J., Shrestha, R., Ding, J., Zheng, H., Mu, C., Wu, J., et al. (2016). Genome-wide association study and QTL mapping reveal genomic loci associated with fusarium ear rot resistance in tropical maize germplasm. *G3* 6, 3803–3815. doi: 10.1534/g3.116.034561

Choudhary, M., Kumar, P., Kumar, P., Sheoran, S., Zunjare, R. U., and Jat, B. S. (2023). "Molecular breeding for drought and heat stress in maize: revisiting the progress and achievements" in *QTL mapping in crop improvement* (Elsevier), 57–74.

Chukwudi, U. P., Kutu, F. R., and Mavengahama, S. (2021). Maize response to combined heat and water stresses under varying growth conditions. *Agron. J.* 113, 4672–4689. doi: 10.1002/agj2.20820

Collins, N. C., Tardieu, F., and Tuberosa, R. (2008). Quantitative trait loci and crop performance under abiotic stress: where do we stand? *Plant Physiol.* 147, 469–486. doi: 10.1104/pp.108.118117

Crossa, J., Pérez-Rodríguez, P., Cuevas, J., Montesinos-López, O., Jarquín, D., De Los Campos, G., et al. (2017). Genomic selection in plant breeding: methods, models, and perspectives. *Trends Plant Sci.* 22, 961–975. doi: 10.1016/j.tplants.2017.08.011

Dekkers, J. (2007). Prediction of response to marker-assisted and genomic selection using selection index theory. *J. Anim. Breed. Genet.* 124, 331–341. doi: 10.1111/j.1439-0388.2007.00701.x

Deutsch, C. A., Tewksbury, J. J., Tigchelaar, M., Battisti, D. S., Merrill, S. C., Huey, R. B., et al. (2018). Increase in crop losses to insect pests in a warming climate. *Science* 361, 916–919. doi: 10.1126/science.aat3466

Dias, K. O. D. G., Gezan, S. A., Guimarães, C. T., Nazarian, A., da Costa e Silva, L., Parentoni, S. N., et al. (2018). Improving accuracies of genomic predictions for drought tolerance in maize by joint modeling of additive and dominance effects in multi-environment trials. *Heredity* 121, 24–37. doi: 10.1038/s41437-018-0053-6

Elshire, R. J., Glaubitz, J. C., Sun, Q., Poland, J. A., Kawamoto, K., Buckler, E. S., et al. (2011). A robust, simple genotyping-by-sequencing (GBS) approach for high diversity species. *PLoS One* 6:e19379. doi: 10.1371/journal.pone.0019379

Ertiro, B. T., Labuschagne, M., Olsen, M., Das, B., Prasanna, B. M., and Gowda, M. (2020). Genetic dissection of nitrogen use efficiency in tropical maize through genome-wide association and genomic prediction. *Front. Plant Sci.* 11:474. doi: 10.3389/fpls.2020.00474

Fisher, M., Abate, T., Lunduka, R. W., Asnake, W., Alemayehu, Y., and Madulu, R. B. (2015). Drought tolerant maize for farmer adaptation to drought in sub-Saharan Africa: determinants of adoption in eastern and southern Africa. *Clim. Chang.* 133, 283–299. doi: 10.1007/s10584-015-1459-2

Gilmour, A. R., Gogel, B. J., Cullis, B. R., and Thompson, R. (2009). *ASReml User Guide Release 3.0 VSN International Ltd, Hemel Hempstead, HP1 1ES, UK*. Available at: https://vsni.co.uk/

Glaubitz, J. C., Casstevens, T. M., Lu, F., Harriman, J., Elshire, R. J., Sun, Q., et al. (2014). TASSEL-GBS: a high capacity genotyping by sequencing analysis pipeline. *PLoS One* 9:e90346. doi: 10.1371/journal.pone.0090346

Gopalakrishna, K. N., Hugar, R., Rajashekar, M. K., Jayant, S. B., Talekar, S. C., and Virupaxi, P. C. (2023). Simulated drought stress unravels differential response and different mechanisms of drought tolerance in newly developed tropical field corn inbreds. *PLoS One* 18:e0283528. doi: 10.1371/journal.pone.0283528

Gowda, M., Beyene, Y., Makumbi, D., Semagn, K., Olsen, M. S., Bright, J. M., et al. (2018). Discovery and validation of genomic regions associated with resistance to maize lethal necrosis in four biparental populations. *Mol. Breed.* 38, 1–16. doi: 10.1007/s11032-018-0829-7

Gowda, M., Das, B., Makumbi, D., Babu, R., Semagn, K., Mahuku, G., et al. (2015). Genome-wide association and genomic prediction of resistance to maize lethal necrosis disease in tropical maize germplasm. *Theor. Appl. Genet.* 128, 1957–1968. doi: 10.1007/s00122-015-2559-0

Gowda, M., Makumbi, D., Das, B., Nyaga, C., Kosgei, T., Crossa, J., et al. (2021). Genetic dissection of *Striga hermonthica* (Del.) Benth. Resistance via genome-wide association and genomic prediction in tropical maize germplasm. *Theor. Appl. Genet.* 134, 941–958. doi: 10.1007/s00122-020-03744-4

Habte, E., Marenya, P., Beyene, F., and Bekele, A. (2023). Reducing susceptibility to drought under growing conditions as set by farmers: the impact of new generation drought tolerant maize varieties in Uganda. *Front. Sustain. Food Syst.* 6:854856. doi: 10.3389/fsufs.2022.854856

He, L., Xiao, J., Rashid, K. Y., Jia, G., Li, P., Yao, Z., et al. (2019). Evaluation of genomic prediction for pasmo resistance in flax. *Int. J. Mol. Sci.* 20:359. doi: 10.3390/ijms20020359

Hu, X., Wang, G., Du, X., Zhang, H., Xu, Z., Wang, J., et al. (2021). QTL analysis across multiple environments reveals promising chromosome regions associated with yield-related traits in maize under drought conditions. *Crop J.* 9, 759–766. doi: 10.1016/j.cj.2020.10.004

Huang, C., Qin, A., Gao, Y., Ma, S., Liu, Z., Zhao, B., et al. (2023). Effects of water deficit at different stages on growth and ear quality of waxy maize. *Front. Plant Sci.* 14:1069551. doi: 10.3389/fpls.2023.1069551

Khan, S. U., Zheng, Y., Chachar, Z., Zhang, X., Zhou, G., Zong, N., et al. (2022). Dissection of maize drought tolerance at the flowering stage using genome-wide association studies. *Genes* 13:564. doi: 10.3390/genes13040564

Kibe, M., Nair, S. K., Das, B., Bright, J. M., Makumbi, D., Kinyua, J., et al. (2020a). Genetic dissection of resistance to gray leaf spot by combining genome-wide association, linkage mapping, and genomic prediction in tropical maize germplasm. *Front. Plant Sci.* 11:572027. doi: 10.3389/fpls.2020.572027

Kibe, M., Nyaga, C., Nair, S. K., Beyene, Y., Das, B., Bright, J. M., et al. (2020b). Combination of linkage mapping, GWAS, and GP to dissect the genetic basis of common rust resistance in tropical maize germplasm. *Int. J. Mol. Sci.* 21:6518. doi: 10.3390/ijms21186518

Kimutai, C., Ndlovu, N., Chaikam, V., Ertiro, B. T., Das, B., Beyene, Y., et al. (2023). Discovery of genomic regions associated with grain yield and agronomic traits in bi-parental populations of maize (*Zea mays*. L) under optimum and low nitrogen conditions. *Front. Genet.* 14:1266402. doi: 10.3389/fgene.2023.1266402

Kosambi, D. D. (1944). The estimation of map distance from recombination values. *Ann. Eugenics* 12, 172–175,

Li, C., Sun, B., Li, Y., Liu, C., Wu, X., Zhang, D., et al. (2016). Numerous genetic loci identified for drought tolerance in the maize nested association mapping populations. *BMC Genomics* 17, 1–11. doi: 10.1186/s12864-016-3170-8

Li, S., Zhang, C., Lu, M., Yang, D., Qian, Y., Yue, Y., et al. (2020). QTL mapping and GWAS for field kernel water content and kernel dehydration rate before physiological maturity in maize. *Sci. Rep.* 10:13114. doi: 10.1038/s41598-020-69890-3

Liu, W., Gowda, M., Steinhoff, J., Maurer, H. P., Würschum, T., Longin, C. F. H., et al. (2011). Association mapping in an elite maize breeding population. *Theor. Appl. Genet.* 123, 847–858. doi: 10.1007/s00122-011-1631-7

Liu, B., Zhang, B., Yang, Z., Liu, Y., Yang, S., Shi, Y., et al. (2021). Manipulating ZmEXPA4 expression ameliorates the drought-induced prolonged anthesis and silking interval in maize. *Plant Cell* 33, 2058–2071. doi: 10.1093/plcell/koab083

Lobell, D. B., Schlenker, W., and Costa-Roberts, J. (2011). Climate trends and global crop production since 1980. *Science* 333, 616–620. doi: 10.1126/science.1204531

Lunduka, R. W., Mateva, K. I., Magorokosho, C., and Manjeru, P. (2019). Impact of adoption of drought-tolerant maize varieties on total maize production in south eastern Zimbabwe. *Clim. Dev.* 11, 35–46. doi: 10.1080/17565529.2017.1372269

Mathew, I., Shimelis, H., Shayanowako, A. I. T., Laing, M., and Chaplot, V. (2019). Genome-wide association study of drought tolerance and biomass allocation in wheat. *PLoS One* 14:e0225383. doi: 10.1371/journal.pone.0225383

Meng, L., Li, H., Zhang, L., and Wang, J. (2015). QTL IciMapping: integrated software for genetic linkage map construction and quantitative trait locus mapping in biparental populations. *Crop J.* 3, 269–283. doi: 10.1016/j.cj.2015.01.001

Muroyiwa, B., Masinda, N., and Mushunje, A. (2022). Smallholder farmers' adaptation strategies to mitigate the effect of drought on maize production in OR Tambo District municipality. *Afr. J. Sci. Technol. Innov. Dev.* 14, 459–471. doi: 10.1080/20421338.2020.1847385

Ndlovu, N., Kachapur, R. M., Beyene, Y., Das, B., Makumbi, D., Spillane, C., et al. (2024). Linkage mapping and genomic prediction of grain quality traits in tropical maize (*Zea mays* L.). *Front. Genet.* 15:1353289. doi: 10.3389/fgene.2024.1353289

Ndlovu, N., Spillane, C., McKeown, P. C., Cairns, J. E., Das, B., and Gowda, M. (2022). Genome-wide association studies of grain yield and quality traits under optimum and low-nitrogen stress in tropical maize (*Zea mays* L.). *Theor. Appl. Genet.* 135:4351. doi: 10.1007/s00122-022-04224-7

Nikolić, A., Anđelković, V., Dodig, D., Mladenović-Drinić, S., Kravić, N., and Ignjatović-Micić, D. (2013). Identification of QTL-s for drought tolerance in maize, II: yield and yield components. *Genetika* 45, 341–350. doi: 10.2298/GENSR1302341N

Osuman, A. S., Badu-Apraku, B., Karikari, B., Ifie, B. E., Tongoona, P., and Danquah, E. Y. (2022). Genome-wide association study reveals genetic architecture and candidate genes for yield and related traits under terminal drought, combined heat and drought in tropical maize germplasm. *Genes* 13:349. doi: 10.3390/genes13020349

Prasanna, B., Nair, S. K., Babu, R., Gowda, M., Zhang, X., Xu, Y., et al. (2020). "Increasing genetic gains in maize in stress-prone environments of the tropics" in *Genomic designing of climate-smart cereal crops*. Springer, Cham, 97–132. doi: 10.1007/978-3-319-93381-8_397–132

R Core Team (2023). *R: A language and environment for statistical computing*. Vienna, Austria: R Foundation for Statistical Computing.

Riedelsheimer, C., and Melchinger, A. E. (2013). Optimizing the allocation of resources for genomic selection in one breeding cycle. *Theor. Appl. Genet.* 126, 2835–2848. doi: 10.1007/s00122-013-2175-9

Sah, R., Chakraborty, M., Prasad, K., Pandit, M., Tudu, V., Chakravarty, M., et al. (2020). Impact of water deficit stress in maize: phenology and yield components. *Sci. Rep.* 10:2944. doi: 10.1038/s41598-020-59689-7

Sallam, A., Alqudah, A. M., Dawood, M. F., Baenziger, P. S., and Börner, A. (2019). Drought stress tolerance in wheat and barley: advances in physiology, breeding and genetics research. *Int. J. Mol. Sci.* 20:3137. doi: 10.3390/ijms20133137

Sallam, A., Eltaher, S., Alqudah, A. M., Belamkar, V., and Baenziger, P. S. (2022). Combined GWAS and QTL mapping revealed candidate genes and SNP network controlling recovery and tolerance traits associated with drought tolerance in seedling winter wheat. *Genomics* 114:110358. doi: 10.1016/j.ygeno.2022.110358

Sanguineti, M., Tuberosa, R., Landi, P., Salvi, S., Maccaferri, M., Casarini, E., et al. (1999). QTL analysis of drought-related traits and grain yield in relation to genetic variation for leaf abscisic acid concentration in field-grown maize. *J. Exp. Bot.* 50, 1289–1297. doi: 10.1093/jxb/50.337.1289

Sarkar, B., Varalaxmi, Y., Vanaja, M., RaviKumar, N., Prabhakar, M., Yadav, S. K., et al. (2023). Mapping of QTLs for morphophysiological and yield traits under water-deficit stress and well-watered conditions in maize. *Front. Plant Sci.* 14:1124619. doi: 10.3389/fpls.2023.1124619

Schwarz, G. (1978). Estimating the dimension of a model. *Ann. Stat.*, 6, 461–464. doi: 10.1214/aos/1176344136

Sehgal, A., Sita, K., Siddique, K. H., Kumar, R., Bhogireddy, S., Varshney, R. K., et al. (2018). Drought or/and heat-stress effects on seed filling in food crops: impacts on functional biochemistry, seed yields, and nutritional quality. *Front. Plant Sci.* 9:1705. doi: 10.3389/fpls.2018.01705

Seleiman, M. F., Al-Suhaibani, N., Ali, N., Akmal, M., Alotaibi, M., Refay, Y., et al. (2021). Drought stress impacts on plants and different approaches to alleviate its adverse effects. *Plan. Theory* 10:259. doi: 10.3390/plants10020259

Silva, P. C., Sánchez, A. C., Opazo, M. A., Mardones, L. A., and Acevedo, E. A. (2022). Grain yield, anthesis-silking interval, and phenotypic plasticity in response to changing environments: evaluation in temperate maize hybrids. *Field Crop Res.* 285:108583. doi: 10.1016/j.fcr.2022.108583

Sitonik, C., Suresh, L. M., Beyene, Y., Olsen, M. S., Makumbi, D., Oliver, K., et al. (2019). Genetic architecture of maize chlorotic mottle virus and maize lethal necrosis through GWAS, linkage analysis and genomic prediction in tropical maize germplasm. *Theor. Appl. Genet.* 132, 2381–2399. doi: 10.1007/s00122-019-03360-x

Tesfaye, K., Sonder, K., Caims, J., Magorokosho, C., Tarekegn, A., Kassie, G. T., et al. (2016). Targeting drought-tolerant maize varieties in southern Africa: A geospatial crop modeling approach using big data. *International Food and Agribusiness Management Review*. 19, 1–18. Available at: https://hdl.handle.net/10568/76332

Thirunavukkarasu, N., Hossain, F., Arora, K., Sharma, R., Shiriga, K., Mittal, S., et al. (2014). Functional mechanisms of drought tolerance in subtropical maize (*Zea mays* L.) identified using genome-wide association mapping. *BMC Genomics* 15, 1–12. doi: 10.1186/1471-2164-15-1182

Wallace, J. G., Zhang, X., Beyene, Y., Semagn, K., Olsen, M., Prasanna, B. M., et al. (2016). Genome-wide association for plant height and flowering time across 15 tropical maize populations under managed drought stress and well-watered conditions in sub-Saharan Africa. *Crop Sci.* 56, 2365–2378. doi: 10.2135/cropsci2015.10.0632

Wang, B., Liu, C., Zhang, D., He, C., Zhang, J., and Li, Z. (2019). Effects of maize organ-specific drought stress response on yields from transcriptome analysis. *BMC Plant Biol.* 19, 1–19. doi: 10.1186/s12870-019-1941-5

Wu, X., Feng, H., Wu, D., Yan, S., Zhang, P., Wang, W., et al. (2021). Using high-throughput multiple optical phenotyping to decipher the genetic architecture of maize drought tolerance. *Genome Biol.* 22, 1–26. doi: 10.1186/s13059-021-02377-0

Würschum, T., Liu, W., Gowda, M., Maurer, H., Fischer, S., Schechert, A., et al. (2012). Comparison of biometrical models for joint linkage association mapping. *Heredity* 108, 332–340. doi: 10.1038/hdy.2011.78

Würschum, T., Reif, J. C., Kraft, T., Janssen, G., and Zhao, Y. (2013). Genomic selection in sugar beet breeding populations. *BMC Genet.* 14, 1–8. doi: 10.1186/1471-2156-14-85

Yuan, Y., Cairns, J. E., Babu, R., Gowda, M., Makumbi, D., Magorokosho, C., et al. (2019). Genome-wide association mapping and genomic prediction analyses reveal the genetic architecture of grain yield and flowering time under drought and heat stress conditions in maize. *Front. Plant Sci.* 9:1919. doi: 10.3389/fpls.2018.01919

Zaidi, P., Seetharam, K., Krishna, G., Krishnamurthy, L., Gajanan, S., Babu, R., et al. (2016). Genomic regions associated with root traits under drought stress in tropical maize (*Zea mays* L.). *PLoS One* 11:e0164340. doi: 10.1371/journal.pone.0164340

Zhang, A., Chen, S., Cui, Z., Liu, Y., Guan, Y., Yang, S., et al. (2022). Genomic prediction of drought tolerance during seedling stage in maize using low-cost molecular markers. *Euphytica* 218:154. doi: 10.1007/s10681-022-03103-y

Zhang, Q., Liu, H., Wu, X., and Wang, W. (2020). Identification of drought tolerant mechanisms in a drought-tolerant maize mutant based on physiological, biochemical and transcriptomic analyses. *BMC Plant Biol.* 20: 315. doi: 10.1186/s12870-020-02526-w

Zhao, Y., Gowda, M., Liu, W., Würschum, T., Maurer, H. P., Longin, F. H., et al. (2012). Accuracy of genomic selection in European maize elite breeding populations. *Theor. Appl. Genet.* 124, 769–776. doi: 10.1007/s00122-011-1745-y

Zhao, X., Peng, Y., Zhang, J., Fang, P., and Wu, B. (2018). Identification of QTLs and meta-QTLs for seven agronomic traits in multiple maize populations under well-watered and water-stressed conditions. *Crop Sci.* 58, 507–520. doi: 10.2135/cropsci2016.12.0991

Zhao, X., Zhang, J., Fang, P., and Peng, Y. (2019). Comparative QTL analysis for yield components and morphological traits in maize (*Zea mays* L.) under water-stressed and well-watered conditions. *Breed. Sci.* 69, 621–632. doi: 10.1270/jsbbs.18021

Zhou, B., Zhou, Z., Ding, J., Zhang, X., Mu, C., Wu, Y., et al. (2018). Combining three mapping strategies to reveal quantitative trait loci and candidate genes for maize ear length. *Plant Genome* 11:170107. doi: 10.3835/plantgenome2017.11.0107

frontiers | Frontiers in Sustainable Food Systems

TYPE Original Research
PUBLISHED 17 June 2024
DOI 10.3389/fsufs.2024.1389970

OPEN ACCESS

EDITED BY
Md Khairul Alam,
Bangladesh Agricultural Research Institute, Bangladesh

REVIEWED BY
Amar Kant Kushwaha,
Central Institute for Subtropical Horticulture (ICAR), India
Muhammad Imran,
King Abdulaziz University, Saudi Arabia

*CORRESPONDENCE
Neeraj Kumar
✉ neeraj0490@gmail.com
Chellapilla Bharadwaj
✉ drchbharadwaj@gmail.com

RECEIVED 22 February 2024
ACCEPTED 28 May 2024
PUBLISHED 17 June 2024

CITATION
Harish D, Pappula Reddy SP, Kumar N, Bharadwaj C, Kumar T, Parida S, Patil BS, Kumar S, Jain PK, Kumar Y and Varshney RK (2024) Integrating multilocus genome-wide association studies in chickpea landraces to discern the genetics of drought tolerance.
Front. Sustain. Food Syst. 8:1389970.
doi: 10.3389/fsufs.2024.1389970

Integrating multilocus genome-wide association studies in chickpea landraces to discern the genetics of drought tolerance

D. Harish[1,2], Sneha Priya Pappula Reddy[1,3], Neeraj Kumar[1]*, Chellapilla Bharadwaj[1]*, Tapan Kumar[1,4], Swaroop Parida[5], Basavanagowda S. Patil[1], Sudhir Kumar[1], Pradeep K. Jain[6], Yogesh Kumar[7] and Rajeev K. Varshney[8]

[1]ICAR-Indian Agricultural Research Institute, New Delhi, India, [2]ICAR-Directorate of Floricultural Research, Pune, India, [3]The UWA Institute of Agriculture, The University of Western Australia, Perth, WA, Australia, [4]ICARDA-FLRP, Amlah, Madhya Pradesh, India, [5]National Institute of Plant Genome Research, New Delhi, India, [6]ICAR-National Institute of Plant Biotechnology, New Delhi, India, [7]ICAR-Indian Institute of Pulses Research, Kanpur, Uttar Pradesh, India, [8]State Agricultural Biotechnology Centre, Murdoch University, Murdoch, WA, Australia

In chickpea breeding, drought is a major concern and a complex trait controlled by several genes. To develop drought-tolerant varieties, it is essential to use the available germplasm and genomic resources. Over the years, the landraces have proven to be a good source for the dissection of genes for different yield and yield-related traits. The present investigation for marker–trait associations (MTAs) and candidate gene identification was conducted by studying 125 chickpea landraces collected from the West Asia and North Africa (WANA) region, along with 4 varieties suitable for irrigated and rainfed environments. This study analyzed 13 physio-morphological traits in 2 consecutive years at two isolated locations (IARI, New Delhi, and Dharwad). A strong correlation coefficient was observed between the trait seed yield (SY) and biological yield (BY) under both conditions. The Drought Susceptibility Index (DSI) ranged from 0.02 to 1.84 and 0.10 to 2.04 at the IARI, New Delhi and Dharwad locations, respectively. The genotypic data of 6,367 single nucleotide polymorphisms (SNPs) distributed across the genome were used for genetic diversity study, population structure, and genome-wide association study (GWAS). The average polymorphic information content (PIC) value observed was 0.25, and the average linkage disequilibrium (LD) decay distance was 152,269 bp across the genome. A total of four subgroups were observed within the population for genotypic data. Fixed and random model Circulating Probability Unification (FarmCPU) was used for the GWAS analysis, which considered both fixed- and random-effect models. A total of 52 significant SNPs were reported in both irrigated and rainfed conditions at low locations; 7 SNPs were associated with more than one trait, which may have pleiotropic effects. Significant SNPs were annotated in the pulse database. The identified genomic region found in or near MTA under rainfed conditions encodes for guard cell hydrogen peroxide-resistant1 (GHR1), late embryogenesis-abundant, E3 ubiquitin-protein ligase, walls are thin1 (WAT1), and beta-galactosidase that are known to be associated with drought tolerance.

KEYWORDS

GWAS, candidate gene, genetic diversity, population structure, GAPIT, TASSEL

Introduction

Chickpea (*Cicer arietinum* L.) is a globally cultivated legume, with an area of 15 million ha and a production of 15 million tons (FAOSTAT, 2021). It is a cool-season crop, predominantly grown in arid and semi-arid climatic conditions with residual soil moisture (Thudi et al., 2014). It is also a vital source of protein, dietary fiber, and essential minerals (Bar-El Dadon et al., 2017). In the past century, the average global temperature has increased by 1.2°C and is estimated to rise further by 3°C by 2,100 (Schneider et al., 2007). Due to these climatic changes, the frequency, severity, and duration of drought periods are estimated to increase progressively (Cramer et al., 2011). Among the 100 meta-analysis studies of 13 legumes, chickpea stands seventh with a significant difference in drought tolerance measured in terms of yield reduction (Daryanto et al., 2015). More than 50% of yield losses were reported by terminal drought or end-season drought alone (Ahmad et al., 2005). Over the past three decades, chickpea cultivation has shifted from cooler to warmer regions in India (Krishnamurthy et al., 2013) and the productivity of chickpea is expected to be further reduced. As per the Vision 2050 document of the Indian Council of Agricultural Research (ICAR)–Indian Institute of Pulses Research (IIPR), approximately 16–17.5 million tons of chickpeas need to be produced from an area of approximately 10.5 million ha with an average productivity of 1.5–1.7 tons/ha (Dixit et al., 2019). The chickpea genome (size ~700 Mb) has been sequenced, and the whole-length genome sequence is available for desi (Jain et al., 2013; Parween et al., 2015), kabuli (Varshney et al., 2013), and wild species, *C. reticulum* (Gupta et al., 2017). With the availability of well-developed genomic resources in chickpeas and the advances in the cost-effective next-generation sequencing technology, genome-wide association mapping is the best method to discover a large amount of variability available in the population. The availability and accessibility of genomic resources make it possible to identify unique alleles and haplotypes associated with agronomic traits (Varshney et al., 2019). The precise integration of genome-wide sequence information, to that of phenotypic variation for yield component trait, abiotic, or disease tolerance, allows capturing accessions with low-frequency variants (Roorkiwal et al., 2020). The QTL hotspot for drought tolerance with a phenotypic variation of >50% was identified on chromosome 4, by using QTL analysis along with SSR and GBS markers (Varshney et al., 2014; Jaganathan et al., 2015). The addition of more SNPs was done to fine map QTL-hotspot to ~300-kb region, and 26 genes were reported in the region with the help of QTL bin-mapping and gene enrichment strategies (Kale et al., 2015). The introgression of these QTL hotspots has led to increased seed yield and enhanced drought tolerance in three elite chickpea cultivars (Bharadwaj et al., 2021). Recent efforts were made by Li et al. (2018) to identify the marker–trait association for drought tolerance by incorporating GWAS and genomic selection (GS) in 132 chickpea varieties. In order to augment the available genomic resources in chickpeas and to accelerate the chickpea breeding program for drought tolerance, our present investigation of GWAS was carried out in 129 chickpea landraces (collected from the WANA region) for the identification of candidate genes for drought tolerance.

Materials and methods

Plant materials and experimental design

The experimental material consisted of 129 chickpea genotypes, including 125 landraces collected from the WANA (West Asia and North Africa) region, and 4 varieties. The experiment was conducted at two isolated locations, *viz.* IARI, New Delhi (28.080^{0}N and 77.120°E), and Dharwad (15.4589^{0}N and 75.0078°E) during 2 consecutive years, 2017–18 and 2018–19, under irrigated and rainfed conditions, respectively. No supplementary irrigation was given for the rainfed environment. The supplementary irrigation was given at the critical growth stage (initiation of pod formation) under an irrigated environment. The month-wise rainfall data are provided in Supplementary Table S1. The 10 morphological traits, namely, days to 50% flowering (DFF), plant height (PH), number of primary branches (NPB), number of secondary branches (NSB), number of pods per plant (NPP), biological yield (BY), the Harvest Index (HI), 100 seed weight (100SW), seed yield (SY), and the Drought Susceptible Index (DSI) and three physiological traits, namely, relative water content (RWC), the Membrane Stability Index (MSI), and canopy temperature depression (CTD) were recorded for both the experimental trials, across the years. The seed yield and biological yield were recorded in 10 plants per genotype, and CTD was measured with the help of an infrared thermometer.

The Drought Susceptibility Index (DSI) was calculated as follows (Fischer and Maurer, 1978):

$$DSI = (1 - Y_S/Y_N)/(1 - Y_S/Y_N)$$

where Y_S and Y_N are the mean yields of individual genotypes under rainfed and irrigated conditions and y_S and y_N are the mean yields of all genotypes under rainfed and irrigated conditions.

The MSI was calculated using the formula (Blum and Ebercon, 1981) as below:

$$MSI = \left(1 - \frac{C1}{C2}\right) X\,100$$

For the estimation of MSI, ~400 mg of fresh leaf sample was taken in a test tube containing 10 mL distilled water and kept in a water bath at 45°C for 30 min, and conductivity was measured (C1). Similarly, the test tubes were placed again at 100°C for 10 min and the conductivity (C2) was measured after allowing it to cool to room temperature.

The relative water content (RWC) was estimated according to Barrs and Weatherley (1962).

$$RWC = \left(\text{Fresh Weight} - \text{Dry Weight}\right) / \left(\text{Turgid Weight} - \text{Dry Weight}\right) X\,100$$

The fresh weight was recorded for the leaf samples of all genotypes, and then they were kept in a Petri dish filled with distilled water for 4 h, so as to record the turgid weight. Thereafter, the samples were

placed in a dry-air oven set at 60°C for 72 h to record the dry weight of the sample.

Analysis variance across location and year is calculated in the R environment. The Best linear Unbiased Predictions (BLUPs) were calculated by using the phenotype version 0.1.0 package, and Metan version 1.16.0 was used to calculate the correlation coefficient and to draw a correlation plot (Olivoto and Lucio, 2020) in R version 4.1.1.

Genotyping of plant material

A total of 16,983 SNPs were filtered from 16 k Illumina GBS resequencing data for 129 genotypes. After excluding the markers with minor allele frequency (MAF) <0.05 in TASSEL version 5 (Bradbury et al., 2007), a total of 6,367 markers were retained for further genetic diversity and genome-wide association study.

Genetic diversity and population structure analysis

The molecular genetics diversities such as gene diversity (GD), polymorphic information content (PIC), and heterozygosity were calculated using PowerMarker 3.25 (Liu and Muse, 2005). The population structure for 6,367 SNPs was analyzed with the 1 to 10 assumed number of subgroups (K) for each run with 100,000 Markov Chain Monte Carlo iteration and a burn-in 10,000 steps in Structure 2.3.4 (Pritchard et al., 2000). The optimum number of clusters was determined by plotting ΔK against the natural logarithms of probability data [LnP(K)] Structure Harvester (Earl and vonHoldt, 2012). The PCA was incorporated in the package Genomic Association and Prediction Integrated Tool Version 3 under the R environment (Wang and Zhang, 2021), and the analysis was performed. The extent of linkage disequilibrium between the SNP markers was analyzed by calculating the r^2 values in TASSEL v5 (Bradbury et al., 2007). Only r^2 values with $p < 0.05$ within each chromosome were considered for LD decay analysis. The non-linear regression curve was used for the estimation of LD decay (Hill and Weir, 1988). LD decay plot was drawn with the help of LD (r^2) and physical distance (bp) by using the script in R version 4.1.1 (David et al., 2001).

Genome-wide association mapping

The genome-wide association analysis for 6,367 SNPs was performed using a multilocus GWAS model, *viz.*, Fixed and random model and Circulating Probability Unification (FarmCPU) (Liu et al., 2016) using GAPIT version 3 (Wang and Zhang, 2021) in R software. Both the fixed-effect model (FEM) and random-effect model (REL) are utilized in this model, and it is considered the most efficient as it eliminates confounding issues arising due to population structure, kinship, multiple testing, etc. (Gahlaut et al., 2021). To identify the significant SNPs, the Bonferroni-corrected *p*-value at 1 (−log *p*-value = 3.8) was considered as the threshold p-value (Kohli et al., 2020). Only the SNPs with above this value were declared as significant MTAs. A mixed linear model in TASSEL was to calculate the phenotypic variation explained (PVE) (Bradbury et al., 2007). The Manhattan plot was generated from qqman version 0.1.8 (Turner, 2018).

Exploration of candidate gene

To explore putative candidate genes, LD decay along the individual chromosome was considered to retrieve sequence flanking significant MTAs, searched against the NCBI (National Center for Biotechnology Information) reference genome ASM33114v1. The Chickpea pulse database[1] was used for the annotation of significant MTAs.

Results

Screening of chickpea genotypes for morpho-physiological traits under irrigated and rainfed environment

In total, 129 chickpea genotypes were evaluated for 10 morphological and 3 physiological traits under differing water regimes and were found to have a wide range of variability. The analysis of variance (ANOVA) of all morphological traits under irrigated and rainfed environments across the location and year was estimated, and a mean sum of squares and their significance are presented in Supplementary Table S2. The ANOVA reveals that the genotype–environmental interaction was significant at $p < 0.001$ for all the morphological traits except NPP, BY, and HI for genotype × year interaction in both irrigated and rainfed conditions. This indicates that the environmental influence on the performance of the genotypes. The genotypic × location interaction effect was significant for all the traits in both irrigated and rainfed conditions. This shows the genotypes studied had wide variability, and they performed differently across the locations. The DSI for IARI, New Delhi, environment varied from 0.02 to 1.84 while for the Dharwad environment was 0.10 to 2.04. Boxplot was drawn to compare the mean value of morphological traits under different environmental conditions, and the reduction in the mean value of all traits studied was observed in rainfed compared to the irrigated conditions in both locations (Figure 1). Pearson's correlation analysis is summarized in Figure 2, which reveals the significant correlation among most of the traits in both rainfed and irrigated environments. Furthermore, the seed yield is positively associated with the traits NPB, NSB, NPP, BY, HI, and 100SW in both irrigated and rainfed environments and negatively associated with the DFF and PH. A strong correlation was observed between the trait SY and BY with correlation coefficients of 0.934, 0.932, 0.919, and 0.941 in the E1, E2, E3, and E4 environment, respectively, which showed that healthy plant biomass will retain yield even in drought condition (Kashiwagi et al., 2013; Li et al., 2018). The boxplot for three physiological traits, *viz.*, RWC, MSI, and CTD is presented in Figure 3, reduced in the mean value of traits observed in rainfed condition compared to irrigated condition.

1 https://www.pulsedb.org/blast/report/

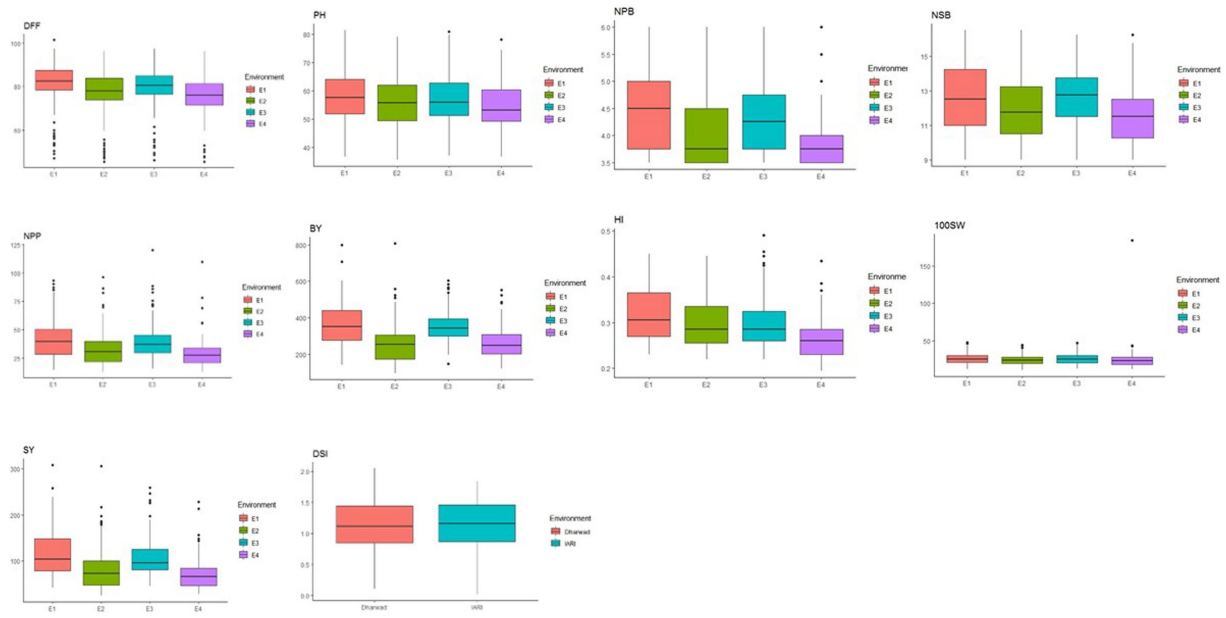

FIGURE 1
Box plot for morphological traits studied under different environments: E1, IARI irrigated; E2, IARI rainfed; E3, Dharwad irrigated; E4, Dharwad rainfed; DFF, days to 50% flowering; PH, plant height; NPB, number of primary branches; NSB, number of secondary branches; NPP, number of pods per plant; BY, biological yield; HI, Harvest Index; 100SW, 100 seed weight; SY, seed yield; DSI, Drought Susceptible Index.

Genetic diversity, linkage disequilibrium, and population structure

A total of 6,367 SNPs were considered for the study after excluding the SNPs with minor allele frequency (MAF) of <0.05 from 16,983 SNPs. The distribution of SNPs across the chromosome ranged from 438 in chromosome 8 to 1,480 in chromosome 4. The percentage of transitions (A/G and C/T) was higher at 0.53% than 0.47% of A/C, A/T, G/C, and G/T transversions. The average genetic distance was 0.33 with a range from 0.095 to 0.611. The average PIC value was 0.25 with a range from 0.09 to 0.53, and the average heterozygosity was 0.11. The LD and LD decay of all 8 chickpea chromosomes are presented in Table 1. The average LD across the genome was 0.14, and in the individual chromosomes, it varied from 0.06 in chromosome 5 to 0.22 in chromosome 8. The maximum SNP pairs with a *p*-value of <0.05 were on chromosome 4 (12477), and the minimum SNP pairs were on chromosome 5 (697). The whole genome LD decay distance was 152,269 bp (Figure 4), above which LD decay was observed. The LD decay distance of individual chromosomes ranged from 81,535 on chromosome 5 to 225,588 on chromosome 6. The SNP density per chromosome ranged from 9.80SNPS/Mb in Chromosome 5 to 30.24 SNPs/Mb in Chromosome 4.

The 129 chickpea genotypes were clustered into subpopulations based on the Bayesian clustering approach and plotted as cluster k and delta K. The maximum delta K was observed on cluster 4 (Figure 5), concluding that 129 chickpea genotypes were divided into 4 subpopulations by using the admixture method in STRUCTURE software and computing the result into online Structure HarveSter (Evanno et al., 2005). The individual genotypes were included in the subpopulation based on their highest share of the membership coefficient. Based on the membership coefficient, the four subpopulations namely SubPop1, SubPop2, SubPop3, and SubPop4 have 54, 42, 18, and 15 genotypes, respectively, in their clusters (Figure 5 and Supplementary Table S3). The fixation index of 0.56, 0.52, 0.44, and 0.58 was recorded in SubPop1, SubPop2, SubPop3, and SubPop4, respectively. The allele-frequency divergence of SubPop1 from SubPop2 was 0.19, from SubPop3 was 0.12, and from SubPop4 0.23; the divergence of SubPop2 from SubPop3 was 0.15 and from SubPop4 was 0.19; and the divergence of SubPop3 from SubPop4 was 0.17. The average distance between the individuals within the subpopulation was 0.18, 0.19, 0.23, and 0.19 in SubPop1, SubPop2, SubPop3, and SubPop4, respectively. The kinship matrix obtained from SNPs, varied from −0.52 to 2.07. The diversity among 129 chickpea genotypes, as shown in the kinship matrix heatmap (Figure 6A), by using PCA (Figure 6C) and percentage variation, explained each PCA (Figure 6B). The PCA and kinship showed the presence of a high level of diversity in the panel used.

Genome-wide association mapping for irrigated and rainfed environments

The analysis of significantly associated SNPs ($p < 1.5E-04$) resulted in a total of 49 SNPs for morphological traits, excluding NPB, and three for physiological traits, in both irrigated and rainfed environments at two locations (Table 2). For the morphological traits studied, 8 SNPs were reported for both irrigated and rainfed environments, 27 SNPs for the rainfed environment, and 10 SNPs for the irrigated environment. A maximum number of 21 SNPs showed significant association with 100SW explained 0.003–17.184% phenotypic variation followed by 10 SNPs with SY explained 0.002–28.75% phenotypic variation and 7 SNPs with NPP explained 0.001 to 30.969% phenotypic variation. In total, seven SNPs were found to be associated with more than one trait (Supplementary Table S4).

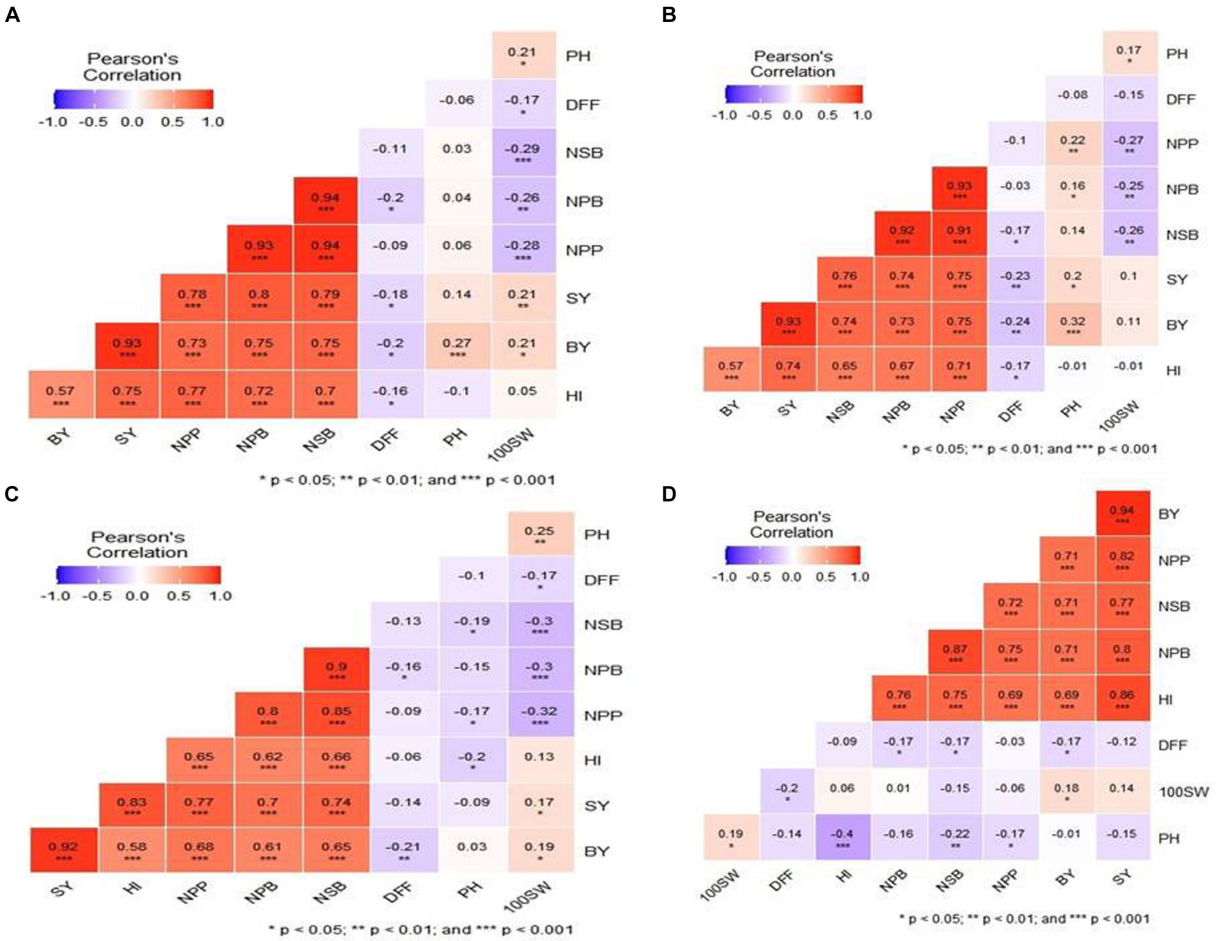

FIGURE 2
Correlation coefficient (*r*) plot for morphological traits in different water regimes. **(A)** IARI irrigated. **(B)** IARI rainfed. **(C)** Dharwad rainfed, and **(D)** Dharwad irrigated environment (top to bottom in clockwise).

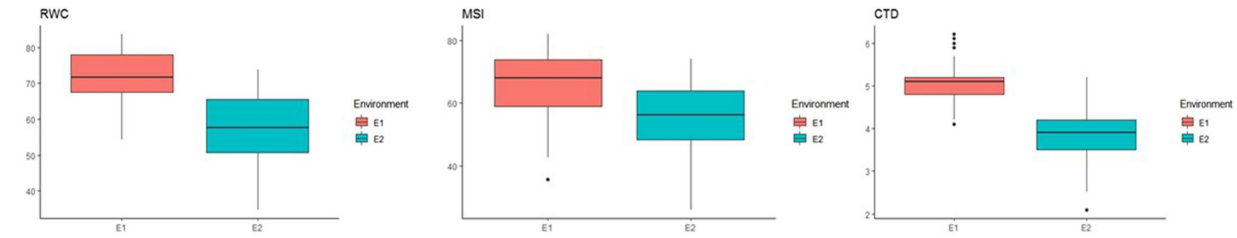

FIGURE 3
Box plot 3 physiological traits RWC (relative water content), MSI (Membrane Stability Index), and CTD (canopy temperature depression) at E1—IARI irrigated and E2—IARI rainfed.

Two significant SNPs for DSI, one each under IARI, New Delhi, located on Ca8:8904366 (Figure 7A) and Dharwad located on Ca1:7500524 (Figure 7B). For physiological traits studies, two SNPs were found to be significant for RWC (Ca3:13202989) and CTD (Ca4:25809665) in an irrigated environment, and one SNP for CTD (Ca5:31164539) for a rainfed environment at IARI, New Delhi (Figure 7C). The Manhattan plot for 100SW and SY under the rainfed condition for both the locations IARI, New Delhi, and Dharwad, are presented in Figure 8. The SNP located on Ca1:43273961 was found to be associated with a greater number of traits (NPB, NPP, BY, and SY) followed by SNP on Ca1:43273962, associated with NPB, NPP, and SY and SNP located on Ca8:13745335 associated with NPP, BY, and SY, which indicates the pleiotropic effect.

TABLE 1 Distribution of SNPs, SNP pairs ($p < 0.05$), LD (r2), and LD decay on all eight chromosomes of chickpea.

Chromosome	Number of SNPs	SNP density (per Mb)	SNP pair in LD ($p < 0.05$)	Average LD (r^2)	LD decay distance (bp)
1	1,014	20.98	5,506	0.14	87,707
2	585	15.98	4,107	0.13	82,456
3	572	14.33	3,621	0.15	216,852
4	1,480	30.24	12,477	0.15	130,725
5	470	9.80	697	0.06	81,535
6	942	15.85	5,273	0.16	225,588
7	866	17.85	4,908	0.12	117,169
8	438	26.59	3,705	0.22	582,792

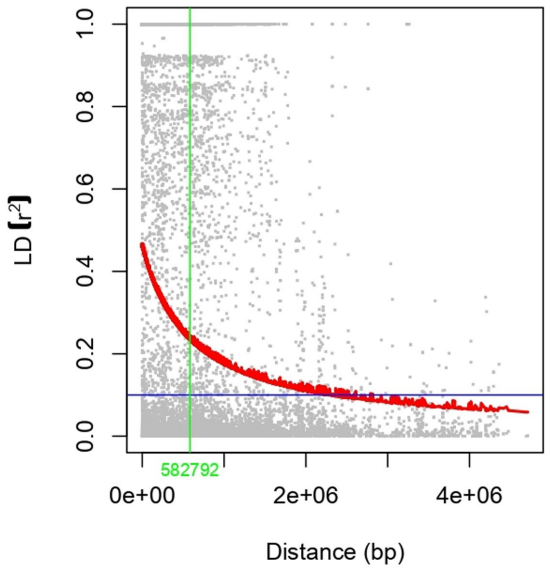

FIGURE 4
Genome-wide Linkage Disequilibrium plot of the entire genome of chickpea. The *x*-axis represents distance (bp), and the *y*-axis represents LD (r^2). The intersection between the horizontal and vertical lines represents the LD decay distance.

Putative candidate gene identification for marker–trait associations

The significant SNP associations with different traits were further used for the identification of putative candidates based on the position of SNPs. LD decay across individual chromosomes was considered to retrieve a flanking sequence of significant SNPs from the NCBI database and functionally annotated based on CDC Frontier v1 functional annotation (Varshney et al., 2013) from the pulse database (Supplementary Data S1). The identified MTA Ca1:7500524 associated with traits IARI_DSI (9.58E-05) and E4_NPP ($p < 1.10$E-04) explains 6.915 and 10.648% phenotypic variance found in or near probable coding region encodes for probable LRR receptor-like serine/threonine-protein kinase At4g20940 (Ca_08003), and another significant MTA for Dharwad_DSI (7.24E-05) located at Ca8:8904366 explains 9.816% phenotypic variance, colocalized with the gene encodes for threonine–tRNA ligase, mitochondrial 1-like (Ca_11521). The MTA Ca3:32706215 for E1_100SW ($p < 3.0$E-04), E1_100SW ($p < 3.0$E-04), and E2_SY (7.24E-10) explain the phenotypic variation of 6.453, 4.818, and 4.361%, respectively, colocalized with the gene zinc finger BED domain-containing protein DAYSLEEPER-like (Ca_12000). The MTA Ca4:30258567 had associations with E4_NPP ($p < 7.97$E-05) and E4_BY ($p < 1.30$E-04) explaining 30.969 and 22.205% phenotypic variations, respectively, and encodes for 11 kDa late embryogenesis abundant protein-like (Ca_14189). The MTA Ca5:28886131 for E4_100SW ($p < 6.16$E-05) explains the phenotypic variation of 14.511% and is colocalized in or near gene encodes for protein WAT1-related protein-like (Ca_17987). MTA Ca7:41673233 was found to be colocalized with gene encodes for the beta-galactosidase (Ca_17987) and was associated with E2_100SW ($p < 1.88$E-05) explaining the phenotypic variation of 6.830%. MTA Ca7:31317611 for E4_100SW ($p < 1.2$E-04) explains the phenotypic variation of 19.740%, found near or in gene encodes for putative proline-rich protein APG isolog, GDSL esterase/lipase APG (Ca_10127). MTA Ca1:2252356 for E2_SY ($p < 8.43$E-07) found in or near gene encodes for E3 ubiquitin-protein ligase AIRP2-like (Ca_00281) explains 13.853% phenotypic variance. MTA Ca5:47684292 for E2_SY ($p < 2.96$E-07) encodes with the protein FAR1-RELATED SEQUENCE 7-like and sugar transport protein 10-like (Ca_24737) explains 7.161% phenotypic variance. MTA Ca4:30308719 for E2_BY ($p < 1.45$E-04) found in or near gene encodes for UDP-glycosyltransferase (Ca_23901) explains a phenotypic variance of 17.974%. MTA Ca5:31164539 for E2_CTD ($p < 7.56$E-05) explains phenotypic variance of 13.406%, found in or near gene encodes for protein U-box domain-containing protein 44-like (Ca_04820), and is also capable of functioning as E3 ubiquitin-protein ligase (Raab et al., 2009).

Discussion

The chickpea grown in the Indian subcontinent has a narrow genetic base (Bharadwaj et al., 2011b), and the use of various accessions/donor parents in the breeding program would increase the sensitivity of chickpea productivity toward biotic and abiotic stress (Muehlbauer and Sarker, 2017). The study on the linkage mapping in the intraspecific populations (*desi* × *kabuli*) from the STMs proved the potential of using genomic resources in chickpea

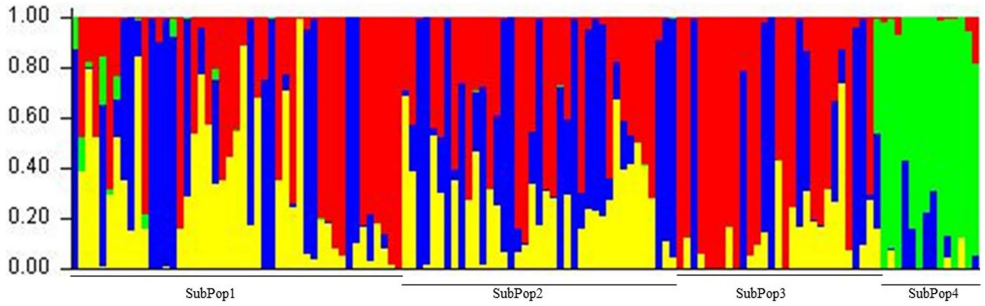

FIGURE 5
Population structure of 129 Chickpea genotypes. Delta K shows four subpopulation by Evanno's method; the peak observed at $k = 4$.

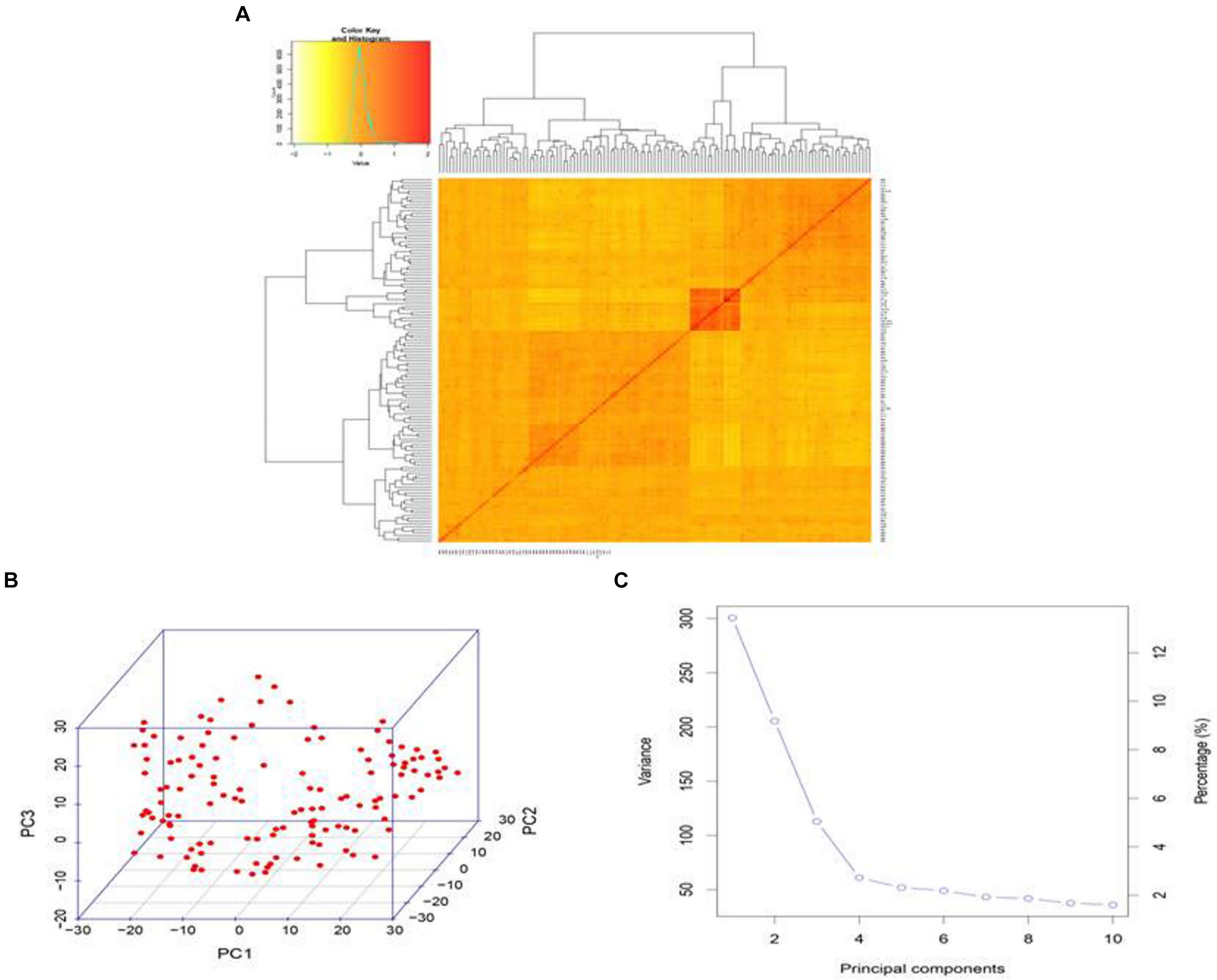

FIGURE 6
Molecular diversity and genetic structure of 129 chickpea genotypes. **(A)** Kinship matrix heatmap. **(C)** Scree plot depicting significant PCs. **(B)** The 3D graph depicting the distribution of genotypes along the three (top to bottom in clockwise).

breeding (Bharadwaj et al., 2011a). The breeding program could be accelerated by supplementing conventional breeding efforts with genomics-assisted breeding (GAB) (Varshney et al., 2007). Sequence cost curtailed as an advance in the next-generation sequencing technology (NGS) (Varshney et al., 2005) and the availability of chickpea draft genome (Jain et al., 2013; Varshney et al., 2013; Gupta et al., 2017) have led to the development of genotyping-by-sequencing-based marker, which can be effectively used for genome-wide association analysis for identification of marker–trait associations (MTAs).

10.3389/fsufs.2024.1389970

TABLE 2 Fifty-two SNPs which are associated with different traits.

Traits	Environment	SNP	Chromosome	Position	SNP allele	*P*-value	Rsquare value
PH	E1	Ca4:10030134	4	10,030,134	A/G	1.2E-04	11.511
	E3	Ca1:1225254	1	1,225,254	T/G	2.72E-05	7.870
		Ca4:10030134	4	10,030,134	A/G	9.52E-05	12.475
	E4	Ca4:10030134	4	10,030,134	A/G	1.2E-04	13.195
		Ca6:14042859	6	14,042,859	A/T	1.10E-04	7.920
DFF	E3	Ca8:1612982	8	1,612,982	A/C	1.4E-04	12.281
	E4	Ca8:1612982	8	1,612,982	A/C	1.4E-05	13.855
NPB	E2	Ca1:10191516	1	10,191,516	A/G	1.10E-04	17.863
		Ca1:10191517	1	10,191,517	G/T	1.10E-04	17.863
		Ca7:35258029	7	35,258,029	G/T	1.30E-04	10.232
	E4	Ca1:43273961	1	43,273,961	C/T	9.1E-06	3.074
		Ca1:43273962	1	43,273,962	A/G	9.1E-06	3.074
		Ca6:32262855	6	32,262,855	C/T	1.89E-05	0.002
		Ca7:6075124	7	6,075,124	T/G	1.20E-04	20.577
NPP	E2	Ca8:13745335	8	13,745,335	A/G	1.39E-05	0.001
	E3	Ca1:43273961	1	43,273,961	C/T	3.5E-05	1.698
		Ca1:43273962	1	43,273,962	G/T	3.5E-05	1.698
		Ca6:32262855	6	32,262,855	C/T	6.2E-05	0.001
		Ca6:52065393	6	52,065,393	C/A	4.60E-04	27.384
	E4	Ca1:43273961	1	43,273,961	C/T	1.33E0.5	4.239
		Ca1:43273962	1	43,273,962	G/T	1.33E0.5	4.239
		Ca1:7500524	1	7,500,524	T/C	1.10E-04	10.468
		Ca4:30258567	4	30,258,567	C/A	7.97E-05	30.969
		Ca6:32262855	6	32,262,855	C/T	7.85E05	0.004
BY	E1	Ca8:13745335	8	13,745,335	A/G	1.14E-04	0.001
	E2	Ca1:43273961	1	43,273,961	C/T	3.94E-07	21.337
		Ca4:30308719	4	30,308,719	C/A	1.45E-05	17.974
		Ca5:6290453	5	6,290,453	G/A	6.41E-06	3.230
	E4	Ca4:30258567	4	30,258,567	C/A	1.30E-04	22.205
HI	E1	Ca3:4878351	3	4,878,351	G/T	1.3E-04	12.007
100SW	E1	Ca1:11225828	1	11,225,828	C/T	1.4E-04	7.527
		Ca1:46749206	1	46,749,206	T/G	1.2E-04	3.608
		Ca3:31454799	3	31,454,799	G/T	1.1E-04	4.610
		Ca3:32706215	3	32,706,215	A/C	3.0E-04	6.453
		Ca4:24729101	4	24,729,101	T/G	1.4E-04	3.892
		Ca5:47775117	5	47,775,117	T/G	1.4E-04	5.936
		Ca6:10136954	6	10,136,954	A/C	1.19E-04	4.124
		Ca6:1288709	6	1,288,709	T/G	3.84E-05	7.853
		Ca8:2029341	8	2,029,341	T/G	7.20E-06	6.951
		Ca8:5352551	8	5,352,551	T/G	5.44E-05	6.904

(Continued)

TABLE 2 (Continued)

Traits	Environment	SNP	Chromosome	Position	SNP allele	*P*-value	Rsquare value
	E2	Ca1:13043346	1	13,043,346	T/A	4.88E-05	0.037
		Ca2:7633564	2	7,633,564	G/T	4.01E-05	0.003
		Ca4:11040108	4	11,040,108	C/T	1.28E-05	4.626
		Ca6:1288709	6	1,288,709	T/G	1.02E-11	7.882
		Ca6:26383440	6	26,383,440	A/C	1.08E-06	3.478
		Ca6:30001391	6	30,001,391	C/T	1.2E-05	5.684
		Ca7:41673233	7	41,673,233	A/C	1.88E-05	6.830
	E3	Ca1:11225828	1	11,225,828	C/T	3.64E-05	7.360
		Ca3:32706215	3	32,706,215	A/C	3.0E-04	4.818
		Ca4:4605340	4	4,605,340	A/C	6.79E-05	6.668
		Ca6:1288709	6	1,288,709	T/G	3.84E-05	5.617
		Ca8:2029341	8	2,029,341	T/G	7.47E-05	5.401
	E4	Ca2:11246842	2	11,246,842	G/A	6.13E-05	0.098
		Ca4:11113277	4	11,113,277	A/C	4.53E-05	1.030
		Ca5:23161492	5	23,161,492	A/T	5.07E-05	0.0490
		Ca5:28886131	5	28,886,131	T/C	6.16E-05	14.511
		Ca7:31317611	7	31,317,611	T/G	1.2E-04	19.740
		Ca8:11631836	8	11,631,836	C/T	3.24E-05	17.184
SY	E2	Ca1:2252356	1	2,252,356	C/T	8.43E-07	13.853
		Ca3:32706215	3	32,706,215	A/C	7.24E-10	4.361
		Ca4:27268301	4	27,268,301	G/A	1.08E-05	18.167
		Ca4:3280217	4	3,280,217	G/A	2.41E-05	4.151
		Ca5:32598221	5	32,598,221	C/A	3.33E-05	12.660
		Ca5:47684292	5	47,684,292	A/G	2.96E-07	7.161
	E4	Ca1:43273961	1	43,273,961	C/T	7.44E-05	11.377
		Ca1:43273962	1	43,273,962	A/G	7.44E-05	11.377
		Ca6:10116403	6	10,116,403	A/T	1.4E-04	28.750
		Ca8:13745335	8	13,745,335	A/G	2.43E-05	0.002
DSI	IARI, New Delhi	Ca1:7500524	1	7,500,524	T/C	9.58E-05	6.915
	Dharwad	Ca8:8904366	8	8,904,366	A/G	7.24E-05	9.816
RWC	E1	Ca3:13202989	3	13,202,989	C/T	4.14E-05	0.197
CTD	E1	Ca4:25809665	4	25,809,665	T/C	9.82E-05	6.066
	E2	Ca5:31164539	5	31,164,539	T/C	7.56E-05	13.406

E1, IARI irrigated; E2, IARI rainfed; E3, Dharwad irrigated; E4, Dharwad rainfed. *R2 Values calculated from the mixed linear model using TASSEL, DFF (days), days to 50% flowering; PH (cm), plant height; NPB, number of primary branches; NPP, number of pods per plants; BY (g/plot), biological yield; HI, Harvest Index; 100SW (g), 100 seed weight; and SY(g/plot), seed yield.

Morphological traits studied under different environments

The significance of the genotypic and environment main effect from analysis of variance implicates the presence of more variability in this germplasm for different traits, and also, the significance of interaction effects reveals the differential response of these genotypes across the environments. A strong correlation with SY and BY in all four environments implies that plant growth and development have a direct impact on seed yield. The strong correlations between seed and biomass in both the irrigated and stress treatments at vegetative and reproductive stages (Sachdeva et al., 2022). The DSI was the best used indices to identify drought-tolerant lines (Fischer and Maurer, 1978), in the earlier investigation, also used the DSI as a selection index to identify drought-tolerant genotypes in chickpeas (Sachdeva et al., 2018).

Genetic diversity of SNPs

Half of SNPs studies have a PIC value of more than 0.25; this indicates sufficient diversity of these markers. The average PIC

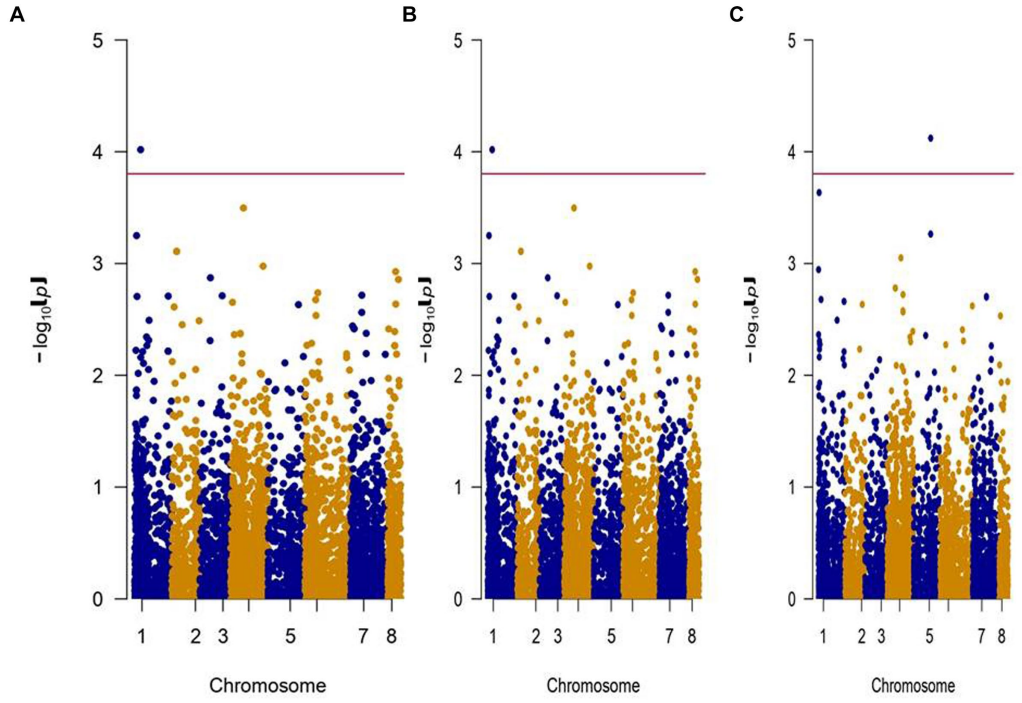

FIGURE 7
Manhattan Plot represents chromosome on the X-axis and −log (p) value on the Y-axis. **(A)** DSI—IARI, New Delhi. **(B)** DSI—Dharwad. **(C)** CTD—IARI, Rainfed (Left to Right).

value of 0.32 was reported for SNP markers, and more than half of the SNP markers showed PIC values higher than 0.25; these SNP markers were used in chickpeas for genome diversity, population structure, and linkage analysis (Farahani et al., 2019). The average genetic distance between the individual was calculated between the genotypes, the average GD between genotypes was 0.32 with more than 81% of genotype pairs having a genetic distance above 0.25, implicating the presence of high genetic variability between the genotypes. The genome-wide LD decay estimated for the present investigation is on par with the previous association studies of chickpeas for complex yield traits (Kujur et al., 2015; Upadhyaya et al., 2016). The greater number of genotypes had a lower kinship value (<0.5) (a lower kinship value indicates diverse genotypes, while a higher kinship value indicates a similar genotype) (Dodds et al., 2015).

Putative candidate genes for drought tolerance

LD decay distance along individual chromosomes was considered to retrieve a flanking sequence of significant MTAs ($p < 1.5E\text{-}04$), selected region searched for the identification of candidate genes including start and stop position, BLAST sequence description, InterPro IDs, Gene ontology terms, and accessions in pulse database. "QTL-hotspot" harboring several drought-tolerant traits has been identified in the biparental mapping population ICCRIL03 (ICC 4958 × ICC 1882) and ICCRIL04 (ICC 283 × ICC 8261) (Varshney et al., 2014). Furthermore, this "QTL-hotspot" region was refined to ~14 cM from the original ~29 cM (Jaganathan et al., 2015); later, it was fine-mapped to ~300 Kb (13,239,546–13,547,009) (Kale et al., 2015); in this study, we do not find any significant MTAs in this QTL-hotspot. Gene present in or near significant MTAs associated with different traits under different environments was found to be encoded for different proteins; based on the available literature, some of the MTAs reported have been known to play a role in drought tolerance mechanisms. The protein probable LRR receptor-like serine/threonine-protein kinase At4g20940 [Guard 211 Cell Hydrogen Peroxide-Resistant1 (GHR1)], found in or near MTA for IARI_DSI and E4_NPP, is reported to be involved in drought tolerance in Arabidopsis by regulating the level of aliphatic glucosinolates (GLSs) by involving in auxin signaling and also stomatal regulation (Salehin et al., 2019); one QTL "QR3dsi02" for DSI explaining 13.00% phenotypic variation was reported in biparental mapping population ICC4958 × ICC 1882 (Jaganathan et al., 2015). The genomic region of MTA for E4_NPP and E4_BY encodes LEA (Late embryonic abundant protein). These proteins contribute toward antioxidant activity, metal ion binding, membrane and protein stabilization, hydration buffering, and DNA and RNA interaction and are known to protect plant metabolism against abiotic stresses (Shao et al., 2005). Genomic region with MTA for E4_100SW encodes WAT1 protein localized, which acts as an auxin transporter and is involved in the auxin homeostasis (Ranocha et al., 2013). MTA for E2_SY encodes with the protein FAR1-RELATED SEQUENCE 7-like and sugar transport protein 10-like. FRS genes like FRS7 and FRS12 and the loss of function could result in early flowering plants with overly elongated hypocotyls mainly in short days in Arabidopsis (Ritter et al., 2017). Two SNPs at different locations are found to be associated with the SY found with the protein sugar transporter. Earlier studies reported that the sugar transporter genes serve as signaling molecules in

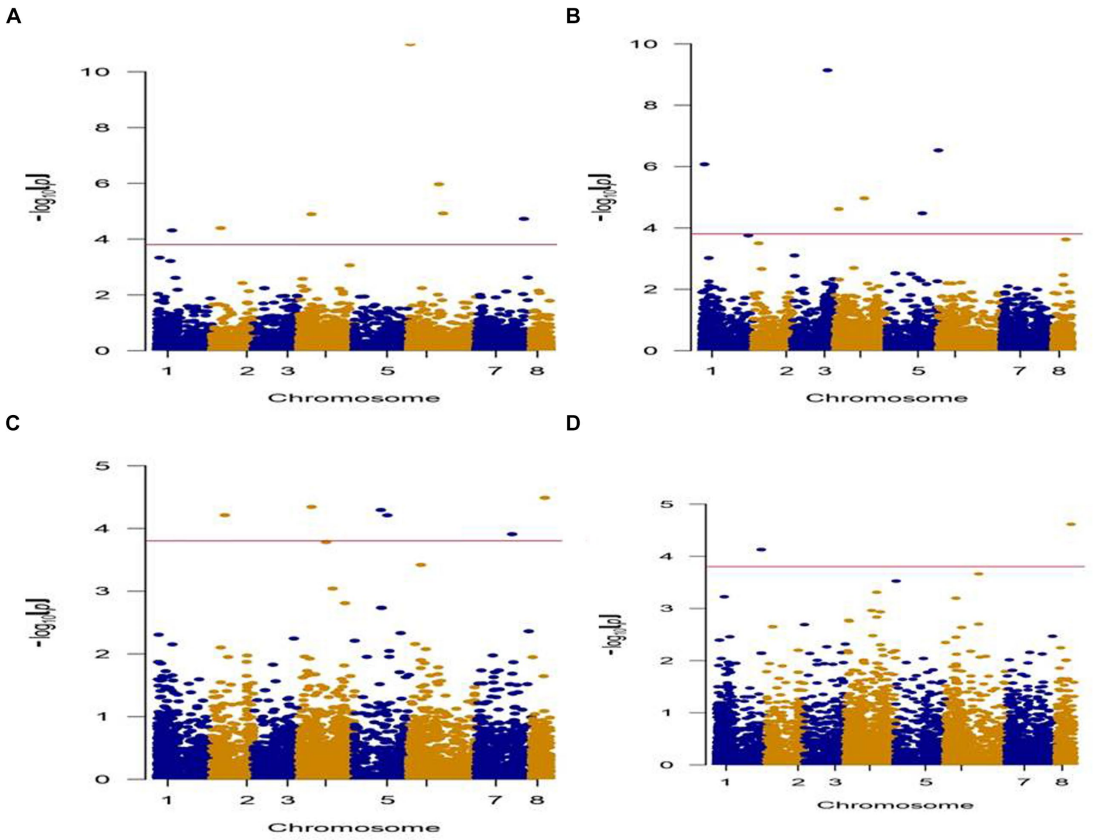

FIGURE 8
Manhattan Plot represents chromosome on the X-axis and −log (p) value on the Y-axis. **(A)** IARI, RF-100SW. **(B)** IARI, RF-SY. **(C)** Dharwad, RF-100SW. **(D)** Dharwad, RF-SY.

Arabidopsis (Wobus and Weber, 1999). In Arabidopsis, the sugar transporter gene induces subcellular modification, cellular signal alteration, enhanced biomass of Arabidopsis seeds, and early plant development (Wingenter et al., 2010). Investigation of drought tolerance in chickpeas using GWAS and genomic selection reported a significant association of SNPs in several auxin-related genes and sugar transporters with yield and yield-related traits under drought-prone environments (Li et al., 2018). MTA for E2_100SW encodes β-galactosidase protein that plays a major role in water stress. During senescence, the increase in the activity of β-galactosidase and loss of photosynthesis was observed in the leaves of Arabidopsis. In the background of loss of photosynthesis, this protein was found to be involved in the production of sugars that could serve for the execution of energy-dependent senescence (Pandey et al., 2017). The MTA for E4_100SW colocalized with the gene encodes putative proline-rich protein APG isolog and GDSL esterase/lipase APG. Some of the PRP genes such as the proline-rich protein-encoding gene (CcHyPRP) isolated from pigeon peas (*Cajanus cajan*) could be induced by various stresses (Priyanka et al., 2010). SNP marker-associated plant height under the rainfed condition located near GDSL esterases and lipases (GELPs) was reported in a study of GWAS for drought tolerance in multiple environments (Istanbuli et al., 2024). The overexpression of the GDSL-type pepper lipase gene in Arabidopsis during seed germination and plant growth showed drought tolerance and differential expression of drought- and abscisic acid (ABA)-inducible genes (Hong et al., 2008). MTA that encodes E3 ubiquitin-protein ligase AIRP2-like, AtAIRP2 in Arabidopsis, reported to play ABA-mediated drought stress responses (Cho et al., 2011). SNP associated with 100 seed weight encodes gene LRR receptor-like kinase family protein, and SNP associated with plant height encodes for E3 ubiquitin-protein ligase RNF185-like was reported in a study of high-resolution mapping of drought tolerance in chickpea using MAGIC population (Thudi et al., 2024). The MTA encoding to UDP-glycosyltransferases was found to be associated with E2_BY. Some of the UDP-glycosyltransferases, such as UGT79B2 and UGT79B3, contribute to cold, salt, and drought stress tolerance via modulating anthocyanin accumulation (Li et al., 2017). The protein U-box domain-containing protein 44, localized with the SNP associated with E2_CTD, has been reported to prevent premature senescence in Arabidopsis plants (Raab et al., 2009).

The present study demonstrates that several MTAs identified for different traits including yield, physiological, and drought indices recorded across locations, seasons, and different stress conditions. Identified genomic region colocalized with these MTAs encodes for proteins that are known for drought tolerance. However, to validate their functionality, further investigation via gene expression analysis or gene knock-out studies is imperative. Moreover, enhancing the scope of research by including large accessions and encompassing more locations and seasons could be considered to improve these findings. Once validated, these insights serve as good candidates for

climate-resilient breeding for the improvement of drought tolerance in chickpeas.

Data availability statement

The original contributions presented in the study are included in the article/Supplementary material, further inquiries can be directed to the corresponding authors.

Author contributions

DH: Data curation, Investigation, Methodology, Software, Validation, Writing – original draft. SPP: Investigation, Methodology, Writing – original draft. NK: Data curation, Formal analysis, Investigation, Methodology, Software, Validation, Writing – review & editing. CB: Conceptualization, Funding acquisition, Investigation, Methodology, Project administration, Resources, Supervision, Visualization, Writing – review & editing. TK: Data curation, Investigation, Methodology, Writing – review & editing. SP: Data curation, Methodology, Software, Writing – review & editing. BP: Formal analysis, Investigation, Methodology, Writing – review & editing. SK: Data curation, Investigation, Methodology, Writing – review & editing. PJ: Conceptualization, Data curation, Validation, Writing – review & editing. YK: Investigation, Methodology, Writing – review & editing. RV: Funding acquisition, Methodology, Resources, Supervision, Validation, Writing – review & editing.

Funding

The author(s) declare that financial support was received for the research, authorship, and/or publication of this article. DH received his funding for a doctoral fellowship from ICAR-IARI, whereas the experiment was partly supported by the funds of ICAR-IARI, CRP (12-143D) Molecular Breeding (Chickpea), DBT (24-752) and DBT AISRF (24-557) Programme.

Acknowledgments

DH acknowledges the funding support from the ICAR-IARI for his doctoral fellowship. All the authors acknowledge the funding from ICAR-CRP and DBT AISRF.

Conflict of interest

The authors declare that the research was conducted in the absence of any commercial or financial relationships that could be construed as a potential conflict of interest.

The reviewer AK declared a shared parent affiliation with the authors to the handling editor at the time of review.

Publisher's note

Supplementary material

The Supplementary material for this article can be found online at: https://www.frontiersin.org/articles/10.3389/fsufs.2024.1389970/full#supplementary-material

References

Ahmad, F., Gaur, P. M., and Croser, J. (2005) in *Chickpea (Cicer arietinum L.) in genetic resources, chromosome engineering, and crop improvement—Grain legumes*. eds. R. J. Singh and P. P. Jauhar (Boca Raton, FL: CRC Press), 187–217.

Bar-El Dadon, S., Abbo, S., and Reifen, R. (2017). Leveraging traditional crops for better nutrition and health - the case of chickpea. *Trends Food Sci. Technol.* 64, 39–47. doi: 10.1016/j.tifs.2017.04.002

Barrs, H. D., and Weatherley, P. E. (1962). A re-examination of the relative turgidity technique for estimating water deficits in leaves. *Aust. J. Biol. Sci.* 15, 413–428. doi: 10.1071/BI9620413

Bharadwaj, C., Chauhan, S., Yadav, S., Tara, T., Singh, R., Kumar, J., et al. (2011a). Molecular marker-based linkage map of chickpea (*Cicer arietinum*) developed from desi × kabuli cross. *Indian J. Agric. Sci.* 80, 947–951.

Bharadwaj, C., Srivastava, R., Chauhan, S. K., Satyavathi, C. T., Kumar, J., Faruqui, A., et al. (2011b). Molecular diversity and phylogeny in geographical collection of chickpea (*Cicer* sp.) accessions. *J. Genet.* 92, 94–100. doi: 10.1007/s12041-011-0114-6

Bharadwaj, C., Tripathi, S., Soren, K. R., Thudi, M., Singh, R., Sheoran, S., et al. (2021). Introgression of "QTL-hotspot" region enhances drought tolerance and grain yield in three elite chickpea cultivars. *Plant Genome* 14:e20076. doi: 10.1002/tpg2.20076

Blum, A., and Ebercon, A. (1981). Cell membrane stability as a measure of drought and heat tolerance in wheat. *Crop Sci.* 21, 43–47. doi: 10.2135/cropsci1981.0011183X002100010013x

Bradbury, P. J., Zhang, Z., Kroon, D. E., Casstevens, T. M., Ramdoss, Y., and Buckler, E. S. (2007). TASSEL: software for association mapping of complex traits in diverse samples. *Bioinformatics* 23, 2633–2635. doi: 10.1093/bioinformatics/btm308

Cho, S. K., Ryu, M. Y., Seo, D. H., Kang, B. G., and Kim, W. T. (2011). The Arabidopsis RING E3 ubiquitin ligase AtAIRP2 plays combinatory roles with AtAIRP1 in abscisic acid-mediated drought stress responses. *Plant Physiol.* 157, 2240–2257. doi: 10.1104/pp.111.185595

Cramer, G. R., Urano, K., Delrot, S., Pezzotti, M., and Shinozaki, K. (2011). Effects of abiotic stress on plants: a systems biology perspective. *BMC Plant Biol.* 11, 163–176. doi: 10.1186/1471-2229-11-163

Daryanto, S., Wang, L., and Jacinthe, P. A. (2015). Global synthesis of drought effects on food legume production. *PLoS One* 10:e0127401. doi: 10.1371/journal.pone.0127401

David, L. R., Jeffry, M. T., Yoshihiro, M., Larissa, M. W., Sherry, R. W., John, D., et al. (2001). Structure of linkage disequilibrium and phenotypic associations in the maize genome. *Proc. Natl. Acad. Sci.* 98, 11479–11484. doi: 10.1073/pnas.201394398

Dixit, G. P., Srivastava, A. K., and Singh, N. P. (2019). Marching towards self-sufficiency in chickpea. *Curr. Sci.* 116, 239–242. doi: 10.18520/cs/v116/i2/239-242

Dodds, K. G., McEwan, J. C., Brauning, R., Anderson, R. A., Van Stijn, T. C., Kristjánsson, T., et al. (2015). Construction of relatedness matrices using genotyping-by-sequencing data. *BMC Genomics* 16:1047. doi: 10.1186/s12864-015-2252-3

Earl, D. A., and vonHoldt, B. (2012). Structure harvester: a website and program for visualizing structure output and implementing the Evanno method. *Cons. Genet. Res.* 4, 359–361. doi: 10.1007/s12686-011-9548-7

Evanno, G., Regnaut, S., and Goudet, J. (2005). Detecting the number of clusters of individuals using the software structure: a simulation study. *Mol. Ecol.* 14, 2611–2620. doi: 10.1111/j.1365-294x.2005.02553.x

FAOSATAT (2021). *Crops and livestock products*. Available at: http://www.fao.org/faostat/en/#data/QCL

Farahani, S., Maleki, M., Mehrabi, R., Kanouni, H., Scheben, A., Batley, J., et al. (2019). Whole genome diversity, population structure, and linkage disequilibrium analysis of chickpea (*Cicer arietinum* L.) genotypes using genome-wide DArTseq-based SNP markers. *Genes* 10:676. doi: 10.3390/genes10090676

Fischer, K. S., and Maurer, R. (1978). Drought resistance in spring wheat cultivars. I. Grain yield responses. *Aust. J. Agric. Res.* 29, 897–912. doi: 10.1071/AR9780897

Gahlaut, V., Jaiswal, V., Balyan, H. S., Joshi, A. K., and Gupta, P. K. (2021). Multi-locus GWAS for grain weight-related traits under rain-fed conditions in common wheat (*Triticum aestivum* L.). *Front. Plant Sci.* 12:758631. doi: 10.3389/fpls.2021.758631

Gupta, S., Nawaz, K., Parween, S., Roy, R., Sahu, K., Pole, A. K., et al. (2017). Draft genome sequence of *Cicer reticulatum* L., the wild progenitor of chickpea provides a resource for agronomic trait improvement. *DNA Res.* 24, 1–10. doi: 10.1093/dnares/dsw042

Hill, W. G., and Weir, B. S. (1988). Variances and covariance of squared linkaged is equilibria in finite populations. *Theor. Popul. Biol.* 33, 54–78. doi: 10.1016/0040-5809(88)90004-4

Hong, J. K., Choi, H. W., Hwang, I. S., Kim, D. S., Kim, N. H., Choi, D. S., et al. (2008). Function of a novel GDSL-type pepper lipase gene, CaGLIP1, in disease susceptibility and abiotic stress tolerance. *Planta* 227, 539–558. doi: 10.1007/s00425-007-0637-5

Istanbuli, T., Nassar, A. E., Abd El-Maksoud, M. M., Tawkaz, S., Alsamman, A. M., and Hamwieh, A. (2024). Genome-wide association study reveals SNP markers controlling drought tolerance and related agronomic traits in chickpea across multiple environments. *Front. Plant Sci.* 15:1260690. doi: 10.3389/fpls.2024.1260690

Jaganathan, D., Thudi, M., Kale, S., Azam, S., Roorkiwal, M., Gaur, P. M., et al. (2015). Genotyping-by-sequencing based intra-specific genetic map refines a "QTL-hotspot" region for drought tolerance in chickpea. *Mol. Gen. Genomics.* 290, 559–571. doi: 10.1007/s00438-014-0932-3

Jain, M., Misra, G., Patel, R. K., Priya, P., Jhanwar, S., Khan, A. W., et al. (2013). A draft genome sequence of the pulse crop chickpea (*Cicer arietinum* L.). *Plant J.* 74, 715–729. doi: 10.1111/tpj.12173

Kale, S., Jaganathan, D., Ruperao, P., Chen, C., Punna, R., Kudapa, H., et al. (2015). Prioritization of candidate genes in "*QTL-hotspot*" region for drought tolerance in chickpea (*Cicer arietinum* L.). *Sci. Rep.* 5:15296. doi: 10.1038/srep15296

Kashiwagi, J., Krishnamurthy, L., Gaur, P. M., Upadhyaya, H. D., Varshney, R. K., and Tobita, S. (2013). Traits of relevance to improve yield under terminal drought stress in chickpea (*C. arietinum* L.). *Field Crop Res.* 145, 88–95. doi: 10.1016/j.fcr.2013.02.011

Kohli, P. S., Kumar Verma, P., Verma, R., Parida, S. K., Thakur, J. K., and Giri, J. (2020). Genome wide association study for phosphate deficiency responsive root hair elongation in chickpea. *Funct. Integr. Genomics* 20, 775–786. doi: 10.1007/s10142-020-00749-6

Krishnamurthy, L., Kashiwagi, J., Upadhyaya, H. D., Gowda, C. L. L., Gaur, P. M., Singh, S., et al. (2013). Partitioning coefficient – a trait that contributes to drought tolerance in chickpea. *Field Crop Res.* 149, 354–365. doi: 10.1016/j.fcr.2013.05.022

Kujur, A., Bajaj, D., Upadhyaya, H. D., Das, S., Ranjan, R., Shree, T., et al. (2015). A genome-wide SNP scan accelerates trait-regulatory genomic loci identification in chickpea. *Sci. Rep.* 5:11166. doi: 10.1038/srep11166

Li, P., Li, Y. J., Zhang, F. J., Zhang, G. Z., Jiang, X. Y., Yu, H. M., et al. (2017). The Arabidopsis UDP-glycosyltransferases UGT79B2 and UGT79B3, contribute to cold, salt and drought stress tolerance via modulating anthocyanin accumulation. *Plant J.* 89, 85–103. doi: 10.1111/tpj.13324

Li, Y., Ruperao, P., Batley, J., Edwards, D., Khan, T., Colmer, T. D., et al. (2018). Investigating drought tolerance in chickpea using genome-wide association mapping and genomic selection based on whole-genome resequencing data. *Front. Plant Sci.* 9:190. doi: 10.3389/fpls.2018.00190

Liu, X., Huang, M., Fan, B., Buckler, E. S., and Zhang, Z. (2016). Iterative usage of fixed and random effect models for powerful and efficient genome-wide association studies. *PLoS Genet.* 12, 1–24. doi: 10.1371/journal.pgen.1005767

Liu, K., and Muse, S. V. (2005). PowerMarker: an integrated analysis environment for genetic marker analysis. *Bioinformatics* 21, 2128–2129. doi: 10.1093/bioinformatics/bti282

Muehlbauer, F. J., and Sarker, A. (2017). *Economic importance of chickpea: production, value, and world trade in the chickpea genome*. Cham: Springer, 5–12.

Olivoto, T., and Lucio, A. D. (2020). Metan: an R package for multi-environment trial analysis. *Methods Ecol. Evol.* 11, 783–789. doi: 10.1111/2041-210X.13384

Pandey, J. K., Dash, S. K., and Biswal, B. (2017). Loss in photosynthesis during senescence is accompanied by an increase in the activity of β-galactosidase in leaves of *Arabidopsis thaliana*: modulation of the enzyme activity by water stress. *Protoplasma* 254, 1651–1659. doi: 10.1007/s00709-016-1061-0

Parween, S., Nawaz, K., Roy, R., Pole, A. K., Suresh, B. V., Misra, G., et al. (2015). An advanced draft genome assembly of a desi type chickpea (*Cicer arietinum* L.). *Sci. Rep.* 5:12806. doi: 10.1038/srep12806

Pritchard, J. K., Stephens, M., and Donnelly, P. (2000). Inference of population structure using multilocus genotype data. *Genetics* 155, 945–959. doi: 10.1093/genetics/155.2.945

Priyanka, B., Sekhar, K., Reddy, V. D., and Rao, K. V. (2010). Expression of pigeonpea hybrid-441 proline-rich protein encoding gene (CcHyPRP) in yeast and Arabidopsis affords multiple abiotic stress 442 tolerance. *Plant Biotechnol. J.* 8, 76–87. doi: 10.1111/j.1467-7652.2009.00467.x

Raab, S., Drechsel, G., Zarepour, M., Hartung, W., Koshiba, T., Bittner, F., et al. (2009). Identification of a novel E3 ubiquitin ligase that is required for suppression of premature senescence in Arabidopsis. *Plant J.* 59, 39–51. doi: 10.1111/j.1365-313X.2009.03846.x

Ranocha, P., Dima, O., Nagy, R., Felten, J., Corratgé-Faillie, C., Novák, O., et al. (2013). Arabidopsis WAT1 is a vacuolar auxin transport facilitator required for auxin homoeostasis. *Nat. Commun.* 4:2625. doi: 10.1038/ncomms3625

Ritter, A., Inigo, S., Fernandez-Calvo, P., Heyndrickx, K. S., Dhondt, S., Shi, H., et al. (2017). The transcriptional repressor complex FRS7-FRS12 regulates flowering time and growth in *Arabidopsis*. *Nat. Commun.* 8:15235. doi: 10.1038/ncomms15235

Roorkiwal, M., Bharadwaj, C., Barmukh, R., Dixit, G. P., Gaur, P. M., Chaturvedi, S. K., et al. (2020). Integrating genomics for chickpea improvement: achievements and opportunities. *Theor. Appl. Genet.* 133, 1703–1720. doi: 10.1007/s00122-020-03584-2

Sachdeva, S., Bharadwaj, C., Patil, B. S., Pal, M., Roorkiwal, M., and Varshney, R. K. (2022). Agronomic performance of chickpea affected by drought stress at different growth stages. *Agronomy* 12:995. doi: 10.3390/agronomy12050995

Sachdeva, S., Bharadwaj, C., Sharma, V., Patil, B. S., Soren, K. R., Roorkiwal, M., et al. (2018). Molecular and phenotypic diversity among chickpea (*Cicer arietinum*) genotypes as a function of drought tolerance. *Crop Pasture Sci.* 69, 142–153. doi: 10.1071/CP17284

Salehin, M., Li, B., Tang, M., Katz, E., Song, L., Ecker, J. R., et al. (2019). Auxin-sensitive aux/IAA proteins mediate drought tolerance in Arabidopsis by regulating glucosinolate levels. *Nat. Commun.* 10:4021. doi: 10.1038/s41467-019-12002-1

Schneider, S. H., Semenov, S., Patwardhan, A., Burton, I., Magadza, C. H. D., Oppenheimer, M., et al. (2007). "Assessing key vulnerabilities and the risk from climate change. climate change 2007: impacts, adaptation and vulnerability" in *Contribution of Working Group II to the Fourth Assessment Report of the Intergovernmental Panel on Climate Change*. eds. M. L. Parry, O. F. Canziani, J. P. Palutikof, P. J. van der Linden and C. E. Hanson (UK: Cambridge University Press, Cambridge), 779–810.

Shao, H. B., Liang, Z. S., and Shao, M. A. (2005). LEA proteins in higher plants: structure, function, gene expression and regulation. *Colloids Surf. B* 45, 131–135. doi: 10.1016/j.colsurfb.2005.07.017

Thudi, M., Gaur, P. M., Krishnamurthy, L., Mir, R. R., Kudapa, H., Fikre, A., et al. (2014). Genomics-assisted breeding for drought tolerance in chickpea. *Funct. Plant Biol.* 41, 1178–1190. doi: 10.1071/FP13318

Thudi, M., Samineni, S., Li, W., Boer, M. P., Roorkiwal, M., Yang, Z., et al. (2024). Whole genome resequencing and phenotyping of MAGIC population for high resolution mapping of drought tolerance in chickpea. *Plant Genome* 17:e20333. doi: 10.1002/tpg2.20333

Turner, S. (2018). Qqman: an R package for visualizing GWAS results using Q-Q and Manhattan plots. *J. Open Source Soft.* 3:731. doi: 10.21105/joss.00731

Upadhyaya, H. D., Bajaj, D., Narnoliya, L., Das, S., Kumar, V., Gowda, C. L., et al. (2016). Genome-wide scans for delineation of candidate genes regulating seed-protein content in chickpea. *Front. Plant Sci.* 7:302. doi: 10.3389/fpls.2016.00302

Varshney, R. K., Graner, A., and Sorrells, M. E. (2005). Genomics-assisted breeding for crop improvement. *Trends Plant Sci.* 10, 621–630. doi: 10.1016/j.tplants.2005.10.004

Varshney, R. K., Hoisington, D. A., Upadhyaya, H. D., Gaur, P. M., Nigam, S. N., Saxena, K., et al. (2007). "Molecular genetics and breeding of grain legume crops for the semi-arid tropics" in *Genomics-assisted crop improvement. Vol II. Genomics applications in crops*. eds. R. K. Varshney and R. Tuberosa (The Netherlands: Springer), 207–242.

Varshney, R. K., Pandey, M. K., Bohra, A., Singh, V. K., Thudi, M., and Saxena, R. K. (2019). Toward the sequence-based breeding in legumes in the post-genome sequencing era. *Theor. Appl. Genet.* 132, 797–816. doi: 10.1007/s00122-018-3252-x

Varshney, R. K., Song, C., Saxena, R. K., Azam, S., Yu, S., Sharpe, A. G., et al. (2013). Draft genome sequence of chickpea (*Cicer arietinum*) provides a resource for trait improvement. *Nat. Biotechnol.* 31, 240–246. doi: 10.1038/nbt.2491

Varshney, R. K., Thudi, M., Nayak, S. N., Gaur, P. M., Kashiwagi, J., Krishnamurthy, L., et al. (2014). Genetic dissection of drought tolerance in chickpea (*Cicer arietinum* L.). *Theor. Appl. Genet.* 127, 445–462. doi: 10.1007/s00122-013-2230-6

Wang, J., and Zhang, Z. (2021). GAPIT version 3: boosting power and accuracy for genomic association and prediction. *Genom. Proteom. Bioinform.* 19, 629–640. doi: 10.1016/j.gpb.2021.08.005

Wingenter, K., Schulz, A., Wormit, A., Wic, S., Trentmann, O., Hoermiller, I. I., et al. (2010). Increased activity of the vacuolar monosaccharide transporter TMT1 alters cellular sugar partitioning, sugar signaling, and seed yield in Arabidopsis. *Plant Physiol.* 154, 665–677. doi: 10.1104/pp.110.162040

Wobus, U., and Weber, H. (1999). Sugars as signal molecules in plant seed development. *Biol. Chem.* 380, 937–944. doi: 10.1515/bc.1999.116

frontiers | Frontiers in Sustainable Food Systems

TYPE Original Research
PUBLISHED 07 August 2024
DOI 10.3389/fsufs.2024.1418554

OPEN ACCESS

EDITED BY
Kamal Krishna Pal,
Directorate of Groundnut Research (ICAR-DGR), India

REVIEWED BY
Marco E. Mng'ong'o,
Mbeya University of Science and Technology, Tanzania
Satya Sundar Bhattacharya,
Tezpur University, India
Fırat Baran,
Batman University, Türkiye

*CORRESPONDENCE
Anas Iqbal
✉ anasiqbal@scau.edu.cn
Xiangru Tang
✉ tangxr@scau.edu.cn

RECEIVED 16 April 2024
ACCEPTED 24 July 2024
PUBLISHED 07 August 2024

CITATION
Iqbal A, Khan R, Hussain Q, Imran M, Mo Z, Hua T, Adnan M, Abid I, Rizwana H, Soliman Elshikh M, El Sabagh A, Lal R and Tang X (2024) Vermicompost application enhances soil health and plant physiological and antioxidant defense to conferring heavy metals tolerance in fragrant rice.
Front. Sustain. Food Syst. 8:1418554.
doi: 10.3389/fsufs.2024.1418554

Vermicompost application enhances soil health and plant physiological and antioxidant defense to conferring heavy metals tolerance in fragrant rice

Anas Iqbal[1,2]*, Rayyan Khan[3], Quaid Hussain[4], Muhammad Imran[1], Zhaowen Mo[1], Tian Hua[1], Muhammad Adnan[2], Islem Abid[5], Humaira Rizwana[6], Mohamed Soliman Elshikh[6], Ayman El Sabagh[7], Rattan Lal[8] and Xiangru Tang[1]*

[1]State Key Laboratory for Conservation and Utilization of Subtropical Agro-Bioresources, College of Agriculture, South China Agricultural University, Guangzhou, China, [2]Department of Agriculture, The University of Swabi, Swabi, Pakistan, [3]Key Laboratory of Crop Cultivation and Physiology, College of Agriculture, Guangxi University, Nanning, China, [4]College of Life Sciences and Oceanography, Shenzhen University, Shenzhen, China, [5]Centre of Excellence in Biotechnology Research, King Saud University, Riyadh, Saudi Arabia, [6]Department of Botany and Microbiology, College of Science, King Saud University, Riyadh, Saudi Arabia, [7]Department of Agronomy, Faculty of Agriculture, Kafrelsheikh University, Kafrelsheikh, Egypt, [8]CFAES Rattan Lal Center for Carbon Management and Sequestration, The Ohio State University, Columbus, OH, United States

Cadmium (Cd) contamination in agricultural soils and its accumulation in plant organs have become a global issue due to its harmful effects on human health. The *in-situ* stabilizing technique, which involves using organic amendments, is commonly employed for removing Cd from agricultural soils. Thus, the current study investigated the effect of vermicompost (VC) on soil properties and plant physio-biochemical attributes, leaf ultrastructure analysis, antioxidant defense mechanisms, and grain yields of two different fragrant rice cultivars, Xiangyaxiangzhan (XGZ) and Meixiangzhan-2 (MXZ-2), under Cd-stress conditions. The results showed that Cd toxicity deteriorates soil quality, the plant's photosynthetic apparatus, and the plant's antioxidant defense mechanism. Moreover, under Cd stress, both cultivars produced significantly lower ($p < 0.05$) rice grain yields compared to non-Cd stress conditions. However, the VC application alleviated the Cd toxicity and improved soil qualitative traits, such as soil organic carbon, available nitrogen, total nitrogen, phosphorus, and potassium. Similarly, VC amendments improved leaf physiological activity, photosynthetic apparatus function, antioxidant enzyme activities and its related gene expression under Cd stress These enhancements led to increased grain yields of both fragrant under Cd toxicity. The addition of VC mitigated the adverse effects of Cd on the leaf chloroplast structure by reducing Cd uptake and accumulation in tissues. This helped prevent Cd-induced peroxidation damage to leaf membrane lipids by increasing the activities of antioxidant enzymes such as ascorbate peroxidase (APX), catalase (CAT), peroxidase (POD), and superoxide dismutase (SOD). On average across the growth stages, the Pos-Cd + VC3 treatment increased SOD, APX, CAT, and POD activities by122.2 and 112.5%, 118.6, and 120.6%, 44.6 and 40.6%, and 38.6 and 33.2% in MXZ-2 and XGZ, respectively, compared to the plants treated with Pos-Cd treated alone. Enhancements in leaf physiological activity and plant antioxidant enzyme activity strengthen the plant's antioxidant defense mechanism against Cd toxicity. In

addition, correlation analysis showed a strong relationship between the leaf net photosynthetic rate and soil chemical attributes, suggesting that improved soil fertility enhances leaf physiological activity and boosts rice grain yields. Of the treatments, Pos-Cd + VC3 proved to be the most effective treatment in terms of enhancing soil health and achieving high fragrant rice yields. Thus, the outcomes of this study show that the addition of VC in Cd-contaminated soils could be useful for sustainable rice production and safe utilization of Cd-polluted soil.

KEYWORDS

antioxidant-encoding genes, cadmium toxicity, fragrant rice, leaf physiological activity, soil fertility, vermicompost

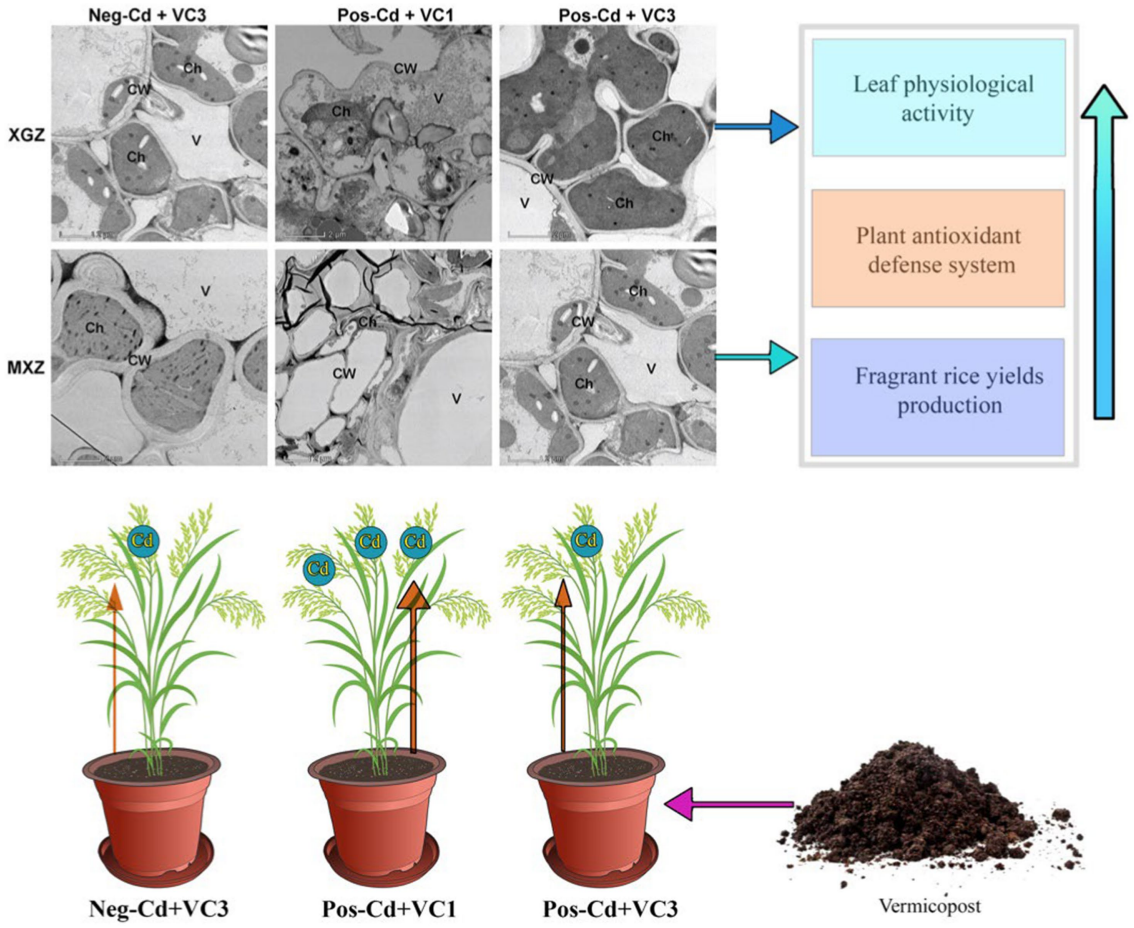

GRAPHICAL ABSTRACT

1 Introduction

Heavy metals, especially Cd, pose significant hazards due to their high toxicity and propensity for substantial uptake and accumulation in cereal grains (Singh et al., 2020). The Cd accumulation in arable soil is caused by industrial processes such as waste discharge, fertilization, mining, and smelting (Islam et al., 2017; Tang et al., 2019; Seleiman et al., 2020). Cd is more soluble and mobile than other metals, making it easily absorbed by plants, translocated within them, and deposited in various plant parts (Chen Q. et al., 2018; Chen Y. et al., 2018; Adil et al., 2020). Furthermore, Cd is commonly non-recyclable and difficult to remove from the soil, and it can migrate to cereal grains via the soil–plant-food cycle, thereby posing health hazards to humans (Rizwan et al., 2016; Seleiman et al., 2020). The Cd inputs and availability in soil adversely affect soil microbial biodiversity and its associated ecosystem function (Xue et al., 2017; Haider et al., 2021; Iqbal et al., 2024a). Cadmium garnered a lot of attention in arable soil because of its toxicity, availability, and persistence in living organisms (Rizwan et al., 2016; Huang et al., 2019).

Additionally, high Cd levels in arable fields may affect soil health, physiochemical characteristics, and plant metabolism, resulting in lower crop growth and reduced productivity (Mitra et al., 2018; Iqbal et al., 2023a). Cd also inhibits plant photosynthesis and reduces plant uptake of essential mineral nutrients, resulting in a decrease in agricultural output (Tran and Popova, 2013; Chen Q. et al., 2018; Chen Y. et al., 2018). In addition, Cd toxicity in plants can produce physiological, biochemical, and physical changes, including reduction in root growth, stomatal density, and chlorosis (Bari et al., 2019; Huybrechts et al., 2020). The plant photosynthetic apparatus is often more vulnerable to Cd-induced damage. Plant chlorophyll is essential for photosynthesis, and any decrease in plant chlorophyll production due to Cd toxicity declines the photosynthesis process (Li et al., 2010; Parmar et al., 2013). Cd stress affects mitochondrial function in plants by affecting redox control and promoting the generation of additional reactive oxygen species (ROS), that damage membrane lipids and alter overall metabolic activity (Chen Q. et al., 2018; Chen Y. et al., 2018; Huybrechts et al., 2020). The ROS generated under stress is responsible for cellular oxidative injury and genotoxicity (Gallego et al., 2012; Khan et al., 2022). As a result, Cd, one of the most harmful contaminants, demands special attention to regulate its mobility in arable soils.

Rice is an important cereal crop for about 3.5 billion people worldwide (Dabral et al., 2019). Rice is a key ingredient and staple diet for Chinese people (Chauhan et al., 2017). The majority of Cd in the food channel could come from agricultural products, and Cd in soil plants accumulates up by roots and finally enters the food, posing health concerns to the human immunological, neurological, and reproductive organs (Parmar et al., 2013; Adil et al., 2020). *In situ* stabilization technique, using organic additions such as cattle fertilizer, biochar, and compost, is an environmentally friendly approach to preventing Cd (Hamid et al., 2020; Ullah et al., 2020; Yuan et al., 2022; Ali et al., 2022a,b,c; Iqbal et al., 2024b). However, these techniques are ineffective and problematic because of the accompanying costs and additional pollutants (Shaheen and Rinklebe, 2015; Pramanik et al., 2018). In addition, according to Igalavithana et al. (2017) the use of these organic fertilizers alone might enhance the risk of arsenic pollution; for instance, applying wood bark organic biochar increases exchangeable arsenic in soil by 84.5%.

Vermicompost (VC), is the product of the decomposition process using species of worms, usually white worms, red wigglers, and other earthworms to create a mixture of decomposing vegetables, food waste and vermicas (Charan et al., 2024). The VC, a nutrient-rich fertilizer, is turning more common for heavy metal-contaminated arable soil rehabilitation (Wang et al., 2018; Zhang et al., 2020). Alam et al. (2020) found that VC is more beneficial and effective than wasted mushroom and organic fertilizer for reducing Cd and other metals accumulation and uptake in plants. Earthworms can accumulate various heavy metals such as Cd, Pb, Hg, and Zn, and store it in benign forms in the chloragogenous tissues (Song et al., 2015). The peak absorption rate of 170.65 mg/g of Cd^{2+} on VC indicates that VC is a possible *in situ* sorbent for Cd-polluted soil (Zhu et al., 2017). Moreover, VC treatment may affect soil physical and biochemical parameters and alter the chemical composition of Cd in soils, reducing Cd bioavailability in soils by adsorption, immobilization, and precipitation (Bradham et al., 2018; Cambier et al., 2019). After soil application, VC provides polysaccharides, the release of mucus from earthworms and microorganisms, and improves soil physical structure, i.e., aeration, porosity, aggregate stability, and drainage, all of which are beneficial to crop root growth, as well as nutrient uptake by plants (Lim et al., 2015; Hussain et al., 2021). VC is a rich source of plant micronutrients and macronutrients, hence adding VC improved the mineral elements in soils, resulting in increased plant growth and production (Maji et al., 2017; Dubey et al., 2020; Goswami et al., 2024). However, limited studies have evaluated VC's effects on paddy soil properties, fragrant rice Cd uptake, plant physiological and antioxidant defense function, and rice production under Cd toxicity.

Given previous consideration, this research investigated the application of VC as a soil conditioner, which is a potential remediation technique in Cd-polluted fields. We used aromatic rice cultivars MXZ-2 and XGZ, which are popular in southern China due to their pleasant flavor (Luo H. et al., 2020; Luo Y. et al., 2020; Zhang et al., 2022). Rice, a semi-aquatic tropical plant grown on marshy lands, is very susceptible to Cd uptake and accumulation in organs (Wu et al., 2014). The presence of Cd in arable soil is common, particularly in China, it can be absorbed by rice plants. This metal accumulates in the grains, posing a significant threat to both the quality and nutritional value of rice. This contamination adversely affects human health and crop production (Zeng et al., 2019; Adil et al., 2024). High concentrations of Cd in rice grains not only alter their taste and texture but also diminish their nutritional content (Bin Rahman and Zhang, 2023). Consumption of Cd-contaminated rice grains can lead to health issues such as kidney damage, skeletal abnormalities, and potentially cancer (Song et al., 2015). Therefore, addressing Cd toxicity in rice cultivation is crucial for ensuring the food safety and nutritional security of communities globally. In this study, we applied VC as a composite material in Cd-contaminated soil to counteract the negative impacts of Cd on soil fertility, plant physiological and biochemical attributes, and grain yield. To the best of our knowledge, there is a lake of knowledge regarding the measured variables in this study in the context of soil and fragrant rice crops relative to different VC amendments under Cd toxicity conditions. The main objectives of the study were: (1) to investigate the impacts of VC on soil environmental parameters and soil fertility (2) to assess the role of VC in plant physiology, especially its impact on photosynthetic performance and leaf ultrastructure (i.e., chloroplast, cell wall, and vacuole), and biochemical attributes (3) to explore the effect of VC application on fragrant-rice yield and the role of soil fertility in plant physiological and biochemical activity. The present work hypothesized that applying VC can improve soil health which in turn increases plant physiological activity and antioxidant defense systems under Cd toxicity. This work will produce a conceptual framework for safe and sustainable crop production in Cd-contaminated soils.

2 Materials and methods

2.1 Experimental place and basic soil qualities

A pot study was carried out at the South China Agriculture University Research Station. The soil of the experimental site (0–15 cm) is slightly acidic, with a pH of 5.88. Furthermore, the soil has 23.75 g kg^{-1} organic matter, 1.18 g kg^{-1} TN, 145.40 mg kg^{-1} available

N, and 0.98 g kg^{-1} phosphorus. Supplementary Table S1 also includes details about the soil's qualities.

2.2 Experimental details

In the present research, we used two different fragrant rice varieties, MXZ-2 and XGZ, which respond differently to Cd-stress conditions (Imran et al., 2020). Both cultivars were obtained from the College of Agriculture, South China Agriculture University. The experiment was conducted in complete block design in the early season of 2023 (March–July). The soil was obtained to a depth of 15 cm from the paddy field and then placed into plastic pots. Further, it was ensured that all pots contained the same size and weight of soil to minimize experimental error. The recommended dose of VC was applied 1 week ago from seedling transplantation. The applied VC was manufactured by Hubei Tianhenjia Biological Environmental Protection Technology Co., Ltd., Wuxue City, Hubei Province, China; it consisted of 34.90% organic matter, 1.48% TN, 2.76% P_2O_2, and 1.00% K_2O, and had a pH of 7.6. Three VC rates, such as VC1 = 0 t ha^{-1}, VC2 = 3 t ha^{-1}, and VC3 = 6 t $ha^{-1,}$ and two doses of Cd (Cd, 0 and 50 mg Cd kg^{-1}) were tested. The study included six treatments: (1) Neg-Cd + VC1 = 0 mg Cd + 0 t ha^{-1} VC, (2) Neg-Cd + VC2 = 0 mg Cd + 3 t ha^{-1} VC, (3) Neg-Cd + VC3 = 0 mg Cd + 6 t ha^{-1} VC, (4) Pos-Cd + VC1 = 50 mg Cd + 0 t ha^{-1} VC, (5) Pos-Cd + VC2 = 50 mg Cd + 3 t ha^{-1} VC, and (6) Pos-Cd + VC3 = 50 mg Cd + 6 t ha^{-1} VC. The seeds of the fragrant rice cultivars were used as a test crop and cultivated in a plastic pot, with each pot containing three hills. The seedlings were transplanted into pots in mid-March, and the rice crops were harvested in mid-July. The NPK dose was 300:150:300 (kg ha^{-1}) 1.80 g of N was used as urea, 0.90 g of P_2O_2 as superphosphate, and 2.20 g of potassium chloride. Uniform flooding irrigation was maintained from the planting of seedlings to physiological maturity to establish anaerobic conditions in the pots. Usual farming practices, such as insecticide and pesticide application, were applied in all treatments.

2.3 Sampling and analysis

2.3.1 Soil chemical attributes

A core sampler was used to gather soil samples at a depth of 15 cm before to seedlings and after harvest. The samples were then separated into two separate portions, one half for soil nutritional evaluations and the other for molecular analysis and stored at −80°C. Soil organic C (SOC) was examined using the $K_2Cr_2O_7$-H_2SO_4 oxidation method posted by Wang et al. (2003). Furthermore, the Ohyama (1991) approach was employed for TN. The TN was determined using Jackson's (1956) micro-Kjeldahl technique. Finally, Lu's (2000) techniques evaluated soil pH, AN, TP, and TK.

2.3.2 Rice grain yield and leaf physiological attributes

At maturity, rice plants from the pot were picked to examine grain yield adjusted to 14% moisture content. Moreover, at the tillering and heading stages, several gaseous exchange parameters were examined, including transpiration rate (Tr), net photosynthetic rate (Pn), intercellular CO_2 concentration (Ci), and stomatal conductance (gs). On a sunny day, a transportable photosynthesis machine (Li-6800, Li-COR USA) was utilized to measure photosynthesis.

Fresh leaf samples (size 1 mm^2) were chosen for transmission electron microscope (TEM) analysis. Small slices of leaves, about 1–3 mm, were fixed in 4% glutaraldehyde (v/v) in 0.2 mol/L PBS (sodium phosphate buffer, pH 7.2) for 6–8 h, then in 1% OsO4 for 1 h, and finally in 0.2 mol/L PBS (pH 7.2) for 1–2 h. Dehydration was performed in a graded ethanol series (50, 60, 70, 80, 90, and 100%), followed by acetone, before samples were filtered and embedded in Spurr's resin. Finally, ultra-thin sections (80 nm) were produced and placed on copper grids for TEM imaging (Roland and Vian, 1991).

2.3.3 Antioxidant enzyme activities

The antioxidant enzymes, such as superoxide dismutase (SOD), peroxidase (POD), catalase (CAT), and ascorbate peroxidase (APX) activities in fresh leaves were determined by using previously described by Wu et al. (2003). Briefly, fresh rice leaves were homogenized using sodium phosphate buffer (50 mM, pH 7.5). The homogenized sample was centrifuged at 12,000 rpm for 10 min at 4°C. The supernatant was then collected and used for subsequent assays. In the enzyme extract, the measurement of the activity of SOD was done using the enzyme solution containing methionine (750 mM), NBT (5.2 mM), EDTA (0.1 mM) and PBS (50 mM). The enzymatic activities of SOD, POD, CAT, and APX were measured as previously reported procedures (Jiang and Zhang, 2001).

2.3.4 Total RNA extraction and qRT-PCR analysis

Total RNA was isolated from the samples using TRIzol reagent (Invitrogen, Carlsbad, California, United States). The qRT-PCR was then evaluated using the Pfafflfl (2001) technique, as previously reported. Rice ACTIN (Os03g50885) was utilized as a reference gene for relative quantification. Supplementary Table S1 provides information about nucleotide sequences and specific annealing temperatures. Three biological repetitions were employed, and expressions were calculated by normalizing the Ct value for every gene compared to the ACTIN value. Quantification was done using the $2^{-\Delta\Delta Ct}$ approach, as indicated in the previous study (Pfafflfl, 2001).

2.3.5 Measurements of MDA and H_2O_2

Leaf malondialdehyde (MDA) content during the vegetative and reproductive was measured by the previously reported method (Velikova et al., 2000). To measure MDA contents, fresh rice leaves were sampled and immediately homogenized in 0.1% (w/v) cold TCA, and the homogenate was centrifuged at 12,000 g for 20 min at 4°C. The reaction mixture contained 0.5 mL of supernatant, and 2.5 mL of 0.5% thiobarbituric acid (TBA) solution (dissolved in 20% TCA). The reaction mixture was boiled for 30 min, and then rapidly cooled and centrifuged for 5 min at 12,000 × g. The difference between the absorbance values at 532 and 600 nm with an extinction coefficient of 155 mM cm 1 was applied to calculate the MDA contents. In addition, hydrogen peroxide (H_2O_2) was investigated from the fresh samples by the technique recommended earlier (Bates et al., 1973). Fresh leaf samples (0.2 g) were crushed in liquid nitrogen and homogenized with 1 mL of 0.1% trichloroacetic acid (TCA) and centrifuged at 12,000 g for 20 min (4°C) for the measurement of hydrogen peroxide (H_2O_2). The reaction mixture was comprised of 0.5 mL of potassium phosphate buffer (pH 6.8, 100 mM), 1 mL potassium iodide (1 M), and 0.5 mL supernatant. The H_2O_2 contents

were measured by spectrophotometer (UV–VIS 2550, Shimadzu, Japan) at 390 nm.

2.3.6 Assessment of proline and protein level

As stated in earlier studies, the amount of proline in fresh leaves was determined using Bradford's (1976) technique The solution was purified with 5 mL of toluene, and the absorption of red chromophore in the methanol component was obtained at the 520 nm range. Fresh leaves (0.1 g) were standardized in 50 mM sodium phosphate buffer (1 mM EDTA-Na2, 2% polyvinyl pyrrolidine-40) and spun at 10,000 × g for 15 min at 4°C and finally, the reaction solution was scanned at 595 nm for final protein content.

2.3.7 Determination of plant cd content

The dried samples were grinded and processed at a 4:1 (v/v) ratio in HNO_3 and $HClO_4$ before being diluted up to 25 mL. Then, Cd levels in rice organs were subsequently analyzed with a flame atomic absorption spectrometer as earlier advised by Cao et al. (2014).

2.4 Statistical analysis

The results collected on soil chemical attributes and fragrant rice physiological, biochemical attributes and grain yield were analyzed using relevant ANOVA procedures for completely randomized design, using Statistix 8.1 software (Analytical Software). Before analysis, results were normalized using the arcsine function. Tukey's *post-hoc* test was conducted to compare multiple means for variables with significant influence from experimental factors.

3 Results

3.1 Effect of VC on soil fertility

The addition of VC considerably enhanced soil chemical characteristics, including SOC, pH, AN, TN, TP, and TK as compared to sole Cd-stressed soil: Pos-Cd + VC1 (Table 1). The application mitigated the adverse effects of Cd on soil health, and the effect was most pronounced in all evaluated parameters at high VC amendments. Off the treatments, the non-Cd stressed soil (Neg-Cd + VC3) had higher values for soil qualitative features (i.e., pH, TN, AN, and SOC), while the solo Pos-Cd soil had the lowest values. Related to Pos-Cd + VC1, Pos-Cd + VC3 enhanced soil SOC, pH, TN, and AN by 5.78, 43.13, 178.54, and 11.38%, respectively, in Cd-contaminated soil. Likewise, low VC input increased each examined variable, although not as much as compared to VC amendments under Cd toxicity.

3.2 Effect of VC on leaf gas exchange attributes and grain yield

Fragrant rice verities, XGZ and MXZ-2, showed substantial variations in photosynthesis rate with VC application in a Cd stress condition (Figures 1, 2). In Cd-contaminated soil, the VC treatment improved leaf photosynthetic characteristics such as *Pn*, Tr, gs, and Ci. In addition, the treatments followed a similar pattern across both development phases. Pos-Cd + VC3 enhanced *Pn* and Tr by 60.66 and 42.44%, correspondingly, in MXZ-2 and 66.40 and 42.44% in the XGZ, as related compared to the High VC treatment: Pos-Cd + VC3, as shown in Figure 1. Similarly, low-VC-treated pots considerably boosted leaf physiological activity over Cd-stressed plants.

Across the growth, differences in gs and Ci were also substantially higher compared with Cd-stressed plants (Figures 2A–D). Across the growth stages, the Pos-Cd + VC3 enhanced gs and Ci by 60.64 and 15.30%, correspondingly, in MXZ-2 and 56.45 and 15.80%, in XGZ cultivars under Cd toxicity. Similarly, low VC-treated plants significantly ($p < 0.05$) increased gs and Ci than only Cd-stressed plants. Furthermore, findings showed that XGZ was more resilient to Cd stress than the MXZ-2 cultivar.

3.3 Leaf ultrastructure analysis under Cd toxicity

Plant growth and development depend primarily on cell elongation and division. In the present study, the plant physiological, biochemical, and yield improved with the addition of VC amendments. Thus, Pos-Cd + VC1, Pos-Cd + VC3, and Neg-Cd + VC3 treated plants were selected for leaf ultrastructure (TEM) analysis and analyzed the changes in the ultrastructure cells of fragrant rice leaves (Figure 3). The leaf ultrastructure analysis showed that the Cd toxicity damages the shape and size of the cell relative to High VC-treated plants: Pos-Cd + VC3 and Neg-Cd + VC3. Under no Cd stress conditions (no Cd) supplemented with vermicomposting (Neg-Cd + VC3), chloroplasts in XGZ and MXZ-2 exhibited well-organized grana and stroma lamellae,

TABLE 1 The impact of vermicompost on soil chemical composition in Cd contaminated soil.

Treatment	pH	SOC (g kg^{-1})	TN (g kg^{-1})	AN (mg kg^{-1})	TP (g kg^{-1})	TK (g kg^{-1})
Neg-Cd + VC1	5.95 ± 0.86 e	11.20 ± 1.42 e	1.12 ± 0.16 d	146.52 ± 12.54 d	0.94 ± 0.02 d	17.40 ± 1.04 c
Neg-Cd + VC2	6.23 ± 0.64 b	14.12 ± 1.40 c	1.28 ± 0.62 b	158.09 ± 14.62 b	1.18 ± 0.02 b	19.06 ± 2.22 b
Neg-Cd + VC3	6.30 ± 0.62 a	16.44 ± 2.02 a	1.38 ± 0.10 a	178.50 ± 15.78 a	1.28 ± 0.04 a	23.34 ± 2.20 a
Pos-Cd + VC1	5.94 ± 0.74 d	11.05 ± 1.08 d	1.08 ± 0.06 e	140.16 ± 12.70 e	0.92 ± 0.03 d	13.35 ± 1.08 d
Pos-Cd + VC2	6.05 ± 0.36 c	12.05 ± 1.70 d	1.14 ± 0.08 c	155.55 ± 10.50 c	0.98 ± 0.03 c	16.46 ± 1.64 d
Pos-Cd + VC3	6.24 ± 0.54 b	14.64 ± 2.12 b	1.30 ± 0.18 b	156.06 ± 12.50 b	1.20 ± 0.03 b	18.98 ± 1.84 b

Cd, Cadmium; VC, vermicompost; SOC, soil organic carbon; TN, total nitrogen; AN, available nitrogen; TP, total phosphorous; TK, total potassium. Neg-Cd + VC1 = 0 mg Cd + 0 t ha^{-1} VC, Neg-Cd + VC2 = 0 mg Cd + 3 t ha^{-1} VC, Neg-Cd + VC3 = 0 mg Cd + 6 t ha^{-1} VC, Pos-Cd + VC1 = 50 mg Cd + 0 t ha^{-1} VC, Pos-Cd + VC2 = 50 mg Cd + 3 t ha^{-1} VC, Pos-Cd + VC3 = 50 mg Cd + 6 t ha^{-1} VC. Tukey tests were used to assess the treatment means. The lettering was done by the Tukey HSD test at 5%. Statistics reveal that the values in the column with similar letters are statistically ($p < 0.05$) the same.

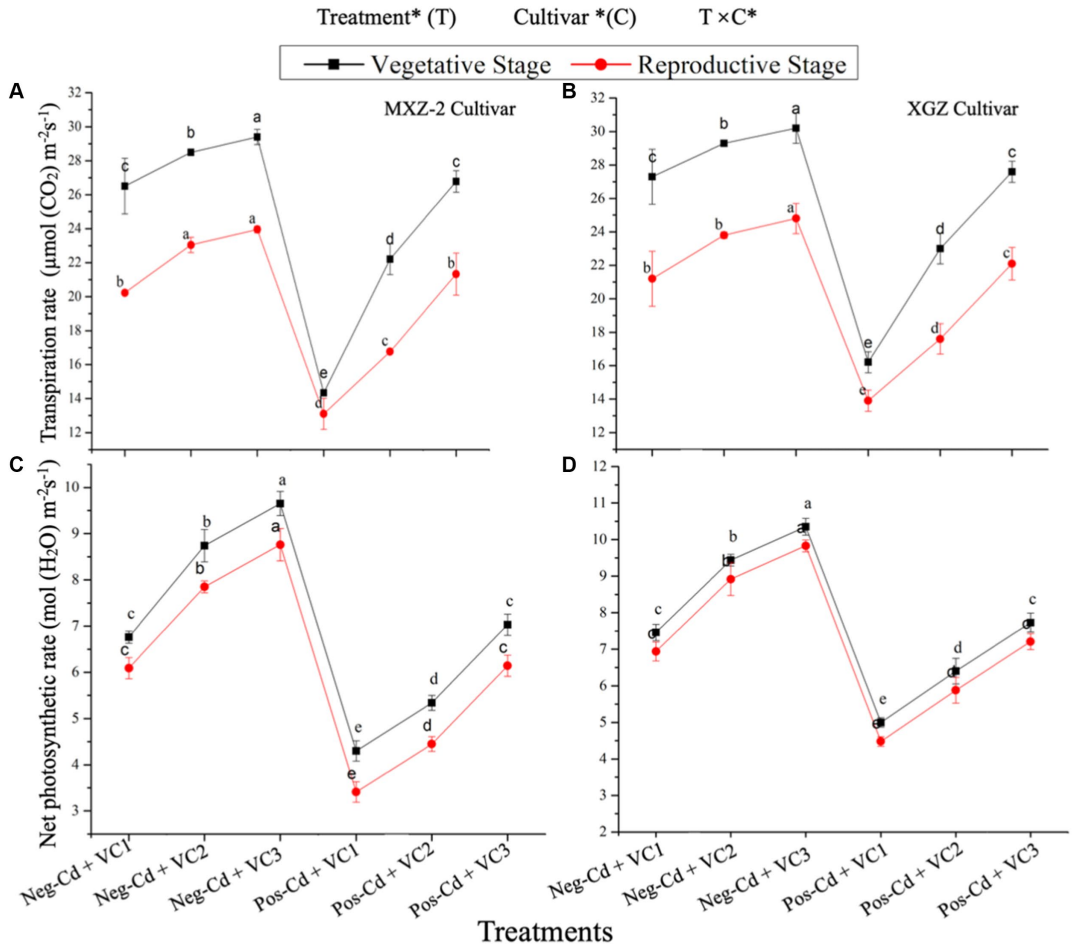

FIGURE 1
Effect of vermicompost application on net photosynthetic rate **(A,B)** and transpiration rate **(C,D)** of rice MXZ-2 and XGZ at different growth periods under Cd toxicity. Tukey analyses were performed to compare the means of the treatments, and the findings were interpreted using a simple test based on the Tukey HSD test at ($p < 0.05$). Error bars are standard errors of the mean. At $p < 0.05$, bars with different letters show significant ($p < 0.05$) differences among the treatments. ** and * indicate significance level at 1% and 5%, correspondingly. See Table 1 for treatment combination details.

developing complete thylakoid membrane systems. However, under Cd stress (Pos-Cd + VC1), chloroplast morphology changed gradually from oblong round to expanding spindle-like shapes, with severe deformities observed in MGZ-2 such as irregular shapes with distorted plastids and dissolution of grana lamellae. In contrast, the changes in chloroplasts (thylakoid and grana lamellae) were less severe in XGZ under Cd stress. Following vermicomposting under Cd stress (Pos-Cd + VC3), chloroplasts and thylakoid membranes in MXZ-2 partially recovered, while chloroplast structures in XGZ resembled those in plants under Neg-Cd + VC3 conditions. Resultantly, vermicomposting application eased the negative effects of Cd on chloroplast structure in both varieties (XGZ and MXZ-2) of fragrant rice.

3.4 Effect of VC application on enzyme activity

Antioxidant-related enzyme activities were investigated to determine the role of VC additions in mitigating Cd-induced oxidative stress in both varieties (Figures 4, 5). The findings demonstrated that Cd stress significantly reduced the antioxidant enzyme activity of rice cultivars than non-Cd stressed plants. Leaf antioxidants enzyme production changed substantially across cultivars, with XGZ exhibiting a slighter drop, indicating that it is more resistant to the Cd stress. Surprisingly VC application reduced Cd toxicity under High VC treatments while increasing antioxidant enzyme activities in leaves under Cd pollution. Across the development phases, the treatments followed a similar pattern. Averaged throughout development stages, Pos-CD + VC3 treatment substantially increased SOD (122.55 and 114.46%), POD (38.65 and 36.23%), CAT (42.46 and 45.66%), and APX (112.22 and 126.45%) activities in MXZ-2 and XGZ rice, respectively, related to Pos-Cd treated plants alone. Similarly, low VC-treated pots had significantly higher antioxidant enzyme activity than Cd-stressed plants.

3.5 Effect of VC application on the antioxidant genes expression pattern

In the current study, the expression patterns of antioxidant-related genes of both fragrant rice cultivars are shown in Figures 6, 7. The gene expression levels were altered by various VC treatments under Cd

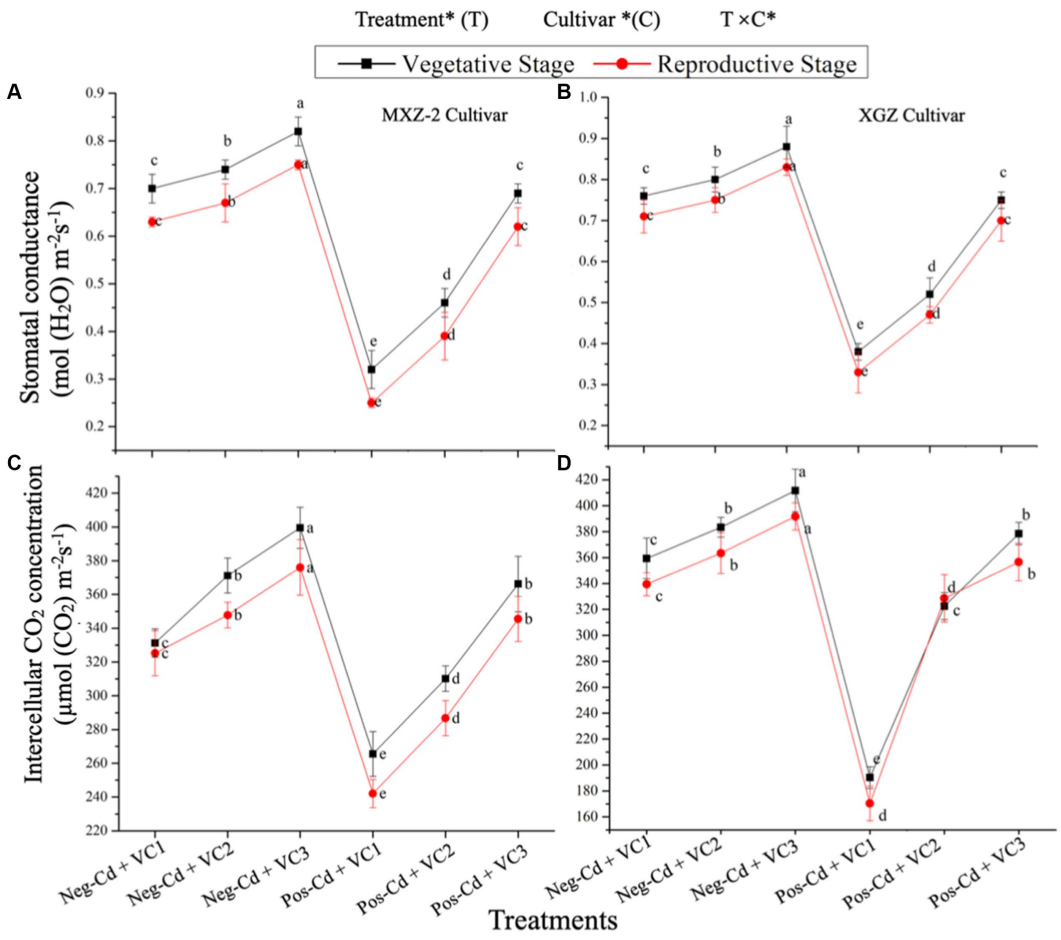

FIGURE 2
Effect of vermicompost application on leaf stomatal conductance **(A,B)** and intercellular CO2 concentration **(C,D)** of rice cultivars, i.e., MXZ-2 and XGZ at different growth periods under Cd toxicity. Tukey analyses were performed to relate the means of the treatments, and the findings were interpreted based on the Tukey HSD test at ($p < 0.05$). At $p < 0.05$, bars with distinct letters show significant differences among treatments. ** and * indicate significance level at 1% and 5%, respectively. See Table 1 for treatment combination details.

intoxication. In both cultivars, Cd-stressed plants had considerably lower expression patterns of genes (such as *OsPOD, OsSOD, OsCAT*, and *OsAPX*) than Neg-Cd plants. However, High-VC treatment reduced Cd toxicity in plants and elevated the pattern of genes related to the plant defense system. Pos-Cd + VC3 substantially enhanced transcript levels *OsPOD* (82.36 and 920.28%), *OsSOD* (88.68 and 68.65%), *OsCAT* (122.55 and 145.85%), and *OsAPX* (97.34 and 85.75%) in MXZ-2 and XGZ, relative to Pos-CD + VC1, averaged throughout development stages. Similarly, the other VC-treated plants showed significant increases in the transcription level of antioxidant-related genes.

3.6 Effect of VC application on protein and proline level

Soluble protein and proline production were significantly different with the use of VC under Cd toxicity (Table 2). Both cultivars had significant variations in protein and proline content. The results showed that the Cd toxicity significantly enhanced proline levels in both stages when compared to Neg-Cd experienced plants. However, the VC modifications reduced Cd stress and lowered proline synthesis. Proline production followed a consistent pattern across development stages, and when Pos-Cd + VC3 was applied, leaf proline concentration dropped by 65.44 and 55.44% in XGZ and MXZ-2 cultivars, correspondingly, compared to Pos-Cd plants. Likewise, lesser VC addition significantly reduced proline content when compared to Cd-stressed plants. In compared to proline, the Pos-Cd plants significantly reduced the soluble protein concentration. Soluble protein levels increased linearly from the vegetative to reproductive development phases. In comparison to Pos-Cd + VC1, Pos-Cd + VC3 treated pots increased leaf total protein content by 36.22 and 42.88% in XGZ and MXZ-2 cultivars, respectively (Table 2). Additionally, the results revealed that MXZ-2 had lower proline content and soluble protein than XGZ, suggesting that MXZ-2 is more vulnerable to stress conditions.

3.7 Influence of VC application on MDA and H_2O_2 contents under toxicity

The current findings showed that VC treatment considerably reduced the concentrations of MDA and H_2O_2 in both varieties under Cd conditions (Table 3). XGZ and MXZ-2 showed substantial

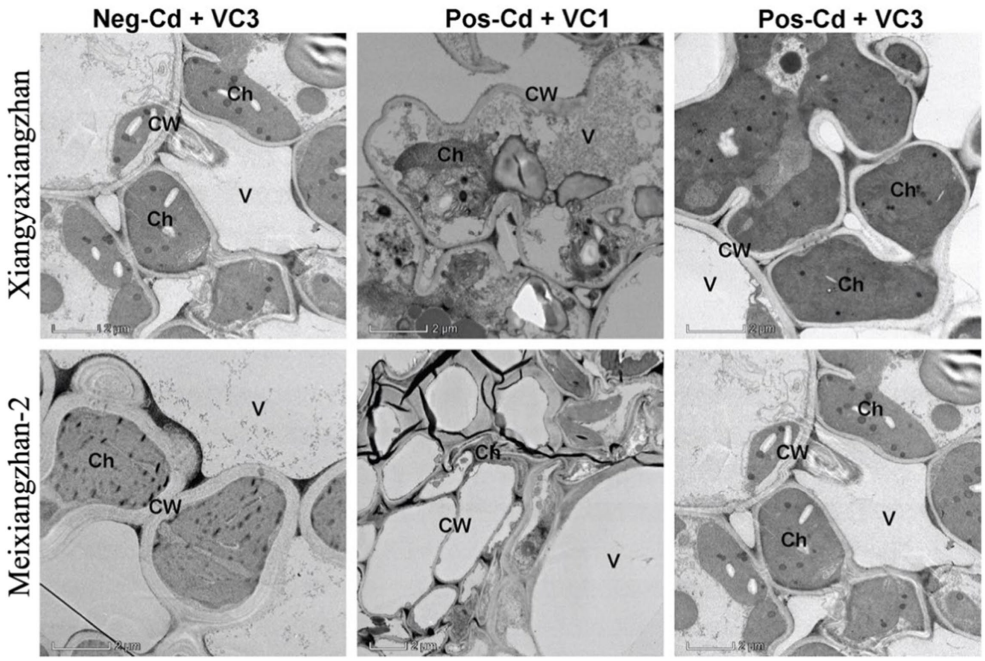

FIGURE 3
Effect of VC application on leaf ultrastructure analysis of rice cultivars such as Xiangyaxiangzhan and Meixiangzhan-2 under Cd toxicity. CW, cell wall; Ch, chloroplast; V, Vacuole. See Table 1 for treatment combination details.

($p < 0.05$) variations for leaf MDA and H_2O_2 levels. In contrast, solo Cd-stressed plants significantly elevated MDA and H_2O_2 levels in both rice cultivars' leaves. Sole Cd-stressed treatment (Pos-Cd + VC1) substantially raised the level of MDA by 68.42 and 82.66% and H_2O_2 by 72.66 and 82.34%, respectively, in XGZ and MXZ-2 cultivars (Table 3). Moreover, the outcomes revealed that the concentrations MDA and of H_2O_2 in MXZ-2 were greater than in XGZ, showing that the XGZ cultivar is more resistant to Cd pollution compared to MXZ.

3.8 Influence of VC amendments on Cd uptake in plant different organs and rice grain yield

The accumulation of Cd in several organs (root, stem + leaves, and grains) of both rice varieties is significantly ($p < 0.05$) higher in Cd stress plants (Table 4). However, the use of VC reduced Cd-related toxicity and significantly lowered Cd uptake in rice different organs. The Cd content in roots was higher than shoots and grains. Off the treatments, Neg-Cd + VC3 had the minimum Cd accumulation rice plant organs, whereas Pos-Cd + VC1 had the greatest levels. The use of VC significantly lowered Cd concentrations in roots, leaves, stems, and grain. Relative to Pos-Cd, the High VC (Pos-Cd + VC3) decreased the uptake of Cd in the MXZ-2 rice cultivar by 35.66, 46.65, and 73.55% in roots, shoots, and grains, respectively. Similarly, relative to Pos-Cd, the High-VC3 treatment reduced Cd absorption in XGZ cultivar by 33.45, 43.88, and 70.66% in roots, shoots, and grains, correspondingly. The data demonstrated that a high VC dosage significantly decreased Cd uptake in rice plants. Furthermore, the results showed that MXZ-2 accumulated more Cd than XGZ, implying that the aromatic rice XGZ is more resistant to Cd contamination soil than MXZ-2.

Additionally, the Cd stress reduced the fragrant rice yield and productivity. However, the VC application improved the rice yield and productivity; off the treatment, Neg-Cd + VC3 resulted in a higher rice grain yield. In addition, Pos-Cd + VC3 enhanced grain yield by 40.2% in MXZ-2 and 41.40% in the XGZ cultivar as compared to Pos-Cd + VC1 (Table 4). Similarly, low-VC-treated pots considerably improved the rice grain yield under Cd toxicity.

3.9 Relationship between soil properties, leaf net photosynthetic rate and antioxidant enzyme activity

A linear regression analysis were conducted to assess the role of soil quality in improving plant physiological activity and antioxidant defense system in the present study (Figure 8). A positive correlation was noted between the soil chemical traits, such as SOC and TN content with leaf net photosynthetic rate (Figures 8A,B). Furthermore, the correlation analysis showed that the SOC and TN were highly positively correlated with the net photosynthetic rate ($R^2 = 0.63^*$; Figure 8A) and ($R^2 = 0.60^*$; Figure 8B), respectively. The regression analysis exhibited that the improvements in leaf physiological activity are directly associated with soil quality, suggesting that higher soil health results in higher plant physiological activity. In addition, the correlation study among net photosynthetic levels and antioxidant enzyme activity also showed a highly positive correlation (Figure 9). The analysis showed that the photosynthetic rate was highly strongly correlated with the antioxidant enzyme activity (i.e., SOD; $R^2 = 0.84^{**}$; Figure 9A, POD; $R^2 = 0.92^{**}$; Figure 9B, CAT; $R^2 = 0.90^{**}$; Figure 9C,

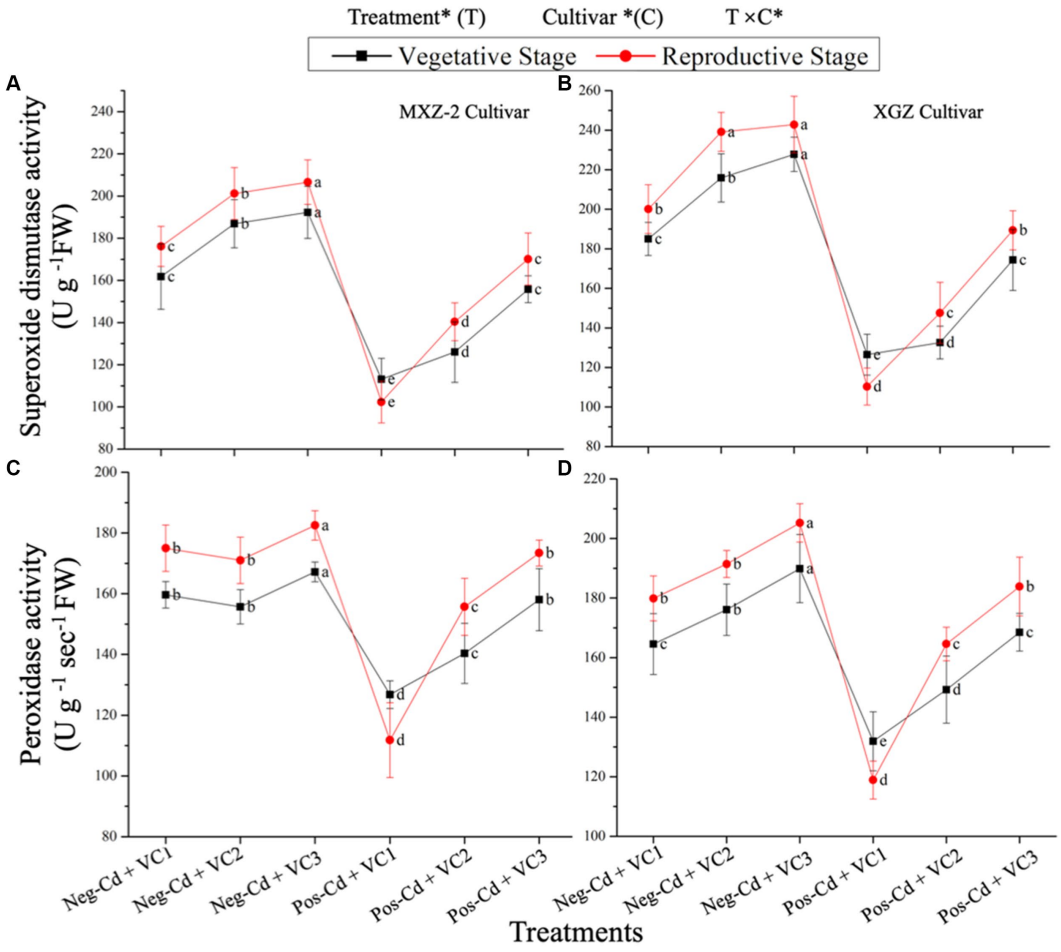

FIGURE 4
Effect of vermicompost application on the activity of superoxide dismutase **(A,B)** peroxidase **(C,D)** enzymes in the leaves of rice cultivars, i.e., MXZ-2 and XGZ at different growth periods under Cd toxicity conditions. Tukey analyses were performed to relate the means of the treatments, and the findings were interpreted based on the Tukey HSD test at ($p < 0.05$). Error bars are standard errors of the mean. At $p < 0.05$, bars with distinct letters show significant differences among the treatments. ** and * indicate significance level at 1% and 5%, respectively. See Table 1 for treatment combination details.

and APX; $R^2 = 0.80^{**}$; Figure 9D). These analyses displayed that the improvement in leaf physiological activity is directly related to plant antioxidant defense systems. Thus, the improvements in plant antioxidant systems and physiological performance are related to soil health and fertility.

4 Discussion

The physio-biochemical and antioxidant defense systems of plants are all disrupted by heavy metal pollution, particularly Cd toxicity. This results in significant yield reductions and losses in yield production and quality, which act as a serious risk to human health via the food chain (Liang et al., 2017). *In situ* stabilization, which involves immobilizing Cd through the application of organic fertilizers such as cattle dung, vermicompost, and biochar, is an effective and environmentally benign method recently (Ali et al., 2020; Hamid et al., 2020). In the present investigation, we examined how VC amendments affected the chemical properties of the paddy soil, the physio-biochemical features of the plants, the antioxidant defense systems, and the leaf ultrastructure of fragrant rice grown in soil contaminated with Cd.

4.1 Soil properties

According to Table 1 of this investigation, the use of VC greatly improved the soil qualitative characteristics under Cd toxicity. We noted that VC biodegrades improve soil quality and slowly release of plant-required nutrients throughout plant growth. The higher pH values were noted under VC amendments addition as compared to non-VC treated soil. According to Ni et al. (2018), nitrification generates H^+ and lowers soil pH when synthetic N fertilizer is used only. The acidic characteristics of synthetic N may cooperate in reducing soil pH (Iqbal et al., 2019; Adekiya et al., 2020). On the other hand, soil acidity was greatly decreased by adding organic N additions (Iqbal et al., 2021a,b, 2023b). Likewise, in this study, the addition of VC significantly enhanced the pH of the soil (Table 1). This could be explained by the fact that the hydroxyl ions (OH^-) from a-charged functional group in organic additions and the hydrolysis of $CaCO_3$

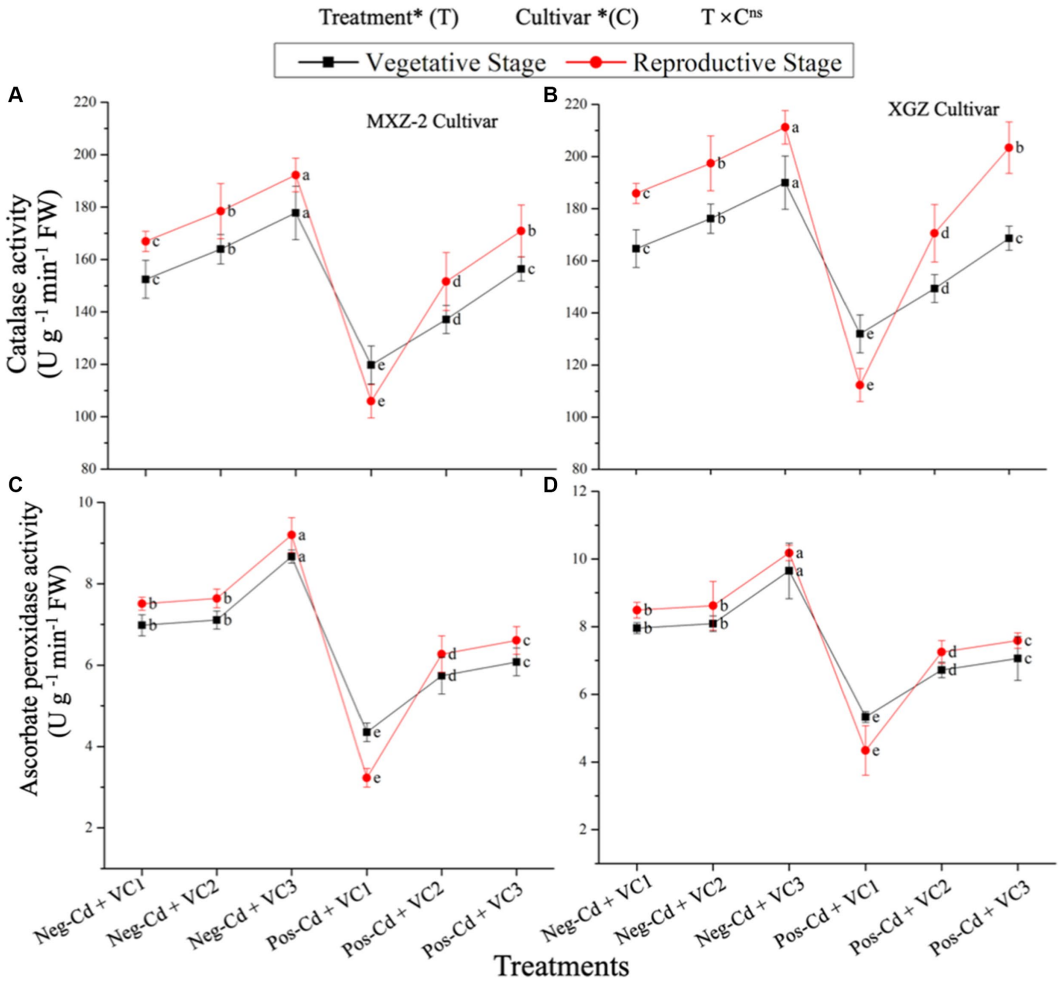

FIGURE 5
Effect of vermicompost application on the activity of catalase **(A,B)** and ascorbate peroxidase **(C,D)** enzymes of rice cultivars, i.e., MXZ-2 and XGZ at different growth periods. Tukey analyses were performed to relate the means of the treatments, and the findings were interpreted using a simple test based on the Tukey HSD test at ($p < 0.05$). Error bars are standard errors of the mean. At $p < 0.05$, bars with different letters show significant differences among the treatments. ** and * indicate significance at 1% and 5%, respectively. See Table 1 for treatment combination details.

produce hydroxyl ions (OH^-) that interact with H^+ ions to increase the pH of the soil. These hydroxyl ions include phenolic, hydroxyl, and carboxyl groups (Gul et al., 2015). Most growing plants would benefit from the pH of the soil being adjusted by the VC to a roughly neutral level (Fernández-Bayo et al., 2009).

Additionally, the addition of VC significantly improved the soil nutrient status in the present study. The possible explanation for this is the fact that the organic compost has a high ratio of organic matter and other essential plant nutrients (Tejada et al., 2010; Iqbal et al., 2023a,b). According to Liang et al. (2017), heavy metals typically do not melt or migrate readily in high-pH soil. Thus, it is possible that the higher soil pH caused by the application of VC fertilizer played an important role in slowing Cd migration in the soil in this experiment. Furthermore, the addition of VC improved soil nutrient availability, leading to greater plant growth and productivity in the current study (Table 1). The application of VC facilitates the secretion of mucus by earthworms, polysaccharides, and microorganisms, all of which improve the soil's physical structure, which is important for plant root growth and nutrient uptake (Lim et al., 2015). In conclusion, vermicomposting enriches the soil with beneficial microbes, enzymes, and humic acids, hence improving soil structure and water retention capacity (Iqbal et al., 2023a). This increases nutrient availability to plants, allowing stronger root development and better nutrient uptake (Iqbal et al., 2024b). Furthermore, the VC addition enhances soil biodiversity by promoting the beneficial microbes which in turn enhances plant growth directly by production of plant growth-regulating hormones and enzymes and indirectly by controlling plant pathogens, nematodes, and other pests, thereby enhancing plant health and minimizing yield loss (Pathma and Sakthivel, 2012). Interestingly, its slow release of nutrients provides long-term fertility, decreasing the demand for artificial fertilizers and minimizing environmental effects (Pathma and Sakthivel, 2012). Overall, the use of VC improves soil fertility while also encouraging sustainable farming practices by promoting long-term soil health and productivity.

4.2 Leaf physiological and plant biochemical attributes

Photosynthesis is the main element of plant physiological activity and productivity by enhancing crop growth and biomass

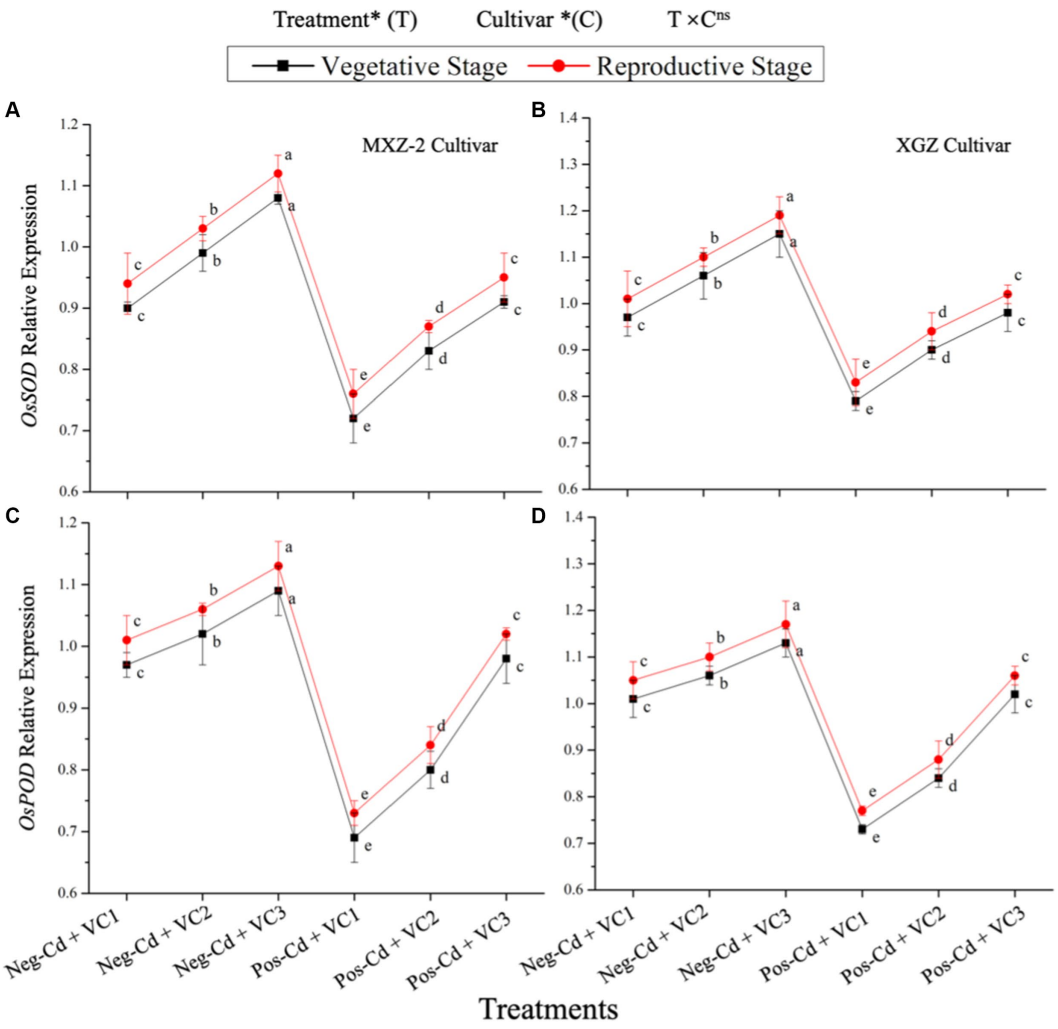

FIGURE 6
Effect of VC application on the relative expression of *OsSOD* **(A,B)** and *OsPOD* **(C,D)** of rice cultivars, i.e., MXZ-2 and XGZ at different growth stages. Tukey analyses were performed to relate the means of the treatments, and the findings were interpreted using a simple test based on the Tukey HSD test at ($p < 0.05$). Error bars are standard errors of the mean of the treatments. At $p < 0.05$, bars with distinct letter show significant differences among the treatments. ** and * indicate significance at 1% and 5%, respectively. See Table 1 for treatment combinations details.

accumulation (Khan et al., 2017; Iqbal et al., 2020; Ali et al., 2021). In the present study, the VC enhanced the plant photosynthetic efficiency, including, Tr, g_s, and Ci, in VC-treated plants as compared to non-VC-treated plants under Cd stress (Figures 1, 2). The enhancement in leaf photosynthetic activity induced under VC application could be primarily attributed to the improved soil fertility (Table 1), faster release of soil nutrients from VC in the early growth stages and gradual and slow release of crop-related nutrients from VC throughout the crop period (Yang et al., 2015; Luo H. et al., 2020; Luo Y. et al., 2020; Iqbal et al., 2022). Photosynthesis experienced a strong reaction to water and soil health (Makoto and Koike, 2007). A sufficient supply of water and nutrients will decrease the number of water-soluble nutrients and the stress-inducing root-sourced signal (ABA), which will open the stomata on leaves and increase their water potential and physiological activity (Daszkowska-Golec and Szarejko, 2013). In addition, the linear regression analysis in the present study also showed a highly positive relation between soil chemical traits and leaf photosynthetic activity (Figure 8). Aslam et al. (2020), reported that the application of VC improves the plant's morphological and physiological attributes.

The VC addition enhances crop growth, yield, and quality due to its plant growth-promoting characteristics. VC stimulates plant emergence because of the availability of essential plant nutrients (Iqbal et al., 2024a,b). According to Khan et al. (2021), antioxidants can lessen oxidative damage and reactive oxidative stress in plants, which is important for plant defense systems. Under the Cd stress condition, the plant's physiological and biochemical attributes significantly ($p < 0.05$) reduced in the current study (Figures 4, 5). Furthermore, the Cd toxicity damaged leaf ultrastructure components such as cell wall, chloroplast, and vacuoles (Figure 3). However, the VC addition counteracted the Cd toxicity and healed the plant's oxidative damage, which may be linked to an increase in the activity of antioxidant enzymes and the expression of genes encoding antioxidants (Figures 4–7). According to earlier research, SOD, POD, CAT, and APX protected plants against oxidative plant

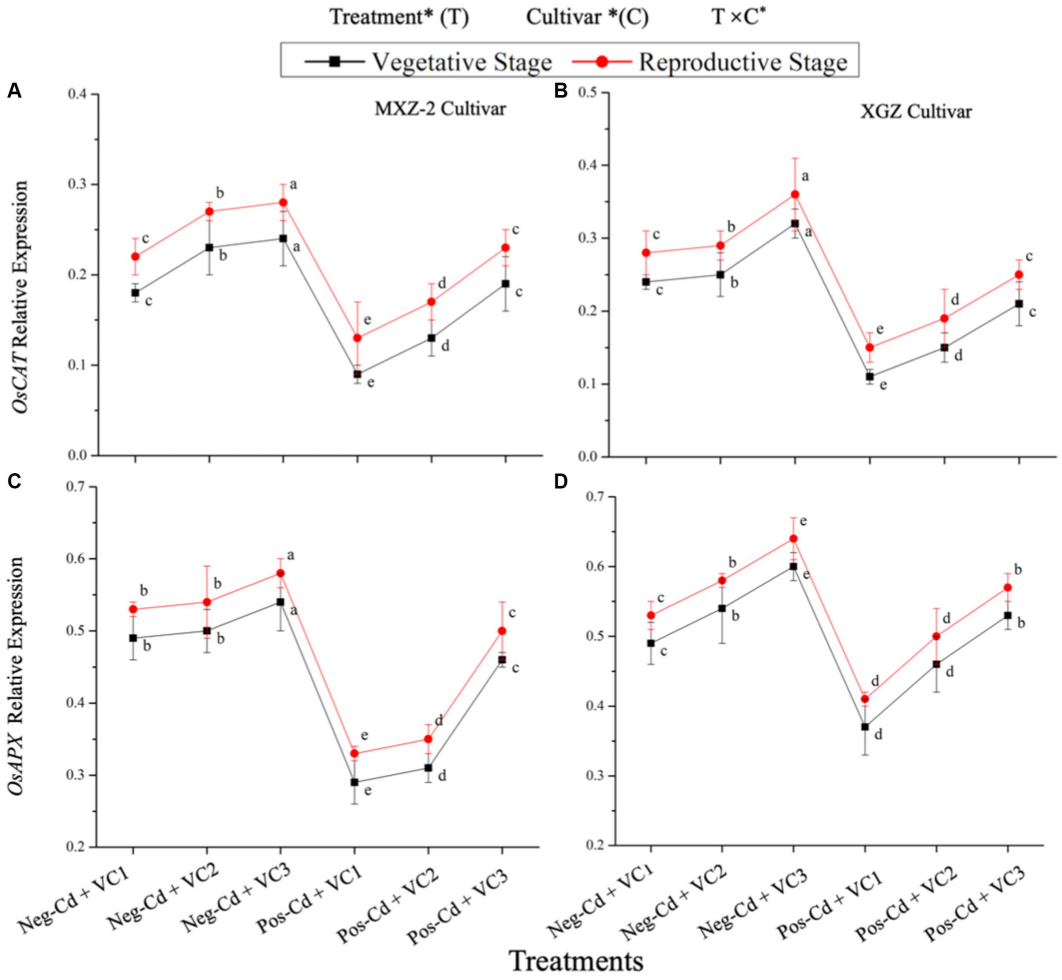

FIGURE 7
Effect of VC application on the relative expression of *OsCAT* **(A,B)** and *OsAPX* **(C,D)** of rice cultivars, i.e., MXZ-2 and XGZ at different growth periods. Tukey tests were performed to relate the means of the treatments, and the findings were interpreted using a simple test based on the Tukey HSD test at ($p < 0.05$). Error bars are standard errors of the mean. At $p < 0.05$, bars with distinct letter show significant ($p < 0.05$) differences among the treatments. ** and * indicate significance at 1% and 5%, respectively. See Table 1 for details treatment combinations.

damage by acting as antioxidant enzymes (Hasanuzzaman et al., 2020; Moustafa-Farag et al., 2020). In this study, we also found that pots containing Cd had lower SOD activity. This could be the case as SOD, which reduces reactive oxidative stress and transforms hazardous O2 into less toxic H_2O_2, is the antioxidant system's first line of defense (Anjum et al., 2011). Similarly, a similar pattern was observed in the activity of CAT, which protects plant cells by turning O_2 into the less toxic H_2O_2, thereby reducing oxidative stress (Sanchez-Casas and Klessig, 1994; Iqbal et al., 2023a,b). The procedure involved in eliminating O_2 and the increased formation of H_2O_2 and MDA in the current investigation may be the cause of the significant decline in antioxidant enzyme activity under Cd stress (Table 3). On the other hand, both aromatic rice varieties' antioxidant enzyme activity was enhanced by VC addition, which may have been a major factor in improving plant growth and antioxidant defense system. Moreover, the results of the linear regression analysis demonstrated that increased leaf physiological activity enhanced the antioxidant defense system and leaf ultrastructure, including the cell wall, chloroplast, and vacuole (Figures 3–5). Additionally, the expression level of antioxidants encoding genes is strongly elevated in plants treated with VC (Figures 6, 7). According to Gao et al. (2013), VC enhances the activity of antioxidant enzymes and so helps in the production of crops by shielding the leaf chloroplast structure from reactive O_2.

Plant cytoplasm contains a substance called proline, which regulates osmotic pressure by altering the water potential of cells (Muneer et al., 2011). In this study, under Cd-stress situations, leaf proline content was boosted significantly (Table 2). Plant proline levels are elevated by heavy metal stress, especially Cd toxicity because stressed plants are more resilient (Bauddh and Singh, 2012). Plant protein degradation may be linked to an increase in proline content and plant damage may be reflected in an increase in proline levels in plant tissue (Palma et al., 2002). Our results are consistent with Elmer and White (2018) and Cao et al. (2014) who reported that the increased protease activity caused protein deficiency under Cd stress conditions. Similar findings were stated by other researchers that the production of soluble protein is significantly affected by stress conditions, particularly by Cd stress

TABLE 2 Effect of VC application on proline and soluble protein content of different rice cultivars under Cd toxicity.

		Vegetative stage		Reproductive stage	
	Treatments	Proline content (μg g^{-1} FW)	Soluble protein (mg g^{-1} FW)	Proline content (μg g^{-1} FW)	Soluble protein (mg g^{-1} FW)
	Neg-Cd + VC1	19.34 ± 2.12 d	401.16 ± 12.33b	22.99 ± 1.86 c	435.45 ± 12.44 b
	Neg-Cd + VC2	18.87 ± 3.21 d	403.75 ± 22.24 b	19.44 ± 1.50 d	438.66 ± 22.25 b
MXZ-2	Neg-Cd + VC3	13.83 ± 1.45 e	423.32 ± 18.45 a	15.43 ± 1.22 e	457.64 ± 15.64 a
	Pos-Cd + VC1	21.23 ± 1.67 a	356.45 ± 14.45 e	28.88 ± 2.36 a	245.53 ± 12.30 e
	Pos-Cd + VC2	18.34 ± 2.44 b	375.44 ± 16.66d	25.99 ± 1.90 b	353.32 ± 14.34 d
	Pos-Cd + VC3	16.24 ± 2.22 c	390.28 ± 12.68 d	23.06 ± 2.22 c	414.55 ± 18.80 c
	Average	17.98 b	391.64 a	22.77b	401.75a
	Neg-Cd + VC1	20.63 ± 1.23 c	385.34 ± 14.44 c	25.85 ± 2.40 c	437.58 ± 19.34 b
	Neg-Cd + VC2	18.16 ± 1.22 d	415.94 ± 18.34 b	26.38 ± 1.66 d	431.17 ± 16.87 b
XGZ	Neg-Cd + VC3	17.90 ± 1.55 d	435.55 ± 16.22 a	23.34 ± 1.70 e	459.78 ± 22.32 a
	Pos-Cd + VC1	24.52 ± 2.23 a	318.68 ± 17.78 e	39.74 ± 2.22 a	311.76 ± 18.23 d
	Pos-Cd + VC2	21.63 ± 1.96 b	387.23 ± 12.20 d	27.85 ± 1.88 b	411.46 ± 15.44 c
	Pos-Cd + VC3	19.95 ± 1.45 c	392.46 ± 15.44 c	25.38 ± 2.11 c	426.69 ± 20.22 b
	Average	21.27 a	403.87a	28.65 a	414.57 a
	ANOVA				
	Treatment (T)	**	**	**	**
	Cultivar (C)	*	ns	*	ns
	T × C	ns	ns	ns	ns

Results are the averages of three replications, and Tukey tests were used to compare the treatment mean. The lettering was done using the Tukey HSD test at 5%. Cd, Cadmium; VC, vermicompost. ns, non-significant; ** and * are significant at 1% and 5%, correspondingly. See Table 1 for treatment combinations.

(Palma et al., 2002; Cao et al., 2014). However, the VC application alleviated the adverse effect of Cd on plants and greatly increased the protein content in the leaves of rice in the present study (Table 2). According to our findings, adding VC amendments to the soil improved its fertility, which in turn improved the physiological and biochemical processes of the plant by facilitating the uptake and accumulation of vital nutrients. Moreover, the VC application lowered the leaf proline content and strengthened plant defense systems due to improved plant physiological activity, indicating a moderating effect in preserving plant osmotic balance under Cd-contaminated soil (Table 2). The results of the linear regression analysis also demonstrated a strong and positive correlation between plant antioxidant defense systems and the leaf net photosynthetic rate (Figure 9).

The present research demonstrated that increased MDA and H_2O_2 generation were indicative of enhanced oxidative damage and leaf ultrastructure in the plant under Cd stress (Table 3). However, by lowering Cd uptake and aggregation in rice organs, VC treatments lessened the harmful effects of Cd (Table 4). Adding VC to soils not only gives plants vital nutrients for growth but also acts as a soil additive by causing heavy metals in the soil to become more complex, soluble, and precipitated. The VC reduces the mobility and uptake of Cd in plants (Huang et al., 2018). Therefore, by enhancing plant growth and antioxidant defense systems, the VC significantly decreased MDA and H_2O_2 in rice leaf organs. This suggests that the VC application lessened intracellular membrane disruptions caused by Cd throughout plant growth and development.

4.3 Cd accumulation in rice plant's different organs and grain yield

In the current study, the use of VC dramatically decreased the absorption and content of Cd in rice in organs, including the roots, shoots, and grains (Table 4). The organic VC treatment, which reduced the accessibility and mobility of Cd in arable soil, is mostly responsible for this behavior. By enhancing the complexation and precipitation of metals in farming soil, VC addition can serve as a soil additive, giving plants nutrients and organic matter while simultaneously reducing their mobility and availability of heavy metals (Deng et al., 2017). However, VC amendments, because of its vast surface area, high cation exchange capacity, and richness in active functional groups, VC may be considered a promising treatment for stabilizing heavy metals in soil (Wang et al., 2018; Ding et al., 2021). When compared to soils that have not been treated with VC, the possibility of Cd absorption and uptake n in plant roots is therefore much decreased. Additionally, Wan et al. (2020) noted that supplying more organic fertilizers significantly decreased the amount of Cd in rice grain, ranging from 7.8 to 79.3%. In a similar vein, Tang et al. (2015) discovered that adding organic amendments decreased the amount of metal in *B. chinezsis* plant roots and shoots growing in acidic soil.

In the present study, the addition of VC significantly increased fragrant rice yields in Cd-stressed soil (Table 4). Improvements in crop production and quality are closely associated with enhancements in soil physiochemical and biological properties (Iqbal et al., 2021a,b). Organic fertilizers enhance soil health and fertility, which increases plant growth, crop yield, and yield elements (Ali et al., 2020; Iqbal et al., 2022). In this

10.3389/fsufs.2024.1418554

TABLE 3 Effect of VC application on H_2O_2 and MDA content of different fragrant rice cultivars (i.e., MXZ-2 and XGZ) under Cd toxicity.

		Vegetative stage		Reproductive Stage	
	Treatments	H_2O_2 ($\mu g\ g^{-1}$ FW)	MDA ($\mu g\ g^{-1}$ FW)	H2O2 ($\mu g\ g^{-1}$ FW)	MDA ($\mu g\ g^{-1}$ FW)
	Neg-Cd + VC1	16.44 ± 1.32 d	11.95 ± 0.88 c	19.87 ± 1.22 d	18.34 ± 1.02 c
	Neg-Cd + VC2	15.53 ± 0.98 e	10.70 ± 0.84 d	17.18 ± 1.08 e	15.05 ± 0.88 d
MXZ-2	Neg-Cd + VC3	14.47 ± 1.58 e	10.46 ± 1.10 e	16.99 ± 0.98 e	14.95 ± 0.94 d
	Pos-Cd + VC1	26.72 ± 2.34 a	18.98 ± 2.12 a	37.70 ± 2.66 a	26.74 ± 1.88 a
	Pos-Cd + VC2	22.66 ± 1.88 b	14.38 ± 1.54 b	29.98 ± 2.14 b	22.15 ± 1.22 b
	Pos-Cd + VC3	19.77 ± 1.20 c	12.05 ± 1.44 c	23.34 ± 1.88 c	18.34 ± 0.98 c
	Average	19.68b	12.80 a	24.30 a	20.24 a
	Neg-Cd + VC1	15.53 ± 0.92 d	10.14 ± 0.72 c	21.40 ± 1.55 d	13.80 ± 0.86 d
	Neg-Cd + VC2	13.03 ± 0.88 e	8.84 ± 0.54 d	19.44 ± 0.82 e	13.91 ± 0.45 d
XGZ	Neg-Cd + VC3	12.99 ± 1.08 e	8.80 ± 0.66 d	16.24 ± 1.20 f	12.24 ± 0.58 e
	Pos-Cd + VC1	28.76 ± 1.34 a	16.34 ± 1.22 a	40.34 ± 3.24 a	25.55 ± 1.44 a
	Pos-Cd + VC2	21.64 ± 0.88 b	14.34 ± 0.98 b	36.22 ± 2.22 b	22.70 ± 1.22 b
	Pos-Cd + VC3	18.30 ± 1.08 c	10.22 ± 0.88 c	26.76 ± 1.66 c	16.66 ± 0.98 c
	Average	21.12a	11.70 b	30.05 b	18.78 b
	ANOVA				
	Treatment (T)	**	**	**	**
	Cultivar (C)	*	*	*	*
	T × C	ns	ns	ns	ns

Results are the means of three replications, and Tukey tests were used to compare the treatment mean. The lettering was done using the Tukey HSD test at 5%. The HSD Tukey test reveals significant variations among values with different letters ($p < 0.05$). Cd, Cadmium; VC, vermicompost. ns, non-significant; ** and * are significant at 1% and 5%, correspondingly. See Table 1 for details treatment combinations.

TABLE 4 The effect of VC uses on Cd accumulation in aromatic rice varieties in various organs and grain yield under Cd stress.

		Cd content ($\mu g\ g^{-1}$ DW)			
	Treatments	Root	Stem + leaf	Grain	Grain yield (g pot^{-1})
	Neg-Cd + VC1	22.83 ± 1.55d	10.87 ± 0.67d	0.15 ± 0.01d	75.08 ± 4.40 d
	Neg-Cd + VC2	20.24 ± 1.30e	9.78 ± 0.78e	0.12 ± 0.02e	95.80 ± 8.82 b
MXZ-2	Neg-Cd + VC3	10.76 ± 0.78f	8.423 ± 0.65f	0.09 ± 0.01f	120.35 ± 10.40 a
	Pos-Cd + VC1	214.76 ± 10.40a	42.875 ± 3.45a	1.56 ± 0.05a	65.40 ± 6.70 e
	Pos-Cd + VC2	189.95 ± 8.48b	36.96 ± 1.10b	0.98 ± 0.05b	79.46 ± 7.60 c
	Pos-Cd + VC3	156.98 ± 5.36c	28.88 ± 2.82c	0.76 ± 0.02c	92.35 ± 8.20 b
	Average	102.60 a	22.95a	0.61a	88.05b
	Neg-Cd + VC1	18.86 ± 1.35e	8.86 ± 0.86d	0.12 ± 0.02d	78.25 ± 4.45 d
	Neg-Cd + VC2	14.44 ± 1.33d	7.12 ± .88e	0.10 ± 0.02e	97.85 ± 7.85 b
XGZ	Neg-Cd + VC3	10.75 ± .77f	6.45 ± 0.44f	0.08 ± 0.01f	122.35 ± 11.45 a
	Pos-Cd + VC1	188.70 ± 10.42a	45.84 ± 3.40a	1.25 ± 0.04a	68.44 ± 6.50 e
	Pos-Cd + VC2	178.98 ± 8.85b	30.98 ± 2.18b	0.96 ± 0.03b	82.40 ± 7.80 c
	Pos-Cd + VC3	125.22 ± 5.38c	20.88 ± 1.80c	0.45 ± 0.02c	96.86 ± 8.20 b
	Average	89.50b	20.02b	0.49b	90.95a
	ANOVA				
	Treatments (T)	**	**	**	**
	Cultivar (T)	*	*	*	*
	T × C	ns	ns	ns	ns

Values are the means of three replications, and Tukey tests were used to compare the treatment mean. The lettering was done using the Tukey HSD test at 5%. The HSD Tukey test reveals significant differences between values with different letters ($p < 0.05$). Cadmium (Cd) and vermicompost (VC) are non-significant; * and ** are significant at 5% and 1%, respectively. See Table 1 for details treatment combination.

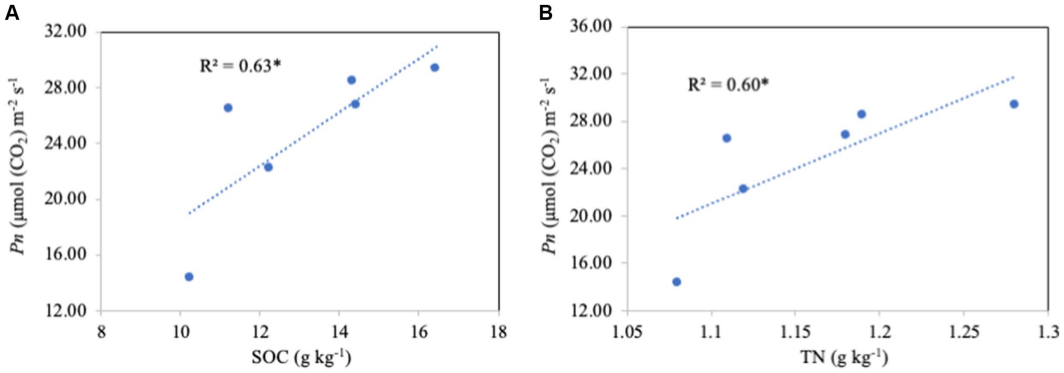

FIGURE 8
Linear regression analysis between soil organic carbon (SOC) and total nitrogen (TN) with leaf net photosynthetic rate (*Pn*) under VC application in a Cd-contaminated soil ($n = 6$). *$P < 0.05$.

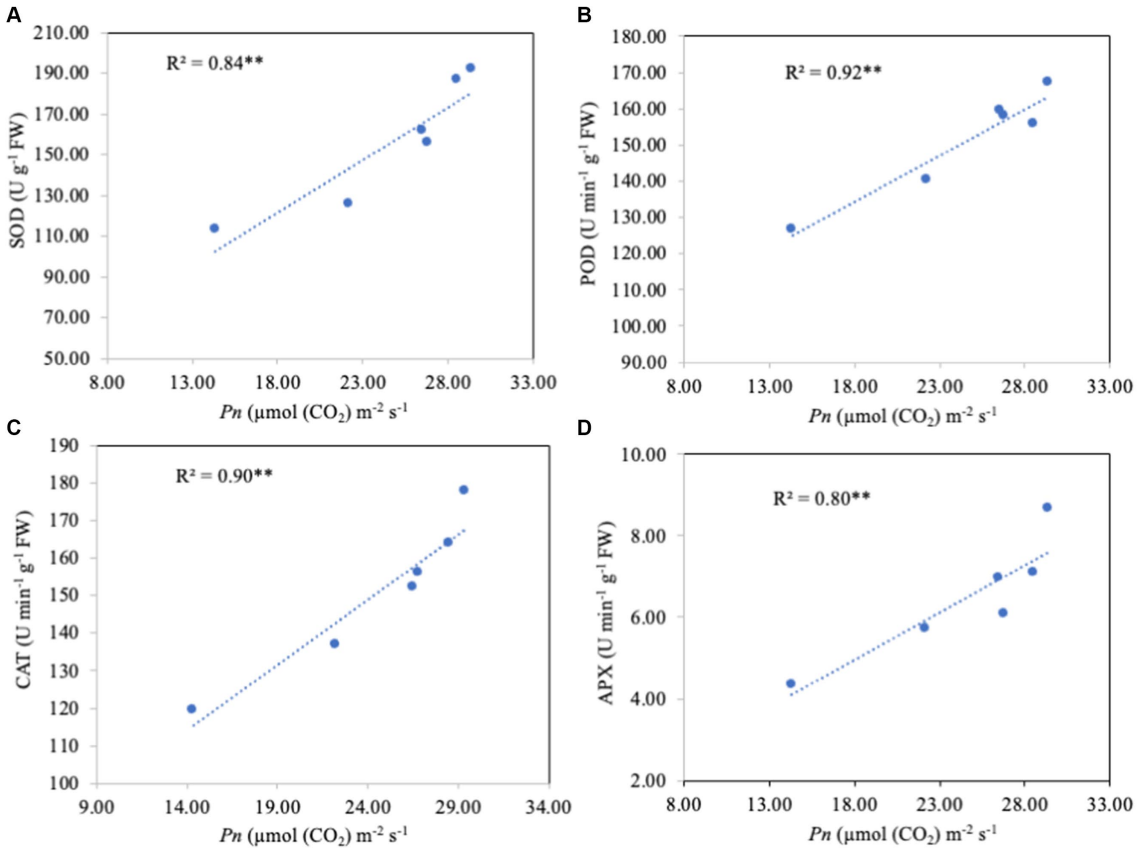

FIGURE 9
Linear regression analysis of leaf net photosynthetic rate (*Pn*) with antioxidant enzyme activity [i.e., SOD **(A)**, POD **(B)**, CAT **(C)**, and APX **(D)**] under the application in a Cd-contaminated soil ($n = 6$). **$P < 0.01$.

study, increased soil nutritional values were found in VC-treated soil (Table 1), which improved aromatic rice growth, physiological activity, and yield by giving the necessary nutrients across the growing period. This was supported by linear regression, which revealed that soil chemical features were highly positively related to leaf physiological traits (Figure 8). Iqbal et al. (2022) found that differences in yield are positively linked with soil biochemical state. Thus, variations in rice yield and yield components are largely dependent on soil health and nutrition.

5 Conclusion

This study aimed to determine how VC application reduced the adverse impacts of Cd toxicity on soil health and fragrant rice growth and grain yield. The results showed that the soil quality and physiological and metabolic efficiency of the fragrant rice cultivars were adversely affected by Cd toxicity. Moreover, under Cd stress, there was an increase in proline, MDA, and H_2O_2 production, as well

as Cd uptake and accumulation in rice organs, particularly in the roots and leaves. However, the VC application alleviated the Cd toxicity on soil health and plant physiological and biochemical attributes. The application of VC simultaneously immobilized Cd in paddy soil and enhanced the chemical characteristics of the soil due to its vast surface area, high cation exchange capacity, and richness in active functional groups and nutrients. Our findings concluded that the addition of VC enhances plant growth and production by promoting soil fertility which in turn enhances plant nutrient uptake and reduces Cd toxicity. Overall, the use of VC improves soil fertility while also encouraging sustainable farming practices by decreasing the demand for synthetic fertilizers and promoting long-term soil health and crop productivity.

Data availability statement

The original contributions presented in the study are included in the article/Supplementary material, further inquiries can be directed to the corresponding authors.

Author contributions

AI: Conceptualization, Methodology, Project administration, Supervision, Visualization, Data curation, Formal analysis, Investigation, Software, Writing – original draft. RK: Methodology, Formal analysis, Software, Validation, Visualization, Writing - review & editing. QH: Formal analysis, Methodology, Software, Validation, Writing – review & editing, Conceptualization, Data curation, Investigation, Visualization. MI: Methodology, Formal analysis, Software, Validation, Visualization, Resources, Writing - review & editing. ZM: Conceptualization, Data curation, Investigation, Methodology, Software, Writing – review & editing, Project administration, Resources, Supervision. TH: Data curation, Formal analysis, Methodology, Software, Supervision, Visualization, Writing – review & editing, Project administration, Resources. MA: Conceptualization, Formal analysis, Methodology, Software, Supervision, Writing – review & editing, Data curation, Visualization. IA: Formal analysis, Funding acquisition, Methodology, Resources, Software, Supervision, Validation, Writing – review & editing. HR: Funding acquisition, Methodology, Supervision, Writing – review & editing, Conceptualization, Formal analysis, Project administration, Software. MS: Conceptualization, Methodology, Project administration, Supervision, Validation, Writing – review & editing, Formal analysis, Funding acquisition, Resources, Software, Visualization. AE: Writing – review & editing, Funding acquisition, Methodology, Resources, Supervision, Validation. RL: Conceptualization, Methodology, Project administration, Supervision, Validation, Writing – review & editing. XT: Writing – review & editing.

Funding

The author(s) declare that financial support was received for the research, authorship, and/or publication of this article. Our work was supported by the Guangzhou Science and Technology Project (202103000075) and the Talent Introduction and Research Program of South China Agriculture University (41000-222106).

Acknowledgments

The authors extended their appreciation to the Researcher Supporting Project Number (RSPD2024R745), King Saud University, Riyadh, Saudi Arabia. In addition, we want to thank our South China Agriculture University Research Station collaborators for their research assistance.

Conflict of interest

The authors declare that the research was conducted in the absence of any commercial or financial relationships that could be construed as a potential conflict of interest.

Publisher's note

Supplementary material

The Supplementary material for this article can be found online at: https://www.frontiersin.org/articles/10.3389/fsufs.2024.1418554/full#supplementary-material

References

Adekiya, A. O., Agbede, T. M., Ejue, W. S., Aboyeji, C. M., Dunsin, O., Aremu, C. O., et al. (2020). Biochar, poultry manure and NPK fertilizer: sole and combine application effects on soil properties and ginger (*Zingiber officinale* roscoe) performance in a tropical Alfisol. *Open Agricult.* 5, 30–39. doi: 10.1515/opag-2020-0004

Adil, M. F., Sehar, S., Chen, G., Chen, Z. H., Jilani, G., Chaudhry, A. N., et al. (2020). Cadmium-zinc crosstalk delineates toxicity tolerance in rice via differential genes expression and physiological/ultrastructural adjustments. *Ecotoxicol. Environ. Saf.* 190:110076. doi: 10.1016/j.ecoenv.2019.110076

Adil, M. F., Sehar, S., Ma, Z., Tahira, K., Askri, S. M. H., el-Sheikh, M. A., et al. (2024). Insights into the alleviation of cadmium toxicity in rice by nano-zinc and *Serendipita indica*: modulation of stress-responsive gene expression and antioxidant defense system activation. *Environ. Pollut.* 350:123952. doi: 10.1016/j.envpol.2024.123952

Alam, M., Hussain, Z., Khan, A., Khan, M. A., Rab, A., Asif, M., et al. (2020). The effects of organic amendments on heavy metals bioavailability in mine impacted soil and associated human health risk. *Sci. Hortic.* 262:109067. doi: 10.1016/j.scienta.2019.109067

Ali, I., Adnan, M., Ullah, S., Zhao, Q., Iqbal, A., He, L., et al. (2022a). Biochar combined with nitrogen fertilizer: a practical approach for increasing the biomass digestibility and yield of rice and promoting food and energy security. *Biofuels Bioprod. Biorefin.* 16, 1304–1318. doi: 10.1002/bbb.2334

Ali, I., Iqbal, A., Ullah, S., Muhammad, I., Yuan, P., Zhao, Q., et al. (2022b). Effects of biochar amendment and nitrogen fertilizer on RVA profile and rice grain quality attributes. *Food Secur.* 11:625. doi: 10.3390/foods11050625

Ali, I., Ullah, S., He, L., Zhao, Q., Iqbal, A., Wei, S., et al. (2020). Combined application of biochar and nitrogen fertilizer improves rice yield, microbial activity and N-metabolism in a pot experiment. *PeerJ* 8:e10311. doi: 10.7717/peerj.10311

Ali, I., Yuan, P., Ullah, S., Iqbal, A., Zhao, Q., Liang, H., et al. (2022c). Biochar amendment and nitrogen fertilizer contribute to the changes in soil properties and microbial communities in a paddy field. *Front. Microbiol.* 13:834751. doi: 10.3389/fmicb.2022.834751

Ali, I., Zhao, Q., Wu, K., Ullah, S., Iqbal, A., Liang, H., et al. (2021). Biochar in combination with nitrogen fertilizer is a technique: to enhance physiological and morphological traits of Rice (*Oryza sativa* L.) by improving soil physio-biochemical properties. *J. Plant Growth Regul.* 41, 2406–2420. doi: 10.1007/s00344-021-10454-8

Aslam, Z., Ahmad, A., Bellitürk, K., Iqbal, N., Idrees, M., Ur Rehman, W., et al. (2020). Effects of vermicompost, vermi-tea and chemical fertilizer on morpho-physiological characteristics of tomato (*Solanum lycopersicum*) in Suleymanpasa District, Tekirdag of Turkey. *Pure Appl. Biol.* 9, 1920–1931. doi: 10.19045/bspab.2020.90205

Anjum, N., Umar, S., Iqbal, M., Khan, N. (2011). Cadmium causes oxidative stress in mung bean by affecting the antioxidant enzyme system and ascorbate-glutathione cycle metabolism. *Russ. J. Plant Physiol*, 58:92–99.

Bari, M. A., Akther, M. S., Reza, M. A., and Kabir, A. H. (2019). Cadmium tolerance is associated with the root-driven coordination of cadmium sequestration, iron regulation, and ROS scavenging in rice. *Plant Physiol. Biochem.* 136, 22–33. doi: 10.1016/j.plaphy.2019.01.007

Bates, L. S., Waldren, R. A., and Teare, I. D. (1973). Rapid determination of free proline for water-stress studies. *Plant Soil* 39, 205–207. doi: 10.1007/BF00018060

Bauddh, K., and Singh, R. P. (2012). Growth, tolerance efficiency and phytoremediation potential of *Ricinus communis* (L.) and *Brassica juncea* (L.) in salinity and drought affected cadmium contaminated soil. *Ecotoxicol. Environ. Saf.* 85, 13–22. doi: 10.1016/j.ecoenv.2012.08.019

Bin Rahman, A. R., and Zhang, J. (2023). Trends in rice research: 2030 and beyond. *Food Energy Secur.* 12:e390. doi: 10.1002/fes3.390

Bradford, M. M. (1976). A rapid and sensitive method for the quantitation of microgram quantities of protein utilizing the principle of protein-dye binding. *Anal. Biochem.* 72, 248–254. doi: 10.1016/0003-2697(76)90527-3

Bradham, K. D., Diamond, G. L., Nelson, C. M., Noerpel, M., Scheckel, K. G., Elek, B., et al. (2018). Long-term in situ reduction in soil lead bioavailability measured in a mouse model. *Environ. Sci. Technol.* 52, 13908–13913. doi: 10.1021/acs.est.8b04684

Cambier, P., Michaud, A., Paradelo, R., Germain, M., Mercier, V., Guérin-Lebourg, A., et al. (2019). Trace metal availability in soil horizons amended with various urban waste composts during 17 years–monitoring and modelling. *Sci. Total Environ.* 651, 2961–2974. doi: 10.1016/j.scitotenv.2018.10.013

Cao, F., Wang, R., Cheng, W., Zeng, F., Ahmed, I. M., Hu, X., et al. (2014). Genotypic and environmental variation in cadmium, chromium, lead and copper in rice and approaches for reducing the accumulation. *Sci. Total Environ.* 496, 275–281. doi: 10.1016/j.scitotenv.2014.07.064

Charan, K., Bhattacharyya, P., and Bhattacharya, S. S. (2024). Vermitechnology transforms hazardous red mud into benign organic input for agriculture: insights on earthworm-microbe interaction, metal removal, and soil-crop improvement. *J. Environ. Manag.* 354:120320. doi: 10.1016/j.jenvman.2024.120320

Chauhan, B. S., Jabran, K., and Mahajan, G. (2017). Rice production worldwide. Berlin, Heidelberg: Springer.

Chen, Y., Jiang, Y., Huang, H., Mou, L., Ru, J., Zhao, J., et al. (2018). Long-term and high-concentration heavy-metal contamination strongly influences the microbiome and functional genes in Yellow River sediments. *Sci. Total Environ.* 637-638, 1400–1412. doi: 10.1016/j.scitotenv.2018.05.109

Chen, Q., Lu, X., Guo, X., Pan, Y., Yu, B., Tang, Z., et al. (2018). Differential responses to cd stress induced by exogenous application of cu, Zn or ca in the medicinal plant *Catharanthus roseus*. *Ecotoxicol. Environ. Saf.* 157, 266–275. doi: 10.1016/j.ecoenv.2018.03.055

Dabral, S., Varma, A., Choudhary, D. K., Bahuguna, R. N., and Nath, M. (2019). Biopriming with Piriformospora indica ameliorates cadmium stress in rice by lowering oxidative stress and cell death in root cells. *Ecotoxicol. Environ. Saf.* 186:109741. doi: 10.1016/j.ecoenv.2019.109741

Daszkowska-Golec, A., and Szarejko, I. (2013). Open or close the gate–stomata action under the control of phytohormones in drought stress conditions. *Front. Plant Sci.* 4:138. doi: 10.3389/fpls.2013.00138

Deng, X., Wu, C., Li, Q., and Li, W., (2017). Effect of vermicompost on soil enzyme activity of coastal saline soil in water spinach plantation. In 2017 6th international conference on energy, environment and sustainable development (ICEESD 2017), 419–422). Atlantis Press.

Ding, Z., Kheir, A. M., Ali, O. A., Hafez, E. M., ElShamey, E. A., Zhou, Z., et al. (2021). A vermicompost and deep tillage system to improve saline-sodic soil quality and wheat productivity. *J. Environ. Manag.* 277:111388. doi: 10.1016/j.jenvman.2020.111388

Dubey, R. K., Dubey, P. K., Chaurasia, R., Singh, H. B., and Abhilash, P. C. (2020). Sustainable agronomic practices for enhancing the soil quality and yield of *Cicer arietinum* L. under diverse agroecosystems. *J. Environ. Manag.* 262:110284. doi: 10.1016/j.jenvman.2020.110284

Elmer, W., and White, J. C. (2018). The future of nanotechnology in plant pathology. *Annu. Rev. Phytopathol.* 56, 111–133. doi: 10.1146/annurev-phyto-080417-050108

Fernández-Bayo, J. D., Nogales, R., and Romero, E. (2009). Assessment of three vermicomposts as organic amendments used to enhance diuron sorption in soils with low organic carbon content. *Eur. J. Soil Sci.* 60, 935–944. doi: 10.1111/j.1365-2389.2009.01176.x

Gallego, S. M., Pena, L. B., Barcia, R. A., Azpilicueta, C. E., Iannone, M. F., Rosales, E. P., et al. (2012). Unravelling cadmium toxicity and tolerance in plants: insight into regulatory mechanisms. *Environ. Exp. Bot.* 83, 33–46. doi: 10.1016/j.envexpbot.2012.04.006

Gao, J., Xu, G., Qian, H., Liu, P., Zhao, P., and Hu, Y. (2013). Effects of nano-TiO2 on photosynthetic characteristics of Ulmus elongata seedlings. *Environ. Pollut.* 176, 63–70. doi: 10.1016/j.envpol.2013.01.027

Goswami, L., Ekblad, A., Choudhury, R., and Bhattacharya, S. S. (2024). Vermi-converted tea industry coal ash efficiently substitutes chemical fertilization for growth and yield of cabbage (*Brassica oleracea var. capitata*) in an alluvial soil: a field-based study on soil quality, nutrient translocation, and metal-risk remediation. *Sci. Total Environ.* 907:168088. doi: 10.1016/j.scitotenv.2023.168088

Gu, J. F., Zhou, H., Tang, H. L., Yang, W. T., Zeng, M., Liu, Z. M., et al. (2019). Cadmium and arsenic accumulation during the rice growth period under in situ remediation. *Ecotoxicol. Environ. Saf.* 171, 451–459. doi: 10.1016/j.ecoenv.2019.01.003

Gul, S., Whalen, J. K., Thomas, B. W., Sachdeva, V., and Deng, H. (2015). Physico-chemical properties and microbial responses in biochar-amended soils: mechanisms and future directions. *Agric. Ecosyst. Environ.* 206, 46–59. doi: 10.1016/j.agee.2015.03.015

Haider, F. U., Liqun, C., Coulter, J. A., Cheema, S. A., Wu, J., Zhang, R., et al. (2021). Cadmium toxicity in plants: impacts and remediation strategies. *Ecotoxicol. Environ. Saf.* 211:111887. doi: 10.1016/j.ecoenv.2020.111887

Hamid, Y., Tang, L., Hussain, B., Usman, M., Lin, Q., Rashid, M. S., et al. (2020). Organic soil additives for the remediation of cadmium contaminated soils and their impact on the soil-plant system: a review. *Sci. Total Environ.* 707:136121. doi: 10.1016/j.scitotenv.2019.136121

Hasanuzzaman, M., Bhuyan, M. B., Zulfiqar, F., Raza, A., Mohsin, S. M., Mahmud, J. A., et al. (2020). Reactive oxygen species and antioxidant defense in plants under abiotic stress: revisiting the crucial role of a universal defense regulator. *Antioxidants* 9:681. doi: 10.3390/antiox9080681

Huang, Y., Wang, L., Wang, W., Li, T., He, Z., and Yang, X. (2019). Current status of agricultural soil pollution by heavy metals in China: a meta-analysis. *Sci. Total Environ.* 651, 3034–3042. doi: 10.1016/j.scitotenv.2018.10.185

Huang, L. M., Yu, G. W., Zou, F. Z., Long, X. X., and Wu, Q. T. (2018). Shift of soil bacterial community and decrease of metals bioavailability after immobilization of a multi-metal contaminated acidic soil by inorganic-organic mixed amendments: a field study. *Appl. Soil Ecol.* 130, 104–119. doi: 10.1016/j.apsoil.2018.05.014

Hussain, N., Chatterjee, S. K., Maiti, T. K., Goswami, L., das, S., Deb, U., et al. (2021). Metal induced non-metallothionein protein in earthworm: a new pathway for cadmium detoxification in chloragogenous tissue. *J. Hazard. Mater.* 401:123357. doi: 10.1016/j.jhazmat.2020.123357

Huybrechts, M., Hendrix, S., Bertels, J., Beemster, G. T., Vandamme, D., and Cuypers, A. (2020). Spatial analysis of the rice leaf growth zone under controlled and cadmium-exposed conditions. *Environ. Exp. Bot.* 177:104120. doi: 10.1016/j.envexpbot.2020.104120

Igalavithana, A. D., Park, J., Ryu, C., Lee, Y. H., Hashimoto, Y., Huang, L., et al. (2017). Slow pyrolyzed biochars from crop residues for soil metal (loid) immobilization and microbial community abundance in contaminated agricultural soils. *Chemosphere* 177, 157–166. doi: 10.1016/j.chemosphere.2017.02.112

Imran, M., Hussain, S., el-Esawi, M. A., Rana, M. S., Saleem, M. H., Riaz, M., et al. (2020). Molybdenum supply alleviates the cadmium toxicity in fragrant rice by modulating oxidative stress and antioxidant gene expression. *Biomol. Ther.* 10:1582. doi: 10.3390/biom10111582

Iqbal, A., Ali, I., Yuan, P., Khan, R., Liang, H., Wei, S., et al. (2022). Combined application of manure and chemical fertilizers alters soil environmental variables and improves soil fungal community composition and rice grain yield. *Front. Microbiol.* 13:856355. doi: 10.3389/fmicb.2022.856355

Iqbal, A., He, L., Ali, I., Ullah, S., Khan, A., Khan, A., et al. (2020). Manure combined with chemical fertilizer increases rice productivity by improving soil health, post-anthesis biomass yield, and nitrogen metabolism. *PLoS One* 15:e0238934. doi: 10.1371/journal.pone.0238934

Iqbal, A., He, L., Khan, A., Wei, S., Akhtar, K., Ali, I., et al. (2019). Organic manure coupled with inorganic fertilizer: an approach for the sustainable production of rice by

improving soil properties and nitrogen use efficiency. *Agronomy* 9:651. doi: 10.3390/agronomy9100651

Iqbal, A., He, L., McBride, S. G., Ali, I., Akhtar, K., Khan, R., et al. (2021a). Manure applications combined with chemical fertilizer improves soil functionality. Microbial biomass and rice production in a paddy field. *Agro* 114, 1431–1446. doi: 10.1002/agj2.20990

Iqbal, A., Hussain, Q., Mo, Z., Hua, T., Mustafa, A. E. Z. M., and Tang, X. (2024a). Vermicompost supply enhances fragrant-Rice yield by improving soil fertility and eukaryotic microbial community composition under environmental stress conditions. *Microorganisms* 12:1252. doi: 10.3390/microorganisms12061252

Iqbal, A., Khan, A., Green, S. J., Ali, I., He, L., Zeeshan, M., et al. (2021b). Long-term straw mulching in a no-till field improves soil functionality and rice yield by increasing soil enzymatic activity and chemical properties in paddy soils. *J. Plant Nutr. Soil Sci.* 184, 622–634. doi: 10.1002/jpln.202100089

Iqbal, A., Ligeng, J., Mo, Z., Adnan, M., Lal, R., Zaman, M., et al. (2024b). Substation of vermicompost mitigates cd toxicity, improves rice yields and restores bacterial community in a cd-contaminated soil in southern China. *J. Hazard. Mater.* 465:133118. doi: 10.1016/j.jhazmat.2023.133118

Iqbal, A., Mo, Z., Pan, S. G., Qi, J. Y., Hua, T., Imran, M., et al. (2023a). Exogenous TiO2 nanoparticles alleviate cd toxicity by reducing cd uptake and regulating plant physiological activity and antioxidant defense Systems in Rice (*Oryza sativa* L.). *Meta* 13:765. doi: 10.3390/metabo13060765

Iqbal, A., Tang, X., Ali, I., Yuan, P., Khan, R., Khan, Z., et al. (2023b). Integrating low levels of organic fertilizer improves soil fertility and rice yields in paddy fields by influencing microbial communities without increasing CH4 emissions. *Appl. Soil Ecol.* 189:104951. doi: 10.1016/j.apsoil.2023.104951

Islam, M. N., Taki, G., Nguyen, X. P., Jo, Y. T., Kim, J., and Park, J. H. (2017). Heavy metal stabilization in contaminated soil by treatment with calcined cockle shell. *Environ. Sci. Pollut. Res.* 24, 7177–7183. doi: 10.1007/s11356-016-8330-5

Jackson, M. L. (1956). Soil chemical analysis-advanced course, published by the author. Wisconsin: Madison, 991.

Jiang, M., and Zhang, J. (2001). Effect of abscisic acid on active oxygen species, antioxidative defence system and oxidative damage in leaves of maize seedlings. *Plant Cell Physiol.* 42, 1265–1273. doi: 10.1093/pcp/pce162

Khan, M. N., Li, Y., Khan, Z., Chen, L., Liu, J., Hu, J., et al. (2021). Nanoceria seed priming enhanced salt tolerance in rapeseed through modulating ROS homeostasis and α-amylase activities. *J. Nanobiotechnol.* 19, 1–19. doi: 10.1186/s12951-021-01026-9

Khan, A., Najeeb, U., Wang, L., Tan, D. K. Y., Yang, G., Munsif, F., et al. (2017). Planting density and sowing date strongly influence growth and lint yield of cotton crops. *Field Crop Res.* 209, 129–135. doi: 10.1016/j.fcr.2017.04.019

Khan, S., Sehar, Z., Fatma, M., Mir, I. R., Iqbal, N., Tarighat, M. A., et al. (2022). Involvement of ethylene in melatonin-modified photosynthetic-N use efficiency and antioxidant activity to improve photosynthesis of salt grown wheat. *Physiol. Plant.* 174:e13832. doi: 10.1111/ppl.13832

Liang, L., Liu, W., Sun, Y., Huo, X., Li, S., and Zhou, Q. (2017). Phytoremediation of heavy metal contaminated saline soils using halophytes: current progress and future perspectives. *Environ. Rev.* 25, 269–281. doi: 10.1139/er-2016-0063

Lim, S. L., Wu, T. Y., Lim, P. N., and Shak, K. P. Y. (2015). The use of vermicompost in organic farming: overview, effects on soil and economics. *J. Sci. Food Agric.* 95, 1143–1156. doi: 10.1002/jsfa.6849

Li, J., Lu, Y., Shim, H., Deng, X., Lian, J., Jia, J., et al. (2010). Use of the BCR sequential extraction procedure for the study of metal availability to plants. *J. Environ. Monit*. 12, 466–471. doi: 10.1039/B916389A

Lu, R. K. (2000). Analytical methods of soil and Agrochemistry. Beijing: China Agricultural Science and Technology Press.

Luo, H., He, L., Du, B., Pan, S., Mo, Z., Duan, M., et al. (2020). Biofortification with chelating selenium in fragrant rice: effects on photosynthetic rates, aroma, grain quality and yield formation. *Field Crop Res.* 255:107909. doi: 10.1016/j.fcr.2020.107909

Luo, Y., Iqbal, A., He, L., Zhao, Q., Wei, S., Ali, I., et al. (2020). Long-term no-tillage and straw retention management enhances soil bacterial community diversity and soil properties in southern China. *Agronomy* 10:1233. doi: 10.3390/agronomy10091233

Maji, D., Misra, P., Singh, S., and Kalra, A. (2017). Humic acid rich vermicompost promotes plant growth by improving microbial community structure of soil as well as root nodulation and mycorrhizal colonization in the roots of *Pisum sativum*. *Appl. Soil Ecol.* 110, 97–108. doi: 10.1016/j.apsoil.2016.10.008

Makoto, K., and Koike, T. (2007). Effects of nitrogen supply on photosynthetic and anatomical changes in current-year needles of *Pinus koraiensis* seedlings grown under two irradiances. *Photosynthetica* 45, 99–104. doi: 10.1007/s11099-007-0015-3

Mitra, S., Pramanik, K., Sarkar, A., Ghosh, P. K., Soren, T., and Maiti, T. K. (2018). Bioaccumulation of cadmium by Enterobacter sp. and enhancement of rice seedling growth under cadmium stress. *Ecotoxicol. Environ. Saf.* 156, 183–196. doi: 10.1016/j.ecoenv.2018.03.001

Moustafa-Farag, M., Mahmoud, A., Arnao, M. B., Sheteiwy, M. S., Dafea, M., Soltan, M., et al. (2020). Melatonin-induced water stress tolerance in plants: recent advances. *Antioxidants* 9:809. doi: 10.3390/antiox9090809

Muneer, S., Qadri, T. N., and Siddiqi, T. O. (2011). Cytogenetic and biochemical investigations to study the response of *Vigna radiata* to cadmium stress. *African J. Plant Sci.* 5, 183–192.

Ni, K., Shi, Y. Z., Yi, X. Y., Zhang, Q. F., Fang, L., Ma, L. F., et al. (2018). Effects of long-term nitrogen application on soil acidification and solution chemistry of a tea plantation in China. *Agric, Ecosyst Environ* 252:74–82. doi: 10.1016/j.agee.2017.10.004

Ohyama, T. (1991). Analytical procedures of N, P, K contents in plant and manure materials using H2SO4-H2O2 Kjeldahl digestion method. *Bull. Facul. Agric. Niigata Univ.* 43, 111–120.

Palma, J. M., Sandalio, L. M., Corpas, F. J., Romero-Puertas, M. C., McCarthy, I., and del Río, L. A. (2002). Plant proteases, protein degradation, and oxidative stress: role of peroxisomes. *Plant Physiol. Biochem.* 40, 521–530. doi: 10.1016/S0981-9428(02)01404-3

Parmar, P., Kumari, N., and Sharma, V. (2013). Structural and functional alterations in photosynthetic apparatus of plants under cadmium stress. *Bot. Stud.* 54, 1–6. doi: 10.1186/1999-3110-54-45

Pathma, J., and Sakthivel, N. (2012). Microbial diversity of vermicompost bacteria that exhibit useful agricultural traits and waste management potential. *Springerplus* 1, 1–19. doi: 10.1186/2193-1801-1-26

Pfafflfl, M. W. (2001). A new mathematical model for relative quantifification in real-time RT–PCR. *Nucleic Acids Res.* 29:e45, 45e–445e. doi: 10.1093/nar/29.9.e45

Pramanik, K., Mitra, S., Sarkar, A., and Maiti, T. K. (2018). Alleviation of phytotoxic effects of cadmium on rice seedlings by cadmium resistant PGPR strain *Enterobacter aerogenes* MCC 3092. *J. Hazard. Mater.* 351, 317–329. doi: 10.1016/j.jhazmat.2018.03.009

Rizwan, M., Ali, S., Abbas, T., Zia-ur-Rehman, M., Hannan, F., Keller, C., et al. (2016). Cadmium minimization in wheat: a critical review. *Ecotoxicol. Environ. Saf.* 130, 43–53. doi: 10.1016/j.ecoenv.2016.04.001

Roland, J. C., and Vian, B. (1991). 1–general preparation and staining of thin sections. *Electron. Microsc. Plant Cells* 40, 1–66.

Sanchez-Casas, P., and Klessig, D. F. (1994). A salicylic acid-binding activity and a salicylic acid-inhibitable catalase activity are present in a variety of plant species. *Plant Physiol.* 106, 1675–1679. doi: 10.1104/pp.106.4.1675

Seleiman, M. F., Ali, S., Refay, Y., Rizwan, M., Alhammad, B. A., and El-Hendawy, S. E. (2020). Chromium resistant microbes and melatonin reduced Cr uptake and toxicity, improved physio-biochemical traits and yield of wheat in contaminated soil. *Chemosphere* 250:126239. doi: 10.1016/j.chemosphere.2020.126239

Shaheen, S. M., and Rinklebe, J. (2015). Impact of emerging and low cost alternative amendments on the (im) mobilization and phytoavailability of cd and Pb in a contaminated floodplain soil. *Ecol. Eng.* 74, 319–326. doi: 10.1016/j.ecoleng.2014.10.024

Singh, P., Singh, I., and Shah, K. (2020). Alterations in antioxidative machinery and growth parameters upon application of nitric oxide donor that reduces detrimental effects of cadmium in rice seedlings with increasing days of growth. *S. Afr. J. Bot.* 131, 283–294. doi: 10.1016/j.sajb.2020.02.022

Song, W. E., Chen, S. B., Liu, J. F., Chen, L., Song, N., Li, N., et al. (2015). Variation of cd concentration in various rice cultivars and derivation of cadmium toxicity thresholds for paddy soil by species-sensitivity distribution. *J. Integr. Agric.* 2015, 1845–1854. doi: 10.1016/S2095-3119(14)60926-6

Tang, X., Li, X., Liu, X., Hashmi, M. Z., Xu, J., and Brookes, P. C. (2015). Effects of inorganic and organic amendments on the uptake of lead and trace elements by *Brassica chinensis* grown in an acidic red soil. *Chemosphere* 119, 177–183. doi: 10.1016/j.chemosphere.2014.05.081

Tang, J., Zhang, J., Ren, L., Zhou, Y., Gao, J., Luo, L., et al. (2019). Diagnosis of soil contamination using microbiological indices: a review on heavy metal pollution. *J. Environ. Manag.* 242, 121–130. doi: 10.1016/j.jenvman.2019.04.061

Tejada, M., Gómez, I., Hernández, T., and García, C. (2010). Utilization of vermicomposts in soil restoration: effects on soil biological properties. *Soil Sci. Soc. Am. J.* 74, 525–532. doi: 10.2136/sssaj2009.0260

Tran, T. A., and Popova, L. P. (2013). Functions and toxicity of cadmium in plants: recent advances and future prospects. *Turk. J. Bot.* 37, 1–13. doi: 10.3906/bot-1112-16

Ullah, S., Liang, H., Ali, I., Zhao, Q., Iqbal, A., Wei, S., et al. (2020). Biochar coupled with contrasting nitrogen sources mediated changes in carbon and nitrogen pools, microbial and enzymatic activity in paddy soil. *J. Saudi Chem. Soc.* 24, 835–849. doi: 10.1016/j.jscs.2020.08.008

Velikova, V., Yordanov, I., and Edreva, A. J. (2000). Oxidative stress and some antioxidant systems in acid rain-treated bean plants: protective role of exogenous polyamines. *Plant Sci.* 151, 59–66. doi: 10.1016/S0168-9452(99)00197-1

Wan, Y., Huang, Q., Wang, Q., Yu, Y., Su, D., Qiao, Y., et al. (2020). Accumulation and bioavailability of heavy metals in an acid soil and their uptake by paddy rice under continuous application of chicken and swine manure. *J. Hazard. Mater.* 384:121293. doi: 10.1016/j.jhazmat.2019.121293

Wang, S., Tian, H., Liu, J., and Pan, S. (2003). Pattern and change of soil organic carbon storage in China: 1960s–1980s. *Tellus Ser. B Chem. Phys. Meteorol.* 55, 416–427. doi: 10.1034/j.1600-0889.2003.00039.x

Wang, Y., Xu, Y., Li, D., Tang, B., Man, S., Jia, Y., et al. (2018). Vermicompost and biochar as bio-conditioners to immobilize heavy metal and improve soil fertility on cadmium contaminated soil under acid rain stress. *Sci. Total Environ.* 621, 1057–1065. doi: 10.1016/j.scitotenv.2017.10.121

Wu, M., Wang, P. Y., Sun, L. G., Zhang, J. J., Yu, J., Wang, Y. W., et al. (2014). Alleviation of cadmium toxicity by cerium in rice seedlings is related to improved photosynthesis, elevated antioxidant enzymes and decreased oxidative stress. *Plant Growth Regul.* 74, 251–260. doi: 10.1007/s10725-014-9916-x

Wu, F., Zhang, G., and Dominy, P. (2003). Four barley genotypes respond differently to cadmium: lipid peroxidation and activities of antioxidant capacity. *Environ. Exp. Bot.* 50, 67–78. doi: 10.1016/S0098-8472(02)00113-2

Xue, S., Shi, L., Wu, C., Wu, H., Qin, Y., Pan, W., et al. (2017). Cadmium, lead, and arsenic contamination in paddy soils of a mining area and their exposure effects on human HEPG2 and keratinocyte cell-lines. *Environ. Res.* 156, 23–30. doi: 10.1016/j.envres.2017.03.014

Yang, B., Xiong, Z., Wang, J., Xu, X., Huang, Q., and Shen, Q. (2015). Mitigating net global warming potential and greenhouse gas intensities by substituting chemical nitrogen fertilizers with organic fertilization strategies in rice–wheat annual rotation systems in China: a 3-year field experiment. *Ecol. Eng.* 81, 289–297. doi: 10.1016/j.ecoleng.2015.04.071

Yuan, P., Li, X., Ni, M., Cao, C., Jiang, L., Iqbal, A., et al. (2022). Effects of straw return and feed addition on the environment and nitrogen use efficiency under different nitrogen application rates in the rice–crayfish system. *Plant Soil* 475, 411–426. doi: 10.1007/s11104-022-05376-7

Zeng, S., Ma, J., Yang, Y., Zhang, S., Liu, G. J., and Chen, F. (2019). Spatial assessment of farmland soil pollution and its potential human health risks in China. *Sci. Total Environ.* 687, 642–653. doi: 10.1016/j.scitotenv.2019.05.291

Zhang, W., Du, W., Wang, F., Xu, H., Zhao, T., Zhang, H., et al. (2020). Comparative study on Pb^{2+} removal from aqueous solutions using biochars derived from cow manure and its vermicompost. *Sci. Total Environ.* 716:137108. doi: 10.1016/j.scitotenv.2020.137108

Zhang, J., Sun, X., Xu, M., Zhao, X., Yang, C., Li, K., et al. (2022). A self-amplifying ROS-sensitive prodrug-based nanodecoy for circumventing immune resistance in chemotherapy-sensitized immunotherapy. *Acta Biomater.* 149, 307–320. doi: 10.1016/j.actbio.2022.06.035

Zhu, W., Du, W., Shen, X., Zhang, H., and Ding, Y. (2017). Comparative adsorption of Pb2+ and Cd2+ by cow manure and its vermicompost. *Environ. Pollut.* 227, 89–97. doi: 10.1016/j.envpol.2017.04.048

frontiers | Frontiers in Sustainable Food Systems

TYPE Original Research
PUBLISHED 29 August 2024
DOI 10.3389/fsufs.2024.1431339

OPEN ACCESS

EDITED BY
Aliza Pradhan,
National Institute of Abiotic Stress Management (ICAR), India

REVIEWED BY
Dibakar Roy,
National Bureau of Soil Survey and Land Use Planning (ICAR), India
Susanta Jena,
Indian Institute of Water Management (ICAR), India

*CORRESPONDENCE
Hongjian Fan
✉ 201820828@stumail.nwu.edu.cn

RECEIVED 11 May 2024
ACCEPTED 13 August 2024
PUBLISHED 29 August 2024

CITATION
Fan H, Xue L and Ma H (2024) Optimization of planting date and irrigation strategy for sustainable cotton production.
Front. Sustain. Food Syst. 8:1431339.
doi: 10.3389/fsufs.2024.1431339

Optimization of planting date and irrigation strategy for sustainable cotton production

Hongjian Fan[1,2,3]*, Lu Xue[4] and Hao Ma[5]

[1]Land Engineering Technology Transformation Center, Shaanxi Provincial Land Engineering Construction Group Co., Ltd., Xi'an, China, [2]Land Engineering Technology Innovation Center, Ministry of Natural Resources, Shaanxi Provincial Land Engineering Construction Group Co., Ltd., Xi'an, China, [3]Institute of Land Engineering and Technology, Shaanxi Provincial Land Engineering Construction Group Co., Ltd., Xi'an, China, [4]College of Life Science, Yulin University, Yulin, China, [5]School of Electronic Information, Xijing University, Xi'an, China

Introduction: The study aims to evaluate the impact of climatological factors on rice yield and methane emissions in Southern Shaanxi's rice cultivation areas, with the goal of informing effective Climate-Smart Agriculture (CSA) strategies.

Methods: A three-year longitudinal analysis (2017-2019) was conducted, examining the correlation between rice productivity and weather conditions within the agricultural ecosystem. Data on rice yields and methane emissions were collected and analyzed to determine patterns and trends.

Results: Significant correlations were identified between rice yield and weather conditions, with favorable weather for rice growth correlating with higher methane emissions. Methane emissions were particularly high during the vegetative and reproductive stages of rice growth, peaking 60 to 90 days after transplanting. Average emissions for this period were 245.2±80.1 kg CH4 ha-1 in 2017, 274.2±93.9 kg CH4 ha-1 in 2018, and 339.6±50.3 kg CH4 ha-1 in 2019. Total cumulative methane emissions over the entire rice cultivation period were 635.0±177.2 kg CH4 ha-1 in 2017, 661.2±239.2 kg CH4 ha-1 in 2018, and 679.4±205.4 kg CH4 ha-1 in 2019, with no statistically significant interannual differences.

Discussion: The findings highlight the need to balance the goals of reducing greenhouse gas emissions for climate change mitigation with the enhancement of rice yield within CSA practices. The organic link between rice productivity and methane emissions under varying weather conditions suggests that an integrated approach to CSA is essential, considering climate adaptability, productivity, and greenhouse gas reduction. The study's results contribute to a deeper scientific understanding of local agricultural ecosystems and provide a basis for developing management techniques for CSA.

Conclusion: An integrated approach to CSA that takes into account the interplay between rice yield, methane emissions, and climatological factors is crucial for achieving sustainable agricultural practices in Southern Shaanxi. The study's insights can guide the development of strategies that enhance both rice productivity and environmental sustainability.

KEYWORDS

AquaCrop model, irrigation quota, planting date, predicting yield, climate change

1 Introduction

With the extensive application of sub-surface drip irrigation, Xinjiang has become China's largest producer of high-quality cotton (Ren et al., 2021; Ding et al., 2023). According to statistics, in 2021, the cotton planting area in Xinjiang was 2.5061 million hectares, with a production of 5.129 million tons, accounting for 82.76 and 89.50% of the national total, respectively. The unique climatic environment of Xinjiang is conducive to the growth and high-quality, high-yield production of cotton (Feng et al., 2017; Zhou et al., 2024). However, water scarcity limits the sustainable production of cotton. Moreover, climate change exacerbates the pressure on the Earth's available water resources. The Fifth Assessment Report by the Intergovernmental Panel on Climate Change (IPCC) indicates that from 2003 to 2012, the global average surface temperature rose by 0.78°C compared to the period from 1850 to 1900, and it is projected to increase by 4.8°C by 2,100. Precipitation in arid regions may decrease, while it may increase in humid areas. In the northwest region of China, by the end of the 21st century (2081–2,100), under extreme conditions, the average temperature may change by 1.5–2.0°C, and the average precipitation may change by 10 to 20%. The warming may lead to an increase in crop evapotranspiration, resulting in a 70–90% increase in irrigation water demand (Tanasijevic et al., 2014; Saadi et al., 2015; Li et al., 2020). Climate change directly affects cotton yield by damaging morphological development and plant growth, which is undoubtedly a double blow to the sustainable production of cotton in Xinjiang (Chen and Dong, 2016; Khalid et al., 2023). Therefore, measures should be taken to mitigate the impact of climate change on agricultural production, such as selecting the optimal planting time for crops (Bisbis et al., 2018) and formulating irrigation strategies to ensure improved water productivity (Kang et al., 2017).

Considering the complexity of the agricultural ecosystem and the limitations of field experiments, using crop growth models to simulate crop growth processes and yields is an important approach to addressing the impacts of climate change and human activities and achieving water-saving and increased agricultural production (Zou et al., 2020; Surendran et al., 2021). Crop growth models are quantitative and dynamic mechanistic models that integrate knowledge and research results from disciplines such as crop physiology, ecology, agricultural meteorology, and soil science to describe crop production. They have been widely used in predicting crop production potential and guiding agricultural irrigation, fertilization, and cultivation management practices (Zinkernagel et al., 2020). The AquaCrop model, developed by the Food and Agriculture Organization (FAO) of the United Nations, is a water-driven crop growth model specifically designed for arid and semi-arid regions in developing countries in Africa and Asia (Kim and Kaluarachchi, 2015; Foster et al., 2017). It transforms water productivity into biomass and then into yield through the harvest index, with advantages such as fewer input parameters, a wide range of applications, and high accuracy (Kim and Kaluarachchi, 2015; Foster et al., 2017; Zinkernagel et al., 2020). Previously, scholars have applied the AquaCrop model to crops such as wheat (Andarzian et al., 2011; Jin et al., 2014), barley (Araya et al., 2010), quinoa (Abrha et al., 2012), soybeans (Khoshravesh et al., 2013), corn (Abedinpour et al., 2012), cotton (Linker et al., 2016), and sugar beets (Stricevic et al., 2011), conducting research on crop growth, development, biomass, and yield under different irrigation systems (Greaves and Wang, 2016), irrigation methods (Geerts et al., 2010), and covering methods (Sandhu and Irmak, 2019). However, there are few reports on how to optimize irrigation strategies and adjust planting dates to improve the sustainability and profitability of cotton production under limited available water resources. Although the AquaCrop model has been localized in arid and semi-arid regions and has made certain progress in verification and application, there is less research on the growth and yield of cotton in arid regions, such as southern Xinjiang, and its response to climate change. Therefore, this study takes the cotton under mulch drip irrigation in the oasis area as the research object, localizes the parameters of the AquaCrop model, verifies the applicability of the model in simulating the growth and yield of cotton under mulch drip irrigation, simulates the impact of different irrigation and planting dates on the accumulation of cotton biomass and yield based on 30 years of meteorological data from 1988 to 2017, and analyzes the stability and sustainability of cotton yield. The aim is to provide a basis for optimizing irrigation strategies and adjusting planting dates to improve the sustainability and profitability of cotton production under limited water resources.

2 Materials and methods

2.1 Experimental area overview

The experimental area is located in Aksu City, near the confluence of the three main sources of the Tarim River (Aksu River, Yarkand River, and Hotan River) in the plain desert oasis, which belongs to a typical inland extremely arid climate. The multi-year average precipitation is 50 mm, the annual evaporation is 2,218 mm, the annual average sunshine duration is 2,950 h, the frost-free period averages 207 days, and the annual average temperature is 11.3°C, making it a typical irrigated agricultural area.

2.2 Field experiments

Starting from the cotton bud stage, the irrigation frequency was determined using meteorological information, and irrigation was conducted when the difference between the evapotranspiration and precipitation reached 30 mm (Conaty et al., 2015). Currently, the irrigation

TABLE 1 Cotton irrigation scheduling in 2017 and 2018.

Irrigation date (mm-dd)		Irrigation quota (mm)		
2017	2018	T_1	T_2	T_3
06–07	06–16	24	30	36
06–17	06–26	24	30	36
06–23	07–06	24	30	36
07–03	07–13	24	30	36
07–10	07–19	24	30	36
07–14	07–26	24	30	36
07–25	08–03	24	30	36
07–31	08–08	24	30	36
08–06	08–14	24	30	36
08–13	08–20	24	30	36
08–20	08–26	24	30	36
Total amount (mm)		264	330	396

quota for cotton under mulch drip irrigation in southern Xinjiang is around 30 mm, with slight variations across different regions, but the difference is not significant. Based on this, three irrigation quotas for cotton under mulch drip irrigation were set, namely T1: 30×0.8=24 mm, T2: 30×1.0=30 mm, T3: 30×1.2=36 mm, as shown in Table 1. Each treatment was replicated three times, totaling nine plots.

The cotton sowing date in 2017 was April 3, and all cotton was harvested by October 1. In 2018, the sowing date was April 15, and all cotton was harvested by October 12. The cotton variety was "Xin Lu Zhong 46," and the experimental plot area was 154 square meters. The planting pattern was 1 film, 2 rows, and 6 rows, with row spacing of 10 cm + 66 cm + 10 cm + 66 cm + 10 cm, and plant spacing of 10 cm, as shown in Figure 1. The drip tape specification was φ16, with a drip head spacing of 20 cm and a rated flow of 3.0 $L{\cdot}h^{-1}$, at a pressure of 0.1 MPa. Fertilization, pesticide spraying, and other agronomic practices were implemented according to local conventional practices.

2.3 AquaCrop model and scenario simulation

2.3.1 Model principle

The AquaCrop model is composed of meteorological, soil, crop, and management modules, which can simulate biomass and yield based on the amount of water lost from the canopy through transpiration under controlled environmental conditions (Stricevic et al., 2011). Seed cotton yield (Y, $t{\cdot}hm^{-2}$) is shown in Equation 1:

$$Y = B{\cdot}HI \tag{1}$$

Where B is the biomass at harvest ($t{\cdot}hm^{-2}$), and HI is the harvest index (%), which is the percentage of seed cotton yield to the aboveground dry biomass.

The total biomass for the entire growth season is the water productivity (WP*, $g{\cdot}m^{-2}$) multiplied by the ratio of daily average transpiration (Tr, mm) to the reference crop evapotranspiration (ET_0, mm), as shown in Equations 2 and 3:

$$B = WP^{*}{\cdot}\sum\frac{T_r}{ET_0} \tag{2}$$

$$T_r = K_S{\cdot}CC^{*}{\cdot}K_{CTr,x}{\cdot}ET_0 \tag{3}$$

Where K_S is the soil water stress coefficient that integrates the effects of waterlogging, stomatal closure, and early senescence; CC* is the canopy cover percentage considering the effects of canopy shading and air movement; $K_{CTr,x}$ is the crop coefficient for maximum plant transpiration; ET_0 is the reference crop evapotranspiration, calculated using the FAO Penman–Monteith method; WP* is the crop water productivity adjusted for atmospheric CO_2 concentration and climate, which is the crop water productivity divided by the crop evapotranspiration under standard evapotranspiration conditions.

2.3.2 Model database

2.3.2.1 Meteorological data

Meteorological data were continuously measured by a standard automatic weather station (Hobo, United States) located near the experimental site, recording data every 10 min. The meteorological data for the 2017 and 2018 experimental periods are shown in Figure 2.

2.3.2.2 Soil data

Table 2 shows the soil physical property data obtained from soil samples taken before cotton sowing, as determined by the Key Laboratory of Crop Water and Regulation, Ministry of Agriculture and Rural Affairs, and input into the AquaCrop model to generate a soil data file.

2.3.2.3 Field management data

Management data include irrigation plans and field management. Irrigation data are based on actual irrigation times and quotas (Table 1) to establish an irrigation parameter database. Field management data for weed control, pest management, fertilization, and covering are created using local cotton field management practices to create a field management database.

2.3.3 Model evaluation

The outputs of the AquaCrop model are evaluated using the root mean square error (RMSE), normalized root mean square error

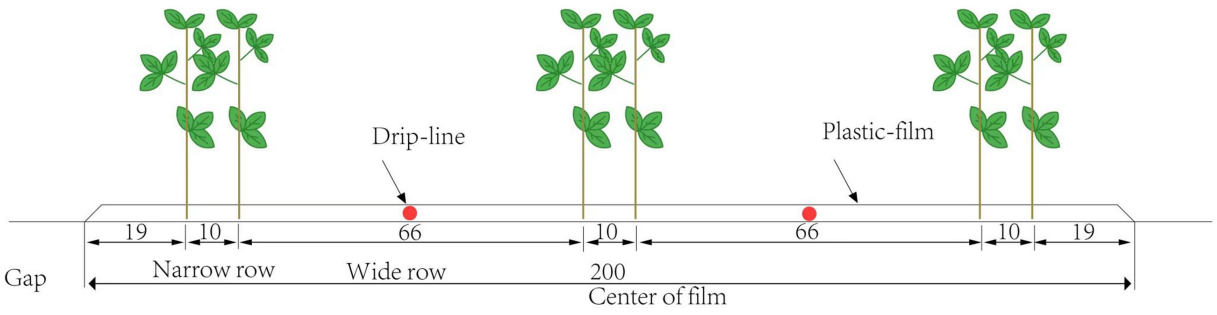

FIGURE 1
Schematic diagram of cotton planting pattern (unit: cm).

10.3389/fsufs.2024.1431339

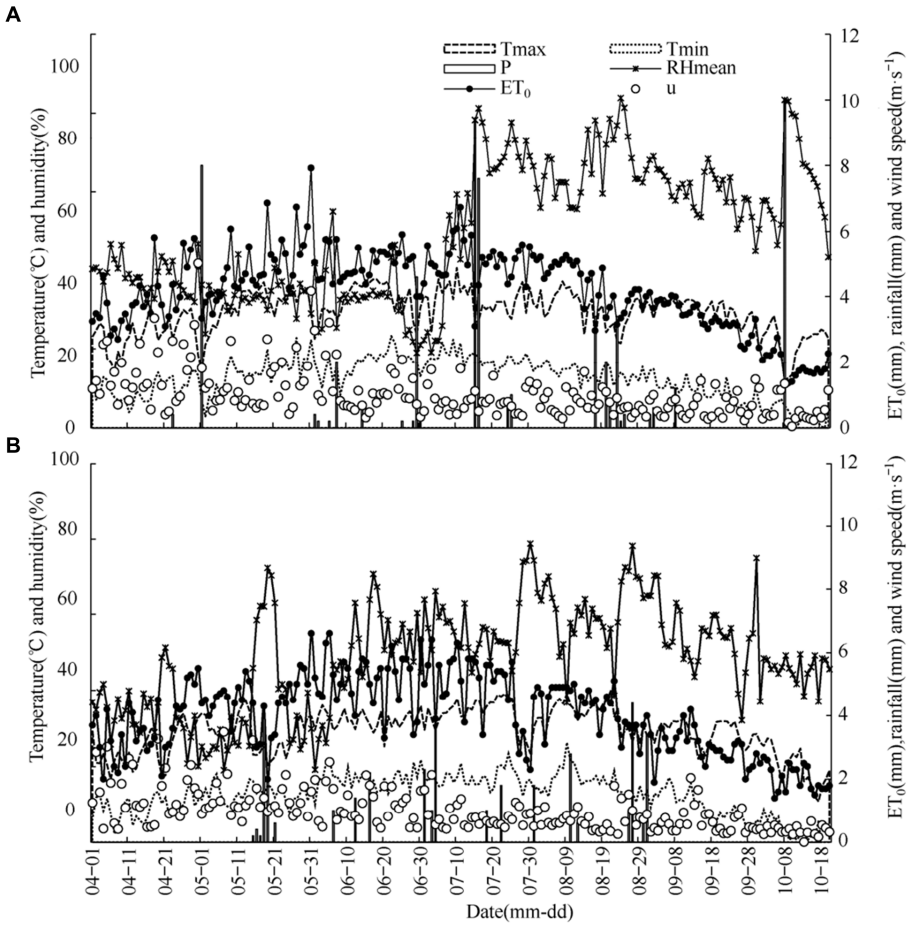

FIGURE 2
Daily change process of meteorological data in cotton growing season in 2017 **(A)** and 2018 **(B)**.

TABLE 2 Daily change process of meteorological data in cotton growing season in 2017(a) and 2018(b).

Soil depth (cm)	Soil bulk density ($g \cdot cm^{-3}$)	Field capacity ($g \cdot g^{-1}$)	Saturated water content ($g \cdot g^{-1}$)	Wilting coefficient ($g \cdot g^{-1}$)	Clay (%)	Silt (%)	Sand (%)
0–20	1.60	0.21	0.24	0.10	2.43	41.49	56.08
20–40	1.55	0.24	0.30	0.10	2.56	41.40	56.05
40–60	1.58	0.25	0.33	0.12	2.88	42.82	54.29
60–80	1.59	0.25	0.32	0.13	2.60	41.40	56.00

(NRMSE), synergy index (d), and relative error (RE), as shown in Equations 4–7:

$$RMSE = \left[\sum_{i=1}^{n}\frac{(P_i - O_i)^2}{n}\right]^{\frac{1}{2}} \quad (4)$$

$$NRMSE = \left[\sum_{i=1}^{n}\frac{(P_i - O_i)^2}{n}\right]^{\frac{1}{2}} \times \frac{100}{\bar{O}} \quad (5)$$

$$d = 1 - \left[\frac{\sum_{i=1}^{n}(P_i - O_i)^2}{\sum_{i=1}^{n}\left(\left|P_i - \bar{O}\right| + \left|O_i - \bar{O}\right|\right)^2}\right] \quad (6)$$

$$RE = \frac{P_i - O_i}{O_i} \times 100 \quad (7)$$

Where P_i is the predicted value, O_i is the measured value, $\bar{O}$ is the average of the measured values, and n is the number of

samples. The smaller the NRMSE, the higher the simulation accuracy; NRMSE <10% indicates excellent simulation effect; 10% < NRMSE <20% indicates good simulation effect; 20% < NRMSE <30% indicates reasonable simulation effect; NRMSE >30% indicates poor simulation effect. The smaller the RE, the higher the simulation accuracy. The closer d is to 1, the higher the model's accuracy.

2.3.4 Scenario simulation

Based on the cotton irrigation quota of 30 mm and the sowing date at the beginning of April in the southern Xinjiang oasis, with slight variations across different regions, six irrigation levels were set: 18 mm (TS1), 24 mm (TS2), 30 mm (TS3), 36 mm (TS4), 45 mm (TS5), and 54 mm (TS6) for a total of six irrigation quotas. Five planting date treatments were set as March 23 (D1), April 3 (D2), April 13 (D3), April 23 (D4), and May 3 (D5), as detailed in Table 3.

TABLE 3 Simulation scenarios set in AquaCrop model.

Irrigation treatment (mm)	Planting date
TS1	D1
	D2
	D3
	D4
	D5
TS2	D1
	D2
	D3
	D4
	D5
TS3	D1
	D2
	D3
	D4
	D5
TS4	D1
	D2
	D3
	D4
	D5
TS5	D1
	D2
	D3
	D4
	D5
TS6	D1
	D2
	D3
	D4
	D5

2.4 Evaluation of yield sustainability

Using the meteorological data from 1988 to 2017 (sourced from the China Meteorological Administration), the AquaCrop model was used to simulate the yield of cotton under different irrigation and sowing scenarios. The sustainability of cotton production was evaluated using the Sustainability Index (SYI), with higher values indicating better sustainability; the stability of yield was represented by the coefficient of variation (CV), with higher CV values indicating lower stability. Equations 8 and 9 are as follows:

$$SYI = \left(Y_{mean} - S\right) / Y_{\max} \tag{8}$$

$$CV = S / Y_{mean} \times 100 \tag{9}$$

Where Y_{mean} is the average yield (t·hm^{-2}), S is the standard deviation of yield, and Y_{max} is the maximum yield (t·hm^{-2}).

3 Results

3.1 AquaCrop model cotton parameter tuning results

Based on the calibration procedure by Vanuytrecht et al. (2014), the AquaCrop crop growth model outputs for canopy cover, aboveground biomass, soil moisture, cotton yield, and evapotranspiration (ET) were calibrated using the 2018 field trial data. The 2017 field trial data were used for validation. The statistical error indicators (Table 4) were used to select the parameter corresponding to the smallest error as the crop parameter for this variety. The results are shown in Table 5. It can be seen from the table that, compared with the recommended parameter values in the model, all parameter values for the Xin Lu Zhong 46 cotton variety were adjusted to some extent, except for the "upper limit temperature." As shown in Table 4, the simulation accuracy for canopy cover, aboveground biomass, and soil moisture in 2018 was relatively high, with the NRMSE for each treatment being less than 15%, and both d and R^2 approaching 1. For the simulation of cotton yield and ET, the NRMSE was less than 10%, R^2 approached 1, and the d value was relatively low. The table also shows that, compared with the 2017 field trial data, the AquaCrop model overestimated the canopy cover rate, aboveground biomass, and soil moisture, with an average RE of 10.15, 8.80, and 0.45%, respectively, while it underestimated the actual transpiration and yield of cotton for each treatment, with an average RE of −7.46% and −1.18%. The comprehensive analysis indicates that the AquaCrop model can accurately simulate the canopy cover, aboveground biomass, and seed cotton yield of cotton.

3.2 Simulation results of cotton biomass and yield under different irrigation and planting scenarios

Using the meteorological data from 1988 to 2017 and based on the AquaCrop model, the effects of irrigation and planting dates on the aboveground biomass and yield of cotton in the oasis area were simulated

TABLE 4 Calibration and validation of AquaCrop model.

Indicator	Treatment	RMSE		NRMSE (%)		*d*		R^2		RE (%)	
		2017	2018	2017	2018	2017	2018	2017	2018	2017	2018
Canopy cover (%)	T_1	5.90	2.95	10.00	4.86	0.98	1.00	0.98	0.99	13.66	5.61
	T_2	2.33	3.71	3.71	6.07	1.00	0.99	1.00	0.98	4.14	4.82
	T_3	5.85	2.80	9.50	4.48	0.99	1.00	0.98	0.99	12.66	3.68
Biomass (t·ha^{-1})	T_1	0.62	0.073.	10.36	1.23	0.99	1.00	0.99	1.00	4.17	−0.41
	T_2	0.90	0.37	14.98	6.24	0.98	1.00	0.99	0.99	7.97	3.68
	T_3	1.07	0.80	17.36	12.57	0.98	0.98	0.96	0.94	14.27	3.34
Soil moisture (%)	T_1	1.09	0.90	5.63	4.93	0.91	0.91	0.85	0.72	−1.46	−0.28
	T_2	0.98	1.15	4.63	5.82	0.95	0.89	0.88	0.74	1.14	1.26
	T_3	1.37	1.56	5.89	7.28	0.90	0.87	0.72	0.66	1.66	3.29
Yield (t·ha^{-1})	T_1	0.56	0.42	9.42	7.82	0.38	0.35	0.81	0.82	−8.60	7.39
	T_2	0.48	0.54	7.27	9.33	0.30	0.25	0.81	0.82	−7.00	9.18
	T_3	0.56	0.36	7.90	5.85	0.42	0.30	0.81	0.82	−6.79	5.66
ET (mm)	T_1	13.34	34.82	3.14	9.23	0.12	0.28	0.87	0.87	−0.26	9.02
	T_2	11.99	29.98	2.58	7.09	0.41	0.15	0.87	0.87	1.24	6.87
	T_3	27.33	17.35	5.20	3.59	0.41	0.44	0.87	0.87	−4.51	−2.85

TABLE 5 Crop parameters of AquaCrop model.

Description and unit	Default value	Calibrated value
Canopy decline coefficient at senescence (%·d^{-1})	2.9	5.2
Maximum crop coefficient	1.10	1.15
Maximum effective rooting depth (m)	2.0	0.8
Water productivity normalized for ET_0 and CO^2 (g·m^{-2})	15	18
Reference harvest index (%)	35	34
Leaf growth threshold p-upper	0.20	0.35
Leaf growth threshold p-lower	0.70	0.65
Stomatal conductance threshold p-upper	0.65	0.35
Soil water depletion threshold for senescence acceleration	0.75	0.60
Base temperature Tbase (°C)	12	15
Upper temperature Tupper (°C)	35	35

(Figure 3). Figure 3A shows that when the planting date is the same, cotton yield increases with the increase in the irrigation quota. The cotton yield for treatments TS2-TS6 increased by 18.7, 34.6, 45.9, 51.9, and 52.3%, respectively, compared to treatment TS1. For planting dates D1–D3, treatments TS5 and TS6 significantly outperformed TS1–TS4, while for dates D4 and D5, treatments TS4–TS6 significantly outperformed TS1–TS3, but there was no significant difference between treatments TS4–TS6. Figure 3A also shows that under the same irrigation quota, cotton yield changes regularly with the delay in planting dates. The yield for treatments TS1 and TS2 increased with delayed planting dates, with D4 and D5 significantly outperforming D1 and D2. For treatments TS3–TS6, cotton yield first increased and then decreased with delayed planting dates, with TS5–TS6 treatments reaching peak yields at D2, significantly outperforming D5, while TS3–TS4 treatments reached peak yields at D4 and D3, respectively.

Figure 3B shows that when the planting date is the same, the trend of change in cotton biomass with the increase in irrigation quota is consistent with that of yield. That is, under the same planting date, as the irrigation quota increases, cotton biomass tends to increase. The biomass for treatments TS2–TS6 increased by 15.4, 29.5, 39.6, 45.8, and 16.7%, respectively, compared to TS1, with TS5–TS6 treatments significantly outperforming TS1–TS3. Figure 3B also shows that the biomass for TS1 increased with delayed planting dates, with D4 and D5 significantly outperforming D1; for TS2–TS4, as the planting date was delayed, the biomass first increased and then decreased, with D4 significantly outperforming D1 under TS2–TS3 irrigation, while under TS4 irrigation, D5 was significantly lower than D1; for TS5–TS6, the biomass decreased with delayed planting dates, with D1–D3 significantly outperforming D4. Overall, a higher irrigation quota is beneficial

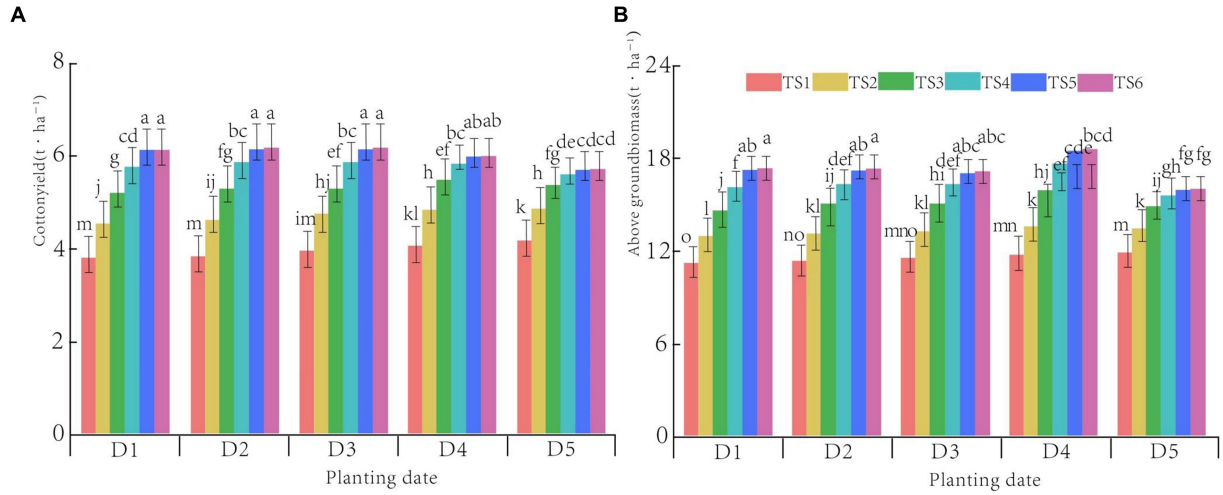

FIGURE 3
Comparison of simulation results of cotton yield and aboveground biomass at different sowing dates using different irrigation systems simulated by the AquaCrop model (Average value in 1988–2017). **(A)** Cotton yield under different scenarios; **(B)** Aboveground biomass under different scenarios. Lowercase indicates the significance difference among treatments at the 0.05 level. The short line represents the standard error.

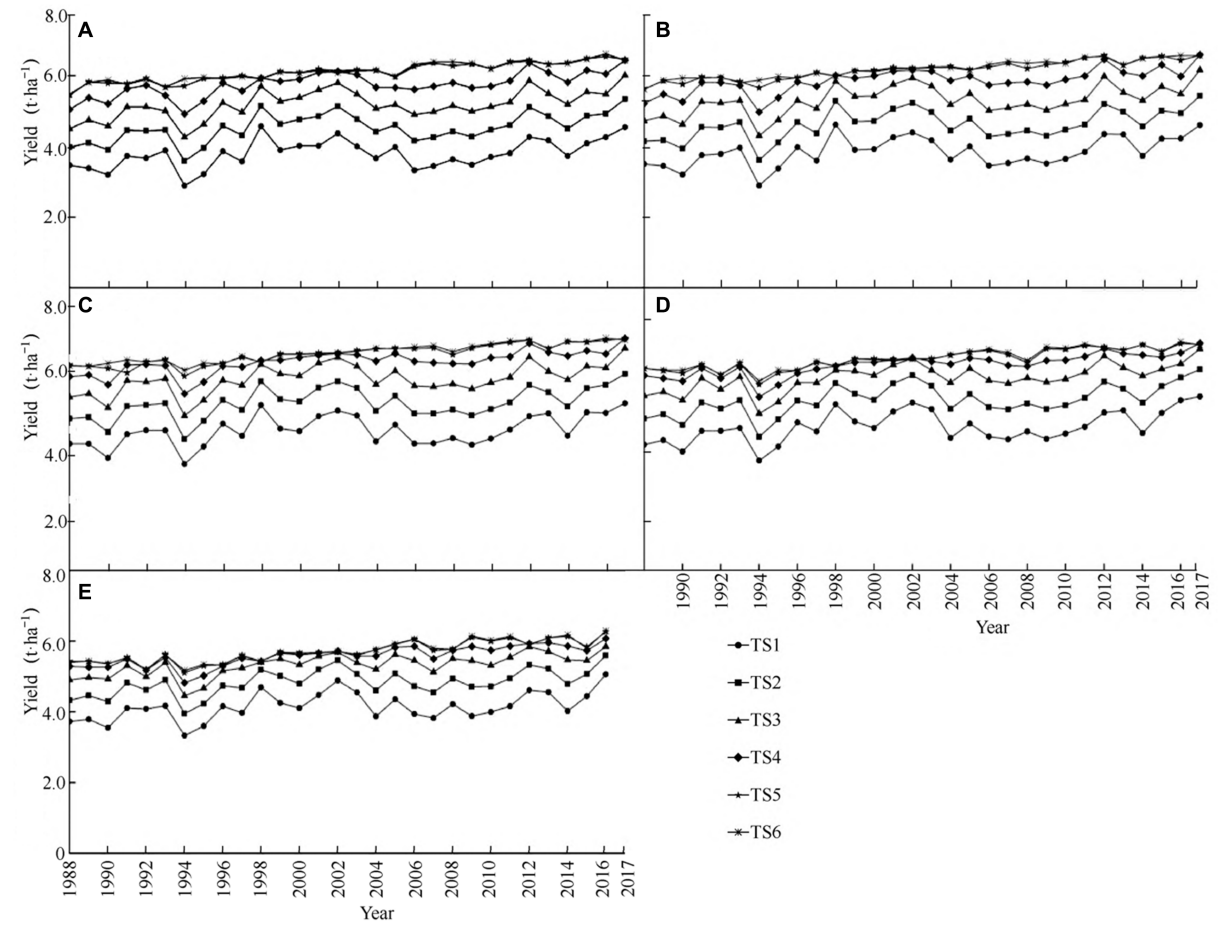

FIGURE 4
Comparison of annual change in cotton yield under different scenarios from 1988 to 2017. **(A)** Scenario TS1; **(B)** Scenario TS2; **(C)** Scenario TS3; **(D)** Scenario TS4; **(E)** Scenario TS5. Note: The standard error is represented by the short line in each graph.

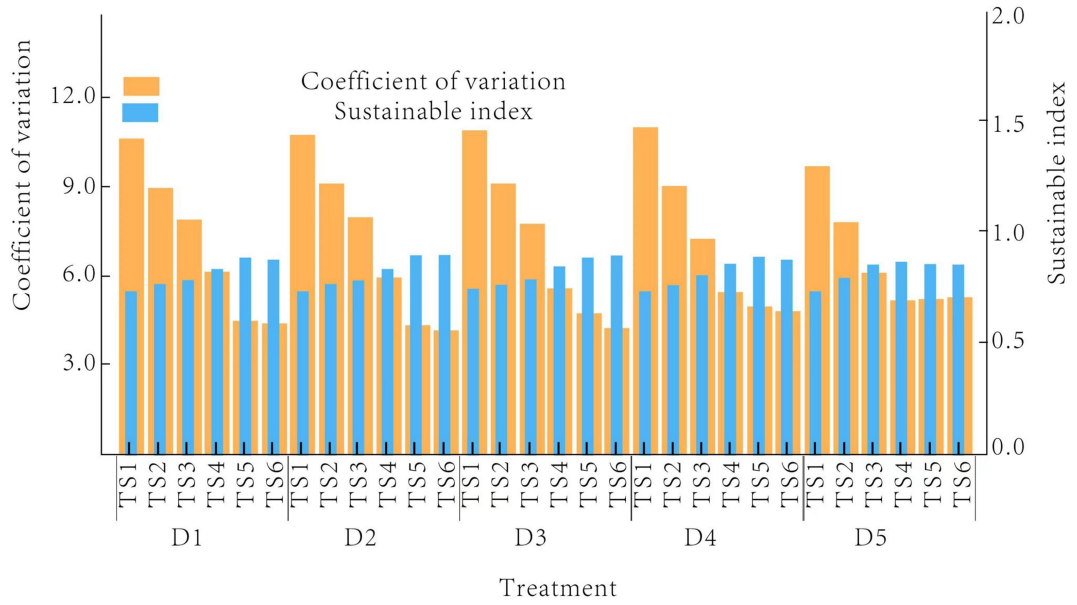

FIGURE 5
Comparison on variation coefficient and sustainable index of annual cotton yield in different scenarios from 1988 to 2017.

TABLE 6 Comparison of actual and model-predicted cotton yield, biomass, and evapotranspiration.

Year	Actual yield (t/ha)	Model predicted yield (t/ha)	Actual biomass (t/ha)	Model predicted biomass (t/ha)	Actual ET (mm)	Model predicted ET (mm)
2017	2.5	2.45	15.0	14.8	450	460
2018	2.7	2.65	16.5	16.3	480	475

for the formation of cotton biomass and yield, while the response to different irrigation quotas varies with planting dates.

3.3 Evaluation of sustainability and stability of simulated cotton yield under different scenarios

The interannual variability, stability, and sustainability of cotton yield from 1988 to 2017 are shown in Figures 4, 5. It can be seen from the figures that the amplitude of interannual variability in cotton yield (Figures 4A–E) decreases with the increase in irrigation quota. Treatments TS5 and TS6 had higher stability, with an average variation coefficient (CV) of 4.6 and 4.8%, respectively, which is a reduction of 55.0 and 56.6% compared to treatment TS1. The sustainability of cotton production also increased with the increase in irrigation quota, with the average Sustainability Index (SYI) for treatments TS4–TS6 being greater than 0.8, indicating good sustainability. It can also be seen that the interannual stability of cotton yield increases with delayed planting dates, with an average CV of 5.94% for treatment D5, which is a reduction of 7.1% compared to D1. The impact of different planting dates on the sustainability of cotton production is relatively small, with the average SYI for treatments TS1–TS6 being greater than 0.8. The comprehensive analysis shows that the planting date has a smaller impact on the stability and sustainability of cotton production, while the impact of irrigation is greater.

3.4 Model performance evaluation

Table 6 presents the results of our AquaCrop model simulations against field measurements obtained from the 2017 and 2018 growing seasons. Each entry in the table reflects the average values derived from three replicate plots for each irrigation treatment and planting date combination.

4 Discussion

Predicting yield is increasingly important for optimizing irrigation and improving the sustainability and profitability of production under limited available water resources (Angella et al., 2016). To understand the impact of climate change on the yield of oasis cotton under different irrigation and planting dates, this study calibrated and validated the crop and irrigation parameters in the AquaCrop model using 2 years of data from 2017 to 2018. The simulation results were statistically analyzed using RE, NRMSE, d, and R^2 to test the accuracy and precision of the model (Wang et al., 2020). The results show that the AquaCrop model can effectively simulate the biomass and yield of

cotton under different irrigation and planting dates, with NRMSE for each treatment being less than 20%, and both *d* and R^2 approaching 1. The RE for ET and seed cotton yield prediction were −4.5 to 1.2% and −8.6% to −6.8%, respectively. The comprehensive analysis indicates that although the AquaCrop model underestimated ET and cotton yield, and overestimated canopy cover, aboveground biomass, and soil moisture, it proved the accuracy of the model for scenario analysis calibration and validation, consistent with the findings of Voloudakis et al. (2015) and Li et al. (2019).

Crop production is directly dependent on climate conditions, which determine the sources and productivity of agricultural activities (Ahmadi et al., 2021). This study used climate data from 1988 to 2017 to simulate 30 years of cotton production under 30 scenarios. The results show that the planting date has a smaller impact on the stability and sustainability of cotton production, but the stability and sustainability increase with the increase in irrigation quota, indicating that increasing the irrigation quota can effectively mitigate the impact of climate change on crop yield (Niu et al., 2016). The simulation shows that cotton biomass and seed cotton yield increase with the increase in irrigation quota. There was no significant difference in the biomass and seed cotton yield between treatments TS5 and TS6, which is close to the results obtained by Tan et al. (2018), who concluded that the suitable irrigation quota for cotton under mulch drip irrigation in southern Xinjiang is 406–462 mm. The difference may be due to different climates, soil textures, and irrigation water quality, suggesting that too much or too little irrigation is not conducive to high cotton yield, while an appropriate amount of irrigation is more beneficial for increasing cotton yield. This is because appropriate moisture is beneficial for the accumulation of aboveground biomass, while excessive irrigation causes leaching of fertilizers, leading to low fertilizer absorption and utilization efficiency, affecting the nutritional and reproductive growth of cotton, and thus reducing cotton yield (Read et al., 2006; Dong et al., 2010).

Choosing the appropriate planting date can improve water use and is an economically feasible, simple, and effective strategy to reduce the impact of climate change (Srivastava et al., 2022). The simulation shows that planting at the end of March and the beginning of April under conditions TS5–TS6 is beneficial for the formation of cotton biomass and yield. This is because late planting delays the cotton growth cycle, and the lower temperatures in the later stages are not conducive to boll development. At the same time, a larger irrigation quota leads to cotton being green and late-maturing, making it difficult to form effective yield. In water-scarce areas, it is possible to irrigate appropriately during the critical water demand period of cotton to avoid affecting the later yield formation of cotton. Under conditions TS1–TS2, planting at the end of April and the beginning of May is more conducive to the formation of cotton biomass and yield. Although late planting delays the cotton growth cycle, the higher soil temperature can meet the good emergence and rapid growth of cotton in the early stage, while the lower irrigation quota advances the cotton growth period, promotes early maturity of cotton, increases the proportion of flowers before frost, and is beneficial for ensuring yield.

Upon reviewing the Table 6, it is evident that the model predictions closely mirror the actual field measurements, with discrepancies generally within acceptable margins. For instance, the model-predicted yields slightly underestimated the actual yields, which may be attributed to the model's conservative approach to simulating crop response to water stress. The slight overestimation of evapotranspiration by the model could be indicative of its sensitivity to microclimatic variations that are not fully captured by standard meteorological data. Nonetheless, the overall trend and magnitude of the model predictions are consistent with observed values, validating the model's utility for strategic planning in cotton production under similar environmental conditions. The minor discrepancies between actual and predicted data also highlight areas for further refinement of the model, such as incorporating more localized microclimate data or considering the impact of other abiotic and biotic factors on crop growth and water use.

At present, the common planting dates in the southern Xinjiang region are from mid-March to mid-April, with slight differences across various regions due to climate influences. Planting at the end of April and the beginning of May is a strategy to cope with future climate change and water scarcity (Braunack et al., 2012), but later planting dates may not conform to actual production. Further research should be conducted in the future to explore the mitigation effects of delayed planting under early-maturing varieties and cultivation models on water scarcity and production stability and sustainability under climate change.

5 Conclusion

The AquaCrop model can accurately simulate cotton canopy cover, aboveground biomass, and seed cotton yield. The stability and sustainability of cotton production are less affected by planting dates and increase with the increase in irrigation quotas. When planting dates are the same, cotton aboveground biomass and yield increase with the increase in irrigation quotas. An irrigation quota of 495 mm can achieve higher irrigation water efficiency and ensure that cotton yield is not significantly reduced. For regions with abundant water resources, planting can be considered at the end of March and the beginning of April, while for water-scarce regions, planting at the end of April to the beginning of May can achieve higher yields, but the use of early-maturing varieties and corresponding cultivation models should be considered.

Data availability statement

The original contributions presented in the study are included in the article/supplementary material, further inquiries can be directed to the corresponding author.

Author contributions

HF: Conceptualization, Data curation, Formal analysis, Funding acquisition, Writing – original draft, Writing – review & editing. LX: Investigation, Methodology, Project administration, Resources, Writing – original draft, Writing – review & editing. HM: Conceptualization, Data curation, Formal analysis, Funding acquisition, Writing – original draft, Writing – review & editing.

Funding

The author(s) declare that financial support was received for the research, authorship, and/or publication of this article. This

research was funded by the Postdoctoral Research Funding Program of Shaanxi Province (2023BSHEDZZ238), the High-level Talents Scientific Research Start-up Fund Project of Yulin University (2023GK13), the "New Star of Science and Technology" Talent Program of Yulin (CXY-2022-137), the Natural Science Research Project of the Education Department in Shaanxi Province of China (22JK0636).

Conflict of interest

Hongjian Fan was employed by Shaanxi Provincial Land Engineering Construction Group Co., Ltd.

The remaining authors declare that the research was conducted in the absence of any commercial or financial relationships that could be construed as a potential conflict of interest.

Publisher's note

All claims expressed in this article are solely those of the authors and do not necessarily represent those of their affiliated organizations, or those of the publisher, the editors and the reviewers. Any product that may be evaluated in this article, or claim that may be made by its manufacturer, is not guaranteed or endorsed by the publisher.

References

Abedinpour, M., Sarangi, A., Rajput, T. B. S., Singh, M., Pathak, H., and Ahmad, T. (2012). Performance evaluation of AquaCrop model for maize crop in a semi-arid environment. *Agric. Water Manag.* 110, 55–66. doi: 10.1016/j.agwat.2012.04.001

Abrha, B., Delbecque, N., Raes, D., Tsegay, A., Todorovic, M., Heng, L., et al. (2012). Sowing strategies for barley (*Hordeum vulgare* L.) based on modelled yield response to water with AquaCrop. *Exp. Agric.* 48, 252–271. doi: 10.1017/S0014479711001190

Ahmadi, M., Etedali, H. R., and Elbeltagi, A. (2021). Evaluation of the effect of climate change on maize water footprint under RCPs scenarios in Qazvin plain, Iran. *Agric. Water Manag.* 254:106969. doi: 10.1016/j.agwat.2021.106969

Andarzian, B., Bannayan, M., Steduto, P., Mazraeh, H., Barati, M. E., Barati, M. A., et al. (2011). Validation and testing of the AquaCrop model under full and deficit irrigated wheat production in Iran. *Agric. Water Manag.* 100, 1–8. doi: 10.1016/j.agwat.2011.08.023

Angella, G., García Vila, M., López, J. M., Barraza, G., Salgado, R., Prieto Angueira, S., et al. (2016). Quantifying yield and water productivity gaps in an irrigation district under rotational delivery schedule. *Irrig. Sci.* 34, 71–83. doi: 10.1007/s00271-015-0486-0

Araya, A., Habtu, S., Hadgu, K. M., Kebede, A., and Dejene, T. (2010). Test of AquaCrop model in simulating biomass and yield of water deficient and irrigated barley (*Hordeum vulgare*). *Agric. Water Manag.* 97, 1838–1846. doi: 10.1016/j.agwat.2010.06.021

Bisbis, M. B., Gruda, N., and Blanke, M. (2018). Potential impacts of climate change on vegetable production and product quality – a review. *J. Clean. Prod.* 170, 1602–1620. doi: 10.1016/j.jclepro.2017.09.224

Braunack, M. V., Bange, M. P., and Johnston, D. B. (2012). Can planting date and cultivar selection improve resource use efficiency of cotton systems? *Field Crop Res.* 137, 1–11. doi: 10.1016/j.fcr.2012.08.018

Chen, Y., and Dong, H. (2016). Mechanisms and regulation of senescence and maturity performance in cotton. *Field Crop Res.* 189, 1–9. doi: 10.1016/j.fcr.2016.02.003

Conaty, W. C., Mahan, J. R., Neilsen, J. E., Tan, D. K. Y., Yeates, S. J., and Sutton, B. G. (2015). The relationship between cotton canopy temperature and yield, fibre quality and water-use efficiency. *Field Crop Res.* 183, 329–341. doi: 10.1016/j.fcr.2015.08.010

Ding, B., Cao, H., Zhang, J., Bai, Y., He, Z., Guo, S., et al. (2023). Biofertilizer application improved cotton growth, nitrogen use efficiency, and yield in saline water drip-irrigated cotton fields in Xinjiang, China. *Ind. Crops Prod.* 205:117553. doi: 10.1016/j.indcrop.2023.117553

Dong, H., Kong, X., Li, W., Tang, W., and Zhang, D. (2010). Effects of plant density and nitrogen and potassium fertilization on cotton yield and uptake of major nutrients in two fields with varying fertility. *Field Crop Res.* 119, 106–113. doi: 10.1016/j.fcr.2010.06.019

Feng, L., Dai, J., Tian, L., Zhang, H., Li, W., and Dong, H. (2017). Review of the technology for high-yielding and efficient cotton cultivation in the northwest inland cotton-growing region of China. *Field Crop Res.* 208, 18–26. doi: 10.1016/j.fcr.2017.03.008

Foster, T., Brozović, N., Butler, A. P., Neale, C. M. U., Raes, D., Steduto, P., et al. (2017). AquaCrop-OS: an open source version of FAO's crop water productivity model. *Agric. Water Manag.* 181, 18–22. doi: 10.1016/j.agwat.2016.11.015

Geerts, S., Raes, D., and Garcia, M. (2010). Using AquaCrop to derive deficit irrigation schedules. *Agric. Water Manag.* 98, 213–216. doi: 10.1016/j.agwat.2010.07.003

Greaves, G. E., and Wang, Y.-M. (2016). Assessment of FAO AquaCrop model for simulating maize growth and productivity under deficit irrigation in a tropical environment. *Water* 8:557. doi: 10.3390/w8120557

Jin, X., Feng, H., Zhu, X., Li, Z., Song, S., Song, X., et al. (2014). Assessment of the AquaCrop model for use in simulation of irrigated winter wheat canopy cover, biomass, and grain yield in the North China plain. *PLoS One* 9:e86938. doi: 10.1371/journal.pone.0086938

Kang, S., Hao, X., Du, T., Tong, L., Su, X., Lu, H., et al. (2017). Improving agricultural water productivity to ensure food security in China under changing environment: from research to practice. *Agric. Water Manag.* 179, 5–17. doi: 10.1016/j.agwat.2016.05.007

Khalid, N., Aqeel, M., Noman, A., and Fatima Rizvi, Z. (2023). Impact of plastic mulching as a major source of microplastics in agroecosystems. *J. Hazard. Mater.* 445:130455. doi: 10.1016/j.jhazmat.2022.130455

Khoshravesh, M., Mostafazadeh-Fard, B., Heidarpour, M., and Kiani, A.-R. (2013). AquaCrop model simulation under different irrigation water and nitrogen strategies. *Water Sci. Technol.* 67, 232–238. doi: 10.2166/wst.2012.564

Kim, D., and Kaluarachchi, J. (2015). Validating FAO AquaCrop using Landsat images and regional crop information. *Agric. Water Manag.* 149, 143–155. doi: 10.1016/j.agwat.2014.10.013

Li, Z., Fang, G., Chen, Y., Duan, W., and Mukanov, Y. (2020). Agricultural water demands in Central Asia under 1.5°C and 2.0°C global warming. *Agric. Water Manag.* 231:106020. doi: 10.1016/j.agwat.2020.106020

Li, F., Yu, D., and Zhao, Y. (2019). Irrigation scheduling optimization for cotton based on the AquaCrop model. *Water Resour. Manag.* 33, 39–55. doi: 10.1007/s11269-018-2087-1

Linker, R., Ioslovich, I., Sylaios, G., Plauborg, F., and Battilani, A. (2016). Optimal model-based deficit irrigation scheduling using AquaCrop: a simulation study with cotton, potato and tomato. *Agric. Water Manag.* 163, 236–243. doi: 10.1016/j.agwat.2015.09.011

Niu, G., Li, Y. P., Huang, G. H., Liu, J., and Fan, Y. R. (2016). Crop planning and water resource allocation for sustainable development of an irrigation region in China under multiple uncertainties. *Agric. Water Manag.* 166, 53–69. doi: 10.1016/j.agwat.2015.12.011

Read, J. J., Reddy, K. R., and Jenkins, J. N. (2006). Yield and fiber quality of upland cotton as influenced by nitrogen and potassium nutrition. *Eur. J. Agron.* 24, 282–290. doi: 10.1016/j.eja.2005.10.004

Ren, F., Yang, G., Li, W., He, X., Gao, Y., Tian, L., et al. (2021). Yield-compatible salinity level for growing cotton (*Gossypium hirsutum* L.) under mulched drip irrigation using saline water. *Agric. Water Manag.* 250:106859. doi: 10.1016/j.agwat.2021.106859

Saadi, S., Todorovic, M., Tanasijevic, L., Pereira, L. S., Pizzigalli, C., and Lionello, P. (2015). Climate change and Mediterranean agriculture: impacts on winter wheat and tomato crop evapotranspiration, irrigation requirements and yield. *Agric. Water Manag.* 147, 103–115. doi: 10.1016/j.agwat.2014.05.008

Sandhu, R., and Irmak, S. (2019). Assessment of AquaCrop model in simulating maize canopy cover, soil-water, evapotranspiration, yield, and water productivity for different planting dates and densities under irrigated and rainfed conditions. *Agric. Water Manag.* 224:105753. doi: 10.1016/j.agwat.2019.105753

Srivastava, R. K., Mequanint, F., Chakraborty, A., Panda, R. K., and Halder, D. (2022). Augmentation of maize yield by strategic adaptation to cope with climate change for a future period in eastern India. *J. Clean. Prod.* 339:130599. doi: 10.1016/j.jclepro.2022.130599

Stricevic, R., Cosic, M., Djurovic, N., Pejic, B., and Maksimovic, L. (2011). Assessment of the FAO AquaCrop model in the simulation of rainfed and supplementally irrigated maize, sugar beet and sunflower. *Agric. Water Manag.* 98, 1615–1621. doi: 10.1016/j.agwat.2011.05.011

Surendran, U., Raja, P., Jayakumar, M., and Subramoniam, S. R. (2021). Use of efficient water saving techniques for production of rice in India under climate change scenario: a critical review. *J. Clean. Prod.* 309:127272. doi: 10.1016/j.jclepro.2021.127272

Tan, S., Wang, Q., Zhang, J., Chen, Y., Shan, Y., and Xu, D. (2018). Performance of AquaCrop model for cotton growth simulation under film-mulched drip irrigation in southern Xinjiang, China. *Agric. Water Manag.* 196, 99–113. doi: 10.1016/j.agwat.2017.11.001

Tanasijevic, L., Todorovic, M., Pereira, L. S., Pizzigalli, C., and Lionello, P. (2014). Impacts of climate change on olive crop evapotranspiration and irrigation requirements in the Mediterranean region. *Agric. Water Manag.* 144, 54–68. doi: 10.1016/j.agwat.2014.05.019

Vanuytrecht, E., Raes, D., Steduto, P., Hsiao, T. C., Fereres, E., Heng, L. K., et al. (2014). AquaCrop: FAO's crop water productivity and yield response model. *Environ. Model Softw.* 62, 351–360. doi: 10.1016/j.envsoft.2014.08.005

Voloudakis, D., Karamanos, A., Economou, G., Kalivas, D., Vahamidis, P., Kotoulas, V., et al. (2015). Prediction of climate change impacts on cotton yields in Greece under eight climatic models using the AquaCrop crop simulation model and discriminant function analysis. *Agric. Water Manag.* 147, 116–128. doi: 10.1016/j.agwat.2014.07.028

Wang, X., Wang, H., Si, Z., Gao, Y., and Duan, A. (2020). Modelling responses of cotton growth and yield to pre-planting soil moisture with the CROPGRO-cotton model for a mulched drip irrigation system in the Tarim Basin. *Agric. Water Manag.* 241:106378. doi: 10.1016/j.agwat.2020.106378

Zhou, Y., Li, F., Xin, Q., Li, Y., and Lin, Z. (2024). Historical variability of cotton yield and response to climate and agronomic management in Xinjiang, China. *Sci. Total Environ.* 912:169327. doi: 10.1016/j.scitotenv.2023.169327

Zinkernagel, J., Maestre-Valero, J., Seresti, S. Y., and Intrigliolo, D. S. (2020). New technologies and practical approaches to improve irrigation management of open field vegetable crops. *Agric. Water Manag.* 242:106404. doi: 10.1016/j.agwat.2020.106404

Zou, M., Kang, S., Niu, J., and Lu, H. (2020). Untangling the effects of future climate change and human activity on evapotranspiration in the Heihe agricultural region, Northwest China. *J. Hydrol.* 585:124323. doi: 10.1016/j.jhydrol.2019.124323

frontiers | Frontiers in Sustainable Food Systems

TYPE Original Research
PUBLISHED 17 October 2024
DOI 10.3389/fsufs.2024.1444246

OPEN ACCESS

EDITED BY
Aliza Pradhan,
National Institute of Abiotic Stress Management (ICAR), India

REVIEWED BY
Jiban Shrestha,
Nepal Agricultural Research Council, Nepal
Huailin Zhou,
Chinese Academy of Meteorological Sciences, China
Wuxia Bi,
China Institute of Water Resources and Hydropower Research, China

*CORRESPONDENCE
Juliang Jin
✉ JINJL66@hfut.edu.cn

RECEIVED 05 June 2024
ACCEPTED 04 October 2024
PUBLISHED 17 October 2024

CITATION
Cui Y, Tang H, Zhou Y, Jin J and Jiang S (2024) Accumulative and adaptive responses of maize transpiration, biomass, and yield under continuous drought stress. *Front. Sustain. Food Syst.* 8:1444246. doi: 10.3389/fsufs.2024.1444246

Accumulative and adaptive responses of maize transpiration, biomass, and yield under continuous drought stress

Yi Cui[1], Huiyan Tang[1], Yuliang Zhou[1], Juliang Jin[1]* and Shangming Jiang[2]

[1]School of Civil Engineering, Hefei University of Technology, Hefei, China, [2]Key Laboratory of Water Conservancy and Water Resources of Anhui Province, Water Resources Research Institute of Anhui Province and Huaihe River Commission, Ministry of Water Resources, Hefei, China

Introduction: Continuous drought stress aggravates agricultural losses and threats food security. However, the responses of crops to continuous drought stress remain uncertain.

Methods: To make up the limitations of field experiment and achieve the setting of multiple continuous drought stress scenarios, AquaCrop model is calibrated and validated using field experiment data of summer maize in 2017 and 2018 seasons. Then, the whole growth processes under different continuous drought stress scenarios at two growth stages of maize are simulated. The quantitative responses of transpiration (*Tr*), biomass accumulation, and yield formation to continuous drought stress are analyzed.

Results and discussion: The results show that when the maize encounters serious drought at the seedling stage, the reduction rates of *Tr* at the jointing stage, the tasseling stage, and the milking stage are 57.45%, 43.61%, and 5.24%, respectively. Drought stress at a growth stage of maize not only have negative impacts on transpiration and biomass accumulation at this stage, but also have after-effects on these elements at the subsequent stages. In addition, continuous serious drought at the seedling and jointing stages reduces yield by 100%, which is higher than the sum of the loss rates at these two stages [>33.30% + 24.16%)], while the loss rate due to continuous light drought is lower than the sum [20.66% < (18.80% + 12.45%)]. The impact of continuous drought stress at two growth stages generally exceeds the sum of the impacts of the two single stages. Nevertheless, drought at the seedling stage promotes the adaptability of maize to drought, alleviating the negative impacts of light drought at the jointing stage, while the adaptability disappears when drought at the jointing stage is serious. Therefore, in the actual production of maize, serious drought at the seedling stage should be avoided to ensure seed survival. Meanwhile, continuous drought at the seedling and jointing stages should be prevented to reduce the severe accumulative effects, which guides drought disaster reduction and sustainable agricultural production.

KEYWORDS

responses to continuous drought stress, accumulative effect, adaptive effect, food security, sustainable agricultural production, summer maize, Huaibei Plain

1 Introduction

In recent years, the frequency, intensity, and scope of drought disasters have increased prominently due to global climate change and human activities (Ge et al., 2021). As a result, drought disasters have become one of the major bottlenecks restricting economic development and social stability in many countries and regions (Ali et al., 2020; Zhang et al., 2020; Zhou et al., 2022). Since the 21st century, global drought disasters have become increasingly severe. Due to the location of the eastern monsoon region, continuous droughts occur more frequently during successive seasons and years in China (Chang et al., 2016; Salgotra and Chauhan, 2023). For example, in 2006, there was a four-season continuous drought in southwest China. In 2022, the Yangtze River Basin had experienced a rare drought in summer, autumn, and winter. As agricultural production is highly dependent on climatic conditions, the negative impacts of drought on agricultural production are the most obvious and direct (Mondol et al., 2021). In addition, continuous drought that spans several growth stages has a more serious negative impact on crop growth and yield formation. It has been estimated that global crop production loss due to drought has reached about $30 billion over the past decade (Gupta et al., 2020). Furthermore, there is an average annual grain loss of 2.31×10^{10} kg due to drought from 2001 to 2021 in China (Cui et al., 2023). Thus, drought disasters have become one of the most significant threats to global food security and regional stable development (Zhang et al., 2004; Hussain et al., 2023), the research on the impacts of continuous drought stress on crops is conducive to agricultural drought risk management.

The impact of drought on crops is a complex process that closely relates to the drought intensity, drought duration, and crop growth stage of drought occurrence (Wang et al., 2023; Li et al., 2024). Moreover, the continuous drought at several stages further complicates the impact (Ors et al., 2021). Currently, numerous studies have been conducted on the impacts of drought on crop physiology and growth indicators. For instance, the influences of different levels and durations of drought on crops (Dao et al., 2023), the impacts of drought on different organs of crops (Shafi et al., 2023), and the influences of drought at different stages (Lamin-Samu et al., 2021). However, most studies concentrate on the effects of drought at a single growth stage of crops, and there are few studies on the lasting impact of drought at a certain stage and the cumulative impact of continuous drought during several stages (Zhang et al., 2015).

Due to the complexity of crop responses under different drought conditions, it is difficult to accurately describe and quantify the effects of drought on the crop growth process. Crop models can mechanistically simulate important physiological and growth processes such as photosynthesis, transpiration, and biomass accumulation of crops under various drought conditions (Tojo Soler et al., 2013; Irmak et al., 2024). The entire process of crop growth under continuous drought at different growth stages can be simulated more conveniently using a crop model after the localization by field experiments. The commonly used crop models include DSSAT (Guo et al., 2016), APSIM (Wang et al., 2022), and AquaCrop (Greaves and Wang, 2016), etc. AquaCrop model is a crop model developed by the Food and Agriculture Organization of the United Nations (FAO), it can reflect the responses mechanism of crops to drought (Li et al., 2022). Driven by water factors, AquaCrop model can effectively separate crop transpiration from soil evaporation and is most suitable for simulating crop in response to drought (Razzaghi et al., 2017). Meanwhile, this model has a user-friendly interface and requires only a few input parameters (Xie et al., 2023). AquaCrop model has been widely used to forecast crop yield and dry matter amount under different water conditions (Ćosić et al., 2017). It has also been employed to simulate soil water content and canopy coverage for determining crop water requirements (Voloudakis et al., 2015), and to evaluate the impact of irrigation scheduling on crop growth (Corbari et al., 2021).

Maize is one of the world's major crops (Zhu et al., 2021; Ge et al., 2024) and sustainable maize production plays a vital role in meeting the rapidly growing global food demand and ensuring national food security (Peng et al., 2023a). Since 2001, maize has surpassed rice as the world's second-largest cereal. In 2021, China is the world's second-largest producer of maize, with about 4.32×10^7 ha of planting area, and the yield reaches 2.72×10^{11} kg, accounting for 22% of total global production. Furthermore, the Huaibei Plain is one of the leading areas for maize cultivation in China (Wei et al., 2019), with one-third of the national planting area. Nevertheless, this region is located in the transitional region of temperate and subtropical climate, with a large interannual variation and an uneven distribution of precipitation within a year, frequent continuous droughts, which seriously limits the maize production.

Continuous drought events severely threaten global food security and regional stable development. As maize is one of the world's important crops, the study on the quantitative effects of continuous drought stress on its growth process and yield formation, thus revealing the complex response mechanism of crops to continuous drought stress, is the foundation for evaluating grain drought losses and agricultural drought risk. In addition, it is assumed that all summer maize plants grow consistently without randomness such as gene mutations, plant growth is only affected by drought stress, without diseases, pests, and high temperatures, and plants can pollinate and bear fruit normally in this research. The current contributions of this study are as follows: (1) calibrating and verifying the AquaCrop model by using two seasons of field experiments of summer maize at Xinmaqiao Experimental Station in Bengbu City, Huaibei Plain, China; (2) selecting a base year and designing the continuous drought stress scenarios at two growth stages of maize by changing the precipitation in the base year, and using the calibrated AquaCrop model to simulate the maize growth processes under different drought stress scenarios; (3) analysing the quantitative responses of maize to various continuous droughts at two growth stages, including plant transpiration, dry matter accumulation, and yield formation. And revealing the complex phenomena such as the after-effect of drought at a growth stage and the accumulative and adaptive effects of continuous drought stress on maize. This study can provide a scientific decision-making basis for maize production and disaster reduction under the current trend of continuous and serious drought. It is conducive to promoting regional sustainable agricultural development and providing support for ensuring global food security.

2 Materials and methods

In this paper, we conduct a study on the quantitative responses of summer maize to continuous drought stress at two growth stages by combining field experiments and AquaCrop model. Figure 1 illustrates the process. The AquaCrop model is calibrated and verified using the field experiment data of summer maize in 2017 and 2018. Then, various continuous drought scenarios at two growth stage are set up, and the growth process of maize under different scenarios are simulated. Finally, the quantitative responses of summer maize to

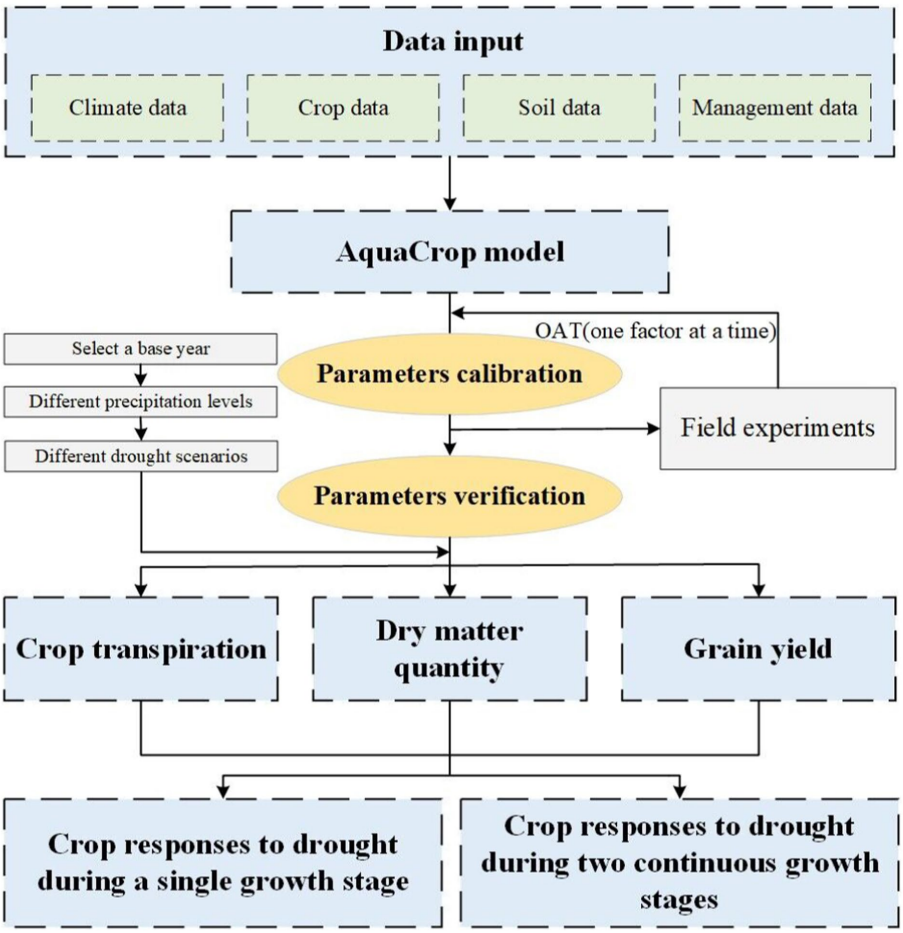

FIGURE 1
Flowchart of the study on quantitative responses of maize to continuous drought stress at two growth stages.

continuous drought stress at two growth stage are analyzed, including crop transpiration, dry matter accumulation, and yield formation.

2.1 Study area

The study is based on two seasons of field experiment data from the Xinmaqiao Agricultural Water Experiment Station. The experiment station is located in the Xinmaqiao Town, Bengbu City, Huaibei Plain (117°22′E, 33°09′N), on the north bank of the middle reaches of the Huai River (Figure 2). The average elevation of the station is 19.7 m, the annual average temperature is 14.9°C, the annual sunshine time is 2,170 h, and the annual average precipitation is 911 mm and the evapotranspiration is 916 mm. The soil in the station is the typical Shajiang black soil of the Huaibei Plain, which is clayey, poorly structured, solid, fissure-developed, with poor soil water retention, and susceptible to drought (Cui et al., 2019). The site has sufficient sunshine to meet the needs of summer maize production. However, because the station is located in the climatic transition zone between the north and south, there are large inter-annual variations in precipitation and uneven distribution within a year. As a result, drought disasters frequently occur and seriously restrict the maize production. Accordingly, the natural geographic conditions and maize production of this station are typical of the Huaibei Plain region. Therefore, the selected area in this study is representative.

2.2 Summer maize field experiments

Summer maize experiments are conducted at the Xinmaqiao Experiment Station. The plants are cultivated in pit plots, which are sown on June 9 and harvested on September 21 in 2017. The size of each plot is 2.00 m (length) × 3.33 m (width) × 2.30 m (depth), and the sowing density is 48,000 plants/hm^2. After sowing, 500 g of compound fertilizer (N 15%, P_2O_5 15%, K_2O 15%) and 200 g of urea are applied to promote the growth of seeds. In 2018, a field experiment is conducted. The plants are sown on June 15 and harvested on September 27. Each field plot has an area of 4.00 m (length) × 6.00 m (width), and the sowing density is 65,000 plants/hm^2. A total of 700 g compound fertilizer and 300 g urea are applied to each field plot after sowing. In addition, three groups of replications are set up for both seasons.

The summer maize varieties in 2017 and 2018 are "Long Ping 206," and the experimental designs are both under rain-fed conditions, the soil water content during the experimental period is only supplemented by precipitation (Figure 3). Based on the actual growth processes of maize observed in the experiments, and the whole growth period of maize is divided into four stages: seedling, jointing, tasseling, and milking stages. Furthermore, the soil water content at different depths (10, 20, 30, 40, and 60 cm) at each growth stage is measured, and the plant samples are selected randomly to measure the dry matter amount at the end of each stage and seed weight at harvest.

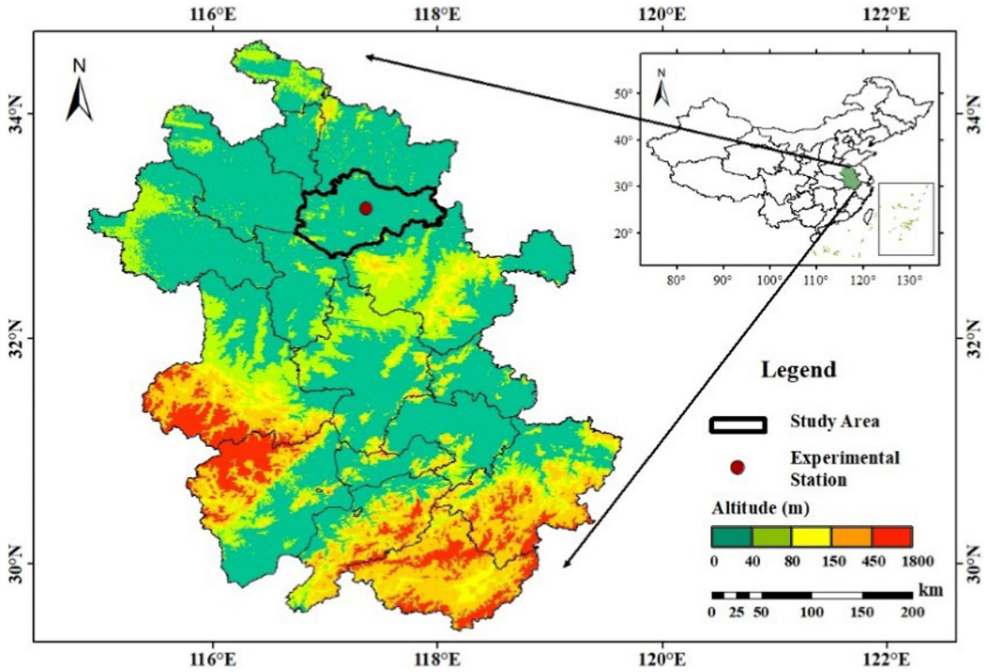

FIGURE 2
Location of study area.

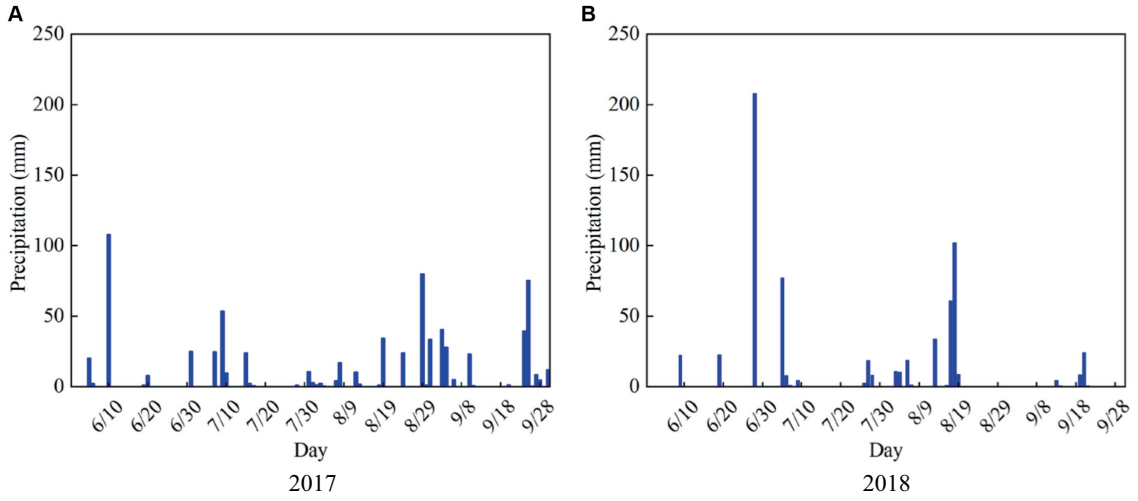

FIGURE 3
Daily precipitation from June to September in **(A)** 2017 and **(B)** 2018 growing seasons of summer maize in the study area.

2.3 AquaCrop model input

AquaCrop model includes a weather module, a crop module, a soil module, and a field management module (Dercas et al., 2022; Alvar-Beltrán et al., 2023). The meteorological data input to the model in this study mainly consisted of daily precipitation, maximum and minimum temperatures, relative humidity, average wind speed, sunshine duration, and CO_2 concentration during the whole growth period of summer maize in 2017 and 2018. The meteorological data used are obtained from the automatic weather station located at the Xinmaqiao experiment site. The CO_2 concentration is obtained using the Mauna Loa. CO_2 data that provided in AquaCrop model. For the crop parameters of the model, we obtain the more sensitive crop genetic parameters first by referring to the default values in the FAO Crop Handbook (Hsiao et al., 2009), and then calibrate them using the field experimental data. The non-sensitive parameters are determined by referring to the FAO Crop Handbook and the relevant studies (Cui et al., 2021; Zhang et al., 2023). The experimental data in 2017 are used to calibrate model parameters, while those in 2018 are used for validation. The soil of the experimental station is typical Shajiang black soil in the Huaibei Plain. The AquaCrop model soil parameters are set with reference to the measured results of the experimental station and existing research of Shajiang black soil (Chen et al., 2020). Due to that two seasons of summer maize experiments are conducted under

rain-fed conditions, the field management parameters meet the normal growth requirements of plant.

2.4 AquaCrop model calibration and validation

The calibration and validation of AquaCrop model is an important step in conducting scenario simulations, and the reliability and accuracy of simulated results are dominated by highly sensitive crop genetic parameters. The OAT (one factor at a time) method (Daniel, 2012) is a fast and effective method of parameter sensitivity analysis by changing only one parameter at a time and selecting it based on the correlation between the change of parameter and that of simulation result. In this study, combining the field experiment data of summer maize at Xinmaqiao Experimental Station in 2017 with existing research (Cui et al., 2022), and referring to the FAO Crop Handbook (Hsiao et al., 2009), the OAT method is adopted to calibrate some of the sensitive crop genetic parameters using dry matter amount and grain yield as the objective functions and to derive locally adapted model parameters. Furthermore, the observed results of summer maize field experiment in 2018 are used to verify the calibrated AquaCrop model.

2.5 Data analysis

To evaluate the reliability of the calibrated AquaCrop model, R-Square (R^2) Equation 1, absolute relative error (*ARE*) Equation 2, and relative root mean square error (*RRMSE*) Equation 3 are used, ensuring the accuracy of model parameters (Lu et al., 2022):

$$R^2 = 1 - \frac{\sum_{i=1}^{n}\left(Obs_i - Sim_i\right)^2}{\sum_{i=1}^{n}\left(Obs_i - \overline{Obs}\right)^2} \quad (1)$$

where n is the number of samples of the output variable (dry matter amount during the growth process of maize in this study); Sim_i is the simulated value of dry matter amount for the ith sample ($i = 1$, 2, 3, 4, 5) of the AquaCrop model; Obs_i is the observed value of the ith sample from the maize field experiments; $\overline{Obs}$ is the average value of all samples of the output variable. The closer the value of R^2 is to 1, the more accurate the simulation results are.

$$ARE = \frac{\left|Sim_i - Obs_i\right|}{Obs_i} \quad (2)$$

$$RRMSE = \frac{\sqrt{\frac{1}{k}\sum_{i=1}^{k}\left(Sim_i - Obs_i\right)^2}}{\overline{Obs}} \quad (3)$$

where k is the number of samples of the output variable (dry matter amount and grain yield at harvest of maize in this study); Sim_i is the simulated value of dry matter amount (or grain yield) at harvest for the ith sample ($i = 1$, 2 indicates 2017 and 2018 seasons, respectively) of the AquaCrop model; Obs_i is the observed value of the ith sample from the maize field experiments. The smaller the value of *ARE* or *RRMSE*, the closer the simulated value is to the observed result and the more accurate the calibrated AquaCrop model is.

2.6 Drought stress scenarios setting

To quantify the responses of maize to continuous drought stress at two growth stages, the calibrated and validated AquaCrop model is used to simulate the whole growth processes of maize under various drought stress scenarios.

The continuous drought stress scenarios at two growth stages of maize designed in this study are as follows: Firstly, the years without drought during the whole growth period of summer maize (June–September) from 1960 to 2019 are selected based on the results of drought identification in the study area (Bengbu City) (Wei et al., 2021). Then, combined with the water consumption of summer maize at each growth stage under sufficient water supply condition, and the year in which the precipitation and the water consumption of maize at each stage are close is considered as the base year. In this study, by analyzing and comparing, 2015 year is chosen as the base year, and the drought stress scenarios are designed by changing the amount of precipitation at each stage of maize in this year.

Table 1 shows the continuous drought stress scenarios at two growth stages of summer maize. The scenarios are designed to set three situations of no drought, light drought, and serious drought stress at one growth stage of maize, and additional three situations of no drought, light drought, and serious drought stress at the next stage, for a total of 21 scenarios. Moreover, no drought is defined as 100% of the precipitation in the base year, light and serious drought are defined as 70% and 40% of the precipitation in the base year, respectively. The actual meteorological data (maximum and minimum temperatures, relative humidity, average wind speed, etc.) in the base year and the precipitation data under various scenarios are input into the calibrated and validated AquaCrop model to simulate the whole growth processes of summer maize under different continuous drought conditions at two growth stages.

3 Results and discussion

3.1 Calibration and validation results of AquaCrop model

This study combines the research on AquaCrop model parameters (Li et al., 2022), selects the sensitive crop genetic parameters of summer maize, and uses the OAT method to calibrate (2017) and validate (2018) the parameters (Table 2). The soil water content, dry matter amount, and grain yield of maize are used as the outputs. Furthermore, the accuracy of the AquaCrop model parameters after calibration are evaluated using the *ARE* and *RRMSE*.

The comparison between the simulated and observed results of relative soil water content during the growth process of maize in 2017 and 2018 are shown in Figure 4. It can be seen that the simulated and measured values of soil water content at different growth stages of maize in the two seasons are similar, meanwhile, the trends and

TABLE 1 Scenarios of continuous drought stress at two growth stages of summer maize.

Scenario number	Percentage of the precipitation in the base year				Drought stress scenario
	Seeding stage [a]	Jointing stage	Tasseling stage	Milking stage	
1	100%	100%	100%	100%	CK
2	100%	70%	100%	100%	S0 + J1
3	100%	40%	100%	100%	S0 + J2
4	70%	100%	100%	100%	S1 + J0
5	70%	70%	100%	100%	S1 + J1
6	70%	40%	100%	100%	S1 + J2
7	40%	100%	100%	100%	S2 + J0
8	40%	70%	100%	100%	S2 + J1
9	40%	40%	100%	100%	S2 + J2
10	100%	100%	70%	100%	J0 + T1
11	100%	100%	40%	100%	J0 + T2
12	100%	70%	70%	100%	J1 + T1
13	100%	70%	40%	100%	J1 + T2
14	100%	40%	70%	100%	J2 + T1
15	100%	40%	40%	100%	J2 + T2
16	100%	100%	100%	70%	T0 + M1
17	100%	100%	100%	40%	T0 + M2
18	100%	100%	70%	70%	T1 + M1
19	100%	100%	70%	40%	T1 + M2
20	100%	100%	40%	70%	T2 + M1
21	100%	100%	40%	40%	T2 + M2

[a]S, J, T, and M represents the seedling stage, the jointing stage, the tasseling stage, and the milking stage, respectively; and 0, 1, and 2 represents no drought stress, light drought stress, and serious drought stress, respectively.

TABLE 2 Calibrated crop parameters of summer maize for Bengbu City in AquaCrop model.

Parameters		Unit	Value
Canopy	Maximum canopy cover	%	90.0
	Canopy growth coefficient	%/day	14.9
	Canopy decline coefficient	%/day	11.3
Root zone	Maximum effective root depth	m	1.8
	Root zone expansion coefficient	cm/day	2.1
Yield	Reference harvest index	%	48.0
	Duration of harvest index	day	38
	Duration of flowering	day	16
	Shape factor of the influence coefficient of water stress on stomatal control		5.80
	Soil moisture depletion threshold leading to pollination failure (upper limit)		0.78

distributions of soil water content at different depths (10, 20, 30, 40, and 60 cm) are basically consistent.

The simulated and observed results of dry matter amount during the whole growth period of maize in 2017 and 2018 are shown in Figure 5. It indicates that the simulated dry matter amount in the two seasons are close to the observed values, with R^2 values of 0.91 and 0.96, respectively. The values of *ARE* between the simulated and observed dry matter amount at harvest are 2.55 and 7.15%, respectively, and the *RRMSE* is 5.54% (Table 3). Thus, the calibrated AquaCrop model accurately simulates the growth process of maize, and the model parameters are reliable.

The values of *ARE* between the simulated and observed grain yield in 2017 and 2018 are 0.21 and 1.99%, respectively, and the *RRMSE* is 1.51% (Table 3). There is a high simulation accuracy using the AquaCrop model.

It can be seen that the calibrated and validated AquaCrop model can accurately simulate the water supply and demand process of summer maize, and the obtained genetic parameters of maize in the

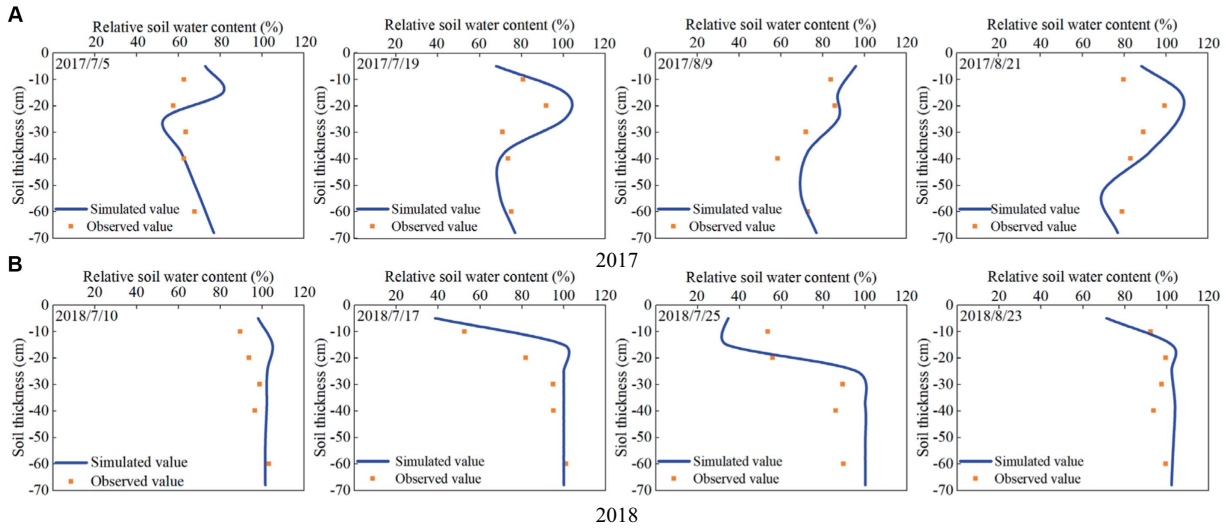

FIGURE 4
Simulated and observed relative soil water content during the growth process of summer maize in **(A)** 2017 and **(B)** 2018.

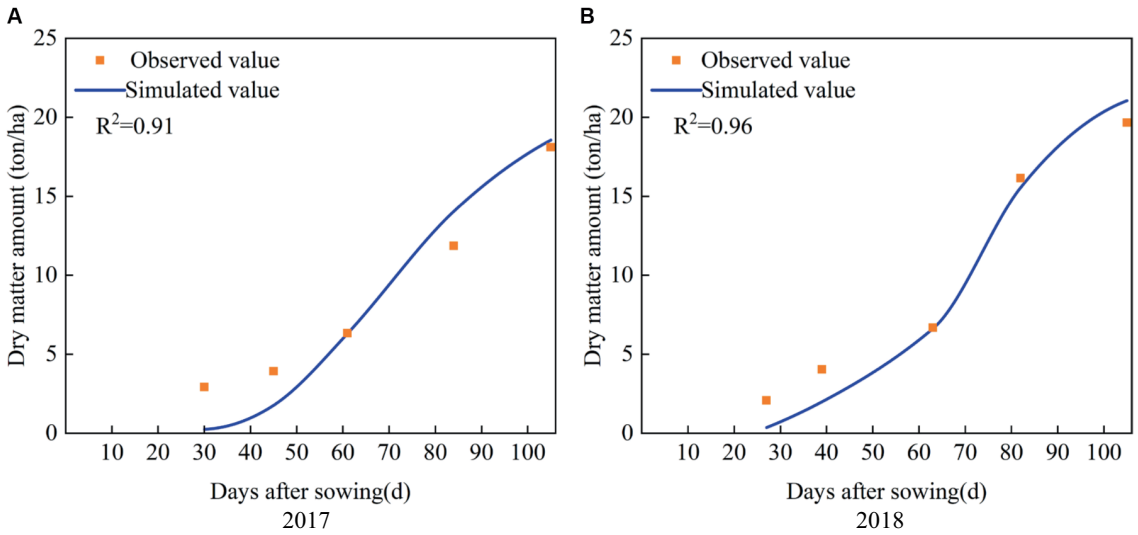

FIGURE 5
Simulated and observed dry matter amount during the whole growth period of summer maize in **(A)** 2017 and **(B)** 2018.

TABLE 3 The values of *ARE* and *RRMSE* between the simulated and observed dry matter amount at harvest and gain yield of summer maize.

Cropping season	Dry matter amount at harvest				Grain yield			
	Sim (ton/ha)	*Obs* (ton/ha)	*ARE*	*RRMSE*	*Sim* (ton/ha)	*Obs* (ton/ha)	*ARE*	*RRMSE*
2017 (calibration)	18.56	18.10	2.55%	5.54%	9.01	8.99	0.21%	1.51%
2018 (validation)	21.06	19.65	7.15%		10.11	10.32	1.99%	

Huaibei Plain are reasonable, which ensures the simulation reliability of the growth processes of maize under drought stress scenarios subsequently.

AquaCrop model has a high fit in simulating maize evapotranspiration, biomass, and yield under different water conditions in the Nebraska (Lu et al., 2022), Uganda (Zizinga et al., 2024), North China Plain (Wu et al., 2024), and Huaibei Plain (Cui et al., 2022). However, Zhou et al. (2024) found that the difference in the total dried yield when using the rain-fed treatment was obvious in 2018 for the North China Plain by AquaCrop model. The reason is that the climate in this area in 2018 is an extreme outlier, with little rainfall and frequent strong winds, while the model cannot take these factors into account. In this study, the precipitation is not extreme (Figure 3) and climate is normal in 2018 for the Huaibei Plain, thus

the simulated dry matter and grain yield are close to the measured values (Table 3). Accordingly, the extreme or unusual climatic conditions should be considered when adopting AquaCrop model.

3.2 Quantitative response of maize transpiration to drought stress

3.2.1 Response of transpiration to drought stress at a single growth stage

Figure 6 shows the transpiration (*Tr*) under continuous light and serious drought at two growth stages of maize. (1) Maize suffers light and serious drought at the seedling stage, *Tr* at this single stage decreases by 40.00 and 78.57%, respectively, compared with that under no drought (Figure 6A); *Tr* decreases by 20.00 and 44.26% at the jointing stage, respectively (Figure 6B); *Tr* decreases by 5.45 and 15.67% at the tasseling stage, respectively (Figure 6C); and *Tr* decreases by 2.00 and 10.44% at the milking stage, respectively (Figure 6C). The proportion of *Tr* reduction under drought condition is the highest at the seedling stage, followed by the jointing stage, tasseling stage, and milking stage. It indicates that drought at a certain growth stage of maize causes a reduction in plant transpiration at this stage, and the more serious the drought stress, the more obvious the reduction.

The effect of drought at the seedling stage is the most severe. Tang et al. (2018) showed that maize canopy increased significantly after 40 d of planting, reflecting that the transpiration was vigorous during the seedling and jointing stages, thus the transpiration was markedly affected by drought at these two stages. Yuan et al. (2019) found that drought caused the close of leaf stomata of summer maize, which resulted in the reduction of plant transpiration, and the reduction increased with the intensity of drought. These results are consistent with the findings of this study. (2) Serious drought at the seedling stage causes the reduction of *Tr* at the jointing stage, the tasseling

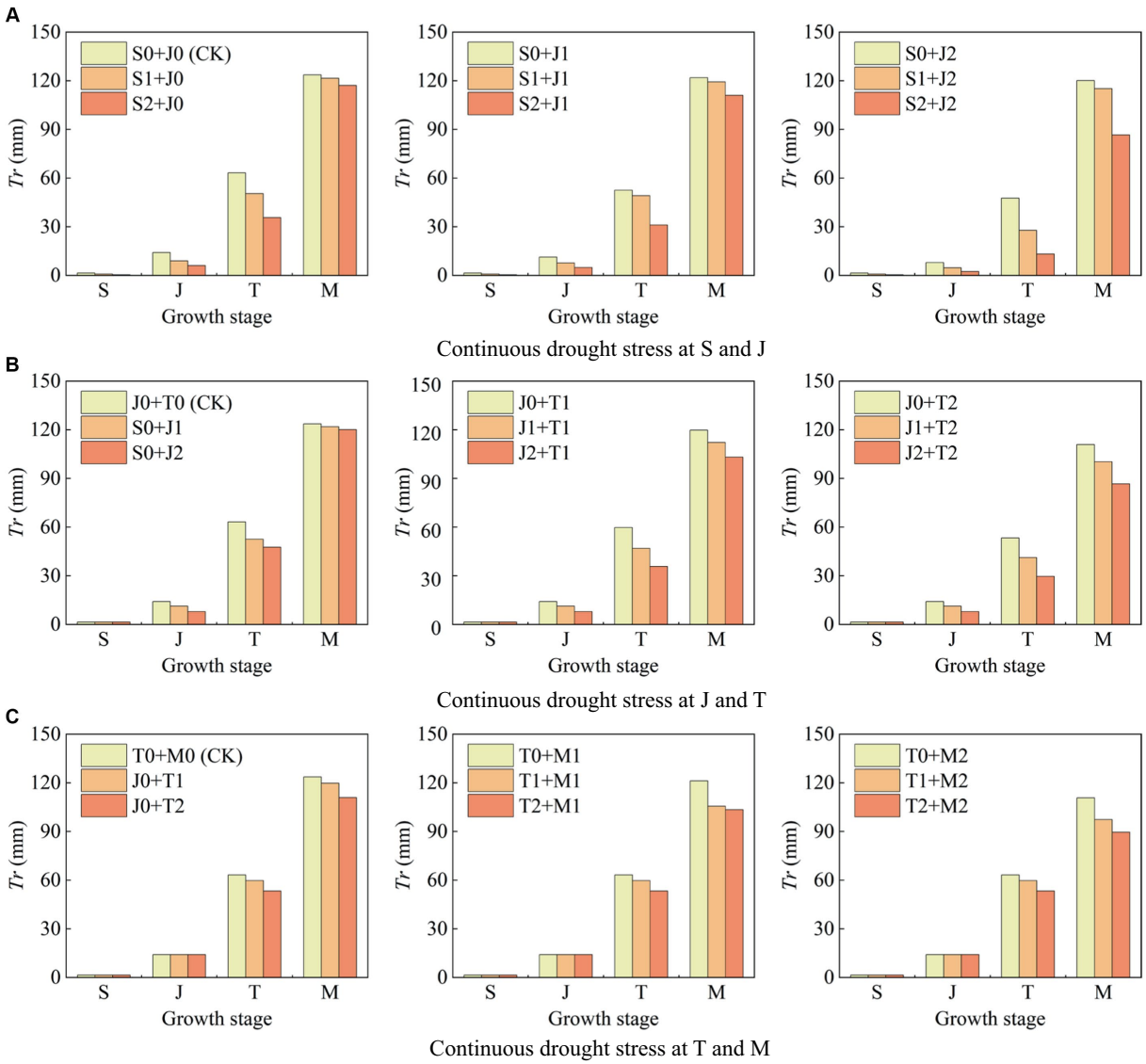

FIGURE 6
Transpiration (*Tr*) at each growth stage of summer maize under continuous drought stress at **(A)** S and J, **(B)** J and T, and **(C)** T and M (S, seedling stage; J, jointing stage; T, tasseling stage; M, milking stage; and 0, no drought stress; 1, light drought stress; 2, serious drought stress).

stage, and the milking stage by 57.45, 43.61, and 5.24%, respectively (Figure 6A); serious drought at the jointing stage reduces *Tr* at the tasseling stage and the milking stage by 24.68 and 2.84% (Figure 6B); and serious drought at the tasseling stage reduces *Tr* at the milking stage by 10.29% (Figure 6C). It indicates that when maize is subjected to drought at a growth stage, the drought not only affects plant transpiration at this stage, but also that the drought impact is continuous and causes the reduction of *Tr* at the subsequent stages, which is the after-effect of drought.

Similarly, Hao et al. (2010) found that drought at the early stage of maize had a lasting impact on transpiration at the later stage. Cui et al. (2020) conducted pot experiments and discovered that when soybean suffered from mild drought at the seedling stage, the evapotranspiration at the branching stage, the flowering-podding stage, and the seed-filling stage reduced by 14.80, 13.23, and 6.12%, respectively, compared with those under full irrigation.

3.2.2 Response of transpiration to continuous drought stress at two growth stages

It can be found that drought at a growth stage of maize has an after-effect on *Tr* in the following stages (Figure 6). Therefore, the impact of continuous drought stress should be fully reflected by the change in *Tr* during the whole growth period. Figure 7 shows the reduction rate of *Tr* under continuous drought stress at two growth stages of maize.

1 The reduction rate of *Tr* during the whole growth period is 21.37% when the maize is subjected to serious drought at the seedling stage, and that is 12.53% under serious drought at the jointing stage; while the reduction rate of *Tr* under continuous serious drought at these two stages is 49.40%, which is higher than the sum of the reduction rates caused by serious drought at the two single stages (>21.37% + 12.53%) (Figure 7A). The reduction rate of *Tr* under continuous serious drought at the jointing stage and the tasseling stages is 37.96% (>12.53% + 11.18%) (Figure 7B). Furthermore, the reduction rate of *Tr* under continuous serious drought at the tasseling stage and the milking stages is 21.75% (>11.18% + 6.38%) (Figure 7C). It indicates that the adverse effect of continuous drought at two growth stages on *Tr* basically exceeds the sum of the effects of drought at the two single stages for summer maize. Moreover, continuous serious drought at the seedling and jointing stages has the most obvious impact on *Tr*.

2 The reduction rate of *Tr* is 10.23% when the maize is subjected to light drought at the seedling stage, and that is 7.52% under light drought at the jointing stage; while the reduction rate of *Tr* under continuous light drought at these two stages is 12.56%, which is lower than the sum of the reduction rates caused by light drought at the two single stages (<10.23% + 7.52%). Similarly, for serious drought at the seedling stage, the reduction rate of *Tr* is 21.37, and for light drought at the jointing stage, the reduction rate of *Tr* is 7.52%, while for serious drought at the seedling stage and light drought at the jointing stage, the reduction rate of *Tr* is 27.29% (<21.37% + 7.52%). It shows that the negative effect of continuous drought at the seedling and jointing stages on *Tr* is less than the sum of the effects of drought at the two single stages. It can be explained that drought at the seedling stage has endowed the maize with an adaptability to drought, which alleviates the negative effect of light drought at the jointing stage on transpiration. However, the adaptability has disappeared when the plant encounters serious drought at the jointing stage. For instance, as shown in Figure 7A, the reduction rate of *Tr* under continuous drought at the seedling and jointing stages is larger than the sum of the reduction rates of *Tr* under drought at the two single stages for maize.

The reduction in maize transpiration caused by drought is primarily due to decreased stomatal conductance (Kinoshita et al., 2021) and an impaired photosynthetic apparatus (Munnus and Millar, 2023). Additionally, there are a series of adaptive changes in physiology and metabolism after early drought for maize (Ru et al., 2023), and the leaves have the ability to recover rapidly but the ability is limited (Yao et al., 2012). Nevertheless, when the plant is subjected to severe drought at a growth stage or continuous serious drought, it may lead to that some photosynthetic apparatus and functions are difficult to recover and irreversibly damaged. Therefore, in this study, drought at a growth stage of summer maize causes reductions of transpiration at the subsequent stages. Meanwhile, compared with the impact on transpiration caused by drought at a single growth stage, continuous drought has a more serious effect.

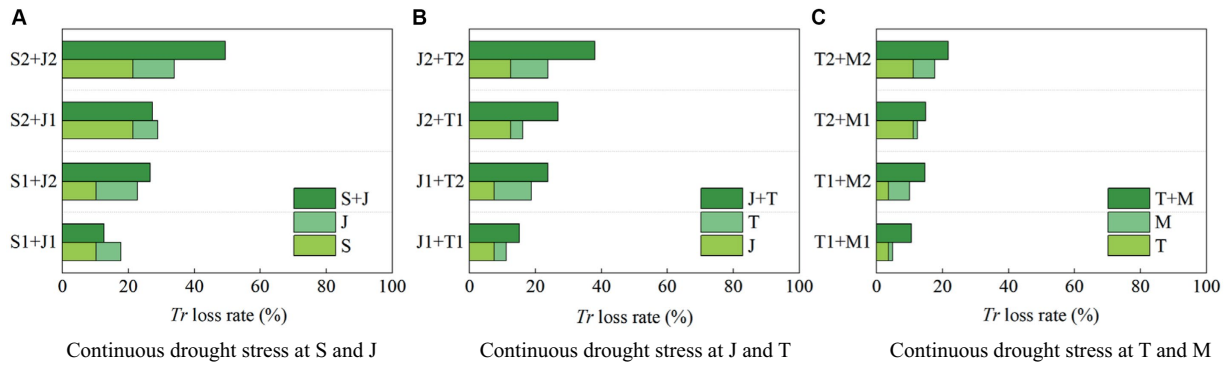

FIGURE 7
The reduction rates of transpiration (*Tr*) during the whole growth period of summer maize under continuous drought stress at **(A)** S and J, **(B)** J and T, and **(C)** T and M (S, seedling stage; J, jointing stage; T, tasseling stage; M, milking stage; and 0, no drought stress; 1, light drought stress; 2, serious drought stress).

3.3 Quantitative response of maize dry matter accumulation to drought stress

3.3.1 Response of dry matter accumulation to drought stress at a single growth stage

Figure 8 shows the dry matter accumulation at each growth stage of maize under different continuous drought stress.

1 The dry matter accumulation of maize under light drought and serious drought at the seedling stage decreases by 40.61 and 58.10%, respectively, compared to that with no drought (Figure 8A). Moreover, the values are 17.94 and 30.05% for the jointing stage (Figure 8B), 9.68 and 18.76% for the tasseling stage (Figure 8C), and 7.33 and 13.02% for the milking stage, respectively (Figure 8C). It can be seen that the reduction proportion of dry matter accumulation caused by drought at the seedling stage is the greatest, followed by the jointing stage, the tasseling stage, and the milking stage. It indicates that drought at a growth stage of maize causes a reduction in dry matter accumulation at this stage, and the more serious the drought, the larger the reduction. Photosynthesis is the source of dry matter for maize (Peng et al., 2023b). Zhang et al. (2018) found that under water deficit condition, the dry matter of maize is decreased due to the inhibition of light capture, which is consistent with the results of this study.

2 Serious drought at the seedling stage reduces the dry matter accumulation at the jointing, the tasseling stage, and the milking stage by 56.76, 49.28, and 23.82%, respectively (Figure 8A); serious drought at the jointing stage reduces the

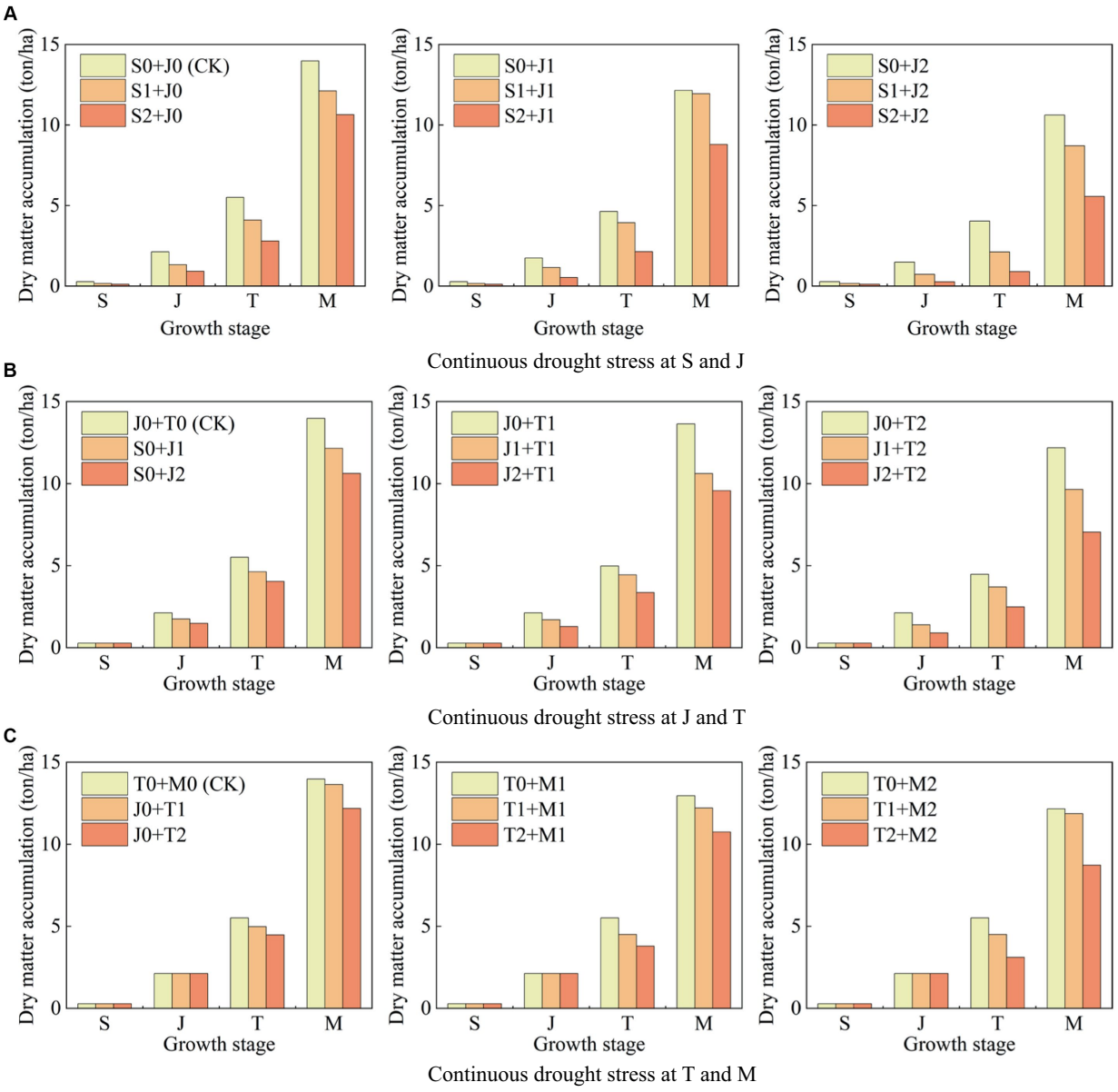

FIGURE 8
Dry matter accumulation at each growth stage of summer maize under continuous drought stress at **(A)** S and J, **(B)** J and T, and **(C)** T and M (S, seedling stage; J, jointing stage; T, tasseling stage; M, milking stage; and 0, no drought stress; 1, light drought stress; 2, serious drought stress).

dry matter accumulation at the tasseling stage and the milking stage by 26.69 and 24.00%, respectively (Figure 8B); serious drought at the tasseling stage reduces the dry matter accumulation at the milking stage by 12.82% (Figure 8C). It reflects that drought at a growth stage of summer maize does not only affect the plant growth at this stage, but the negative impact is continuous, resulting in the reductions of biomass at the following stages. The serious drought at the seedling stage has the most severe impact on maize growth at the jointing stage.

Consistent with this study, Hao et al. (2010) found that maize senescence was accelerated by serious drought in the late seedling and early jointing stages. In addition, Cui et al. (2020) obtained that when soybean was under mild drought at the seedling stage, the biomass accumulations at the branching stage and the flowering-podding stage reduced by 24.01 and 11.49%, respectively, compared with those under no drought stress.

3.3.2 Response of dry matter accumulation to continuous drought stress at two growth stages

It can be seen that drought at a growth stage of summer maize has an after-effect on dry matter accumulation at the later stages, so the dry matter amount at harvest can be used to analyze the impact of continuous drought more accurately. Figure 9 shows the loss rates of dry matter amount at harvest under different scenarios of continuous drought stress at two growth stages for summer maize, compared with that under no drought stress.

1 The loss rate of dry matter amount at harvest is 33.85% when the maize encounters serious drought at the seedling stage, and that is 24.97% when the plant is subjected to serious drought at the jointing stage; while the loss rate under continuous serious drought at these two stages is 68.74%, which is higher than the sum of the loss rates caused by serious drought at the two single stages (>33.85% + 24.97%) (Figure 9A). The loss rates of dry matter amount are 24.97 and 12.91% under serious drought at the jointing stage and the tasseling stage, respectively, while the loss rate under continuous serious drought at these two stages is 51.13% (>24.97% + 12.91%) (Figure 9B). Moreover, the loss rates of dry matter amount are 12.91 and 8.32% for serious drought at the tasseling stage and the milking stage, respectively, while the loss rate for continuous serious drought at these two stages is 35.06% (>12.91% + 8.32%) (Figure 9C). It shows that the adverse impact on biomass of continuous drought at two growth stages is basically more serious than the sum of the impacts of drought at the two single stages for maize. Furthermore, the most severe impact is caused by continuous serious drought at the seedling and jointing stages.

2 The loss rates of dry matter amount at harvest are 19.13 and 14.13% under light drought at the seedling stage and the jointing stage, respectively, while the loss rate under continuous light drought at these two stages is 21.46%, which is less than the sum of the loss rates induced by light drought at the two single stages (<19.13% + 14.13%). Additionally, the loss rate under serious drought at the seedling stage is 33.85, and that under light drought at the jointing stage is 14.13%, while the loss rate caused by serious drought at the seedling stage and light drought at the jointing stage is 47.10% (<33.85% + 14.13%). It reflects that a degree of adaptability to drought for maize has been promoted by drought at the seedling stage, alleviating the impact of light drought at the jointing stage. However, the adaptability has disappeared when the drought at the jointing stage becomes serious.

Drought at different growth stages affects crop biomass accumulation differently. Yao et al. (2012) found that dry matter accumulation of maize was adaptive to drought, but it was detrimental to plant growth if the drought was severe. In addition, drought tolerance is limited at the seedling stage of maize, which is due to that during this stage the growth and development of plant has just began, and part physiological functions have not completed. Therefore, serious drought at the seedling stage has the greatest after-effect on plant growth and biomass accumulation of maize.

Drought accelerates the leaf senescence and decreases the photosynthetic capacity, thus impeding dry matter accumulation for summer maize (Hu et al., 2023). The substantial changes in biochemical and physiological processes under drought conditions decelerate or halt the growth and cause biomass suppression (Gupta et al., 2020). These are consistent with the lasting reductions of dry matter amount caused by drought at a growth stage and exceeded reductions caused by continuous drought for maize. Furthermore,

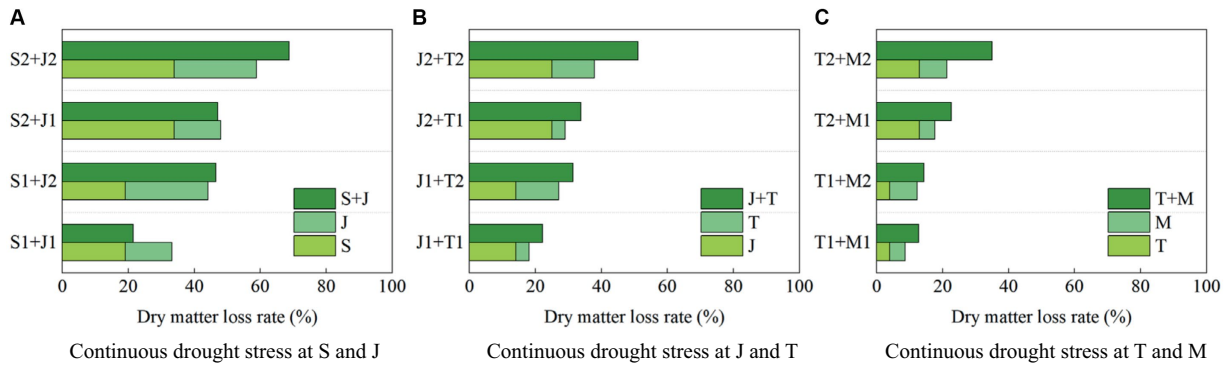

FIGURE 9
The loss rates of dry matter amount at harvest of summer maize under continuous drought stress at **(A)** S and J, **(B)** J and T, and **(C)** T and M (S, seedling stage; J, jointing stage; T, tasseling stage; M, milking stage; and 0, no drought stress; 1, light drought stress; 2, serious drought stress).

among the initial response to drought is stomatal closure, which triggers a series of biochemical and physiological reactions to boost plant defense mechanisms (including antioxidant formation and increased osmolyte accumulation) and maintain the photosynthetic rate (Gusain et al., 2024; Sato et al., 2024). These explain the adaptability of maize plant induced by drought at the seedling stage.

3.4 Quantitative response of maize yield to drought stress

3.4.1 Response of yield to drought stress at a single growth stage

The yield loss rates of summer maize under continuous drought stress at two growth stages are shown in Figure 10. The yield loss rates induced by light and serious drought at the seedling stage are 18.80 and 33.30, respectively, compared with that with no drought (Figure 10A), those for the jointing stage are 12.78 and 24.16%, respectively (Figure 10B), those for the tasseling stage are 3.65 and 12.22%, respectively (Figure 10C), and those for the milking stage are 1.02 and 7.44%, respectively (Figure 10C). The yield loss rates is largest under drought conditions at the seedling stage, followed by the jointing stage, the tasseling stage, and the milking stage. Thus drought at a growth stage of maize causes the yield loss, and the more serious the drought, the more significant the loss.

3.4.2 Response of yield to continuous drought stress at two growth stages

When the maize is subjected to serious drought at the seedling stage and the jointing stage, the yield loss rates are 33.30 and 24.16%, respectively, while when the plant encounters continuous serious drought at these two stages, the loss rate is 100%, which is higher than the sum of the loss rates induced by drought at the two single stages (>33.30% + 24.16%) (Figure 10A). When the maize suffers serious drought at the jointing stage and the tasseling stage, the yield loss rates are 24.16 and 12.12%, respectively, while the loss rate under continuous serious drought at these two stages is 50.16% (>24.16% + 12.12%) (Figure 10B). Furthermore, serious drought at the tasseling stage and the milking stage reduce yield by 12.22 and 7.44%, respectively, while continuous serious drought at these two stages causes yield loss by 33.28% (>12.22% + 7.44%) (Figure 10C). It shows that the negative impact on yield formation of continuous drought at two stages for maize is basically more severe than the sum of the impacts induced by drought at the two single stages. In addition, the maximum yield loss rate is caused by continuous serious drought at the seedling and jointing stages, reaching 100%. The loss rate is 50.16% due to continuous serious drought at the jointing and tasseling stages. These can be explained that the growth of maize at the seedling stage is vigorous, and at this period the reproductive organs have not developed and have less resistance to drought stress, so drought at the seedling and jointing stages causes serious yield loss, which is consistent with the study of Zou et al. (2023).

The yield loss rate are 18.80 and 12.78% when the maize is subjected to light drought at the seedling stage and the jointing stage, respectively, while the loss rate caused by continuous drought at these two stage is 20.66% (<18.80% + 12.45%). It reflects that the negative impact of continuous light drought at the seedling and jointing stages on maize yield formation is less than the sum of the impacts of drought induced by the two single stages. The maize plant has been adaptive to drought at the jointing stage after light drought at the seedling stage. In addition, serious drought at the seedling stage reduces yield by 100% regardless of light or serious drought at the jointing stage, indicating that serious drought at the seedling stage causes irreversible impact on the growth of maize. It is also mentioned in the study of Liu (2015), who found that appropriate drought at the seedling stage could promote maize growth, but prolonged or serious drought stress had caused serious yield reduction or even no harvest.

Maize is tall and broad-leaved, extreme drought at planting could cause leaves to curl and stunt growth. Additionally, high temperatures caused by drought could inhibit the induction of flowering in male flowers and cause factors that interfere with pollen development (Kim and Lee, 2023). These are consistent with the high yield losses caused by drought at the seedling stage and the tasseling stage for summer maize in this study. Furthermore, Hou et al. (2024) found that concurrent drought would induce larger yield gaps, which would be, on average, 2–30% higher than single-type drought, which is consistent with the exceeded reduction of maize yield caused by continuous drought.

The after-effect of drought at different growth stages of summer maize on dry matter partitioning (DMP) are various, and that of drought during vegetative period enlarges and drastically induces the reduction of harvest index (HI), which is larger than that of drought

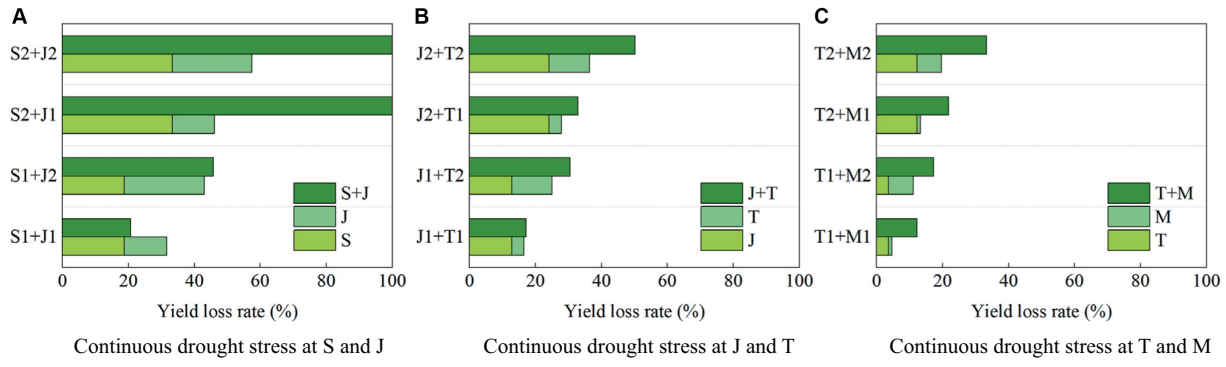

FIGURE 10
The yield loss rates under continuous drought stress of summer maize at two growth stages at **(A)** S and J, **(B)** J and T, and **(C)** T and M (S, seedling stage; J, jointing stage; T, tasseling stage; M, milking stage; and 0, no drought stress; 1, light drought stress; 2, serious drought stress).

during reproductive period, demonstrating obvious alleviation in the previous adverse impacts on DMP and HI (Cai et al., 2023). In addition, the resilience of maize is strong after rewatering under light drought then leaf biomass and root growth could be enhanced, thus improving yield (Jing et al., 2023). These explain the larger grain yield losses caused by drought at the seedling stage and the joint stage (vegetative period) than those caused by drought at the tasseling stage and the milking stage (reproductive period), and also the less yield loss caused by continuous light drought at the seedling and jointing stages in this study.

4 Conclusion

In this study, the quantitative responses of plant transpiration, dry matter accumulation, and yield formation to continuous drought stress at two growth stages of summer maize are analyzed. The main conclusions are as follows:

1 Drought stress at a single growth stage of summer maize has negative impacts on plant transpiration and biomass accumulation at this stage, and the more serious the drought stress, the more significant the impacts. Meanwhile, drought stress at a stage has after-effects on maize transpiration and biomass at the subsequent stages.
2 The impact of continuous drought stress at two growth stages of maize generally exceeds the sum of the impacts of drought at the two single stages, especially continuous serious drought at the seedling and jointing stages, which causes the most severe accumulative effects on plant transpiration, biomass accumulation, and yield formation.
3 Drought at the seedling stage promotes the adaptability of maize, alleviating the negative impacts of light drought at the jointing stage, while the adaptability disappears when drought at the jointing stage becomes serious.

Therefore, in the actual production of summer maize, serious drought at the seedling stage should be avoided to ensure seed survival, and meanwhile, continuous drought stress, especially that at the seedling and jointing stages should be prevented to reduce the accumulative effect and unrecoverable impact. It is conducive to conduct drought disaster prevention planning and irrigation allocation, ensuring normal growth and reduce drought losses of maize. Additionally, climate change impacts (e.g., CO_2 concentration and climate pattern) could be considered in crop growth simulation, field experiments of continuous drought would be carried out if the natural climate meets the conditions, and a more detailed growth stage division of maize in setting continuous drought stress scenarios in future work.

Data availability statement

The original contributions presented in the study are included in the article/supplementary material, further inquiries can be directed to the corresponding author.

Author contributions

YC: Formal analysis, Funding acquisition, Methodology, Writing – original draft. HT: Formal analysis, Investigation, Visualization, Writing – original draft. YZ: Funding acquisition, Methodology, Supervision, Writing – review & editing. JJ: Conceptualization, Funding acquisition, Supervision, Writing – review & editing. SJ: Investigation, Supervision, Writing – review & editing.

Funding

The author(s) declare that financial support was received for the research, authorship, and/or publication of this article. This study was supported by the National Natural Science Foundation of China (Grant nos. 52109009, U2240223, 42271084, and 52379006), the Natural Science Foundation of Anhui Province, China (Grant no. 2308085US06), and the Fundamental Research Funds for the Central Universities (Grant no. JZ2024HGTB0208).

Acknowledgments

The authors sincerely appreciate the reviewers and editors comments to improve the manuscript.

Conflict of interest

The authors declare that the research was conducted in the absence of any commercial or financial relationships that could be construed as a potential conflict of interest.

Publisher's note

Referencess

Ali, S. A., Khatun, R., Ahmad, A., and Ahmad, S. N. (2020). Assessment of cyclone vulnerability, hazard evaluation and mitigation capacity for analyzing cyclone risk using GIS technique: a study on Sundarban biosphere reserve, India. *Earth Syst. Environ.* 4, 71–92. doi: 10.1007/s41748-019-00140-x

Alvar-Beltrán, J., Saturnin, C., Grégoire, B., Camacho, J. L., Dao, A., Migraine, J. B., et al. (2023). Using AquaCrop as a decision-support tool for improved irrigation management in the Sahel region. *Agric. Water Manag.* 287:108430. doi: 10.1016/j.agwat.2023.108430

Cai, F., Mi, N., Ming, H., Zhang, Y., Zhang, H., Zhang, S., et al. (2023). Responses of dry matter accumulation and partitioning to drought and subsequent rewatering at different growth stages of maize in Northeast China. *Front. Plant Sci.* 14:1110727. doi: 10.3389/fpls.2023.1110727

Chang, J., Li, Y., Wang, Y., and Yuan, M. (2016). Copula-based drought risk assessment combined with an integrated index in the Wei River basin, China. *J. Hydrol.* 540, 824–834. doi: 10.1016/j.jhydrol.2016.06.064

Chen, L., Li, F., Li, W., Ning, Q., Li, J., Zhang, J., et al. (2020). Organic amendment mitigates the negative impacts of mineral fertilization on bacterial communities in Shajiang black soil. *Appl. Soil Ecol.* 150:103457. doi: 10.1016/j.apsoil.2019.103457

Corbari, C., Charfi, I. B., and Mancin, M. (2021). Optimizing irrigation water use efficiency for tomato and maize fields across Italy combining remote sensing data and the AquaCrop model. *Hydrology.* 8:39. doi: 10.3390/hydrology8010039

Ćosić, M., Stričević, R., Djurović, N., Moravčević, D., Pavlović, M., and Todorović, M. (2017). Predicting biomass and yield of sweet pepper grown with and without plastic film mulching under different water supply and weather conditions. *Agric. Water Manag.* 188, 91–100. doi: 10.1016/j.agwat.2017.04.006

Cui, Y., Jiang, S., Jin, J., Ning, S., and Feng, P. (2019). Quantitative assessment of soybean drought loss sensitivity at different growth stages based on S-shaped damage curve. *Agric. Water Manag.* 213, 821–832. doi: 10.1016/j.agwat.2018.11.020

Cui, Y., Lin, H., Xie, Y., and Liu, S. (2021). Application study of crop yield prediction based on AquaCrop model in black soil region of Northeast China. *Acta Agron. Sin.* 47, 159–168. doi: 10.3724/SP.J.1006.2021.03016

Cui, Y., Ning, S., Jin, J., Jiang, S., Zhou, Y., and Wu, C. (2020). Quantitative lasting effects of drought stress at a growth stage on soybean evapotranspiration and aboveground biomass. *Water* 13:18. doi: 10.3390/w13010018

Cui, Y., Tang, H., Jin, J., Zhou, Y., Jiang, S., and Chen, M. (2022). System structure—based drought disaster risk assessment using remote sensing and field experiment data. *Remote Sens.* 14:5700. doi: 10.3390/rs14225700

Cui, Y., Zhou, Y., Jin, J., Jiang, S., Wu, C., and Ning, S. (2023). Spatiotemporal characteristics and obstacle factors identification of agricultural drought disaster risk. A case study across Anhui Province, China. *Agric. Water Manag.* 289:108554. doi: 10.1016/j.agwat.2023.108554

Daniel, C. (2012). One-at-a-time plans. *J. Am. Stat. Assoc.* 68, 353–360. doi: 10.1080/01621459.1973.10482433

Dao, J., Xing, Y., Chen, C., Chen, M., and Wang, Z. (2023). Adaptability of rhizosphere bacterial communities of drought-resistant sugarcane varieties under different degrees of drought stress. *Microbiol. Spectr.* 11:e0118423. doi: 10.1128/spectrum.01184-23

Dercas, N., Dalezios, N. R., Stamatiadis, S., Evangelou, E., Glampedakis, A., Mantonanakis, G., et al. (2022). AquaCrop simulation of winter wheat under different N management practices. *Hydrology.* 9:56. doi: 10.3390/hydrology9040056

Ge, D., Gao, X., and Wei, X. (2024). Changes in spatiotemporal drought characteristics from 1961 to 2017 in northeastern maize-growing regions, China. *Irrig. Sci.* 42, 163–177. doi: 10.1007/s00271-023-00893-4

Ge, W., Han, J., Zhang, D., and Wang, F. (2021). Divergent impacts of droughts on vegetation phenology and productivity in the Yungui plateau. Southwest China. *Ecol. Indic.* 127:107743. doi: 10.1016/j.ecolind.2021.107743

Greaves, G. E., and Wang, Y. (2016). Assessment of FAO AquaCrop model for simulating maize growth and productivity under deficit irrigation in a tropical environment. *Water* 8:557. doi: 10.3390/w8120557

Guo, E., Zhang, J., Wang, Y., Si, H., and Zhang, F. (2016). Dynamic risk assessment of waterlogging disaster for maize based on CERES-maize model in Midwest of Jilin Province, China. *Nat. Hazards* 83, 1747–1761. doi: 10.1007/s11069-016-2391-0

Gupta, A., Rico-Medina, A., and Caño-Delgado, A. I. (2020). The physiology of plant responses to drought. *Science* 368, 266–269. doi: 10.1126/science.aaz7614

Gusain, S., Kumari, K., and Joshi, R. (2024). Physiological, hormonal and molecular dynamics of root system architectural response to drought stress signaling in crops. *Rhizosphere.* 31:100922. doi: 10.1016/j.rhisph.2024.100922

Hao, S., Guo, X., and Wang, W. (2010). Aftereffects of water stress on corn growth at different stages. *Trans. Chin. Soc. Agric. Eng.* 26, 71–75. doi: 10.3969/j.issn.1002-6819.2010.07.012

Hou, M., Li, Y., Biswas, A., Chen, X., Xie, L., Liu, D., et al. (2024). Concurrent drought threatens wheat and maize production and will widen crop yield gaps in the future. *Agric. Syst.* 220:104056. doi: 10.1016/j.agsy.2024.104056

Hsiao, T., Heng, L., Steduto, P., Rojas-Lara, B., Raes, D., and Fereres, E. (2009). AquaCrop—the FAO crop model to simulate yield response to water: III. Parameterization and testing for maize. *Agron. J.* 101, 448–459. doi: 10.2134/agronj2008.0218s

Hu, J., Zhao, X., Gu, L., Liu, P., Zhao, B., Zhang, J., et al. (2023). The effects of high temperature, drought, and their combined stresses on the photosynthesis and senescence of summer maize. *Agric. Water Manag.* 289:108525. doi: 10.1016/j.agwat.2023.108525

Hussain, A., Jadoon, K. Z., Rahman, K. U., Shang, S., Shahid, M., Ejaz, N., et al. (2023). Analyzing the impact of drought on agriculture: evidence from Pakistan using standardized precipitation evapotranspiration index. *Nat. Hazards* 115, 389–408. doi: 10.1007/s11069-022-05559-6

Irmak, S., Amiri, E., Bazkiaee, P. A., and Araji, H. A. (2024). Evaluation of CERES-maize model for simulating maize phenology, grain yield, soil-water, evapotranspiration, and water productivity under different nitrogen levels and rainfed, limited, and full irrigation conditions. *Irrig. Sci.* 42, 551–573. doi: 10.1007/s00271-023-00909-z

Jing, L., Weng, B., Yan, D., Zhang, S., Bi, W., and Yan, S. (2023). The persistent impact of drought stress on the resilience of summer maize. *Front. Plant Sci.* 14:1016993. doi: 10.3389/fpls.2023.1016993

Kim, K. H., and Lee, B. M. (2023). Effects of climate change and drought tolerance on maize growth. *Plan. Theory* 12:3548. doi: 10.3390/plants12203548

Kinoshita, T., Toh, S., and Torii, K. U. (2021). Chemical control of stomatal function and development. *Curr. Opin. Plant Biol.* 60:102010. doi: 10.1016/j.pbi.2021.102010

Lamin-Samu, A. T., Mohamed, F., Muhammad, A., and Lu, G. (2021). Morpho-physiological and transcriptome changes in tomato anthers of different developmental stages under drought stress. *Cells* 10:1809. doi: 10.3390/cells10071809

Li, B., Qin, L., Qi, H., Wang, J., Dang, Y., Lv, M., et al. (2024). Assessing the effects of drought on rainfed maize water footprints based on remote sensing approaches. *J. Sci. Food Agric.* 104, 1154–1165. doi: 10.1002/JSFA.13000

Li, F., Zhang, M., and Liu, Y. (2022). Quantitative research on drought loss sensitivity of summer maize based on AquaCrop model. *Nat. Hazards* 112, 1065–1084. doi: 10.1007/S11069-022-05218-W

Liu, L. (2015). The influence of drought on the growth and yield of maize. *Agric. Sci. Technol. Equipment* 11, 6–7. doi: 10.3969/j.issn.1674-1161.2015.11.003

Lu, Y., Wei, C., McCabe, M. F., and Sheffild, J. (2022). Multi-variable assimilation into a modified AquaCrop model for improved maize simulation without management or crop phenology information. *Agric. Water Manag.* 266:107576. doi: 10.1016/j.agwat.2022.107576

Mondol, M. A. H., Zhu, X., Dunkerley, D., and Henley, B. J. (2021). Observed meteorological drought trends in Bangladesh identified with the effective drought index (EDI). *Agric. Water Manag.* 255:107001. doi: 10.1016/j.agwat.2021.107001

Munnus, R., and Millar, A. H. (2023). Seven plant capacities to adapt to abiotic stress. *J. Exp. Bot.* 74, 4308–4323. doi: 10.1093/jxb/erad179

Ors, S., Ekinci, M., Yildirim, E., Sahin, U., Turan, M., and Dursun, A. (2021). Interactive effects of salinity and drought stress on photosynthetic characteristics and physiology of tomato (*Lycopersicon esculentum* L.) seedlings. *S. Afr. J. Bot.* 137, 335–339. doi: 10.1016/j.sajb.2020.10.031

Peng, J., Lu, L., Noor, M., Li, S., Ma, W., and Wang, J. (2023b). Mid-season lodging modulates photosynthesis, evapotranspiration, and dry matter accumulation and distribution simulated by the optimized model in maize. *Front. Ecol. Evol.* 11:1178609. doi: 10.3389/fevo.2023.1178609

Peng, Q., Shen, R., Li, X., Ye, T., Dong, J., Fu, Y., et al. (2023a). A twenty-year dataset of high-resolution maize distribution in China. *Sci. Data.* 10:658. doi: 10.1038/S41597-023-02573-6

Razzaghi, F., Zhou, Z., Andersen, M., and Plauborg, F. (2017). Simulation of potato yield in temperate condition by the AquaCrop model. *Agric. Water Manag.* 191, 113–123. doi: 10.1016/j.agwat.2017.06.008

Ru, C., Hu, X., Chen, D., and Wang, W. (2023). Droughts and thermo-priming enhance acclimation to later drought and heat stress in maize seedlings by improving leaf physiological activity. *Agronomy* 13:1124. doi: 10.3390/agronomy13041124

Salgotra, R. K., and Chauhan, B. S. (2023). Ecophysiological responses of rice (*Oryza sativa* L.) to drought and high temperature. *Agronomy* 13:1877. doi: 10.3390/agronomy13071877

Sato, H., Mizoi, J., Shinozaki, K., and Yamaguchi-Shinozaki, K. (2024). Complex plant responses to drought and heat stress under climate change. *Plant J.* 117, 1873–1892. doi: 10.1111/tpj.16612

Shafi, S., Shafi, I., Zaffar, A., Zaffar, S. M., Shikari, A. B., Ranjan, A., et al. (2023). The resilience of rice under water stress will be driven by better roots: evidence from root phenotyping, physiological, and yield experiments. *Plant Stress* 10:100211. doi: 10.1016/j.stress.2023.100211

Tang, D., Feng, Y., Gong, D., Hao, W., and Cui, N. (2018). Evaluation of artificial intelligence models for actual crop evapotranspiration modeling in mulched and non-mulched maize croplands. *Comput. Electron. Agric.* 152, 375–384. doi: 10.1016/j.compag.2018.07.029

Tojo Soler, C. M., Suleiman, A., Anothai, J., Flitcroft, I., and Hoogenboom, D. (2013). Scheduling irrigation with a dynamic crop growth model and determining the relation between simulated drought stress and yield for peanut. *Irrig. Sci.* 31, 889–901. doi: 10.1007/s00271-012-0366-9

Voloudakis, D., Karamanos, A., Economou, G., Kalivas, D., Vahamidis, P., Kotoulas, V., et al. (2015). Prediction of climate change impacts on cotton yields in Greece under eight climatic models using the AquaCrop crop simulation model and discriminant function analysis. *Agric. Water Manag.* 147, 116–128. doi: 10.1016/j.agwat.2014.07.028

Wang, C., Guo, E., Wang, Y., Jirigala, B., Kang, Y., and Zhang, Y. (2023). Spatiotemporal variations in drought and waterlogging and their effects on maize yields at different growth stages in Jilin Province, China. *Nat. Hazards* 118, 155–180. doi: 10.1007/s11069-023-05996-x

Wang, Y., Lv, J., Sun, H., Zuo, H., Gao, H., Qu, Y., et al. (2022). Dynamic agricultural drought risk assessment for maize using weather generator and APSIM crop models. *Nat. Hazards* 114, 3083–3100. doi: 10.1007/s11069-022-05506-5

Wei, Y., Jin, J., Cui, Y., Ning, S., Fei, Z., Wu, C., et al. (2021). Quantitative assessment of soybean drought risk in Bengbu city based on disaster loss risk curve and DSSAT. *Int. J. Disaster Risk Reduc.* 56:102126. doi: 10.1016/j.ijdrr.2021.102126

Wei, Y., Jin, J., Jiang, S., Ning, S., Cui, Y., and Zhou, Y. (2019). Simulated assessment of summer maize drought loss sensitivity in Huaibei plain, China. *Agronomy* 9:78. doi: 10.3390/agronomy9020078

Wu, Y., Leng, P., and Ren, C. (2024). Assessing net irrigation needs in maize–wheat rotation farmlands on the North China plain: implications for future climate scenarios. *Agronomy* 14:1144. doi: 10.3390/agronomy14061144

Xie, Z., Kong, J., Tang, M., Luo, Z., Li, D., Liu, R., et al. (2023). Modelling winter rapeseed (*Brassica napus* L.) growth and yield under different sowing dates and densities using AquaCrop model. *Agronomy* 13:367. doi: 10.3390/agronomy13020367

Yao, C., Zhang, S., and Yan, X. (2012). Effects of drought and re-watering on photosynthetic characteristics of maize leaf. *Res. Soil Water Conserv.* 19, 278–283.

Yuan, H., Jiang, S., Yang, J., and Liu, J. (2019). The response regularity of maize under drought stress based on physiological indexes. *Water Saving Irrigation.* 5, 5–10. doi: 10.3969/j.issn.1007-4929.2019.05.002

Zhang, C., Chao, J., Tang, M., Lin, W., Ding, D., and Feng, H. (2023). Improving maize growth and development simulation by integrating temperature compensatory effect under plastic film mulching into the AquaCrop model. *Crop J.* 11, 1559–1568. doi: 10.1016/j.cj.2023.05.008

Zhang, J., He, Y., Wang, J., Zhao, Y., and Wang, C. (2015). Impact simulation of drought at different growth stages on grain formation and yield of maize. *Chin. J. Agrometeorol.* 36, 43–49. doi: 10.3969/j.issn.1000-6362.2015.01.006

Zhang, X., Lei, L., Lai, J., Zhao, H., and Song, W. (2018). Effects of drought stress and water recovery on physiological responses and gene expression in maize seedlings. *BMC Plant Biol.* 18:68. doi: 10.1186/s12870-018-1281-x

Zhang, J., Okada, N., Tatano, H., and Hayakawa, S. (2004). Damage evaluation of agro-meteorological hazards in the maize-growing region of Songliao plain, China: case study of Lishu county of Jilin Province. *Nat. Hazards* 31, 209–232. doi: 10.1023/B:NHAZ.0000020263.98345.a0

Zhang, Q., Yao, Y., Li, Y., Huang, J., Ma, Z., Wang, Z., et al. (2020). Causes and changes of drought in China: research progress and prospects. *J. Meteorol. Res.* 34, 460–481. doi: 10.1007/s13351-020-9829-8

Zhou, R., Jin, J., Cui, Y., Ning, S., Bai, X., Zhang, L., et al. (2022). Agricultural drought vulnerability assessment and diagnosis based on entropy fuzzy pattern recognition and subtraction set pair potential. *Alex. Eng. J.* 61, 51–63. doi: 10.1016/j.aej.2021.04.090

Zhou, D., Wang, H., Wang, X., Wang, F., Zhang, J., and Ma, D. (2024). Evaluation of AquaCrop's ability to simulate water stress based on 2-year case study of maize crop. *Agronomy* 14:354. doi: 10.3390/agronomy14020354

Zhu, X., Xu, K., Liu, Y., Guo, R., and Chen, L. (2021). Assessing the vulnerability and risk of maize to drought in China based on the AquaCrop model. *Agric. Syst.* 189:103040. doi: 10.1016/j.agsy.2020.103040

Zizinga, A., Mwanjalolo, J. G. M., Tietjen, B., Martins, M. A., and Bedadi, B. (2024). Maize yield under a changing climate in Uganda: long-term impacts for climate smart agriculture. *Reg. Environ. Chang.* 24:34. doi: 10.1007/s10113-024-02186-8

Zou, Z., Cheng, C., and Shen, S. (2023). Effects of meteorological conditions and irrigation levels during different growth stages on maize yield in the Jing-Jin-Ji region. *Sustain. For.* 15:3485. doi: 10.3390/su15043485

frontiers | Frontiers in Sustainable Food Systems

TYPE Original Research
PUBLISHED 23 October 2024
DOI 10.3389/fsufs.2024.1477210

OPEN ACCESS

EDITED BY
Aliza Pradhan,
National Institute of Abiotic Stress Management (ICAR), India

REVIEWED BY
Khushboo Rani,
Indian Institute of Soil Science (ICAR), India
Arjun Tayade,
Central Institute for Cotton Research (ICAR), India

*CORRESPONDENCE
Sheetal Sharma
✉ sheetalhpkvv@gmail.com
Arti Bhatia
✉ arti.bhatia@icar.gov.in

RECEIVED 07 August 2024
ACCEPTED 09 October 2024
PUBLISHED 23 October 2024

CITATION
Chakrabarti B, Sharma S, Mishra AK, Kannojiya S, Kumar V, Bandyopadhyay SK and Bhatia A (2024) Application of additional dose of N could sustain rice yield and maintain plant nitrogen under elevated ozone (O_3) and carbon dioxide (CO_2) condition. *Front. Sustain. Food Syst.* 8:1477210. doi: 10.3389/fsufs.2024.1477210

Application of additional dose of N could sustain rice yield and maintain plant nitrogen under elevated ozone (O_3) and carbon dioxide (CO_2) condition

Bidisha Chakrabarti[1], Sheetal Sharma[2]*, Ajay Kumar Mishra[2], Sudha Kannojiya[1], V. Kumar[1], S. K. Bandyopadhyay[1] and Arti Bhatia[1]*

[1]Division of Environment Science, ICAR-Indian Agricultural Research Institute, New Delhi, India, [2]International Rice Research Institute, New Delhi, India

Introduction: Global food security is challenged by the increasing levels of air pollutants like ozone (O_3) through their impacts on crop productivity. The present study was conducted to quantify the interactive effect of elevated ozone (O_3) and carbon dioxide (CO_2), on different rice varieties in northern India.

Methods: An experiment was conducted in Genetic H field, Environment science, IARI for two consecutive years (2020 and 2021) during the *kharif* season, to quantify the impact of elevated O_3 and CO_2 interaction on productivity, and plant N in three rice varieties (Pusa basmati 1121, Nagina 22, IR64 Drt1) under different nitrogen (N) management practices. Rice crop was grown in Free Air Ozone-Carbon dioxide Enrichment rings (FAOCE) rings with two levels of O_3 (elevated 60 $\pm$10ppb and ambient) and two levels of CO_2 (elevated, 550$\pm$25 ppm and ambient) concentration and their interaction with two N fertilizer treatments i.e., 100% RDN (recommended dose of N) and 125% RDN.

Results and discussion: Elevated O_3 significantly decreased physiological parameters like photosynthesis rate, stomatal conductance and transpiration rate of the crop. Grain yield reduced by 7.2-7.5%, in Pusa Basmati 1121 and from 6.9-9% in IR64 Drt1 varieties in elevated O_3 treatment as compared to ambient treatment. Yield reduction in Nagina 22 variety was not significant in elevated O_3 treatment. Elevated CO_2 concentration of 550 ppm was able to fully compensate the yield loss in Nagina 22 variety and partially compensate (3.9-8.0%) in Pusa Basmati 1121 and IR64 Drt1 varieties. Grain N concentration in rice varieties decreased by 10.8-14.7% during first year and by 7.8-20.6% during second year in elevated O_3 plus CO_2 interaction treatment than ambient. Grain N uptake also decreased (13.2-17.1% in first year and 4.5-22.8% in second year) in elevated O_3 plus CO_2 interaction treatment as compared to ambient. Application of additional 25% of recommended dose of N improved grain N concentration, grain N uptake as well as available N of soil as compared to 100% RDN treatment in elevated O_3 plus CO_2 interaction treatment. Additional 25% N dose could help in sustaining rice productivity and quality under elevated O_3 and CO_2 condition.

KEYWORDS

elevated O_3, elevated CO_2, N management, plant nitrogen, rice variety

Introduction

Air pollution is only one of several environmental issues that threaten food production. Tropospheric ozone (O_3) is one of the major air pollutants harmful to plants (Feng et al., 2015). The O_3 pollution is expected to worsen in the future due to a warmer climate, depending on the location, and increased anthropogenic emissions of O_3 precursors.

Following the Industrial Revolution, the percentage of ground-level O_3 has been steadily rising, reaching 35–40 ppb globally. In the 21st century, it may continue to rise more rapidly in developing countries with fast-growing economies (Proietti et al., 2016). The tropospheric O_3 level might exceed 70 ppb by 2050, according to the Environmental Protection Agency, if worldwide emissions of O_3 precursors continue at their current rate (Pfister et al., 2014). Tropospheric O_3 concentrations are increasing at a higher rate in tropical regions due to favorable conditions for O_3 formation (Agrawal et al., 2003; Tiwari et al., 2008). Following the mid-1990s, the decadal increase in tropospheric O_3 levels has been 2–14% in the tropics, 2–7% in northern mid-latitude areas, and 8–14% in the South Asian region (IPCC, 2021). Tropospheric O_3 is created as a secondary pollutant in the atmosphere through photochemical interactions between volatile organic compounds (VOCs) and nitrogen oxides (NOx) in the presence of sunlight (Lefohn et al., 2017). Due to increased economic growth accompanied by higher NOx and VOC emissions, tropospheric O_3 levels are rising and are expected to continue to do so across the Asian region, leading to more crop losses (Ashmore, 2005). The O_3 concentration ranged from 45 to 65 ppb across the Indian region (David and Nair, 2013; Deb Roy et al., 2009). In most regions of the world, ozone is now the most significant air pollutant that has a detrimental effect on the growth and productivity of crops. Tropospheric O_3 is also a greenhouse gas (GHG) and contributes to climate change (Feng et al., 2019). Exposure to O_3 leads to stomatal closure, which limits carbon dioxide (CO_2) and water uptake by plants, further compromising photosynthetic efficiency and causing reduced growth and decreased grain filling in crop plants (Feng and Kobayashi, 2009). Several studies have quantified the impact of O_3 on crop development and yield (Ainsworth, 2008; Mills et al., 2018; Tai et al., 2014; Yadav et al., 2021). There are reports of reduced photosynthesis rates, leaf senescence, and changes in assimilate partitioning in plants due to exposure to elevated levels of O_3 (Mina et al., 2016; Tomer et al., 2015). Increased concentrations of surface O_3 diminish carbon storage in vegetation, leading to reduced growth and yield of crops (Tai et al., 2014). On the other hand, elevated atmospheric CO_2 concentrations lead to the accumulation of carbon, thereby increasing crop growth and also reducing plant nitrogen (N) and protein content (Abebe et al., 2016; Chakrabarti et al., 2020; Raj et al., 2019). The global average concentration of CO_2 has increased from 280 ppm to 409.7 ppm (NOAA, ESRI, 2019). An increase in atmospheric CO_2 concentrations improves the growth and productivity of crop plants (Bhatia et al., 2012; Singh et al., 2013; Deryng et al., 2016).

The world's most important food crop, rice, is vulnerable to a variety of contaminants, especially air pollutants such as tropospheric O_3. Global food security is likely to suffer if the productivity of rice declines. Elevated tropospheric O_3 levels cause stress to rice plants during both the vegetative and reproductive stages, affecting their physiology, yield, and grain quality. According to Xia et al. (2021), major food crops, such as rice, wheat, and maize, are less tolerant to elevated O_3 than trees, such as spruce, silver fir, and pine. Elevated O_3 levels can alter physiological processes in crop plants, leading to changes in crop morphology and reduced crop growth (Bhatia et al., 2013).

Some reports elevated O_3 levels reduced yield by 11.4–12.3% compared to ambient levels in rice crops (Bhatia et al., 2011). Pandey et al. (2018) observed that grain yield and grain N content in wheat decreased under elevated O_3 concentrations. Along with reduced plant growth and productivity, higher O_3 levels also affect grain quality in crops as it is a strong oxidant and reduces important physiological processes in plants (Avnery et al., 2011; Broberg et al., 2015). Some researchers have reported that protein content in crops gets negatively affected by elevated O_3, but to a lesser extent than grain yield (Broberg et al., 2015; Grünhage et al., 2012). The interactive effect of elevated O_3 and CO_2 on crop growth, yield, and plant nutrient content will differ from the individual effect of O_3. Phothi et al. (2016) reported that elevated CO_2 levels would mitigate the negative impact of elevated tropospheric O_3 in rice crops. A simultaneous increase in both O_3 and CO_2 concentrations could nullify the negative effects of elevated O_3 on the ecosystem (Bhatia et al., 2012). Therefore, the negative effects of elevated tropospheric O_3 would be overestimated if the impact of elevated CO_2 concentrations is not considered (Xia et al., 2021).

Crop productivity is affected by the availability of N supplied to plants through various sources, including inorganic fertilizers. The interaction between O_3 and CO_2 will also affect the nutrient levels in crops (Phothi et al., 2016). As crop growth is reduced under elevated O_3 conditions (Pleijel et al., 2014), the demand and uptake of nutrients will also get altered under such situations, thereby reducing total nutrient content in plants. A study comprising data analysis of peer-reviewed literature depicted that the translocation of nitrogen from straw and leaves to grain in wheat crops was negatively affected by O_3. As N fertilizer use efficiency is reduced under elevated O_3 conditions, the risk of N losses from agroecosystems increases (Broberg et al., 2017). Elevated O_3 also affects soil microbial function and N transformation in the soil (Chen et al., 2015; Wu et al., 2016), which could, in turn, affect nutrient availability and uptake in plants. As crop productivity is often limited by nitrogen, N management becomes very crucial, especially under changing climatic conditions (Bhatia et al., 2010). A study by Singh et al. (2009) showed that the application of 1.5 times of recommended NPK can help ameliorate the negative effects of elevated tropospheric O_3 in mustard crops.

Estimating the effects of crop loss caused by tropospheric O_3 is crucial for nations, such as India, that are experiencing rapid urbanization and population growth. A few studies have investigated the interactive effects of elevated O_3 and CO_2 on crop plants. However, studies on elevated O_3 and CO_2 interactions with rice productivity and plant N are very limited. In addition, most studies were conducted earlier using open-top chambers (OTCs). It is imperative to conduct studies on the interaction between elevated levels of O_3 and CO_2 in open-field conditions, as such research is rarely reported. There is a need for a better understanding of cultivar-specific responses to elevated O_3 and CO_2 interactions to identify suitable adaptation options in rice under ozone stress conditions. In addition, N management strategies need to be formulated to sustain crop productivity and quality under elevated O_3 and CO_2 conditions. The hypothesis is that elevated O_3 and CO_2 can negatively affect rice productivity and quality. An additional N dose may counteract the

harmful effects by improving growth, yield, and plant N uptake under elevated O_3 and CO_2 conditions. Therefore, the following study was conducted using a free air ozone and carbon dioxide enrichment (FAOCE) facility under open-field conditions (1) to quantify the yield and N uptake in rice varieties under the interaction of elevated O_3 and CO_2 and (2) to investigate the effect of an increased N dose on the yield and plant N in rice under elevated O_3 and CO_2 conditions.

Materials and methods

Experimental site

A field experiment was conducted during the *kharif* season (July–October) for two consecutive years, i.e., 2020 and 2021, inside free air O_3 and CO_2 enrichment (FAOCE) rings located at the experimental farm of the-Indian Agricultural Research Institute (ICAR), New Delhi (28°35'N and 77°12′E) India. The mean temperatures during the cropping season were 29.5°C in the first and 29.1°C in the second year of the study. Three different rice varieties, Pusa Basmati 1121, Nagina 22, and IR64 Drt1, were grown in crates inside the free air ozone and carbon dioxide enrichment (FAOCE) facility. Pusa Basmati 1509 is a popular basmati variety of rice in the northwestern Indo-Gangetic Plain (IGP). It is known for its long, slender grains and distinct aroma. IR64 DRT1 is a high-yielding, drought-tolerant rice variety that is resistant to major pests and diseases and can be grown in different agro-climatic conditions. Nagina 22 is a short-duration rice variety adaptable to various abiotic stresses and also resistant to pests and diseases. The rice varieties were grown under ambient and elevated (60 ppb) O_3 levels, as well as ambient and elevated (550 ± 25 ppm) CO_2 concentrations. The ambient CO_2 concentration ranged from 398 to 421 ppm and from 404 to 420 ppm in 2020 and 2021, respectively. The elevated CO_2 concentration ranged from 518 to 570 ppm and from 526 to 575 ppm in the FAOCE rings in 2020 and 2021, respectively. The 5 m diameter FAOCE rings were effective in exposing the crops to elevated O_3 and CO_2 under natural field conditions. Air mixed with CO_2 was supplied at the canopy level through perforated pipes with laser-drilled holes (0.3 mm in diameter) inside the ring from commercial-grade compressed 30 kg pure CO_2 gas cylinders. The release of CO_2 inside the rings was controlled by the opening and closing of the solenoid valves depending on the wind speed and direction (Yadav et al., 2021). Ozone generators were used to convert atmospheric oxygen (O_2) into O_3, which was then released inside the rings with the help of flappers through a common duct placed perpendicular to the rings (Yadav et al., 2019). Air samples were drawn from the center of the rings, and the CO_2 concentration was measured using a CO_2 analyzer (NDIR, Topak United States), while the O_3 concentration was measured using an O_3 analyzer (2B Technologies). The CO_2 and O_3 concentrations in the rings were automatically logged in the computer by microprocessors through digital input and output modules on a real-time basis. The crops were exposed to elevated CO_2 and O_3 for 7 h (10.00 am to 17.00 pm). Four rings were used for the study: (1) ambient CO_2 and O_3, (2) ambient O_3 and elevated CO_2, (3) elevated O_3 and ambient CO_2, and (4) elevated O_3 and elevated CO_2. Rice seedlings (30 days old) were transplanted into crates (42 cm × 63 cm) filled with 40 kg of soil inside the FAOCE rings during the second week of July. The crops were fertilized with two doses of N: the recommended dose of N (RDN) (120 kg ha^{-1}) and 125% of the recommended dose of N (150 kg ha^{-1}). Phosphorus (P) and potassium (K) were applied at the rate of 60 kg ha^{-1}. Half of the N dose and the total amount of P and K were applied at the time of transplanting. The remaining half of the N dose was applied in two equal splits at the maximum tillering and flowering stages of the crops. In total, there were 24 treatments, each with three replications.

Measurements of the crop growth parameters

Gas exchange parameters, such as photosynthesis rate, stomatal conductance, and transpiration rate, were measured using the Portable Photosynthesis System IRGA (LI-6400XT, LiCOR, United States) at the maximum tillering stage of the crops. The observations were recorded on physiologically active, fully expanded leaves exposed to the sun between 9:00 AM to 11:00 AM. The flow rate of input air was set at 300 μmol s^{-1}, and photosynthetically active radiation (PAR) was set at 1,000 μmol m^{-2} s^{-1}. The reference CO_2 concentration was maintained at 410 ppm. Ten readings were recorded for each observation in each treatment. The number of tillers per hill was also counted for each treatment. The plant samples were harvested at maturity and air-dried, and the weights of the grain and straw were recorded. The number of grains per panicle was counted after harvesting the crops for each treatment.

Soil and plant sample collection and analysis

Soil samples were collected at the flowering stage. Available N in the soil was estimated using the Subbiah and Asija (1956) method. The soil was distilled with alkaline $KMnO_4$ (potassium permanganate) and NaOH (sodium hydroxide) solutions, and the amount of liberated NH_3 (ammonia) was estimated by titration with standard H_2SO_4 (sulphuric acid). The plant samples were collected after harvesting the crops. The rice grains were separated from the straw biomass, and the samples were dried in an oven at 65 ± 2°C for 72 h. The nitrogen concentration in the grain and straw samples was determined using the method described by Jackson (1956). The plant samples were digested using concentrated H_2SO_4 and a digestion mixture in a micro Kjeldahl digestion block. The digested samples were distilled with NaOH, and the liberated NH_3 was absorbed in H_3BO_3 (boric acid) and then titrated against standard H_2SO_4. The grain N uptake (mg $plant^{-1}$) was then calculated by multiplying the grain weight/plant by the grain N concentration, as described by Cowan et al. (2021).

Statistical analysis

The experiment was a factorial, completely randomized design with 24 treatments, each having three replicates. Four factorial (CO_2 level, O_3 level, variety, and N dose) analysis of variance (ANOVA) was carried out using SAS (ver. 9.3) statistical package (SAS Institute Inc., CA, United States). Tukey's honestly significant difference (HSD) test at the 5% level of significance was performed to check if the differences were statistically significant.

Results

Effect of elevated O_3 and CO_2 on the rice physiology

The photosynthesis rates varied among the different rice varieties, ranging from 23.1 to 36.1 µmol CO_2 m^{-2} s^{-1} in the first year and from 23.2 to 35.1 µmol CO_2 m^{-2} s^{-1} in the second year under the recommended N dose (Figures 1a,b). Pusa Basmati 1121 exhibited a significant decrease in the photosynthesis rates, dropping from 30.3 to 26.5 µmol CO_2 m^{-2} s^{-1} in the first year and from 31.1 to 27.9 µmol CO_2 m^{-2} s^{-1} in the second year. In the case of IR64 Drt1, the photosynthesis rate was significantly lower under the elevated O_3 levels compared to the ambient levels in the second year. Conversely, there was no notable reduction in the photosynthesis rates for the Nagina 22 variety over both years under the elevated O_3 conditions. The elevated CO_2 concentration exhibited a positive impact on the photosynthesis rates of all rice varieties. However, the interactive treatment of elevated O_3 and CO_2 still maintained the photosynthesis rates similar to those under the ambient condition. The application of additional N positively influenced the photosynthesis rates across all treatments. When 25% additional N was applied, the photosynthesis

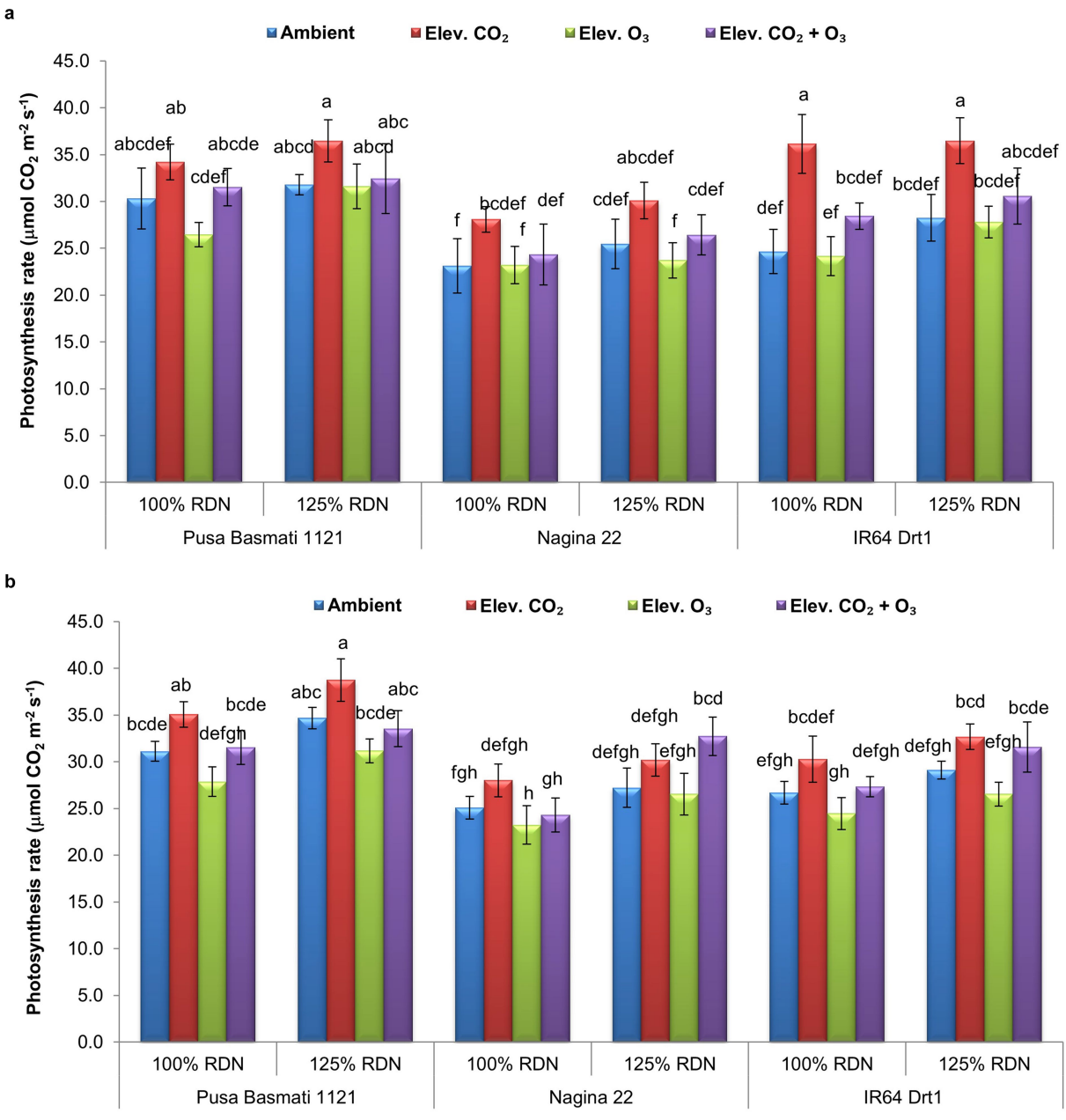

FIGURE 1
Photosynthesis rates (µmol CO_2 m^{-2} s^{-1}) in the rice varieties under the elevated O_3 and CO_2 conditions during the (a) first and (b) second year. Columns with different letters are significantly different ($p \leq 0.05$). The error bars represent the standard deviation of the data, indicating the variability around the mean.

rates in the elevated O_3 treatment became comparable to those in the ambient treatment.

Stomatal conductance in the rice varieties decreased in the presence of the elevated O_3 and elevated O_3 plus CO_2 treatments compared to the ambient treatment. In the treatments with the recommended N application, stomatal conductance ranged from 0.31 to 0.42 m mol H_2O m^{-2} s^{-1} in Pusa Basmati 1121, 0.29 to 0.31 m mol H_2O m^{-2} s^{-1} in Nagina 22, and 0.33 to 0.41 m mol H_2O m^{-2} s^{-1} in IR64 Drt1 under the ambient conditions (Figures 2a,b). However, stomatal conductance decreased in the elevated O_3 plus CO_2 treatment, ranging from 0.24 to 0.30 m mol H_2O m^{-2} s^{-1} in Pusa Basmati 1121, 0.22 to 0.24 m mol H_2O m^{-2} s^{-1} in Nagina 22, and 0.29 to 0.30 m mol H_2O m^{-2} s^{-1} in IR64 Drt1. Furthermore, the elevated O_3 and elevated O_3 plus CO_2 treatments significantly reduced transpiration rates in the Pusa Basmati 1121 and IR64 Drt1 varieties. Over the two-year study, the transpiration rates in Pusa Basmati 1121 ranged from 12.3 to 16.4 m mol H_2O m^{-2} s^{-1} in the ambient treatment, while decreasing to 9.5 from 11.9 H_2O m^{-2} s^{-1} in the elevated O_3 treatment (Figures 3a,b). Similarly, in the IR64 Drt1 variety, the transpiration rates ranged from 14.5 to 15.0 m mol H_2O m^{-2} s^{-1} in the ambient treatment, but in the elevated O_3 treatment, they ranged from 9.5 to 11.8 m mol H_2O m^{-2} s^{-1}.

Effect of elevated O_3 and CO_2 on rice yield

The elevated O_3 level significantly decreased the grain yield of the Pusa Basmati 1121 and IR64 Drt1 varieties in both years of the study. The grain yield was reduced by 7.2–7.5%, in Pusa Basmati 1121 and by 6.9–9% in IR64 Drt1 in the elevated O_3 treatment as compared to the ambient treatment (Figure 4). In the Nagina 22 variety, there was a reduction in the yield by 4.4% in the elevated O_3 treatment compared to the ambient treatment during the first year. However, in the second year, there was no reduction in the grain yield of this variety under the elevated O_3 condition. Nagina 22 is a stress-tolerant variety, which is why an increase in the O_3 levels had little to no effect on it. In the present study, the reduction in the grain yield in the elevated O_3 treatment was attributed to a lower number of panicles per hill and

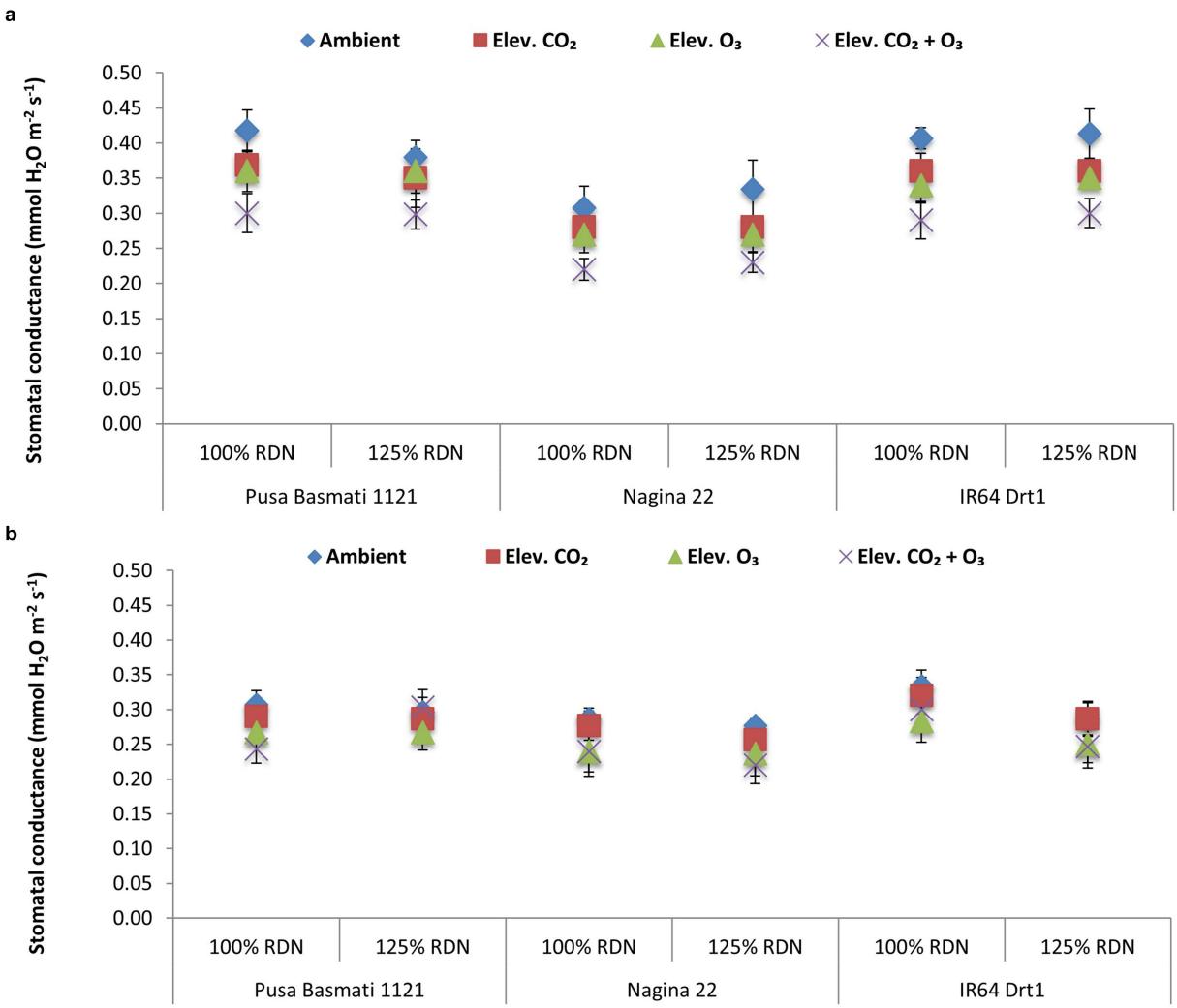

FIGURE 2
Stomatal conductance (mmol H_2O m^{-2} s^{-1}) in the rice varieties under the elevated O_3 and CO_2 conditions during the (a) first and (b) second year. The error bars represent the standard deviation of the data, indicating the variability around the mean.

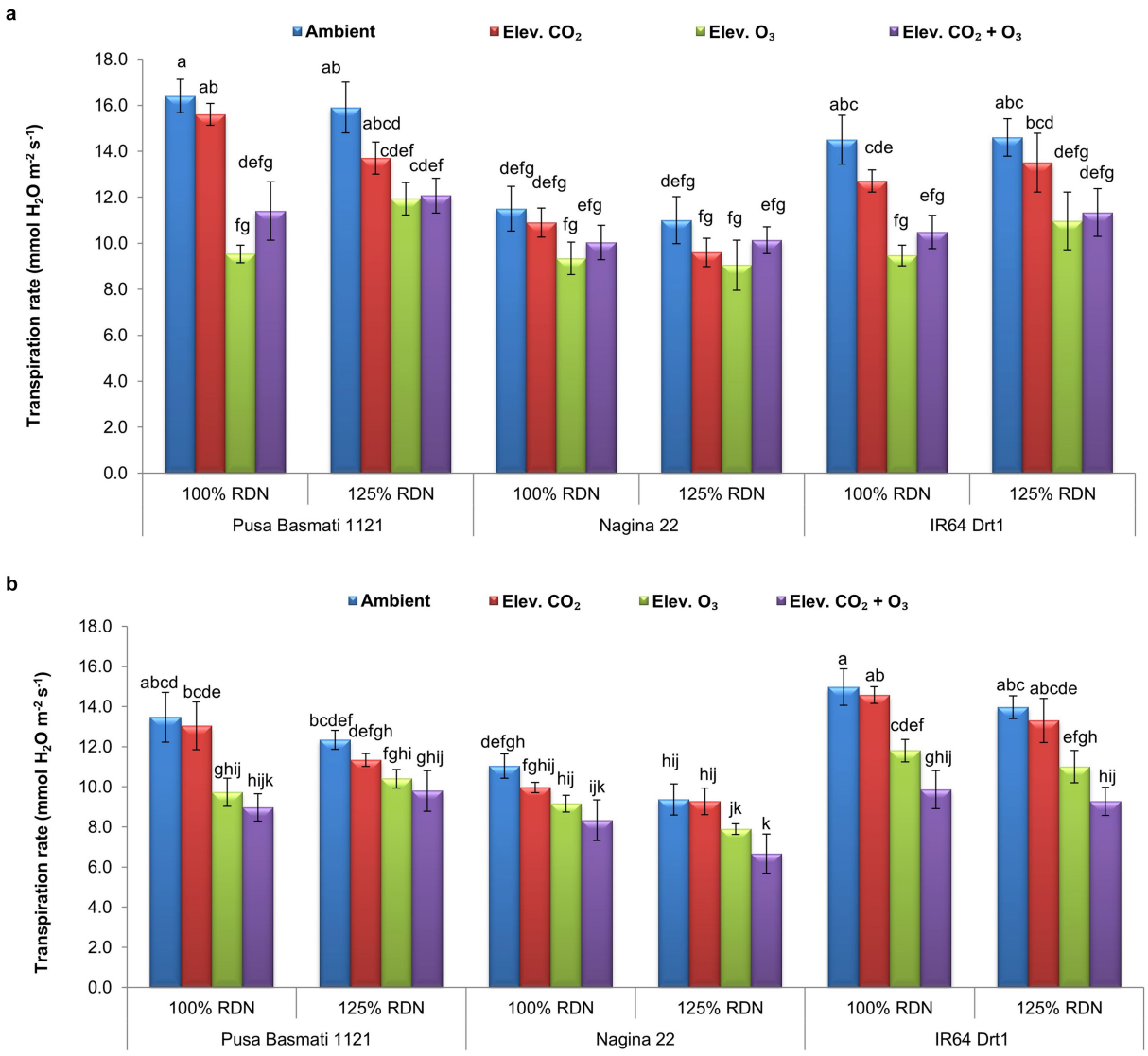

FIGURE 3
Transpiration rates (mmol H_2Om^{-2} s^{-1}) in the rice varieties under the elevated O_3 and CO_2 conditions during the (a) first and (b) second year. Columns with different letters are significantly different ($p \leq 0.05$). The error bars represent the standard deviation of the data, indicating the variability around the mean.

fewer grains per panicle under the elevated O_3 condition. Under the ambient condition, the number of grains per panicle ranged from 101 to 111 among the different rice varieties, while in the elevated O_3 treatment, the number of grains per panicle ranged from 95 to 101 (Table 1). The number of panicles per hill also decreased in the elevated O_3 treatment compared to the ambient treatment. In the ambient treatment, the number of panicles per hill ranged from 14 to 17, while in the elevated O_3 treatment, it decreased from 15 to 13.

In the elevated O_3 plus elevated CO_2 treatment, the grain yield was 2.9–3.4% lower than in the ambient treatment for the Pusa Basmati 1121 variety. This shows that the increased CO_2 concentration of 550 ppm was able to compensate for 3.9–4.6% yield loss in the Pusa Basmati 1121 variety. In the IR64 Drt1 variety, the grain yield in the elevated O_3 plus elevated CO_2 treatment was 3.4% lower than in the ambient during the first year of the study. However, during the second year, the yield was 1.1% higher than in the ambient treatment for this variety. The Nagina 22 variety recorded higher yields in the elevated O_3 plus elevated CO_2 treatment compared to the ambient treatment in both years. The application of a higher N dose also helped in preventing the yield loss in the rice varieties under the elevated O_3 concentration. In the treatment with elevated O_3 plus CO_2, along with 125% of the RDN, the grain yield of the Pusa Basmati 1121 variety increased by 11–13% compared to the ambient treatment (Figure 4). Similarly, in the IR64 Drt1 variety, the yield increased by 9–10%, and in the Nagina 22 variety, it increased by 6–7% in this treatment.

The grain number per panicle also increased in the elevated CO_2 plus elevated O_3 treatment compared to that in the elevated O_3 treatment. The elevated CO_2 level increased the photosynthesis rates of the crops, which led to greater biomass accumulation and subsequently more grains, resulting in higher crop yields. The application of a higher dose of N also increased the grain number in all three rice varieties, which led to higher crop yields. In the elevated

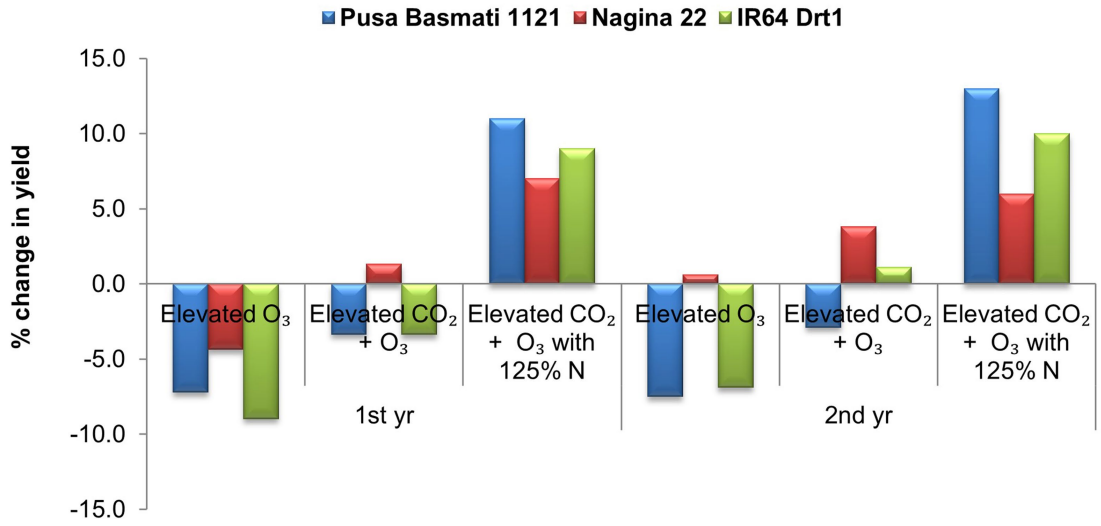

FIGURE 4
Percent change in the yield in the rice varieties under the elevated O_3 and CO_2 conditions.

TABLE 1 Effect of the elevated CO_2, O_3 and N treatments on the yield parameters of rice.

Variety	O_3	CO_2	Panicles hill^{-1}		Panicles hill^{-1}		Grains panicle^{-1}		Grains panicle^{-1}	
			First year		Second year		First year		Second year	
			100% RDN	125% RDN	100% RDN	125% RDN	100% RDN	125% RDN	100% RDN	125% RDN
PB1121	Ambient	Ambient	16.4 ± 1.8^{def}	20.2 ± 0.2^{abcd}	16.4 ± 0.5^{cdef}	18.3 ± 0.7^{abcd}	111.4 ± 3.8^{abcde}	120.4 ± 2.9^{ab}	104.9 ± 3.1^{bcd}	116.1 ± 4.5^{abc}
		Elevated	20.2 ± 25.4^{abcd}	23.3 ± 0.6^{a}	18.0 ± 1.2^{cde}	22.0 ± 0.9^{ab}	115.7 ± 6.1^{abcd}	124.9 ± 4.0^{a}	112.2 ± 3.6^{abcd}	119.3 ± 2.9^{ab}
	Elevated	Ambient	14.1 ± 1.5^{f}	18.5 ± 0.9^{abcd}	14.0 ± 1.1^{efg}	17.2 ± 1.6^{cde}	96.5 ± 3.9^{e}	105.5 ± 3.4^{bcde}	94.9 ± 3.1^{f}	101.1 ± 3.0^{cde}
		Elevated	17.4 ± 0.2^{cde}	18.8 ± 0.4^{abcd}	16.0 ± 0.8^{defg}	18.5 ± 0.8^{abcd}	106.8 ± 4.8^{bcde}	113.9 ± 6.6^{abcd}	98.9 ± 1.9^{def}	106.2 ± 1.7^{bcd}
Nagina 22	Ambient	Ambient	14.9 ± 0.5^{ef}	18.5 ± 0.8^{abcd}	13.7 ± 0.7^{fg}	16.1 ± 1.1^{cdef}	106.3 ± 2.0^{bcde}	113.3 ± 3.9^{abcd}	100.7 ± 1.3^{def}	114.0 ± 2.3^{abcd}
		Elevated	17.3 ± 0.5^{cde}	21.8 ± 0.8^{abc}	16.5 ± 0.4^{cdef}	19.2 ± 2.1^{abc}	114.9 ± 6.0^{abcd}	117.6 ± 4.2^{abc}	109.8 ± 3.3^{abcde}	116.5 ± 0.9^{abc}
	Elevated	Ambient	14.4 ± 0.6^{f}	17.7 ± 0.9^{cde}	12.5 ± 0.8^{g}	15.1 ± 1.3^{defg}	97.0 ± 1.2^{e}	104.1 ± 4.2^{cde}	98.1 ± 3.6^{ef}	105.5 ± 3.1^{bcd}
		Elevated	16.4 ± 0.5^{def}	18.0 ± 1.0^{cde}	14.0 ± 0.5^{efg}	15.9 ± 1.1^{defg}	106.3 ± 2.0^{bcde}	110.8 ± 8.9^{abcde}	99.8 ± 1.5^{def}	110.8 ± 3.7^{abcde}
IR64 Drt1	Ambient	Ambient	14.9 ± 0.6^{ef}	18.7 ± 0.6^{abcde}	17.1 ± 0.6^{cdef}	19.1 ± 10^{abc}	106.8 ± 5.9^{bcde}	110.5 ± 5.4^{abcde}	106.8 ± 0.9^{bcd}	114.3 ± 4.6^{abcd}
		Elevated	19.2 ± 1.1^{abcd}	23.1 ± 1.2^{ab}	19.7 ± 0.4^{abc}	22.8 ± 0.3^{a}	108.8 ± 4.0^{abcde}	118.5 ± 2.5^{abc}	118.3 ± 1.2^{ab}	125.2 ± 5.5^{a}
	Elevated	Ambient	14.3 ± 0.7^{f}	18.1 ± 1.1^{cde}	15.4 ± 0.7^{defg}	17.5 ± 0.5^{cde}	96.1 ± 2.0^{e}	102.4 ± 3.1^{cde}	100.6 ± 1.0^{def}	107.7 ± 2.7^{bcd}
		Elevated	17.0 ± 1.2^{def}	19.5 ± 1.1^{abcd}	16.2 ± 0.1^{cdef}	19.1 ± 0.5^{abc}	100.1 ± 7.3^{de}	108.3 ± 2.5^{bcde}	105.1 ± 3.1^{bcd}	113.3 ± 3.9^{abcd}

Numbers in each column represent the mean values along with their standard deviation. Means with at least one letter in common are not statistically significant ($p \leq 0.05$).

O_3 treatment, the application of a higher N dose also helped in increasing the panicle number and grain number, thereby increasing the grain yield to a certain extent.

Effect of elevated O_3 and CO_2 on the plant N

The responses of the grain N concentration (%) in the rice varieties to the elevated CO_2 and O_3 treatments are shown in Figure 5a. In the 100% recommended N applied treatments, the grain N concentration ranged from 1.20–1.36% under the ambient condition, with a mean value of 1.30%. The grain N concentration significantly decreased in the elevated CO_2 and elevated O_3 plus CO_2 interaction treatment compared to the ambient treatment. In the elevated O_3 plus CO_2 interaction treatment, the grain N concentration ranged from 1.07–1.18%, with a mean value of 1.13%. The application of an additional 25% of N improved the grain N concentration in both years. When the additional N dose was applied, the grain N concentration ranged from 1.25–1.33% in the elevated O_3 plus CO_2 interaction treatments, with a mean value of 1.29%. The grain N concentration was higher in the Pusa Basmati 1121 and IR64 Drt1 varieties than in the Nagina 22 variety.

Elevated O_3 also reduced the grain N uptake of the rice varieties compared to the ambient treatment. In the ambient treatment, the grain N uptake ranged from 189 to 269 mg hill^{-1}, with a mean value

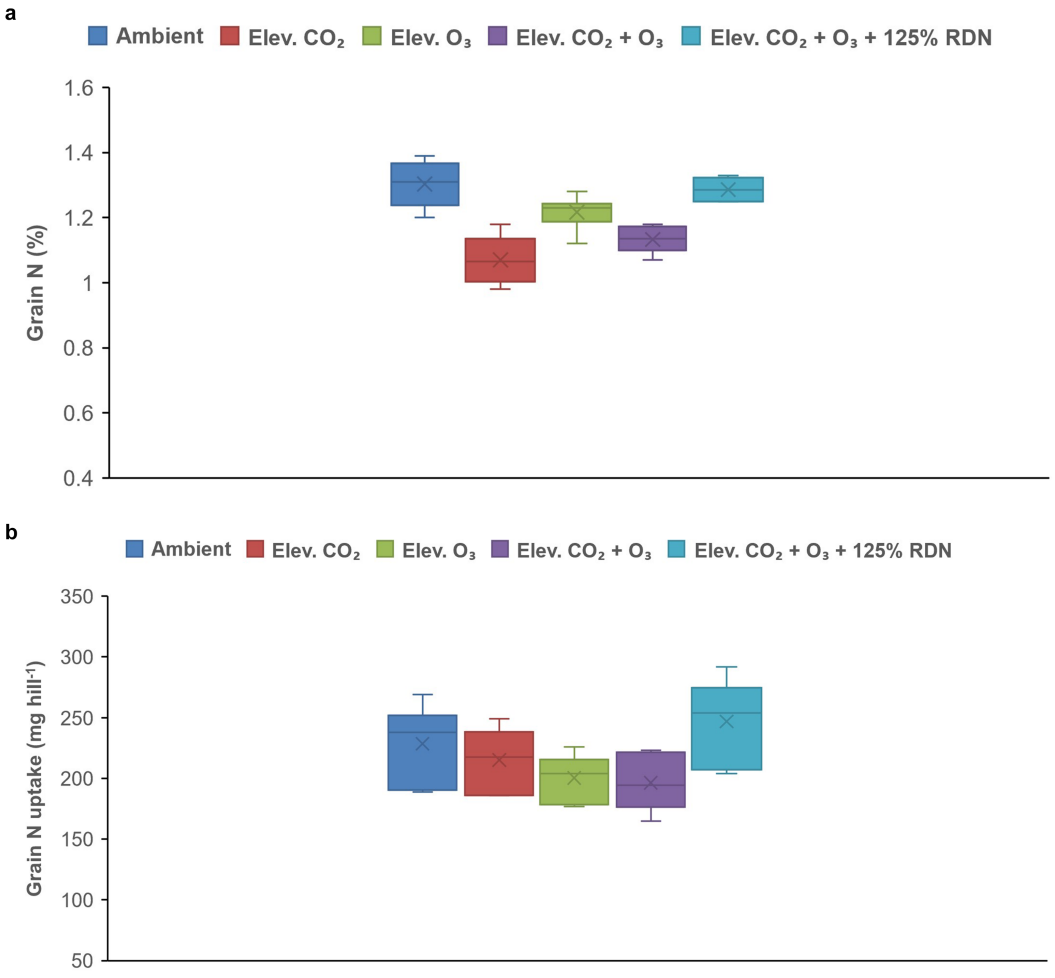

FIGURE 5
(a) Grain nitrogen concentration (%) and (b) grain N uptake (mg hill^{-1}) in the rice varieties under the elevated O_3 and CO_2 conditions. The bottom and top of the whiskers denote the first and third quartiles, respectively. The line inside the box represents the median line.

of 229 mg hill^{-1} in the treatment with the 100% RDN (Figure 5b). In the elevated O_3 plus CO_2 interaction treatment, the grain N uptake decreased and ranged from 165 to 223 mg hill^{-1}, with a mean value of 196 mg hill^{-1}. The application of a higher N dose increased the grain N uptake in the rice varieties. In the elevated O_3 plus CO_2 interaction treatment, the grain N uptake was even higher than in the ambient treatment. It ranged from 204 to 292 mg hill^{-1}, with a mean value of 247 mg hill^{-1}. The grain N uptake was greater in the Pusa Basmati 1121 and IR64 Drt1 varieties than in the Nagina 22 variety. The application of an additional 25% of N increased the grain N uptake by 30.2–40.8% in Pusa Basmati 1121, by 15.3–22.3% in Nagina 22, and by 21.7% in the IR64 Drt1 variety of the rice crops (Table 2).

Effect of elevated O_3 and CO_2 on the soil available N

In the ambient treatment, the soil available N ranged from 176.4–204.2 kg ha^{-1} in the first year and from 135.2–151.7 kg ha^{-1} in the second year among the different rice varieties with the recommended dose of the N application (Table 2). In the elevated O_3 plus CO_2 interaction treatment, the soil available N was lower than in the ambient treatment in both years of the study. The soil available N was also found to be lower in the elevated CO_2 treatment compared to the ambient treatment. The application of a higher dose of N increased the available N content of the soil. In the elevated O_3 plus CO_2 interaction treatment, the application of an additional 25% of N increased the soil available N by 5.3–14.9% in Pusa Basmati 1121, by 6.3–9.0% in Nagina 22 and by 16–16.9% in IR64 Drt1 of the rice crops.

Discussion

Tropospheric O_3 is a secondary air pollutant generated through photochemical reactions among precursors such as nitrogen oxides (NOx), volatile organic compounds (VOCs), and carbon monoxide (CO), primarily released from anthropogenic activities (Broberg et al., 2015). Several researchers have reported the substantial impact of elevated O_3 levels on crop productivity and quality (Singh et al., 2018; Yadav et al., 2019). The results from the current study showed that elevated O_3 reduced the photosynthesis rates of the Pusa Basmati 1121 and IR64 Drt1 varieties of the rice crop, while the elevated O_3 plus CO_2

10.3389/fsufs.2024.1477210

TABLE 2 Effect of the elevated CO_2, O_3, and N treatments on the grain N uptake and soil available N of the rice varieties.

Variety	O_3	CO_2	Grain N uptake (mg hill^{-1})		Grain N uptake (mg hill^{-1})		Soil available N (kg ha^{-1})		Soil available N (kg ha^{-1})	
			First year		Second year		First year		Second year	
			100% RDN	125% RDN	100% RDN	125% RDN	100% RDN	125% RDN	100% RDN	125% RDN
PB1121	Ambient	Ambient	269.3 ± 17.9^{cde}	382.4 ± 24.1^{a}	241.5 ± 4.1^{bcdefg}	296.9 ± 4.5^{ab}	179.8 ± 9.6^{abc}	202.5 ± 18.1^{ab}	135.2 ± 4.2^{cde}	149.1 ± 8.1^{bcde}
		Elevated	249.1 ± 14.7^{cdef}	374.6 ± 21.4^{ab}	232.6 ± 18.4^{cdefgh}	279.5 ± 13.8^{abc}	147.5 ± 9.1^{c}	172.8 ± 4.8^{abc}	118.0 ± 5.7^{e}	136.5 ± 4.5^{bcde}
	Elevated	Ambient	226.4 ± 14.5^{cdef}	288.3 ± 16.2^{bcd}	196.6 ± 17.9^{gh}	240.3 ± 7.4^{bcdefg}	172.5 ± 5.4^{abc}	194.2 ± 9.8^{abc}	129.0 ± 2.1^{cde}	139.9 ± 4.0^{bcde}
		Elevated	223.4 ± 11.1^{cdef}	292.2 ± 13.9^{abcd}	186.4 ± 16.8^{gh}	261.2 ± 18.6^{bcde}	167.1 ± 11.0^{abc}	175.6 ± 7.2^{abc}	120.2 ± 6.8^{de}	138.1 ± 7.4^{bcde}
Nagina 22	Ambient	Ambient	190.6 ± 15.0^{ef}	254.2 ± 20.1^{cdef}	188.6 ± 13.2^{gh}	233.5 ± 4.5^{cdefgh}	176.4 ± 6.7^{abc}	185.6 ± 13.2^{abc}	151.7 ± 6.9^{abc}	166.9 ± 1.9^{ab}
		Elevated	186.0 ± 18.4^{ef}	258.3 ± 20.8^{cde}	186.4 ± 24.4^{gh}	244.0 ± 16.1^{bcdefg}	169.3 ± 9.6^{abc}	162.5 ± 10.2^{bc}	129.0 ± 1.5^{cde}	140.4 ± 4.0^{bcde}
	Elevated	Ambient	179.2 ± 7.5^{ef}	203.0 ± 5.9^{def}	177.1 ± 6.1^{h}	251.9 ± 10.3^{abcdef}	170.4 ± 2.8^{abc}	162.9 ± 13.0^{bc}	137.8 ± 5.7^{bcde}	150.4 ± 10.1^{abcd}
		Elevated	165.4 ± 22.0^{f}	204.0 ± 4.6^{def}	180.1 ± 5.4^{h}	207.6 ± 7.8^{gh}	157.8 ± 6.1^{bc}	171.8 ± 7.5^{abc}	136.7 ± 3.3^{bcde}	145.4 ± 6.3^{bcde}
IR64 Drt1	Ambient	Ambient	235.2 ± 7.7^{cdef}	300.3 ± 22.2^{abc}	245.6 ± 8.0^{bcdefg}	305.0 ± 16.2^{a}	204.2 ± 10.0^{ab}	216.7 ± 11.1^{a}	144.9 ± 4.9^{bcde}	172.6 ± 6.4^{a}
		Elevated	201.8 ± 10.7^{def}	260.2 ± 2.7^{cde}	235.3 ± 4.5^{cdefgh}	305.5 ± 18.8^{a}	147.5 ± 9.5^{c}	168.9 ± 7.7^{abc}	119.1 ± 4.9^{e}	143.7 ± 6.5^{bcde}
	Elevated	Ambient	211.3 ± 8.2^{cdef}	247.0 ± 18.7^{cdef}	212.2 ± 7.0^{defgh}	263.1 ± 10.3^{bcde}	162.5 ± 10.2^{bc}	166.8 ± 8.3^{abc}	136.4 ± 5.6^{bcde}	154.1 ± 6.8^{abc}
		Elevated	203.0 ± 7.3^{def}	270.0 ± 16.4^{cde}	221.0 ± 5.3^{cdefgh}	269.1 ± 15.7^{bcd}	161.7 ± 6.6^{bc}	188.9 ± 7.7^{abc}	134.9 ± 3.0^{cde}	157.8 ± 9.7^{abc}

Numbers in each column represent the mean values along with their standard deviation. Means with at least one letter in common are not statistically significant ($p \leq 0.05$).

treatment was able to maintain the photosynthesis rates of the crops. The elevated O_3 and elevated O_3 plus CO_2 treatments significantly reduced the stomatal conductance and transpiration rates of the Pusa Basmati 1121 and IR64 Drt1 varieties. Previous studies have also indicated that elevated O_3 could hinder photosynthetic carbon acquisition in crops (Guidi et al., 2001; Morgan et al., 2003; Singh et al., 2009; Bhatia et al., 2012). There are reports that elevated CO_2 concentrations reduce stomatal conductance and transpiration rates in rice crops (Maity et al., 2023; Zhang et al., 2022). The elevated O_3 level substantially decreased the yield of the Pusa Basmati 1121 and IR64 Drt1 varieties. In contrast, the Nagina 22 variety demonstrated comparatively less or no yield reduction. Nagina 22 is known for its stress tolerance, and the results indicate that the increase in the O_3 concentration had minimal to no effect on its yield. Such yield losses under the O_3 exposure occurred due to the reduction in photosynthesis, which reduced the supply of assimilates required for reproductive development and seed growth (Feng et al., 2010). Tatsumi et al. (2019) also reported that brown rice yield was significantly reduced under elevated O_3 concentrations. A similar decrease in grain yield with exposure to elevated O_3 concentrations was reported for wheat cultivars in north India (Daripa et al., 2016; Yadav et al., 2019). In our study, an elevated CO_2 concentration of 550 ppm was able to partially mitigate the reduction in the grain yield due to increased O_3 exposure in the Pusa Basmati 1121 and IR64 Drt1 varieties, while it fully compensated for the yield reduction in the Nagina 22 variety. Elevated CO_2 has a fertilization effect on crops, which has helped compensate for yield losses in different rice varieties. The yield loss in the Nagina 22 variety, which is stress-tolerant, was already less than the other varieties. Therefore, the reduction in the yield in Nagina 22 was fully compensated under the elevated CO_2 plus O_3 treatment. Various researchers have earlier reported the beneficial effects of increased CO_2 levels in terms of increasing yields in different crops (Dey et al., 2017; Kobayashi et al., 1999; Pramanik et al., 2018; Sanyal et al., 2023). Bhatia et al. (2021) observed that a high CO_2 concentration of 554 ppm was able to counter the harmful impacts of O_3 exposure on yield and nutrient content in chickpeas. A study conducted with rice showed that elevated CO_2 could counter yield reduction due to O_3 exposure by more than 40% (Kumar et al., 2021).

The application of a 25% higher dose of N increased the photosynthesis rates and different yield parameters, such as the number of panicles and the number of grains per panicle, in the rice crops, thereby increasing the yield to a certain extent under the elevated O_3 concentration. According to Chen et al. (2018), decreased photosynthesis in nitrogen-deficient leaves increases the yield sensitivity of crops to high O_3 concentrations. Therefore, the increased dose of N had a positive effect on the yield parameters of the rice crops even under the elevated O_3 condition. The beneficial impact of higher N doses was also reported by Raj et al. (2019), who observed that increased atmospheric CO_2 concentrations and higher N doses synergistically contributed to an increase in the panicle number, thereby improving the yield of rice crops.

The elevated O_3 plus CO_2 interaction decreased the grain N concentration and N uptake in the rice varieties compared to the ambient condition. As O_3 is a strong oxidant, it harmfully affects important physiological functions in plants, which leads to reduced quality in crops (Avnery et al., 2011). Similar findings have been reported by earlier researchers, who found that protein content in plants is negatively affected by increased O_3 (Broberg et al., 2015;

Grünhage et al., 2012). Broberg et al. (2017) reported that O_3 impairs the N translocation from straw to grain, thereby reducing the N use efficiency of crops. In addition, the applied N fertilizer is used less efficiently under elevated O_3, leading to adverse effects on grain protein content in crops. Under elevated CO_2 conditions, higher photosynthesis rates lead to greater carbon assimilation in rice, thereby reducing plant N concentrations due to the dilution effect (Kim et al., 2001). Reports indicate that protein content and N content in plants, especially cereal crops, decrease under elevated CO_2 conditions (Abebe et al., 2016; Chakrabarti et al., 2020; Raj et al., 2019).

Soil available N is also negatively affected by elevated O_3 and CO_2 treatment, which may be attributed to increased N losses from crop fields under elevated O_3 (Broberg et al., 2017). Under O_3 exposure, plant photosynthesis and grain filling duration are shortened (Gelang et al., 2000), which reduces the nutrient uptake period and increases the likelihood of greater N loss from the soil. Earlier studies (Chakrabarti et al., 2020; Maity et al., 2020) have also reported a decrease in soil available N under elevated CO_2 conditions due to increased crop growth resulting in higher N demand by the crop. As plant photosynthesis is hampered under increased O_3 concentrations, reduced photosynthates in the roots affect the root system and various soil processes (Chen et al., 2008). This may further affect soil N transformation rates (Wu et al., 2016), thereby lowering the available N status in the soil. The application of a higher N dose increased both the grain N uptake and soil available N in rice. As the crop growth was greater under the higher N doses, this generated more aboveground and belowground biomass of the crops. This might have led to increased microbial activity in the rhizosphere, leading to enhanced availability of N to the plants.

The study showed that although the negative effects of elevated O_3 on the rice yield were negated by the elevated CO_2 concentration, the adverse effect of elevated O_3 on the grain N content could not be compensated for. The response of rice to elevated CO_2 may be limited when nitrogen levels are sub-optimal. However, the decrease in plant N could be alleviated to a certain extent by applying higher doses of N (Maity et al., 2020). Our study showed that the application of the 25% RDN improved both the grain N concentration and grain N uptake, as well as soil available N, in the rice crops under the elevated O_3 and CO_2 interaction.

Conclusion

The grain yield of the rice varieties decreased under the elevated O_3 condition. An elevated CO_2 concentration of 550 ppm was able to compensate for the yield loss by 3.9–4.6% in the Pusa Basmati 1121 rice variety and by 4.6–8.0% in the IR64 Drt1 variety. Although elevated CO_2 was able to compensate for the yield loss due to elevated O_3, the N content in the rice grains was further reduced in the elevated O_3 plus CO_2 treatment. The application of an additional 25% of the recommended dose of N improved the grain N uptake by 15.3–40.8% in the different rice varieties compared to the 100% RDN in the elevated O_3 plus CO_2 interaction treatment. The study shows that nitrogen in rice grains and soil available N will decrease under elevated O_3 plus CO_2 conditions. An elevated CO_2 concentration of 550 ppm will be able to compensate for yield loss to a certain extent, but grain quality will further deteriorate in the elevated O_3 plus CO_2 treatment. The application of an additional 25% of the recommended dose of N could help in sustaining rice yield and also maintaining plant and soil N under elevated O_3 and CO_2 conditions in the future. However, the response of rice varieties to elevated O_3 and CO_2 might vary with different climate types. Therefore, the findings of the study could be further improved by testing different N fertilizer formulations to suggest the best N management options for the sustaining productivity and quality of rice under elevated O_3 and CO_2 conditions.

Data availability statement

The raw data supporting the conclusions of this article will be made available by the authors, without undue reservation.

Author contributions

BC: Formal analysis, Investigation, Project administration, Visualization, Writing – original draft, Writing – review & editing. SS: Funding acquisition, Project administration, Writing – review & editing. AM: Funding acquisition, Project administration, Writing – review & editing. SK: Investigation, Writing – original draft. VK: Methodology, Writing – original draft. SB: Conceptualization, Writing – review & editing. AB: Conceptualization, Formal analysis, Writing – review & editing, Project administration, Supervision.

Funding

The author(s) declare that financial support was received for the research, authorship, and/or publication of this article. The authors acknowledged the funding provided by the ICAR-IRRI project, which supported this work and the publication of the manuscript. The facilities for carrying out this study were funded and maintained by the National Innovations in Climate Resilient Agriculture, NICRA project (IARI-12-115).

Acknowledgments

The authors would like to thank the ICAR-Indian Agricultural Research Institute, New Delhi, for providing the facilities for conducting the study.

Conflict of interest

The authors declare that the research was conducted in the absence of any commercial or financial relationships that could be construed as a potential conflict of interest.

Publisher's note

References

Abebe, A., Pathak, H., Singh, S. D., Bhatia, A., Harit, R. C., and Kumar, V. (2016). Growth, yield and quality of maize with elevated atmospheric carbon dioxide and temperature in north–West India. *Agric. Ecosyst. Environ.* 218, 66–72. doi: 10.1016/j.agee.2015.11.014

Agrawal, M., Singh, B., Rajput, M., Marshall, F., and Bell, J. N. B. (2003). Effect of air pollution on peri-urban agriculture: a case study. *Environ. Pollut.* 126, 323–329. doi: 10.1016/S0269-7491(03)00245-8

Ainsworth, E. A. (2008). Rice production in a changing climate: a metaanalysis of responses to elevated carbon dioxide and elevated ozone concentration. *Glob. Change Biol.* 14, 1642–1650. doi: 10.1111/j.1365-2486.2008.01594.x

Ashmore, M. R. (2005). Assessing the future global impacts of ozone on vegetation. *Plant Cell Environ.* 28, 949–964. doi: 10.1111/j.1365-3040.2005.01341.x

Avnery, S., Mauzerall, D. L., Liu, J., and Horowitz, L. W. (2011). Global crop yield reductions due to surface ozone exposure: 1. Year 2000 crop production losses and economic damage. *Atmos. Environ.* 45, 2284–2296. doi: 10.1016/j.atmosenv.2010.11.045

Bhatia, A., Ghosh, A., Kumar, V., Tomer, R., Singh, S. D., and Pathak, H. (2011). Effect of elevated tropospheric ozone on methane and nitrous oxide emission from rice soil in North India. *Agric. Ecosyst. Environ.* 144, 21–28. doi: 10.1016/j.agee.2011.07.003

Bhatia, A., Kumar, V., Kumar, A., Tomer, R., Singh, B., and Singh, S. D. (2013). Effect of elevated ozone and carbon dioxide interaction on growth and yield of maize. *Maydica* 58, 291–298.

Bhatia, A., Mina, U., Kumar, V., Tomer, R., Kumar, A., Chakrabarti, B., et al. (2021). Effect of elevated ozone and carbon dioxide interaction on growth, yield, nutrient content and wilt disease severity in chickpea grown in northern India. *Heliyon* 7:e06049. doi: 10.1016/j.heliyon.2021.e06049

Bhatia, A., Pathak, H., Aggarwal, P. K., and Jain, N. (2010). Trade-off between productivity enhancement and global warming potential of rice and wheat in India. *Nutr. Cycl. Agroecosys.* 86, 413–424. doi: 10.1007/s10705-009-9304-5

Bhatia, A., Tomer, R., Kumar, V., Singh, S. D., and Pathak, H. (2012). Impact of tropospheric ozone on crop growth and productivity–a review. *J. Sci. Indust. Res.* 71, 97–112.

Broberg, M. C., Feng, Z. Z., Xin, Y., and Pleijel, H. (2015). Ozone effects on wheat grain quality – a summary. *Environ. Pollut.* 197, 203–213. doi: 10.1016/j.envpol.2014.12.009

Broberg, M. C., Uddling, J., Mills, G., and Pleijel, H. (2017). Fertilizer efficiency in wheat is reduced by ozone pollution. *Sci. Total Environ.* 607-608, 876–880. doi: 10.1016/j.scitotenv.2017.07.069

Chakrabarti, B., Singh, S. D., Bhatia, A., Kumar, V., and Harit, R. C. (2020). Yield and nitrogen uptake in wheat and chickpea grown under elevated carbon dioxide level. *Natl. Acad. Sci. Lett.* 43, 109–113. doi: 10.1007/s40009-019-00816-y

Chen, C. T., Lee, C. L., and Yeh, D. M. (2018). Effects of nitrogen, phosphorus, potassium, calcium, or magnesium deficiency on growth and photosynthesis of eustoma. *Hortic. Sci.* 53, 795–798. doi: 10.21273/HORTSCI12947-18

Chen, Z., Wang, X., Feng, Z., Xiao, Q., and Duan, X. (2008). Impact of elevated O_3 on soil microbial community function under wheat crop. *Water Air Soil Pollut.* 198, 189–198.

Chen, Z., Wang, X., and Shang, H. (2015). Structure and function of rhizosphere and non-rhizosphere soil microbial community respond differently to elevated ozone in field planted wheat. *J. Environ. Sci. (China)* 32, 126–134. doi: 10.1016/j.jes.2014.12.018

Cowan, N., Bhatia, A., Drewer, J., Jain, N., Singh, R., Tomer, R., et al. (2021). Experimental comparison of continuous and intermittent flooding of rice in relation to methane, nitrous oxide and ammonia emissions and the implications for nitrogen use efficiency and yield. *Agric. Ecosyst. Environ.* 319:107571. doi: 10.1016/j.agee.2021.107571

Daripa, A., Bhatia, A., Ojha, S., Tomer, R., Chattaraj, S., Singh, K. P., et al. (2016). Chemical and natural plant extract in ameliorating negative impact of tropospheric ozone on wheat crop: a case study in a part of semiarid north West India. *Aerosol Air Qual. Res.* 16, 1742–1756. doi: 10.4209/aaqr.2014.10.0263

David, L. M., and Nair, P. R. (2013). Tropospheric column O_3 and NO_2 over the Indian region observed by ozone monitoring instrument (OMI): seasonal changes and long-term trends. *Atmos. Environ.* 65, 25–39. doi: 10.1016/j.atmosenv.2012.09.033

Deb Roy, S., Beig, G., and Ghude, S. D. (2009). Exposure plant response of ambient ozone over the tropical Indian region. *Atmos. Chem. Phys.* 9, 5253–5260. doi: 10.5194/acp-9-5253-2009

Deryng, D., Elliott, J., Folberth, C., Müller, C., Pugh, T. A. M., Boote, K. J., et al. (2016). Regional disparities in the beneficial effects of rising CO_2 concentrations on crop water productivity. *Nat. Clim. Chang. Lett.* 6, 786–790. doi: 10.1038/nclimate2995

Dey, S. K., Chakrabarti, B., Prasanna, R., Singh, S. D., Purakayastha, T. J., Datta, A., et al. (2017). Productivity of mungbean (*Vigna radiata*) with elevated carbon dioxide at various phosphorus levels and cyanobacteria inoculation. *Legum. Res.* 40, 497–505.

Feng, Z., Hu, E., Wang, X., Jiang, L., and Liu, X. (2015). Ground-level O_3 pollution and its impacts on food crops in China: a review. *Environ. Pollut.* 199, 42–48. doi: 10.1016/j.envpol.2015.01.016

Feng, Z., and Kobayashi, K. (2009). Assessing the impacts of current and future concentrations of surface ozone on crop yield with meta-analysis. *Atmos. Environ.* 43, 1510–1519. doi: 10.1016/j.atmosenv.2008.11.033

Feng, Z. Z., Kobayashi, K., Li, P., Xu, Y. S., Tang, H. Y., Guo, A. H., et al. (2019). Impacts of current ozone pollution on wheat yield in China as estimated with observed ozone, meteorology and day of flowering. *Atmos. Environ.* 217:116945.

Feng, Z. Z., Pang, J., Kobayashi, K., Zhu, J., and Ort, D. R. (2010). Differential responses in two varieties of winter wheat to elevated ozone concentration under fully open-air field conditions. *Glob. Change Biol.* doi: 10.1111/j.1365-2486.2010.02184.X

Gelang, J., Pleijel, H., Sild, E., Danielsson, H., Younis, S., and Sellden, G. (2000). Rate and duration of grain filling in relation to flag leaf senescence and grain yield in spring wheat (*Triticum aestivum*) exposed to different concentrations of ozone. *Physiol. Plant.* 110, 366–375. doi: 10.1111/j.1399-3054.2000.1100311.x

Grünhage, L., Pleijel, H., Mills, G., Bender, J., Danielsson, H., Lehmann, Y., et al. (2012). Updated stomatal flux and flux-effect models for wheat for quantifying effects of ozone on grain yield, grain mass and protein yield. *Environ. Pollut.* 165, 147–157. doi: 10.1016/j.envpol.2012.02.026

Guidi, L., Nali, C., Lorenzini, G., Filppi, F., and Soladatini, G. F. (2001). Effect of chronic ozone fumigation on the photosynthetic process of poplar clones showing different sensitivity. *Environ. Pollut.* 113, 245–254. doi: 10.1016/S0269-7491(00)00194-9

IPCC (2021). "Climate change 2021: the physical science basis" in Contribution of working group I to the sixth assessment report of the intergovernmental panel on climate change. eds. V. Masson-Delmotte, P. Zhai, A. Pirani, S. L. Connors, C. Péan and S. Bergeret al. (Cambridge, United Kingdom and New York, NY, USA: Cambridge University Press).

Jackson, M. L. (1956). *Soil chemical analysis - advanced course*. Madison, WI: Published by the author, Dep. of Soil Science, Univ. of Wisconsin.

Kim, H. Y., Lieffering, M., Miura, S., Kobayashi, K., and Okada, M. (2001). Growth and nitrogen uptake of CO_2-enriched rice under field conditions. *New Phytol.* 150, 223–229. doi: 10.1046/j.1469-8137.2001.00111.x

Kobayashi, K., Okada, M., and Kim, H. Y. (1999). "The free air CO_2 enrichment (FACE) with rice in Japan" in World food security and crop production technologies for tomorrow. eds. T. Horie, S. Geng, T. Amano, T. Inamura and T. Shiraiwa (Kyoto University, Kyoto, Japan: Graduate School of Agriculture), 213–215.

Kumar, R., Bhatia, A., Chakrabarti, B., Kumar, V., Tomer, R., Sharma, D. K., et al. (2021). Effect of elevated ozone and carbon dioxide on growth and yield of rice (*Oryza sativa*). *Indian J. Agric. Sci.* 91, 1607–1611. doi: 10.56093/ijas.v91i11.118540

Lefohn, A. S., Malley, C. S., Simon, H., Wells, B., Xu, X., Zhang, L., et al. (2017). Responses of human health and vegetation exposure metrics to changes in ozone concentration distributions in the European Union, United States, and China. *Atmos. Environ.* 152, 123–145. doi: 10.1016/j.atmosenv.2016.12.025

Maity, P. P., Chakrabarti, B., Bhatia, A., Kumar, S. N., Purakayastha, T. J., Chakraborty, D., et al. (2023). Co-elevation of atmospheric CO_2 and temperature affect instantaneous and intrinsic water use efficiency of rice varieties. *J. Agrometeorol.* 25, 404–409. doi: 10.54386/jam.v25i3.2243

Maity, P. P., Chakrabarti, B., Purakayastha, T. J., Bhatia, A., Saha Das, N. D., Jatav, R. S., et al. (2020). Do elevated CO_2 and temperature affect organic nitrogen fractions and enzyme activities in soil under rice crop? *Soil Res.* 58, 400–410. doi: 10.1071/SR19270

Mills, G., Sharps, K., Simpson, D., Pleijel, H., Broberg, M., Uddling, J., et al. (2018). Ozone pollution will compromise efforts to increase global wheat production. *Glob. Change Biol.* 24, 3560–3574. doi: 10.1111/gcb.14157

Mina, U., Fuloria, A., and Aggarwal, R. (2016). Effect of ozone and antioxidants on wheat and its pathogen—Bipolaris sorokininana. *Cereal Res. Comm.* 44, 594–604. doi: 10.1556/0806.44.2016.039

Morgan, P. B., Ainsworth, E. A., and Long, S. P. (2003). How does elevated ozone impact soybean? A meta analysis of photosynthesis, growth and yield. *Plant Cell Environ.* 26, 1317–1328. doi: 10.1046/j.0016-8025.2003.01056.x

NOAA, ESRI (2019). Mauna Loa CO_2 Annual Mean Data.

Pandey, A. K., Ghosh, A., Agrawal, M., and Agrawal, S. B. (2018). Effect of elevated ozone and varying levels of soil nitrogen in two wheat (*Triticum aestivum* L.) cultivars: growth, gas-exchange, antioxidant status, grain yield and quality. *Ecotoxicol. Environ. Saf.* 158, 59–68. doi: 10.1016/j.ecoenv.2018.04.014

Pfister, G. G., Walters, S., Lamarque, J. F., Fast, J., Barth, M. C., Wong, J., et al. (2014). Projections of future summertime ozone over the US. *J. Geophys. Res. Atmos.* 119, 5559–5582. doi: 10.1002/2013JD020932

Phothi, R., Umponstira, C., Sarin, C. S. W., and Nabheerong, N. (2016). Combining effects of ozone and carbon dioxide application on photosynthesis of Thai jasmine rice (*Oryza sativa* L.) cultivar Khao Dawk Mali 105. *Aus. J. Crop Sci.* 10, 591–597. doi: 10.21475/ajcs.2016.10.04.p7595x

Pleijel, H., Danielsson, H., Simpson, D., and Mills, G. (2014). Have ozone effects on carbon sequestration been overestimated? A new biomass response function for wheat. *Biogeosciences* 11, 4521–4528. doi: 10.5194/bg-11-4521-2014

Pramanik, P., Chakrabarti, B., Bhatia, A., Singh, S. D., Mridha, N., and Krishnan, P. (2018). Effect of elevated carbon dioxide on soil hydrothermal regimes and growth of maize crop (*Zea mays* L.) in semi-arid tropics of indo-Gangetic Plains. *Environ. Monit. Assess.* 190:661. doi: 10.1007/s10661-018-6988-5

Proietti, C., Anav, A., De Marco, A., Sicard, P., and Vitale, M. (2016). A multi-sites analysis on the ozone effects on gross primary production of European forests. *Sci. Total Environ.* 556, 1–11. doi: 10.1016/j.scitotenv.2016.02.187

Raj, A., Chakrabarti, B., Pathak, H., Singh, S. D., Mina, U., and Purakayastha, T. J. (2019). Growth, yield and nitrogen uptake in rice crop grown under elevated carbon dioxide and different doses of nitrogen fertilizer. *Indian J. Exp. Biol.* 57, 181–187.

Sanyal, S., Chakrabarti, B., Bhatia, A., Kumar, S. N., Purakayastha, T. J., Kumar, D., et al. (2023). Response of aestivum and durum wheat varieties to elevated CO_2 and temperature under OTC condition. *J. Agrometeorol.* 25, 498–502. doi: 10.54386/jam.v25i4.2366

Singh, P., Agrawal, M., and Agrawal, S. B. (2009). Evaluation of physiological, growth and yield responses of a tropical oil crop (*Brassica campestris* L. var. Kranti) under ambient ozone pollution at varying NPK levels. *Environ. Pollut.* 157, 871–880. doi: 10.1016/j.envpol.2008.11.008

Singh, S. D., Chakrabarti, B., Muralikrishna, K. S., Chaturvedi, A. K., Kumar, V., Mishra, S., et al. (2013). Yield response of important field crops to elevated air temperature and CO_2 levels. *Indian J. Agri. Sci.* 83, 1009–1012.

Singh, E., Rai, R., Pandey, B., and Agrawal, M. (2018). Development of resistance in two wheat cultivars against constant fumigation of ozone. *Proc. Natl. Acad. Sci. India Sect. B Biol. Sci.* 88, 1121–1134. doi: 10.1007/s40011-017-0849-9

Subbiah, B., and Asija, G. L. (1956). A rapid procedure for estimation of available nitrogen in soils. *Curr. Sci.* 25, 259–260.

Tai, A. P. K., Val Martin, M., and Heald, C. L. (2014). Threat to future global food security from climate change and ozone air pollution. *Nat. Clim. Chang.* 4, 817–821. doi: 10.1038/nclimate2317

Tatsumi, K., Abiko, T., Kinose, Y., Inagaki, S., and Izuta, T. (2019). Effects of ozone on the growth and yield of rice (*Oryza sativa* L.) under different nitrogen fertilization regimes. *Environ. Sci. Pollut. Res. Int.* 26, 32103–32113. doi: 10.1007/s11356-019-06358-6

Tiwari, S., Rai, R., and Agrawal, M. (2008). Annual and seasonal variations in tropospheric ozone concentrations around Varanasi. *Int. J. Remote Sens.* 29, 4499–4514. doi: 10.1080/01431160801961391

Tomer, R., Bhatia, A., Kumar, V., Kumar, A., Singh, R., Singh, B., et al. (2015). Impact of elevated ozone on growth, yield and nutritional quality of two wheat species in northern India. *Aerosol Air Qual. Res.* 15, 329–340. doi: 10.4209/aaqr.2013.12.0354

Wu, H., Li, Q., Lu, C., Zhang, L., Zhu, J., Dijkstra, F. A., et al. (2016). Elevated ozone effects on soil nitrogen cycling differ among wheat cultivars. *Appl. Soil Ecol.* 108, 187–194. doi: 10.1016/j.apsoil.2016.08.015

Xia, L., Lam, S. K., Kiese, R., Chen, D., Luo, Y., van Groenigen, K. J., et al. (2021). Elevated CO_2 negates O_3 impacts on terrestrial carbon and nitrogen cycles. *One Earth* 4, 1752–1763. doi: 10.1016/j.oneear.2021.11.009

Yadav, A., Bhatia, A., Yadav, S., Kumar, V., and Singh, B. (2019). The effects of elevated CO_2 and elevated O_3 exposure on plant growth, yield and quality of grains of two wheat cultivars grown in North India. *Heliyon* 5:e02317. doi: 10.1016/j.heliyon.2019.e02317

Yadav, A., Bhatia, A., Yadav, S., Singh, A., Tomer, R., Harit, R., et al. (2021). Growth, yield and quality of maize under ozone and carbon dioxide interaction in north West India. *Aerosol Air Qual. Res.* 21:200194. doi: 10.4209/aaqr.2020.05.0194

Zhang, C., Li, Y., Yu, Z., Wang, G., Liu, X., Liu, J., et al. (2022). Co-elevation of atmospheric [CO_2] and temperature alters photosynthetic capacity and instantaneous water use efficiency in rice cultivars in a cold-temperate region. *Front. Plant Sci.* 13:1037720. doi: 10.3389/fpls.2022.1037720

frontiers | Frontiers in Sustainable Food Systems

TYPE Original Research
PUBLISHED 13 November 2024
DOI 10.3389/fsufs.2024.1446308

OPEN ACCESS

EDITED BY
Aliza Pradhan,
National Institute of Abiotic Stress Management (ICAR), India

REVIEWED BY
Ahmed A. A. Aioub,
Zagazig University, Egypt
Sushil Sudhakar Changan,
Indian Agricultural Research Institute (ICAR), India

*CORRESPONDENCE
Sazada Siddiqui
✉ sasdeky@kku.edu.sa

RECEIVED 09 June 2024
ACCEPTED 28 October 2024
PUBLISHED 13 November 2024

CITATION
Siddiqui S (2024) Effects of cypermethrin on morphological, physiological and biochemical attributes of *Cicer arietinum* (Fabales: Fabaceae).
Front. Sustain. Food Syst. 8:1446308.
doi: 10.3389/fsufs.2024.1446308

Effects of cypermethrin on morphological, physiological and biochemical attributes of *Cicer arietinum* (Fabales: Fabaceae)

Sazada Siddiqui*

Department of Biology, College of Science, King Khalid University, Abha, Saudi Arabia

Cypermethrin, a synthetic pyrethroid, is a widely employed pesticide in large-scale commercial agriculture and domestic settings to control pests and boost crop yields. Despite its effectiveness in controlling pests, concerns persist about the potential ecological and human health impacts associated with its use. In the present study, the impact of cypermethrin on different parameters, including growth indices, pollen morphology and pollen fertility, chlorophyll and carotenoid content, hydrogen peroxide (H_2O_2) scavenging, lipid peroxidation (MDA concentration), superoxide dismutase (SOD), and catalase (CAT) activities, was investigated in *Cicer arietinum* L. The results showed that plants exhibited decreasing trends in plant height, number of branches, pods, and seeds per plant as cypermethrin concentrations increased. These changes resulted in significant reductions in the overall yield of the plants. The percentage of wrinkled pollen significantly increased with higher concentrations of cypermethrin and longer exposure durations. Exposure to cypermethrin showed significant variations in pollen fertility of *C. arietinum* at different concentrations and time intervals in comparison to control, which had a baseline pollen fertility of 79.12% ± 4.59. Chlorophyll and carotenoid content of *C. arietinum* were considerably affected by cypermethrin, indicative of potential disturbances in essential photosynthetic processes crucial for plant health. Further, with increasing concentrations of cypermethrin ranging from 100 mg/L to 500 mg/L, noticeable effects were observed on $H_2O_{2\_}$ scavenging, MDA concentration, SOD and CAT activities of *C. arietinum* in dose-dependent manner. Further, it was found that the duration of exposure and concentration of cypermethrin played a crucial role in exacerbating these detrimental effects. The findings of the present study raise concerns regarding the harmful effects of agricultural pesticides like cypermethrin and highlight the need for more research on the nutritional value of products derived from plants and seeds exposed to these agents.

KEYWORDS

cypermethrin, growth indices, chlorophyll content, lipid peroxidation, *Cicer arietinum* L

1 Introduction

The world is grappling with the dual challenge of a rapidly growing population and diminishing food resources, prompting global concerns (Ridwan et al., 2022; Rajak et al., 2023). The intensified development of the global economy has resulted in a surge in pesticide production and usage. In agriculture, pesticides are common chemical substances that are used to eradicate weeds, insects, and other pests (Sharma et al., 2020; Kenko et al., 2023; Gautam et al., 2023). They are an essential component of modern agricultural practices and play a crucial role in safeguarding crops and enhancing yields, as approximately 45% of annual food production is lost due to pest invasions (Borowik et al., 2023a,b; Skubała et al., 2024).

However, the widespread use of pesticides poses significant threats to ecosystems, human health, and other biotic elements of the environment (Khan et al., 2023; Liess and Gröning, 2024). Cypermethrin is a widely employed pesticide in large-scale commercial agriculture and domestic settings to control pests and boost crop yields (Nath et al., 2024). Classified as an extremely effective synthetic type II pyrethroid, cypermethrin is recognized as a valuable pesticide in agricultural, horticultural, and aquatic systems, having comparatively less noxiousness to non-target animals (Liu et al., 2009; Baruah et al., 2024). Cypermethrin has very low vapor pressure and solubility in water, but it is highly soluble in a wide range of organic solvents. It primarily targets sodium channels and adenosine triphosphatase in pests (Çavuşoğlu, 2011). Despite its effectiveness, concerns persist about the potential ecological and human health impacts associated with the use of cypermethrin and similar pesticides (Çavuşoğlu, 2011). Methods for the determination of residues of cypermethrin in foods and in the environment are well established. In most substrates, the practical limit of determination of is 0.01 mg/kg (World Health Organization, 1989).

Several crop plants, like *Crepis capillaries*, *Vicia faba*, *Hordeum vulgare*, *Pisum sativum*, *Allium cepa*, and *Cicer arietinum*, have been identified as bioindicators for evaluating the biological effects of chemicals from diverse sources (Sheikh et al., 2020; Hoseiny-Rad and Aivazi, 2020). Chickpea (*Cicer arietinum* L.) stands out as the second most cultivated legume globally, following soybeans (Pang et al., 2017). Although estimates vary, Nedumaran et al. (2015) reported cultivation at 11 million hectares with a production of 8 million tons, positioning chickpea as the third most crucial food legume ever grown. Beyond its role as a significant food source for both humans and animals, chickpea contributes substantially to soil fertility conservation, especially in dry, rain-fed regions, through symbiotic nitrogen fixation (Sharma, 2012; Angaji et al., 2013). However, chickpea faces challenges due to its limited competitiveness with weeds, attributed to its sluggish growth and constrained development of leaf area in the initial phases of growth (Hoseiny-Rad and Aivazi, 2020).

Previous research has explored the effects of various pesticides on plants, such as the accumulation of atrazine in rice plants, leading to toxic reactions through the over-formation of reactive oxygen species (ROS) and activation of plant safety mechanisms (Zhang et al., 2014). Yin et al. (2008) found that isoproturon delayed wheat plant growth and impacted various physiological processes, inducing oxidative stress. In our current investigation, we examined the impact of cypermethrin on different parameters in chickpea plants. This involved analyzing growth patterns, pollen fertility, and pollen morphology, as well as investigating potential alterations in the antioxidant structure and photosynthetic procedure in cypermethrin-induced stress. We specifically assessed hydrogen peroxide (H_2O_2) -scavenging, malondialdehyde (MDA) levels, catalase (CAT), and superoxide dismutase (SOD) activity, in addition to chlorophyll and carotenoid levels. Our primary objective was to develop a comprehensive understanding of how cypermethrin influences critical aspects of *Cicer arietinum* development and biochemistry.

2 Methodology

2.1 Procurement of chemical and seeds

Cypermethrin (CAS No. 52315-07-8) was purchased from Sigma Chemicals Ltd., USA. *Cicer arietinum* seeds were obtained from a certified dealer in Abha, Aseer Region, KSA.

2.2 Agroclimatic conditions of the experimental site

The studies were carried out in the Department of Botany, Science College, Alfarra Campus, King Khalid University, Abha, Saudi Arabia. Abha is 2,270 meters above sea level and situated in the southern region of Saudi Arabia, near Aseer. Abha's high elevation gives it a semi-arid climate. Abha, Asir, Saudi Arabia is located at latitude 18.216797 and longitude 42.503765.

2.3 Plant materials and treatments

Fresh and vigorous seeds were surface sterilized using a 5% NaOCl solution for 10 min. Post-sterilization, the seeds were carefully rinsed multiple times with distilled water. Subsequently, the seeds were divided into distinct groups, each comprising 100 seeds. The experimental treatments involved subjecting the seeds to five different concentrations (100 mg/L, 200 mg/L, 300 mg/L, 400 mg/L and 500 mg/L) of a 250 ml cypermethrin solution, with exposure durations of 1 and 3 h. For control group (0) 100 seeds were treated with distilled water. Following treatment, the seeds were permitted to germinate on petri plates containing damp cotton, maintained at a controlled temperature in the dark for 24 h. The germination status of the seeds was then assessed, and the resulting sprouts were utilized for subsequent growth and yield investigations. Additionally, another set of seeds for each concentration was planted in earthen pots to facilitate biochemical studies. These seeds were grown in greenhouse conditions. The temperature and humidity in a greenhouse were 64 to 75°F and approximately 80%, respectively. In parallel, plants in the control group, devoid of any exposure, were cultivated to serve as a basis for comparative analysis. The entire experiment was replicated three times under consistent conditions to ensure the reliability and repeatability of the results.

2.4 Growth studies

Growth parameters were examined on 14-day-old seedlings. The studied growth parameters include Plant height, number of branches, number and length of pods, number of seeds per pod, along with their weights and total yield.

2.5 Pollen studies

An examination of 100 pollens from each treatment was conducted to assess fertility, pollen morphology, and shape. The pollens were categorized based on their shape and dimensions in equatorial and polar views, following the classification method proposed by Erdtman (1966). For determining pollen viability, a total of 100 pollen grains from each group were observed under a light microscope. The viability level was assessed by a solution of 2, 3, 5-triphenyl tetrazolium chloride (TTC) (Norton, 1966).

To conduct this viability test, a drop of TTC solution was kept on a slide, and pollens were spread using a brush, followed by the placement of a cover slip. After the application of TTC, counting was done, and the pollens were categorized into three sets based on staining density. Pollen exhibiting a dark red stain were considered viable; those with a light red stain were categorized as semi-viable; and unstained pollens were classified as non-viable, following the criteria established by Eti (1991) and Stosser (1984).

2.6 Photosynthetic pigment measurement

The chlorophyll estimation was carried out using the Acetone method, following Arnon (1949). Chlorophyll extraction was performed in 80% acetone, and absorbance was measured at wavelengths of 663 nm and 645 nm. Chlorophyll and carotenoid content were calculated by Khan et al. (2019).

2.7 Hydrogen peroxide (H_2O_2) scavenging effects

The assessment of hydrogen peroxide scavenging activity was conducted following the technique stated by Ruch et al. (1989), employing spectrophotometry at 230 nm. Leaf extracts in methanol were prepared at 100 μg/mL concentration and then mixed with a H_2O_2 solution (0.6 mL; 40 mM) in phosphate buffer (PB) having a pH of 7.4. The volume of the final solution was adjusted to 3 mL, and the mixture was kept in incubation for 10 min. PB solution with no H_2O_2 was kept as a reference. At 230 nm, absorbance was measured for all compounds. The degree of H_2O_2 scavenging by plant extracts was subsequently calculated by Khan et al. (2019).

2.8 Lipid peroxidation

Rao and Sresty (2000) were followed for the estimation of lipid peroxidation. 0.2 g of frozen leaf sections were homogenized in 2 mL of 0.1% trichloroacetic acid (TCA) and subjected to centrifugation at 10,000 rpm for 10 min to precipitate the remains. Supernatant aliquots were then added to 4 mL of 20% TCA with 0.5% thiobarbituric acid and 100 μL of butylated hydroxyl toluene in 4% ethanol. The mixture was incubated for 1 h at 90°C, later cooled in an ice bath and subsequently centrifuged at 10,000 rpm for 5 min. The supernatant and the unspecific turbidity of the sample were measured at 532 nm and 600 nm, respectively. This turbidity value was subtracted from the absorbance at 532 nm. A solution of 0.25% TBA in 10% TCA served as a blank reference. The content of TBA reactive substances was depicted as nmol/g fresh weight by means of an extinction coefficient of 155 mM^{-1} cm^{-1}.

2.9 Superoxide dismutase (SOD) and catalase (CAT) activity

Total CAT activity was examined by quantifying the intake of H_2O_2 at 240 nm, following the technique described by Gallego et al. (1996). The enzymatic actions of both SOD and CAT were stated as units per milligram of protein (U mg^{-1} protein). The measurement of SOD activity was conducted following Khan et al. (2019) with slight modifications.

2.10 Statistical analysis

One way ANOVA using SPSS software (version 16.0, SPSS Inc., Chicago, IL, USA) was applied to find the significance of differences in variables. The changes were considered statistically significant at $p < 0.05$. All the outcomes are expressed as mean ± standard error.

3 Results

3.1 Effects of cypermethrin on growth and development of *C. arietinum*

Table 1, Figure 1 show the impact of diverse cypermethrin concentrations from 100 mg/L to 500 mg/L on several growth parameters of *C. arietinum*. In both 1 and 3 h exposures to increasing concentrations of cypermethrin, noticeable adverse effects were observed on various growth parameters of *C. arietinum*. Relative to the control group, the plants exhibited decreasing trends in plant height (21.04% in 1 h; 25.32% in 3 h), branches (31.48% in 1 h; 37.23% in 3 h), pods (13.87% in 1 h; 17.33% in 3 h), and seeds per plant (40.45% in 1 h; 44.87% in 3 h), as cypermethrin concentrations increased. These changes resulted in significant reductions in the overall yield of the plants (14.95% in 1 h; 40.53% in 3 h). Furthermore, negative consequences extended to individual seed quality, as evidenced by a decrease in pod length (72.54% in 1 h; 64.07% in 3 h) and the weight of seeds (14.61% in 1 h; 10.24% in 3 h).

3.2 Effects of cypermethrin on pollen morphology of *C. arietinum*

Cypermethrin has a notable detrimental effect on the pollen morphology of *C. arietinum*, as evidenced by increased wrinkled pollen, a higher proportion of pollen without visible pores, and an elevated occurrence of abnormal pollen shapes. Table 2, Figure 2 illustrate the impact of various concentrations of cypermethrin (100 mg/L to 500 mg/L) and different exposure durations (1 h and

TABLE 1 Impact on the growth and yield of *C. arietinum* treated with cypermethrin for 1 and 3 h.

Concentration (mg/L)	Plant height (cm)	No. of branches per plant	No. of pods per plant	Length per pod (cm)	No. of seeds per pod	Total no. of seeds per plant	100 seeds weight (g)	Total yield per plant (gm)
1 h								
0	55.367 ± 2.72	4.86 ± 0.49	49.53 ± 2.65	3.06 ± 0.16	4.12 ± 0.46	97.05 ± 4.08	5.13 ± 0.40	4.48 ± 0.65
100 mg/L	59.53 ± 4.74	3.94 ± 0.68^{c}	48.46 ± 2.82	2.12 ± 0.13^{b}	3.67 ± 0.54	81.75 ± 4.41^{b}	4.24 ± 0.56^{b}	3.91 ± 0.89
200 mg/L	48.84 ± 4.31^{b}	3.82 ± 0.67^{c}	47.43 ± 3.88	0.96 ± 0.34^{b}	3.66 ± 0.68	72.64 ± 3.65^{b}	4.28 ± 0.59^{b}	3.31 ± 0.68
300 mg/L	46.57 ± 0.32^{b}	3.76 ± 0.83^{b}	45.43 ± 3.26^{c}	0.92 ± 0.35^{b}	3.32 ± 0.69^{C}	68.73 ± 4.16^{b}	4.20 ± 0.61^{b}	3.48 ± 0.61
400 mg/L	44.46 ± 5.88^{b}	3.62 ± 0.91^{b}	43.53 ± 2.89^{b}	0.77 ± 0.27^{b}	3.43 ± 0.49	60.88 ± 5.86^{b}	4.62 ± 0.46	3.71 ± 0.55
500 mg/L	43.71 ± 4.66^{b}	3.33 ± 0.71^{b}	42.66 ± 3.38^{b}	0.84 ± 0.28^{b}	3.43 ± 0.68	57.79 ± 4.19^{b}	4.38 ± 0.64^{c}	3.81 ± 0.60
3 h								
0	45.26 ± 2.72	3.76 ± 0.39	39.63 ± 2.35	2.06 ± 0.16	3.00 ± 0.46	87.06 ± 3.08	4.10 ± 0.30	3.38 ± 0.55
100 mg/L	39.53 ± 4.74^{c}	2.93 ± 0.57^{b}	38.36 ± 3.58	1.00 ± 0.13^{b}	2.66 ± 0.54	71.85 ± 5.42^{b}	3.94 ± 0.46	2.81 ± 0.79
200 mg/L	38.93 ± 4.31^{c}	2.83 ± 0.67^{b}	37.33 ± 3.77	0.86 ± 0.34^{b}	2.46 ± 0.58	62.74 ± 5.64^{b}	3.88 ± 0.49	2.51 ± 0.68^{c}
300 mg/L	36.46 ± 4.32^{b}	2.86 ± 0.73^{b}	35.63 ± 4.46	0.82 ± 0.35^{b}	0.33 ± 0.59^{C}	58.83 ± 4.15^{b}	3.80 ± 0.51	2.28 ± 0.71^{b}
400 mg/L	34.46 ± 5.88^{b}	2.50 ± 0.80^{b}	35.63 ± 3.89^{b}	0.67 ± 0.27^{b}	0.26 ± 0.39^{b}	50.98 ± 4.81^{b}	3.72 ± 0.56	2.11 ± 0.65^{b}
500 mg/L	33.80 ± 4.66^{b}	2.36 ± 0.68^{b}	32.76 ± 2.38^{b}	0.74 ± 0.28^{b}	0.20 ± 0.58^{b}	47.99 ± 5.09^{b}	3.68 ± 0.60	2.01 ± 0.50^{b}

$^{c}p < 0.05$; $^{b}p < 0.01$ compared to control group. Data are mean of three replicates ± SE, 0 = Control group.

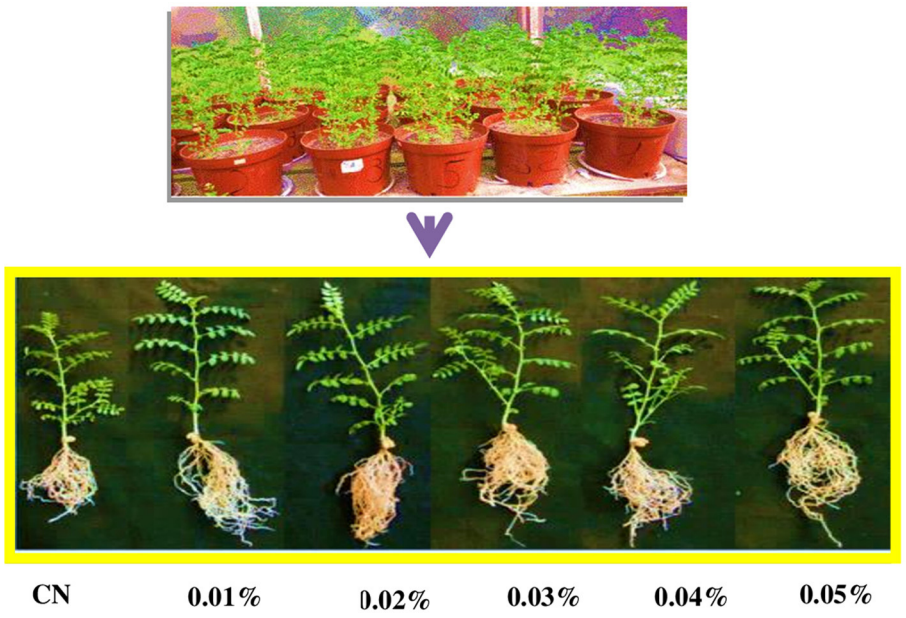

FIGURE 1
Effect on morphology of *C. arietinum*. treated with cypermethrin for 1 and 3 h.

3 h) on the pollen morphology of *C. arietinum*. In comparison to control, the percentage of wrinkled pollen significantly increased with higher concentrations of cypermethrin (with 3.71 ± 1.47 in control group to 40.35 ± 4.58; $p < 0.01$ at 500 mg/L for 1 h) and longer exposure durations (with 2.77 ± 1.27 in control to 31.75 ± 5.37; $p < 0.01$ at 500 mg/L for 3 h). This is evident in all treated groups, indicating a dose-dependent and time-dependent effect on pollen morphology. Treatment with cypermethrin led to a significant rise in the percentage of pollen without visible pores. This effect was more pronounced with increased concentrations and exposure durations (with 2.54 ± 1.45 at control to 26.55 ± 3.39; at 500 mg/L for 1 h and, with 2.78 ± 0.91 at control

to 51.37 ± 4.53; at 500 mg/L for 3 h) highlighting the adverse impact of cypermethrin on the structural integrity of pollen grains. Similarly, the percentage of pollen with abnormal shapes displayed a significant rise in relation to cypermethrin treatment in Table 2.

TABLE 2 Impact on the pollen morphology of *C. arietinum* treated with cypermethrin for 1 and 3 h.

Concentration (mg/L)	Wrinkled pollen (%)	Pollen without visible pore (%)	Pollen with abnormal shape (%)
1 h			
0	3.71 ± 1.47	2.54 ± 1.45	1.23 ± 0.04
100 mg/L	14.75 ± 3.52^b	17.55 ± 2.15^b	8.77 ± 2.17^b
200 mg/L	20.65 ± 4.23^b	25.75 ± 3.22^b	14.22 ± 3.52^b
300 mg/L	27.15 ± 2.78^b	32.88 ± 4.55^b	17.32 ± 2.13^b
400 mg/L	35.25 ± 3.11^b	40.77 ± 3.22^b	20.45 ± 3.45^b
500 mg/L	40.35 ± 4.58^b	45.23 ± 4.58^b	26.55 ± 3.39^b
3 h			
0	2.77 ± 1.27	2.78 ± 0.91	2.34 ± 0.09
100 mg/L	10.77 ± 3.17^b	20.75 ± 3.74^b	10.45 ± 2.75^b
200 mg/L	15.15 ± 3.75^b	27.68 ± 4.25^b	19.75 ± 4.23^b
300 mg/L	23.45 ± 4.65^b	34.99 ± 3.75^b	25.85 ± 3.75^b
400 mg/L	27.45 ± 4.23^b	45.95 ± 4.35^b	31.78 ± 4.23^b
500 mg/L	31.75 ± 5.37^b	51.37 ± 4.53^b	35.88 ± 3.15^b

$^a p < 0.05$; $^b p < 0.01$ compared to control group. Data are mean of three replicates ±SE, 0 = Control group.

3.3 Effects of cypermethrin on pollen fertility of *C. arietinum*

Exposure to cypermethrin showed significant variations in pollen fertility of *C. arietinum* at different concentrations and time intervals in comparison to the control, which had a baseline pollen fertility of 79.12% ± 4.59. After a 1 h exposure, lower concentrations of cypermethrin slightly increased the pollen fertility of *C. arietinum* compared to the control, with concentrations of 100 mg/L and 200 mg/L resulting in increased pollen fertility to 84.54% ± 6.23 and 80.14% ± 5.73, respectively. However, higher concentrations exhibited a significant decline in the fertility of pollens, with 500 mg/L showing the maximum reduction in the fertility of pollens with a pollen fertility of 65.57% ± 4.32 ($p < 0.01$). In the 3 h exposure, a similar but non-significant pattern was observed. It was observed that the two-time intervals (1 h and 3 h) revealed distinct effects of cypermethrin on the pollen fertility of *C. arietinum*. For instance, after 1 h of exposure, a concentration of 300 mg/L demonstrated a significant reduction in pollen fertility to 73.12% ± 4.42, whereas at 3 h of exposure with the same concentration, a pollen fertility rate of 70.78% ± 6.12 was observed, and similar trends were observed for other concentrations as well (Figures 3, 4). The decrease in the percentage of fertile pollen with increasing dosage is likely attributable to the toxic effects of cypermethrin on pollen.

3.4 Effects of cypermethrin on leaf pigments of *C. arietinum*

Chlorophyll (Figure 5A) and carotenoid content (Figure 5B) of *C. arietinum* were considerably affected by cypermethrin, indicative of potential disturbances in essential photosynthetic processes

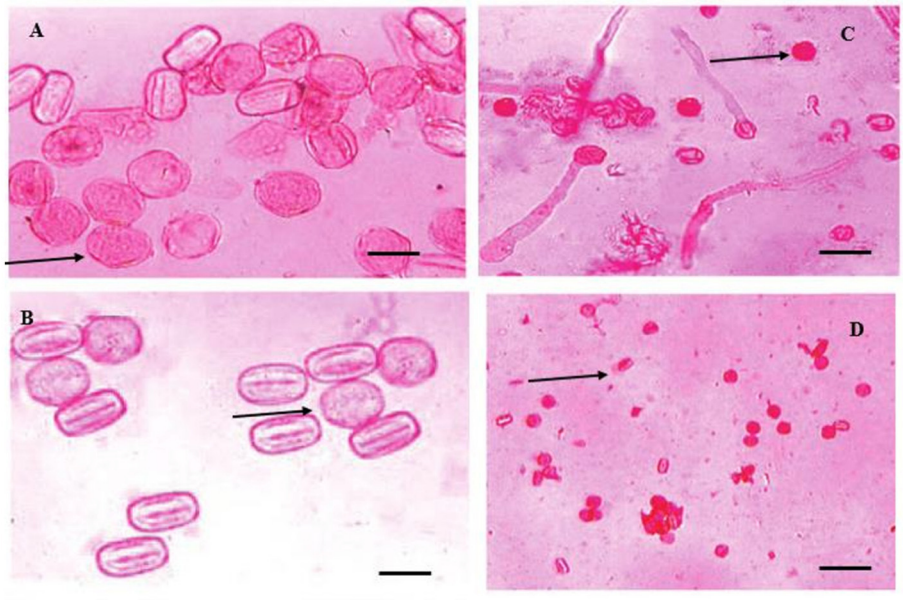

FIGURE 2
Impact on pollen morphology of *C. arietinum* treated with cypermethrin for 1 and or 3 h in PMCs. **(A)** Wrinkled pollen grain; **(B, C)** Pollen without visible pore; **(D)** Pollen with abnormal shape. Scale bars = 10 μM; bars = 10 μM.

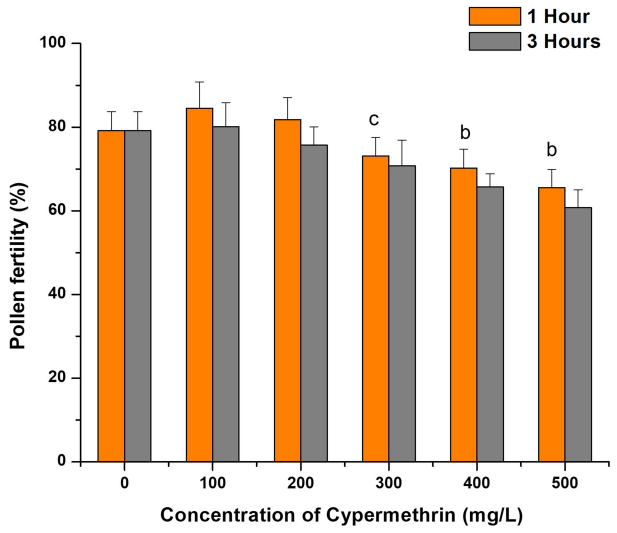

FIGURE 3
Effect of cypermethrin on pollen fertility *C. arietinum* for 1 and 3 h.$^{c}p < 0.05$; $^{b}p < 0.01$ compared to control group. Data are mean of three replicates ±SE, 0 = Control group.

crucial for plant health. Upon exposure to cypermethrin for 1 h, a visible dose-dependent response was observed with a 12.5% decrease at 500 mg/L in comparison to the control. Overall, a statistically significant reduction in chlorophyll content was noted as the concentration of cypermethrin increased in Figure 5A. Concentrations equal to or exceeding 200 mg/L exhibited a noteworthy decline in chlorophyll content compared to the control group. Similarly, after a 3 h exposure, a dose-dependent decrease in chlorophyll content was evident, with all concentrations ranging from 100 mg/L to 500 mg/L displaying statistically significant reductions compared to the control, with an 18.75% reduction at 500 mg/L in Figure 5A. These findings emphasize the concentration-dependent and exposure duration-dependent impact of cypermethrin on the chlorophyll content of *C. arietinum*.

Cypermethrin exposure also adversely affected the carotenoid content of *C. arietinum* indicating potential disruptions in essential pigment concentrations crucial for plant health. Following a 1 h exposure, a concentration dependent decrease in carotenoid content was observed, with a 58.9% decrease at 500 mg/L Similarly, after a 3 h exposure, a concentration-dependent decline in carotenoid content was evident across all concentrations compared to the control group, with a 54.1% decrease at 500 mg/L. The consistent and statistically significant differences highlight the concentration-dependent and exposure duration-dependent effects of cypermethrin on the carotenoid content of the plant in Figure 5B.

3.5 Effects of cypermethrin on H_2O_2–scavenging, MDA, SOD, and CAT activities *C. arietinum*

Figures 6A–D show the effect of different cypermethrin concentrations from 100 mg/L to 500 mg/L on various biochemical parameters such as H_2O_2 scavenging (Figure 6A), lipid peroxidation concentration (MDA; Figure 6B), superoxide dismutase (SOD) activity (Figure 6C) and catalase (CAT) activity (Figure 6D) on *C. arietinum* for 1 and 3 h. In both 1 and 3 h exposures to increasing concentrations of cypermethrin ranging from 100 mg/L to 500 mg/L, noticeable enhanced effects were observed on various parameters such as hydrogen peroxide scavenging, MDA, SOD and CAT activity of C. *arietinum* in a dose-dependent manner, which is very significantly increased ($p < 0.01$) when compared to control.

4 Discussion

This implies that cypermethrin not only impacts the overall productivity of the plants but also affects the characteristics of the produced seeds. Interestingly, the duration of exposure played a crucial role in exacerbating these detrimental effects. The 3 h exposure to cypermethrin demonstrated a more pronounced negative influence on all measured growth parameters compared to the 1 h exposure. This suggests that prolonged exposure to cypermethrin intensifies its impact on the growth and reproductive aspects of chickpea plants. The findings align with results obtained by Obidola et al. (2019) in cowpea, indicating a common sensitivity of leguminous crops to cypermethrin. Ramzan et al. (2022) have also found that cypermethrin has the most toxic effects on growth parameters like root length, stem length, and dry weight in *Helianthus annus* and *Brassica juncea*. A very strong negative correlation was found between the concentration of cypermethrin and plant height in 1 h treatment (−0.88) and 3 h treatment (−0.95). Increased exposures to pesticides reduce the photosynthetic capacity of the plants by inhibiting PSII, which in turn reduces the overall growth of the plant (Ramzan et al., 2022; Borowik et al., 2023a; Khurshid et al., 2024).

Higher concentrations and longer durations were associated with a greater incidence of abnormal pollen shapes, suggesting a disruptive influence on the typical morphology of *C. arietinum* pollen. It has been found that pesticides have direct negative effects on the morphology and anatomy of pollens (Wrońska–Pilarek et al., 2023). It is well known that the generative reproduction organs of plants are more susceptible to stress than the vegetative portions. Because of this, pollen is frequently used to evaluate the harmful effects of xenobiotics (Zanelli et al., 2023).

This toxic impact becomes more pronounced at higher dosages, and the observed reduction in fertile pollens compared to the control may have negative implications for the long-term productivity and quality of chickpeas (Çali, 2009). Similar negative effects on pollen viability were reported in eggplants exposed to a combination of two organophosphate insecticides and a dinitro herbicide. Furthermore, the fungicide propiconazole was found to adversely affect pollen germination and pollen tube growth in *Tradescantia virginiana*. Regardless of the type or dosage of herbicide used, pesticide treatment reduces the viability of pollen grains in both laboratory testing and field observations (Wrońska–Pilarek et al., 2023), and thus the significance of adequate pollination and fertilization in economically important crops is emphasized in various studies.

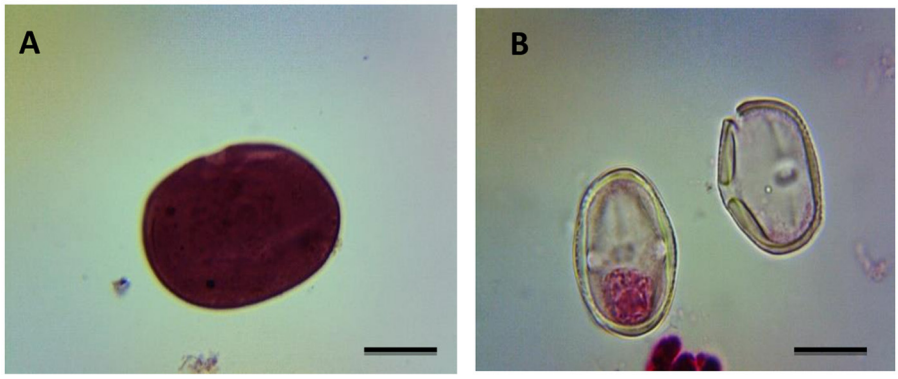

FIGURE 4
Impact on pollen fertility of *C. arietinum* treated with cypermethrin for 1 and 3 h in PMCs. **(A)** Fertile pollen grain in PMCs; **(B)** Sterile pollen grain in PMCs of *C. arietinum*; bars =10 μM.

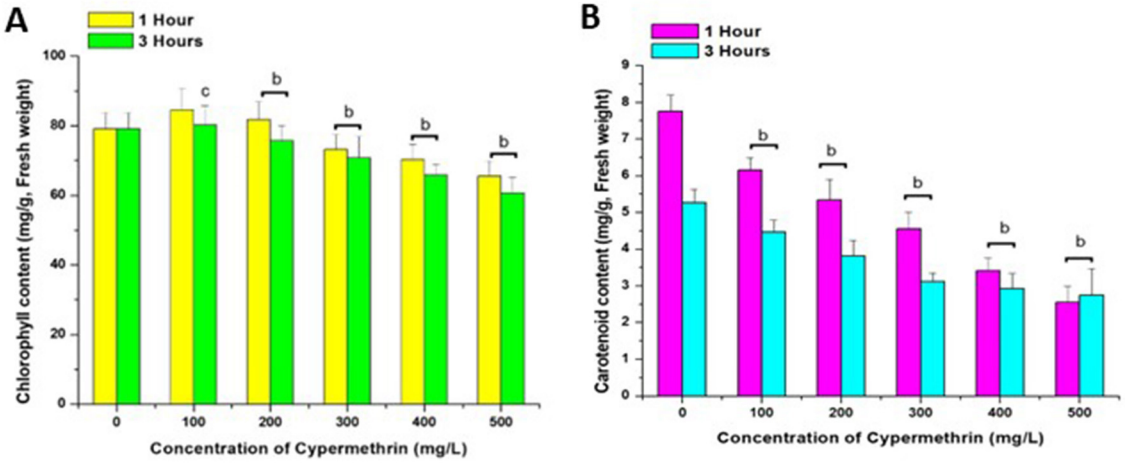

FIGURE 5
Effect of Cypermethrin on chlorophyll **(A)** and carotenoids **(B)** on *C. arietinum* for 1 and 3 h. $^{c}p < 0.05$; $^{b}p < 0.01$ compared to control group. Data are mean of three replicates ±SE, 0 = Control group.

In pigment investigations, when the concentration of cypermethrin increased, the chlorophyll content in *C. ariteinum* leaves reduced considerably. Reduced pigment content can be attributed to various factors, and several studies have revealed a decrease in chlorophyll content in responses to increased stress (Chen et al., 2024; Skubała et al., 2024; Somtrakoon et al., 2024).

The carotenoid contents in this study reduced when treated with cypermethrin, although at a slower rate than the contents of chlorophyll. Cypermethrin not only caused pigment degradation but also lowered the biosynthesis mechanism, as seen by the decrease in carotenoid concentration. It is well-established that carotenoids play a vital role in protecting cells against photooxidation by assisting in the dissipation of excessive excitation energy (Vuković et al., 2021; Gautam et al., 2023). Cypermethrin not only induces the dilapidation of pigments but hampers their biosynthesis process by inhibiting membrane bound enzymes (Stelzer and Gordon, 1988; Michelangeli et al., 1990; Çavuşoğlu, 2011; Somtrakoon et al., 2024; Ariola and Ramize, 2024).

In our study, we observed a gradual increase in both SOD and CAT activities in treated populations as the concentration of cypermethrin increased in comparison to the control group. The significant rise in SOD and CAT activity at maximum concentration suggests an augmented generation of ROS. This increase leads to the transformation of superoxide anion free radicals into H_2O_2, as indicated by the elevated hydrogen peroxide scavenging observed in our results. According to Ayhan et al. (2024), the presence of hazardous chemicals causes serious oxidative damage to various cell structures and biomolecules. Antioxidant enzymes like CAT and SOD can cause oxidative damage and SOD is an essential part of antioxidative mechanisms in cell metabolism.

To evaluate oxidative stress-induced harm to lipid membranes, we monitored the change in malondialdehyde

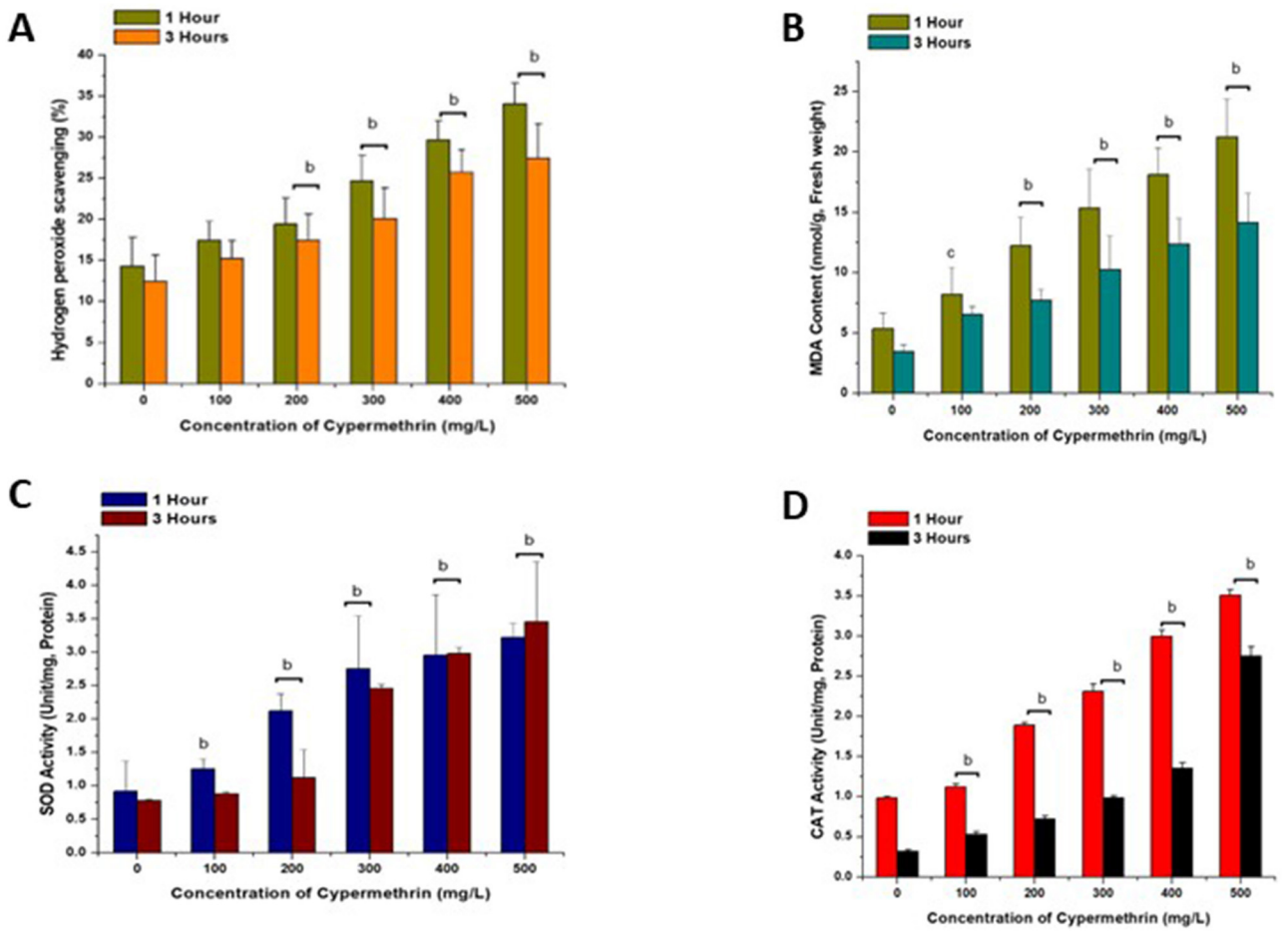

FIGURE 6
Effect of cypermethrin on Hydrogen peroxide scavenging **(A)**, lipid peroxidation **(B)**, SOD **(C)** and CAT **(D)** activities, on *C. arietinum* for 1 and 3 h. $^{c}p < 0.05$; $^{b}p < 0.01$ compared to control group. Data are mean of three replicates ± SE, 0 = Control group.

(MDA) concentration. Higher levels of MDA indicate increased cellular harm and the presence of oxidative stress (Khan et al., 2019). Our findings revealed a concentration-dependent response to cypermethrin, with elevated MDA levels observed. Interestingly, we observed a trend where longer exposure durations tended to lower SOD and CAT activities (Figures 6C, D). This was evident in the comparison between the 1 and 3 h treatments, suggesting a potential adaptation or regulation mechanism in response to prolonged cypermethrin exposure. Several studies have consistently demonstrated that plants have developed intricate antioxidant defense mechanisms relying on enzymes like SOD and CAT to neutralize free radicals and peroxides (Sharma et al., 2024). The enzyme SOD serves as the primary defense against reactive oxygen species (ROS) generated during oxidative stress (Khan et al., 2019). The augmentation of stress tolerance in plants under various stressful conditions is closely linked to an elevation in the activity of antioxidant enzymes (Aioub et al., 2021; Khurshid et al., 2024).

5 Conclusion

The present study aimed to develop a comprehensive understanding of how cypermethrin influences critical aspects of development and biochemistry in *C. arietinum*. The results of this investigation showed that cypermethrin can alter and negatively affect the morphology, biochemistry, and physiological aspects of *C. arietinum*. The duration of exposure and concentration of cypermethrin played a crucial role in exacerbating these detrimental effects. Our concerns regarding the harmful effects of agricultural pesticides like cypermethrin should be raised by these results, which also highlight the need for more research on the nutritional value of products derived from plants and seeds exposed to these agents. In order to achieve high crop yields, traditional intensive cropping systems heavily utilize chemical fertilizers, plant growth regulators, and pesticides. However, increased use of chemical pesticides on agricultural crops has raised a number of economic, ecological and health concerns. Governments in developed nations are establishing goals to limit the use of

pesticides as awareness of this issue grows, but the adoption and scope of organic farming are growing more slowly, despite the efforts of various organizations to support it. This low adoption rate can be explained by a variety of factors, including the information given to farmers and their perceptions of the production risk associated with the new technology. So, more robust efforts are needed in this direction.

Data availability statement

The original contributions presented in the study are included in the article/supplementary material, further inquiries can be directed to the corresponding author.

Author contributions

SS: Conceptualization, Data curation, Formal analysis, Funding acquisition, Investigation, Methodology, Project administration, Resources, Software, Supervision, Validation, Visualization, Writing – original draft, Writing – review & editing.

Funding

The author(s) declare financial support was received for the research, authorship, and/or publication of this article. The author extends their appreciation to the Deanship of Research and Graduate Studies at King Khalid University for funding this work through a Large Group Project under grant number (RGP2/49/45).

Conflict of interest

The author declares that the research was conducted in the absence of any commercial or financial relationships that could be construed as a potential conflict of interest.

Publisher's note

All claims expressed in this article are solely those of the authors and do not necessarily represent those of their affiliated organizations, or those of the publisher, the editors and the reviewers. Any product that may be evaluated in this article, or claim that may be made by its manufacturer, is not guaranteed or endorsed by the publisher.

References

Aioub, A. A., Zuo, Y., Aioub, A. A., and Hu, Z. (2021). Biochemical and phytoremediation of Plantago major L. to protect tomato plants from the contamination of cypermethrin pesticide. *Environ. Sci. Pollut. Res.* 28, 43992–44001. doi: 10.1007/s11356-021-13853-2

Angaji, S. A., Najafi, F., Khavarinejad, R. A., and Soltani, E. (2013). The analysis of gene expression to identify interaction of gibberellic acid and salinity using differential display-PCR in chickpea (*Cicer arietinum* L.). *Adv. Environ. Biol.* 7, 1058–1063.

Ariola, B., Ramize, H. and Kathelina, K. (2024). Different level of tolerance to herbicides is displayed by l. cultivars depending on herbicide category and mode of application. *EuroBiotech J.* 8, 44–54. doi: 10.2478/ebtj-2024-0005

Arnon, D. I. (1949). Copper enzymes in isolated chloroplasts. Polyphenoloxidase in Beta vulgaris. *Plant Physiol.* 24:1. doi: 10.1104/pp.24.1.1

Ayhan, B. S., Macar, T. K., Macar, O., Yalçin, E., Çavuşoglu, K., and Özkan, B. (2024). A comprehensive analysis of royal jelly protection against cypermethrin-induced toxicity in the model organism *Allium cepa* L., employing spectral shift and molecular docking approaches. *Pest. Biochem. Physiol.* 203:105997. doi: 10.1016/j.pestbp.2024.105997

Baruah, P., Srivastava, A., Mishra, Y., and Chaurasia, N. (2024). Modulation in growth, oxidative stress, photosynthesis, and morphology reveals higher toxicity of alpha-cypermethrin than chlorpyrifos towards a non-target green alga at high doses. *Environm. Toxicol. Pharmacol.* 2024:104376. doi: 10.1016/j.etap.2024.104376

Borowik, A., Wyszkowska, J., Zaborowska, M., and Kucharski, J. (2023a). Impact of cypermethrin (Arpon G) on soil health and zea mays growth: a microbiological and enzymatic study. *Agriculture* 13:2261. doi: 10.3390/agriculture13122261

Borowik, A., Wyszkowska, J., Zaborowska, M., and Kucharski, J. (2023b). The impact of permethrin and cypermethrin on plants, soil enzyme activity, and microbial communities. *Int. J. Mol. Sci.* 24:2892. doi: 10.3390/ijms24032892

Çali, I. Ö. (2009). Effects of a fungicide on pollen morphology and fertility of tomato (*Lycopersicon esculentum* Mill.). *Bang. J. Botany* 38, 7–11. doi: 10.3329/bjb.v38i1.5112

Çavuşoğlu, K. (2011). Investigation of toxic effects of the glyphosate on Allium cepa. *J. Agric. Sci.* 17, 131–142.

Chen, P., Niu, M., Qiu, Y., Zhang, Y., Xu, J., Wang, R., et al. (2024). Physiological effects of maize stressed by HPPD inhibitor herbicides via multi-spectral technology and two-dimensional correlation spectrum technology. *Ecotoxicol. Environ. Saf.* 272:116087. doi: 10.1016/j.ecoenv.2024.116087

Erdtman, G. (1966). *Pollen Morphology and Plant Taxonomy Angiosperms*. New York: Hafner Publishing Co., 553.

Eti, S. (1991). Bazi meyve tür çeşitlerinde degişik in vitro testler yardimiyla çiçek tozu canlilik ve çimlenme yeteneklerinin belirlenmesi. *Çukurova Univ. Ziraat Fak. Der.* 6, 69–81.

Gallego, S. M., Benavides, M. P., and Tomaro, M. L. (1996). Effect of heavy metal ion excess on sunflower leaves: evidence for involvement of oxidative stress. *Plant Sci.* 121, 151–159. doi: 10.1016/S0168-9452(96)04528-1

Gautam, H., Singh, S., Prashad, H., Kumar, A., Choudhary, A., Kaur, H., et al. (2023). "Pesticide toxicity and their impact on plant growth, active constituents and productivity," in *Plants and their Interaction to Environmental Pollution* (London: Elsevier), 231–252.

Hoseiny-Rad, M., and Aivazi, A. A. (2020). Biochemical and cytogenetic effects of Imazethapyr on *Cicer arietinum* L. *J. Appl. Biol. Biotechnol.* 8, 73–77. doi: 10.7324/JABB.2020.80212

Kenko, D. B. N., Ngameni, N. T., Awo, M. E., Njikam, N. A., and Dzemo, W. D. (2023). Does pesticide use in agriculture present a risk to the terrestrial biota? *Sci. Total Environm.* 861:160715. doi: 10.1016/j.scitotenv.2022.160715

Khan, B. A., Nadeem, M. A., Nawaz, H., Amin, M. M., Abbasi, G. H., Nadeem, M., et al. (2023). "Pesticides: impacts on agriculture productivity, environment, and management strategies," in *Emerging Contaminants and Plants: Interactions, Adaptations and Remediation Technologies* (Cham: Springer International Publishing), 109–134.

Khan, Z., Shahwar, D., Ansari, M. K. Y., and Chandel, R. (2019). Toxicity assessment of anatase (TiO2) nanoparticles: A pilot study on stress response alterations and DNA damage studies in Lens culinaris Medik. *Heliyon* 5:e02069. doi: 10.1016/j.heliyon.2019.e02069

Khurshid, A., Inayat, R., Basit, A., Mobarak, S. H., Gui, S. H., and Liu, T. X. (2024). Effects of thiamethoxam on physiological and molecular responses to potato plant (*Solanum tuberosum*), green peach aphid (*Myzus persicae*) and parasitoid (*Aphidius gifuensis*). *Pest Managem. Sci.* 80, 3000–3009. doi: 10.1002/ps.8006

Liess, M., and Gröning, J. (2024). Latent pesticide effects and their mechanisms. *Sci. Total Environm.* 909:168368. doi: 10.1016/j.scitotenv.2023.168368

Liu, T. F., Wang, T., Sun, C., and Wang, Y. M. (2009). Single and joint toxicity of cypermethrin and copper on Chinese cabbage (Pakchoi) seeds. *J. Hazard. Mater.* 163, 344–348. doi: 10.1016/j.jhazmat.2008.06.099

Michelangeli, F., Robson, M. J., East, J. M., and Lee, A. G. (1990). The conformation of pyrethroids bound to lipid bilayers. *Biochimica et biophysica acta (bba)-biomembranes* 1028, 49–57. doi: 10.1016/0005-2736(90)90264-O

Nath, U., Puzari, A., and Jamir, T. (2024). Toxicological assessment of synthetic pesticides on physiology of *Phaseolus vulgaris L.* and *Pisum sativum L.* along with their correlation to health hazards: a case study in south-west Nagaland, India. *J. Saudi Soc. Agric. Sci*. 23, 300–311. doi: 10.1016/j.jssas.2024.01.001

Nedumaran, S., Abinaya, P., Jyosthnaa, P., Shraavya, B., Parthasarathy, R., and Bantilan, C. (2015). "Grain legumes production, consumption and trade trends in developing countries," in *Working Paper Series No. 60. ICRISAT Research Program, Markets, Institutions and Policies* (Patancheru: International Crops Research Institute for the Semi-Arid Tropics), 64.

Norton, J. D. (1966). Testing of plum pollen viability with Tetrazolium salts. *Proc. Amer. Soc. Hort. Sci.* 89:132–134.

Obidola, S. M., Ibrahim, I., Yaroson, A. Y., and Henry, U. I. (2019). Phytotoxicity of cypermethrin pesticide on seed germination, growth and yield parameters of cowpea (Vigna unguiculata). *Asian J. Agricult. Horticult. Res.* 3, 1–10. doi: 10.9734/ajahr/2019/v3i229995

Pang, J., Turner, N. C., Khan, T., Du, Y.-L., Xiong, J.-L., Colmer, T. D., et al. (2017). Response of chickpea (*Cicer arietinum* L.) to terminal drought: leaf stomatal conductance, pod abscisic acid concentration, and seed set. *J. Exp. Bot*. 68, 1973–1985. doi: 10.1093/jxb/erw153

Rajak, P., Roy, S., Ganguly, A., Mandi, M., Dutta, A., Das, K., et al. (2023). Agricultural pesticides–Friends or foes to biosphere? *J. Hazardous Mater. Adv.* 10:100264. doi: 10.1016/j.hazadv.2023.100264

Ramzan, M., Akram, M., Rahi, A. A., Mubashir, M., Ali, L., Fahad, S., et al. (2022). Physio-biochemical, anatomical and functional responses of *Helianthus annuus* L. and *Brassica juncea* (Linn) to cypermethrin pesticide exposure. *J. King Saud Univers.-Sci.* 34:102210. doi: 10.1016/j.jksus.2022.102210

Rao, K. M., and Sresty, T. V. S. (2000). Antioxidative parameters in the seedlings of pigeonpea (*Cajanus cajan* (L.) Millspaugh) in response to Zn and Ni stresses. *Plant Sci.* 157, 113–128. doi: 10.1016/S0168-9452(00)00273-9

Ridwan, Q., Anjum, N., Rashid, S., Akhter, F., and Hanief, M. (2022). "Plant-microbe interactions in agro-ecological perspectives and degradation of pesticides," in *Bioremediation and Phytoremediation Technologies in Sustainable Soil Management* (Palm Bay, Florida: Apple Academic Press), 129–158.

Ruch, R. J., Cheng, S. J., and Klaunig, J. E. (1989). Prevention of cytotoxicity and inhibition of intercellular communication by antioxidant catechins isolated from Chinese green tea. *Carcinogenesis* 10, 1003–1008. doi: 10.1093/carcin/10.6.1003

Sharma, A., Sharma, S. K., Singh, N., Maurya, V., Kaur, S., Kumar, R., et al. (2024). "Pesticides-mediated ROS generation in plants," in *Pesticides in a Changing Environment* (London: Elsevier), 179–202.

Sharma, A., Shukla, A., Attri, K., Kumar, M., Kumar, P., Suttee, A., et al. (2020). Global trends in pesticides: a looming threat and viable alternatives. *Ecotoxicol. Environ. Saf.* 201:110812. doi: 10.1016/j.ecoenv.2020.110812

Sharma, P. (2012). Influence of pesticide-treated seeds on survival of Mesorhizobium sp. Cicer, symbiotic efficiency and yield in chickpea. *Plant Prot. Sci.* 48, 37–43. doi: 10.17221/54/2010-PPS

Sheikh, N., Patowary, H., and Laskar, R. A. (2020). Screening of cytotoxic and genotoxic potency of two pesticides (malathion and cypermethrin) on *Allium cepa* L. *Mol. Cellular Toxicol.* 16, 291–299. doi: 10.1007/s13273-020-00077-7

Skubała, K., Styburski, J., and Chowaniec, K. (2024). Combined effect of fungicide, herbicide and plant elicitor used in apple orchards on non-target epiphytic moss *Hypnum cupressiforme*. *Environm. Pollut.* 342:123133. doi: 10.1016/j.envpol.2023.123133

Somtrakoon, K., Thala, C., Thinnok, C., Thumjan, C., and Chouychai, W. (2024). Using plant growth regulators to stimulate growth of napier grass under atrazine contamination. *Soil Sedim. Contamin.* 23, 1–17. doi: 10.1080/15320383.2023.2301042

Stelzer, K. J., and Gordon, M. A. (1988). Interactions of pyrethroids with gramicidin-containing liposomal membranes. *Biochimica et Biophysica Acta (BBA)-Biomembranes* 938, 114–120. doi: 10.1016/0005-2736(88)90128-9

Stosser, R. (1984). Untersuchungen uber die befruchtungsbiologie and pollen production innerhalb der gruppe Prunus domestica. *Erwerbobstbau* 26, 110–115.

Vuković, S., Žunić, A., Maksimović, I., Lazić, S., Šunjka, D., Žunić, V., et al. (2021). Insecticide-induced changes of photosynthetic pigments content in peach leaves. *Pak. J. Agri. Sci.* 58, 1705–1710. doi: 10.21162/PAKJAS/21.1066

World Health Organization (1989). *International Programme on Chemical Safety & WHO Task Group Meeting on Environmental Health Criteria for Cypermethrin. Cypermethrin/published under the joint sponsorship of the United Nations Environment Programme, the International Labour Organisation, and the World Health Organization*. Geneva: World Health Organization.

Wrońska–Pilarek, D., Maciejewska–Rutkowska, I., Lechowicz, K., Bocianowski, J., Hauke–Kowalska, M., Baranowska, M., et al. (2023). The effect of herbicides on morphological features of pollen grains in *Prunus serotina* Ehrh. in the context of elimination of this invasive species from European forests. *Scient. Rep*. 13:4657. doi: 10.1038/s41598-023-31010-2

Yin, X., Jiang, L., Song, N., and Yang, H. (2008). Toxic reactivity of wheat (*Triticum aestivum*) plants to herbicide isoproturon. *J. Agric. Food. Chem.* 56, 4825–4831. doi: 10.1021/jf800795v

Zanelli, D., Carniel, F. C., Fortuna, L., Pavoni, E., González, V. J., Vázquez, E., et al. (2023). Interactions of airborne graphene oxides with the sexual reproduction of a model plant: when production impurities matter. *Chemosphere* 312:137138. doi: 10.1016/j.chemosphere.2022.137138

Zhang, J. J., Lu, Y. C., Zhang, J. J., Tan, L. R., and Yang, H. (2014). Accumulation and toxicological response of atrazine in rice crops. *Ecotoxicol. Environm. Safety* 102, 105–112.

frontiers | Frontiers in Sustainable Food Systems

TYPE Review
PUBLISHED 04 December 2024
DOI 10.3389/fsufs.2024.1458552

OPEN ACCESS

EDITED BY
Aliza Pradhan,
National Institute of Abiotic Stress Management (ICAR), India

REVIEWED BY
Zhou Li,
Sichuan Agricultural University, China
Hanamant Halli,
National Institute of Abiotic Stress Management (ICAR), India

*CORRESPONDENCE
Puchang Wang
✉ wangpuchang@163.com

†These authors have contributed equally to this work

RECEIVED 02 July 2024
ACCEPTED 18 November 2024
PUBLISHED 04 December 2024

CITATION
Wang R, Gao Y, Li J, Wang X, Yang Y, Huang H, Zhou Z, Wang P and Zhao L (2024) Drought and heat stress studies in perennial ryegrass: a bibliometric analysis 1994–2024. *Front. Sustain. Food Syst.* 8:1458552. doi: 10.3389/fsufs.2024.1458552

Drought and heat stress studies in perennial ryegrass: a bibliometric analysis 1994–2024

Rui Wang[1†], Yang Gao[2†], Junqin Li[1], Xiangtao Wang[1], Yuting Yang[1], Haiyan Huang[1], Zijun Zhou[1], Puchang Wang[1*] and Lili Zhao[3]

[1]School of Life Sciences, Guizhou Normal University, Guiyang, Guizhou, China, [2]School of Karst Science, Guizhou Normal University, Guiyang, Guizhou, China, [3]College of Animal Science, Guizhou University, Guiyang, Guizhou, China

Perennial ryegrass (*Lolium perenne* L.) is a key forage species in warm temperate to subtropical regions worldwide. Climate change poses significant challenges to agriculture, particularly through drought and heat stress, which adversely affect ryegrass yield and may be further exacerbated by global warming. Despite numerous research achievements in recent years, a comprehensive bibliometric analysis of the literature on drought and heat stress in perennial ryegrass is lacking. This study provides a quantitative analysis of relevant literature published from 1994 to 2024, utilizing the Web of Science database to evaluate global research trends and priorities. The results indicate a consistent annual growth in publication output, with China and the United States being major contributors, and the journal *Crop Science* publishing the most papers. Keyword analysis shows that "growth," "endophytic fungi," and "yield" are most frequently used in drought stress research, while "growth," "gene," and "leaf" are common in heat stress research. Over the past 30 years, research has mainly focused on phenotype, response mechanisms, and drought and heat resistance techniques in perennial ryegrass. Endophyte have become a hot topic in drought stress research in recent years and have also gained attention in heat stress research, suggesting future research directions in this area. Furthermore, there is a need to strengthen research on the molecular mechanisms associated with drought stress in ryegrass, as well as to explore molecular responses to heat stress. The research trend shows increasing attention to the interaction between drought and heat stress, indicating it will become an important direction for future studies. The findings of this study offer valuable insights for guiding future research on perennial ryegrass under drought and heat stress conditions and provide useful information for researchers in related fields.

KEYWORDS

perennial ryegrass, drought stress, heat stress, bibliometrics, response mechanism

1 Introduction

Global climate change represents a serious worldwide challenge, with wide-ranging impacts, especially in agriculture. This phenomenon has profoundly affected agricultural systems by altering temperature patterns and water availability (Gong et al., 2020; Leisner, 2020). According to climate change projections, greenhouse gas emissions may lead to a global average temperature rise of 1.5–2°C, which is expected to cause more frequent and prolonged droughts in most crop-growing areas around the world (Naidoo, 2022; Zandalinas et al., 2021). In crop production, rising temperatures not only exacerbate drought problems but also increase the frequency and intensity of heat waves. These factors collectively pose significant

and direct threats to ecosystems and agricultural production (Gornall et al., 2010; Mittler, 2006). These impacts not only challenge current agricultural production but also present severe tests for future food security and agricultural sustainability.

In the coming decades, global agriculture is expected to experience more severe impacts of climate change, with increased frequency and intensity of heat and drought events. These stresses could result in crop yield losses of up to 60%, depending onfactors such as the crop type, developmental stage, and the severity, type, and duration of the stress (Jedmowski et al., 2015). Drought affects crop growth by impacting nutrient and water relationships, photosynthesis, and assimilate allocation, ultimately leading to significant decreases in crop yield (Farooq et al., 2009; Praba et al., 2009). The severity of drought-induced damage is often unpredictable, influenced by factors such as rainfall patterns, soil water retention capacity, and water loss due to evapotranspiration (Huang et al., 2024). Similarly, heat stress induces a series of morphological, biochemical, and physiological changes that greatly affect plant growth and development (Anjum et al., 2011). Generally, when temperatures exceed the optimal growth range of plants by 5–10°C, irreversible cellular oxidative damage occurs, especially affecting photosystems I (PSI) and photosystems II (PSII) (Pucciariello et al., 2012; Wahid and Close, 2007; Zhao et al., 2021), leading to delayed growth and wilting (Zhao et al., 2021). Heat stress can also disrupt carbohydrate metabolism and negatively affect critical reproductive processes, including stamen and pollen development, ovule fertilization, fruit set, and seed development, ultimately leading to yield losses in various crops (Kotak et al., 2007; Liu et al., 2019; Ozga et al., 2017; Schauberger et al., 2017; Wahid et al., 2007).

Drought and heat frequently occur simultaneously, and in combination with low atmospheric humidity, drought can increase the vapor pressure deficit (VPD), accelerating the loss of water from both soil and plant tissues. To counteract increased VPD, plants usually close their stomata, which is a conservative strategy but often insufficient to meet the demands of transpirational cooling, resulting in increased tissue and canopy temperatures (Prasad et al., 2008). Similarly, water deficits caused by thermal stress require evaporative cooling to mitigate temperature effects, but under drought conditions, controlling evaporative cooling to prevent water loss makes plants more sensitive to heat stress (Craufurd et al., 2013; Steinmeyer et al., 2013). Due to certain physiological characteristics that adapt to stress, such as canopy temperature, plants may adopt similar regulatory pathways when facing drought and heat stress (Reynolds et al., 2007).

Perennial ryegrass (*Lolium perenne* L.) is a high-quality forage and turf grass native to Europe, Asia, and North Africa, with a cultivation history of over 100 year (Xie et al., 2020). Due to its ease of cultivation and low maintenance requirements, perennial ryegrass has been widely planted in warm temperate and subtropical regions worldwide (Yu et al., 2021). Fresh perennial ryegrass is palatable and rich in nutrients, benefiting animal digestion and absorption; its hay is rich in crude protein and contains various amino acids, vitamins, and other nutrients, aligning with sustainable animal husbandry practices (Sun et al., 2020; Zhang et al., 2020). In dairy production, perennial ryegrass is superior to many other feeds in terms of corrected milk solids and fat per hectare, and it can tolerate grazing with uniform distribution across different seasons, playing an important role in livestock production (Chapman et al., 2023; Ding et al., 2023; Janke et al., 2015). However, due to its wide geographical distribution and perennial characteristics, perennial ryegrass is highly susceptible to various environmental stresses, including drought and heat. These factors are the main limiting factors affecting its growth and productivity throughout its lifecycle (Huang et al., 2014; Zhou and Abaraha, 2007). During the sowing and seedling stages, autumn drought may prevent normal germination and growth; in the mature stage, heat and drought stress in summer may hinder its survival through the season (Shen et al., 2008; Wang et al., 2016). Drought stress leads to decreased forage quality and biomass, causing premature leaf yellowing and senescence (Rogers et al., 2019). When summer temperatures exceed 38°C, high heat can disrupt the balance between development and growth, leading to accelerated metabolic and physiological changes (Lei and Huang, 2022; Wang et al., 2016). These environmental stresses exceed the optimal growth conditions for perennial ryegrass, resulting in decreased forage yield and quality (Wang et al., 2016). Therefore, addressing global climate change (such as frequent droughts and heats) has become a key challenge in the cultivation and management of perennial ryegrass (Armstead et al., 2006; Mohammadi et al., 2017; Thomas et al., 1999). Therefore, numerous studies have emerged on drought and heat stress in perennial ryegrass, underscoring the importance of synthesizing this growing body of research to identify current trends and future development directions.

Bibliometrics provides theoretical and methodological tools for evaluating the scientific productivity, academic impact, and research frontiers of countries, institutions, or disciplines (Ninkov et al., 2022; Zhang et al., 2024). It integrates mathematics, statistics, and literature studies, focusing on a comprehensive system of quantitative knowledge. By reviewing the history of research in a particular field, bibliometric analysis offers valuable insights into the evolution of research hotspots, the establishment of collaborative networks, and the identification of emerging research directions (Zhang et al., 2024). Compared with traditional literature reviews and meta-analyses, bibliometric analysis can more comprehensively reveal the current status, frontiers, and potential future trends of a given research field (Zhou et al., 2024). However, currently, there are no reports on bibliometric research concerning drought and heat stress in perennial ryegrass. Although there is a substantial body of literature in related fields, the quantitative characteristics, development patterns, and internal relationships of this research remain unclear. To systematically and objectively summarize global research results on drought and heat stress in perennial ryegrass, this study employed mainstream bibliometric software and methods to review research progress across various growth stages of perennial ryegrass between 1994 and 2024. This process provides a deep understanding of the history and current status of drought and heat resistance research in perennial ryegrass and offers guidance for future research directions.

2 Materials and methods

2.1 Database and search strategy

This study conducted a comprehensive search of the Web of Science Core Collection (WoSCC) database. For research on drought in perennial ryegrass, the following search terms were used: ("perennial ryegrass" OR "*Lolium perenne* L." OR "*Lolium perenne*") AND ("drought" OR "drought tolerance" OR "drought stress" etc.). For

studies on heat stress in perennial ryegrass, the search terms were: ("perennial ryegrass" OR "*Lolium perenne* L." OR "*Lolium perenne*") AND ("heat" OR "heat tolerance" OR "heat stress" etc.). The search period spanned from January 1, 1994, to October 16, 2024. There were no restrictions on language, document type, or data category during the retrieval process. Initial screening of search results based on correlation analysis. The titles, keywords, and abstracts of literature obtained from the search results were checked to determine their relevance to perennial ryegrass. After excluding irrelevant publications, the final selection included English articles and reviews. The literature selection process and the research framework are detailed in Figure 1. A total of 680 publications on drought research of perennial ryegrass and 204 publications on heat stress research of perennial ryegrass were selected and output in text format for further analysis.

2.2 Data analysis

VOSviewer software (version 1.6.15) was used to analyze publication types, years, countries, institutions, journal sources, co-cited journals, and keywords co-occurrences. Data were summarized and analyzed using Microsoft Excel 2016, and relevant charts were generated. Clustering analysis was performed with VOSviewer to produce social network maps, where node size indicates the importance or frequency, and the thickness of connecting lines represents the strength of associations. Additionally, the Bibliometrix package in R was utilized to analyze author influence and trends in key keyword changes. This comprehensive approach provided an in-depth understanding of the research progress in the field of drought and heat stress in perennial ryegrass, including various bibliometric indicators such as the number of publications and citation counts.

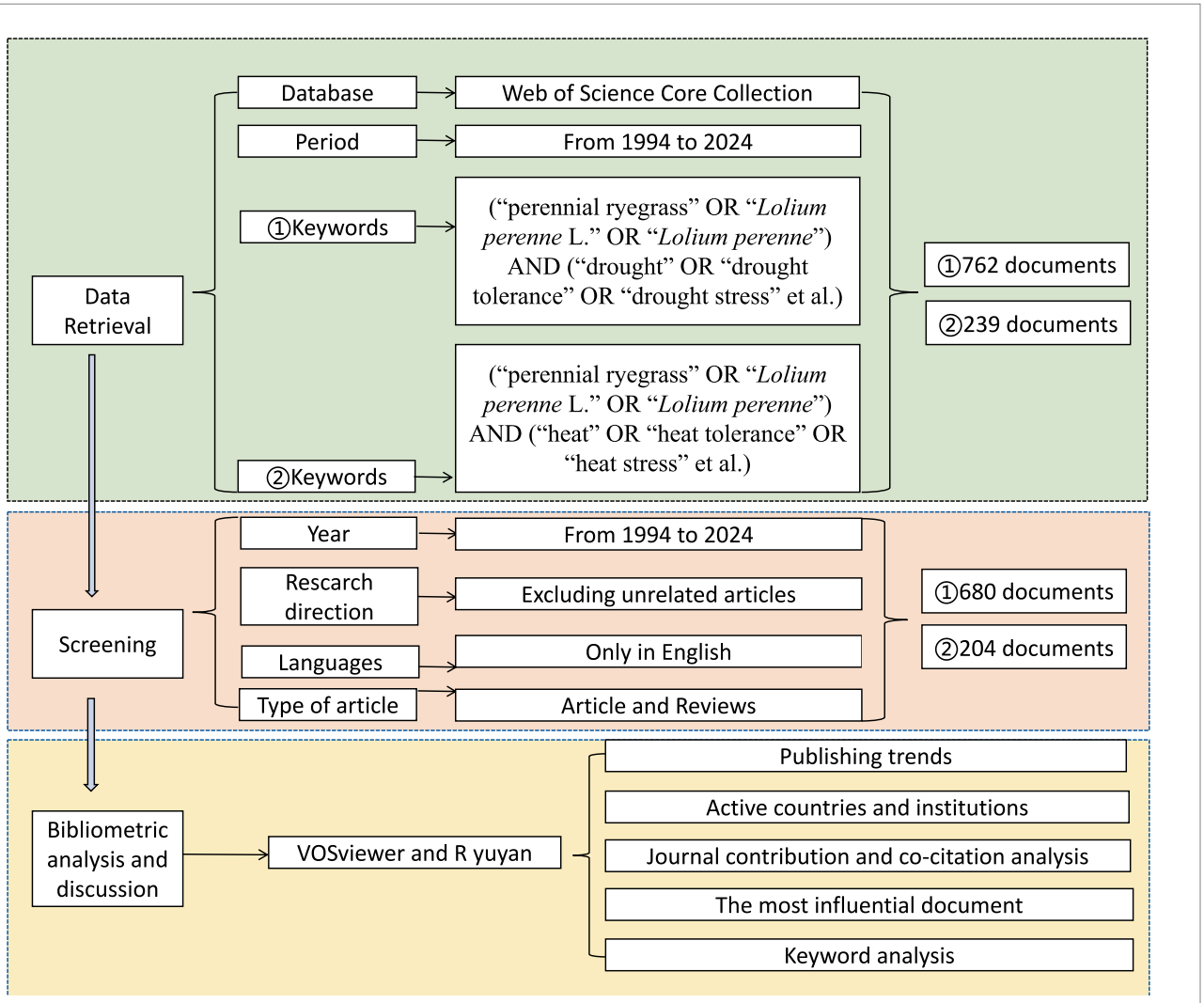

FIGURE 1
Flowchart illustrating the search strategy and publication filtering steps.

3 Results

3.1 Publication trends

Core indicators for evaluating academic publications include the number of publications and their citation frequency. Figure 2 shows an increasing trend in the number of publications on drought and heat stress in perennial ryegrass worldwide from 1994 to 2024. Over the past 30 years, the average number of citations per article has steadily increased and then stabilized. This trend may be partly due to newly published articles gradually replacing earlier works, as current research often takes longer to accumulate higher citation counts.

The number of articles in drought research is significantly higher than in heat stress research, indicating that the academic community places greater emphasis on drought studies. The overall number of articles is rising, reflecting increasing academic interest in drought and heat stress in perennial ryegrass. This trend may signify that, as climate change and environmental challenges become more prominent, related research fields are receiving more attention and resource investment.

3.2 Active countries and institutions

3.2.1 Analysis of influential countries/regions and global cooperation

Figure 3A presents the differences and collaborative trends among countries involved in drought research on perennial ryegrass. Based on data from Supplementary Table S1, the graph shows 33 countries with over five published articles and their collaborative relationships. The United States ranks first globally with 182 published articles, the largest number of nodes, the widest range of domain relationships (the highest TLS), and the highest citation count of 7,658. China follows closely with 127 articles and 2,354 citations. New Zealand ranks third with 80 papers and 1,938 citations.

Figure 3B presents the distribution and cooperation among countries in heat stress research on perennial ryegrass. Using data from Supplementary Table S2, the graph shows 30 countries with over two published articles and their collaborative relationships. The United States leads with 67 published articles, the widest domain relationships (the highest TLS), and 1,973 citations. China, as the second-largest node, has 58 articles and 1,606 citations. New Zealand ranks third with 22 articles.

These findings indicate that both China and the United States have made significant quantitative contributions to drought and heat stress research on perennial ryegrass. However, in drought research, the citation rate of Chinese articles is significantly lower than that of the United States, possibly due to a number of lower-value scientific articles. Therefore, promoting innovative exploration and reducing repetitive research is particularly important.

3.2.2 Quantitative analysis of productive and influential institutions

Figure 4A, along with Supplementary Table S3, shows the literature coupling relationships among institutions in drought research. Research institutions in New Zealand, France, the United States, and China form the core of scientific output. Massey University leads with 31 articles and occupies a central position in the network (the highest TLS). Following is the French National Institute for Agricultural Research (INRA) with 21 articles and Rutgers University with 19 articles. Notably, Aarhus University, Sichuan Agricultural University, Lanzhou University, and the University of Florida, although not in global research hubs, have significant scientific output and collaborations with numerous institutions. However, the depth and closeness of these collaborations need further strengthening.

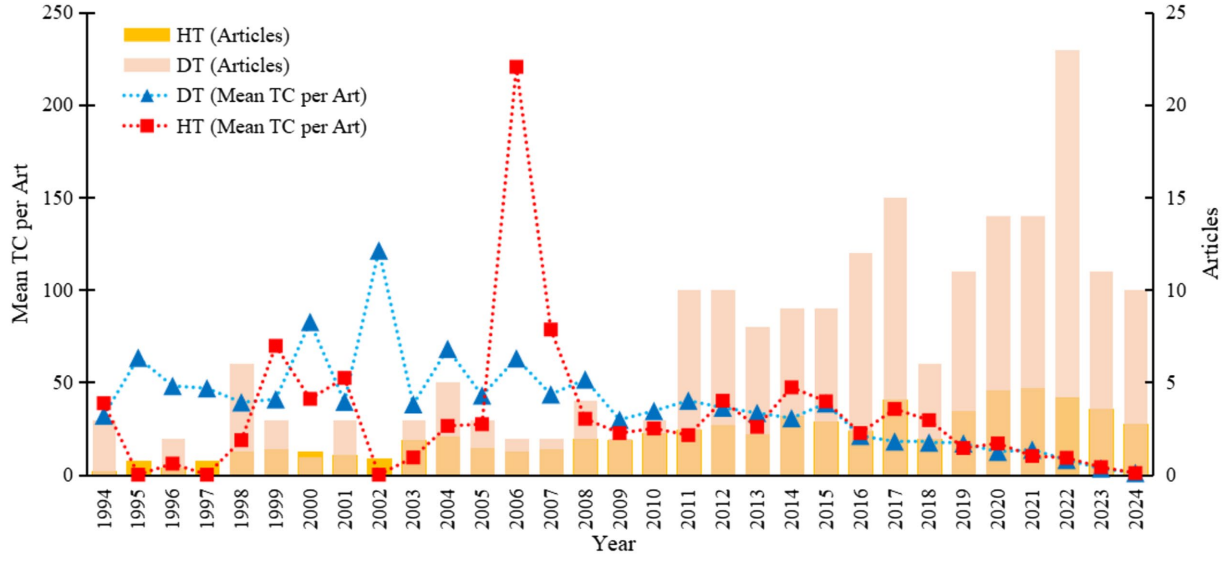

FIGURE 2
Annual trends in publications and citations related to drought and heat stress in perennial ryegrass (1994–2024). DT: drought stress; HT: heat stress; Mean TC per Art: average total citations per article.

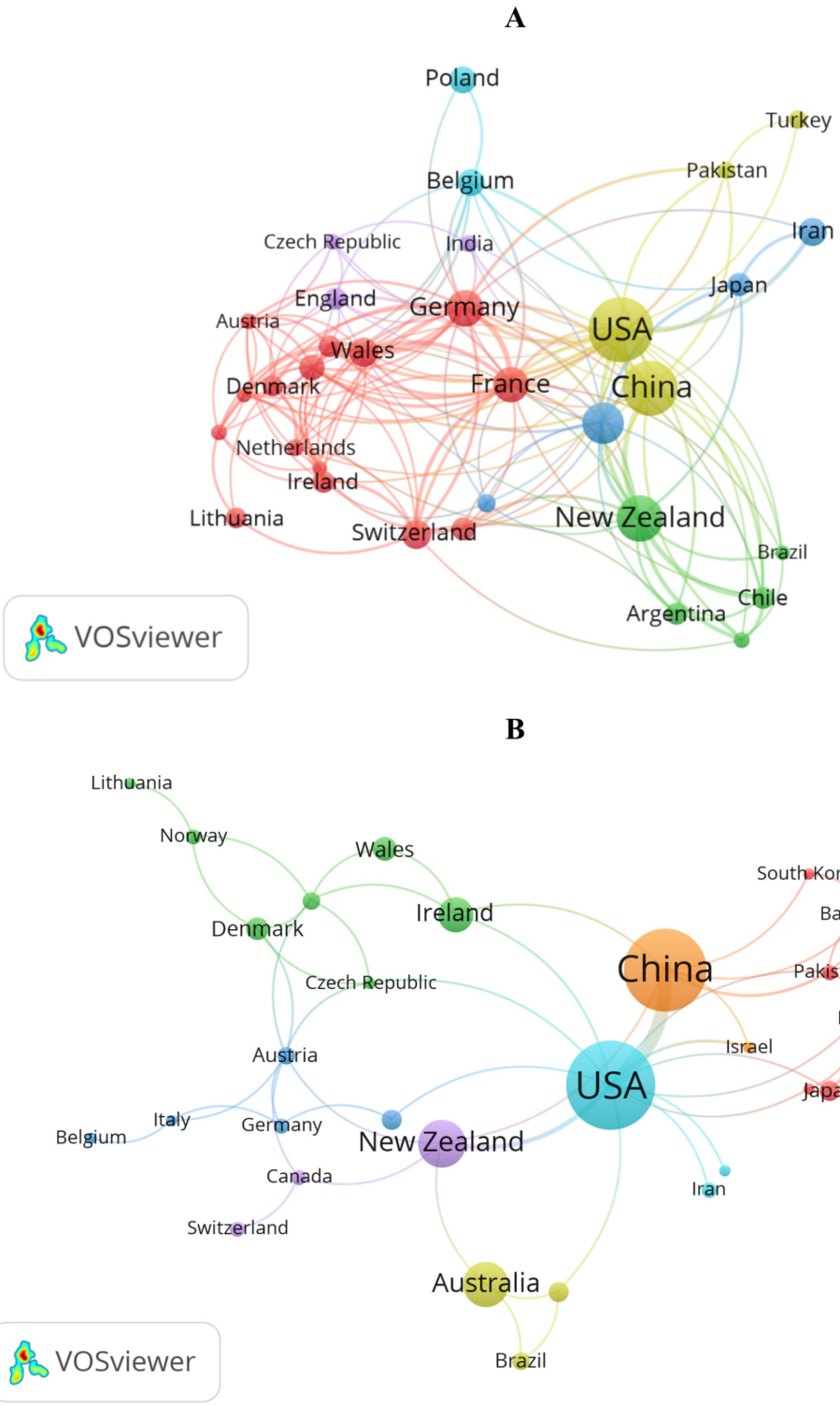

FIGURE 3
Knowledge maps of research on perennial ryegrass in countries: **(A)** drought stress; **(B)** heat stress.

Figure 4B, using data from Supplementary Table S4, presents the inter-institutional literature coupling analysis in heat stress research. Institutions in China, the United States, and Australia are the main contributors. Rutgers University ranks first with 15 articles and serves as a central node (the highest TLS). The Chinese Academy of Sciences and Nanjing Agricultural University each have 13 articles, playing key roles in China's academic network. The University of Melbourne, Teagasc, and AgResearch Limited have also contributed significantly but need to enhance cooperation intensity with other institutions.

The analysis presented in Figures 3, 4 underscores the dominant roles of China and the United States in research on drought and heat stress in perennial ryegrass. Future research efforts should focus on

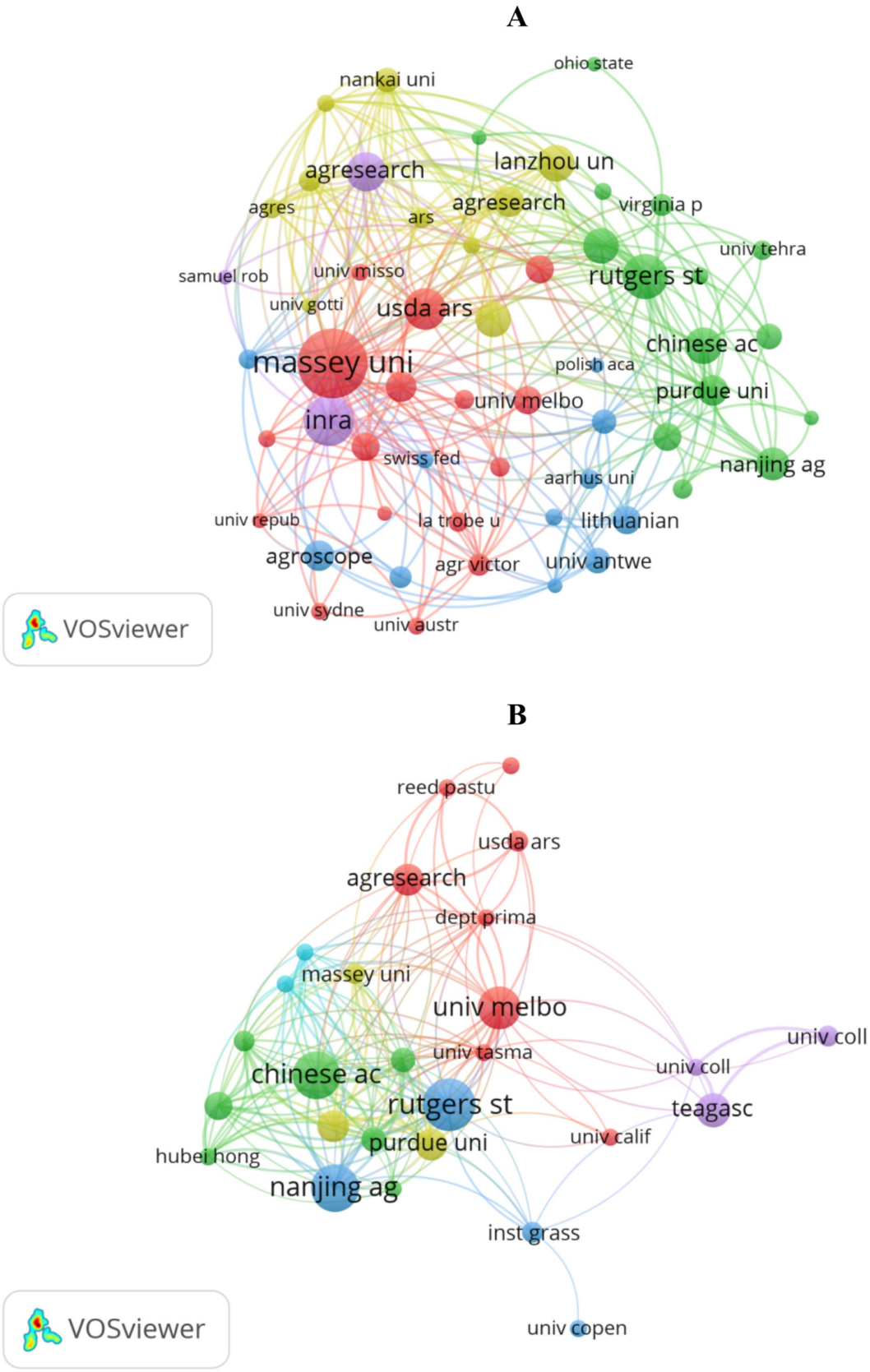

FIGURE 4
Institutional collaboration networks in perennial ryegrass research: **(A)** drought stress; **(B)** heat stress.

expanding cross-regional and interdisciplinary collaborations to enhance scientific impact.

3.3 Journal contribution and co-citation analysis

Figure 5A and Supplementary Table S5 present a co-citation analysis of 262 journals in drought research. *Crop Science* is the largest node with 1,516 citations, followed closely by *New Phytologist* with 1,101 citations and *Plant Physiology* with 960 citations. The map displays four clusters (red, green, blue, yellow), corresponding to environmental change and agriculture, plant physiology and genetics, microbial-plant interactions, and plant breeding and biotechnology. This demonstrates that drought resistance research covers forage production, breeding and genetics, physiological metabolism, molecular genetics, and biotechnology.

In heat stress research, Figure 5B and Supplementary Table S6 show that *Crop Science* is the most influential journal with 438 citations, followed by *Plant Physiology* with 537 citations and the Journal of *Experimental Botany* with 259 citations. The map divides into five clusters (red, green, blue, yellow, purple), representing plant growth and physiological changes, grass development and utilization, environmental changes and agricultural research, plant physiology and biochemistry, and cell tissue structure. These research results indicate that the study of drought and heat stress on perennial ryegrass covers a wide range of fields, and *Crop Science* plays a crucial role in this research area.

3.4 Most influential papers

In drought research, Supplementary Table S7 lists the top 30 most cited papers published in 24 journals. Clay and Schardl (2002) article, cited 887 times in the Web of Science database, is particularly noteworthy. It reveals the role of endophytic fungi in perennial ryegrass, emphasizing how their infection can improve drought tolerance, photosynthetic rate, and growth. Reviewing these articles shows that the first two mainly explored the effects of drought stress on growth and yield. Articles ranked 3–13 focused on physiological and biochemical responses, such as photosynthesis and hormone mechanisms. Articles ranked 14–18 delved into molecular mechanisms. Researchers also examined management strategies under drought stress, such as mixed planting (Article 19) and fertilization (Article 20). In the context of climate change, the symbiotic relationship between endophytic fungi and perennial ryegrass, especially their role in promoting plant growth and enhancing drought resistance, has become a research focus in academia (Articles 21–29). The last paper discussed drought resistance differences among varieties. These studies highlight critical research directions, involving yield, physiological and biochemical reactions, molecular regulation mechanisms, and breeding and cultivation techniques for drought resistance.

In heat stress research, the top 30 most cited articles were published in 18 journals (Supplementary Table S8). Xu et al. (2006), whose paper ranked first with 367 citations, examining physiological and biochemical responses under heat stress. Zhang et al. (2017), cited 202 times, explored melatonin's biological functions under heat stress and its interaction with plant hormones. Kauffman et al. (2007) investigated plant hormones' effects on photosynthetic capacity, membrane thermal stability, and heat tolerance. Summarizing these papers reveals that three focused on growth and yield effects under heat stress. Eight highly cited articles studied physiological and biochemical reactions, like osmotic regulation and oxidative stress responses. Sixteen highly cited papers analyzed molecular regulatory mechanisms. Researchers also emphasized agronomic management techniques, such as fertilization. These studies not only reveal the effects of heat stress on plant physiology and molecular levels, but also emphasize the importance of improving crop heat tolerance through agronomic management techniques, providing a scientific basis for addressing climate change.

3.5 Analysis of research hotspots and evolutionary trends

3.5.1 Most common and trending keywords in drought resistance research

Figure 6A displays the 20 most frequent keywords. The keyword "drought stress" has the highest frequency at 627 times, followed by "perennial ryegrass" (338 times), "growth" (183 times), "fungal endophyte" (147 times), "yield" (118 times), "CO_2" (68 times), "root" (45 times), "leaf" (43 times), and "photosynthesis" (37 times). This indicates the significance of studying drought stress effects on growth and yield, and the interaction mechanisms between endophytic fungi and perennial ryegrass.

The co-occurrence network (Figure 6B) identifies 198 keywords that appeared at least three times, grouped into four clusters: (1) Red cluster focuses on growth and physiological responses, including keywords such as "yield," "endophytes," "photosynthesis," "drought survival strategies," "physiological responses." (2) Green cluster centers on plant hormones and molecular research, featuring keywords like "abscisic acid," "hormone metabolism," "antioxidant enzymes," "Arabidopsis," "gene expression," "molecular identification." (3) Blue cluster emphasizes breeding-related topics, including "interspecific hybridization," "breeding," and "genotype." (4) Yellow cluster concentrates endophytes and stress responses, such as "fungal endophytes," "seed germination," and "environmental pressure." This network analysis offers a comprehensive understanding of key themes. Based on Supplementary Table S7, current drought resistance research focuses on phenotype, response mechanisms, and tolerance enhancement strategies.

3.5.2 Most common and trending keywords in heat resistance research

Figure 7A shows the 20 most frequent terms in heat stress research. "Heat stress" has the highest frequency at 141 times, followed by "perennial ryegrass" (69 times), "growth" (31 times), "gene" (20 times), "leaf" (20 times), "yield" (18 times), "Arabidopsis" (18 times), and "water-use" (16 times). This underscores the importance of studying heat stress effects on growth and molecular mechanisms.

The co-occurrence network (Figure 7B) identifies 84 keywords that appeared at least twice, grouped into five clusters: (1) Red cluster focuses on physiology, biochemistry, molecular mechanisms, and breeding, including keywords like "abscisic acid," "Arabidopsis," "genes," "heat shock proteins," and "antioxidant enzymes." (2) Green

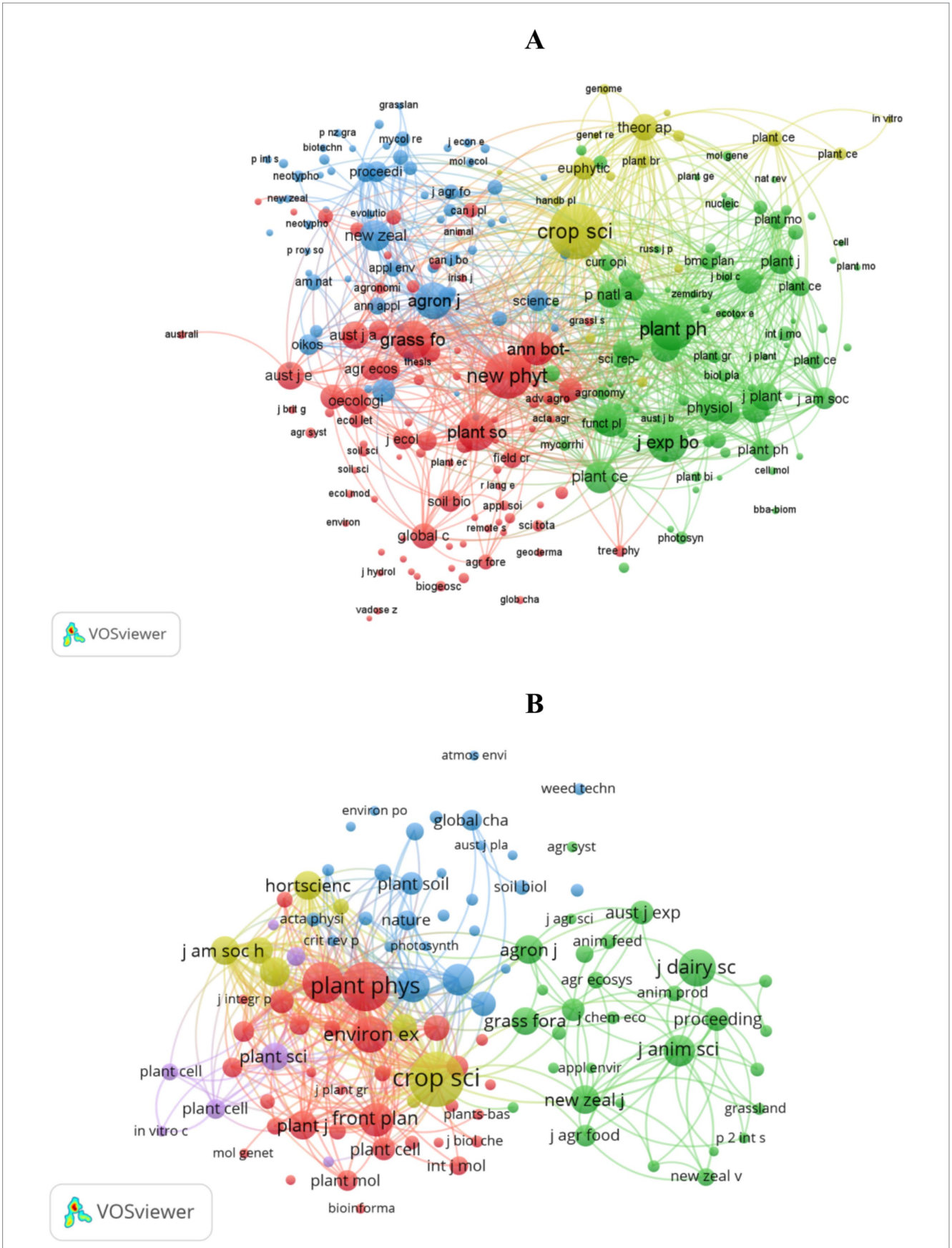

FIGURE 5
Co-citation knowledge maps of journals publishing research on perennial ryegrass: **(A)** drought stress; **(B)** heat stress.

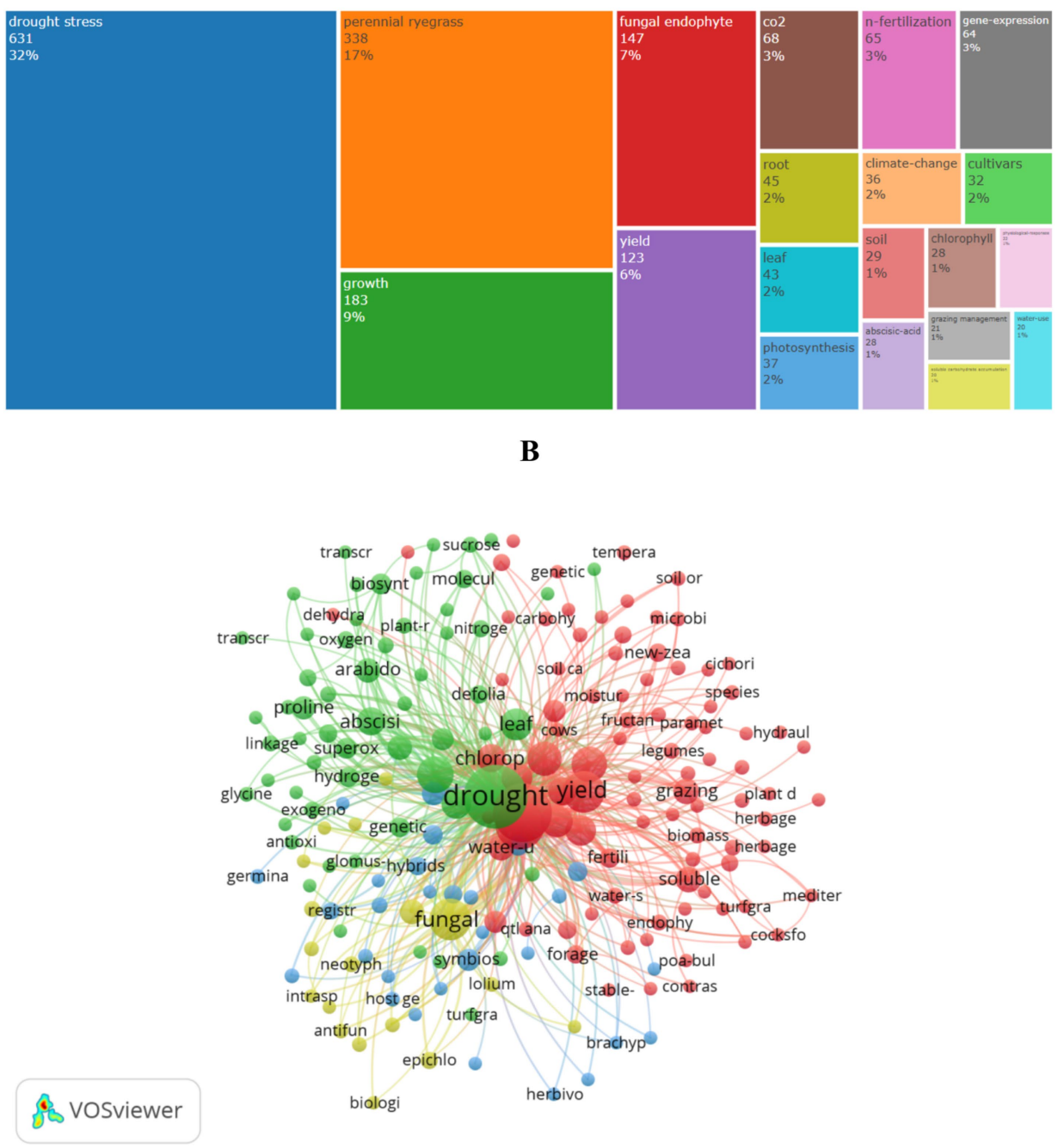

FIGURE 6
Keywords in drought research on perennial ryegrass: **(A)** most common keywords; **(B)** co-occurrence network.

cluster centers on plant growth under climate change, featuring keywords like "climate change," "CO_2," "perennial ryegrass," "cell membrane stability," and "germination." (3) Blue cluster highlights endophytic fungi and organic compounds, such as "endophytic fungi," "alkaloids," "ergot alkaloids," and "chemical composition." (4) Yellow cluster focuses on plant organic components, including "carbohydrate reserves," "nutritional value," and "plant components." (5) Purple cluster features keywords related to "Temperature and humidity index." Based on Supplementary Table S8, heat stress research emphasizes phenotype, response mechanisms, and tolerance enhancement strategies.

3.5.3 Evolution of research themes

Figure 8A shows the analysis for drought stress from 1994 to 2024, divided into three periods: 1994–2004, 2005–2014, and 2015–2024. In the initial stage (1994–2004), six key themes were identified, with "gene expression" being the most relevant and persistent across all periods. In the second period (2005–2014), themes like "drought

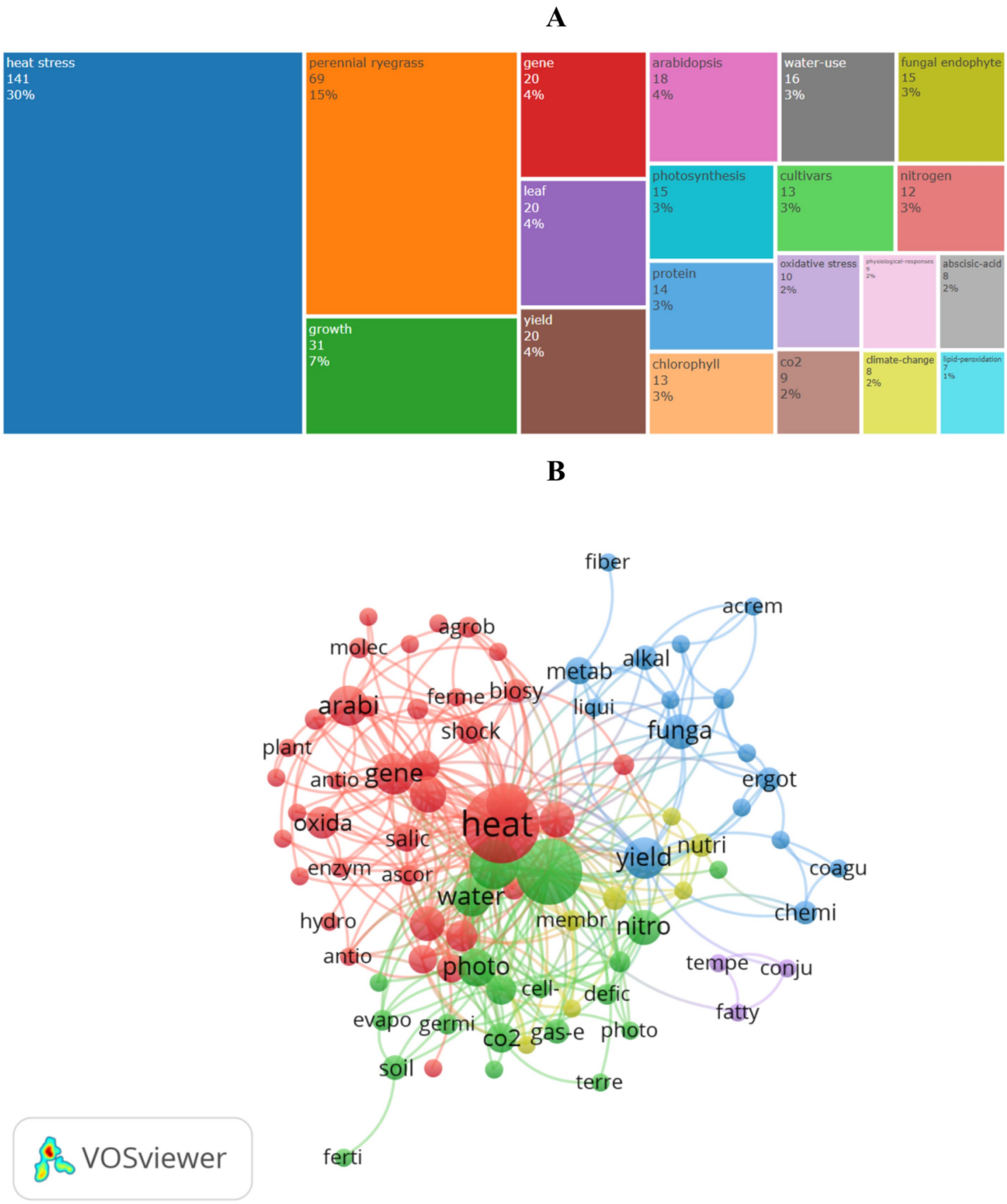

FIGURE 7
Keyword analysis in heat stress research on perennial ryegrass: **(A)** most common keywords; **(B)** co-occurrence network.

stress," "yield," "abscisic acid," "oxidative stress," "protein," and "molecular characterization" emerged. "Drought stress" and "yield" showed high correlation, indicating a strong link between drought stress research and yield changes. In the third period (2015–2024), an increase in keyword variety indicates broader research fields. Notable keywords include "fungal endophyte," "germination," and "gene expression." The shift from phenotypic studies to physiological, biochemical, and drought resistance improvement highlights gene expression as a consistent focus. The emergence of "fungal endophyte" suggests a future research direction. Current frontiers in drought resistance research include gene expression and endophytic fungi.

Similarly, Figure 8B presents heat stress research evolution. In the initial stage, key themes were "yield," "perennial ryegrass," and "CO_2." In the second period, themes like "heat stress," "oxidative stress,"

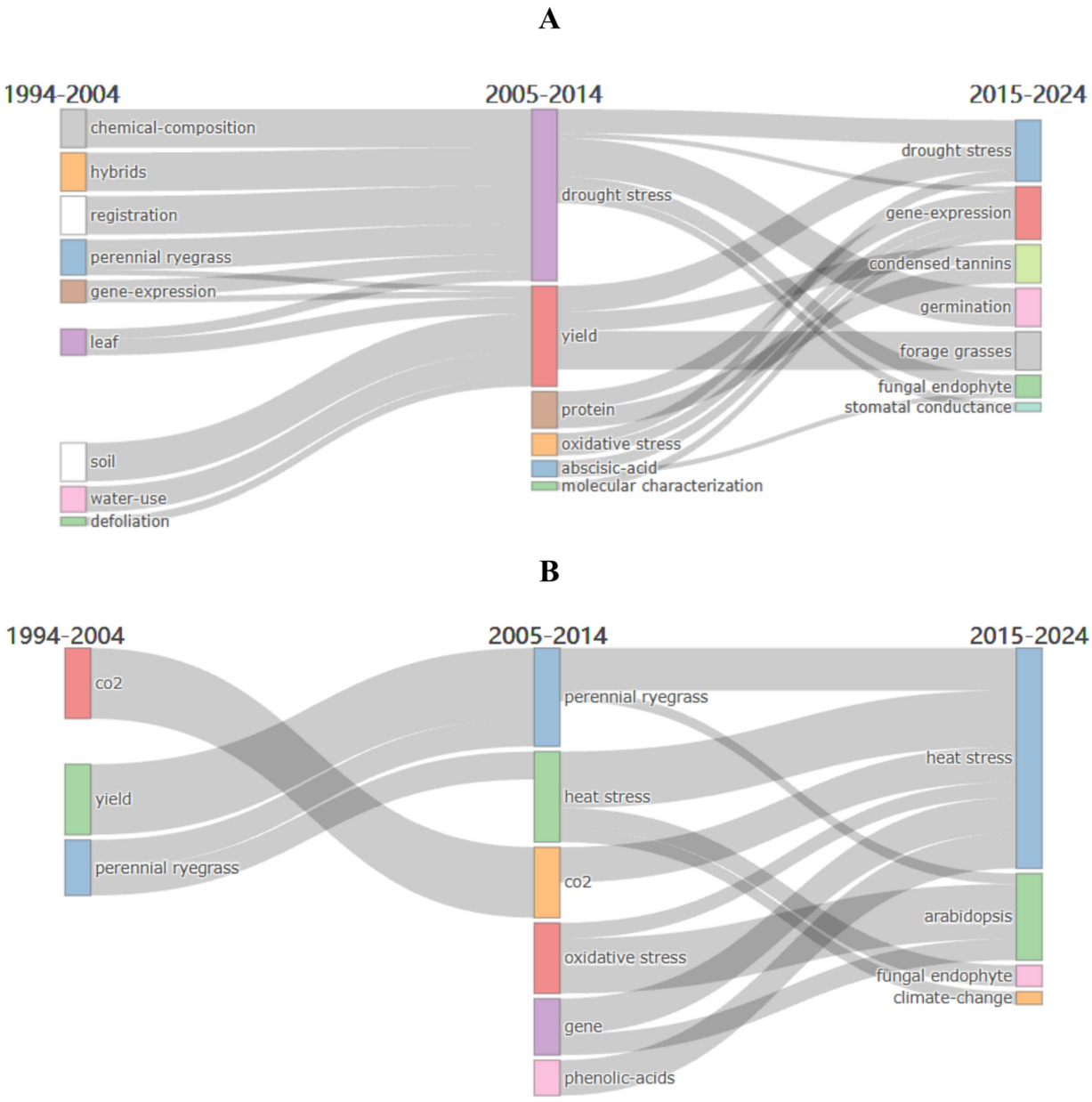

FIGURE 8
Evolution of research themes in perennial ryegrass: **(A)** drought stress; **(B)** heat stress.

"gene," and "phenolic acids" emerged, with "heat stress" highly correlated with these words. In the third period, new themes like "fungal endophyte," "Arabidopsis," and "climate change" appeared, indicating that "fungal endophyte" may become a future focus.

4 Discussion

The challenges posed by global climate change continue to escalate, particularly the sustained rise in environmental temperatures, which poses a serious threat to food security and crop production (Basavaraj and Rane, 2020; Shah et al., 2017). Extreme weather events such as droughts and heat waves are expected to become more frequent and intense, serving as major factors limiting the growth, geographical distribution, and yield of perennial ryegrass (Pan et al., 2018; Wang et al., 2017; Yu et al., 2013). Therefore, understanding the effects of drought and heat stress on perennial ryegrass, current research progress, and future research directions is crucial for improving its cultivation management and yield (Liu and Jiang, 2010; Yu et al., 2015). In this study, we employed bibliometric methods to analyze all English academic publications, including articles and reviews, on drought and heat stress in perennial ryegrass over the past 30 years. The bibliometric analysis shows that research in this field mainly focuses on three aspects: the effects of drought and heat stress on phenotypic changes in perennial ryegrass growth, potential response mechanisms, and studies on drought and heat resistance technologies.

4.1 Phenotypic changes

4.1.1 Effects of drought and heat stress on seed germination

The development of seeds and the growth of seedlings depend on suitable soil conditions, which vary depending on the plant type and include factors such as humidity and temperature levels (Reed et al., 2022). Drought and rising soil temperatures often have negative effects on the germination of crop seeds, involving complex physiological metabolic activities such as enzyme activity and cell division within the seeds (Huchzermeyer et al., 2022; Wafa'a, 2010). For perennial ryegrass, sufficient water is crucial for seed germination; water not only promotes enzyme absorption and activation but, when lacking, leads to delayed germination, thereby affecting the success rate of the entire germination process (Xiong et al., 2024). Additionally, different varieties of perennial ryegrass exhibit significant differences in drought resistance. For example, a study comparing the germination of four varieties under drought conditions showed that the "Solstice II" variety exhibited superior germination and seedling growth abilities under drought stress (Yilmaz and Kisakurek, 2021). Heat stress can also reduce enzyme activity and interfere with metabolic processes related to seed germination (Iqbal et al., 2024). High soil temperatures intensify transpiration, reduce the effectiveness of seed moisture, and thus delay the germination process (Zou et al., 2023). The ideal growth temperature range for perennial ryegrass is 15–24°C; beyond this range, an increase in temperature creates heat stress, limiting its application in temperate regions. Under heat stress conditions, seedling characteristics of perennial ryegrass—such as relative germination rate, germination index, vitality index, and root and seedling length—generally show a downward trend. When the temperature rises to 35°C, the germination rate sharply decreases, and the inhibitory effect of heat stress on root and stem growth becomes increasingly evident (Javaid et al., 2022). Moreover, the combined effect of drought and heat stress severely inhibits the normal physiological functions of perennial ryegrass seedlings, leading to wilting (Rahman et al., 2022).

4.1.2 Effects of drought and heat stress on yield and phenotype

Drought and heat stress adversely affect the growth and developmental stages of perennial ryegrass, leading to significant decreases in yield. Under such environmental pressures, perennial ryegrass exhibits notable phenotypic adaptive changes to address these challenges. Under drought stress, the lack of soil moisture directly affects plant growth and development. When perennial ryegrass experiences drought stress, its root water absorption capacity is hindered, disrupting the balance between root water uptake and canopy transpiration. As drought stress intensifies, parameters such as leaf relative water content, dark respiration rate, wilting coefficient, tiller number, and biomass of both aboveground and root systems show decreasing trends (Patel et al., 2015). Studies have shown that under severe water scarcity, drought stress can reduce the yield of fresh grass and hay by 45 and 28%, respectively (Shariatipour et al., 2022), decrease the annual harvest frequency from four to three, and reduce ryegrass biomass by up to 79% (Kemesyte et al., 2017). Water shortages in arid environments significantly alter plant morphology, revealing their drought resistance potential and water-use efficiency to some extent (Su et al., 2007). Faced with drought stress, plants typically reduce excessive water consumption by decreasing aboveground biomass while correspondingly increasing underground biomass. This strategic redistribution of biomass helps roots absorb water more effectively, thereby enhancing plant adaptability to drought stress (Huang et al., 2014; Yang et al., 2014). The root system, as a key organ for water and nutrient uptake and soil resource utilization, plays a crucial role in growth and biomass accumulation and is the first part to perceive and respond to water deficits (Wasaya et al., 2018). Under drought conditions, perennial ryegrass resists stress by forming smaller and thicker leaves and expanding the total surface area of its roots to absorb more water. Even in extreme drought conditions, increases in root length and area reveal special adaptive strategies adopted by plants in arid environments, even though root deformities and reduced numbers may occur (Jones et al., 1980).

Under heat stress conditions, when perennial ryegrass plants are subjected to high temperatures above 35°C, this extreme temperature can directly lead to plant death; leaf color changes from emerald green to withered yellow, ultimately turning brown (Chen et al., 2023; Rahman et al., 2022). Heat stress can significantly deteriorate the growth status of ryegrass plants, initially manifested as damage at the junction of the penultimate and antepenultimate leaf sheaths. Simultaneously, some leaves begin to wilt, and their color gradually turns yellow from the base to the tip, followed by damage symptoms on lodging and aging leaves. If stress persist, these injuries become irreversible, ultimately leading to decreased forage coverage (Kauffman et al., 2007; Lei et al., 2022; Yang et al., 2014). During the maturation stage, heat stress can significantly reduce the effective number of spikes per unit area. It hinders the vegetative growth of ryegrass and inhibits material transport, leading to significant decreases in pollen grain weight and protein content, seriously affecting reproductive growth. This results in reduced grain numbers per ear, affecting grain plumpness and thousand-grain weight, and ultimately decreasing yield (Jung et al., 2021). To adapt to high-temperature environments, plants cope with heat stress through a series of complex morphological adjustments. Under heat stress, plants may exhibit specific thermomorphogenic traits such as elongation of hypocotyls and petioles, growth of hypocotyl leaves, and early flowering, which contribute to enhancing photosynthesis and reproductive capacity under heat stress (Kan et al., 2023). Heat stress also leads to an increase in specific leaf area, while leaf thickness, cell layers, and chlorophyll content decrease accordingly. Heat stress intensify transpiration in leaves, increasing the risk of water loss. Therefore, plants may develop smaller and denser stomata to reduce water loss caused by transpiration (Higuchi et al., 1999). Perennial ryegrass enhances its heat tolerance through adaptive changes such as reducing plant height, narrowing leaf width, shortening leaf length, and reducing leaf area (Yang et al., 2024).

4.2 Response mechanism

4.2.1 Physiological mechanisms of perennial ryegrass in response to drought and heat stress

4.2.1.1 Photosynthesis

In arid environments, the diffusion of carbon dioxide through stomata and mesophyll tissues is limited, leading to a decrease in CO_2 concentration within photosynthetic cells and subsequently reducing

carbon fixation (Chaves et al., 2009). Under high-temperature conditions, both carbon fixation and photoreactions are adversely affected. The carbon-fixing enzyme ribulose-1,5-bisphosphate carboxylase/oxygenase (Rubisco) has a dual function, but its specificity for CO_2 decreases with increasing temperature. This change enhances photorespiration, which not only consumes energy but also releases CO_2, thereby reducing the efficiency of net photosynthesis (Moore et al., 2021). The chlorophyll content in leaves is directly related to photosynthetic potential and reflects the plant's adaptability to drought stress. Drought stress leads to gradual loss of leaf water and stomatal closure, weakening the plant's ability to absorb CO_2. This results in the deactivation of the PSII reaction center, affecting the transfer of photosynthetic electrons and energy conversion, ultimately reducing overall photosynthetic efficiency (Gunasekera and Berkowitz, 1993; Medrano et al., 2010). Drought stress also increases the non-photochemical quenching of chlorophyll fluorescence (NPQ) by 15 to 47%, which helps protect PSII reaction centers from damage caused by excess energy (Koscielniak et al., 2006). Research has shown that under drought stress, the ratio of chlorophyll a to chlorophyll b increases, which helps ensure the electron supply to PSII and aligns with the excitation rate of PSI (Ashraf et al., 2011).

Under heat stress, the chlorophyll content of ryegrass decreases, relative conductivity increases, electrolyte leakage rate rises, and stomatal conductance, instantaneous water-use efficiency, and light energy-use efficiency decrease (Zhang et al., 2020). The ultrastructure of leaf cells undergoes significant changes, including chloroplast expansion, structural damage, morphological alterations, and an increase in the number of mitochondria and lipid bodies to adapt to high-temperature environments (Xu et al., 2006). Additionally, perennial ryegrass slows down chlorophyll degradation by inhibiting genes involved in chlorophyll catabolism, such as chlorophyll-a oxygenase, thereby delaying heat-induced leaf senescence (Jespersen et al., 2016; Zhang et al., 2019; Zhang et al., 2016). Studies have shown that inhibiting genes involved in chlorophyll degradation, such as pheophorbide a oxygenas, can effectively slow down the aging process of perennial ryegrass leaves under heat stress (Zhang et al., 2019). Chlorophyll a is crucial for enhancing heat tolerance, and reducing the expression of the chlorophyll catabolism gene *LpNOL* or applying chlorophyll derivatives can inhibit heat-induced leaf senescence (Yu et al., 2022; Zhang et al., 2019). Chlorophyll fluorescence, as a sensitive physiological indicator, can accurately reflect the maximum quantum efficiency (Fv/Fm) of PSII. Maintaining high chlorophyll content and fluorescence levels can help improve photosynthetic efficiency and enhance plant heat tolerance (Pan et al., 2018; Zhu et al., 2022). Moreover, the combined effects of drought and heat stress on photosynthesis are believed to be synergistic, as stomatal closure not only limits carbon fixation but may also lead to excess energy, exacerbating photodamage in the photosystems (Sato et al., 2024).

4.2.1.2 Generation and protective responses to reactive oxygen species

Under drought and heat stress, oxidative stress indicators—such as reactive oxygen species (ROS), hydrogen peroxide, and lipid peroxidation—in perennial ryegrass significantly increase, especially under combined stress conditions (Rahman et al., 2022). In chloroplasts, the reaction centers of PSI and PSII are the main sites for ROS generation; when excess light energy is present, they generate superoxide (Edreva, 2005). Mitochondria are another source of ROS production, where O_2^- is produced through electron leakage from complexes I and III under abiotic stress conditions (Choudhury et al., 2017). Due to the similar processes inducing ROS production under drought and heat stress, their combination synergistically increases ROS levels (Li et al., 2014). To prevent oxidative damage, plants activate ROS-scavenging mechanisms, including enzymes such as superoxide dismutase (SOD), catalase (CAT), ascorbate peroxidase, and glutathione peroxidase, as well as antioxidants like ascorbic acid and glutathione (Kuzniak, 2002). Drought and heat stress typically trigger these defense processes, but different stress conditions lead to variations in ROS levels and the induction of ROS detoxification genes, indicating specific ROS responses under specific stress combinations (Choudhury et al., 2017; Zandalinas et al., 2018). Under drought conditions, perennial ryegrass adapts by increasing the activity of SOD and CAT (Fu and Huang, 2001). Zhang et al. (2015) found that under drought treatment, resistant varieties had lower malondialdehyde (MDA) content and less cell membrane damage. To resist oxidative stress under heat stress, plants activate their antioxidant defense systems (Hamilton et al., 2012), where SOD and CAT prevent MDA accumulation, balance free radical production and scavenging, and enhance plant heat tolerance (Huang et al., 2014; Xu et al., 2011). Under adverse stresses like drought and heat, the activities of peroxidase (POD), SOD, and CAT in ryegrass leaves are enhanced, promoting ROS metabolism balance in cells and improving cell membrane stability, thereby alleviating stress-induced damage (Wang et al., 2022; Wang et al., 2019).

4.2.1.3 Role of osmoregulation

Under drought and heat stress, plant cells maintain osmotic balance by regulating substances such as proline, soluble sugars, and proteins. Studies have found that MDA content in different forage is positively correlated with stress degree, reflecting cell membrane damage; increased proline content enhances the drought tolerance of ryegrass (Chen and Murata, 2011; Jafari et al., 2019). As an osmotic regulator, soluble sugars increase under drought stress, helping plants adapt to arid environments. Under extreme drought conditions, increasing the content of hexose and sucrose in leaf sheaths reduces osmotic potential and enhances drought resistance in perennial ryegrass (Karsten and Macadam, 2001) Perennial ryegrass resists heat stress by maintaining high levels of proline and soluble sugar content (Sun et al., 2020). By maintaining appropriate levels of carbohydrates, including soluble sugars and fructooligosaccharides, plants protect their photosynthetic apparatus from thermal damage, maintain osmotic balance and membrane stability, and slow down leaf senescence (Wang and Xiong, 2016).

4.2.1.4 Regulatory effects of plant hormones

Recent studies have shown that endogenous and exogenous plant hormones play important roles in mitigating damage caused by drought and heat stress. Hormones such as abscisic acid (ABA), cytokinins (CK), and melatonin (MT) are key in the drought and heat resistance mechanisms of perennial ryegrass. ABA, as a key hormone induced by drought, regulates numerous drought-responsive genes and occupies a central position in abiotic stress signaling (Choi et al., 2000). MT pretreatment significantly slowed the decline in forage quality, photochemical efficiency, and relative water content of perennial ryegrass under drought stress, as well as the increase in relative conductivity and MDA content. MT maintains cell membrane

stability by enhancing the activity of SOD, CAT, and peroxidase (Li and Du, 2019).

Under heat stress, ABA content increases, inducing the expression of resistance genes, reducing ROS damage to cell membranes, protecting plants from photoinhibition, and enhancing high-temperature tolerance (Abro et al., 2023). Cytokinins enhance the activity of membrane-protective enzymes like SOD, eliminate free radicals, reduce lipid peroxidation, maintain membrane fatty acid ratios, and protect cell membrane integrity (Wang, 2000). Maintaining stable levels of indole-3-acetic acid (IAA) and salicylic acid (SA), as well as delaying the increase of ABA and the decrease of gibberellin (GA_3), can help improve plant heat tolerance (Li et al., 2020). Cytokinin and ethylene inhibitors alleviate premature leaf senescence under heat stress by upregulating the expression of *LpWRKY69* and *LpWRKY70* (Chen and Huang, 2022). In perennial ryegrass treated with MT, the expression of ABA synthesis pathway genes is inhibited, while the expression of CK synthesis and signaling pathway genes is upregulated, inhibiting heat-induced leaf senescence (Zhang et al., 2017). Exogenous MT application alleviates growth inhibition and leaf senescence caused by heat stress, manifested by increased tiller number, plant height, leaf chlorophyll content, and decreased transcription levels of senescence-related genes *LpSAG12.1* and *Lph3* (Zhang et al., 2017).

4.2.2 Molecular mechanisms of perennial ryegrass response to drought and heat stress

4.2.2.1 Drought-induced responses: gene expression and signal transduction

When plants face drought stress, they activate a series of complex molecular coping strategies involving numerous genes and signaling pathways. Sensors such as G protein-coupled receptors (GPCRs) and receptor-like kinases (RLKs) on the cell membrane detect external drought signals and trigger the expression of drought-responsive genes through signal transduction networks. In this chain reaction, secondary messengers like Ca^{2+}, ROS, ABA, and transcription regulators play crucial roles (Mahmood et al., 2020). For example, *GmCIPK2* enhances plant drought resistance by increasing ABA content and expression of drought-related genes, playing a role in ABA-mediated stomatal closure (Xu et al., 2021). The *MAP3K18* kinase activated by ABA can directly interact with *SnRK2.6* kinase and PP2C phosphatase *ABI1*, participating in the regulation of stomatal opening and closing in Arabidopsis and improving plant drought resistance (Tajdel et al., 2016). *OsCIPK23* RNAi transgenic plants show high sensitivity to drought (Li et al., 2014); *MAPKs* activate SnRK2s through phosphorylation, regulating the expression of drought stress response genes (Mahmood et al., 2020). In combating drought stress, perennial ryegrass adopts complex regulatory strategies, including significantly enhanced expression of transcription factors, kinases, and E3 ubiquitin ligases, promoting ABA and stress signal transduction (Wang et al., 2023). Amiard et al. (2003) found that inositol-1-phosphate synthase (INPS) and galactinol synthase (GOLS) play key roles in regulating the content of raffinose and stachyose under drought stress. Foito et al. (2009) identified functional genes regulated under drought stress through metabolomics and transcriptomics analysis. The cytochrome P450 gene *LpCYP72A15*, as a potential gene for osmotic stress tolerance, demonstrates excellent antioxidant and osmoregulatory abilities, effectively enhancing drought tolerance in ryegrass (Xing et al., 2024). In arid environments, adaptive variations of genotypes such as "Accelerate," "Icon," and "Haymaker" form an important foundation for ryegrass drought tolerance (Majeed et al., 2023). Genome-wide association studies (GWAS) have shown that under drought stress, late embryogenesis abundant protein 3 (*LpLEA3*) and superoxide dismutase (*LpFeSOD*) play crucial roles in maintaining leaf water balance (Yu et al., 2013).

Determining the role of drought-responsive genes in perennial ryegrass adaptation through genetic transformation is significant for elucidating its drought resistance mechanisms. Transcription factors are regulatory proteins that respond to drought stress by modulating gene expression at the transcriptional level. Plants activate or inhibit specific transcription factors through MAPK and CDPK cascade signal transduction pathways, affecting cis-regulatory elements of stress-related genes to enhance or inhibit their transcription. These transcription factors include *MYB*, *NAC*, *WRKY*, and *ERF/DREB*, playing important roles in plant responses to drought stress (Baillo et al., 2019). Genes responsible for transcriptional regulation, ROS scavenging, and osmoregulation of soluble sugars and proline in perennial ryegrass seedlings (such as *DREB*, *NAC*, *MYB*) are crucial under drought stress (Demirkol et al., 2023; Liu and Jiang, 2010). In Arabidopsis, overexpression of the bZIP transcription factor *AREB1* increases sensitivity to ABA and enhances drought tolerance (Fujita et al., 2005). Previous studies have shown that transgenic perennial ryegrass overexpressing *LpHIB1* exhibits better drought tolerance, including higher relative water content, leaf water potential, chlorophyll content, and photosynthetic rate, indicating that *HUB1* may play an important role in abiotic stress tolerance (Patel et al., 2015). Recent research shows that expressing the rice *miR408* gene in perennial ryegrass through genetic modification can enhance drought tolerance, possibly related to leaf morphology adjustment and improved antioxidant capacity (Hang et al., 2021). Additionally, *LpP5CS* (pyrroline-5-carboxylate synthase) plays a crucial role in various stress responses and is a potential candidate gene for stress-related molecular breeding in perennial ryegrass. Overexpression of *LpP5CS* in tobacco plants, especially the mutant form *LpP5CS^F128A* not inhibited by proline feedback, enhances tolerance to drought stress (Cao et al., 2015). Using a yeast ectopic expression system, *LpSAPK9* was identified as a candidate positive regulatory factor for drought tolerance. *LpSAPK9* showed distinct expression changes in drought-tolerant ryegrass varieties, indicating that its expression level is related to drought tolerance. These results contribute to further analysis of *LpSAPKs* for molecular breeding of ryegrass and related grass species (Xing et al., 2022).

4.2.2.2 Heat-induced responses: gene expression and signal transduction

Identifying key regulatory genes affecting heat tolerance and exploring their mechanisms of adaptation provides references for improving heat tolerance in perennial ryegrass. The process of plant response to heat stress is complex, involving interactions among numerous transcription factors and signaling molecules, forming a regulatory network (Zhang et al., 2020). The homeodomain leucine zipper (HD-Zip) transcription factor family plays an important role in regulating plant development and responding to abiotic stresses, including heat stress. RT-PCR results showed that the expression levels of *LpHOX6*, *LpHOX8*, and *LpHOX24* (HD-Zip I transcription factors) in perennial ryegrass were negatively correlated with heat

tolerance, while *LpHOX21* expression was positively correlated (Wang et al., 2019). Dai et al. (2017) found through sequencing and methylation analysis using sodium bisulfite that the P450 gene *LpCYP72A161* in perennial ryegrass is epigenetically regulated under heat stress. Zhang et al. (2020) conducted heat tolerance identification and molecular marker experiments on 98 varieties and found that four chlorophyll catabolism genes (*LpNYC1*, *LpNOL*, *LpSGR*, and *LpPPH*) were closely related to heat tolerance. Additionally, heterologous expression of perennial ryegrass *LpHSFC1b* in Arabidopsis can significantly improve heat resistance in transgenic Arabidopsis (Sun et al., 2020). This study provides new insights into the epigenetic regulation of perennial ryegrass genes under heat stress.

In addition to transcriptional regulation, post-transcriptional and post-translational regulations play important roles in plant responses to heat stress. MicroRNAs (miRNAs) participate in heat stress responses by regulating transcription factor activity. Under high-temperature conditions, *miRNA398* in Arabidopsis promotes the accumulation of heat shock transcription factors (*HSFs*) by inhibiting three ROS-scavenging enzymes, thereby enhancing heat tolerance (Guan et al., 2013). Overexpression of *miRNA160* in Arabidopsis can inhibit *ARF10*, *ARF16*, and *ARF17*, activate a series of downstream heat shock protein (HSP) genes, and enhance heat tolerance (Lin et al., 2018). The expression of *HSFA1* in Arabidopsis is also feedback-regulated by small RNAs. miR398 induced by *HSFA1* inhibits the expression of ROS-scavenging genes *CSD1* (copper/zinc superoxide dismutase 1), *CSD2*, and *CCS1* (copper chaperone of SOD1), leading to excessive ROS accumulation, positively regulating *HSFA1* expression and ultimately affecting heat tolerance (Guan et al., 2013). Studies have also found that *DREB2A* remains stable under high-temperature stress through SUMO modification, helping improve heat tolerance (Wang et al., 2020).

4.2.2.3 Heat shock proteins regulating drought and heat resistance

Plants exposed to high temperatures and/or drought produce excessive free radicals (O_2^-, H_2O_2, OH^-), leading to cell damage and oxidative stress, which inhibit crucial cellular and metabolic processes (Hussain et al., 2019). These combined effects can slow plant growth and even cause wilting or death. Genetic and genomic studies have shown that many proteins and antioxidant genes are involved in plant responses to heat and drought stress (Al Khateeb et al., 2020; Bourgine and Guihur, 2021). These candidate proteins and genes protect plants from abiotic stress through cellular homeostasis, metabolic protein regulation, signal transduction, and antioxidant defense (Rahman et al., 2021; Wang et al., 2004). For example, overexpression of the *TaHsfA6f* gene in Arabidopsis significantly enhances tolerance to heat and drought (Bi et al., 2020). Li et al. (2014) analyzed the GmHsf family in soybean and found that Arabidopsis plants overexpressing *GmHsf-34* exhibited stronger heat and drought tolerance. Ma et al. (2022) identified and characterized 16 putative *Hsf* genes through whole-genome bioinformatics analysis, including eight *HsfA*, five *HsfB*, and three *HsfC* in ryegrass. These genes mostly respond to early heat stress and also to late drought stress. Functional analysis of *LmHSFA5*, induced by high temperature and drought, showed that it may positively regulate heat and drought tolerance by directly activating the expression of *LmHSP18.2* and *LmAPX2* in ryegrass. Rahman et al. (2022) investigated the transcriptional response of HSP and antioxidant genes in perennial ryegrass under combined heat and drought stress. The study showed that oxidative stress indicators significantly increased under combined stress, while *HSP70*, *HSP90-6*, and mitochondrial small *HSP26.2* showed high expression levels. Additionally, up to 90% of Hsfs in sesame have drought responsiveness (Dossa et al., 2016), and *ZmHSF06* has a positive regulatory effect on drought tolerance in Arabidopsis (Li et al., 2015). Jiang et al. (2016) compared responses and gene expression differences of two perennial ryegrass varieties during deficit irrigation and growth recovery. The results showed significant differences in transcription levels of heat shock cognate protein 70 (*HSC70*), iron superoxide dismutase (*FeSOD*), and plasma membrane intrinsic protein 1 (*PIP1*) in leaves and stems, providing important evidence for further exploration of molecular mechanisms in drought resistance.

To resist heat stress, HSPs are induced and act as molecular chaperones to prevent protein denaturation, a process controlled by heat stress transcription factors. In the HSF gene family, the *LpHSFC1b* gene is significantly induced after heat treatment and is a core regulatory gene (Scharf et al., 2018). The *FaHSFC1b* gene of tall fescue and the *LpHSFC1b* gene of perennial ryegrass have been confirmed to be involved in plant heat stress responses. Overexpression of these genes can enhance heat tolerance in transgenic Arabidopsis and promote the expression of *HSFA* genes, *HSP* genes, and ABA synthesis-related gene *NCED* (Sundaram and Rathinasabapathi, 2010; Zhuang et al., 2018). Arabidopsis transformed with the *LpHSFC1b* gene showed decreased electrolyte leakage and MDA content, as well as significantly increased expression of heat stress response genes (Sun et al., 2020). RNA-seq analysis showed that the *HSFA* and *HSFB* subfamilies in ryegrass are closely related to heat tolerance (Yang et al., 2012). After 10 h of high-temperature treatment, about 25% of gene expression in ryegrass leaves showed significant changes, with genes A2, A3, A4, A6, and A9 in the *HSFA* subfamily and B genes in the *HSFB* subfamily significantly upregulated, indicating the important role of *HSFA* and *HSFB* in heat stress adaptation (Wang et al., 2017).

4.3 Strategies to improve drought and heat resistance in perennial ryegrass

4.3.1 Enhancing resistance through exogenous substances

Under drought stress, the water absorption capacity of perennial ryegrass roots may be impaired. However, increasing the root-to-shoot ratio can enhance root water uptake, effectively mitigating the negative effects of drought stress. Adopting appropriate cultivation and management strategies can significantly improve the drought resistance of ryegrass. Although drought stress typically restricts ryegrass growth, appropriate fertilization measures can promote biomass accumulation (Ponce et al., 1993). For instance, applying suitable concentrations of potassium fertilizer in arid environments can significantly improve seed germination rates, increase leaf thickness, and enhance the root-to-shoot ratio, thereby bolstering drought resistance (Hoffman et al., 2010). The application of nitrogen fertilizer has also been shown to significantly increase the dry matter yield of ryegrass and improve feed quality (Abraha et al., 2015). Additionally, the use of silicates can alleviate physiological changes in ryegrass under drought stress, while plant growth regulators can reduce the rate of quality loss under such conditions (Hahn et al., 2008; Mahdavi et al., 2016). Spraying uniconazole has been found to

reduce plant height, promote tillering, and improve stress resistance; foliar application of uniconazole enhances the drought resistance of ryegrass to varying degrees under drought stress (Ma et al., 2009). The application of rice husk biochar (RHB) improves shoot and root growth, increases chlorophyll content, and enhances photosynthetic efficiency, thereby augmenting drought tolerance (Safari et al., 2023). Methyl jasmonate (MeJA) treatment increases endogenous indole-3-acetic acid (IAA) and MeJA levels in ryegrass under drought stress, contributing to increased biomass and improved drought resistance (Wei et al., 2024). Adding sludge to the soil can significantly improve growth rates and osmotic regulation under drought stress, enhance photosynthesis and water-use efficiency, and ultimately strengthen drought resistance (Bermanec et al., 2016).

In summer, moderate application of nitrogen fertilizer can meet the energy needs of plants to resist high temperatures. Adequate phosphorus fertilization helps plants absorb water from deeper soil layers, supplementing the insufficient surface moisture caused by high temperatures. Increasing potassium fertilizer application can enhance the heat resistance of forage, possibly because potassium promotes photosynthesis, accelerates protein and starch synthesis, compensates for excessive consumption of organic matter under high temperatures, and slows the aging process of forage (Gong et al., 1998). The application of plant growth regulators can effectively improve the heat resistance of ryegrass, enabling it to survive hot summer days safely. For example, the use of chemicals such as paclobutrazol (PP_{333}) can enhance plant heat resistance. Xiong et al. (2006) found that spraying PP_{333} at different concentrations on perennial ryegrass significantly reduced leaf emergence rates compared to the control group, while increasing the accumulation of free proline, relative leaf water content, soluble protein content, and enhancing the activities of ascorbic acid, peroxidase, and nitrate reductase. These changes work together to significantly enhance the heat tolerance of perennial ryegrass.

4.3.2 Enhancing resistance through symbiotic bacteria

Perennial ryegrass forms mutually beneficial symbiotic relationships with endophytic fungi. The grass provides space and essential nutrients for the fungi, while endophytic fungi play key roles in promoting plant growth and enhancing resistance to biotic and abiotic stresses (Clay and Schardl, 2002; Gao et al., 2024; Zhao et al., 2024a). The impact of endophytic fungi on the resistance of perennial ryegrass has become an important research topic internationally. Numerous studies have shown that endophytic fungal infections can enhance the drought tolerance of perennial ryegrass (Kane, 2011), reduce damage caused by stress (Deng et al., 2020), and influence tillering (Ravel et al., 1997) and physiological responses. Endophytic fungi enhance the drought resistance of the host by boosting its osmotic regulation and reactive ROS scavenging systems (Ma et al., 2020). Hesse et al. (2003) reported that under drought conditions, endophytic fungi increased the root-to-shoot ratio and root dry weight of ryegrass; subsequent studies found that they significantly increased seed yield.

Endophytic fungi also play crucial roles in plant growth and resistance to environmental stresses like heat stress. They effectively eliminate harmful ROS by inducing antioxidant enzyme production, thereby enhancing the plant's antioxidant defense system. Endophytes can regulate plant hormone levels, promote the synthesis of ABA, and enhance heat tolerance (Ding et al., 2024; Sahu et al., 2022). Research has found that inoculation with Aspergillus oryzae significantly enhances the heat and drought resistance of perennial ryegrass. After treatment with Aspergillus nidulans, ABA content in ryegrass leaves significantly increased, while salicylic acid content decreased (Li et al., 2021; Wei et al., 2023b). Inoculation with arbuscular mycorrhizal (AM) fungi can enhance the antioxidant defense capacity and hormone levels of ryegrass under heat stress. Wei et al. (2023a) found that high-temperature stress significantly inhibited the growth of perennial ryegrass. However, inoculation with AM fungi combined with melatonin treatment upregulated the expression of melatonin synthesis genes in the ryegrass root system, increased endogenous melatonin content, enhanced antioxidant enzyme activity, reduced oxidative damage, and improved osmotic regulation ability, thereby enhancing heat tolerance (Zhao et al., 2022).

4.3.3 Breeding and cultivating superior varieties

4.3.3.1 Drought-resistant breeding strategies

Cultivating drought-resistant varieties is fundamental to improving plant drought tolerance. With the development of modern biotechnology, breeding research on perennial ryegrass has gained new opportunities and methods. Traditional breeding techniques, such as introduction, hybridization, and selection, have long improvement cycles and limited genetic material (Ahmar et al., 2020). Advances in biotechnology have provided new possibilities for cultivating drought-tolerant varieties.

Introduction is an important method for developing ryegrass production by bringing in excellent varieties from abroad or other regions, conducting adaptability assessments, and evaluating their suitability for promotion in specific areas. Among the 29 ryegrass varieties introduced by Huang et al. (2008) from Germany, "Taurus," "Barfort," "Gemini," "Fastyl," and others showed good adaptability in Sichuan; "Defo," "Prestyl," "Pomerol," and others provided excellent genetic material for breeding new ryegrass varieties, accelerating the breeding process. "Winter Pasture 70" ryegrass exhibits characteristics of drought tolerance, low fertility requirements, and strong stress resistance, with yields surpassing those of Italian ryegrass and perennial ryegrass (Liu et al., 2006). Through introduction, excellent germplasm resources can be obtained. Wild and cultivated ryegrass germplasm resources can be collected and sorted, and through domestication experiments and selective breeding, valuable parents can be provided for breeding new varieties.

As a strictly cross-pollinated plant, perennial ryegrass may achieve trait improvements through mixed selection and single-plant selection methods; cyclical selection can improve ryegrass populations (Sheng and He, 2003). In an experiment conducted by Mo et al. (2009) in Guizhou, excellent plants were selected from the seed breeding population of American varieties. After repeated selection and improvement, the high-yield and high-quality "Guicao No. 1" Italian ryegrass was bred. A comparative study on the drought tolerance of nine perennial ryegrass varieties found that the dry matter content of the Norwegian germplasm was 50% higher than that of the second-best performing germplasm. After six drought cycles, the dry matter content was more than seven times higher than that of the reference variety "Grasslands Impact," demonstrating excellent performance under drought stress (Daliya et al., 2018). A study on the genetic variation of drought resistance in 18 varieties revealed diversity among varieties and inconsistencies between survival rate and growth status.

The "Sopin" variety performed the best under two drought conditions, adapting to drought by regulating starch and sugar metabolism, antioxidant enzyme activity, and transcriptional regulation mechanisms (Wang et al., 2023).

Hybrid breeding, as an effective genetic improvement method, can integrate the excellent traits of both parents. Through gene recombination and interaction, offspring with heterosis surpassing the parents' traits may be bred (Zhao et al., 2024b). For cross-pollinated ryegrass, hybridization between different varieties of the same species is convenient, and interspecific hybridization is also feasible, often resulting in fertile hybrids. Distant hybridization has proven effective for enhancing stress resistance in perennial ryegrass. Liu et al. (2004) confirmed through isoenzyme analysis that "Changjiang No. 2" Italian ryegrass is a hybrid of "Abode" and "Ganxuan No. 1," integrating the excellent qualities of both parents. Studying the drought tolerance of hybrid offspring from perennial ryegrass and tall fescue revealed that drought-tolerant ryegrass varieties could be developed through intergeneric hybridization (Wang and Bughrara, 2008).

Mutation breeding, as an effective means of genetic improvement, has been widely applied in drought-tolerance breeding of perennial ryegrass. Using spatial conditions for mutagenesis can generate high-frequency and significant variations, with most trait variations being heritable. Yan and Zhang (2008) observed the germination rate, phenological period, and agronomic traits of "Changjiang No. 2" Italian ryegrass seeds carried by the "Shijian 8" satellite. They found that the germination rate of the space-exposed seeds reached 98.34%, higher than the control group; the later growth rate was faster, and the coefficient of variation for various agronomic traits was significantly higher than the control. Further research showed that the endogenous hormones, ion content, and nutrient elements of perennial ryegrass seeds infected with endophytic fungi (E+) and uninfected (E−) changed after aerospace mutagenesis, these changes promoted host plant growth and ultimately improved drought resistance (Ma et al., 2020). Dong et al. (2018) successfully obtained mutant strains B9, B10, and B12 with strong drought resistance under drought stress by using EMS to induce mutations in seeds of the perennial ryegrass variety "Prime Minister."

Global research focuses on introducing key functional genes into perennial ryegrass to improve its physiological characteristics. Given that perennial ryegrass is a cross-pollinated crop with high self-incompatibility, achieving homozygous stability of excellent genes is challenging, making genetic improvement relatively difficult. However, advances in biotechnology breeding have brought new hope. The application of genetic engineering, cell fusion, and molecular marker-assisted breeding techniques has improved breeding accuracy and speed, helping cultivate new varieties with ideal traits (Araghi et al., 2014; Foolad et al., 2001). Yang et al. (2006) transformed the *DREB1B* (*CBF1*) gene using a gene gun method and subjected 36 transgenic plants to drought treatment. After 25 days of drought, three plants showed signs of survival, and one revived after rehydration. Han et al. (2007) introduced *DREB1A* and *BADH-CMO* genes into embryogenic callus tissue of perennial ryegrass using gene gun and Agrobacterium-mediated techniques. The transgenic plants obtained showed strong tolerance to drought stress and produced fertile transgenic plants with enhanced drought resistance and normal growth. Zhang et al. (2011) cloned the *Ac-1-FFT* gene from ice grass using transgenic technology and transferred it into ryegrass to cultivate a new variety with enhanced drought resistance. Jaskune et al. (2020) successfully identified single nucleotide polymorphism (SNP) markers adjacent to the Phytochrome B (*PhyB*) and *MYB41* transcription factor genes in perennial ryegrass using genome-wide association studies (GWAS). Research showed that the expression of these genes is closely related to leaf growth and yield under drought stress, playing roles in regulating drought response mechanisms. These SNP markers have the potential to become valuable resources for improving biomass and breeding strategies of perennial ryegrass under drought conditions. Akinroluyo et al. (2021) found through RNA sequencing that tetraploid lines of Italian ryegrass (*Lolium multiflorum*) have higher drought resistance and survival rates than diploid lines due to high expression of functional protein and dehydration protein genes. Additionally, the release of the perennial ryegrass genome has made predictive research based on genomic data possible, aiding in the selection of perennial ryegrass and providing a foundation for breeding other ryegrass species (Byrne et al., 2016).

4.3.3.2 Heat-resistant breeding strategies

To enhance the resistance of perennial ryegrass to heat stress, several strategies can be adopted. Firstly, introducing new ryegrass varieties with excellent heat resistance based on the natural ecological conditions of different regions is considered the most economical and effective way to improve resistance in ryegrass production. Secondly, selecting ryegrass varieties with good heat resistance through hybrid breeding, mutagenesis breeding, biotechnology breeding, or a combination of conventional and biotechnology breeding is a comprehensive strategy to prevent and address susceptibility to high-temperature stress (Kimbeng, 1999; Li et al., 2008; Soliman et al., 2021). Currently, research on heat-resistant breeding of perennial ryegrass mainly focuses on screening germplasm resources. For example, Zhang et al. (2020) subjected 98 varieties to a 24-day heat treatment at 35°C/30°C and evaluated their heat tolerance using eight physiological indicators. They successfully identified five heat-resistant and five heat-sensitive varieties. The study also showed that the perennial ryegrass variety "Emerald" has poor heat tolerance (Sun et al., 2020). Shi et al. (2010) used the conductivity method to determine the heat tolerance of 12 ryegrass varieties and found that "Esquire" and "Granddaddy" exhibited high heat tolerance after heat stress and recovery, demonstrating good heat resistance characteristics. Furthermore, Soliman et al. (2021) successfully cultivated 72 F_1 hybrid offspring by crossbreeding the heat-resistant variety "Kangaroo Valley" with the heat-sensitive variety "Norlea." These offspring exhibit significant additive genetic variation in heat tolerance, providing valuable genetic resources for improving the heat tolerance of perennial ryegrass. In another study, Wang et al. (2016) subjected perennial ryegrass to high-temperature treatment at 40°C for 10 h and, compared with ryegrass under normal growth conditions, used RNA sequencing to identify 52 heat shock transcription factor (HSF) genes. Similarly, Wang et al. (2017) conducted RNA sequencing on perennial ryegrass treated at 35°C for 6 h and identified four candidate genes related to the C_4 carbon fixation pathway. The significant differences in heat tolerance among perennial ryegrass varieties are mainly caused by genetic diversity. Phenotypic and genetic diversity analysis is necessary for in-depth research on heat tolerance mechanisms, screening promising plant materials, and developing effective breeding strategies (Zhu et al., 2022).

5 Conclusion

In this study, we utilized bibliometric methods to comprehensively summarize and analyze the global literature on drought and heat stress in perennial ryegrass over the past 30 years. This analysis clarifies the overall knowledge framework of research in this area and provides a detailed and comprehensive reference for future studies. Our findings indicate a significant upward trend in research output during this period, with China and the United States emerging as major contributors. Notably, the journal *Crop Science* published the highest number of relevant papers. Keyword analysis revealed that "growth," "endophytic fungi," and "yield" are the most frequently used terms in drought stress research, while "growth," "gene," and "leaf" are prevalent in heat stress studies. Research has predominantly focused on phenotypic changes, response mechanisms, and techniques to enhance drought and heat resistance in perennial ryegrass. Endophytic fungi have become a hot topic in recent drought stress research and have also attracted considerable attention in heat stress studies, suggesting that this area may continue to develop in the future. Furthermore, there is a need to strengthen research on the functions and mechanisms of genes related to drought stress in ryegrass and to further explore molecular response mechanisms under heat stress. Trend analysis indicates that the interaction between drought and heat stress is receiving increasing attention, suggesting it will become an important direction for future research. Monitoring the hotspots and frontiers in perennial ryegrass research on drought and heat stress can help effectively identify key turning points and lay the foundation for future studies. The results of this study not only provide guidance for future research on perennial ryegrass under drought and heat stress but also offer valuable information for researchers in related fields.

Author contributions

RW: Writing – review & editing, Writing – original draft, Methodology. YG: Writing – review & editing, Formal analysis. JL: Writing – review & editing, Supervision, Conceptualization. XW: Writing – review & editing, Supervision, Conceptualization. YY: Writing – review & editing, Supervision, Conceptualization. HH: Writing – review & editing, Supervision, Conceptualization. ZZ: Writing – review & editing, Supervision, Conceptualization. PW: Writing – review & editing, Methodology, Funding acquisition. LZ: Writing – review & editing, Supervision, Conceptualization.

Funding

The author(s) declare that financial support was received for the research, authorship, and/or publication of this article. This study was supported by the Natural Science Foundation of China (32260351), State Key Laboratory of Microbial Technology Open Projects Fund (Project no. M2022-14), and Guizhou high-level innovative talents project [Qiankehepingtairencai-GCC (2022)022–1].

Conflict of interest

The authors declare that the research was conducted in the absence of any commercial or financial relationships that could be construed as a potential conflict of interest.

Publisher's note

All claims expressed in this article are solely those of the authors and do not necessarily represent those of their affiliated organizations, or those of the publisher, the editors and the reviewers. Any product that may be evaluated in this article, or claim that may be made by its manufacturer, is not guaranteed or endorsed by the publisher.

Supplementary material

The Supplementary material for this article can be found online at: https://www.frontiersin.org/articles/10.3389/fsufs.2024.1458552/full#supplementary-material

References

Abraha, A. B., Truter, W. F., Annandale, J. G., and Fessehazion, M. K. (2015). Forage yield and quality response of annual ryegrass (*Lolium multiflorum*) to different water and nitrogen levels. *Afr. J. Range For. Sci.* 32, 125–131. doi: 10.2989/10220119.2015.1056228

Abro, A. A., Anwar, M., Javwad, M. U., Zhang, M., Liu, F., Jiménez-Ballesta, R., et al. (2023). Morphological and physio-biochemical responses under heat stress in cotton: overview. *Biotechnol. Rep* 40:e00813. doi: 10.1016/j.btre.2023.e00813

Ahmar, S., Gill, R. A., Jung, K. H., Faheem, A., Qasim, M. U., Mubeen, M., et al. (2020). Conventional and molecular techniques from simple breeding to speed breeding in crop plants: recent advances and future outlook. *Int. J. Mol. Sci.* 21:2590. doi: 10.3390/ijms21072590

Akinroluyo, O. K., Kemesyte, V., Jaskune, K., and Statkeviciute, G. (2021). Candidate-gene expression patterns in diploid and tetraploid *Lolium multiflorum* spp. *multiflorum* cultivars under water deficit. *Zemdirbyste-Agriculture* 108, 363–370. doi: 10.13080/z-a.2021.108.046

Al Khateeb, W., Muhaidat, R., Alahmed, S., Al Zoubi, M. S., Al-Batayneh, K. M., El-Oqlah, A., et al. (2020). Heat shock proteins gene expression and physiological responses in durum wheat (*Triticum durum*) under salt stress. *Physiol. Mol. Biol. Plants* 26, 1599–1608. doi: 10.1007/s12298-020-00850-x

Amiard, V., Morvan-Bertrand, A., Billard, J. P., Huault, C., Keller, F., and Prud'homme, M. P. (2003). Fructans, but not the sucrosyl-galactosides, raffinose and loliose, are affected by drought stress in perennial ryegrass. *Plant Physiol.* 132, 2218–2229. doi: 10.1104/pp.103.022335

Anjum, S. A., Wang, L. C., Farooq, M., Hussain, M., Xue, L. L., and Zou, C. M. (2011). Brassinolide application improves the drought tolerance in maize through modulation of enzymatic antioxidants and leaf gas exchange. *J. Agron. Crop Sci.* 197, 177–185. doi: 10.1111/j.1439-037X.2010.00459.x

Araghi, B., Barati, M., Majidi, M. M., and Mirlohi, A. (2014). Application of half-sib mating for genetic analysis of forage yield and related traits in *Bromus inermis*. *Euphytica* 196, 25–34. doi: 10.1007/s10681-013-1011-2

Armstead, I., Donnison, I., Aubry, S., Harper, J., Hoertensteiner, S., James, C., et al. (2006). From crop to model to crop: identifying the genetic basis of the staygreen mutation in the *Lolium/Festuca* forage and amenity grasses. *New Phytol.* 172, 592–597. doi: 10.1111/j.1469-8137.2006.01922.x

Ashraf, M., Akram, N. A., Al-Qurainy, F., and Foolad, M. R. (2011). Drought tolerance: roles of organic osmolytes, growth regulators, and mineral nutrients. *Adv. Agron.* 111, 249–296. doi: 10.1016/b978-0-12-387689-8.00002-3

Baillo, E. H., Kimotho, R. N., Zhang, Z. B., and Xu, P. (2019). Transcription factors associated with abiotic and biotic stress tolerance and their potential for crops improvement. *Genes.* 10:771. doi: 10.3390/genes10100771

Basavaraj, P. S., and Rane, J. (2020). Avenues to realize potential of phenomics to accelerate crop breeding for heat tolerance. *Plant Physiol.* 25, 594–610. doi: 10.1007/s40502-020-00552-2

Bermanec, V., Vidakovic-Cifrek, Z., Fiket, Z., Tkalec, M., Kampic, S., and Kniewald, G. (2016). Influence of digested wastewater sludge on early growth of the perennial ryegrass (*Lolium perenne* L.). *Environ. Earth Sci.* 75:32. doi: 10.1007/s12665-015-4814-8

Bi, H. H., Zhao, Y., Li, H. H., and Liu, W. X. (2020). Wheat heat shock factor TaHsfA6f increases ABA levels and enhances tolerance to multiple abiotic stresses in transgenic plants. *Int. J. Mol. Sci.* 21:121. doi: 10.3390/ijms21093121

Bourgine, B., and Guihur, A. (2021). Heat shock signaling in land plants: from plasma membrane sensing to the transcription of small heat shock proteins. *Front. Plant Sci.* 12:710801. doi: 10.3389/fpls.2021.710801

Byrne, S. L., Nagy, I., Pfeifer, M., Armstead, I., and Asp, T. (2016). A synteny-based draft genome sequence of the forage grass *Lolium perenne*. *Plant J.* 84, 816–826. doi: 10.1111/tpj.13037

Cao, L., Han, L., Zhang, H. L., Xin, H. B., Imtiaz, M., Yi, M. F., et al. (2015). Isolation and characterization of pyrroline-5-carboxylate synthetase gene from perennial ryegrass (*Lolium perenne* L.). *Acta Physiol. Plant.* 37, 1–9. doi: 10.1007/s11738-015-1808-9

Chapman, D. F., Ludemann, C., Wims, C. M., and Kuhn-Sherlock, B. (2023). The contribution of perennial ryegrass (*Lolium perenne* L.) breeding to whole pasture productivity under dairy cattle grazing in New Zealand. 2. Rates of gain in production traits and economic value. *Grass Forage Sci.* 78, 85–100. doi: 10.1111/gfs.12589

Chaves, M. M., Flexas, J., and Pinheiro, C. (2009). Photosynthesis under drought and salt stress: regulation mechanisms from whole plant to cell. *Ann. Bot.* 103, 551–560. doi: 10.1093/aob/mcn125

Chen, W., and Huang, B. R. (2022). Cytokinin or ethylene regulation of heat-induced leaf senescence involving transcriptional modulation of WRKY in perennial ryegrass. *Physiol. Plantarum.* 174:e13766. doi: 10.1111/ppl.13766

Chen, T. H. H., and Murata, N. (2011). Glycinebetaine protects plants against abiotic stress: mechanisms and biotechnological applications. *Plant Cell Environ.* 34, 1–20. doi: 10.1111/j.1365-3040.2010.02232.x

Chen, Y., Sun, Y. Y., Wan, H., Chen, L., Cao, L., Zhao, B. Y., et al. (2023). Integrative analysis of transcriptome and yeast screening system identified heat stress-responding genes in ryegrass. *Environ. Exp. Bot.* 210:105333. doi: 10.1016/j.envexpbot.2023.105333

Choi, H., Hong, J., Ha, J., Kang, J., and Kim, S. Y. (2000). ABFs, a family of ABA-responsive element binding factors. *J. Biol. Chem.* 275, 1723–1730. doi: 10.1074/jbc.275.3.1723

Choudhury, F. K., Rivero, R. M., Blumwald, E., and Mittler, R. (2017). Reactive oxygen species, abiotic stress and stress combination. *Plant J.* 90, 856–867. doi: 10.1111/tpj.13299

Clay, K., and Schardl, C. (2002). Evolutionary origins and ecological consequences of endophyte symbiosis with grasses. *Am. Nat.* 160, S99–S127. doi: 10.1086/342161

Craufurd, P. Q., Vadez, V., Jagadish, S. K., Prasad, P. V., and Zaman-Allah, M. (2013). Crop science experiments designed to inform crop modeling. *Agric. For. Meteorol.* 170, 8–18. doi: 10.1016/j.agrformet.2011.09.003

Dai, Y., Mao, P., Tao, X., Wang, Y., Wei, C. M., and Ma, X. R. (2017). Flexible shift on gene body methylation and transcription of *LpCYP72A161* exposed to temperature stress in perennial ryegrass. *Environ. Exp. Bot.* 143, 29–37. doi: 10.1016/j.envexpbot.2017.08.002

Daliya, C., Hofmann, R. W., Alan, S., Sathish, P., Winefield, C. S., and Moot, D. J. (2018). Intraspecific differences in long-term drought tolerance in perennial ryegrass. *PLoS One* 13:e0194977. doi: 10.1371/journal.pone.0194977

Demirkol, G., Felek, A. F., Asci, O. O., and Yilmaz, N. (2023). Physiological and transcriptional status of genetically diverse perennial ryegrass (*Lolium perenne* L.) populations under drought stress. *Plant Genet. Resour.* 21, 331–339. doi: 10.1017/s1479262123000795

Deng, J., Li, F., and Duan, T. Y. (2020). *Claroideoglomus etunicatum* reduces leaf spot incidence and improves drought stress resistance in perennial ryegrass. *Australasian Plant Path.* 49, 147–157. doi: 10.1007/s13313-020-00685-w

Ding, L. L., Chen, H., Wei, X., Qin, T. Y., Lei, X., Li, J. Y., et al. (2024). Soil cations explain the variation of soil extracellular activities and microbial elemental limitations on subtropical grassland, China. *Polish J. Environ. Stu.* 33, 4061–4070. doi: 10.15244/pjoes/176566

Ding, L. L., Tian, L. L., Li, J. Y., Zhang, Y. J., Wang, M. Y., and Wang, P. C. (2023). Grazing lowers soil multifunctionality but boosts soil microbial network complexity and stability in a subtropical grassland of China. *Front. Microbiol.* 13:1027097. doi: 10.3389/fmicb.2022.1027097

Dong, W. K., Lu, X. P., Jiang, H. Y., and Ma, H. L. (2018). Ems mutagenesis and drought tolerant evaluation of *Loium perenne* L. *J. Nuclear Agric. Sci.* 32, 1889–1897. doi: 10.11869/j.issn.100-8551.2018.10.1889

Dossa, K., Diouf, D., and Cisse, N. (2016). Genome-wide investigation of Hsf genes in sesame reveals their segmental duplication expansion and their active role in drought stress response. *Front. Plant Sci.* 7:1522. doi: 10.3389/fpls.2016.01522

Edreva, A. (2005). Generation and scavenging of reactive oxygen species in chloroplasts: a submolecular approach. *Agric. Ecosyst. Environ.* 106, 119–133. doi: 10.1016/j.agee.2004.10.022

Farooq, M., Wahid, A., Kobayashi, N., Fujita, D., and Basra, S. M. A. (2009). Plant drought stress: effects, mechanisms and management. *Agron. Sustain. Dev.* 29, 185–212. doi: 10.1051/agro:2008021

Foito, A., Byrne, S. L., Shepherd, T., Stewart, D., and Barth, S. (2009). Transcriptional and metabolic profiles of *Lolium perenne* L. genotypes in response to a PEG-induced water stress. *Plant Biotechnol. J.* 7, 719–732. doi: 10.1111/j.1467-7652.2009.00437.x

Foolad, M. R., Zhang, L. P., and Lin, G. Y. (2001). Identification and validation of QTLs for salt tolerance during vegetative growth in tomato by selective genotyping. *Genome* 44, 444–454. doi: 10.1139/gen-44-3-444

Fu, J. M., and Huang, B. R. (2001). Involvement of antioxidants and lipid peroxidation in the adaptation of two cool-season grasses to localized drought stress. *Environ. Exp. Bot.* 45, 105–114. doi: 10.1016/S0098-8472(00)00084-8

Fujita, Y., Fujita, A. M., Satoh, C. R., Maruyama, C. K., Parvez, A. M. M., and Seki, A. M. (2005). AREB1 is a transcription activator of novel abre-dependent ABA signaling that enhances drought stress tolerance in Arabidopsis. *Plant Cell* 17:3470, –3488. doi: 10.1105/tpc.105.035659

Gao, Y., Zhang, Y. J., Wang, P. C., and Zhao, L. L. (2024). Structure and diversity of endophytic bacteria in maize seeds and germinating roots. *Microorganisms.* 12:1348. doi: 10.3390/microorganisms12071348

Gong, M., Li, Y. J., and Chen, S. Z. (1998). Abscisic acid-induced thermotolerance in maize seedlings is mediated by calcium and associated with antioxidant systems. *J. Plant Physiol.* 153, 488–496. doi: 10.1016/S0176-1617(98)80179-X

Gong, Z. Z., Xiong, L. M., Shi, H. Z., Yang, S. H., and Zhu, J. K. (2020). Plant abiotic stress response and nutrient use efficiency. *Sci. China Life Sci.* 63:635, –674. doi: 10.1007/s11427-020-1683-x

Gornall, J., Betts, R., Burke, E., Clark, R., Camp, J., Willett, K., et al. (2010). Implications of climate change for agricultural productivity in the early twenty-first century. *Philos. T. R. Soc. B.* 365, 2973–2989. doi: 10.1098/rstb.2010.0158

Guan, Q. M., Lu, X. Y., Zeng, H. T., Zhang, Y. Y., and Zhu, J. H. (2013). Heat stress induction of *miR398* triggers a regulatory loop that is critical for thermotolerance in Arabidopsis. *Plant J.* 74, 840–851. doi: 10.1111/tpj.12169

Gunasekera, D., and Berkowitz, G. A. (1993). Use of transgenic plants with ribulose-1, 5-bisphosphate carboxylase/oxygenase antisense DNA to evaluate the rate limitation of photosynthesis under water stress. *J. Plant Physiol.* 103, 629–635. doi: 10.1104/pp.103.2.629

Hahn, H., McManus, M. T., Warnstorff, K., Monahan, B. J., Young, C. A., Davies, E., et al. (2008). Neotyphodium fungal endophytes confer physiological protection to perennial ryegrass (*Lolium perenne* L.) subjected to a water deficit. *Environ. Exp. Bot.* 63, 183–199. doi: 10.1016/j.envexpbot.2007.10.021

Hamilton, C. E., Gundel, P. E., Helander, M., and Saikkonen, K. (2012). Endophytic mediation of reactive oxygen species and antioxidant activity in plants: a review. *Fungal Divers.* 54, 1–10. doi: 10.1007/s13225-012-0158-9

Han, L. B., Li, X., Liu, J., and Zeng, H. M. (2007). "Drought-tolerant transgenic perennial ryegrass (*Lolium perenne* L.) obtained via particle bombardment gene transformation of CBF3/DREB1A gene," in *II International Conference on Turfgrass Science and Management for Sports Fields*, 273–282.

Hang, N., Shi, T. R., Liu, Y. R., Ye, W. X., Taier, G., Sun, Y., et al. (2021). Overexpression of *Os-microRNA408* enhances drought tolerance in perennial ryegrass. *Physiol. Plantarum.* 172, 733–747. doi: 10.1111/ppl.13276

Hesse, U., Schöberlein, W., Wittenmayer, L., Förster, K., Warnstorff, K., Diepenbrock, W., et al. (2003). Effects of neotyphodium endophytes on growth, reproduction and drought-stress tolerance of three *Lolium perenne* L. genotypes. *Grass Forage Sci.* 58, 407–415. doi: 10.1111/j.1365-2494.2003.00393.x

Higuchi, H., Sakuratani, T., and Utsunomiya, N. (1999). Photosynthesis, leaf morphology, and shoot growth as affected by temperatures in cherimoya (*Annona cherimola* mill.) trees. *Sci. Hortic.* 80, 91–104. doi: 10.1016/S0304-4238(98)00221-0

Hoffman, L., Ebdon, J. S., Dest, W. M., and DaCosta, M. (2010). Effects of nitrogen and potassium on wear mechanisms in perennial ryegrass: I. Wear tolerance and recovery. *Crop Sci.* 50, 357–366. doi: 10.2135/cropsci2008.08.0473

Huang, B. R., DaCosta, M., and Jiang, Y. W. (2014). Research advances in mechanisms of turfgrass tolerance to abiotic stresses: from physiology to molecular biology. *Crit. Rev. Plant Sci.* 33, 141–189. doi: 10.1080/07352689.2014.870411

Huang, X. Q., Ke, S. Y., and Liu, Y. (2008). Comparative studies on adaptability of Germany ryegrass in Sichuan. *Pratac. Sci.* 25, 60–65. doi: 10.3969/j.issn.1001-0629.2008.10.013

Huang, H. Y., Wang, X. T., Li, J. Q., Gao, Y., Yang, Y. T., Wang, R., et al. (2024). Trends and directions in oats research under drought and salt stresses: a bibliometric analysis (1993–2023). *Plan. Theory* 13:1902. doi: 10.3390/plants13141902

Huang, L. K., Yan, H. D., Jiang, X. M., Yin, G. H., Zhang, X. Q., Qi, X., et al. (2014). Identification of candidate reference genes in perennial ryegrass for quantitative RT-PCR under various abiotic stress conditions. *PLoS One* 9:e93724. doi: 10.1371/journal.pone.0093724

Huchzermeyer, B., Menghani, E., Khardia, P., and Shilu, A. (2022). Metabolic pathway of natural antioxidants, antioxidant enzymes and ROS providence. *Antioxidants.* 11:761. doi: 10.3390/antiox11040761

Hussain, H. A., Men, S. N., Hussain, S., Chen, Y. L., Ali, S., Zhang, S., et al. (2019). Interactive effects of drought and heat stresses on morphophysiological attributes, yield, nutrient uptake and oxidative status in maize hybrids. *Sci. Rep.* 9:3890. doi: 10.1038/s41598-019-40362-7

Iqbal, B., Zhao, X., Khan, K. Y., Javed, Q., Nazar, M., Khan, I., et al. (2024). Microplastics meet invasive plants: unraveling the ecological hazards to agroecosystems. *Sci. Total Environ.* 906:167756. doi: 10.1016/j.scitotenv.2023.167756

Jafari, S., Garmdareh, S. E. H., and Azadegan, B. (2019). Effects of drought stress on morphological, physiological, and biochemical characteristics of stock plant (*Matthiola incana* L.). *Sci. Hortic.* 253, 128–133. doi: 10.1016/j.scienta.2019.04.033

Janke, V. D. C., Botha, P. R., Meeske, R., and Truter, W. F. (2015). Grazing capacity, milk production and milk composition of kikuyu over-sown with annual or perennial ryegrass. *Afr. J. Range For. Sci.* 32, 143–151. doi: 10.2989/10220119.2015.1052096

Jaskune, K., Aleliunas, A., Statkeviciute, G., Kemesyte, V., Studer, B., and Yates, S. (2020). Genome-wide association study to identify candidate loci for biomass formation under water deficit in perennial ryegrass. *Front. Plant Sci.* 11:570204. doi: 10.3389/fpls.2020.570204

Javaid, M. M., Mahmood, A., Alshaya, D. S., AlKahtani, M. D. F., Waheed, H., Wasaya, A., et al. (2022). Influence of environmental factors on seed germination and seedling characteristics of perennial ryegrass (*Lolium perenne* L.). *Sci. Rep.* 12:9522. doi: 10.1038/s41598-022-13416-6

Jedmowski, C., Ashoub, A., Momtaz, O., and Brüggemann, W. (2015). Impact of drought, heat, and theircombination on chlorophyll fluorescence and yield ofwild barley (*Hordeum spontaneum*). *J. Bot.* 2015, 1–9. doi: 10.1155/2015/120868

Jespersen, D., Zhang, J., and Huang, B. (2016). Chlorophyll loss associated with heat-induced senescence in bentgrass. *Plant Sci.* 249, 1–12. doi: 10.1016/j.plantsci.2016.04.016

Jiang, Y. W., Cui, Y., Pei, Z. Y., Liu, H. F., and Sun, S. J. (2016). Growth response and gene expression to deficit irrigation and recovery of two perennial ryegrass accessions contrasting in drought tolerance. *HortScience* 51, 921–926. doi: 10.21273/hortsci.51.7.921

Jones, M. B., Leafe, E. L., and Stiles, W. (1980). Water stress in field-grown perennial ryegrass. I. Its effect on growth, canopy photosynthesis and transpiration. *Ann. Appl. Biol.* 96, 87–101. doi: 10.1111/j.1744-7348.1980.tb04772.x

Jung, S., Estrella, N., Pfaffl, M. W., Hartmann, S., Ewald, F., and Menzel, A. (2021). Correction: impact of elevated air temperature and drought on pollen characteristics of major agricultural grass species. *PLoS One* 16:e0261879. doi: 10.1371/journal.pone.0261879

Kan, Y., Mu, X. R., Gao, J., Lin, H. X., and Lin, Y. S. (2023). The molecular basis of heat stress responses in plants. *Mol. Plant* 16, 1612–1634. doi: 10.1016/j.molp.2023.09.013

Kane, K. H. (2011). Effects of endophyte infection on drought stress tolerance of *Lolium perenne* accessions from the Mediterranean region. *Environ. Exp. Bot.* 71, 337–344. doi: 10.1016/j.envexpbot.2011.01.002

Karsten, H. D., and Macadam, J. W. (2001). Effect of drought on growth, carbohydrates, and soil water use by perennial ryegrass, tall fescue, and white clover. *Crop Sci.* 41, 156–166. doi: 10.2135/cropsci2001.411156x

Kauffman, G. L. III, Kneivel, D. P., and Watschke, T. L. (2007). Effects of a biostimulant on the heat tolerance associated with photosynthetic capacity, membrane thermostability, and polyphenol production of perennial ryegrass. *Crop Sci.* 47, 261–267. doi: 10.2135/cropsci2006.03.0171

Kemesyte, V., Statkeviciute, G., and Brazauskas, G. (2017). Perennial ryegrass yield performance under abiotic stress. *Crop Sci.* 57, 1935–1940. doi: 10.2135/cropsci2016.10.0864

Kimbeng, C. A. (1999). Genetic basis of crown rust resistance in perennial ryegrass, breeding strategies, and genetic variation among pathogen populations: a review. *Aust. J. Exp. Agr.* 39, 361–378. doi: 10.1071/ea98111

Koscielniak, J., Filek, W., and Biesaga-Koscielniak, J. (2006). The effect of drought stress on chlorophyll fluorescence in *Lolium-Festuca* hybrids. *Acta Physiol. Plant.* 28, 149–158. doi: 10.1007/s11738-006-0041-y

Kotak, S., Larkindale, J., Lee, U., Vierling, E., and Scharf, K. D. (2007). Complexity of the heat stress response in plants. *Curr. Opin. Plant Biol.* 10, 310–316. doi: 10.1016/j.pbi.2007.04.011

Kuzniak, E. (2002). Transgenic plants: an insight into oxidative stress tolerance mechanisms. *Acta Physiol. Plant.* 24, 97–113. doi: 10.1007/s11738-002-0027-3

Lei, S. H., and Huang, B. R. (2022). Metabolic regulation of α-ketoglutarate associated with heat tolerance in perennial ryegrass. *Plant Physiol. Bioch.* 190, 164–173. doi: 10.1016/j.plaphy.2022.09.005

Lei, S. H., Rossi, S., and Huang, B. R. (2022). Metabolic and physiological regulation of aspartic acid-mediated enhancement of heat stress tolerance in perennial ryegrass. *Plan. Theory* 11:199. doi: 10.3390/plants11020199

Leisner, C. P. (2020). Review: climate change impacts on food security- focus on perennial cropping systems and nutritional value. *Plant Sci.* 293:110412. doi: 10.1016/j.plantsci.2020.110412

Li, B. F., and Du, H. M. (2019). Mechanism analysis of melatonin pretreatment to improve drought tolerance of perennial ryegrass (*Lolium perenne*). *Pratac Sci.* 36, 666–676. doi: 10.11829/j.issn.1001-0629.2018-0397

Li, N., Euring, D., Cha, J. Y., Lin, Z., Lu, M. Z., Huang, L. J., et al. (2021). Plant hormone-mediated regulation of heat tolerance in response to global climate change. *Front. Plant Sci.* 11:627969. doi: 10.3389/fpls.2020.627969

Li, X., Han, L. B., and Liu, J. (2008). Review on transgenic breeding and biosafety of perennial ryegrass (*Lolium perenne* L.). *Chin. J. Grassland.* 32, 91–95. doi: 10.3724/SP.J.1035.2008.00091

Li, M., Jannasch, A. H., and Jiang, Y. (2020). Growth and hormone alterations in response to heat stress in perennial ryegrass accessions differing in heat tolerance. *J. Plant Growth Regul.* 39, 1022–1029. doi: 10.1007/s00344-019-10043-w

Li, J., Long, Y., Qi, G. N., Li, J., Xu, Z. J., Wu, W. H., et al. (2014). The os-akt1 channel is critical for k+ uptake in rice roots and is modulated by the rice cbl1-cipk23 complex. *Plant Cell* 26, 3387–3402. doi: 10.1105/tpc.114.123455

Li, X., Yang, Y. Q., Sun, X. D., Lin, H. M., Chen, J. H., Ren, J., et al. (2014). Comparative physiological and proteomic analyses of poplar (*Populus yunnanensis*) plantlets exposed to high temperature and drought. *PLoS One* 9:e107605. doi: 10.1371/journal.pone.0107605

Li, P. S., Yu, T. F., He, G. H., Chen, M., Zhou, Y. B., Chai, S. C., et al. (2014). Genome-wide analysis of the HSF family in soybean and functional identification of GmHsf-34 involvement in drought and heat stresses. *BMC Genomics* 15:1009. doi: 10.1186/1471-2164-15-1009

Li, H. C., Zhang, H. N., Li, G. L., Liu, Z. H., Zhang, Y. M., Zhang, H. M., et al. (2015). Expression of maize heat shock transcription factor gene *ZmHsf06* enhances the thermotolerance and drought-stress tolerance of transgenic Arabidopsis. *Funct. Plant Biol.* 42, 1080–1091. doi: 10.1071/fp15080

Lin, J. S., Kuo, C. C., Yang, I. C., Tsai, W. A., Shen, Y. H., Lin, C. C., et al. (2018). MicroRNA160 modulates plant development and heat shock protein gene expression to mediate heat tolerance in Arabidopsis. *Front. Plant Sci.* 9:68. doi: 10.3389/fpls.2018.00068

Liu, S. W., and Jiang, Y. W. (2010). Identification of differentially expressed genes under drought stress in perennial ryegrass. *Physiol. Plant.* 139, 375–387. doi: 10.1111/j.1399-3054.2010.01374.x

Liu, Q., Luo, J., and Cao, S. H. (2006). Experiment in the introduction of herbage variety in the southern Shaanxi. *J. Anhui Agric. Sci.* 2, 3373–3374. doi: 10.3969/j.issn.0517-6611.2006.14.068

Liu, J., Xu, L. X., Wang, Y. B., and Han, L. B. (2019). Ethephon treatment reduced mondo grass (*Ophiopogon japonicus*) gas exchange rate and gene expression of Rbcs. *Eur. J. Hortic. Sci.* 84, 106–112. doi: 10.17660/eJHS.2019/84.2.7

Liu, M. X., Zhang, X. Q., and Yang, C. H. (2004). Analysis on the isozyme of annunl ryegrass Changiiang - II and its parents. *Grass Forage Sci.* 2, 20–22. doi: 10.3969/j.issn.1673-8403.2004.11.007

Ma, B. H., Lin, W. H., Gao, M., Wang, X. D., and Tian, P. (2020). Effects of salicylic acid and *Epichloëon* perennial ryegrass (*Lolium perenne*) under drought stress. *Acta Pratacul. Sin.* 29, 135–144. doi: 10.11686/cyxb2019103

Ma, G. J., Shen, J., Yu, H., Huang, X. B., Deng, X. L., Hu, Z. R., et al. (2022). Genome-wide identification and functional analyses of heat shock transcription factors involved in heat and drought stresses in ryegrass. *Environ. Exp. Bot.* 201:104968. doi: 10.1016/j.envexpbot.2022.104968

Ma, Y. H., Song, Y., and Zhang, H. R. (2009). Effects of uniconazole on the drought resistance of perennial ryegrass. *Pratac. Sci.* 26, 169–173. doi: 10.3969/j.issn.1001-0629.2009.05.030

Mahdavi, S., Kafi, M., Fallahi, E., Shokrpour, M., and Tabrizi, L. (2016). Water stress, nano silica, and digoxin effects on minerals, chlorophyll index, and growth in ryegrass. *Int. J. Plant Prod.* 10, 251–264. doi: 10.22069/IJPP.2016.2791

Mahmood, T., Khalid, S., Abdullah, M., Ahmed, Z., Shah, M. K. N., Ghafoor, A., et al. (2020). Insights into drought stress signaling in plants and the molecular genetic basis of cotton drought tolerance. *Cells* 9:105. doi: 10.3390/cells9010105

Majeed, Y., Rasheed, A., Awan, S. I., Xu, Z. J., Javed, S. O., Gillani, S. F. A., et al. (2023). Physicochemical response of alfalfa (*Medicago sativa* L.) and rye grass (*Lolium perenne* L.) genotypes to induce drought stress at seedling stage. *Appl. Ecol. Env. Res.* 21, 3335–3348. doi: 10.15666/aeer/2104_33353348

Medrano, H., Parry, M. A. J., Socias, X., and Lawlor, D. W. (2010). Long term water stress inactivates rubisco in subterranean clover. *Ann. Appl. Biol.* 131, 491–501. doi: 10.1111/j.1744-7348.1997.tb05176.x

Mittler, R. (2006). Abiotic stress, the field environment and stress combination. *Trends Plant Sci.* 11, 15–19. doi: 10.1016/j.tplants.2005.11.002

Mo, B. T., Long, Z. F., Chen, R. X., Luo, J. Y., Yang, F., and Zhang, M. J. (2009). Breeding of Guicao 1 (*Lolium multiflorum*). *Agric. Sci.* 37, 94–95. doi: 10.3969/j.issn.1001-3601.2009.02.035

Mohammadi, M. H. S., Etemadi, N., Arab, M. M., Aalifar, M., and Pessarakli, M. (2017). Molecular and physiological responses of iranian perennial ryegrass as affected by trinexapac ethyl, paclobutrazol and abscisic acid under drought stress. *Plant Physiol. Bioch.* 111, 129–143. doi: 10.1016/j.plaphy.2016.11.014

Moore, C. E., Meacham-Hensold, K., Lemonnier, P., Slattery, R. A., Benjamin, C., Bernacchi, C. J., et al. (2021). The effect of increasing temperature on crop

photosynthesis: from enzymes to ecosystems. *J. Exp. Bot.* 72, 2822–2844. doi: 10.1093/jxb/erab090

Naidoo, S. (2022). Commentary on the contribution of working group iii to the sixth assessment report of the intergovernmental panel on climate change. *S. Afr. J. Sci.* 118, 9–10. doi: 10.17159/sajs.2022/14690

Ninkov, A., Frank, J. R., and Maggio, L. A. (2022). Bibliometrics: methods for studying academic publishing. *Perspect Med. Educ.* 11, 173–176. doi: 10.1007/s40037-021-00695-4

Ozga, J. A., Kaur, H., Savada, R. P., and Reinecke, D. M. (2017). Hormonal regulation of reproductive growth under normal and heat-stress conditions in legume and other model crop species. *J. Exp. Bot.* 68:erw464. doi: 10.1093/jxb/erw464

Pan, C. Z., Ahammed, G. J., Li, X., and Shi, K. (2018). Elevated CO_2 improves photosynthesis under high temperature by attenuating the functional limitations to energy fluxes, electron transport and redox homeostasis in tomato leaves. *Front. Plant Sci.* 9:1739. doi: 10.3389/fpls.2018.01739

Pan, L., Meng, C., Wang, J. P., Ma, X., Fan, X. M., Yang, Z. F., et al. (2018). Integrated omics data of two annual ryegrass (*Lolium multiflorum* L.) genotypes reveals core metabolic processes under drought stress. *BMC Plant Biol.* 18:26. doi: 10.1186/s12870-018-1239-z

Patel, M., Milla-Lewis, S., Zhang, W., Templeton, K., Reynolds, W. C., Richardson, K., et al. (2015). Overexpression of ubiquitin-like *LpHUB1* gene confers drought tolerance in perennial ryegrass. *Plant Biotechnol. J.* 13, 689–699. doi: 10.1111/pbi.12291

Ponce, R. G., Salas, M. L., and Mason, S. C. (1993). Nitrogen use efficiency by winter barley under different climatic conditions. *J. Plant Nutr.* 16, 1249–1261. doi: 10.1080/01904169309364610

Praba, M. L., Cairns, J. E., Babu, R. C., and Lafitte, H. R. (2009). Identification of physiological traits underlying cultivar differences in drought tolerance in rice and wheat. *J. Agron. Crop Sci.* 195, 30–46. doi: 10.1111/j.1439-037X.2008.00341.x

Prasad, P. V. V., Staggenborg, S. A., and Ristic, Z. (2008). Impacts of drought and/or heat stress on physiological, developmental, growth, and yield processes of crop plants. *Resp. Crops Limited Water Understanding Modeling Water Stress Effects Plant Growth Proc.* 1, 301–355. doi: 10.2134/advagricsystmodel1.c11

Pucciariello, C., Banti, V., and Perata, P. (2012). ROS signaling as common element in low oxygen and heat stresses. *Plant Physiol. Bioch.* 59, 3–10. doi: 10.1016/j.plaphy.2012.02.016

Rahman, M. A., Kabir, A. H., Song, Y., Lee, S. H., Hasanuzzaman, M., and Lee, K. W. (2021). Nitric oxide prevents Fe deficiency-induced photosynthetic disturbance, and oxidative stress in alfalfa by regulating Fe acquisition and antioxidant defense. *Antioxidants.* 10:1556. doi: 10.3390/antiox10101556

Rahman, M. A., Kabir, A. H., Song, Y., Lee, S. H., Hasanuzzaman, M., and Lee, K. W. (2022). Heat shock proteins and antioxidant genes involved in heat combined with drought stress responses in perennial rye grass. *Life* 12:1426. doi: 10.3390/life12091426

Ravel, C., Courty, C., Coudret, A., and Charmet, G. (1997). Beneficial effects of *Neotyphodium lolii* on the growth and the water status in perennial ryegrass cultivated under nitrogen deficiency or drought stress. *Agronomie* 17, 173–181. doi: 10.1051/agro:19970304

Reed, R. C., Bradford, K. J., and Khanday, I. (2022). Seed germination and vigor: ensuring crop sustainability in a changing climate. *Heredity* 128, 450–459. doi: 10.1038/s41437-022-00497-2

Reynolds, M. P., Pierre, C. S., Saad, A. S., Vargas, M., and Condon, A. G. (2007). Evaluating potential genetic gains in wheat associated with stress-adaptive trait expression in elite genetic resources under drought and heat stress. *Crop Sci.* 47, S172–S189. doi: 10.2135/cropsci2007.10.0022IPBS

Rogers, M. E., Lawson, A. R., and Kelly, K. B. (2019). Summer production and survival of perennial ryegrass (*Lolium perenne*) and tall fescue (*Festuca arundinacea*) genotypes in northern Victoria under differing irrigation management. *Crop Pasture Sci.* 70, 1163–1174. doi: 10.1071/cp18542

Safari, S., Nazari, F., Vafaee, Y., and Teixeira da Silva, J. A. (2023). Impact of rice husk biochar on drought stress tolerance in perennial ryegrass (*Lolium perenne* L.). *J. Plant Growth Regul.* 42, 810–826. doi: 10.1007/s00344-022-10588-3

Sahu, P. K., Jayalakshmi, K., Tilgam, J., Gupta, A., Nagaraju, Y., Kumar, A., et al. (2022). ROS generated from biotic stress: effects on plants and alleviation by endophytic microbes. *Front. Plant Sci.* 13:1042936. doi: 10.3389/fpls.2022.1042936

Sato, H., Mizoi, J., Shinozaki, K., and Yamaguchi-Shinozaki, K. (2024). Complex plant responses to drought and heat stress under climate change. *Plant J.* 117, 1873–1892. doi: 10.1111/tpj.16612

Scharf, K. D., Berberich, T., Ebersberger, I., and Nover, L. (2018). The plant heat stress transcription factor (Hsf) family: structure, function and evolution. *BBA-Gene Regul. Mech.* 1861:60. doi: 10.1016/j.bbagrm.2017.12.005

Schauberger, B., Archontoulis, S., Arneth, A., Balkovic, J., Ciais, P., Deryng, D., et al. (2017). Consistent negative response of US crops to high temperatures in observations and crop models. *Nat. Commun.* 8:13931. doi: 10.1038/ncomms13931

Shah, F., Bajwa, A. A., Usman, N., Anjum, S. A., Ayesha, F., Ali, Z., et al. (2017). Crop production under drought and heat stress: plant responses and management options. *Front. Plant Sci.* 8:1147. doi: 10.3389/fpls.2017.01147

Shariatipour, N., Heidari, B., Shams, Z., and Richards, C. (2022). Assessing the potential of native ecotypes of *Poa pratensis* L. for forage yield and phytochemical compositions under water deficit conditions. *Sci. Rep.* 12:1121. doi: 10.1038/s41598-022-05024-1

Shen, J. B., Xu, L. Y., Jin, X. Q., Chen, J. H., and Lu, H. F. (2008). Effect of temperature regime on germination of seed of perennial ryegrass (*Lolium perenne*). *Grass Forage Sci.* 63, 249–256. doi: 10.1111/j.1365-2494.2008.00630.x

Sheng, L. X., and He, X. Q. (2003). The development trend, introduction and breeding of forages and feed crops. *Pratac. Sci.* 20, 14–17. doi: 10.3969/j.issn.1001-0629.2003.05.006

Shi, Y. H., Wan, L. Q., Liu, J. N., Wang, Y. Q., Wu, X. M., and Li, X. L. (2010). Semi-lethal high temperature and heat tolerance of twelve varieties of *Lolium perenne*. *Pratac. Sci.* 30, 491–496. doi: 10.3724/SP.J.1142.2010.40491

Soliman, W. S., Abbas, A. M., Novak, S. J., Fujimori, M., Tase, K., and Sugiyama, S. I. (2021). Inheritance of heat tolerance in perennial ryegrass (*Lolium perenne*, Poaceae): evidence from progeny array analysis. *PeerJ.* 9:e11782. doi: 10.7717/peerj.11782

Steinmeyer, F. T., Lukac, M., Reynolds, M. P., and Jones, H. E. (2013). Quantifying the relationship between temperature regulation in the ear and floret development stage in wheat (*Triticum aestivum* L.) under heat and drought stress. *Funct. Plant Biol.* 40, 700–707. doi: 10.1071/fp12362

Su, K., Bremer, D. J., Keeley, S. J., and Fry, J. D. (2007). Effects of high temperature and drought on a hybrid bluegrass compared with Kentucky bluegrass and tall fescue. *Crop Sci.* 47, 2152–2161. doi: 10.2135/cropsci2006.12.0781

Sun, T. X., Shao, K., Huang, Y., Lei, Y. Y., Tan, L. Y., and Chan, Z. L. (2020). Natural variation analysis of perennial ryegrass in response to abiotic stress highlights *LpHSFC1b* as a positive regulator of heat stress. *Environ. Exp. Bot.* 179:104192. doi: 10.1016/j.envexpbot.2020.104192

Sundaram, S., and Rathinasabapathi, B. (2010). Transgenic expression of fern *Pteris vittata* glutaredoxin PvGrx5 in *Arabidopsis thaliana* increases plant tolerance to high temperature stress and reduces oxidative damage to proteins. *Planta* 231, 361–369. doi: 10.1007/s00425-009-1055-7

Tajdel, M., Mitula, F., and Ludwikow, A. (2016). Regulation of Arabidopsis MAPKKK18 by ABI1 and SnRK2, components of the ABA signaling pathway. *Plant Signal. Behav.* 11:e1139277. doi: 10.1080/15592324.2016.1139277

Thomas, H., Morgan, W. G., Thomas, A. M., and Ougham, H. J. (1999). Expression of the stay-green character introgressed into *Lolium temulentum* Ceres from a senescence mutant of *Festuca pratensis*. *Theor. Appl. Genet.* 99, 92–99. doi: 10.1007/s001220051212

Wafa'a, A. (2010). Comparative effects of drought and salt stress on germination and seedling growth of *Pennisetum divisum* (Gmel.) Henr. *Am. J. Appl. Sci.* 7, 640–646. doi: 10.3844/ajassp.2010.640.646

Wahid, A., and Close, T. J. (2007). Expression of dehydrins under heat stress and their relationship with water relations of sugarcane leaves. *Biol. Plant.* 51, 104–109. doi: 10.1007/s10535-007-0021-0

Wahid, A., Gelani, S., Ashraf, M., and Foolad, M. R. (2007). Heat tolerance in plants: an overview. *Environ. Exp. Bot.* 61, 199–223. doi: 10.1016/j.envexpbot.2007.05.011

Wang, S. G. (2000). Roles of cytokinin on stress-resistance and delaying senescence in plants. *Chin. Bullet. Bot.* 17:121. doi: 10.3969/j.issn.1674-3466.2000.02.004

Wang, J. P., and Bughrara, S. S. (2008). Evaluation of drought tolerance for atlas fescue, perennial ryegrass, and their progeny. *Euphytica* 164, 113–122. doi: 10.1007/s10681-008-9669-6

Wang, Y., Dai, Y., Tao, X., Wang, J. Z., Cheng, H. Y., Yang, H., et al. (2016). Heat shock factor genes of tall fescue and perennial ryegrass in response to temperature stress by RNA-Seq analysis. *Front. Plant Sci.* 6:1226. doi: 10.3389/fpls.2015.01226

Wang, F. G., Liu, Y. Y., Shi, Y. Q., Han, D. L., Wu, Y. Y., Ye, W. X., et al. (2020). SUMOylation stabilizes the transcription factor DREB2A to improve plant thermotolerance. *Plant Physiol.* 183, 41–50. doi: 10.1104/pp.20.00080

Wang, K. H., Liu, Y. R., Tian, J. L., Huang, K. Y., Shi, T. R., Dai, X. X., et al. (2017). Transcriptional profiling and identification of heat-responsive genes in perennial ryegrass by RNA-sequencing. *Front. Plant Sci.* 8:1032. doi: 10.3389/fpls.2017.01032

Wang, W. X., Vinocur, B., Shoseyov, O., and Altman, A. (2004). Role of plant heat-shock proteins and molecular chaperones in the abiotic stress response. *Trends Plant Sci.* 9, 244–252. doi: 10.1016/j.tplants.2004.03.006

Wang, R. M., Wang, Z. Q., and Xiang, Z. X. (2019). Effect of exogenous gamma-aminobutyric acid on the antioxidant defense system and phytohormones metabolism under high temperature stress in perennial ryegrass. *Pratac. Sci.* 36, 111–122. doi: 10.11829/j.issn.1001-0629.2018-0133

Wang, H., Wang, D. M., Zhang, Z. Z., Ren, H. X., Huang, W., and Xie, Z. F. (2022). Effects of exogenous melatonin on antioxidant capacity and nutrient uptake of *Lolium perenne* and *Medicago sativa* under drought stress. *J. Appl. Ecol.* 33, 1311–1319. doi: 10.13287/j.1001-9332.202205.004

Wang, R. M., and Xiong, X. Y. (2016). Effect of temperature stress on growth and metabolism in perennial ryegrass. *Acta Pratacul. Sin.* 25:81. doi: 10.11686/cyxb2015563

Wang, D., Zhang, Y. T., Chen, C. Y., Chen, R. X., Bai, X. C., Qiang, Z. Q., et al. (2023). The genetic variation in drought resistance in eighteen perennial ryegrass varieties and the underlying adaptation mechanisms. *BMC Plant Biol.* 23:451. doi: 10.1186/s12870-023-04460-z

Wang, J., Zhuang, L. L., Zhang, J., Yu, J. J., Yang, Z. M., and Huang, B. R. (2019). Identification and characterization of novel homeodomain leucine zipper (HD-zip) transcription factors associated with heat tolerance in perennial ryegrass. *Environ. Exp. Bot.* 160, 1–11. doi: 10.1016/j.envexpbot.2018.12.023

Wasaya, A., Zhang, X. Y., Fang, Q., and Yan, Z. Z. (2018). Root phenotyping for drought tolerance: a review. *Agronomy* 8:241. doi: 10.3390/agronomy8110241

Wei, T., Gao, H., Yang, D. Z., Zhu, G., Zhang, C. P., Wang, B. C., et al. (2024). Effects of methyl jasmonate on physiological characteristics and drought resistance of alfalfa (*Medicago sativa*) and ryegrass (*Lolium perenne* l.). *J. Plant Growth Regul.* 19, 1–18. doi: 10.1007/s00344-024-11469-7

Wei, H. J., He, W. Y., Wang, Y., Tang, M., and Chen, H. (2023a). The effects of arbuscular mycorrhizal fungi and melatonin on the heat tolerance of perennial ryegrass. *Acta Pratacul. Sin.* 32, 126–138. doi: 10.11686/cyxb2023129

Wei, H. J., Li, X., He, W. Y., Kuang, Y. X., Wang, Z. H., Hu, W. T., et al. (2023b). *Arbuscular mycorrhizal* symbiosis enhances perennial ryegrass growth during temperature stress through the modulation of antioxidant defense and hormone levels. *Ind. Crop. Prod.* 195:116412. doi: 10.1016/j.indcrop.2023.116412

Xie, L. J., Teng, K., Tan, P. H., Chao, Y. H., Li, Y. R. Z., Guo, W., et al. (2020). PacBio single-molecule long-read sequencing shed new light on the transcripts and splice isoforms of the perennial ryegrass. *Mol. Gen. Genomics.* 295, 475–489. doi: 10.1007/s00438-019-01635-y

Xing, J., Yang, Y. W., Zhang, Q., Yin, T. C., Zhao, R. J., Hao, G., et al. (2024). A cytochrome P450 gene, *LpCYP72A15*, confers drought tolerance in perennial ryegrass. *Grass Forage Sci.* 79, 4–16. doi: 10.1111/gfs.12642

Xing, J., Zhao, R. J., Zhang, Q., Huang, X. R., Yin, T. C., Zhang, J., et al. (2022). Genome-wide identification and characterization of the *LpSAPK* family genes in perennial ryegrass highlight *LpSAPK9* as an active regulator of drought stress. *Front. Plant Sci.* 13:922564. doi: 10.3389/fpls.2022.922564

Xiong, Z. M., Cai, H., Feng, W. X., and Sun, G. P. (2006). Effects of PP_{333} on heat tolerance of *Lolium perenne* under high temperature stress. *J. Yangzhou Univ.* 27, 98–100. doi: 10.3969/j.issn.1671-4652.2006.04.025

Xiong, X., Dong, J. X., Li, Y. N., Zhu, G. F., and Ding, X. S. (2024). Comparison of drought resistance during germination of four perennial ryegrass varieties. *J. Zhejiang Agric. Sci.* 65, 2132–2137. doi: 10.16178/j.issn.0528-9017.20230740

Xu, L. X., Han, L. B., and Huang, B. R. (2011). Antioxidant enzyme activities and gene expression patterns in leaves of Kentucky bluegrass in response to drought and post-drought recovery. *J. Am. Soc. Hortic. Sci.* 136, 247–255. doi: 10.21273/jashs.136.4.247

Xu, M., Li, H., Liu, Z. N., Wang, X. H., Xu, P., Dai, S. J., et al. (2021). The soybean CBL-interacting protein kinase, GmCIPK2, positively regulates drought tolerance and ABA signaling. *Plant Physiol. Biochem.* 167, 980–989. doi: 10.1016/j.plaphy.2021.09.026

Xu, S., Li, J., Zhang, X., Wei, H., and Cui, L. (2006). Effects of heat acclimation pretreatment on changes of membrane lipid peroxidation, antioxidant metabolites, and ultrastructure of chloroplasts in two cool-season turfgrass species under heat stress. *Environ. Exp. Bot.* 56, 274–285. doi: 10.1016/j.envexpbot.2005.03.002

Yan, H., and Zhang, X. Q. (2008). Study on the space mutagenic effect of two herbage seeds. *J. Anhui Agric. Sci.* 36:580. doi: 10.3969/j.issn.0517-6611.2008.02.043

Yang, F. P., Liang, M. Q., Zhang, L. Q., Chen, X. Q., Zhang, X. D., Wang, G. Y., et al. (2006). Improvement of perennial ryegrass (*Lolium perenne*) tolerance to drought by gene transferring of stress-inducible transcription factor CBF1 gene. *Acta Agric. Boreali-Sinica.* 21, 14–18. doi: 10.3321/j.issn:1000-7091.2006.01.004

Yang, Z. M., Miao, Y. C., Yu, J. J., Liu, J., and Huang, B. R. (2014). Differential growth and physiological responses to heat stress between two annual and two perennial cool-season turfgrasses. *Sci. Hortic.* 170, 75–81. doi: 10.1016/j.scienta.2014.02.005

Yang, D., Zhang, Z. W., Fang, Z. F., Wang, W. L., Wu, S. M., Sun, T. X., et al. (2024). Genome-wide identification and analysis of the HD-zip transcription factors in perennial ryegrass highlight LpHOX22 and LpHOX24 as negative regulators of osmotic and heat stresses. *Environ. Exp. Bot.* 225:105854. doi: 10.1016/j.envexpbot.2024.105854

Yang, Y. J., Zheng, M. Z., Qin, W. Z., Chen, T., Jiang, S. G., and Liu, J. R. (2012). Responses of tall fescue and perennial ryegrass turfgrasses to drought stress and re-watering treatment. *Pratac. Sci.* 29, 370–376.

Yilmaz, M. B., and Kisakurek, S. (2021). Effect of drought stress on germination and early seedling growth of (*Lolium perenne* L.) cultivars. *Ksu. Tarim. Doga. Derg.* 24, 529–538. doi: 10.18016/ksutarimdoga.vi.777692

Yu, X. Q., Bai, G. H., Liu, S. W., Luo, N., Wang, Y., Richmond, D. S., et al. (2013). Association of candidate genes with drought tolerance traits in diverse perennial ryegrass accessions. *J. Exp. Bot.* 64, 1537–1551. doi: 10.1093/jxb/ert018

Yu, X. Q., Pijut, P. M., Byrne, S., Asp, T., Bai, G. H., and Jiang, Y. W. (2015). Candidate gene association mapping for winter survival and spring regrowth in perennial ryegrass. *Plant Sci.* 235, 37–45. doi: 10.1016/j.plantsci.2015.03.003

Yu, G. H., Xie, Z. N., Chen, W., Xu, B., and Huang, B. R. (2022). Knock down of *NON-YELLOW COLOURING 1-like* gene or chlorophyllin application enhanced chlorophyll accumulation with antioxidant roles in suppressing heat-induced leaf senescence in perennial ryegrass. *J. Exp. Bot.* 73, 429–444. doi: 10.1093/jxb/erab426

Yu, G. H., Xie, Z. N., Zhang, J., Lei, S. S., Lin, W. J., Xu, B., et al. (2021). *NOL*-mediated functional stay-green traits in perennial ryegrass (*Lolium perenne* L.) involving multifaceted molecular factors and metabolic pathways regulating leaf senescence. *Plant J.* 106, 1219–1232. doi: 10.1111/tpj.15204

Zandalinas, S. I., Fritschi, F. B., and Mittler, R. (2021). Global warming, climate change, and environmental pollution: recipe for a multifactorial stress combination disaster. *Trends Plant Sci.* 26, 588–599. doi: 10.1016/j.tplants.2021.02.011

Zandalinas, S. I., Mittler, R., Balfagon, D., Arbona, V., and Gomez-Cadenas, A. (2018). Plant adaptations to the combination of drought and high temperatures. *Physiol. Plant.* 162, 2–12. doi: 10.1111/ppl.12540

Zhang, X. Z., Ervin, E. H., Liu, Y. M., Hu, G. F., Shang, C., Fukao, T., et al. (2015). Differential responses of antioxidants, abscisic acid, and auxin to deficit irrigation in two perennial ryegrass cultivars contrasting in drought tolerance. *J. Am. Soc. Hortic. Sci.* 140, 562–572. doi: 10.21273/jashs.140.6.562

Zhang, X. Y., He, J. G., Sun, X. H., and Wu, J. X. (2011). Transformation of *Lolium perenne* with a fructan: fructan 1-fructosyltransferase gene from *Agropyron cristatum* and enhancement of drought tolerance in transgenic plants. *Acta Pratacul. Sin.* 20, 111–118.

Zhang, J., Li, H., Jiang, Y. W., Li, H. B., Zhang, Z. P., Xu, Z. P., et al. (2020). Natural variation of physiological traits, molecular markers, and chlorophyll catabolic genes associated with heat tolerance in perennial ryegrass accessions. *BMC Plant Biol.* 20:520. doi: 10.1186/s12870-020-02695-8

Zhang, Y., Li, J. Q., Wang, X. T., Yang, Y. T., Zhou, Z. J., Deng, X. L., et al. (2024). A bibliometric analysis review of the *pennisetum* (1970–2023). *Front. Sust. Food Syst.* 8:1405684. doi: 10.3389/fsufs.2024.1405684

Zhang, J., Shi, Y., Zhang, X. Z., Du, H. M., Xu, B., and Huang, B. R. (2017). Melatonin suppression of heat-induced leaf senescence involves changes in abscisic acid and cytokinin biosynthesis and signaling pathways in perennial ryegrass (*Lolium perenne* L.). *Environ. Exp. Bot.* 138, 36–45. doi: 10.1016/j.envexpbot.2017.02.012

Zhang, J., Xing, J., Lu, Q. Y., Yu, G. H., Xu, B., and Huang, B. (2019). Transcriptional regulation of chlorophyll-catabolic genes associated with exogenous chemical effects and genotypic variations in heat-induced leaf senescence for perennial ryegrass. *Environ. Exp. Bot.* 167:103858. doi: 10.1016/j.envexpbot.2019.103858

Zhang, J., Yu, G. H., Wen, W. W., Ma, X. Q., Xu, B., and Huang, B. R. (2016). Functional characterization and hormonal regulation of the *PHEOPHYTINASE* gene *LpPPH* controlling leaf senescence in perennial ryegrass. *J. Exp. Bot.* 67, 935–945. doi: 10.1093/jxb/erv509

Zhao, Y. L., Du, H. W., Wang, Y. K., Wang, H. L., Yang, S. Y., Li, C. H., et al. (2021). The calcium-dependent protein kinase ZmCDPK7 functions in heat-stress tolerance in maize. *J. Integr. Plant Biol.* 63, 510–527. doi: 10.1111/jipb.13056

Zhao, L. L., Wang, L. T., Chen, K. K., Sun, H., and Wang, P. C. (2024a). Effects of arbuscular mycorrhizal fungi on the growth and physiological performance of *Sophora davidii* seedling under low-phosphorus stress. *J. Plant Growth Regul.* 43, 2383–2395. doi: 10.1007/s00344-024-11273-3

Zhao, B. S., Yu, S. M., Lu, Y. R., Liu, S. Q., Wang, G. K., and Wang, Y. (2022). Effects of AM Fungi on growth and physiology of *Lolium perenne* under high temperature stress. *Forestry Environ. Sci.* 38, 113–119. doi: 10.3969/j.issn.1006-4427.2022.05.017

Zhao, L. L., Zhao, X., Huang, L., Liu, X. Y., and Wang, P. C. (2024b). Transcriptome analysis of *Pennisetum americanum* × *Pennisetum purpureum* and *Pennisetum americanum* leaves in response to high-phosphorus stress. *BMC Plant Biol.* 24:635. doi: 10.1186/s12870-024-05339-3

Zhou, S. P., and Abaraha, A. (2007). Response to heat stress in warm season and cool season turf grass cultivars. *Sci. Res. Essays* 16, 371–376. doi: 10.1002/pon.1070

Zhou, Z. J., Li, J. Q., Gao, Y., Wang, X. T., Wang, R., Huang, H. Y., et al. (2024). Research on drought stress in *Medicago sativa* L. from 1998 to 2023: a bibliometric analysis. *Front. Plant Sci.* 15:1406256. doi: 10.3389/fpls.2024.1406256

Zhu, Y. Q., Liao, Z. C., Yang, J., Ye, H. T., Han, C. Y., Xu, W. Z., et al. (2022). Genotypic and phenotypic diversity of heat tolerance among and within perennial ryegrass (*Lolium perenne* L.). *Braz. J. Bot.* 45, 1223–1234. doi: 10.1007/s40415-022-00854-9

Zhuang, L. L., Cao, W., Wang, J., Yu, J. G., Yang, Z. M., and Huang, B. R. (2018). Characterization and functional analysis of *FaHsfC1b* from *Festuca arundinacea* conferring heat tolerance in Arabidopsis. *Int. J. Mol. Sci.* 19:2702. doi: 10.3390/ijms19092702

Zou, H., Wang, C. X., Yu, J. Q., Huang, D. F., Yang, R. G., and Wang, R. Z. (2023). Eliminating greenhouse heat stress with transparent radiative cooling film. *Cell Rep. Phys. Sci.* 4:101539. doi: 10.1016/j.xcrp.2023.101539

Frontiers in
Sustainable Food Systems

Exploring sustainable solutions to global food security

Aligned with the UN Sustainable Development Goals, this journal explores the intersection of food systems, science and practice of sustainability including its environmental, economic and social justice dimensions.

Discover the latest Research Topics

See more →

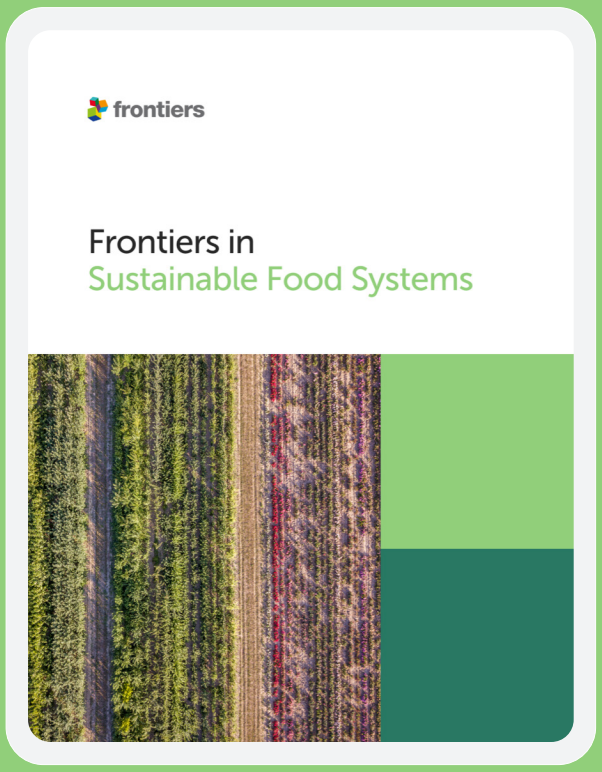

Frontiers

Avenue du Tribunal-Fédéral 34
1005 Lausanne, Switzerland
frontiersin.org

Contact us

+41 (0)21 510 17 00
frontiersin.org/about/contact